Mechanics

A Joint Publication of the Applied Mechanics Division

. . . John Zickel 165
. . . J. W. [illegible] 176
. . . J. W. [illegible] 181
. . . W. S. [illegible] 185
. . . Paul [illegible] 191
. . . Daniel [illegible] 195
. . . R. L. [illegible] 201
. . . Bertram [illegible] 207
. . . T. H. [illegible] 214
. . . P. [illegible] 219
. . . R. G. Thomas 225
. . . A. M. [illegible] 231
. . . M. E. [illegible] 239
. . . E. V. [illegible] Jr. 245
W. G. Hafke and M. B. Dusseau 247
S. C. Lin and G. W. [illegible] 255
R. B. Kemp and W. E. [illegible] 263
. . . L. R. W[illegible] 269
. . . P. G. [illegible] Jr. 276
. . . Z. S. Kuss and E. D. [illegible] 277
. . . E. M. Gaither and W. E. Johnson 284
. . . W. E. [illegible] 287
. . . A. R. Schmitt 293
. . . E. V. [illegible] 298
. . . A. C. Rigg and G. O. [illegible] 304
. . . P. W. [illegible] 307
. . . O. P. Khorlunde[illegible] 313
. . . H. M. [illegible] and E. Pr[illegible] Jr. 319
. . . J. S. [illegible] 314
. . . Eric [illegible] 315
. . . M. L. [illegible] 318
. . . E. P. N. [illegible] 319
. . . H. Dan[illegible] 319
. . . C. C. Chen, N. J. [illegible]
. . . and R. B. [illegible] 329

[illegible] Mechanical Engineers

Journal of Applied Mechanics

Papers Classified to the Transactions by the ASME Applied Mechanics Division

[illegible] M. Hetényi, Secretary

Jesse M. Lessells, Technical Editor

Published Quarterly by

The American Society of Mechanical Engineers

Publication Office, 20th and Northampton Streets, Easton, Pa.
Editorial Department at the Headquarters of the Society, 29 West Thirty-Ninth Street, New York18, N. Y.

OFFICERS OF THE SOCIETY
J. W. Roppes, President

[illegible] C. R. Davis, Secretary

[illegible]

[illegible] K. W. Cunningham, Managing Editor
H. K. Weston, Asst. Managing Editor

No Editor: The Society shall not be responsible for statements or opinions advanced in papers or . . . printed in its publications (B13, Par. 4)

Published quarterly by The American Society of Mechanical Engineers. Publication office at 20th and Northampton Streets, Easton, Pa. The editorial [illegible] 29 West Thirty-Ninth Street, New York 18, N. Y. Cable address, "Dynamic," New York. Price [illegible] $4.00. Add 25c for postage in all countries outside the United States. [illegible] Society, or affiliated societies, and [illegible] Society publications except those they are to be effective on the mailing list. [illegible] Entered as second-class matter [illegible] for membership or subscription advanced in papers or . . . printed in [illegible] March 14, 1933, at the Post Office at Easton, Pa., under the act of August 24, 1912. . . . [illegible] Permission to print from this publication may be made on condition that full credit be [illegible] of publication be stated.

Pretwisted Beams and Columns[1]

By JOHN ZICKEL,[2] SCHENECTADY, N. Y.

A theory is developed for the behavior of pretwisted structural members of thin-walled section with slight initial bending. The stresses are at first determined along and perpendicular to the fibers and are then transformed to stresses in the cross section and along the axis. Although the development is perfectly general the integrations are only indicated for doubly symmetric sections. The buckling of doubly symmetric columns which are initially straight but are pretwisted at a constant rate is treated in detail. The results show that columns of decidedly unequal principal moments of inertia can be strengthened up to 90 per cent, but columns of equal moments of inertia are weakened by initial twist. In analogy to the Euler load of the buckling theory for straight, untwisted columns, a reduced Euler load is defined. The buckling load is the product of this reduced Euler load and a stiffening factor.

Nomenclature

The following nomenclature is used in the paper:

A = area of cross section

$A_1 = 1 + \dfrac{\delta'^2}{G\bar{C}}\,(2G\bar{C}\bar{\rho}^2 - EJ_1\bar{\rho}^2 + EJ_3)$

$A_2 = 1 - 3\delta'^2 J_3/J_1 + \delta'^4 J_4/J_1 - G\bar{C}_7/E\bar{A}\bar{\rho}^2$

$A_3 = (EI_{\xi 1} - 4Z_\eta{}^4\delta'^2)^{-1}$

$A_4 = (EI_{\eta 1} - 4Z_\xi{}^4\delta'^2)^{-1}$

c = additional curvature

c_0 = initial curvature

C = torsional rigidity

E = Young's modulus

$\vec{i}, \vec{\jmath}_\xi, \vec{\jmath}_\eta$ = unit vectors in nonorthogonal co-ordinate system

$\vec{f}$ = vector of stressed fiber

$\vec{f}_0$ = vector of unstressed fiber

G = shear modulus

G_n = stress couple ($n = \xi, \eta, \zeta$)

I_ξ, I_ζ = moment of inertia

k = additional curvature

k_0 = initial curvature

K = ratio of buckling load to modified Euler load

K_z = Ziegler's ratio of buckling load to Euler load

l = co-ordinate along center line of stressed beam-column

L = length of beam-column

M_n = applied moment ($n = x, y, z$)

n = normal to middle curve of cross section

N_n = stress resultant ($n = \xi, \eta, \zeta$)

P_n = point in cross section ($n = 1, 2, 3, 4$)

r = radial distance $\left(r = \sqrt{x^2 + y^2} = \sqrt{\xi^2 + \eta^2}\right)$

R = $(1 + r^2\delta'^2)^{-1}$

s = co-ordinate along middle curve of cross section

t = co-ordinate along center line of unstressed beam-column

T = thickness of section

u, v, w = additional displacements

u_0, v_0 = initial displacements

x, y, z = co-ordinates of unstressed beam-column

x_0, y_0, z_0 = stationary co-ordinates

X, Y, Z = applied forces

$\alpha_{1,2} = {}^1/_4 Z(A_3 + A_4) + \delta_0'^2 \pm \sqrt{{}^1/_4 Z^2(A_3 - A_4)^2 + 2Z\delta_0'^2(A_3 + A_4)}$

$\alpha_3 = (\alpha_1{}^2 + \delta_0'^2 - ZA_3)/2\alpha_1\delta_0' = 2\alpha_1\delta_0'/(\alpha_1{}^2 + \delta_0'^2 - ZA_4)$

$\alpha_4 = (\alpha_2{}^2 + \delta_0'^2 - ZA_3)/2\alpha_2\delta_0' = 2\alpha_2\delta_0'/(\alpha_2{}^2 + \delta_0'^2 - ZA_4)$

$\alpha_5 = {}^1/_2(\alpha_3/\alpha_4 + \alpha_4/\alpha_3)$

β = additional twist

γ = angle in $\vec{f}, \vec{\jmath}_\xi, \vec{\jmath}_\eta$ co-ordinate system

γ_n = direction cosines ($n = 1, 2, 3$)

Γ = Wagner torsion constant

δ = initial twist

δ_0' = constant rate of initial twist

Δ = total initial twist

ϵ_f = strain in stressed fiber

θ = angle between middle curve of cross section and ξ-axis

ξ, η, ζ = co-ordinates of stressed beam-column

$\bar{\xi}^4 = I_{\eta 3}/\bar{A}$

$\bar{\eta}^4 = I_{\xi 3}/\bar{A}$

ρ = polar radius of gyration

$\bar{\rho}^2 = J_1/\bar{A}$

ρ_ξ, ρ_η = radius of gyration about ξ or η-axis

σ_n = normal stress ($n = f, \zeta$)

τ = additional twist per unit length

τ_0 = initial twist per unit length

τ_{sn} = shear stress

φ = torsion function

ψ = stress function

ω = warping displacement

$$C_2 = -\frac{\xi\dfrac{\partial\psi}{\partial\xi}\,(1 - \xi^2 r^2\delta'^4)}{(1 + \xi^2\delta'^2)^{3/2}} - \frac{\eta\dfrac{\partial\psi}{\partial\eta}\,(1 - \eta^2 r^2\delta'^4)}{(1 + \eta^2\delta'^2)^{3/2}}$$

$$C_3 = -\frac{\xi\dfrac{\partial\psi}{\partial\xi}}{\sqrt{1 + \xi^2\delta'^2}} - \frac{\eta\dfrac{\partial\psi}{\partial\eta}}{\sqrt{1 + \eta^2\delta'^2}}$$

$$C_4 = -\frac{\xi^2\dfrac{\partial\psi}{\partial\xi}\,\delta'^2}{\sqrt{1 + \eta^2\delta'^2}} - \frac{\eta^2\dfrac{\partial\psi}{\partial\eta}\,\delta'^2}{\sqrt{1 + \xi^2\delta'^2}}$$

$$C_5 = -\frac{\xi\dfrac{\partial\psi}{\partial\xi}}{\sqrt{1 + \eta^2\delta'^2}} - \frac{\eta\dfrac{\partial\psi}{\partial\eta}}{\sqrt{1 + \xi^2\delta'^2}}$$

---

[1] The results presented in this paper were obtained in the course of research sponsored partly by the Office of Naval Research under Contract N7onr-358, and partly under a grant from the Column Research Council, and the Rhode Island Department of Public Works.

[2] Knolls Atomic Power Laboratory, General Electric Company; formerly, Research Associate, Graduate Division of Applied Mathematics, Brown University, Providence, R. I. At present with Atomic Products Department, General Electric Company, San Jose, Calif.

Contributed by the Applied Mechanics Division and presented at the Diamond Jubilee Annual Meeting, Chicago, Ill., November 13–18, 1955, of The American Society of Mechanical Engineers.

Discussion of this paper should be addressed to the Secretary, ASME, 29 West 39th Street, New York, N. Y., and will be accepted until July 10, 1956, for publication at a later date. Discussion received after the closing date will be returned.

Note: Statements and opinions advanced in papers are to be understood as individual expressions of their authors and not those of the Society. Manuscript received by ASME Applied Mechanics Division, December 29, 1954. Paper No. 55—A-28.

$$C_6 = -\frac{\xi\eta^2\dfrac{\partial\psi}{\partial\xi}\delta'^2}{\sqrt{1+\xi^2\delta'^2}} - \frac{\xi^2\eta\dfrac{\partial\psi}{\partial\eta}\delta'^2}{\sqrt{1+\eta^2\delta'^2}}$$

$$C_7 = -\frac{\xi\eta^2\dfrac{\partial\psi}{\partial\xi}\delta'^2}{(1+\xi^2\delta'^2)^{3/2}} - \frac{\xi^2\eta\dfrac{\partial\psi}{\partial\eta}\delta'^2}{(1+\eta^2\delta'^2)^{3/2}}$$

Integrals

$$\bar{A} = \int_A R^2 dA$$

$$\bar{C} = 1/2\int_A \sqrt{R}C_3\left(1+\sqrt{1+R\xi^2\eta^2\delta'^4}\right)dA$$

$$\overline{\bar{C}} = \int_A \sqrt{R}C_3\left(1-r^2\delta'^2\sqrt{1+R\xi^2\eta^2\delta'^4}\right)dA$$

$$\bar{C}_5 = \int_A R^{3/2}C_5 dA - \int_A R^2 C_4\, dA + \int_A R^2 C_3\sqrt{(1+\xi^2\delta'^2)(1+\eta^2\delta'^2)}\,dA$$

$$\bar{C}_7 = \int_A \Big[R^2(2r^2\delta'^2+\xi^2\eta^2\delta'^4)\sqrt{(1+\xi^2\delta'^2)(1+\eta^2\delta'^2)} + 2r^2\delta'^2\sqrt{1+r^2\delta'^2}\Big]C_5 dA - \int_A R^2\xi^2\eta^2\delta'^4(C_5-C_4)\,dA + \int_A R^2 r^2\delta'^2 C_3\sqrt{(1+\xi^2\delta'^2)(1+\eta^2\delta'^2)}\,dA - \int_A R^{3/2}C_7 dA$$

$$\Phi = \int_A R^2 r^2\xi\eta\varphi dA$$

$$I_{\xi 1} = \int_A R^2\eta^2 dA \qquad I_{\eta 1} = \int_A R^2\xi^2 dA$$

$$I_{\xi 2} = \int_A R^2 r^2\eta^2 dA \qquad I_{\eta 2} = \int_A R^2 r^2\xi^2 dA$$

$$I_{\xi 4} = \int_A R^2 r^4\eta^2 dA \qquad I_{\eta 4} = \int_A R^2 r^4\xi^2 dA$$

$$I_{\xi 3} = \int_A R^{3/2}\eta^2\left[\frac{\xi^2+\xi\dfrac{\partial\varphi}{\partial\eta}}{(1+\xi^2\delta'^2)^{3/2}}(1-\xi^2\delta'^2) + \frac{\eta^2-\eta\dfrac{\partial\varphi}{\partial\xi}}{(1+\eta^2\delta'^2)^{3/2}}(1-\eta^2\delta'^2)\right]dA + \int_A R^2\eta^2\left[\frac{\xi^2+\xi\dfrac{\partial\varphi}{\partial\eta}}{\sqrt{1+\eta^2\delta'^2}}(1-\xi^2\delta'^2+\eta^2\delta'^2) + \frac{\eta^2-\eta\dfrac{\partial\varphi}{\partial\xi}}{\sqrt{1+\xi^2\delta'^2}}(1+\xi^2\delta'^2-\eta^2\delta'^2)\right]dA$$

$$I_{\eta 3} = \int_A R^{3/2}\xi^2\left[\frac{\xi^2+\xi\dfrac{\partial\varphi}{\partial\eta}}{(1+\xi^2\delta'^2)^{3/2}}(1-\xi^2\delta'^2) + \frac{\eta^2-\eta\dfrac{\partial\varphi}{\partial\xi}}{(1+\eta^2\delta'^2)^{3/2}}(1-\eta^2\delta'^2)\right]dA + \int_A R^2\xi^2\left[\frac{\xi^2+\xi\dfrac{\partial\varphi}{\partial\eta}}{\sqrt{1+\eta^2\delta'^2}}(1-\xi^2\delta'^2+\eta^2\delta'^2) + \frac{\eta^2-\eta\dfrac{\partial\varphi}{\partial\xi}}{\sqrt{1+\xi^2\delta'^2}}(1+\xi^2\delta'^2-\eta^2\delta'^2)\right]dA$$

$$J_1 = \int_A R^2 r^2 dA$$

$$J_2 = \int_A R^2 r^2 dA$$

$$J_3 = \int_A R^2 r^4 dA$$

$$J_3 = \int_A R^2 r^4 dA$$

$$J_4 = \int_A R^2 r^6 dA$$

$$\Gamma_1 = \int_A C_2 dA$$

$$\Gamma_2 = \int_A C_7 dA$$

$$\Gamma_3 = \int_A C_3 r^2\sqrt{1+R\xi^2\eta^2\delta'^4}\,dA$$

$$\Gamma_4 = \int_A C_7 r^2\sqrt{1+R\xi^2\eta^2\delta'^4}\,dA$$

$$\Gamma_5 = 1/2\int_A C_2\left(1+\sqrt{1+R\xi^2\eta^2\delta'^4}\right)dA$$

$$\Gamma_6 = 1/2\int_A C_7\left(1+\sqrt{1+R\xi^2\eta^2\delta'^4}\right)dA$$

$$\Gamma_7 = 1/2\int_A \xi\eta\left(\bar{r}_\xi\int_0^\xi\sqrt{R}\,ds + \bar{r}_\eta\int_0^\eta\sqrt{R}\,dn\right)\left(1+\sqrt{1+R\xi^2\eta^2\delta'^4}\right)dA$$

$$\Gamma_8 = 1/2\int_A \xi\eta\left(\bar{r}_\xi\int_0^\xi R^{3/2}r^2 ds + \bar{r}_\eta\int_0^\eta R^{3/2}r^2 dn\right)\left(1+\sqrt{1+R\xi^2\eta^2\delta'^4}\right)dA$$

$$\bar{\Gamma}_1 = \Gamma_1 - \Gamma_3\delta'^2 + 2\Gamma_3\bar{\rho}^2\delta'^2$$

$$\bar{\Gamma}_2 = \Gamma_2 - \Gamma_4\delta'^2 + 2\Gamma_4\bar{\rho}^2\delta'^2$$

When δ is zero everywhere along the beam-column then some of these integrals reduce to standard engineering terms, such as

$\bar{A} = A$ = cross-sectional area

$\bar{C} = \overline{\bar{C}} = C$ = torsional rigidity

$I_{\xi 1} = I_\xi$ = moment of inertia about ξ-axis

$I_{\eta 1} = I_\eta$ = moment of inertia about η-axis

$J_1 = J_2 = J$ = polar moment of inertia

$\Gamma_1 = \bar{\Gamma}_1 = \Gamma$ = Wagner's torsion constant

Introduction

In buckling or bending of ordinary beam-columns the major deflections occur in the direction perpendicular to that of the axis about which the cross section has the smallest moment of inertia. When a beam or column is pretwisted, this axis of least moment of inertia is no longer perpendicular to the direction of deflection at all times and greater moments of inertia are taking effect. Because the deflection in a given direction is a function of the inverse of the moment of inertia about an axis perpendicular to the deflection, it would seem reasonable to expect the deflection of a pretwisted beam-column to be a function of the average of the reciprocals of the affected moments of inertia. Ziegler (1)[3] has, in fact, shown that pretwisted columns of rectangular cross section can be strengthened up to a factor of 2.

The deformations of thin-walled beam-columns can be more easily visualized if these structural members are considered to consist of a great many longitudinal fibers. Wagner (2), Kappus (3), and Goodier (4) have applied this analysis to untwisted columns and thus found a simple derivation of the Wagner constant Γ for nonuniform torsion. In this paper an investigation is presented in which pretwisted beams and columns are analyzed in

[3] Numbers in parentheses refer to the Bibliography at the end of the paper.

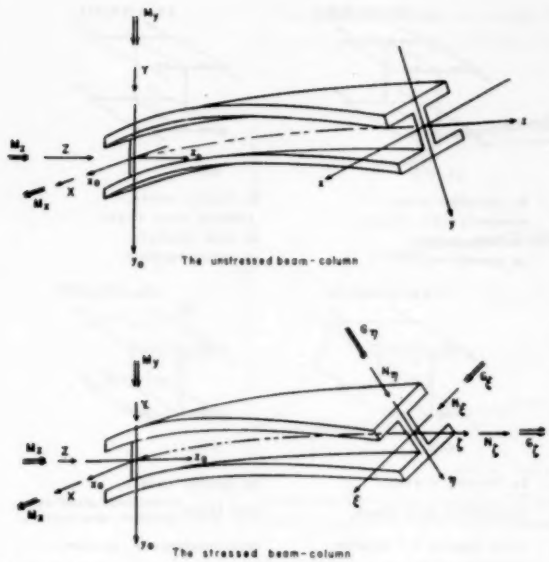

FIG. 1 PRETWISTED BEAM-COLUMN WITH ITS CO-ORDINATE SYSTEMS

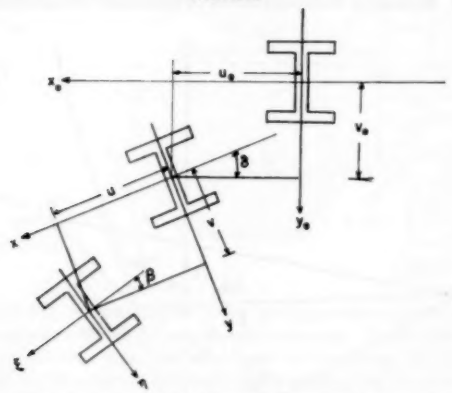

FIG. 2 RELATIONSHIP OF CO-ORDINATE SYSTEMS PROJECTED INTO THE x_0, y_0-PLANE—SCHEMATIC

terms of stresses along the direction of each fiber and perpendicular to it.

KINEMATICS

The configuration of the beam-column is described in terms of three co-ordinate systems, the stationary x_0, y_0, z_0-system, the x, y, z system of the unstressed beam-column and the ξ, η, ζ-system of the stressed beam-column. The x_0, y_0, x, y, ξ, η-directions are taken along the principal axes of the cross sections and the z_0, z, ζ-direction is taken tangent to the line through the shear centers. The three systems are so chosen that they will coincide at one end, Fig. 1. For sake of simplicity doubly symmetric sections are used in this development. The initial displacements of a point on the center line are u_0 and v_0 and the additional displacements are u and v. The projections of the principal axes of one system unto the other, form the angles δ and β, respectively, Fig. 2. The displacement in the z-direction is w if it is due to bending or axial force and ω if it is warping due to torsion. It is assumed that u, v, w, β, u_0, v_0, and δ are functions of arc length only and that all but the last quantity are of small order, so that their products or products of their derivatives are negligible. Tables of direction cosines connecting the three systems are shown in the Appendix. Also described there in terms of displacements and rotations are the initial curvatures c_0 and k_0 and the additional curvatures c and k.

Differentiation with respect to the stressed arc length l is denoted by $'$, the unstressed arc length is called t. Goodier (4) and Sokolnikoff (6) have defined the warping function ω as the product of β' and the torsion function φ. The latter is a function of the cross section only and is related to the stress function by Equation [12].

A differential length of an unstressed fiber between cross sections dt apart, Fig. 3(a), is

$$|f_0| = R^{-1/2}(1 - Rxk_0 + Ryc_0)dt \quad \ldots\ldots\ldots [1]$$

with

$$r = \sqrt{x^2 + y^2}$$

$$R = (1 + r^2\delta'^2)^{-1}$$

The same fiber, after it has been stressed, Fig. 3(b), is of length

$$|f| = R^{-1/2}[1 - R(r^2\delta'^2\beta' + w' + \omega' - \xi k - \xi k_0 + \eta c + \eta c_0)]dl \quad \ldots\ldots\ldots [2]$$

STRESSES

Thus the particular fiber has been strained by an amount

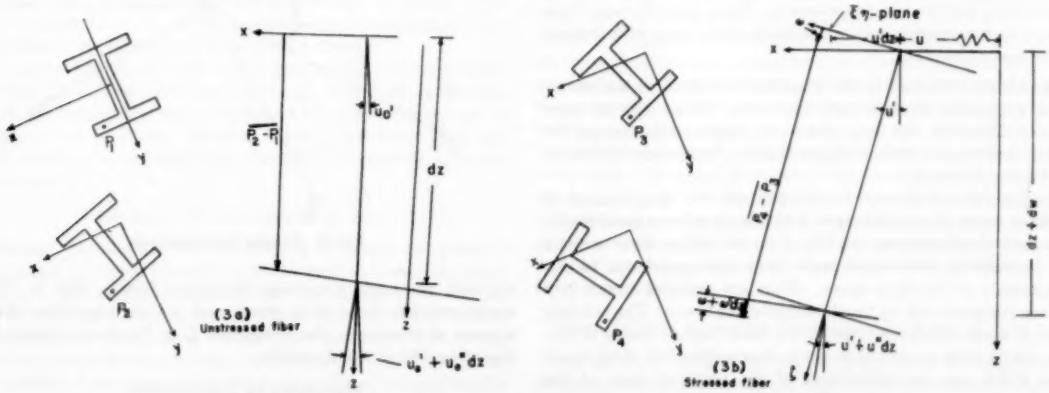

FIG. 3 ORIENTATION OF A FIBER OF INFINITESIMAL LENGTH—SCHEMATIC
(yz-plane not shown.)

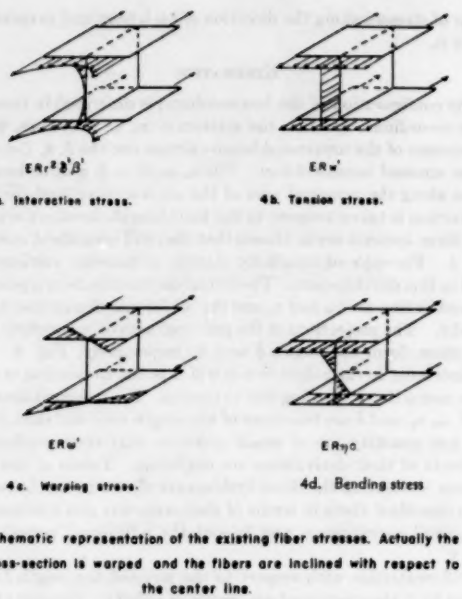
ER$r^2\delta'\beta'$
4a. Interaction stress.
ERw'
4b. Tension stress.
ERω'
4c. Warping stress.
ER$\eta\phi$
4d. Bending stress
Schematic representation of the existing fiber stresses. Actually the cross-section is warped and the fibers are inclined with respect to the center line.

FIG. 4 FIBER STRESSES IN CROSS SECTION OF A PRETWISTED BEAM-COLUMN

$$\epsilon_f = \frac{|f|}{|f_0|} - 1 = R(\delta'\beta' r^2 + w' + \omega - \xi k + \eta c) \ldots . [3]$$

and the corresponding fiber stress is

$$\sigma_f = ER(\delta'\beta' r^2 + w' + \omega' - \xi k + \eta c) \ldots . . . . [4]$$

This stress consists of five components, which are shown schematically in Fig. 4, as follows:

(*a*) The "interaction stress" $ER\,\delta'\beta' r^2$ is due to the interaction of initial and additional twist.

(*b*) The "tension stress" ERw' is uniformly distributed over the cross section.

(*c*) The "warping stress" $ER\omega'$ is antisymmetric in both co-ordinates. In an I-section it varies in each flange from tension to compression.

(*d*) The "bending stresses" $ER\xi k$ and $ER\eta c$ are due to bending about the η and ξ-axes, respectively. They vary linearly from tension to compression but are antisymmetric only with respect to the axis of bending.

The initial twist causes the fibers to be inclined to the center line in proportion to their radial distance. Under uniform compression, therefore, the fiber stresses are concentrated toward the center, and because of their orientation the fibers resist additional twist more effectively.

Wagner (2) and Goodier (4) have shown that the variation of the fiber stress along the length of the beam-column gives rise to secondary shear stresses. In Fig. 5 the secondary shear stresses are pictured in accordance with their correspondence to the components of the fiber stress. They are assumed to act in a surface perpendicular to the direction of the fibers. The primary shear stresses, which are those of the Saint Venant theory of torsion, are likewise presumed to act in that surface but along directions which are the projections of the principal axes of the corresponding cross section. These directions and the direction of the fiber define another co-ordinate system. It is nonorthogo-

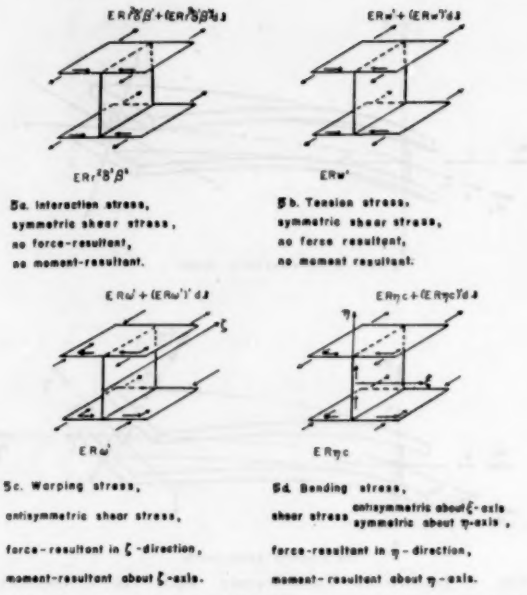
ER$r^2\delta'\beta'$
5a. Interaction stress, symmetric shear stress, no force-resultant, no moment-resultant.
ERw'
5b. Tension stress, symmetric shear stress, no force resultant, no moment resultant.
ERω'
5c. Warping stress, antisymmetric shear stress, force-resultant in ζ-direction, moment-resultant about ζ-axis.
ERηc
5d. Bending stress, shear stress antisymmetric about ξ-axis symmetric about η-axis, force-resultant in η-direction, moment-resultant about η-axis.

FIG. 5 SCHEMATIC REPRESENTATION OF SECONDARY SHEAR STRESSES

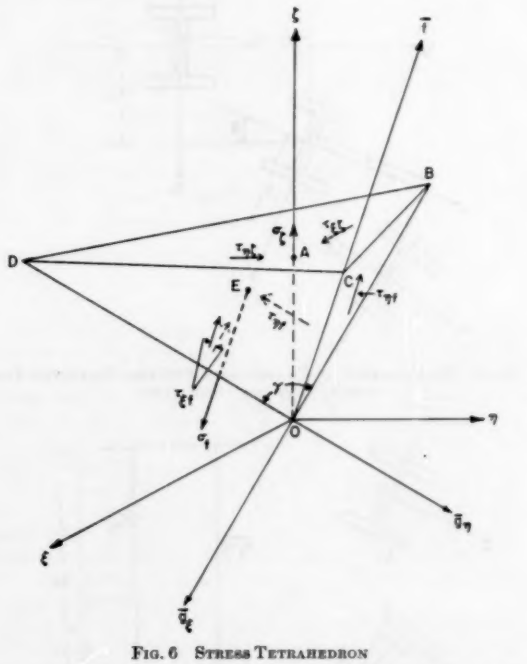

FIG. 6 STRESS TETRAHEDRON

nal with the angle γ between the $\bar{g}_\xi$ and $\bar{g}_\eta$-axes, Fig. 6. The transformation from fiber stress and its corresponding shear stresses to stresses in the orthogonal ξ, η, ζ-system is given by Equation [20] in the Appendix.

EQUATIONS OF EQUILIBRIUM

The stress resultants N_ξ, N_η, N_ζ, and stress couples G_ξ, G_η, G_ζ,

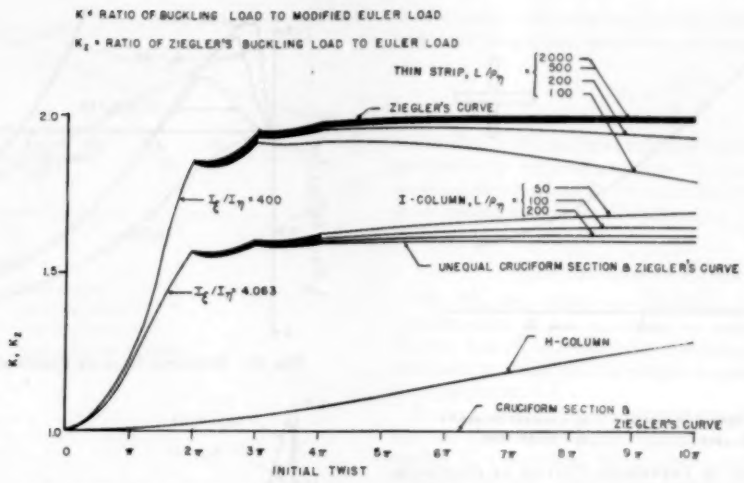

FIG. 7 RATIOS OF BUCKLING LOADS TO MODIFIED EULER LOADS FOR PRETWISTED COLUMNS
(The apparent strengthening shown here is actually offset considerably by the modified Euler load.)

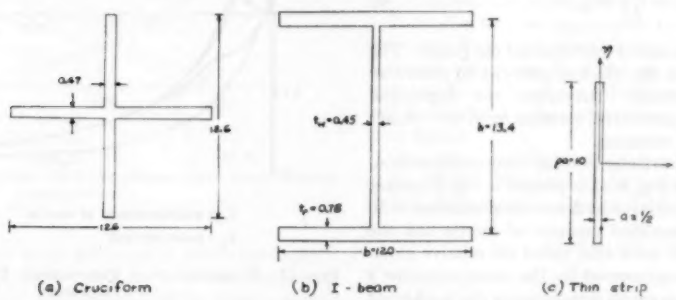

FIG. 8 CROSS SECTIONS

shown in Fig. 1, are obtained by integrating stresses and stresses with moment arms over the cross-sectional area. From these the three equilibrium equations are found by equating the stress couples to the external moments and moments due to external forces. Similarly, the stress resultants can be equated to the external forces. The equation for N_ξ then permits the elimination of both N_ξ and w from the equilibrium equations. The latter reduce to a set of three simultaneous equations in the variables of displacement u and v and the twist β.

No general solution of the equilibrium equations is obtainable, because, in addition to being nonlinear, they have coefficients which are functions of the independent variable l. A number of problems can be solved, however, with comparative ease, and their results give an insight into the effect of pretwisting beams and columns.

EULER OR TRANSVERSE BUCKLING

Perhaps the simplest such problem is a column on spherical seats which is initially straight but pretwisted at a constant rate of twist δ_0'. One end is prevented from rotating about the column axis to avoid rigid-body motion and both ends are held so that no warping stress exists there. With these conditions one of the equations of equilibrium becomes an equation in only the dependent variable β, and its solution shows that the additional twist is proportional to the initial twist. This solution also precludes warping at any section. At the same time it makes the other two equations independent of the additional twist. Their solution leads to a characteristic equation

$$\cos \alpha_1 L \cos \alpha_2 L + \alpha_3 \sin \alpha_1 L \sin \alpha_2 L = 1 \ldots\ldots [5]$$

in which the α's are integral functions of load, pretwist, and cross-sectional area. The buckling load is the smallest (nonzero) characteristic value which satisfies Equation [5]. The equation appears to be identical with Ziegler's (1) Equation [14]. However, the use of fiber stresses causes the α's to be entirely different. As a consequence, Ziegler finds the stiffening effect due to rotation of the cross section, but he does not show the marked and very important weakening effect of rotation per se. The ratio K_z of Ziegler's buckling load to the least Euler load for cross sections with ratios of principal moments of inertia of 1, 4.063, and 400 is shown in Fig. 7. In the following sections thin-walled columns with the same ratios of principal moments of inertia are investigated in terms of fiber stresses and stresses perpendicular to them, and the pronounced weakening effect due to the inclination of the fiber is demonstrated.

CROSS SECTION OF EQUAL PRINCIPAL MOMENTS OF INERTIA

For columns whose cross section is identical in the x and y-direction, such as the cruciform section, the integrals of Equation [5] in the x and y-direction become identical. As a consequence it is possible to solve the equation explicitly for the buckling load

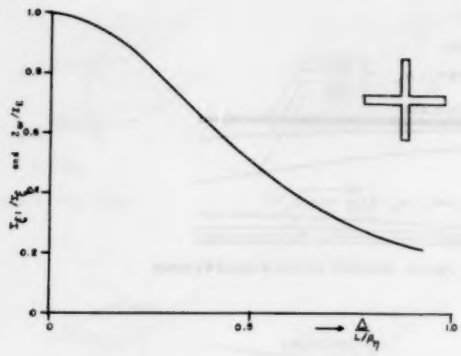

$I_{\xi 1}$ = MODIFIED MOMENT OF INERTIA, I_ξ = MOMENT OF INERTIA
Z_{cr} = BUCKLING LOAD, Z_E = EULER LOAD

FIG. 9 BUCKLING LOAD OF PRETWISTED COLUMN OF CRUCIFORM SECTION

$$Z_{cr} = \frac{\pi^2}{L^2} EI_{\xi 1} \quad \ldots\ldots\ldots\ldots\ldots\ldots [6]$$

where $I_{\xi 1}$ is the modified moment of inertia about the ξ-axis. The adjective "modified" defines the effect of pretwist to otherwise well-known section properties. Hereafter, the expression "buckling load" refers to pretwisted columns only, and "Euler load" to similar untwisted columns.

The ratio of buckling load to Euler load for a cruciform section, with dimensions as shown in Fig. 8(*a*), is plotted in Fig. 9 against $\Delta/(L/\rho_\eta)$, the ratio of total initial twist Δ and the slenderness ratio L/ρ_η. The ratio of the modified moment of inertia and the moment of inertia about the same axis, called the relative modified moment of inertia, is represented by the same curve for a cruciform section only. This graph demonstrates the weakening effect of appreciable initial twist, but it also shows the insignificant effect of small accidental initial twist on the elastic buckling load. For a slenderness ratio of 50 and a pretwist of 2π the buckling load is 90 per cent of the Euler load. For an initial twist of 10π, however, the buckling load is only 21 per cent of the Euler load.

All other columns of equal principal moments of inertia behave like columns of unequal principal moments of inertia, which are treated in the next section.

Cross Section With Unequal Principal Moments of Inertia

Columns of equal moments of inertia about both principal axes cannot be stiffened by pretwist. A column of unequal moments of inertia, however, should become stiffer with initial twist.

A wide-flange I-column, 14 × 12 — 84 lb, is chosen as the first example, but its cross section is idealized to three rectangles, Fig. 8(*b*). Its ratio of principal moments of inertia is 4.06. The ratio of buckling load to the Euler load for slenderness ratios of 50, 100, and 200 are shown in Fig. 10 with the ratio of total initial twist and slenderness ratio as abscissa. The strengthening effect of total pretwists up to 2π is obvious, however, for larger pretwists the buckling load decreases steadily and eventually becomes even less than the Euler load. The curves are not smooth but show the effect of the various buckling modes.

The ratio of buckling load to Euler load, which may be termed the relative stiffness, is found to increase with slenderness ratio. For $L/\rho_\eta = 50$ the maximum relative stiffness is 1.27, for $L/\rho_\eta = 100$ it is 1.48, and for $L/\rho_\eta = 200$ it is 1.64. Although there is a

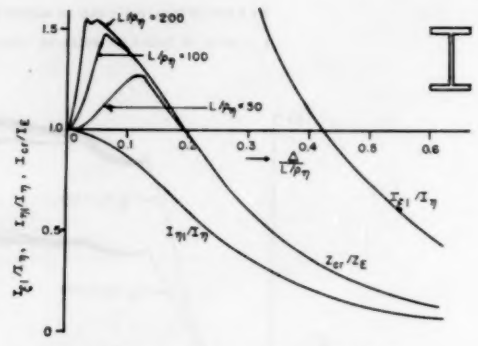

FIG. 10 BUCKLING LOAD OF PRETWISTED I-COLUMN

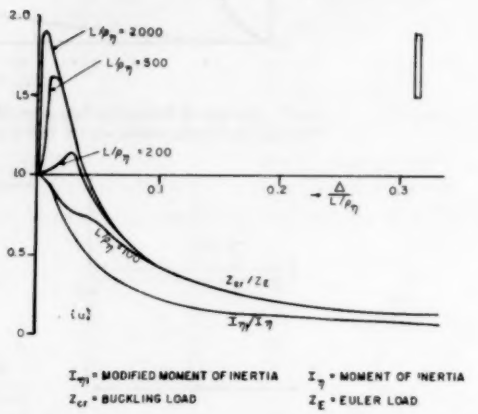

$I_{\eta 1}$ = MODIFIED MOMENT OF INERTIA I_η = MOMENT OF INERTIA
Z_{cr} = BUCKLING LOAD Z_E = EULER LOAD

FIG. 11 BUCKLING OF A PRETWISTED THIN STRIP UNDER COMPRESSION

variation in the strength due to slenderness ratio, the buckling load becomes less than the Euler load when the ratio $\Delta/(L/\rho_\eta)$ becomes greater than 0.2.

Added to Fig. 10 are the ratios of the modified moments of inertia to the smallest moment of inertia. These curves bracket the curves for relative stiffness but the latter approaches the curve of weakest modified moment of inertia for larger pretwists.

As another example, consider a column of a very high ratio of principal moments of inertia, such as a thin strip, Fig. 8(*c*), with a ratio of 400, which may be found useful in instrument design. The relative stiffness of strips of slenderness ratios 100, 200, 500, and 2000 are plotted in Fig. 11. Possibly contrary to expectation, the column with a slenderness ratio of 100 is not stiffened at all. The one with $L/\rho_\eta = 200$ reaches a maximum relative stiffness of 1.13, that of $L/\rho_\eta = 500$ goes up to 1.62, and that of $L/\rho_\eta = 2000$ reaches 1.90 which approaches the factor 2 of Ziegler's investigation. For large pretwists the curves of relative stiffness again approach the curve of the ratio of weakest modified moment of inertia and moment of inertia.

Modified Euler Load—Summary of Transverse Buckling

The curve of relative stiffness for columns with equal moments of inertia demonstrates the weakening effect due to the increasing inclination of the fibers. As the pretwist increases, the fiber stresses concentrate toward the center line, and the flexural rigidity decreases. Columns of unequal principal moments of inertia, however, are strengthened somewhat by the rotation of

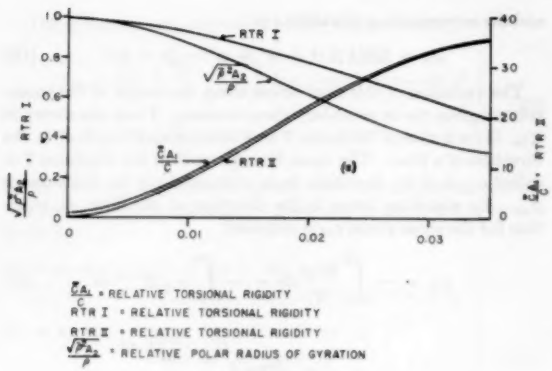
RTR I
RTR II
(a)
$\frac{\bar{C}A_1}{C}$ = RELATIVE TORSIONAL RIGIDITY
RTR I = RELATIVE TORSIONAL RIGIDITY
RTR II = RELATIVE TORSIONAL RIGIDITY
$\frac{\sqrt{\bar{\rho}^2 A_2}}{\rho}$ = RELATIVE POLAR RADIUS OF GYRATION

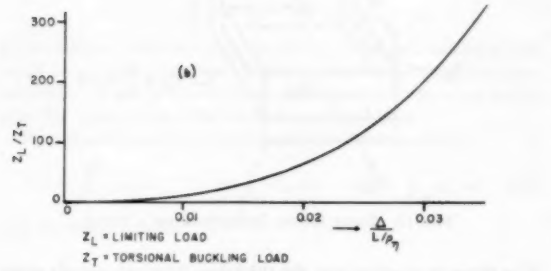

FIG. 12 TORSIONAL FAILURE OF PRETWISTED THIN STRIP UNDER COMPRESSION

the cross section, whereby larger moments of inertia are brought into play. For pretwists greater than 2π very little additional stiffening can be expected because the effect of the larger moment of inertia has been fully utilized.

The weakening of the column appears closely related to the modified moment of inertia about the weak axis. As a consequence, a modified Euler load may be defined by

$$Z_M = \frac{\pi^2}{L^2} EI_{\eta_1} \quad \ldots\ldots [7]$$

However, it should not be confused with the actual buckling load.

The ratio K of the buckling load to the modified Euler load, for all columns which were discussed, is shown in Fig. 7. For initial twists up to 2π the factor K and the previously discussed Ziegler factor K_z are identical. The deviation of K for larger pretwists is a function of the ratio of the modified moments of inertia, but it is small enough for pretwists up to 5π that the factor K_z can be used.

The two phenomena which influence the transverse buckling of columns with thin-walled section can best be summarized into the weakening effect which is expressed in the modified Euler load, and the strengthening effect K which can be read from Fig. 7. Thus the buckling load is given by

$$Z_{cr} = KZ_M \quad \ldots\ldots [8]$$

TORSIONAL FAILURE

A straight, but pretwisted, column which is restrained laterally will fail in torsion when it is compressed. The limiting load is defined as that load for which the additional torsion β becomes infinite, unless the yield point is reached earlier. If the initial twist is of constant rate, then the limiting load is independent of the end conditions, except for freedom to rotate. It is of the form

$$Z_L = \frac{G\bar{C}A_1}{\bar{\rho}^2 A_2} \quad \ldots\ldots [9]$$

where $\bar{C}A_1$ is the modified torsional rigidity and $\sqrt{\bar{\rho}^2 A_2}$ is the modified polar radius of gyration. Expression [9] reduces to the torsional buckling load Z_T for no initial twist. Consequently, for small accidental pretwist, the failure load is the torsional buckling load.

LIMITING LOAD OF A THIN STRIP

The thin strip which was investigated previously for transverse buckling is now examined for perfectly elastic torsional failure. Assume an initial twist of constant rate and let the strip be so held that only relative rotation is possible and that warping is not prevented.

For an untwisted beam-column the torsional rigidity is only a function of the Saint Venant shear stress. The modified torsional rigidity of a pretwisted beam-column, however, has two components. The first, again, is the contribution of the Saint Venant shear stress, the second is due to the fiber stress. The greater the initial twist the greater becomes this second component, because the fibers are more inclined to the center line.

The ratios of these components to the torsional rigidity of an untwisted column are plotted in Fig. 12(*a*). The first component decreases with initial twist but the second component increases very rapidly. The sum is entirely governed by the latter. The relative modified polar radius of gyration is also shown in the same figure.

The ratio of limiting load to torsional buckling load is plotted in Fig. 12(*b*). This curve shows the expected increase in torsional stiffness for a perfectly elastic column.

ACKNOWLEDGMENT

The author is indebted to Prof. D. C. Drucker, chairman of the School of Engineering, Brown University, for his advice and criticism during the preparation of the paper.

BIBLIOGRAPHY

1 "Die Knickung des Verwundenen Stabes," by H. Ziegler, *Schweizerische Bauzeitung*, vol. 66, 1948, p. 463.
2 "Torsion and Buckling of Open Sections," by H. Wagner, NACA TM No. 807, 1936.
3 "Twisting Failure of Centrally Loaded Open-Section Columns in the Elastic Range," by R. Kappus, NACA TM No. 851, 1938.
4 "The Buckling of Compressed Bars by Torsion and Flexure," by J. N. Goodier, Cornell University Engineering Experiment Station, Bulletin No. 27, 1941.
5 "A Treatise on the Mathematical Theory of Elasticity," by A. E. H. Love, Dover Publications, New York, N. Y., 1944, chapter 21.
6 "Mathematical Theory of Elasticity," by I. S. Sokolnikoff, McGraw-Hill Book Company, Inc., New York, N. Y., 1946.

Appendix

MATHEMATICAL DERIVATION

The kinematics of pretwisted beams and columns involves three co-ordinate systems. The x_0, y_0, z_0-system is stationary in space; the x, y, z-system, the system of the unstressed beam-column, rotates with respect to the first one, and the ξ, η, ζ-system, the system of the stressed beam-column, rotates with respect to the second system, Fig. 1. The displacements and rotations, Fig. 2, are assumed to be functions of the center-line distance only and all except the initial twist δ are considered to be quantities of

small order, so that their products and products of their derivatives are negligible.

In accordance with Love's Theory of Naturally Curved Rods (5), the curvatures and twist rates are found to be

$$\left.\begin{aligned} c_0 &= u_0'' \sin\delta - v_0'' \delta \\ k_0 &= u_0'' \cos\delta + v_0'' \sin\delta \\ \tau_0 &= \delta' \\ c &= -(v'' + 2u'\delta' + u\delta'' - v\delta'^2) \\ k &= u'' - 2v'\delta' - v\delta'' - u\delta'^2 \\ \tau &= \beta' \end{aligned}\right\} \quad \ldots\ldots [10]$$

With these values the direction cosines relating the co-ordinate systems become

$$\left.\begin{array}{lccc} & x_0 & y_0 & z_0 \\ x & \cos\delta & \sin\delta & -u_0'\cos\delta - v_0'\sin\delta \\ y & -\sin\delta & \cos\delta & u_0'\sin\delta - v_0'\cos\delta \\ z & u_0' & v_0' & 1 \end{array}\right\} \quad \ldots [11a]$$

$$\left.\begin{array}{lccc} & x & y & z \\ \xi & 1 & \beta & -u' + v\delta' \\ \eta & -\beta & 1 & -v' - u\delta' \\ \zeta & u' - v\delta' & v' + u\delta' & 1 \end{array}\right\} \quad \ldots [11b]$$

$$\left.\begin{array}{lccc} & x_0 & y_0 & z_0 \\ & & & -u' + v\delta' \\ \xi & \xi\cos\delta - \beta\sin\delta & \sin\delta + \beta\cos\delta & -u_0'\cos\delta \\ & & & -v_0\sin\delta \\ & & & -v' - u\delta \\ \eta & -\sin\delta - \beta\cos\delta & \cos\delta - \beta\sin\delta & +u_0'\sin\delta \\ & & & -v_0\cos\delta \\ & (u - v\delta')\cos\delta & (u' - v\delta')\sin\delta & \\ \zeta & -(v' + u\delta')\sin\delta + u_0' & +(v' + u\delta')\times & 1 \\ & & \cos\delta + v_0' & \end{array}\right\} \quad [11c]$$

Together with the additional twist there will be warping of the cross section. This has been defined (4, 6) in terms of the warping function ω, which, in turn, is the product of the torsion function φ and the twist rate β'. The torsion function is also related to the stress function ψ by

$$\left.\begin{aligned} \frac{\partial\psi}{\partial\xi} &= -\frac{\partial\varphi}{\partial\eta} - \xi \\ \frac{\partial\psi}{\partial\eta} &= \frac{\partial\varphi}{\partial\xi} - \eta \end{aligned}\right\} \quad \ldots\ldots [12]$$

In evaluating some of the integrals use is made of either the torsion function or the stress function.

Let P_1 and P_2, Fig. 3(*a*), be two points along the same unstressed fiber whose cross sections are an infinitesimal distance dt apart at the center line. The corresponding fiber distance is then

$$|f_0| = R^{-1/2}(1 - Rxk_0 + Ryc_0)dt \quad \ldots\ldots [13]$$

$$R = (1 + r^2\delta'^2)^{-1}$$

$$r = \sqrt{x^2 + y^2}$$

Assume that the beam-column is stressed. Points P_1 and P_2 then become points P_3 and P_4, Fig. 3(*b*), and the distance between them is

$$|f| = R^{-1/2}[1 - R(\delta'\beta'r^2 + w' + \omega' - \xi k - \xi k_0 + \eta c + \eta c_0]dl \quad \ldots [14]$$

The strain in the fiber is given by

$$\epsilon_f = \frac{|f|}{|f_0|} - 1 = R(\delta'\beta'r^2 + w' + \omega' - \xi k + \eta c) \quad \ldots [15]$$

and the corresponding fiber stress is

$$\sigma_f = ER(\delta'\beta'r^2 + w' + \omega' - \xi k + \eta c) \quad \ldots\ldots [16]$$

The variation of this fiber stress along the length of the beam-column gives rise to secondary shear stresses. These are shown in Fig. 13 for a slice of thickness T and infinitesimal length df in the direction of a fiber. The mean fiber stress over the thickness T is called σ_{fs} and the deviation from average along the thickness is σ_{ss}. By summing forces in the direction of the fiber, an equation for the shear stress τ_{sf} is obtained

$$\tau_{sf} = -\int_0^s \frac{\partial\sigma_{fs}}{\partial f}\,ds = -\int_0^s \sigma_{ss}' R^{-1/2}\,ds \quad \ldots\ldots [17]$$

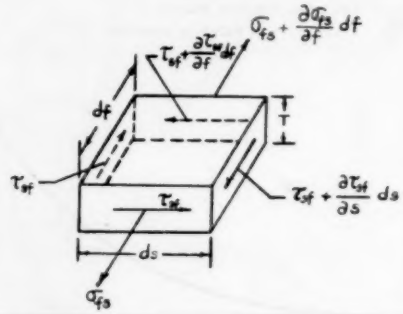

FIG. 13 SLICE ALONG DIRECTION OF A FIBER

This stress is constant over the thickness T for any point s along the middle curve of the cross section. The additional shear stress τ_{nf} is parabolically distributed over the thickness T. It is

$$\tau_{nf} = -\int_0^n R^{-1/2}\sigma_{fn}\,dn \quad \ldots\ldots [18]$$

with n the co-ordinate in the direction of T. Because its integration is limited to the half-thickness, the shear stress τ_{nf} is frequently neglected.

All shear stresses are assumed to act in a plane perpendicular to the direction of the fiber, at the same time the primary shear stresses are presumed to act in the principal directions of the cross section. These directions are given by unit vectors $\vec{g}_\xi$ and $\vec{g}_\eta$, which lie in the $\xi\zeta$ and $\eta\zeta$-planes, respectively, and which are also perpendicular to the fiber direction $\vec{f}$, Fig. 6. The vectors $\vec{g}_\xi$ and $\vec{g}_\eta$ are not mutually perpendicular but enclose the angle γ, given by

$$\gamma = \sin^{-1}(\csc\gamma_1 \csc\gamma_2 \cos\gamma_3) \quad \ldots\ldots [19]$$

The direction cosines between this system and the ξ, η, ζ-system are

$$\left.\begin{array}{lccc} & \xi & \eta & \zeta \\ \vec{g}_\xi & \csc\gamma_2\cos\gamma_3 & 0 & -\cos\gamma_1 \csc\gamma_2 \\ \vec{g}_\eta & 0 & \csc\gamma_1\cos\gamma_3 & -\csc\gamma_1\cos\gamma_2 \\ \vec{f} & \cos\gamma_1 & \cos\gamma_2 & \cos\gamma_3 \end{array}\right\} \quad \ldots [20]$$

with

$$\left.\begin{aligned} \cos\gamma_1 &= -\eta\sqrt{R}\,[\delta' + \beta' - R(\delta'\beta'r^2 + w' + \omega' \\ &\qquad - \xi k - \xi k_0 + \eta c + \eta c_0)] \\ \cos\gamma_2 &= \xi\sqrt{R}\,[\delta' + \beta' - R(\delta'\beta'r^2 + w' \\ &\qquad + \omega' - \xi k - \xi k_0 + \eta c + \eta c_0)] \\ \cos\gamma_3 &= \sqrt{R}\,[1 - R\delta' r^2(\beta' - w' \\ &\qquad - \omega' + \xi k + \xi k_0 - \eta c - \eta c_0)] \end{aligned}\right\} \quad \ldots [21]$$

The shear stresses, expressed in this system, are

$$\left.\begin{aligned}\tau_{\xi f} &= G\beta'\left(\frac{\partial\varphi}{\partial\xi} - \eta\right) + \tau_{s f}\cos\theta - \tau_{n f}\sin\theta \\ \tau_{\eta f} &= G\beta'\left(\frac{\partial\varphi}{\partial\eta} + \xi\right) + \tau_{s f}\sin\theta + \tau_{n f}\cos\theta\end{aligned}\right\} \quad [22]$$

with θ the angle between the middle curve of the cross section and the ξ-axis. The transformation to stresses in the ξ, η, ζ-system is given by

$$\left.\begin{aligned}\sigma_\zeta &= \sigma_f\cos^2\gamma_3 - (\tau_{\xi f}\cos\gamma_1\csc\gamma_3 \\ &\quad + \tau_{n f}\csc\gamma_1\cos\gamma_2)(1+\csc\gamma)\cos\gamma_3 \\ \tau_{\xi\zeta} &= \sigma_f\cos\gamma_1\cos\gamma_3 + \tau_{\xi f}(\csc\gamma_2\cos^2\gamma_3 \\ &\quad - \cos^2\gamma_1\csc\gamma_3\csc\gamma) \\ &\quad - \tau_{\eta f}\cot\gamma_1\cos\gamma_2\csc\gamma \\ \tau_{\eta\zeta} &= \sigma_f\cos\gamma_2\cos\gamma_3 - \tau_{\xi f}\cos\gamma_1\cot\gamma_2\csc\gamma \\ &\quad + \tau_{\eta f}(\csc\gamma_1\cos^2\gamma_3 - \csc\gamma_1\cos^2\gamma_2\csc\gamma)\end{aligned}\right\} \quad [23]$$

In calculating these stresses, products of Young's modulus and small-order quantities were considered finite quantities, and consequently, simple products of small-order quantities when multiplied by Young's modulus are no longer negligible.

With the stresses of Equations [23] the stress resultants

$$N_\xi = \int_A \tau_{\xi\zeta}\,dA, \quad N_\eta = \int_A \tau_{\eta\zeta}\,dA, \quad N_\zeta = \int_A \sigma_\zeta\,dA \quad [24]$$

and the stress couples

$$G_\xi = \int_A \eta\sigma_\zeta dA, \quad G_\eta = \int_A \xi\sigma_\zeta\,dA,$$
$$G_\zeta = \int_A (\xi\tau_{\eta\zeta} - \eta\tau_{\xi\zeta})\,dA \quad [25]$$

are obtained. The integrals simplify appreciably for double symmetric sections, and only those were considered in this paper. Extension to any thin-walled section can be accomplished without too much difficulty.

The stress resultant in the ζ-direction is

$$\left.\begin{aligned}N_\zeta &= E\delta'\beta' J_1 + E\bar{A}w' - 2E(J_2 + J_3\delta'^2)\delta'\beta' w' \\ &\quad + 2EI_{\eta_1}\delta'^2 k\,(k + k_0) + 2EI_{\xi\xi}\delta'^2 c(c + c_0) \\ &\quad - 2G\bar{C}\delta'\beta' + 2E\Gamma_4\beta'''\delta' \\ &\quad - 2E\Gamma_6\beta''\delta'^2\delta'' + G\bar{C}_4\beta' w'\delta'\end{aligned}\right\} \quad [26a]^4$$

In comparison with $E\bar{A}w'$ all terms containing $\beta' w'$ are negligible. Dropping these terms, Equation [26a] can be solved for w'

$$\left.\begin{aligned}w' &= \frac{N_\zeta}{E\bar{A}} - \bar{\rho}^2\delta'\beta' - 2\bar{\eta}^4\delta'^2 c^2 - 2\bar{\xi}^4\delta'^2 k^2 \\ &\quad - 2\bar{\eta}^4\delta'^2 cc_0 - 2\bar{\xi}^4\delta'^2 kk_0 + \frac{2G\bar{C}}{E\bar{A}}\delta'\beta' \\ &\quad - \frac{2\Gamma_5}{\bar{A}}\beta'''\delta' + \frac{2\Gamma_5}{\bar{A}}\beta''\delta'^2\delta''\end{aligned}\right\} \quad [26b]$$

The stress couple about the ξ-axis is

$$\left.\begin{aligned}G_\xi &= EI_{\xi\xi}c - (2EI_{\xi\eta} - 2EI_{\xi 4}\delta'^2 - GI_{\xi 5})\delta'\beta' c \\ &\quad - 4E\Phi\delta'^2\beta'' k + 4EI_{\xi\eta}\delta'^2 w' c + (2EI_{\xi 4}\delta'^2 \\ &\quad + GI_{\xi 5})\delta'\beta' c_0 - 2E\Phi\delta'^2\beta'' k_0 \\ &\quad + 2EI_{\xi\eta}\delta'^2 w' c_0 - 2E\Gamma_7\delta' k' + 2E\Gamma_8\delta'^2\delta'' k\end{aligned}\right\} \quad [27]$$

[4] The symbols representing integrals are defined in the nomenclature.

In comparison with the first term all terms containing products of β', β'', and β''' with c can be neglected. The last two terms, which are due to secondary shear forces, are also negligible because deformations due to shear forces are usually neglected in the theory of bending of beams. By substituting Expression [26b] for w' the final expression for the stress couple G_ξ is obtained

$$\left.\begin{aligned}G_\xi &= (EI_{\xi_1} + 4N_\zeta\bar{\eta}^4\delta'^2)c + 2N_\zeta\bar{\eta}^4\delta'^2 c_0 \\ &\quad - 4E\Phi\delta'^2\beta'' k - 4E\Gamma_4\bar{\eta}^4\delta'^2\beta''' c_0 \\ &\quad + 4E\Gamma_6\bar{\eta}^4\delta'^4\delta''\beta'' c_0 - 2E(\Phi + 2\Gamma_6\bar{\eta}^2\delta'^2\delta'')\delta'^2\beta'' k_0 \\ &\quad + (2EI_{\xi_4}\delta'^2 + GI_{\xi_5} - 2EI_{\xi_5}\bar{\rho}^2\delta'^2 + 4G\bar{C}\bar{\eta}^4\delta'^2)\beta'\delta' c_0\end{aligned}\right\} \quad [27a]$$

By similar reasoning the stress couples G_η and G_ζ are derived

$$\left.\begin{aligned}G_\eta &= (EI_{\eta_1} + 4N_\zeta\bar{\xi}^4\delta'^2)k + 2N_\zeta\bar{\xi}^4\delta'^2 k_0 \\ &\quad - 4E\Phi\delta'^2\beta'' c - 4E\Gamma_6\bar{\xi}^4\delta'^2\beta''' k_0 \\ &\quad - 2E(\Phi + 2\Gamma_6\bar{\xi}^2\delta'\delta'')\delta'^2\beta'' c_0 \\ &\quad + 4E\Gamma_6\bar{\xi}^4\delta'^4\delta''\beta'' k_0 + (2EI_{\eta_4}\delta'^2 + GI_{\eta_5} \\ &\quad - 2EI_{\eta_5}\bar{\rho}^2\delta'^2 + 4G\bar{C}\bar{\xi}^4\delta'^2)\delta'\beta' k_0\end{aligned}\right\} \quad [27b]$$

$$\left.\begin{aligned}G_\zeta &= -E\bar{\Gamma}_1\beta''' + E\bar{\Gamma}_2\delta'\delta''\beta'' + G\bar{C}\beta' \\ &\quad + \left[N_\zeta\left(\bar{\rho}^2 - 3\frac{J_3}{\bar{A}}\delta'^2 + \frac{J_4}{\bar{A}}\delta'^4 + \frac{G\bar{C}_7}{E\bar{A}}\right)\right. \\ &\quad \left. + (2G\bar{C}\bar{\rho}^2 - EJ_1\bar{\rho}^2 + EJ_3)\delta'^2\right]\beta' - E\delta' c^2(I_{\xi_3} + 2I_{\xi_5}\bar{\rho}^2\delta'^2 \\ &\quad - I_{\xi_4}\delta'^2) - E\delta' k^2(I_{\eta_3} + 2I_{\eta_5}\bar{\rho}^2\delta'^2 - I_{\eta_5}\delta'^2) \\ &\quad - E\delta' cc_0(I_{\xi_3} + 2I_{\xi_5}\bar{\rho}^2\delta'^2 - I_{\xi_5}\delta'^2) \\ &\quad - E\delta' kk_0(I_{\eta_3} + 2I_{\eta_5}\bar{\rho}^2\delta'^2 - I_{\eta_4}\delta'^2) + N_\zeta\bar{\rho}^2\delta'\end{aligned}\right\} \quad [27c]$$

From equilibrium considerations the stress resultant N_ζ can be evaluated in terms of the external forces

$$\left.\begin{aligned}N_\zeta &= -X[(u' - v\delta')\cos\delta - (v' + u\delta')\sin\delta + u_0'] \\ &\quad - Y[(u' - v\delta')\sin\delta + (v' + u\delta')\cos\delta + v_0'] - Z\end{aligned}\right\} \quad [28]$$

Likewise, the stress couples can be determined in terms of the external moments and moments due to external forces

$$\left.\begin{aligned}-G_\xi &= M_x(\cos\delta - \beta\sin\delta) + M_y(\sin\delta + \beta\cos\delta) \\ &\quad - M_s(u' - v\delta' + u_0'\cos\delta + v_0'\sin\delta) - Xl(\sin\delta + \beta\cos\delta) \\ &\quad + Yl(\cos\delta - \beta\sin\delta) - Z(v - u_0\sin\delta + v_0\cos\delta)\end{aligned}\right\} \quad [29a]$$

$$\left.\begin{aligned}-G_\eta &= -Mx(\sin\delta + \beta\cos\delta) + My(\cos\delta - \beta\sin\delta) \\ &\quad - M_s(v' + u\delta' - u_0'\sin\delta + v_0'\cos\delta) - Xl(\cos\delta - \beta\sin\delta) \\ &\quad - Yl(\sin\delta + \beta\cos\delta) + Z(u + u_0\cos\delta + v_0\sin\delta)\end{aligned}\right\} \quad [29b]$$

$$\left.\begin{aligned}-G_\zeta &= M_x[(u' - v\delta')\cos\delta - (v' + u\delta')\sin\delta + u_0'] \\ &\quad + M_y[(u' - v\delta')\sin\delta + (v' + u\delta')\cos\delta + v_0'] \\ &\quad + M_s - X[(u' - v\delta')l\sin\delta + (v' + u\delta')l\cos\delta \\ &\quad - u\sin\delta - v\cos\delta - v_0 + v_0'l] + Y[(u' - v\delta')l\cos\delta \\ &\quad - (v' + u\delta')l\sin\delta - u\cos\delta + v\sin\delta - u_0 + u_0'l]\end{aligned}\right\} \quad [29c]$$

If Equation [28] is substituted in Equations [27] and they are then equated to Equations [29], a set of three simultaneous equations is obtained which describes the action of a pretwisted beam-column. The simultaneous equations are in terms of the variables u, v, and β.

For a beam-column which is initially straight and untwisted these simultaneous equations reduce to

$$\left.\begin{aligned}EI_\xi v'' &= M_x + M_y\beta - M_s u' - Zv \\ EI_\eta u'' &= -M_x\beta + M_y - M_s v' - Zu \\ E\Gamma\beta''' + (Z\rho^2 - GC)\beta' &= M_x u' + M_y v'\end{aligned}\right\} \quad [30]$$

which are Goodier's (4) Equations [2.1], [3.1], and [7.1]. These are the equations of the well-known theory of untwisted beam-columns.

Because the simultaneous equations, which are here called "equilibrium equations," are not explicitly solvable it is interesting to investigate some problems for which the complexity is somewhat reduced. A convenient example is a column which is initially straight but twisted at a constant rate.

The only external force is an axial load Z; the other forces are

$$X = Y = 0 \quad \ldots\ldots [31a]$$

and the external moments are

$$M_x = M_y = M_z = 0 \quad \ldots\ldots [31b]$$

The initial deformations are specified by

$$\left.\begin{array}{ll} u_0 = v_0 = 0 & 0 \le l \le L \\ \delta' = \delta_0' = \text{const} & 0 \le l \le L \end{array}\right\} \quad \ldots [31c]$$

These conditions determine the stress resultant

$$N_\zeta = -Z \quad \ldots\ldots [32]$$

and the stress couples

$$G_\xi = Zv, \qquad G_\eta = -Zu, \qquad G_\zeta = 0 \quad \ldots\ldots [33]$$

The equilibrium equations are obtained by equating Expressions [27] to Expressions [33], substituting for N_ζ and, finally, by applying Conditions [31]. This results in

$$\left.\begin{array}{l} EI_{\xi 1}c - Z(v + 4\bar{\eta}^4\delta_0'^2 c) - 4E\Phi\delta_0'^2\beta''k = 0 \\ EI_{\eta 1}k + Z(u - 4\bar{\xi}^4\delta_0'^2 k) - 4E\Phi\delta_0'^2\beta''c = 0 \\ E\Gamma_1\beta''' - (G\bar{C}A_1 - Z\bar{\rho}^2A_2)\beta' = -Z\bar{\rho}^2\delta_0' \end{array}\right\} . \quad [34]$$

Rigid-body motion can be eliminated from the solution by specifying that there can be no lateral displacements at either end and that no additional twist is permissible at one end. If warping at the ends is not restricted, there will be no warping stresses at the ends. Consequently

$$\left.\begin{array}{lll} u = 0 & & \\ v = 0 & u = 0 & \\ & v = 0 & \\ \text{at } l = 0 & & \text{at } l = L \\ \beta = 0 & \beta'' = 0 & \\ \beta' = 0 & & \end{array}\right\} \quad \ldots [35]$$

The solution to the last of Equations [34] with Conditions [35] is given by

$$\beta' = \frac{Z\bar{\rho}^2\delta_0'}{G\bar{C}A_1 - Z\bar{\rho}^2A_2} \quad \ldots\ldots [36]$$

This result shows that the additional twist is proportional to the initial twist and that no warping stress exists anywhere along the column. With Equation [36] the other two equilibrium equations become

$$\left.\begin{array}{l} v'' + (ZA_3 - \delta_0'^2)v + 2u'\delta_0' = 0 \\ u'' + (ZA_4 - \delta_0'^2)u - 2v'\delta_0' = 0 \end{array}\right\} \quad \ldots\ldots [37]$$

where

$$A_3 = (EI_{\xi 1} - 4Z\bar{\eta}^4\delta_0'^2)^{-1}$$
$$A_4 = (EI_{\eta 1} - 4Z\bar{\xi}^4\delta_0'^2)^{-1}$$

The end Conditions [35] can only be satisfied if the determinant

$$\begin{vmatrix} \frac{1}{\alpha_2}\sin\alpha_1 L - \frac{1}{\alpha_4}\sin\alpha_2 L & -\cos\alpha_1 L + \cos\alpha_2 L \\ \cos\alpha_1 L - \cos\alpha_2 L & +\alpha_3\sin\alpha_1 L - \alpha_4\sin\alpha_2 L \end{vmatrix} \equiv 0 \ldots [38]$$

The α's, which are functions of the unknown axial load Z, are defined by

$$\alpha_{1,2} = \frac{1}{2}Z(A_3 + A_4) + \delta_0'^2 \pm \sqrt{\frac{1}{4}Z^2(A_3 - A_4)^2 + 2Z\delta_0'^2(A_3 + A_4)}$$

$$\alpha_3 = \frac{\alpha_1^2 + \delta_0'^2 - ZA_4}{2\alpha_1\delta_0'} = \frac{2\alpha_1\delta_0'}{\alpha_1^2 + \delta_0'^2 - ZA_3}$$

$$\alpha_4 = \frac{\alpha_2^2 + \delta_0'^2 - ZA_4}{2\alpha_2\delta_0'} = \frac{2\alpha_2\delta_0'}{\alpha_2^2 + \delta_0'^2 - ZA_3}$$

$$\alpha_5 = \frac{1}{2}\left(\frac{\alpha_3}{\alpha_4} + \frac{\alpha_4}{\alpha_3}\right)$$

From the determinant the following characteristic equation is obtained

$$\cos\alpha_1 L\cos\alpha_2 L + \alpha_5\sin\alpha_1 L\sin\alpha_2 L = 1 \quad \ldots\ldots [39]$$

The lowest characteristic value of Equation [39] is the buckling load Z_{cr}.

A special case is the column whose cross sections are identical in the ξ and in the η-direction. Then integrals of the cross section are identical in both directions, e.g.

$$I_\xi = I_\eta, \qquad I_{\xi 1} = I_{\eta 1}, \qquad \bar{\xi}^4 = \bar{\eta}^4$$

Consequently, also

$$A_3 = A_4, \qquad \alpha_{1,2} = \sqrt{2A_3} \pm \delta_0', \qquad \alpha_{3,4} = \pm 1$$

and Equation [39] is reduced to

$$\cos(\alpha_1 + \alpha_2)L = 1 \quad \ldots\ldots [40]$$

The smallest characteristic value of this equation is

$$Z_{cr} = \frac{EI_{\xi 1}\pi^2}{L^2}\left(1 + \frac{4\pi^2\bar{\xi}^4\delta_0'^2}{L^2}\right)^{-1} \quad \ldots\ldots [41]$$

For columns with a slenderness ratio of 50 or more the second term within the brackets becomes negligible and the buckling load reduces to

$$Z_{cr} = EI_{\xi 1}\frac{\pi^2}{L^2} \quad \ldots\ldots [42]$$

The ratio of buckling load to Euler load, the relative stiffness of the column, is thus found to be equal to the ratio of the modified moment of inertia to moment of inertia.

When transverse displacements are prevented all along the length of the column, then the first two Equations [34] become identically zero. Solution [36] now leads to the limiting load in torsion for which $\beta = \infty$

$$Z_L = \frac{G\bar{C}A_1}{\bar{\rho}^2A_2} \quad \ldots\ldots [43]$$

Slight deviations from a constant rate of twist do not change this limiting load appreciably, provided $\rho\delta'' \ll \delta'$.

Let the initial twist be given by

$$\delta = \delta_0 l + \sum_{n=1}^{\infty} b_n \sin\frac{n\pi l}{L}$$

With the condition on δ'', $\bar{C}A_1$ and $\bar{\rho}^2A_2$ are still constants for a predetermined twist, and the last Equation [34] becomes

$$E\Gamma_1\beta''' - (G\overline{C}A_1 - Z\overline{\rho}^2A_2)\beta' = -Z\overline{\rho}^2\delta' \quad [44]$$

Again, the limiting load is given by Expression [43].

If the initial twist is very small, then it may be expressed as

$$\delta = \sum_{n=1}^{\infty} a_n \cos\frac{n\pi l}{L} + \sum_{n=1}^{\infty} b_n \frac{n\pi l}{L}\sin\frac{n\pi l}{L} \quad [45]$$

The solution of Equation [44] for this pretwist results in the well-known buckling load in torsion

$$Z_T = \frac{GC}{\rho^2} \quad [46]$$

The modified torsional rigidity

$$\overline{C}A_1 = \overline{C} + 2\overline{C}\overline{\rho}^2\delta'^2 + \frac{E}{G}\delta'^2(J_3 - J_1\overline{\rho}^2) \quad [47]$$

can be separated into two parts in accordance with its derivation. The first two terms are due to the Saint Venant shear stress, and the last term is due to the existing fiber stress. If Expression [47] is divided by the torsional rigidity C, then the relative torsional rigidities I and II are obtained. They are plotted in Fig. 12(*a*), together with their sum. The latter demonstrates the decided increase of torsional rigidity for increasing initial twist.

The Solution of Multiple-Branch Piping-Flexibility Problems by Tensor Analysis

By J. W. SOULE,[1] SWARTHMORE, PA.

A general method of flexibility analysis is presented which, by the use of tensors, makes it possible to derive the equations of performance of highly complex piping systems by a routine procedure.

Nomenclature

The following nomenclature is used in the paper:

E = Young's modulus of elasticity of the pipe material
I = moment of inertia of pipe cross section
I_x = line moment of inertia about x-axis
I_y = line moment of inertia about y-axis
I_z = line moment of inertia about z-axis
I_{xy} = line product of inertia in xy-plane
I_{xz} = line product of inertia in xz-plane
I_{yz} = line product of inertia in yz-plane
S_x = line statical moment about x-axis
S_y = line statical moment about y-axis
S_z = line statical moment about z-axis
l = line length
F_x = force in x-direction
F_y = force in y-direction
F_z = force in z-direction
M_{xy} = moment in xy-plane
M_{xz} = moment in xz-plane
M_{yz} = moment in yz-plane
D_x = deflection in x-direction
D_y = deflection in y-direction
D_z = deflection in z-direction
$D_{\theta xy}$ = angular deflection in xy-plane
$D_{\theta xz}$ = angular deflection in xz-plane
$D_{\theta yz}$ = angular deflection in yz-plane

Introduction

The two-anchor piping-flexibility problem has been the subject of numerous articles and technical papers over the past 15 or 20 years, so that today the solution of such problems is commonplace. The next question which naturally suggests itself to the engineer is as follows: Given the equations expressing the performance of several independent piping configurations, is it possible to combine them to obtain the equations of performance for the given configurations combined into a new and more complicated system in any chosen manner? Fortunately the answer is yes. Electrical engineers have been solving electrical networks in this manner for several years, by tensor analysis. Mechanical and structural engineers have also found tensor analysis to be a useful tool for the solution of highly complicated structures. The results obtained by tensor methods are ideal for application to piping-flexibility problems because they are in a form which allows the given conditions of the problem (deflections) to be varied and the effect of such changes obtained without the necessity of repeating pages of calculations. Once the equations of performance of the combined system have been obtained they may be used repeatedly by merely substituting in the various values for deflections and solving for the corresponding forces and moments at the terminals. It is recommended that the numerical work of solving the equations be carried out on computing machines.

It is not the purpose of this paper to instruct on tensor analysis, but rather to show how it may be applied to the more difficult piping-flexibility problems. The reader is referred to Kron's work (1)[2] for the study of fundamentals of tensor analysis and manipulation of n-way matrices. The reader may also be interested in the method of J. E. Brock (5), which uses matrix algebra but does not use the tensor approach to the problem (Appendix).

Theory

To illustrate the method, a piping system consisting of 6 branches and 5 anchors, as shown in Fig. 1, is to be solved.

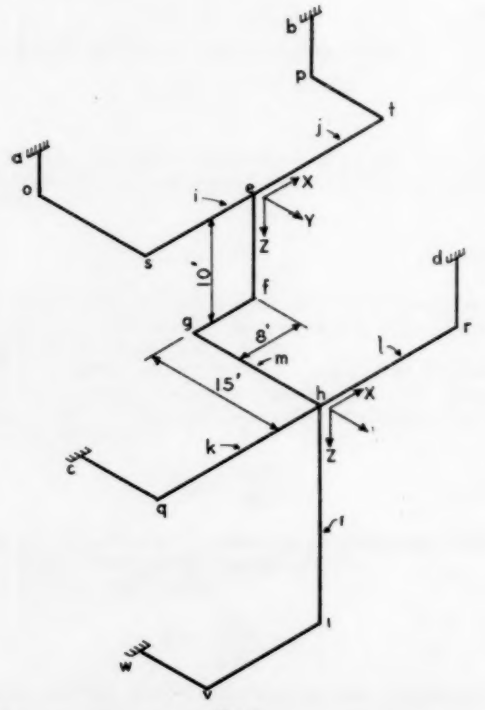

Fig. 1

[1] Designer, United Engineers and Constructors, Inc., Philadelphia, Pa.

Contributed by the Applied Mechanics Division and presented at the Diamond Jubilee Annual Meeting, Chicago, Ill., November 13–18, 1955, of The American Society of Mechanical Engineers.

Discussion of this paper should be addressed to the Secretary, ASME, 29 West 39th Street, New York, N. Y., and will be accepted until July 10, 1956, for publication at a later date. Discussion received after the closing date will be returned.

Note: Statements and opinions advanced in papers are to be understood as individual expressions of their authors and not those of the Society. Manuscript received by ASME Applied Mechanics Division, January 3, 1955. Paper No. 55—A-83.

[2] Numbers in parentheses refer to the Bibliography at the end of the paper.

The first step is to divide the system into its component parts, labeled i, j, k, l, m, n. Considering each branch by itself, reference axes may be set up and the equations for each branch obtained. Fig. 2 shows 4 of the individual branches with their reference axes.

The author prefers to set up the reference axes in the same direction for each branch to avoid confusion. It will also be noticed that the x-axis always appears as abscissa, while the z-axis always appears as ordinate. With these conventions we define a positive moment or angular deflection as one which would rotate the positive abscissa toward the positive ordinate, and a negative moment or angular deflection as one which would rotate the positive ordinate toward the positive abscissa. The equations of one branch, say the i-branch, as derived by the dummy load method (2) are as follows: (Note that the nomenclature is similar to that used by S. W. Spielvogel in his book on piping stress analysis, reference 3.)

$$\frac{I_x}{EI}F_x - \frac{I_{xy}}{EI}F_y - \frac{I_{xz}}{EI}F_z + \frac{S_x}{EI}M_{xy} + \frac{S_z}{EI}M_{xz} = D_x \quad [1]$$

$$-\frac{I_{xy}}{EI}F_x + \frac{I_y}{EI}F_y - \frac{I_{yz}}{EI}F_z - \frac{S_y}{EI}M_{xy} + \frac{S_y}{EI}M_{yz} = D_y \quad [2]$$

$$-\frac{I_{xz}}{EI}F_x - \frac{I_{yz}}{EI}F_y + \frac{I_z}{EI}F_z - \frac{S_z}{EI}M_{xz} - \frac{S_z}{EI}M_{yz} = D_z \quad [3]$$

$$\frac{S_x}{EI}F_x - \frac{S_y}{EI}F_y + \frac{l}{EI}M_{xy} = D_{\theta xy} \quad [4]$$

$$\frac{S_z}{EI}F_x - \frac{S_z}{EI}F_z + \frac{l}{EI}M_{xz} = D_{\theta xz} \quad [5]$$

$$\frac{S_y}{EI}F_y - \frac{S_z}{EI}F_z + \frac{l}{EI}M_{yz} = D_{\theta yz} \quad [6]$$

When computing the coefficients for Equations [1] to [6] it is assumed that, where necessary, allowance has been made for the in-plane and out-of-plane properties of bends or other special features by the application of suitable flexibility constants.

The set of 6 equations for each of the 6 branches may be expressed in matrix form as follows

$$\mathbf{A}_i\mathbf{F}_i = \mathbf{D}_i;\ \mathbf{A}_j\mathbf{F}_j = \mathbf{D}_j, \text{ etc.}$$

The elements of the matrices are shown in Fig. 3. (Throughout the paper bold-face capitals will be used to represent a matrix, a subscript being used to indicate which branch of the piping system is being referred to.)

It should be noted that the forces and moments for the branch i as expressed in Equations [1] to [6] are the external loads applied *to* the branch i at e for given deflections at e. However, the same equations may also represent the forces and moments at e for given deflections at a if the forces and moments are understood to be applied *from* branch i at the point e. This reasoning has also been used for branches j, k, and l, thus simplifying the connection tensor $\mathbf{C}$ and the final equation $\mathbf{Z}'\mathbf{F}' = \mathbf{D}'$, which then expresses the forces at points e and h corresponding to given deflections at a, b, c, and d.

The equation of the "primitive" system which consists of the total 6 systems before interconnection, is $\mathbf{ZF} = \mathbf{D}$, where

$$\mathbf{Z} = \begin{array}{c|cccccc} & i & j & k & l & m & n \\ i & \mathbf{A}_i & & & & & \\ j & & \mathbf{A}_j & & & & \\ k & & & \mathbf{A}_k & & & \\ l & & & & \mathbf{A}_l & & \\ m & & & & & \mathbf{A}_m & \\ n & & & & & & \mathbf{A}_n \end{array} \quad \ldots\ldots [7]$$

$$\mathbf{F} = \begin{array}{|c|} \hline \mathbf{F}_i \\ \mathbf{F}_j \\ \mathbf{F}_k \\ \mathbf{F}_l \\ \mathbf{F}_m \\ \mathbf{F}_n \\ \hline \end{array} \quad \ldots\ldots [8] \qquad \mathbf{D} = \begin{array}{|c|} \hline \mathbf{D}_i \\ \mathbf{D}_j \\ \mathbf{D}_k \\ \mathbf{D}_l \\ \mathbf{D}_m \\ \mathbf{D}_n \\ \hline \end{array} \quad \ldots\ldots [9]$$

The primitive system is illustrated in Fig. 4.

The derived (interconnected) system will have the equation $\mathbf{Z}'\mathbf{F}' = \mathbf{D}'$, and is shown in Fig. 5. The problem is now to find the elements of $\mathbf{Z}'$. To do this we must establish the connection tensor $\mathbf{C}$, which expresses the manner in which the branches have been interconnected. Once $\mathbf{C}$ has been established the $\mathbf{Z}'$ will be found from the formula $\mathbf{Z}' = \mathbf{C}_t\mathbf{Z}\mathbf{C}$. (The subscript t is used throughout the paper to indicate the transposed matrix, a standard convention in matrix algebra.)

In setting up the tensor $\mathbf{C}$ it will be necessary to express the forces and moments at h in terms of those at e. Referring to Fig. 1, it can be seen that the relationship is as follows

$$\left.\begin{aligned} F_{xh} &= F_{xe} \\ F_{yh} &= F_{ye} \\ F_{zh} &= F_{ze} \\ M_{xyh} &= 15F_{xe} + 8F_{ye} + M_{xye} \\ M_{xzh} &= 10F_{xe} + 8F_{ze} + M_{xze} \\ M_{yzh} &= 10F_{ye} - 15F_{ze} + M_{yze} \end{aligned}\right\} \quad [10]$$

Using the foregoing tabulation, we may express $\mathbf{F}_h$ in terms of $\mathbf{F}_e$ as follows: $\mathbf{F}_h = \mathbf{B}\mathbf{F}_e$, where

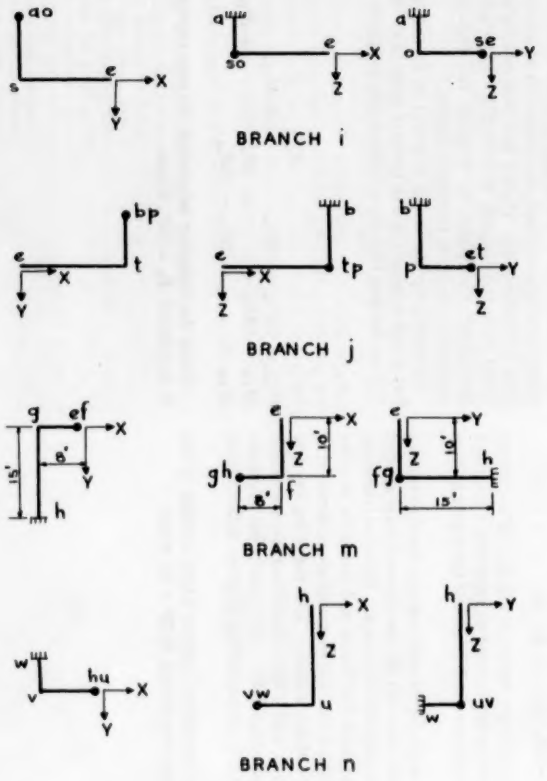

Fig. 2

$$A = \begin{bmatrix} \frac{l_x}{EI} & -\frac{l_{xy}}{EI} & -\frac{l_{xz}}{EI} & \frac{S_x}{EI}\ (\text{XY PLANE}) & \frac{S_x}{EI}\ (\text{XZ PLANE}) & 0 \\ -\frac{l_{xy}}{EI} & \frac{l_y}{EI} & -\frac{l_{yz}}{EI} & -\frac{S_y}{EI}\ (\text{XY PLANE}) & 0 & \frac{S_y}{EI}\ (\text{YZ PLANE}) \\ -\frac{l_{xz}}{EI} & -\frac{l_{yz}}{EI} & \frac{l_z}{EI} & 0 & -\frac{S_z}{EI}\ (\text{XZ PLANE}) & -\frac{S_z}{EI}\ (\text{YZ PLANE}) \\ \frac{S_x}{EI}\ (\text{XY PLANE}) & -\frac{S_y}{EI}\ (\text{XY PLANE}) & 0 & \frac{1}{EI}\ (\text{XY PLANE}) & 0 & 0 \\ \frac{S_x}{EI}\ (\text{XZ PLANE}) & 0 & -\frac{S_z}{EI}\ (\text{XZ PLANE}) & 0 & \frac{1}{EI}\ (\text{XZ PLANE}) & 0 \\ 0 & \frac{S_y}{EI}\ (\text{YZ PLANE}) & -\frac{S_z}{EI}\ (\text{YZ PLANE}) & 0 & 0 & \frac{1}{EI}\ (\text{YZ PLANE}) \end{bmatrix}$$

$$F = \begin{bmatrix} F_x \\ F_y \\ F_z \\ M_{xy} \\ M_{xz} \\ M_{yz} \end{bmatrix} \qquad D = \begin{bmatrix} D_x \\ D_y \\ D_z \\ D_{xxy} \\ D_{oxz} \\ D_{oyz} \end{bmatrix}$$

Fig. 3 Matrix Elements for General 3-Plane 2-Anchor Piping Configuration

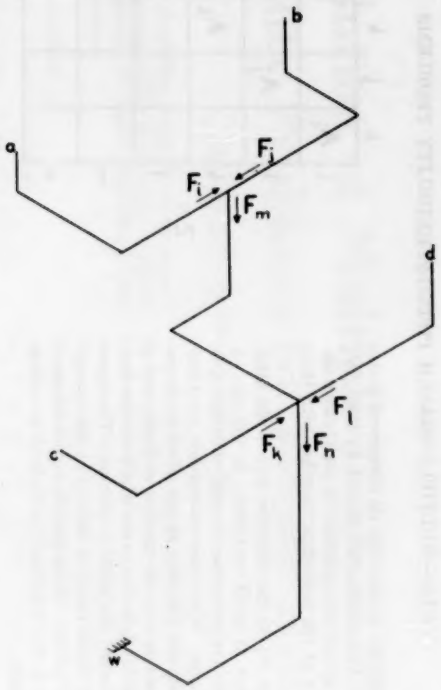

Fig. 4 Primitive System

$$B = \begin{bmatrix} 1 & & & & & \\ & 1 & & & & \\ & & 1 & & & \\ 15 & 8 & & 1 & & \\ 10 & & 8 & & 1 & \\ & 10 & -15 & & & 1 \end{bmatrix} \quad \ldots\ldots\ldots\ldots [11]$$

Referring to Figs. 4 and 5 and writing the old forces in terms of the new, we obtain

$$\left.\begin{aligned} \mathbf{F}_i &= \mathbf{I}\mathbf{F}_i' \\ \mathbf{F}_j &= \mathbf{I}\mathbf{F}_j' \\ \mathbf{F}_k &= \mathbf{I}\mathbf{F}_k' \\ \mathbf{F}_l &= \mathbf{I}\mathbf{F}_l' \\ \mathbf{F}_m &= \mathbf{I}\mathbf{F}_i' + \mathbf{I}\mathbf{F}_j' \\ \mathbf{F}_n &= \mathbf{B}\mathbf{F}_i' + \mathbf{B}\mathbf{F}_j' + \mathbf{I}\mathbf{F}_k' + \mathbf{I}\mathbf{F}_l' \end{aligned}\right\} \quad \ldots\ldots [12]$$

in which **I** is the unit matrix.

Using the relation $\mathbf{F} = \mathbf{CF}'$, we can now establish **C** and **Z′** as shown in Fig. 6.

The variables of the derived system must be chosen so that the number of equations equals the number of unknowns. This is the reason for choosing the axes i', j', k', and l' as the variables for the interconnected system, as shown by the connection tensor **C** in Fig. 6.

Each element of **Z′** is a 6×6 matrix. For the general case it is obvious that for a system of n-anchors the equation $\mathbf{Z'F'} = \mathbf{D'}$ will express the interconnected system as a set of $6(n-1)$ simultaneous equations. For the usual problem **F′** is unknown and **D′** is known from the conditions of the problem, for the present case being the deflections at the ends a, b, c, and d.

The elements of **F′** and **D′** are as follows:

$$\mathbf{F'} = \begin{bmatrix} \mathbf{F}_i' \\ \mathbf{F}_j' \\ \mathbf{F}_k' \\ \mathbf{F}_l' \end{bmatrix} \qquad \mathbf{D'} = \begin{bmatrix} \mathbf{D}_i' \\ \mathbf{D}_j' \\ \mathbf{D}_k' \\ \mathbf{D}_l' \end{bmatrix}$$

Each element of **F′** and of **D′** is a 6×1 matrix.

In closing it should be emphasized that the method is a perfectly general one, and may be applied to any piping configuration by the following routine procedure:

1 Draw the diagram and establish the equation of performance of the primitive system as $\mathbf{ZF} = \mathbf{D}$.

2 Draw a force-flow diagram of the manner in which the system is interconnected, and from it establish the connection tensor **C**, using $\mathbf{F} = \mathbf{CF}'$.

3 Establish **Z′** from $\mathbf{Z'} = \mathbf{C}_t\mathbf{ZC}$.

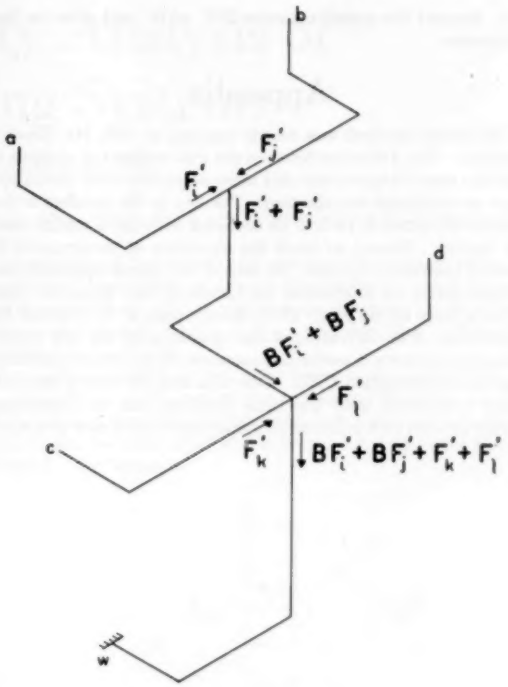

FIG. 5 DERIVED SYSTEM

$$C = \begin{array}{c} \\ i \\ j \\ k \\ l \\ m \\ n \end{array} \begin{array}{c} \begin{array}{cccc} i' & j' & k' & l' \end{array} \\ \begin{bmatrix} \mathbf{I} & & & \\ & \mathbf{I} & & \\ & & \mathbf{I} & \\ & & & \mathbf{I} \\ \mathbf{I} & \mathbf{I} & & \\ \mathbf{B} & \mathbf{B} & \mathbf{I} & \mathbf{I} \end{bmatrix} \end{array} \qquad C_t = \begin{bmatrix} \mathbf{I} & & & & \mathbf{I} & \mathbf{B}_i \\ & \mathbf{I} & & & \mathbf{I} & \mathbf{B}_j \\ & & \mathbf{I} & & & \mathbf{I} \\ & & & \mathbf{I} & & \mathbf{I} \end{bmatrix}$$

$$Z' = C_t Z C = \begin{bmatrix} A_i + A_m + B_i A_m B & A_m + B_i A_n B & B_i A_n & B_i A_n \\ A_m + B_j A_n B & A_j + A_m + B_j A_n B & B_j A_n & B_j A_n \\ A_n B & A_n B & A_k + A_n & A_n \\ A_n B & A_n B & A_n & A_l + A_n \end{bmatrix}$$

FIG. 6

4 Expand the matrix equation $\mathbf{Z'F'} = \mathbf{D'}$, and solve for the unknowns.

Appendix

The tensor method uses matrix algebra, as does Mr. Brock's method. The difference between the two methods of analysis is perhaps more fundamental and more important than would appear on superficial examination. The key to the problem is the connection tensor **C** (not to be confused with the **C**-matrix used by Brock). Having at hand the equations of performance of several individual systems, the user of the tensor approach can always derive an interconnected system of any degree of complexity, since he can easily fill in the elements of the **C** tensor by inspection. The derivation of the equations for the new (interconnected) system is performed *automatically* by merely performing the multiplication $\mathbf{C_i ZC}$. One who uses the matrix method when confronted with the same problem, has no connection tensor to work with and therefore must derive each new and more complicated system by laboriously tracing out the complicated interrelationships existing in the network.

Acknowledgment

The author wishes to acknowledge his appreciation to Mr. Gabriel Kron of the General Electric Company, for his help in checking the tensor equations.

BIBLIOGRAPHY

1 "Tensor Analysis of Networks," by Gabriel Kron, John Wiley & Sons, Inc., New York, N. Y., 1939.

2 "Advanced Mechanics of Materials," by F. B. Seely and J. O. Smith, John Wiley & Sons, Inc., New York, N. Y., 1952, pp. 477–481.

3 "Piping Stress Calculations Simplified," by S. W. Spielvogel, McGraw-Hill Book Company, Inc., New York, N. Y., 1943.

4 "Elementary Matrices," by R. A. Frazer, W. J. Duncan, and A. R. Collar, Cambridge University Press and The Macmillan Company, New York, N. Y., 1947.

5 "A Matrix Method for Flexibility Analysis of Piping Systems," by J. E. Brock, JOURNAL OF APPLIED MECHANICS, Trans. ASME, vol. 74, 1952, p. 501.

Tensor-Flexibility Analysis of Pipe-Supporting Systems

By J. W. SOULE,[1] SWARTHMORE, PA.

A general tensor method of analysis is used to derive the equations of performance of a complete piping system, including effect of pipe weight, supports, and thermal expansion.

Introduction

A COMPANION paper by the author[2] develops a tensor method for obtaining the equations of performance of a general piping system subjected to given deflections. The purpose of the present paper is to extend the method to include the most general case possible in a piping system; namely, that of a system including effects of pipe weight, hangers, guides, and the like, as well as the deflections due to thermal expansion. Hitherto this problem has been too complex to permit solution within practical time limits, except for the extremely simple cases. In general, however, the more complex the problem, the greater the advantage gained by the use of tensor methods.

Theory

The method is best shown by solving a sample problem, which consists of a three-dimensional system with 2 anchors and 2 supports, as shown in Fig. 1. The theory and sign conventions used in the previous paper (hereinafter referred to as Part 1), will also apply in the method which follows. As in Part 1, matrices will be represented by bold-face capitals. Subscripts will be used to indicate which branch is referred to, with the addition of a subscript w where the forces or deflections are due to the pipe weight.

The solution is begun by dividing the system into "branches," starting a new branch at each change in direction or point of constraint. In this problem there are the 8 branches i, j, p, m, n, o, l, r. Co-ordinate axes have been established for each branch, as shown in Figs. 1 and 2.

The flexibility matrices for constraints, such as $\mathbf{A}_p$ and $\mathbf{A}_l$ may be easily written if it is remembered that each element represents the deflection due to a unit force or moment. Which force or moment is meant will be apparent from the position in the matrix. $\mathbf{A}_p$ and $\mathbf{A}_l$ are shown in Figs. 3 and 4.

In order to allow for the effects of the uniform load it will be necessary to consider each horizontal branch as composed of two component branches, one of which is a hypothetical branch which has the properties of a uniformly loaded cantilever, and the other is the actual branch which acts in accordance with the theory of Part 1.

The equation of performance for each cantilever can be written. At branch i for example, $\mathbf{A}_{iw}\mathbf{F}_{iw} = \mathbf{D}_{iw}$ (deflections at a, forces and moments at b). These matrices are shown in Fig. 5. For branch j we will have $\mathbf{A}_{jw}\mathbf{F}_{jw} = \mathbf{D}_{jw}$ (deflections at b, forces and moments at c), and so on.

For vertical members such as n the forces at the one end e may be considered to be the sum of two component branches, one of which is the hypothetical one exerting forces $\mathbf{F}_{nw}$ (the concentrated weight), and the other is the actual branch exerting forces $\mathbf{F}_n$ as in Part 1. For branch n

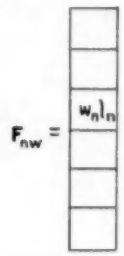

and $\mathbf{A}_{nw} = \mathbf{O}$ (the zero matrix).

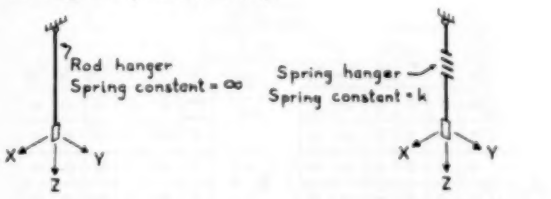

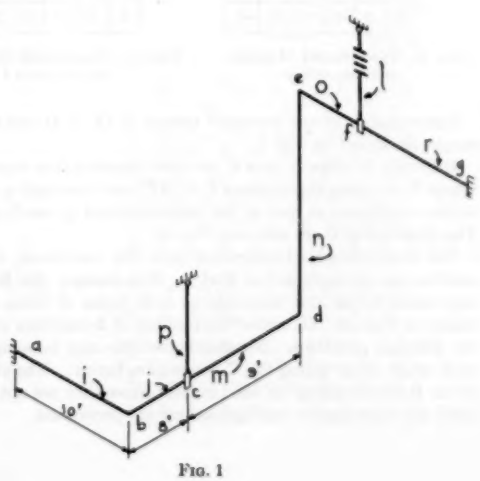

Fig. 1

[1] Designer, United Engineers and Constructors, Inc., Philadelphia, Pa.

[2] "The Solution of Multiple-Branch Piping-Flexibility Problems by Tensor Analysis," by J. W. Soule, published in this issue, pp. 176–180.

Contributed by the Applied Mechanics Division and presented at the Diamond Jubilee Annual Meeting, Chicago, Ill., November 13–18, 1955, of The American Society of Mechanical Engineers.

Discussion of this paper should be addressed to the Secretary, ASME, 29 West 39th Street, New York, N. Y., and will be accepted until July 10, 1956, for publication at a later date. Discussion received after the closing date will be returned.

Note: Statements and opinions advanced in papers are to be understood as individual expressions of their authors and not those of the Society. Manuscript received by ASME Applied Mechanics Division, February 17, 1955. Paper No. 55—A-82.

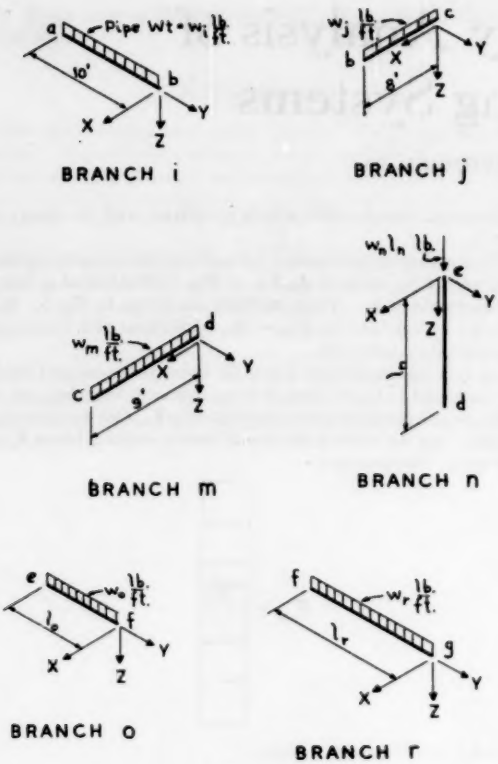

FIG. 2

$A_p =$

F_x	F_y	F_z	M_{xy}	M_{xz}	M_{yz}
∞	0	0	0	0	0
0	∞	0	0	0	0
0	0	0	0	0	0
0	0	0	∞	0	0
0	0	0	0	∞	0
0	0	0	0	0	∞

FIG. 3 FLEXIBILITY MATRIX FOR BRANCH p

$A_l =$

F_x	F_y	F_z	M_{xy}	M_{xz}	M_{yz}
∞	0	0	0	0	0
0	∞	0	0	0	0
0	0	$\frac{1}{k}$	0	0	0
0	0	0	∞	0	0
0	0	0	0	∞	0
0	0	0	0	0	∞

FIG. 4 FLEXIBILITY MATRIX FOR BRANCH l

The equation of the primitive system is $\mathbf{ZF} = \mathbf{D}$ and the elements are shown in Fig. 6.

Referring to Figs. 7 and 8, we can construct the connection tensor $\mathbf{C}$ by using the relation $\mathbf{F} = \mathbf{CF'}$ and considering the fictitious cantilevers as part of the interconnected (primed) system. The elements of $\mathbf{C}$ are shown in Fig. 9.

The $\mathbf{B}$-matrices are constructed from the conditions of static equilibrium, as explained in Part 1. For example, the $\mathbf{B}$-matrix expressing forces and moments at d in terms of those at b is shown in Fig. 10. Of course the number of $\mathbf{B}$-matrices will vary for different problems. Number subscripts may be assigned to each while constructing the $\mathbf{C}$-connection tensor. The elements of the $\mathbf{B}$-matrices may be filled in later, since they are not needed until the final matrix multiplications are performed.

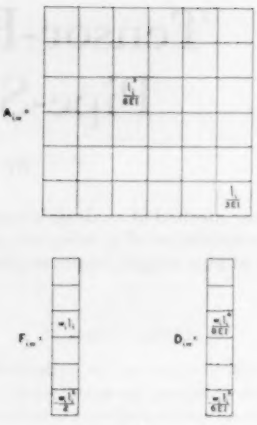

FIG. 5

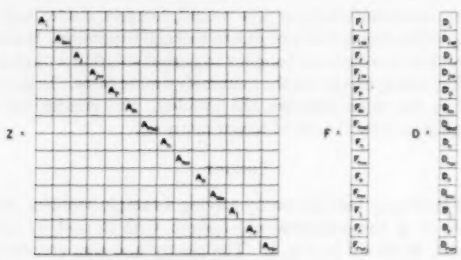

FIG. 6 MATRIX ELEMENTS FOR THE PRIMITIVE SYSTEM

The $\mathbf{Z'}$ matrix can be constructed by using the relation $\mathbf{Z'} = \mathbf{C}_t\mathbf{ZC}$, as shown in Fig. 11.

Referring to Figs. 6, 9, and 11, we see that as a result of performing the matrix multiplication $\mathbf{C}_t\mathbf{ZC}$, each element of $\mathbf{Z'}$ is a 6×6 matrix, as follows

$$\mathbf{Z}_{11}' = \mathbf{A}_i + \tilde{\mathbf{B}}_j\mathbf{A}_j\mathbf{B}_j + \tilde{\mathbf{B}}_n\mathbf{A}_m\mathbf{B}_n + \tilde{\mathbf{B}}_t\mathbf{A}_n\mathbf{B}_t + \tilde{\mathbf{B}}_7\mathbf{A}_o\mathbf{B}_7 + \tilde{\mathbf{B}}_{11}\mathbf{A}_r\mathbf{B}_{11}$$

$$\mathbf{Z}_{12}' = \tilde{\mathbf{B}}_j\mathbf{A}_j\mathbf{B}_j + \tilde{\mathbf{B}}_n\mathbf{A}_m\mathbf{B}_n + \tilde{\mathbf{B}}_t\mathbf{A}_n\mathbf{B}_t + \tilde{\mathbf{B}}_7\mathbf{A}_o\mathbf{B}_7 + \tilde{\mathbf{B}}_{11}\mathbf{A}_r\mathbf{B}_{11}$$

and so on. (Note: Tilde indicates transposed matrix.)

The equation of the interconnected system is $\mathbf{Z'F'} = \mathbf{D'}$, in which

$$\mathbf{F'} = \begin{bmatrix} F_i' \\ F_{iw}' \\ F_{jw}' \\ F_p' \\ F_{mw}' \\ F_{nw}' \\ F_{ow}' \\ F_l' \\ F_{rw}' \end{bmatrix} \qquad \mathbf{D'} = \begin{bmatrix} D_i' \\ D_{iw}' \\ D_{jw}' \\ D_p' \\ D_{mw}' \\ D_{nw}' \\ D_{ow}' \\ D_l' \\ D_{rw}' \end{bmatrix}$$

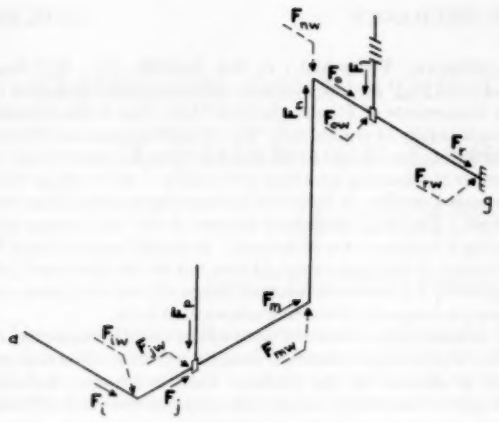

FIG. 7 PRIMITIVE SYSTEM

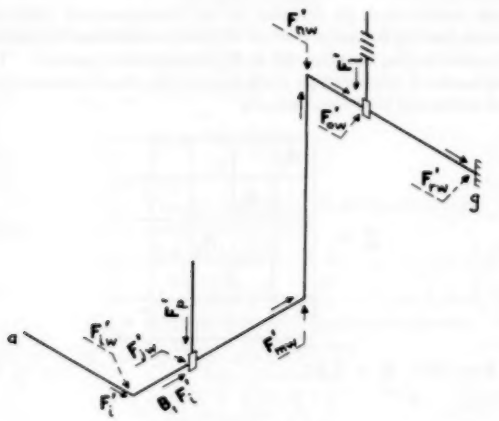

FIG. 8 DERIVED SYSTEM

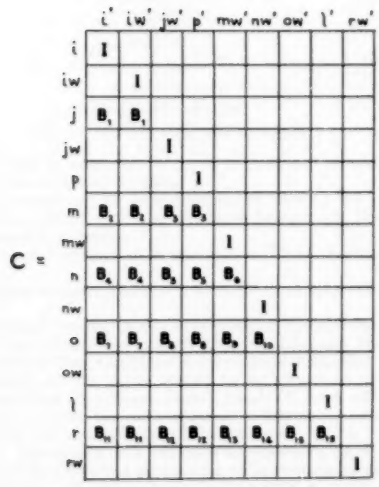

FIG. 9 THE C CONNECTION TENSOR

The elements of $\mathbf{F}_{iw}'$, $\mathbf{F}_{jw}'$, $\mathbf{F}_{mw}'$, etc., are known from the cantilever formulas as before. For example

$$\mathbf{F}'_{iw} = \begin{bmatrix} \\ \\ w_i l_i \\ \\ \\ -\frac{w_i l_i^2}{2} \end{bmatrix}$$

The new (primed) deflections of the hypothetical cantilevers are not needed for our solution, so the elements of $\mathbf{Z}'$ which have the same row number as $\mathbf{D}_{iw}'$, $\mathbf{D}_{jw}'$, etc., need not be computed.

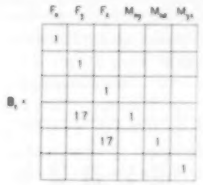

FIG. 10

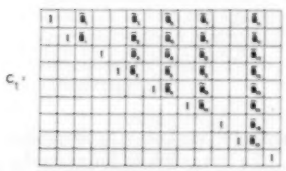

(a)

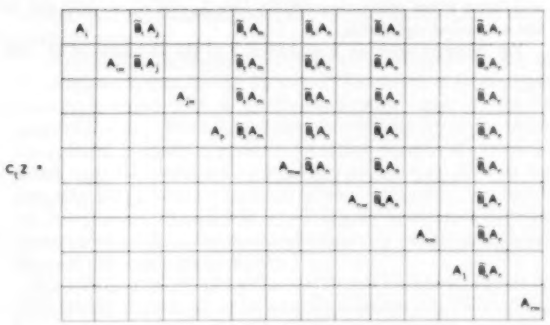

(b)

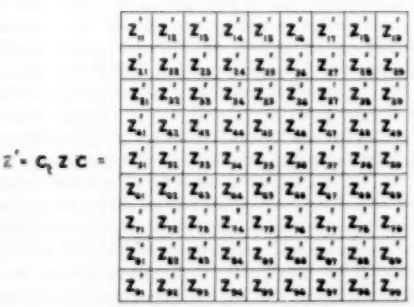

(c)

FIG. 11

The elements of **D′** for the external members are found by releasing the structure at all external terminals except the fixed end *g* and computing the deflections necessary to return them to their known positions after the structure has undergone thermal expansion. The original hypothetical cantilever deflections are subtracted from the deflections so found to form the elements of **D′**, as shown in Fig. 12.

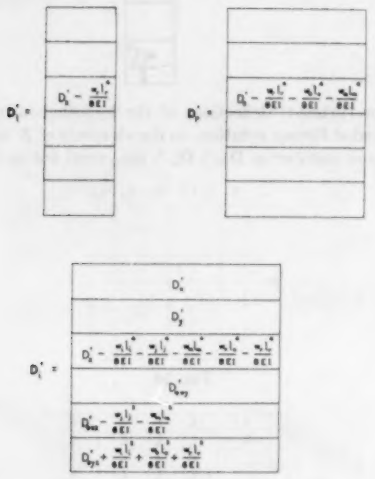

Fig. 12

Certain elements of **F′** are known to be zero from the conditions of the problem. In this problem, for example, all elements are zero except in the *z*-direction for hangers *p* and *l*. These zeros will cause terms containing infinity (see $\mathbf{A}_p$ and $\mathbf{A}_l$) to drop out in the expanded equations.

For hangers such as *p* and *l* some of the elements of **D′** will be unknown. For *p* and *l* in this problem, D_x', D_y', $D_{\theta z x}'$, $D_{\theta z z}'$, and $D_{\theta y z}'$ are indeterminate and of no value in solving for the components of **F′**, and therefore these lines in the expanded equations may be crossed out. The remaining equations will contain the unique solution to the problem. For the present case the number of remaining equations will be $[6(n-1)-10]$, in which *n* equals 4 anchors, so there will be 8 simultaneous equations to be solved. The 10 is subtracted because of the two hangers each having 5 indeterminate deflections. It should be noted that if F_z' for either of the hangers should turn out to act downward (plus sign for F_z'), it means the assumed design will not work, since a rod hanger is incapable of exerting a downward force.

Obviously, much time and labor will be saved by neglecting the effect of pipe weight whenever possible, but the method does provide a solution to the problem when necessary. Including hangers in the solution usually will not cause too much difficulty.

Summary

The tensor method of analysis as developed in Part 1 and in the present paper, solves all problems, from the very simple to the most complicated, by building up an interconnected (derived) system having equation $\mathbf{Z'F'} = \mathbf{D'}$ from a collection of isolated branches having equation $\mathbf{ZF} = \mathbf{D}$ (the primitive system). The fundamental relationships used to perform the interconnection and derive the final equations are

$$\mathbf{Z} = \begin{bmatrix} \mathbf{A}_i & & & & \\ & \mathbf{A}_j & & & \\ & & \mathbf{A}_k & & \\ & & & \ddots & \\ & & & & \ddots \end{bmatrix}$$

$\mathbf{F} = \mathbf{CF'}$; $\mathbf{Z'} = \mathbf{C}_t\mathbf{ZC}$.

Bending and Torsion of Circular Cylinder Cantilever Beams of Cylindrically Aeolotropic Material[1]

By W. S. ERICKSEN,[2] WRIGHT-PATTERSON AIR FORCE BASE, OHIO

This paper deals with the problem of determining the components of stress and displacement associated with the flexure and torsion of a cantilever beam in the form of a hollow circular cylinder of cylindrically aeolotropic material. A solution satisfying the conditions of the theory of elasticity is obtained by the semi-inverse method of Saint Venant.

Nomenclature

The following nomenclature is used in the paper:

a_{pq} = elastic coefficients

$A_{pq} = \dfrac{a_{11}a_{pq} - a_{1p}a_{1q}}{a_{11}}$

$B = \dfrac{A_{22} + 2A_{23} + 2a_{44}}{A_{33}}$

C, D = const

E = Young's modulus of an isotropic material

$e_{zz}, e_{rr}, \ldots, e_{\theta z}$ = components of strain

$F_n = \dfrac{2\delta_n A_{23}(3 - B)}{a_{12} - a_{13}} - \dfrac{(n+1)}{a_{11}}[a_{12} + a_{13}(n+2)]$,* $n = 1, i, j$, where $\delta_1 = 1$ and $\delta_i = \delta_j = 0$

G = shear modulus of an isotropic material

$H_n = \dfrac{2\delta_n A_{23}(3 - B)(2a_{13} - a_{12})}{(a_{12} - a_{13})} + (n+1)[(n+1)(n+2)A_{23} - (A_{22} + A_{23} + a_{44})]$* $n = 1, i, j$, where $\delta_1 = 1$ and $\delta_i = \delta_j = 0$

$I = \dfrac{\pi(r_2^4 - r_1^4)}{4}$

$i = (1 + B)^{1/2} - 1$

$j = -(1 + B)^{1/2} - 1$

$k = (a_{44}/a_{55})^{1/2}$

$K_{pn} = a_{p1}F_n + a_{p2}(n+1) + a_{p3}(n+1)(n+2)$ $n = 1, i, j$; $p = 1, 2, 3$

l = length of cylinder

M = applied torsional moment

n = a summation index that ranges over the values 1, i, and j

P = applied radial force

r_1, r_2 = inner and outer radii, respectively, of cylinder

S_n = coefficients determined by Equations [44]

T_k, T_{-k} = coefficients determined by Equations [54]

u_z, u_r, u_θ = axial, radial, and tangential components of displacement

$u = u_r \cos\theta - u_\theta \sin\theta$

$v = u_r \sin\theta + u_\theta \cos\theta$, $w = u_z$ = components of displacement, rectangular co-ordinates

$x = r\cos\theta$, $y = r\sin\theta$, z = rectangular co-ordinates

z, r, θ = cylindrical co-ordinates

σ = Poisson's ratio of an isotropic material

Σ_n = a symbol indicating summation over indexes n

$\tau_{zz}, \tau_{rr}, \ldots, \tau_{\theta z}$ = components of stress

φ, ψ = stress functions

1 Introduction

The problem that is considered here is that of determining the components of stress and displacement in a long hollow circular cylinder of cylindrically aeolotropic material, one end of which is fixed,[4] and the other subjected to a radially directed force and a torsional moment.

An example of the material of which the cylinder is assumed to be composed is that formed by rolling thin sheets of an isotropic material covered with a bonding substance upon a circular cylindrical core. The axis of the core is evidently one about which the material is axially symmetric. Another example of a material which may be considered cylindrically aeolotropic, at least for purposes of approximate analysis, is wood with circular cylindrical growth rings. Specifically, a cylindrically aeolotropic material is one for which the stress-strain relations may be expressed in the forms of Equations [1] to [6] (2).

It has been pointed out by Carrier (2) that a material cannot be cylindrically aeolotropic at its axis of symmetry. If the material is continuous to this axis, a transition in properties must take place in the vicinity of the axis such that at the axis it is isotropic. An analysis based on the assumption of cylindrical aeolotropy throughout cannot, therefore, be accurate in the vicinity of the longitudinal axis if this axis is contained in the material. This characteristic of the results is exhibited in Formulas [67] and [68], for example, where, if $k < 1$, stresses of infinite magnitude are obtained at the center if the inner radius of the cylinder is taken as zero. The present results are therefore, in general, applicable only if the inner radius of the cylinder is not zero.

In the section which follows the various conditions imposed in the determination of the stress distribution are given together with an outline of the method of analysis. The determination of the stress components is carried out in Section 3 and in Section 4 the components of displacement are listed with results in each case given in terms of the solution of a system of linear algebraic

* The case in which $a_{13} = a_{12}$ so that F_1 and H_1 are undefined is treated in Section 5 of the paper.

[1] The present results were obtained in part by the author while employed at the U. S. Forest Products Laboratory, Madison, Wis., and reported in reference (1).[3]

[2] Associate Professor of Mathematics, USAF Institute of Technology.

[3] Numbers in parentheses refer to the Bibliography at the end of the paper.

Contributed by the Applied Mechanics Division and presented at the Diamond Jubilee Annual Meeting, Chicago, Ill., November 13–18, 1955, of The American Society of Mechanical Engineers.

Discussion of this paper should be addressed to the Secretary, ASME, 29 West 39th Street, New York, N. Y., and will be accepted until July 10, 1956, for publication at a later date. Discussion received after the closing date will be returned.

Note: Statements and opinions advanced in papers are to be understood as individual expressions of their authors and not those of the Society. Manuscript received by ASME Applied Mechanics Division, March 28, 1955. Paper No. 55—A-41.

[4] With limitations discussed in Section 6.

equations. Results for the case $a_{12} = a_{13}$ (two equal Poisson's ratios) are given in Section 5. A discussion of some of the results is given in the final section.

2 Formulation of the Problem

If the components of stress and strain in a cylindrically aeolotropic material are considered as functions of cylindrical co-ordinates, and if the z-axis of the co-ordinate system coincides with the axis of symmetry of the material, the stress-strain relations of the material are of the forms (2)

$$e_{zz} = a_{11}\tau_{zz} + a_{12}\tau_{rr} + a_{13}\tau_{\theta\theta} \quad [1]$$

$$e_{rr} = a_{21}\tau_{zz} + a_{22}\tau_{rr} + a_{23}\tau_{\theta\theta} \quad [2]$$

$$e_{\theta\theta} = a_{31}\tau_{zz} + a_{32}\tau_{rr} + a_{33}\tau_{\theta\theta} \quad [3]$$

$$e_{r\theta} = a_{44}\tau_{r\theta} \quad [4]$$

$$e_{\theta z} = a_{55}\tau_{\theta z} \quad [5]$$

$$e_{zr} = a_{66}\tau_{zr} \quad [6]$$

where the coefficients a_{pq} are constants. These constants are such that $a_{pq} = a_{qp}$. For a material which is isotropic they are given as follows

$$a_{11} = a_{22} = a_{33} = \frac{1}{E}$$

$$a_{12} = a_{13} = a_{23} = -\frac{\sigma}{E}$$

and

$$a_{44} = a_{55} = a_{66} = \frac{1}{2G}$$

In general, each constant is defined by an expression of the same form that it is here, but differs in value from each other constant in the sequence in which it appears.

With components of stress expressed as functions of cylindrical co-ordinates the equations of equilibrium take the well-known forms[4]

$$\frac{\partial \tau_{rr}}{\partial r} + \frac{1}{r}\frac{\partial \tau_{r\theta}}{\partial \theta} + \frac{\partial \tau_{rz}}{\partial z} + \frac{\tau_{rr} - \tau_{\theta\theta}}{r} = 0 \quad [7]$$

$$\frac{1}{r}\frac{\partial \tau_{\theta\theta}}{\partial \theta} + \frac{\partial \tau_{r\theta}}{\partial r} + \frac{\partial \tau_{\theta z}}{\partial z} + \frac{2}{r}\tau_{r\theta} = 0 \quad [8]$$

$$\frac{\partial \tau_{zr}}{\partial r} + \frac{1}{r}\frac{\partial \tau_{\theta z}}{\partial \theta} + \frac{\partial \tau_{zz}}{\partial z} + \frac{1}{r}\tau_{rz} = 0 \quad [9]$$

The equations of compatibility, with components of strain referred to cylindrical co-ordinates, are less familiar. They may be expressed in the forms (4, 5)

$$\frac{\partial^2 e_{rr}}{\partial z^2} + \frac{\partial^2 e_{zz}}{\partial r^2} - 2\frac{\partial^2 e_{rz}}{\partial r \partial z} = 0 \quad [10]$$

$$\frac{1}{r^2}\frac{\partial^2 e_{zz}}{\partial \theta^2} + \frac{\partial^2 e_{\theta\theta}}{\partial z^2} - \frac{2}{r}\frac{\partial^2 e_{\theta z}}{\partial \theta \partial z} + \frac{1}{r}\frac{\partial e_{zz}}{\partial r} - \frac{2}{r}\frac{\partial e_{rz}}{\partial z} = 0 \quad [11]$$

$$\frac{\partial}{\partial z}\left[\frac{\partial e_{r\theta}}{\partial z} - \frac{\partial e_{\theta z}}{\partial r} - \frac{1}{r}\left(\frac{\partial e_{rz}}{\partial \theta} - e_{\theta z}\right)\right] + \frac{1}{r}\frac{\partial^2 e_{zz}}{\partial r \partial \theta} - \frac{1}{r^2}\frac{\partial e_{zz}}{\partial \theta} = 0 \quad [12]$$

$$\frac{\partial}{\partial r}\left[\frac{\partial (re_{\theta\theta})}{\partial r} - \frac{\partial e_{r\theta}}{\partial \theta} - e_{rr}\right] + \frac{\partial}{\partial \theta}\left[\frac{1}{r}\frac{\partial e_{rr}}{\partial \theta} - \frac{\partial e_{r\theta}}{\partial r} - \frac{2}{r}e_{r\theta}\right] = 0 \quad [13]$$

$$\frac{\partial}{\partial r}\left\{\frac{1}{r}\left[\frac{\partial (re_{\theta_z})}{\partial r} - \frac{\partial e_{zr}}{\partial \theta}\right]\right\} = -\frac{\partial}{\partial z}\left[\frac{1}{r}\frac{\partial e_{rr}}{\partial \theta} - \frac{\partial e_{r\theta}}{\partial r} - \frac{2}{r}e_{r\theta}\right] \quad [14]$$

$$\frac{\partial}{\partial \theta}\left\{\frac{1}{r}\left[\frac{\partial (re_{\theta_z})}{\partial r} - \frac{\partial e_{zr}}{\partial \theta}\right]\right\} = \frac{\partial}{\partial z}\left[\frac{\partial (re_{\theta\theta})}{\partial r} - \frac{\partial e_{r\theta}}{\partial \theta} - e_{rr}\right] \quad [15]$$

Let the cylinder be fixed at the base $z = 0$,[4] and be subjected to a force P directed along the radius $\theta = 0$ and a torsional moment M at $z = l$. Then with r_1 and r_2 denoting, respectively, the inner and outer radii of the cylinder, the stress resultants and couples must satisfy the following conditions

$$\int_{r_1}^{r_2}\int_0^{2\pi} (\tau_{zr}\cos\theta - \tau_{\theta_z}\sin\theta) r\, dr\, d\theta = P \quad [16]$$

$$\int_{r_1}^{r_2}\int_0^{2\pi} \tau_{zz} r^2 \cos\theta\, dr\, d\theta = -P(l - z) \quad [17]$$

$$\int_{r_1}^{r_2}\int^{2\pi} \tau_{\theta_z} r^2\, dr\, d\theta = M \quad [18]$$

$$\int_{r_1}^{r_2}\int_0^{2\pi} (\tau_{zr}\sin\theta + \tau_{\theta_z}\cos\theta) r\, dr\, d\theta = 0 \quad [19]$$

$$\int_{r_1}^{r_2}\int_0^{2\pi} \tau_{zz} r^2 \sin\theta\, dr\, d\theta = 0 \quad [20]$$

$$\int_{r_1}^{r_2}\int_0^{2\pi} \tau_{zz} r\, dr\, d\theta = 0 \quad [21]$$

Finally, since the inner and outer curved surfaces of the cylinder are free of stress, the boundary conditions are

$$\tau_{rr} = 0 \text{ at } r = r_1 \text{ and } r = r_2 \quad [22]$$

$$\tau_{r\theta} = 0 \text{ at } r = r_1 \text{ and } r = r_2 \quad [23]$$

$$\tau_{zr} = 0 \text{ at } r = r_1 \text{ and } r = r_2 \quad [24]$$

Among the foregoing conditions, Equation [16] is redundant because its fulfillment is implied by Equations [9], [17], and [24].

The problem is solved by the use of the semi-inverse method of Saint Venant. After assuming forms of the stress components as functions of z it is found that the solution is separated into two parts. The first consists in the determination of τ_{zz}, τ_{rr}, $\tau_{\theta\theta}$, and $\tau_{r\theta}$. This is carried out by applying the first two equilibrium Conditions [7] and [8] and the first four compatibility Conditions [10] to [13] with appropriate boundary and end conditions. The second part consists in the determination of the stress components τ_{θ_z} and τ_{zr} which are linked to the previously determined stress components by the remaining equilibrium and compatibility Conditions [9], [14], and [15].

3 The Analysis

The solution to the problem at hand is obtained by making the assumptions that τ_{θ_z} and τ_{zr} are independent of z and that τ_{zz}, τ_{rr}, $\tau_{\theta\theta}$, and $\tau_{r\theta}$ are linear in z. From Relations [1] to [6] it is seen

[4] Reference (3), p. 202.

that the strain components $e_{\theta\theta}$ and e_{zr} are likewise independent of z and that the remaining strain components are linear in z.

On the basis of the foregoing assumptions, the compatibility Conditions [10], [11], and [12] reduce, respectively, to

$$\frac{\partial^2 e_{zz}}{\partial r^2} = 0 \quad [25]$$

$$\frac{\partial^2 e_{zz}}{\partial \theta^2} + r\frac{\partial e_{zz}}{\partial r} = 0 \quad [26]$$

and

$$r\frac{\partial^2 e_{zz}}{\partial r \partial \theta} - \frac{\partial e_{zz}}{\partial \theta} = 0 \quad [27]$$

A solution of this set of equations is taken in the form

$$e_{zz} = Cr(l - z)\cos\theta \quad [28]$$

where the coefficient C remains to be determined.

If $\tau_{\theta z}$ and τ_{zr} are independent of z, the equilibrium Equations [7] and [8] reduce to

$$\frac{\partial \tau_{rr}}{\partial r} + \frac{1}{r}\frac{\partial \tau_{r\theta}}{\partial \theta} + \frac{\tau_{rr} - \tau_{\theta\theta}}{r} = 0 \quad [29]$$

and

$$\frac{1}{r}\frac{\partial \tau_{\theta\theta}}{\partial \theta} + \frac{\partial \tau_{r\theta}}{\partial r} + \frac{2}{r}\tau_{r\theta} = 0 \quad [30]$$

These equations are solved by the use of a stress function ψ where

$$\tau_{rr} = \frac{1}{r}\frac{\partial \psi}{\partial r} + \frac{1}{r^2}\frac{\partial^2 \psi}{\partial \theta^2} \quad [31]$$

$$\tau_{\theta\theta} = \frac{\partial^2 \psi}{\partial r^2} \quad [32]$$

and

$$\tau_{r\theta} = \frac{1}{r^2}\frac{\partial \psi}{\partial \theta} - \frac{1}{r}\frac{\partial^2 \psi}{\partial r \partial \theta} \quad [33]$$

It is found that the form

$$\psi = R(r)(l - z)\cos\theta \quad [34]$$

is appropriate for determining ψ. A differential equation for the function $R(r)$ in this expression is obtained from compatibility Relation [13] by the following steps: Substitute Equation [28] into [1] and use the resulting equation to eliminate τ_{zz} from Equations [2] and [3]. Thus

$$e_{rr} = A_{23}\tau_{rr} + A_{23}\tau_{\theta\theta} + \frac{Ca_{12}}{a_{11}}(l - z)r\cos\theta \quad [35]$$

and

$$e_{\theta\theta} = A_{23}\tau_{rr} + A_{33}\tau_{\theta\theta} + \frac{Ca_{13}}{a_{11}}(l - z)r\cos\theta \quad [36]$$

These two strain components and $e_{r\theta}$, Equation [4], may now be expressed in terms of ψ by the use of Equations [31], [32], and [33], and finally in terms of $R(r)$, θ, and z by means of Equation [34]. With the use of these expressions Equation [13] yields

$$\frac{d^4R}{dr^4} + \frac{2}{r}\frac{d^3R}{dr^3} - B\left(\frac{1}{r^2}\frac{d^2R}{dr^2} - \frac{1}{r^3}\frac{dR}{dr} + \frac{R}{r^4}\right) = \frac{2C(a_{12} - a_{13})}{ra_{11}A_{23}} \quad [37]$$

The general solution for $R(r)$ is

$$R(r) = S_0 r\log r + S_{-1}r + S_1 r^3 + S_i r^{i+2} + S_j r^{j+2}$$

with

$$S_1 = \frac{C(a_{12} - a_{13})}{2a_{11}A_{23}(3 - B)} \quad [38]$$

This coefficient is now adopted as an unknown in place of its undetermined factor C. Among the remaining coefficients, S_0 is taken as zero because the term to which it belongs yields multiple valued components of displacement, and S_{-1} can be set equal to zero without effect on the stress components, Equations [31], [32], and [33]. The expression for $R(r)$ may then be written

$$R(r) = \Sigma_n S_n r^{n+2} \quad [39]$$

where Σ_n is used to denote summation over the indexes 1, i, and j. In this notation

$$\tau_{zz} = \Sigma_n S_n F_n r^n (l - z)\cos\theta \quad [40]$$

$$\tau_{rr} = \Sigma_n S_n (n + 1)r^n (l - z)\cos\theta \quad [41]$$

$$\tau_{\theta\theta} = \Sigma_n S_n (n + 1)(n + 2)r^n (l - z)\cos\theta \quad [42]$$

and

$$\tau_{r\theta} = \Sigma_n S_n (n + 1)r^n (l - z)\sin\theta \quad [43]$$

The first among these is obtained by using Equations [28], [38], [41], and [42] in Equation [1].

The coefficients S_n may now be evaluated by using Expressions [40], [41], and [43] to impose Conditions [17], [22], and [23]. They are thus determined as the solution of the following system of equations

$$\left.\begin{aligned} &\sum_n \pi S_n F_n \left(\frac{r_2^{n+3} - r_1^{n+3}}{n+3}\right) = -P \\ &\text{and} \\ &\Sigma_n S_n (n+1)r^n = 0 \text{ for } r = r_1 \text{ and for } r = r_2 \end{aligned}\right\} \quad [44]$$

The remaining compatibility Conditions [14] and [15] may be partially integrated by the following steps: With the use of Expressions [40], [41], [42], and [43] in Relations [2], [3], and [4]

$$\frac{\partial(re_{\theta\theta})}{\partial r} - \frac{\partial e_{r\theta}}{\partial \theta} - e_{rr} = U(r)(l - z)\cos\theta \quad [45]$$

where, for reference

$$U(r) = \Sigma_n S_n H_n r^n \quad [46]$$

Then, taking into account the forms of e_{rr} and $e_{r\theta}$ as functions of θ, Equation [13] yields

$$\frac{1}{r}\frac{\partial e_{rr}}{\partial \theta} - \frac{\partial e_{r\theta}}{\partial r} - 2\frac{e_{r\theta}}{r} = -U'(r)(l - z)\sin\theta$$

and Equations [14] and [15] are reduced, respectively, to

$$\frac{\partial}{\partial r}\left\{\frac{1}{r}\left[\frac{\partial(re_{\theta z})}{\partial r} - \frac{\partial e_{zr}}{\partial \theta}\right]\right\} = -U'(r)\sin\theta$$

and

$$\frac{\partial}{\partial \theta}\left\{\frac{1}{r}\left[\frac{\partial(re_{\theta z})}{\partial r} - \frac{\partial e_{zr}}{\partial \theta}\right]\right\} = -U(r)\cos\theta$$

These equations imply

$$\frac{1}{r}\left[\frac{\partial(re_{\theta z})}{\partial r} - \frac{\partial e_{zr}}{\partial \theta}\right] = -U(r)\sin\theta + D \quad [47]$$

where D is a constant.

The final equilibrium Condition [9], using Expression [40], is written

$$\frac{\partial \tau_{rz}}{\partial r} + \frac{1}{r}\tau_{rz} + \frac{1}{r}\frac{\partial \tau_{\theta z}}{\partial \theta} = \Sigma_n S_n F_n r^n \cos\theta \ldots\ldots [48]$$

This equation is solved by the use of the stress function φ where

$$\tau_{zr} = \frac{1}{r}\frac{\partial \varphi}{\partial \theta} + \sum_n \frac{S_n F_n}{n+2} r^{n+1}\cos\theta \ldots\ldots [49]$$

and

$$\tau_{\theta z} = -\frac{\partial \varphi}{\partial r} \ldots\ldots [50]$$

With the substitution of the foregoing expressions into Equations [5] and [6] it is found that

$$\frac{1}{r}\left[\frac{\partial (re_{\theta z})}{\partial r} - \frac{\partial e_{zr}}{\partial \theta}\right] = -a_{55}\left[\frac{\partial^2 \varphi}{\partial r^2} + \frac{1}{r}\frac{\partial \varphi}{\partial r}\right] - a_{55}\left[\frac{1}{r^2}\frac{\partial^2 \varphi}{\partial \theta^2} - \sum_n \frac{S_n F_n}{n+2} r^n \sin\theta\right]$$

By equating the right-hand member of this equation to that of Equation [47] after substituting Equation [46], the following equation for φ is obtained

$$\frac{\partial^2 \varphi}{\partial r^2} + \frac{1}{r}\frac{\partial \varphi}{\partial r} + \frac{k^2}{r^2}\frac{\partial^2 \varphi}{\partial \theta^2} = \sum_n S_n \left(\frac{k^2 F_n}{n+2} + \frac{H_n}{a_{55}}\right) r^n \sin\theta - \frac{D}{a_{55}}$$

This equation has as a solution[6]

$$\varphi = \left[T_k r^k + T_{-k} r^{-k} + \sum_n \frac{S_n\left(\frac{k^2 F_n}{n+2} + \frac{H_n}{a_{55}}\right) r^{n+2}}{(n+2)^2 - k^2}\right] \sin\theta - \frac{Dr^2}{4a_{55}}$$

With the use of this expression Equations [49] and [50] yield, respectively

$$\tau_{zr} = \left\{T_k r^{k-1} + T_{-k} r^{-k-1} + \sum_n \frac{S_n\left[(n+2)F_n + \frac{H_n}{a_{55}}\right] r^{n+1}}{(n+2)^2 - k^2}\right\} \cos\theta \ldots [51]$$

and

$$\tau_{\theta z} = \left\{-kT_k r^{k-1} + kT_{-k} r^{-k-1} - \sum_n \frac{S_n\left[k^2 F_n + \frac{(n+2)H_n}{a_{55}}\right] r^{n+1}}{(n+2)^2 - k^2}\right\} \sin\theta + \frac{Dr}{2a_{55}} \ldots\ldots [52]$$

The coefficients T_k, T_{-k}, and D in these expressions are evaluated by imposing Conditions [18] and [24]. From the former

$$D = \frac{a_{55}M}{I} \ldots\ldots [53]$$

and from the latter conditions

$$T_k r^{k-1} + T_{-k} r^{-k-1} + \sum_n \frac{S_n\left[(n+2)F_n + \frac{H_n}{a_{55}}\right] r^{n+1}}{(n+2)^2 - k^2} = 0$$

for $r = r_1$ and for $r = r_2$ ..... [54]

By noting the forms of Expressions [51] and [52] as functions of θ, it is seen that Condition [19] is satisfied. Likewise τ_{zz}, Expression [40], depends on θ in such a way that the two remaining Conditions [20] and [21] are fulfilled. All of the required conditions have thus been met and the solution, explicit in the solution of the system of Equations [44], [53], and [54], is exact.

4 Components of Displacement

The components of strain are obtained from the stress-strain relations, Equations [1] to [6], by substituting Expressions [40] to [43], [51], and [52] for the components of stress. They are given as follows

$$e_{zz} = S_1 K_{11} r(l - z)\cos\theta \ldots\ldots [55]$$

$$e_{rr} = \Sigma_n S_n K_{2n} r^n (l - z)\cos\theta \ldots\ldots [56]$$

$$e_{\theta\theta} = \Sigma_n S_n K_{3n} r^n (l - z)\cos\theta \ldots\ldots [57]$$

$$e_{r\theta} = \Sigma_n S_n (n+1) a_{44} r^n (l - z)\sin\theta \ldots\ldots [58]$$

$$e_{\theta z} = a_{55}\left\{-kT_k r^{k-1} + kT_{-k} r^{-k-1} - \sum_n \frac{S_n\left[k^2 F_n + \frac{(n+2)}{a_{55}} H_n\right] r^{n+1}}{(n+2)^2 - k^2}\right\} \sin\theta + \frac{a_{55} M r}{2I} \ldots [59]$$

$$e_{zr} = a_{55}\left\{k^2 T_k r^{k-1} + k^2 T_{-k} r^{-k-1} + \sum_n \frac{S_n k^2\left[(n+2)F_n + \frac{H_n}{a_{55}}\right] r^{n+1}}{(n+2)^2 - k^2}\right\} \cos\theta \ldots [60]$$

With these expressions the relations

$$\left.\begin{aligned} e_{zz} &= \frac{\partial u_z}{\partial z}, \quad e_{rr} = \frac{\partial u_r}{\partial r}, \quad e_{\theta\theta} = \frac{1}{r}\frac{\partial u_\theta}{\partial \theta} + \frac{u_r}{r} \\ e_{r\theta} &= \frac{1}{2}\left(\frac{1}{r}\frac{\partial u_r}{\partial \theta} + \frac{\partial u_\theta}{\partial r} - \frac{u_\theta}{r}\right) \\ e_{\theta z} &= \frac{1}{2}\left(\frac{\partial u_\theta}{\partial z} + \frac{1}{r}\frac{\partial u_z}{\partial \theta}\right), \quad e_{zr} = \frac{1}{2}\left(\frac{\partial u_z}{\partial r} + \frac{\partial u_r}{\partial z}\right) \end{aligned}\right\} \ldots [61]$$

yield the components of displacement. It is readily verified with the use of relations among the constants K_{2n}, K_{3n}, H_n, and a_{44} obtained from Equations [13] and [45] that the components of displacement may be expressed as follows

$$u_z = \left[-\frac{S_1 K_{11}(l - z)^2}{2} - \beta + \sum_n \frac{S_n K_{2n} r^{n+1}}{(n+1)(n+2)} + 2a_{55}\left\{kT_k r^{k-1} - kT_{-k} r^{-k-1} + k^2 \sum_n \frac{S_n\left[(n+2)F_n + \frac{H_n}{a_{55}}\right] r^{n+1}}{(n+2)[(n+2)^2 - k^2]}\right\}\right] r\cos\theta - \beta' r\sin\theta + \gamma \ldots\ldots [62]$$

[6] It is assumed that $(n+2)^2 \neq k^2$. If $(n+2)^2 = k^2$ for some index n, a modification in the form of ϕ is necessary.

$$u_r = \left[-\frac{S_1 K_{11}(l-z)^3}{6} + \beta z + \alpha + \sum_n \frac{S_n K_{3n} r^{n+1}(l-z)}{n+1} \right] \cos\theta + (\beta' z + \alpha') \sin\theta \quad [63]$$

$$u_\theta = \left[\frac{S_1 K_{11}(l-z)^3}{6} - \beta z - \alpha + \sum_n \frac{S_n [K_{3n} + 2(n+1)a_{44}]}{n+1} r^{n+1}(l-z) \right] \sin\theta + [\beta' z + \alpha'] \cos\theta + \frac{a_{55} M z r}{I} + \gamma' r \quad [64]$$

The terms with coefficients α, β, γ, α', β', and γ' represent rigid-body displacements, and the coefficients are determined by imposing conditions on these displacements at the end $z = 0$.

5 Results for Material With $a_{13} = a_{12}$

The foregoing results require modification when the material is such that $a_{13} = a_{14}$ because F_1 and H_1 are then undefined. In this case it is necessary to repeat the analysis starting with Equation [37] which is now homogeneous. The results are those given in Sections 3 and 4 with

$$S_1 = S_i = S_j = 0$$

and with

$$S_1 F_1 = -P/I, \quad S_1 H_1 = -a_{12} P/I$$

and

$$S_1 K_{p1} = -a_{p1} P/I$$

Explicit formulas for the components of stress and displacement may then be given as follows

$$\tau_{zz} = -P/Ir(l-z)\cos\theta \quad [65]$$

$$\tau_{rr} = \tau_{\theta\theta} = \tau_{r\theta} = 0 \quad [66]$$

$$\tau_{\theta z} = P/I \left(\frac{3 + \frac{a_{12}}{a_{55}}}{9 - k^2} \right) \left[\left(\frac{k^2 + \frac{3a_{12}}{a_{55}}}{3 + \frac{a_{12}}{a_{55}}} \right) r^2 - \frac{k r_1^{3-k}}{r^{1-k}} - \frac{k r_2^{1+k}}{r^2} \left(\frac{r_2^{3-k} - r_1^{3-k}}{r_2^{1+k} r_1^{1-k} - r_2^{1-k} r_1^{1+k}} \right) (r^{1-k} r_1^{1+k} + r_1^{1-k} r^{1+k}) \right] \sin\theta + Mr/2I \quad [67]$$

$$\tau_{rr} = P/I \left(\frac{3 + \frac{a_{12}}{a_{55}}}{9 - k^2} \right) \left[-r^2 + \frac{r_1^{3-k}}{r^{1-k}} - \frac{r_2^{1+k}}{r^2} \left(\frac{r_2^{3-k} - r_1^{3-k}}{r_2^{1+k} r_1^{1-k} - r_2^{1-k} r_1^{1+k}} \right) \times \left(r^{1-k} r_1^{1+k} - r^{1+k} r_1^{1-k} \right) \right] \cos\theta \quad [68]$$

$$u_z = \frac{P a_{11}}{I} \left\{ \frac{(l-z)^2}{2} - \frac{r^2 a_{12}}{6 a_{11}} + \frac{2k}{9 - k^2} \left(\frac{3a_{55}}{a_{11}} + \frac{a_{12}}{a_{11}} \right) \left[\frac{r_1^{3-k}}{r^{1-k}} - \frac{k r^2}{3} + r_2^{1+k} (r^{-1-k} r_1^{1+k} + r^{-1+k} r_1^{1-k}) \left(\frac{r_2^{3-k} - r_1^{3-k}}{r_2^{1+k} r_1^{1-k} - r_2^{1-k} r_1^{1+k}} \right) \right] - \beta \right\} r\cos\theta - \beta' r \sin\theta + \gamma \quad [69]$$

$$u_r = \frac{P a_{11}}{I} \left[\frac{(l-z)^3}{6} - \frac{r^2 (l-z) a_{12}}{2 a_{11}} + \beta z + \alpha \right] \cos\theta + (\beta' z + \alpha') \sin\theta \quad [70]$$

and

$$u_\theta = \frac{P a_{11}}{I} \left[-\frac{(l-z)^3}{6} - \frac{r^2 (l-z) a_{12}}{2 a_{11}} - \beta z - \alpha \right] \sin\theta + (\beta' z + \alpha') \cos\theta + \gamma' r + \frac{z r M a_{55}}{I} \quad [71]$$

The deflection of the cylinder is obtained from u_r and u_θ in the form

$$u = \frac{P a_{11}}{I} \left[\frac{(l-z)^3}{6} - \frac{(l-z)(x^2 - y^2) a_{12}}{2 a_{11}} + \beta z + \alpha \right] - \frac{z y M a_{55}}{I} - \gamma' y \quad [72]$$

For an isotropic material

$$k = 1, \quad a_{11} = 1/E, \quad \frac{a_{12}}{a_{11}} = -\sigma, \quad \frac{a_{55}}{a_{11}} = \frac{E}{2G}$$

and the formulas of this section reduce to those previously obtained.[7]

6 Discussion of Results

In general, the elastic coefficients a_{pq} are independent of one another. The use of the present results to observe the effect of making one or a combination of these coefficients take on certain limit values is therefore possible. Also, since the thickness of the cylinder is not restricted, applications to thin cylinders may be made. In the use of the results for these purposes, as well as in their application in general, the following limitations should be considered:

1 A formula may not be suitable for use for some value of one of its parameters, such as for $k = 3$ in the formulas of Section 5. In this case, a revision of the analysis for the excepted parameter value is necessary.

2 The results are based on a small deflection theory.

3 The end $z = 0$ is not completely fixed.

In regard to the end fixity it is observed that once the components of stress are determined the components of displacement are also determined except those that represent a rigid-body displacement. It is possible, for example, to impose the conditions

$$\left. \begin{aligned} u_z = 0 \text{ for } z = 0, \quad r = a, \quad 0 \leqq \theta < 2\pi \\ r_1 \leqq a \leqq r_2, \text{ and} \\ u_r = u_\theta = 0 \text{ for } z = 0, \quad r = a, \quad \theta = \pm \frac{\pi}{2} \end{aligned} \right\} \quad [73]$$

which fix the plane of the circle $z = 0$, $r = a$, and two points on it, but no further conditions can then be imposed at $z = 0$. This is usual for solutions of the present type. However, for a cylindrically aeolotropic material the choice of the radius a may have a considerable effect on the deflection. Consider, for example, u Formula [72] with $M = 0$ and evaluated at $z = l$ for the two values $a = r_1$ and $a = r_2$. Write

$$a_{11} = \frac{1}{E_z}, \quad a_{12} = -\frac{\sigma_{zr}}{E_z}, \quad a_{55} = \frac{1}{2G_{\theta z}}, \quad a_{44} = \frac{1}{2G_{zr}}$$

where these coefficients may be interpreted by referring to Equa-

[7] Reference (3), pp. 231 and 254.

tions [1] to [6], and assume $G_{\theta z} = G_{rz}$ so that $k = 1$. Then if $a = r_1$

$$u\Big|_{z=l} = \frac{Pl^3}{3E_z I} - \frac{Pl(r_2^2 - r_1^2)\sigma_{zr}}{2E_z I} + \frac{Pl(3r_2^2 + r_1^2)}{G_{\theta z}\pi(r_2^4 - r_1^4)} \quad [74]$$

and if $a = r_2$

$$u\Big|_{z=l} = \frac{Pl^3}{3E_z I} + \frac{Pl(r_2^2 - r_1^2)\sigma_{zr}}{2E_z I} + \frac{Pl(r_2^2 + 3r_1^2)}{G_{\theta z}\pi(r_2^4 - r_1^4)} \quad [75]$$

The first two terms in each of these formulas represent deflections that are associated with bending, the second being small compared with the first if

$$\frac{r_2^2 - r_1^2}{l^2}$$

is small. The last term in each formula represents a deflection due to shear deformation. When the cylinder walls are thin (r_1 nearly equal to r_2), this term is substantially the same in both formulas. However, if r_1 is small compared with r_2 the last term is three times greater in Equation [74] than it is in Equation [75]. When $G_{\theta z}$ is small compared with E_z this difference in the last terms produces a large discrepancy between values of $u_{z=l}$ obtained from the two formulas. Thus for thick-walled cylinder composed of a material that is weak in shear the choice of the radius a has a large effect on the deflection.

Acknowledgment

The author wishes to acknowledge the use of suggestions made by Dr. B. E. Gatewood[8] in the preparation of this paper.

BIBLIOGRAPHY

1 "The Distribution of Stress in a Wood Pole Bent by a Radial End Load," by W. S. Ericksen, U. S. Forest Products Laboratory Report No. R1933, 1953.

2 "Stress Distributions in Cylindrically Aeolotropic Plates," by G. F. Carrier, JOURNAL OF APPLIED MECHANICS, Trans. ASME, vol. 65, 1943, pp. A-117–A-122.

3 "Mathematical Theory of Elasticity," by I. S. Sokolnikoff, McGraw-Hill Book Company, Inc., New York, N. Y., 1946.

4 "Equations de Compatibilité Pour un Système de Coordonnées Triplex Orthogonaux Quelconques," by F. Odqvist, *Comptes Rendus de l'Académie des Sciences*, vol. 205, 1937, pp. 202–204.

5 "Differential Equations of the Equilibrium of the Theory of Elasticity in the Curvilinear Coordinate System," by T. N. Blinchikov, *Applied Mathematics and Mechanics*, new series, vol. 2, 1939, pp. 407–413.

[8] Professor of Mechanics, USAF Institute of Technology.

On the Torsion of Rectangular Sandwich Plates

By PAUL SEIDE,[1] LOS ANGELES, CALIF.

The torsional rigidity of rectangular sandwich plates of constant thickness is calculated, with cross sections assumed free to warp. The faces are isotropic and of equal thickness while the core may be orthotropic, the axes of orthotropy coinciding with co-ordinate axes of the structure.

Nomenclature

The following nomenclature is used in the paper:

A_m, B_m, C_m = constants in stress function
a = half-thickness of sandwich plate $(h + t)$
b = half-width of sandwich plate
C_1, C_2 = arbitrary constants in boundary conditions
c = width of sandwich plate $(2b)$
D = flexural stiffness per unit width of solid isotropic plate

$$\left(\frac{Et^3}{12(1-\nu^2)}\right)$$

D_0 = flexural stiffness per unit width of sandwich plate with isotropic faces, stiffness of core neglected

$$\left(\frac{2Et^3[(1+h/t)^3-(h/t)^3]}{3(1-\nu^2)}\right)$$

E = Young's modulus of isotropic material
G = shear modulus of isotropic faces

$$\left(\frac{E}{2(1+\nu)}\right)$$

G_{xz}, G_{yz} = shear moduli of orthotropic core
GJ = torsional stiffness or rigidity
h = half-depth of core
k_1 = a function of ζ, given by Table 1 and Fig. 2
l = length of sandwich plate
m, n = integers
T = applied torque
t = thickness of solid plate; individual thickness of sandwich faces
u, v, w = deformation in x, y, z-directions, respectively
x, y, z = co-ordinate axes (see Fig. 1)
Y_n = function of y in stress function
ζ = $2b/t$ or $\sqrt{\frac{G_{yz}}{G_{xz}}}\frac{b}{h}$
θ = rate of twist of unrestrained sandwich plate
ν = Poisson's ratio of face material
τ_{xz}, τ_{yz} = shear stresses
φ = stress function

Subscripts:

c = pertaining to core
f = pertaining to faces

Introduction

The present investigation came about as the result of a request for information on the torsional rigidity of sandwich beams and plates for correlation with the results of torsion tests of balsa-core sandwich beams. While the twisting stiffness of solid rectangular isotropic plates is given adequately by the expression

$$\overline{GJ} = \frac{1}{3}Gt^3c \equiv 2D(1-\nu)c \quad \ldots\ldots\ldots\ldots [1]$$

provided the ratio c/t is greater than about 10, and the ratio l/c is greater than about 4,[2,3] it was not obvious that the stiffness of sandwich plates could be calculated accurately from the corresponding expression for sandwich plates with equal thickness isotropic faces

$$\overline{GJ} = \frac{8}{3}Gt^3c\left[\left(1+\frac{h}{t}\right)^3-\left(\frac{h}{t}\right)^3\right] \equiv 2D_0(1-\nu)c \quad [2]$$

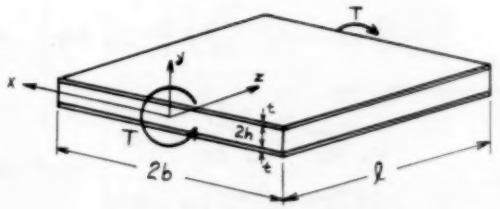

Fig. 1 Sandwich-Plate Notation

or that the same limits of validity would hold. Accordingly, the analysis of the present paper was carried out. Unfortunately, it was found that no realistic correlation between theory and experiment was possible because of excessive experimental errors owing to a faulty test setup, so that only the theoretical analysis is reported herein. Note that the analysis is for a core which extends to the edges of the plate, Fig. 1, corresponding to the test specimens.

---

[1] Member Technical Staff, Guided Missile Research Division, The Ramo-Wooldridge Corporation; formerly Research Engineer, Structural Research Section, Northrop Aircraft, Inc., Hawthorne, Calif.

Contributed by the Applied Mechanics Division and presented at the Diamond Jubilee Annual Meeting, Chicago, Ill., November 13–18, 1955, of The American Society of Mechanical Engineers.

Discussion of this paper should be addressed to the Secretary, ASME, 29 West 39th Street, New York, N. Y., and will be accepted until July 10, 1956, for publication at a later date. Discussion received after the closing date will be returned.

Note: Statements and opinions advanced in papers are to be understood as individual expressions of their authors and not those of the Society. Manuscript received by ASME Applied Mechanics Division, June 30, 1955. Paper No. 55—A-40.

[2] "Torsion and Transverse Bending of Cantilever Plates," by Eric Reissner and Manuel Stein, National Advisory Committee for Aeronautics, Technical Note 2369, 1951.

[3] "Theory of Elasticity," by S. Timoshenko and J. N. Goodier, McGraw-Hill Book Company, Inc., New York, N. Y., second edition, 1951, p. 277.

Torsion With Unrestrained Warping

In accordance with the Saint Venant semi-inverse method, the stresses σ_x, σ_y, σ_z, and τ_{xy} are assumed to vanish in both the core and faces, see Fig. 1. The remaining stresses τ_{xz} and τ_{yz} are then independent of the co-ordinate z and must satisfy the relationship of equilibrium

$$\frac{\partial \tau_{xz}}{\partial x} + \frac{\partial \tau_{yz}}{\partial y} = 0 \quad \ldots\ldots [3]$$

Equation [3] is satisfied by stress functions φ_c for the core and φ_f for the faces (only one stress function is required for both faces because of the symmetry of the cross section) such that

$$\tau_{xz(c)} = \frac{\partial \varphi_c}{\partial y} \qquad \tau_{yz(c)} = -\frac{\partial \varphi_c}{\partial x} \quad \ldots\ldots [4]$$

$$\tau_{xz(f)} = \frac{\partial \varphi_f}{\partial y} \qquad \tau_{yz(f)} = -\frac{\partial \varphi_f}{\partial x} \quad \ldots\ldots [5]$$

The stress functions are functions of x and y only.

Equations for φ_c and φ_f are found by considering displacements of the structure. For both the core and the faces

$$\frac{\partial u}{\partial x} = \frac{\partial v}{\partial y} = \frac{\partial w}{\partial z} = \frac{\partial u}{\partial y} + \frac{\partial v}{\partial x} = 0 \quad \ldots\ldots [6]$$

by virtue of Hooke's law and the assumption of vanishing σ_x, σ_y, σ_z, and τ_{xy}. The equations for u and v are satisfied by assuming that

$$u = -\theta yz; \qquad v = \theta xz \quad \ldots\ldots [7]$$

which implies that each cross section rotates as a rigid body about its centroid so that the center line of the structure remains straight. The warping w is independent of z and must satisfy the following equations

$$\frac{\partial w_c}{\partial x} = \frac{1}{G_{xz}} \tau_{xz(c)} + \theta y \qquad \frac{\partial w_c}{\partial y} = \frac{1}{G_{yz}} \tau_{yz(c)} - \theta x \quad \ldots [8]$$

$$\frac{\partial w_f}{\partial x} = \frac{1}{G} \tau_{xz(f)} + \theta y \qquad \frac{\partial w_f}{\partial y} = \frac{1}{G} \tau_{yz(f)} - \theta x \quad \ldots [9]$$

For compatibility, then

$$\left.\begin{aligned} \frac{1}{G_{xz}} \frac{\partial \tau_{xz(c)}}{\partial y} - \frac{1}{G_{yz}} \frac{\partial \tau_{yz(c)}}{\partial x} &= -2\theta \\ \frac{1}{G} \left(\frac{\partial \tau_{xz(f)}}{\partial y} - \frac{\partial \tau_{yz(f)}}{\partial x} \right) &= -2\theta \end{aligned}\right\} \quad \ldots\ldots [10]$$

or, on substituting Equations [4] and [5] into [10]

$$\frac{\partial^2 \varphi_c}{\partial x^2} + \frac{G_{yz}}{G_{xz}} \frac{\partial^2 \varphi_c}{\partial y^2} = -2G_{yz}\theta \qquad \frac{\partial^2 \varphi_f}{\partial x^2} + \frac{\partial^2 \varphi_f}{\partial y^2} = -2G\theta \quad \ldots [11]$$

The boundary conditions to be satisfied by φ_c and φ_f are as follows:

(a) $\tau_{xz(c)} = \tau_{xz(f)} = 0$ on $x = \pm b$ or $\dfrac{\partial \varphi_c}{\partial y} = \dfrac{\partial \varphi_f}{\partial y} = 0$

(b) $\tau_{yz(f)} = 0$ on $y = \pm(h + t)$ or $\dfrac{\partial \varphi_f}{\partial x} = 0$

(c) $\tau_{yz(c)} = \tau_{yz(f)}$ on $y = \pm h$ or $\dfrac{\partial \varphi_c}{\partial x} = \dfrac{\partial \varphi_f}{\partial x}$

(d) $w_c = w_f$ or $\dfrac{\tau_{xz(c)}}{G_{xz}} = \dfrac{\tau_{xz(f)}}{G}$ on $y = h$ or $\dfrac{\partial \varphi_c}{\partial y} = \dfrac{G_{xz}}{G} \dfrac{\partial \varphi_f}{\partial y}$

Condition (a) is satisfied by

(a′) $\varphi_c = C_1, \quad \varphi_f = C_2$ on $x = \pm b$

Condition (b) is satisfied by

(b′) $\varphi_f = C_2$ on $y = \pm(h + t)$

which takes continuity of φ_f around the face boundary into account. Condition (c) is satisfied by

(c′) $\varphi_c = \varphi_f - C_2 + C_1$ on $y = \pm h$

which takes continuity of φ_c around the core boundary into account.

It will now be shown that the values of C_1 and C_2 may be taken arbitrarily as zero. The value of the applied moment is

$$\left.\begin{aligned} T &= \int_{-b}^{b}\int_{-h}^{h} (\tau_{yz(c)}x - \tau_{xz(c)}y)dx\,dy \\ &\quad + 2\int_{-b}^{b}\int_{h}^{h+t} (\tau_{yz(f)}x - \tau_{xz(f)}y)dx\,dy \\ &= -\left[\int_{-b}^{b}\int_{-h}^{h} \left(x\frac{\partial \varphi_c}{\partial x} + y\frac{\partial \varphi_c}{\partial y} \right) dx\,dy + 2 \right. \\ &\quad \left. \int_{-b}^{b}\int_{h}^{h+t} \left(x\frac{\partial \varphi_f}{\partial x} + y\frac{\partial \varphi_f}{\partial y} \right) dx\,dy \right] \\ &= 2\int_{-b}^{b}\int_{-h}^{h} (\varphi_c - C_1)dx\,dy \\ &\quad + 4\int_{-b}^{b}\int_{h}^{h+t} (\varphi_f - C_2)dx\,dy \end{aligned}\right\} \quad \ldots [12]$$

where conditions (a′), (b′), and (c′) have been used.

Equation [12] and the boundary conditions imply that the solution of the problem is unaffected by the actual values of the constants C_1 and C_2. It is convenient to set these equal to zero, in which case Equation [12] and the boundary conditions (a), (b), and (c) reduce to

$$T = 2\int_{-b}^{b}\int_{-h}^{h} \varphi_c\,dx\,dy + 4\int_{-b}^{b}\int_{h}^{h+t} \varphi_f\,dx\,dy \quad \ldots [13]$$

(a″) $\varphi_c = \varphi_f = 0$ on $x = \pm b$

(b″) $\varphi_f = 0$ on $y = \pm(h + t)$

(c″) $\varphi_f = \varphi_c$ on $y = \pm h$

The solution of Equations [11] subject to conditions (a″), (b″), (c″), and (d) is easily affected by the following method. Let

$$\left.\begin{aligned} \varphi_c &= \sum_{n=1,3,5\ldots}^{\infty} Y_{n(c)}(y) \cos\frac{n\pi x}{2b} \\ \varphi_f &= \sum_{n=1,3,5\ldots}^{\infty} Y_{n(f)}(c) \cos\frac{n\pi x}{2b} \end{aligned}\right\} \quad \ldots\ldots [14]$$

which satisfy conditions (a″) identically. Substitution of Equations [14] into Equations [11] yields

$$\left.\begin{aligned} \sum_{n=1,3,5\ldots}^{\infty} \left[\frac{d^2 Y_{n(c)}}{dy^2} - \left(\frac{n\pi}{2b}\right)^2 \frac{G_{xz}}{G_{yz}} Y_{n(c)} \right] \\ \cos\frac{n\pi x}{2b} = -2G_{xz}\theta \end{aligned}\right\} \quad \ldots [15]$$

$$\left.\begin{aligned}\sum_{n=1,3,5\ldots}^{\infty}\left[\frac{d^2Y_{n(f)}}{dy^2}-\left(\frac{n\pi}{2b}\right)^2 Y_{n(f)}\right]\cos\frac{n\pi x}{2b} &= -2G\theta\end{aligned}\right\}\ldots[15]\ (continued)$$

The multiplication of Equations [15] by $\cos(m\pi x)/(2b)$ and integration over x from $-b$ to b then gives

$$\left.\begin{aligned}\frac{d^2Y_{m(e)}}{dy^2}-\left(\frac{m\pi}{2b}\right)^2\frac{G_{xz}}{G_{yz}}Y_{m(e)} &= -\frac{8(-1)^{\frac{m-1}{2}}}{m\pi}G_{xz}\theta\\ \frac{d^2Y_{m(f)}}{dy^2}-\left(\frac{m\pi}{2b}\right)^2 Y_{m(f)} &= -\frac{8(-1)^{\frac{m-1}{2}}}{m\pi}G\theta\\ m &= 1,3,5,\ldots\end{aligned}\right\}\ldots[16]$$

The solution of Equations [16], noting that φ_e should be symmetrical about the x-axis, is

$$\left.\begin{aligned}Y_{m(e)} &= A_m\cosh\sqrt{\frac{G_{xz}}{G_{yz}}}\frac{m\pi y}{2b}+\frac{32(-1)^{\frac{m-1}{2}}}{m^3\pi^3}G_{xz}b^2\theta\\ Y_{m(f)} &= B_m\cosh\frac{m\pi y}{2b}+C_m\sinh\frac{m\pi y}{2b}\\ &\quad+\frac{32(-1)^{\frac{m-1}{2}}}{m^3\pi^3}Gb^2\theta\\ m &= 1,3,5,\ldots\end{aligned}\right\}\ldots[17]$$

Substitution of Equations [17] into conditions (b''), (c''), and (d) yields three simultaneous equations for A_m, B_m, and C_m of which the solution is

$$A_m=\frac{32(-1)^{\frac{m-1}{2}}}{m^3\pi^3}Gb^2\theta\frac{\left(1-\frac{G_{yz}}{G}\right)\cosh\frac{m\pi t}{2b}-1}{\sqrt{\frac{G_{yz}}{G_{xz}}}\frac{G}{G_{yz}}\sinh\left(\sqrt{\frac{G_{xz}}{G_{yz}}}\frac{m\pi h}{2b}\right)\sinh\frac{m\pi t}{2b}+\cosh\left(\sqrt{\frac{G_{xz}}{G_{yz}}}\frac{m\pi h}{2b}\right)\cosh\frac{m\pi t}{2b}}\quad\ldots[18a]$$

$$B_m=\frac{32(-1)^{\frac{m-1}{2}}}{m^3\pi^3}Gb^2\theta\left[\frac{\left\{\sqrt{\frac{G_{yz}}{G_{xz}}}\sinh\left(\sqrt{\frac{G_{xz}}{G_{yz}}}\frac{m\pi h}{2b}\right)\left[\frac{G}{G_{yz}}\sinh\frac{m\pi h}{2b}+\left(1-\frac{G}{G_{yz}}\right)\sinh\frac{m\pi(h+t)}{2b}\right]-\cosh\left(\sqrt{\frac{G_{xz}}{G_{yz}}}\frac{m\pi h}{2b}\right)\cosh\frac{m\pi h}{2b}\right\}}{\sqrt{\frac{G_{yz}}{G_{xz}}}\frac{G}{G_{yz}}\sinh\left(\sqrt{\frac{G_{xz}}{G_{yz}}}\frac{m\pi h}{2b}\right)\sinh\frac{m\pi t}{2b}+\cosh\left(\sqrt{\frac{G_{xz}}{G_{yz}}}\frac{m\pi h}{2b}\right)\cosh\frac{m\pi t}{2b}}\right]\quad\ldots[18b]$$

$$C_m=-\frac{32(-1)^{\frac{m-1}{2}}}{m^3\pi^3}Gb^2\theta$$

$$\left[\frac{\left\{\sqrt{\frac{G_{yz}}{G_{xz}}}\sinh\left(\sqrt{\frac{G_{xz}}{G_{yz}}}\frac{m\pi h}{2b}\right)\left[\frac{G}{G_{yz}}\cosh\frac{m\pi h}{2b}+\left(1-\frac{G}{G_{yz}}\right)\cosh\frac{m\pi(h+t)}{2b}\right]-\cosh\left(\sqrt{\frac{G_{xz}}{G_{yz}}}\frac{m\pi h}{2b}\right)\sinh\frac{m\pi h}{2b}\right\}}{\sqrt{\frac{G_{yz}}{G_{xz}}}\frac{G}{G_{yz}}\sinh\left(\sqrt{\frac{G_{xz}}{G_{yz}}}\frac{m\pi h}{2b}\right)\sinh\frac{m\pi t}{2b}+\cosh\left(\sqrt{\frac{G_{xz}}{G_{yz}}}\frac{m\pi h}{2b}\right)\cosh\frac{m\pi t}{2b}}\right]\quad\ldots[18c]$$

$$m=1,3,5,\ldots$$

With φ_e and φ_f now known, substitution of Equations [14], [17], and [19] into Equation [13] yields

$$T=\overline{GJ}\theta\quad\ldots[19]$$

where after some rearrangement and transformation of terms is made

$$\overline{GJ}=\frac{1}{3}G_{xz}(2h)^3(2b)\left[1-\frac{192}{\pi^5}\sqrt{\frac{G_{xz}}{G_{yz}}}\frac{h}{b}\sum_{n=1,3,5,\ldots}^{\infty}\frac{1}{n^5}\tanh\left(\frac{n\pi}{2}\sqrt{\frac{G_{yz}}{G_{xz}}}\frac{b}{h}\right)\right]+2\left\{\frac{1}{3}Gt^3(2b)\left[1-\frac{192}{\pi^5}\frac{t/2}{b}\sum_{n=1,3,5,\ldots}^{\infty}\frac{1}{n^5}\tanh\left(\frac{n\pi}{2}\frac{b}{t/2}\right)\right]\right\}+\frac{64}{\pi^5}G(2b)^4\sum_{n=1,3,5,\ldots}^{\infty}\frac{1}{n^5}\left\{\begin{aligned}&\left[\sqrt{\frac{G_{yz}}{G_{xz}}}\tanh\left(\sqrt{\frac{G_{xz}}{G_{yz}}}\frac{n\pi h}{2b}\right)+\tanh\frac{n\pi t}{4b}\right]^2\\ &\frac{G}{G_{yz}}\sqrt{\frac{G_{yz}}{G_{xz}}}\tanh\left(\sqrt{\frac{G_{xz}}{G_{yz}}}\frac{n\pi h}{2b}\right)+\coth\frac{n\pi t}{2b}\end{aligned}\right\}\quad\ldots[20]$$

The function

$$k_1(\zeta)=\frac{1}{3}\left[1-\frac{192}{\pi^5}\frac{1}{\zeta}\sum_{n=1,3,5\ldots}^{\infty}\frac{1}{n^5}\tanh\frac{n\pi}{2}\zeta\right]$$

has been computed and is reported by Timoshenko[3,4] as in Table 1, see also Fig. 2.

The first term of Equation [20] is the twisting stiffness of the orthotropic core alone; the second term is the sum of the torsional rigidities of the two isotropic faces alone. These are a small part of the total rigidity, however, and may be neglected in most cases. The third term gives the effect of the interaction between the faces and core and, although rather complex in appearance, can be easily calculated in most cases since the series involved

[4] "Strength of Materials—Part I," by S. Timoshenko, McGraw-Hill Book Company, Inc., New York, N. Y., second edition, 1940, p. 270.

TABLE 1 VALUES OF ζ AND $k_1(\zeta)$

ζ	$k_1(\zeta)$
1.00	0.1406
1.20	0.166
1.50	0.196
1.75	0.214
2.00	0.229
2.50	0.249
3.00	0.263
4.00	0.281
5.00	0.291
6.00	0.299
8.00	0.307
10.00	0.312
∞	0.333

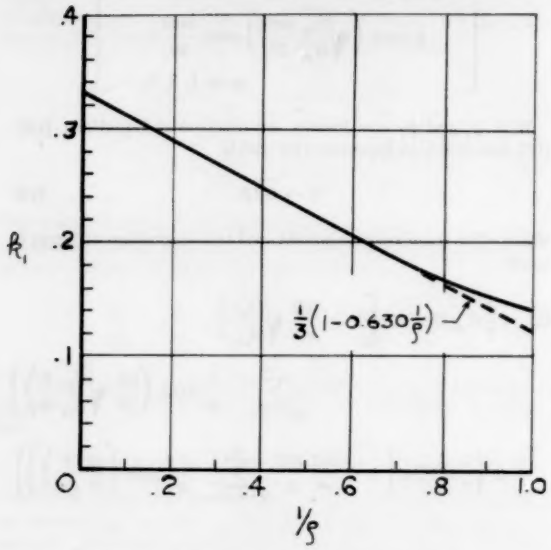

FIG. 2 TORSIONAL STIFFNESS COEFFICIENT

converges rapidly. For the limiting case of an infinitely wide plate, Equation [20] can be shown to reduce to

$$\overline{GJ} = \frac{8}{3}\left[\left(1+\frac{h}{t}\right)^3 + \left(\frac{G_{zz}}{G}-1\right)\left(\frac{h}{t}\right)^3\right] G(2b)t^3 \quad [21]$$

which is identical with Equation [2] except for the term giving the effect of the core.

ILLUSTRATIVE EXAMPLE

As an illustration of the relative magnitudes of the twisting stiffnesses involved in Equations [2], [20], and [21], consider a sandwich plate with the following properties

$$h/t = 10$$

$$b/t = 100$$

$$\frac{G_{zz}}{G_{yz}} = 3/2$$

$$\frac{G_{zz}}{G} = 0.00158$$

The material properties are those for a balsa sandwich core (specific gravity = 0.19) and aluminum faces, the core being oriented so that the grain is parallel to the faces. Then

$$\frac{\overline{GJ}}{G(2b)t^3} = \begin{matrix} 883 \text{ (from Equation [2])} \\ 547 \text{ (from Equation [20])} \\ 887 \text{ (from Equation [21])} \end{matrix}$$

It is thus seen that the use of Equation [2] or [21] can be quite unconservative for a sandwich plate with a b/h ratio as low as 10 when the core extends to the plate edges.

CONCLUSIONS

The computed torsional rigidity of sandwich plates of moderate width-thickness ratio can be quite unconservative if the twisting stiffness constant of sandwich-plate theory is used, since the lower limit of the width-thickness ratio of a sandwich plate for it to be considered infinitely wide is somewhat greater than the value of 10 found for isotropic plates. For a sandwich beam with a particular balsa core, this degree of unconservatism was found to be about 61 per cent when the width-core depth ratio was 10 and the face-core thickness ratio was 10.

On Some Problems in Bending of Thick Circular Plates on an Elastic Foundation[1]

By DANIEL FREDERICK,[2] BLACKSBURG, VA.

The governing equations and solutions for the nonsymmetrical bending of circular plates resting on an elastic foundation are presented using the theory developed by E. Reissner. Also included are two examples in which numerical comparisons have been made with the predictions of the classical theory. These are (*a*) the axially symmetric bending of a finite circular plate on an elastic foundation under a partial uniform loading, and (*b*) the nonsymmetric bending of an infinite plate on an elastic foundation with a rigid circular inclusion.

Introduction

ALTHOUGH the literature contains several thick-plate theories, the theory developed by E. Reissner in 1945 (1, 2, 3)[3] is significant because it provides certain important modifications to the classical thin-plate theory. The Reissner theory which was developed from a variational principle does not require the evaluation of a large number of functions as in most thick-plate theories, and yet includes the effect of shear deformation and normal pressure. In 1949 Green (4) showed that Reissner's theory also could be developed from the equations of elasticity. Another important feature of the theory is that it permits the specification of three boundary conditions for each edge of the plate involving stress resultants or displacements instead of two as in the classical theory. In 1951 Mindlin (5) developed a theory for vibrating plates including the effects of shear deformation and rotatory inertia, analogous to that of Reissner's by proceeding from the equations of elasticity.

Reissner's theory has been applied to the solution of several problems in the static bending of plates. He solved the problem of the bending and twisting of an infinite plate with a circular hole. Naghdi and Rowley (6) extended the theory to include an elastic foundation which reacts with a pressure proportional to the displacement at every point of the foundation and solved two problems involving axially symmetric bending of an infinite plate. Naghdi (7) also studied the problem of the bending and twisting of an infinite plate with an elliptic hole. A more detailed history on Reissner's theory is also found in reference (7).

In this paper, the solutions of some specific problems in the bending of circular plates using the Reissner theory have been obtained. In all cases, the results are compared numerically with the predictions of the classical theory. The examples considered are (*a*) the axially symmetric bending of a finite circular plate on an elastic foundation under a partial uniform loading, and (*b*) the nonsymmetric bending of an infinite plate on an elastic foundation with a rigid circular inclusion.

The Fundamental Equations

To conserve space the notations of reference (3) will be used where possible and frequent reference should be made to that paper.

The co-ordinate system and the usual stress resultants in their positive directions are shown in Fig. 1. Taking the displace-

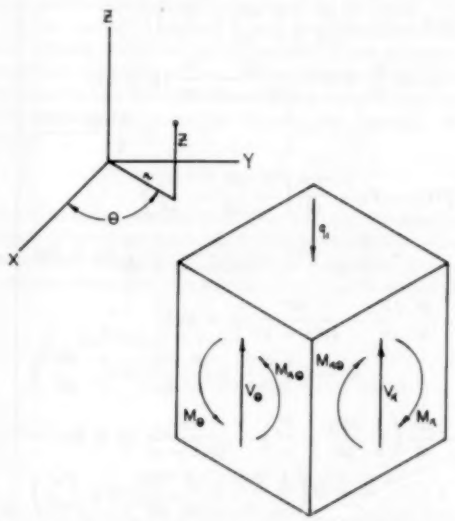

Fig. 1 An Element of the Plate for Cylindrical Co-Ordinates

ments u, v, and w as positive when they act toward the positive ends of the axes r, θ, and z, respectively, they will be assumed to be of the form

$$u = z\alpha_r(r, \theta), \quad v = z\alpha_\theta(r, \theta), \quad \text{and } w = \bar{w}(r, \theta).$$

Here α_r and α_θ are rotations of a line element originally perpendicular to the middle surface about a point in the middle surface and $\bar{w}$ is the vertical displacement for all points on this line. These are defined as

$$\left.\begin{aligned} \alpha_r &= \frac{12}{h^3}\int_{-h/2}^{h/2} uz\,dz, \quad \alpha_\theta = \frac{12}{h^3}\int_{-h/2}^{h/2} vz\,dz, \\ \bar{w} &= \frac{3}{2h}\int_{-h/2}^{h/2} w\left(1 - \frac{4z^2}{h^2}\right)dz \end{aligned}\right\} \quad \ldots [1]$$

It will be further assumed that the components of stress τ_{rz},

---

[1] Based on part of a dissertation submitted to the University of Michigan, in January, 1955, in partial fulfillment of the requirements for the degree of Doctor of Philosophy.

[2] Associate Professor of Applied Mechanics, Virginia Polytechnic Institute.

[3] Numbers in parentheses refer to the Bibliography at the end of the paper.

Contributed by the Applied Mechanics Division and presented at the Diamond Jubilee Annual Meeting, Chicago, Ill., November 13–18, 1955, of The American Society of Mechanical Engineers.

Discussion of this paper should be addressed to the Secretary, ASME, 29 West 39th Street, New York, N. Y., and will be accepted until July 10, 1956, for publication at a later date. Discussion received after the closing date will be returned.

Note: Statements and opinions advanced in papers are to be understood as individual expressions of their authors and not those of the Society. Manuscript received by ASME Applied Mechanics Division, March 7, 1955. Paper No. 55—A-36.

$\tau_{\theta z}$, and σ_z satisfy the equations of equilibrium and hence are given by

$$\left.\begin{aligned} \tau_{rz} &= \frac{3V_r}{2h}\left(1-\frac{4z^2}{h^2}\right), \quad \tau_{\theta z} = \frac{3V_\theta}{2h}\left(1-\frac{4z^2}{h^2}\right), \\ \sigma_z &= -\frac{q_1+q_2}{2} + (q_2-q_1)\left(\frac{3z}{2h}-\frac{2z^3}{h^3}\right) \end{aligned}\right\} \quad \ldots [2]$$

where q_1 is the pressure on the upper face and $q_2 = -k\bar{w}$ (k is the foundation modulus) is the pressure on the lower face of the plate. The stress resultants V_r, V_θ, M_r, M_θ, and $M_{r\theta}$ are defined as in the classical theory and are shear forces and moments per unit of length.

Basic Equations for the Bending of Circular Plates on an Elastic Foundation. From Reissner's variational theorem (3), the basic equations for the bending of a plate on an elastic foundation in polar co-ordinates are

$$\left.\begin{aligned} &D\nabla^4\bar{w} - \beta h^2\nabla^2(q_1+k\bar{w}) + (q_1+k\bar{w}) = 0 \\ &\text{where} \\ &\nabla^2 = \frac{\partial^2}{\partial r^2} + \frac{1}{r}\frac{\partial}{\partial r} + \frac{1}{r^2}\frac{\partial^2}{\partial\theta^2} \\ &\frac{h^2}{10}\nabla^2 V_r - V_r + \frac{h^2}{10}\left(\frac{2}{r}\frac{\partial V_r}{\partial r} + \frac{V_r}{r^2}\right) \\ &\quad = D\frac{\partial}{\partial r}\nabla^2\bar{w} - \frac{h^2}{10(1-\nu)}\frac{\partial}{\partial r}(q_1+k\bar{w}) \\ &\qquad + \frac{h^2}{5}\frac{q_1+k\bar{w}}{r} \\ &\frac{h^2}{10}\nabla^2 V_\theta - V_\theta + \frac{h^2}{10}\left(\frac{2}{r^2}\frac{\partial V_r}{\partial\theta} - \frac{V_\theta}{r^2}\right) \\ &\quad = \frac{D}{r}\frac{\partial}{\partial\theta}\nabla^2\bar{w} - \frac{h^2}{10(1-\nu)}\frac{1}{r}\frac{\partial}{\partial\theta}(q_1+k\bar{w}) \\ &M_r - \frac{h^2}{5}\frac{\partial V_r}{\partial r} - \frac{\nu h^2}{10(1-\nu)}(q_1+k\bar{w}) \\ &\quad = -D\left(\frac{\partial^2\bar{w}}{\partial r^2} + \frac{\nu}{r}\frac{\partial\bar{w}}{\partial r} + \frac{\nu}{r^2}\frac{\partial^2\bar{w}}{\partial\theta^2}\right) \\ &M_\theta - \frac{h^2}{5}\left(\frac{1}{r}\frac{\partial V_\theta}{\partial\theta} + \frac{V_r}{r}\right) - \frac{\nu h^2}{10(1-\nu)}(q_1+k\bar{w}) \\ &\quad = -D\left(\frac{1}{r}\frac{\partial\bar{w}}{\partial r} + \frac{1}{r^2}\frac{\partial^2\bar{w}}{\partial\theta^2} + \nu\frac{\partial^2\bar{w}}{\partial r^2}\right) \\ &M_{r\theta} - \frac{h^2}{10}\left[\frac{1}{r}\frac{\partial V_r}{\partial\theta} + r\frac{\partial}{\partial r}\left(\frac{V_\theta}{r}\right)\right] \\ &\quad = -D(1-\nu)\frac{\partial}{\partial r}\left(\frac{1}{r}\frac{\partial\bar{w}}{\partial\theta}\right) \\ &\alpha_r + \frac{\partial\bar{w}}{\partial r} = \frac{6}{5Gh}V_r, \quad \alpha_\theta + \frac{1}{r}\frac{\partial\bar{w}}{\partial\theta} \\ &\quad = \frac{6}{5Gh}V_\theta, \quad \text{and} \quad \beta = \frac{2-\nu}{10(1-\nu)} \end{aligned}\right\} \quad \ldots [3]$$

These equations reduce to the well-known Reissner equations when $k = 0$.

It may be repeated here that contrary to the classical theory of plates, the boundary conditions are three in number and these are either on the stress resultants or displacements.

Solutions and Applications

Governing Equations for the Axially Symmetric Bending of Circular Plates Resting on an Elastic Foundation. Referring to the basic Equations [3], the governing equations for the axially symmetric bending may be written in the following form. In writing these equations the following notation was introduced

$$\rho = \bar{w} + q_1/k, \quad l^4 = D/k, \quad r = lx, \quad \gamma^2 = \frac{h^2\beta}{l^2}$$

It also was assumed that $(dq_1)/(dr) = 0$

$$\left.\begin{aligned} &\nabla^4\rho - \gamma^2\nabla^2\rho + \rho = 0, \quad \text{where } \nabla^2 = \frac{d^2}{dx^2} + \frac{1}{x}\frac{d}{dx} \\ &M_r/kh^2 = -\frac{l^2}{h^2}\left(\frac{d^2\rho}{dx^2} + \frac{\nu}{x}\frac{d\rho}{dx}\right) \\ &\quad - \frac{1}{5}\frac{d^2}{dx^2}(\nabla^2\rho) + \frac{\gamma^2}{5}\frac{d^2\rho}{dx^2} + \frac{\nu}{10(1-\nu)}\rho \\ &M_\theta/kh^2 = -\frac{1}{5x}\frac{d}{dx}(\nabla^2\rho) + \frac{\gamma^2}{5x}\frac{d\rho}{dx} + \frac{\nu}{10(1-\nu)}\rho \\ &\quad - \frac{l^2}{h^2}\left(\frac{1}{x}\frac{d\rho}{dx} + \nu\frac{d^2\rho}{dx^2}\right) \\ &V_r/kl = \gamma^2\frac{d\rho}{dx} - \frac{d}{dx}(\nabla^2\rho) \end{aligned}\right\} \quad \ldots [4]$$

The boundary conditions associated with these equations are now two in number since the third one is automatically satisfied by virtue of axial symmetry.

(a) *A Circular Plate Subjected to a Partial Uniform Load Resting on an Elastic Foundation.* The case of a finite circular plate resting on an elastic foundation under a partial uniform load will now be considered. It shall be loaded with a constant pressure q_0 over a circular area of radius b and be free on the outer edge, $r = a$. Factoring the first equation of Equations [4] as

$$(\nabla^2 + e^{i\alpha})(\nabla^2 + e^{-i\alpha})\rho = 0, \quad \text{where } \cos\alpha = -\frac{\gamma^2}{2} \quad \ldots [5]$$

its solutions are

$$J_0[x\exp(i\alpha/2)], \quad J_0[x\exp(-i\alpha/2)],$$
$$Y_0[x\exp(i\alpha/2)], \quad Y_0[x\exp(-i\alpha/2)]$$

For the solution of this problem, it is more convenient to use the functions U_0, V_0, $\bar{U}_0$, and $\bar{V}_0$ defined as follows

$$\left.\begin{aligned} U_0 &= \frac{1}{2}\left[J_0(xe^{i\alpha/2}) + J_0(xe^{-i\alpha/2})\right] \\ V_0 &= \frac{1}{2i}\left[J_0(xe^{i\alpha/2}) - J_0(xe^{-i\alpha/2})\right] \\ \bar{U}_0 &= \frac{1}{2}\left[Y_0(xe^{i\alpha/2}) + Y_0(xe^{-i\alpha/2})\right] \\ \bar{V}_0 &= \frac{1}{2i}\left[Y_0(xe^{i\alpha/2}) - Y_0(xe^{-i\alpha/2})\right] \end{aligned}\right\} \quad \ldots [6]$$

The functions $\bar{U}_0$ and $\bar{V}_0$ become infinite at the origin while U_0 and V_0 remain finite there. Hence the solution for the region $0 \leq r \leq b$, which will be indicated by the subscript 1, will be written as

$$\rho_1 = \bar{w}_1 + q_0/k = A_1U_0 + B_1V_0 \quad \ldots [7]$$

Outside of the load $b \leq r \leq a$, which will be indicated by the subscript 2, the solution will be

$$\rho_2 = \bar{w}_2 = A_2U_0 + B_2V_0 + C_2\bar{U}_0 + D_2\bar{V}_0 \quad \ldots [8]$$

For the free edge ($r = a$), the boundary conditions will be

$M_r(a) = 0$ and $V_r(a) = 0$, and at the radius $r = b$ there will be four equations expressing continuity on $\bar{w}$, V_r, M_r, and α_r.

In order to use the tables for Bessel functions of the first and second kind for a complex argument (8, 9), which are tabulated in 5-deg increments, $\alpha/2$ will be chosen as 45, 50, and 55 deg. The case where $\alpha/2 = 45$ deg corresponds to the classical solution if terms containing h^2 in Equations [4] are omitted. For this case, the functions of Equations [6] can be expressed in terms of the Kelvin functions.

Also, since the tables are for functions of zero and first order, the second, third, and fourth derivatives were expressed in terms of U_0, U_1, V_0, V_1, $\mathcal{O}_0$, $\mathcal{O}_1$, $\mathcal{V}_0$, and $\mathcal{V}_1$ through recurrence relations.[4] For the sake of completeness, the final expressions which were used in the calculations are presented as follows

$$\bar{w}_i = A_i U_0 + B_i V_0 + C_i \mathcal{O}_0 + D_i \mathcal{V}_0 - q_0/k$$

$$\frac{d\bar{w}_i}{dr} = -\frac{A_i}{l}[U_1 \cos \alpha/2 - V_1 \sin \alpha/2] - \frac{B_i}{l}[V_1 \cos \alpha/2 + U_1 \sin \alpha/2] - \frac{C_i}{l}[\mathcal{O}_1 \cos \alpha/2 - \mathcal{V}_1 \sin \alpha/2] - \frac{D_i}{l}[\mathcal{V}_1 \cos \alpha/2 + \mathcal{O}_1 \sin \alpha/2]$$

$$(V_r)_i = A_i kl[U_1 \cos \alpha/2 + V_1 \sin \alpha/2] + B_i kl[-U_1 \sin \alpha/2 + V_1 \cos \alpha/2] + C_i kl[\mathcal{O}_1 \cos \alpha/2 + \mathcal{V}_1 \sin \alpha/2] + D_i kl[-\mathcal{O}_1 \sin \alpha/2 + \mathcal{V}_1 \cos \alpha/2]$$

$$(M_r)_i = A_i kh^2 \left\{ \left[\frac{l^2}{h^2} \frac{\nu - 1}{x} - \frac{1}{5x} \right] U_1 \cos \alpha/2 - \left[\frac{1}{5x} + \frac{l^2}{h^2} \frac{\nu - 1}{x} \right] V_1 \sin \alpha/2 + \left[\frac{\nu}{10(1-\nu)} + \frac{1}{5} + \frac{l^2}{h^2} \cos \alpha \right] U_0 - \left[\frac{l^2}{h^2} \sin \alpha \right] V_0 \right\} \quad \ldots [9]$$

$$+ B_i kh^2 \left\{ \left[\frac{l^2}{h^2} \frac{\nu - 1}{x} + \frac{1}{5x} \right] U_1 \sin \alpha/2 + \left[\frac{l^2}{h^2} \frac{\nu - 1}{x} - \frac{1}{5x} \right] V_1 \cos \alpha/2 + \left[\frac{\nu}{10(1-\nu)} + \frac{1}{5} + \frac{l^2}{h^2} \cos \alpha \right] V_0 + \left[\frac{l^2}{h^2} \sin \alpha \right] U_0 \right\}$$

$$+ C_i kh^2 \left\{ \left[\frac{l^2}{h^2} \frac{\nu - 1}{x} - \frac{1}{5x} \right] \mathcal{O}_1 \cos \alpha/2 - \left[\frac{1}{5x} + \frac{l^2}{h^2} \frac{\nu - 1}{x} \right] \mathcal{V}_1 \sin \alpha/2 + \left[\frac{\nu}{10(1-\nu)} + \frac{1}{5} + \frac{l^2}{h^2} \cos \alpha \right] \mathcal{O}_0 - \left[\frac{l^2}{h^2} \sin \alpha \right] \mathcal{V}_0 \right\}$$

$$+ D_i kh^2 \left\{ \left[\frac{l^2}{h^2} \frac{\nu - 1}{x} + \frac{1}{5x} \right] \mathcal{O}_1 \sin \alpha/2 + \left[\frac{l^2}{h^2} \frac{\nu - 1}{x} - \frac{1}{5x} \right] \mathcal{V}_1 \cos \alpha/2 + \left[\frac{\nu}{10(1-\nu)} + \frac{1}{5} + \frac{l^2}{h^2} \cos \alpha \right] \mathcal{V}_0 + \left[\frac{l^2}{h^2} \sin \alpha \right] \mathcal{O}_0 \right\} \quad \ldots [9] \text{ (continued)}$$

NOTE: $(i = 1, 2)$. For $i = 1$ the terms containing C_1 and D_1 are dropped. For $i = 2$ the term containing q_0 is dropped.

Calculations were made for $\nu = 1/3$ and $a/b = 10$. The results for the moment, shear, and deflection at the center of the plate and at the edge of the uniform load are presented in Table 1. Outside of the load, these three quantities decrease and become small.

Table 1 shows that the maximum deflection increases and that the maximum moment decreases as h increases for a plate with a given stiffness and a given foundation modulus. Upon comparing the results with those of Naghdi and Rowley (6) for an infinite plate, in which $b/l = 1$, it can be seen from Fig. 2 that the results are essentially the same for small h/a values. It can be concluded also that the effects of the uniform load upon an infinite plate are more severe than the effects of the same load on a finite plate on the quantities $(\bar{w})_{r=0}$, $(M_r)_{r=0}$, and $(V_r)_{r=b}$ for the a/b values considered.

Nonsymmetric Bending of Circular Plates on an Elastic Foundation. In this section, a method of solving problems of nonsymmetrical bending of circular and ring-shaped plates is considered. The solutions are presented in a series form involving trigonometric functions and Bessel functions with a complex argument.

To find solutions to Equations [3], the first equation will be written as

$$(\nabla^2 + e^{i\alpha})(\nabla^2 + e^{-i\alpha})\rho = 0$$

in which it has been assumed that $\nabla^4 q_1 = 0$ and the notation in Equations [4] has been used. It is now assumed that ρ can be written in a form in which the variables are separable. Following the customary procedure, the solution for ρ may be written as

$$\rho(x, \theta) = \sum_{n=0}^{\infty} [a_n U_n(x) + b_n V_n(x) + c_n \mathcal{O}_n(x) + d_n \mathcal{V}_n(x)] \cos n\theta + \sum_{n=1}^{\infty} [\bar{a}_n U_n(x) + \bar{b}_n V_n(x) + \bar{c}_n \mathcal{O}_n(x) + \bar{d}_n \mathcal{V}_n(x)] \sin n\theta \quad \ldots [10]$$

where $a_n \ldots d_n$, $\bar{a}_n \ldots \bar{d}_n$ are constants and the functions U_n, V_n, $\mathcal{O}_n$, and $\mathcal{V}_n$ are defined as

$$U_n = \frac{1}{2}[J_n(xe^{i\alpha/2}) + J_n(xe^{-i\alpha/2})], \qquad V_n = \frac{1}{2i}[J_n(xe^{i\alpha/2}) - J_n(xe^{-i\alpha/2})]$$

$$\mathcal{O}_n = \frac{1}{2}[Y_n(xe^{i\alpha/2}) + Y_n(xe^{-i\alpha/2})], \qquad \mathcal{V}_n = \frac{1}{2i}[Y_n(xe^{i\alpha/2}) - Y_n(xe^{-i\alpha/2})] \quad \ldots [11]$$

To complete the solutions for the system of Equations [3], the

[4] See Appendix.

TABLE 1 MOMENT, SHEAR, AND DEFLECTION AT CENTER OF PLATE AND EDGE OF UNIFORM LOAD

Deg	h^2/l^2	$(\bar{w})_{r=0}$	$(\bar{w})_{r=1}$	$(V_r)_{r=1}$	$(M_r)_{r=0}$	$(M_r)_{r=1}$
$\alpha/2^* = 45$	0.00000	$-0.30539q_0/k$	$-0.22830q_0/k$	$0.36750ql$	$-0.35238ql^2$	$-0.08559ql^2$
$\alpha/2 = 50$	1.38920	$-0.38274q_0/k$	$-0.25758q_0/k$	$0.34051ql$	$-0.31451ql^2$	$-0.08969ql^2$
$\alpha/2 = 55$	2.73616	$-0.44421q_0/k$	$-0.27976q_0/k$	$0.31918ql$	$-0.28519ql^2$	$-0.09426ql^2$

* Classical theory.

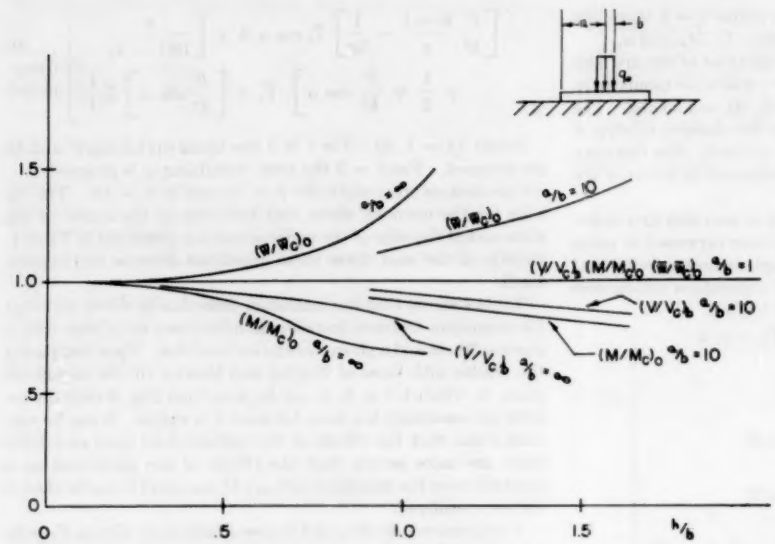

FIG. 2 COMPARISONS FOR AN INFINITE AND A FINITE CIRCULAR PLATE ON AN ELASTIC FOUNDATION

solutions for V_r and V_θ must be found from the second and third equations. These two shears will be written as

$$V_r = (V_r)_P + (V_r)_H \text{ and } V_\theta = (V_\theta)_P + (V_\theta)_H$$

where the particular solutions satisfy the second and third equations of the System [3]. The homogeneous solutions can be found by introducing a function $\phi(r, \theta)$, such that

$$(V_r)_H = \frac{1}{r}\frac{\partial \phi}{\partial \theta} \quad \text{and} \quad (V_\theta)_H = -\frac{\partial \phi}{\partial r} \qquad [12]$$

Then ϕ must be a solution of

$$\frac{h^2}{10}\nabla^2\phi - \phi = 0 \qquad [13]$$

Using the separation of variables technique, the solution for ϕ can be written as

$$\phi(r, \theta) = \sum_{n=0}^{\infty}\left[e_n' I_n\left(\frac{\sqrt{10}}{h}r\right) + f_n' K_n\left(\frac{\sqrt{10}}{h}r\right)\right]\cos n\theta + \sum_{n=1}^{\infty}\left[e_n I_n\left(\frac{\sqrt{10}}{h}r\right) + f_n K_n\left(\frac{\sqrt{10}}{h}r\right)\right]\sin n\theta \qquad [14]$$

where e_n, f_n, e_n', and f_n' are constants and I_n and K_n are the modified Bessel functions of the first and second kind. If $\nabla^2 q_1 = c$ (a constant), then ρ from Equation [10] can be substituted into the right side of the second of Equations [3] and the particular solution $(V_r)_P$ can be found from it. This can be written as

$$\left.\begin{aligned}(V_r)_P &= h_0 U_1 + j_0 V_1 + l_0 \bar{U}_1 + n_0 \bar{V}_1 \\ &+ \sum_{n=1}^{\infty}\left[g_n\frac{U_n}{r} + h_n U_{n+1} + i_n\frac{V_n}{r} + j_n V_{n+1} + k_n\frac{\bar{U}_n}{r} + l_n \bar{U}_{n+1} + m_n\frac{\bar{V}_n}{r} + n_n \bar{V}_{n+1}\right]\cos n\theta \\ &+ \sum_{n=1}^{\infty}\left[\bar{g}_n\frac{U_n}{r} + \bar{h}_n U_{n+1} + \bar{i}_n\frac{V_n}{r} + \bar{j}_n V_{n+1} + \bar{k}_n\frac{\bar{U}_n}{r} + \bar{l}_n \bar{U}_{n+1} + \bar{m}_n\frac{\bar{V}_n}{r} + \bar{n}_n \bar{V}_{n+1}\right]\sin n\theta\end{aligned}\right\} \qquad [15]$$

where the constants $h_n \ldots\ldots n_n$ are related to the constants a_n, b_n, c_n, and d_n by the following equations which also hold for the barred constants

$$\left.\begin{aligned}h_0 &= kl[a_0\cos\alpha/2 - b_0\sin\alpha/2] \\ j_0 &= kl[a_0\sin\alpha/2 + b_0\cos\alpha/2] \\ l_0 &= kl[c_0\cos\alpha/2 - d_0\sin\alpha/2] \\ n_0 &= kl[c_0\sin\alpha/2 + d_0\cos\alpha/2] \\ g_n &= nkl^2[-a_n\cos\alpha + b_n\sin\alpha] \\ h_n &= kl[a_n\cos\alpha/2 - b_n\sin\alpha/2] \\ i_n &= -nkl^2[a_n\sin\alpha + b_n\cos\alpha] \\ j_n &= kl[a_n\sin\alpha/2 + b_n\cos\alpha/2] \\ k_n &= nkl^2[-c_n\cos\alpha + d_n\sin\alpha] \\ l_n &= kl[c_n\cos\alpha/2 - d_n\sin\alpha/2] \\ m_n &= -nkl^2[c_n\sin\alpha + d_n\cos\alpha] \\ n_n &= kl[c_n\sin\alpha/2 + d_n\cos\alpha/2]\end{aligned}\right\} \qquad [16]$$

In a similar fashion, by substituting the expressions for ρ and $(V_r)_P$ into the third of Equations [3], the particular solution, $(V_\theta)_P$ is found to be

$$(V_\theta)_P = -\sum_{n=1}^{\infty}\left[g_n\frac{U_n}{r} + i_n\frac{V_n}{r} + k_n\frac{\bar{U}_n}{r} + m_n\frac{\bar{V}_n}{r}\right]\sin n\theta + \sum_{n=1}^{\infty}\left[\bar{g}_n\frac{U_n}{r} + \bar{i}_n\frac{V_n}{r} + \bar{k}_n\frac{\bar{U}_n}{r} + \bar{m}_n\frac{\bar{V}_n}{r}\right]\cos n\theta \qquad [17]$$

where the constants $g_n \ldots\ldots \bar{m}_n$ are the same as the ones given in Equations [16].

In retrospect, it can be seen that the complete solution to the system of Equations [3] has been found for the case where $\nabla^2 q_1 = c$ in terms of twelve sets of constants, which can be evaluated from the twelve boundary conditions specified for the most general case of a plate in the form of a circular sector. There will be three conditions for each of the two radial edges and three for each of the circular edges. If $\nabla^2 q_1 \neq c$, then the particular solutions must be found by some other method, but the statements above still apply.

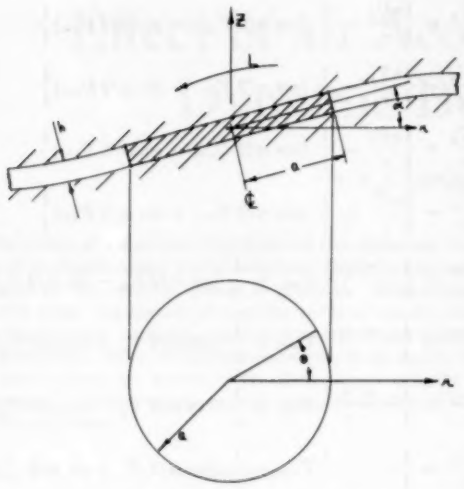

FIG. 3 SKETCH OF A PLATE WITH A RIGID CIRCULAR INCLUSION

(*b*) *An Infinite Plate on a Foundation Bent by Rotation of a Rigid Circular Inclusion.* A rigid disk of radius a is rotated through an angle α as shown in Fig. 3. Since the boundary conditions at infinity require that the deflection, moments, and shears vanish, the solutions for ρ will be expressed in terms of the modified Bessel functions of the first and second kind with an imaginary argument

$$I_n[ix\exp(i\alpha/2)],\quad I_n[ix\exp(-i\alpha/2)]$$

$$K_n[ix\exp(i\alpha/2)] \text{ and } K_n[ix\exp(-i\alpha/2)]$$

The four functions U_n, V_n, $\bar{U}_n$, and $\bar{V}_n$ used previously all become infinite as x approaches infinity. Hence, for this example, the functions U_n^* and V_n^* defined as

$$\left.\begin{aligned} U_n^* &= -\frac{2}{\pi}\,[K_n(ixe^{i\alpha/2}) + K_n(ixe^{-i\alpha/2})] \\ V_n^* &= -\frac{2i}{\pi}\,[K_n(ixe^{i\alpha/2}) - K_n(ixe^{-i\alpha/2})] \end{aligned}\right\} \quad \ldots [18]$$

will be used. Both of these functions approach zero as x approaches infinity. Considering that θ is measured from the r-axis, suitable solutions for w, V_r, and V_θ can be written as

$$\left.\begin{aligned} w &= [c_1U_1^* + d_1V_1^*]\cos\theta \\ V_r &= \left\{ f_1\,\frac{K_1\left(\frac{\sqrt{10}}{h}\,r\right)}{r} + k_1\,\frac{U_1^*}{r} + l_1U_2^* + m_1\,\frac{V_1^*}{r} + n_1V_2^* \right\}\cos\theta \\ V_\theta &= \left\{ f_1\left[\frac{K_1\left(\frac{\sqrt{10}}{h}\,r\right)}{r} + \frac{\sqrt{10}}{h}\,K_0\left(\frac{\sqrt{10}}{h}\,r\right)\right] - k_1\,\frac{U_1^*}{r} - m_1\,\frac{V_1^*}{r} \right\}\sin\theta \end{aligned}\right\} \quad \ldots [19]$$

These solutions were written with the boundary conditions $w(a,\theta) = a\,\alpha\cos\theta$; $\alpha_r(a,\theta) = -\alpha\cos\theta$; and $\alpha_\theta(a,\theta) = \alpha\sin\theta$ in view. The relations between the constants k_1, l_1, m_1, and n_1 and the independent constants c_1 and d_1 are given by the last four of Equations [16] by choosing $n = 1$.

Of particular interest is the magnitude of the moment L required to rotate the disk as a rigid body through an angle α. This is obtained by considering the contributions to the moment of each of the stress resultants M_r, $M_{r\theta}$, and V_r acting on the rim of the disk. It follows that

$$L = \int_0^{2\pi} [aM_r(a,\theta)\cos\theta + aM_{r\theta}(a,\theta)\sin\theta - a^2V_r(a,\theta)\cos\theta]a\theta + \int_0^{2\pi}\int_0^a kar^3\cos^2\theta\,dr\,d\theta \quad \ldots [20]$$

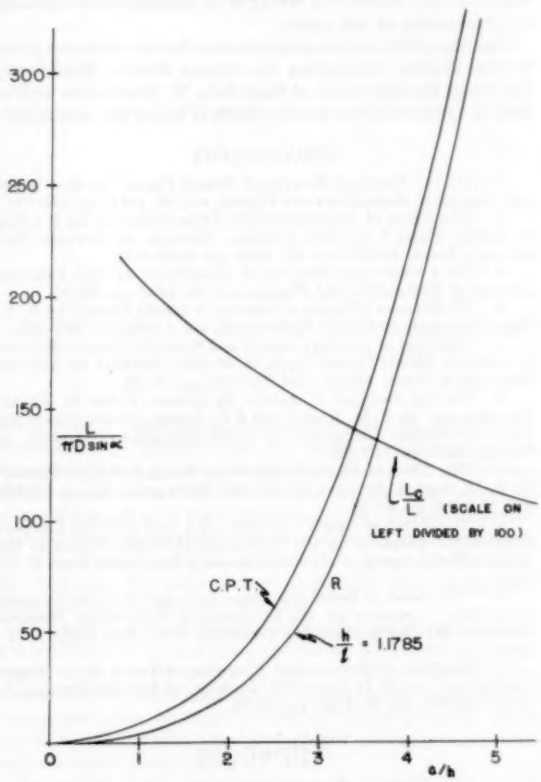

FIG. 4 MOMENT AND L_c/L VERSUS a/h FOR THE RIGID CIRCULAR INCLUSION

The moment L has been calculated for $\alpha/2 = 50$ deg or $h^2/l^2 = 1.389$ and the result has been plotted in Fig. 4, along with the result from the classical theory which was given by Reismann (10). In this figure, L_c denotes the moment required to rotate the disk through the same angle α as obtained from the classical theory. For small a/h values, the ratio L_c/L is the greatest and it gradually decreases as a/h gets larger.

CONCLUSION

The thick-plate theory developed by E. Reissner which includes the effects of shear deformation and normal stress can be used to solve problems in the bending of circular plates on an elastic foundation. For symmetric and antisymmetric problems,

the solutions can be expressed in terms of Bessel functions of zero and first order with a complex argument. Since these have been partially tabulated, numerical calculations can be conveniently carried out for certain cases.

Two specific examples have been considered in this paper and certain numerical results are presented graphically. Since these have been compared with the corresponding values as given by the classical theory, the value of a thickness-length parameter at which the effects of shear deformation and normal pressure must be taken into account can be determined from the figures.

Finally, the solutions to other problems in plate theory may be obtained by using the solutions given in this paper.

Acknowledgments

The author wishes to express appreciation to Prof. Paul M. Naghdi of the University of Michigan for his suggestions regarding the presentation of this paper.

Also, the author expresses appreciation for the assistance given by the Virginia Engineering Experiment Station, Blacksburg, Va., under the supervision of Dean John W. Whittemore, and to Mrs. K. Greever for her patient efforts in typing the manuscript.

BIBLIOGRAPHY

1 "On the Theory of Bending of Elastic Plates," by Eric Reissner, *Journal of Mathematics and Physics*, vol. 23, 1944, pp. 184–191.

2 "The Effect of Transverse Shear Deformation on the Bending of Elastic Plates," by Eric Reissner, JOURNAL OF APPLIED MECHANICS, Trans. ASME, vol. 67, 1945, pp. A-69–A-77.

3 "On a Variational Theorem in Elasticity," by Eric Reissner, *Journal of Mathematics and Physics*, vol. 29, 1950, pp. 90–95.

4 "On Reissner's Theory of Bending of Elastic Plates," by A. E. Green, *Quarterly of Applied Mathematics*, vol. 7, 1949, pp. 223–228.

5 "Influence of Rotatory Inertia and Shear on Flexural Motions of Isotropic, Elastic Plates," by R. D. Mindlin, JOURNAL OF APPLIED MECHANICS, Trans. ASME, vol. 73, 1951, pp. 31–38.

6 "On the Bending of Axially Symmetric Plates on Elastic Foundations," by P. M. Naghdi and J. C. Rowley, Proceedings of the First Midwestern Conference on Solid Mechanics, University of Illinois, 1953, pp. 119–123.

7 "The Effect of Elliptic Holes on the Bending of Thick Plates," by P. M. Naghdi, JOURNAL OF APPLIED MECHANICS, Trans. ASME, vol. 77, 1955, pp. 89–94.

8 "The Table of Bessel Functions $J_0(z)$ and $J_1(z)$ for Complex Arguments," prepared by the Mathematical Tables Project of the Federal Works Agency, Columbia University Press, New York, N. Y., 1943.

9 "The Table of Bessel Functions $Y_0(z)$ and $Y_1(z)$ for Complex Arguments," prepared by the Computation Laboratory, National Bureau of Standards, Columbia University Press, New York, N. Y., 1950.

10 "Bending of Circular and Ring-Shaped Plates on an Elastic Foundation," by H. D. Reismann, JOURNAL OF APPLIED MECHANICS, Trans. ASME, vol. 76, 1954, pp. 45–51.

Appendix

List of Identities

Following is a list of identities on the functions U_n, V_n, $\mathcal{U}_n$, $\mathcal{V}_n$, I_n, and K_n which were used in the solutions of the problems. The identities for the functions U_n^* and V_n^* are the same as those for $\mathcal{U}$ and $\mathcal{V}$

$$\frac{2nl}{r}\left[\cos\alpha/2\ U_n + \sin\alpha/2\ V_n\right] = U_{n+1} + U_{n-1}$$

$$\frac{2nl}{r}\left[\cos\alpha/2\ V_n - \sin\alpha/2\ U_n\right] = V_{n+1} + V_{n-1}$$

$$\frac{2nl}{r}\left[\cos\alpha/2\ \mathcal{U}_n + \sin\alpha/2\ \mathcal{V}_n\right] = \mathcal{U}_{n+1} + \mathcal{U}_{n-1}$$

$$\frac{2nl}{r}\left[\cos\alpha/2\ \mathcal{V}_n - \sin\alpha/2\ \mathcal{U}_n\right] = \mathcal{V}_{n+1} + \mathcal{V}_{n-1}$$

$$\frac{dU_n}{dr} = \left\{\frac{nU_n}{r} - \frac{1}{l}\left[\cos\alpha/2\ U_{n+1} - \sin\alpha/2\ V_{n+1}\right]\right\}$$

$$\frac{dV_n}{dr} = \left\{\frac{nV_n}{r} - \frac{1}{l}\left[\cos\alpha/2\ V_{n+1} + \sin\alpha/2\ U_{n+1}\right]\right\}$$

$$\frac{d\mathcal{U}_n}{dr} = \left\{\frac{n\mathcal{U}_n}{r} - \frac{1}{l}\left[\cos\alpha/2\ \mathcal{U}_{n+1} - \sin\alpha/2\ \mathcal{V}_{n+1}\right]\right\}$$

$$\frac{d\mathcal{V}_n}{dr} = \left\{\frac{n\mathcal{V}_n}{r} - \frac{1}{l}\left[\cos\alpha/2\ \mathcal{V}_{n+1} + \sin\alpha/2\ \mathcal{U}_{n+1}\right]\right\}$$

$$\frac{dU_{n+1}}{dr} = \left\{-\frac{n+1}{r}U_{n+1} + \frac{1}{l}\left[\cos\alpha/2\ U_n - \sin\alpha/2\ V_n\right]\right\}$$

$$\frac{dV_{n+1}}{dr} = \left\{-\frac{n+1}{r}V_{n+1} + \frac{1}{l}\left[\cos\alpha/2\ V_n + \sin\alpha/2\ U_n\right]\right\}$$

$$\frac{d\mathcal{U}_{n+1}}{dr} = \left\{-\frac{n+1}{r}\mathcal{U}_{n+1} + \frac{1}{l}\left[\cos\alpha/2\ \mathcal{U}_n - \sin\alpha/2\ \mathcal{V}_n\right]\right\}$$

$$\frac{d\mathcal{V}_{n+1}}{dr} = \left\{-\frac{n+1}{r}\mathcal{V}_{n+1} + \frac{1}{l}\left[\cos\alpha/2\ \mathcal{V}_n + \sin\alpha/2\ \mathcal{U}_n\right]\right\}$$

$$\frac{d^2U_n}{dr^2} = \left\{\left[\frac{n(n-1)}{r^2} - \frac{\cos\alpha}{l^2}\right]U_n + \frac{\sin\alpha}{l^2}V_n + \frac{\cos\alpha/2}{lr}U_{n+1} - \frac{\sin\alpha/2}{lr}V_{n+1}\right\}$$

$$\frac{d^2V_n}{dr^2} = \left\{\left[\frac{n(n-1)}{r^2} - \frac{\cos\alpha}{l^2}\right]V_n - \frac{\sin\alpha}{l^2}U_n + \frac{\cos\alpha/2}{lr}V_{n+1} + \frac{\sin\alpha/2}{lr}U_{n+1}\right\}$$

$$\frac{d^2\mathcal{U}_n}{dr^2} = \left\{\left[\frac{n(n-1)}{r^2} - \frac{\cos\alpha}{l^2}\right]\mathcal{U}_n + \frac{\sin\alpha}{l^2}\mathcal{V}_n + \frac{\cos\alpha/2}{lr}\mathcal{U}_{n+1} - \frac{\sin\alpha/2}{lr}\mathcal{V}_{n+1}\right\}$$

$$\frac{d^2\mathcal{V}_n}{dr^2} = \left\{\left[\frac{n(n-1)}{r^2} - \frac{\cos\alpha}{l^2}\right]\mathcal{V}_n - \frac{\sin\alpha}{l^2}\mathcal{U}_n + \frac{\cos\alpha/2}{lr}\mathcal{V}_{n+1} + \frac{\sin\alpha/2}{lr}\mathcal{U}_{n+1}\right\}$$

$$\frac{d}{dr}\left[I_n\left(\frac{\sqrt{10}}{h}r\right)\right] = \frac{n}{r}I_n\left(\frac{\sqrt{10}}{h}r\right) + \frac{\sqrt{10}}{h}I_{n+1}\left(\frac{\sqrt{10}}{h}r\right)$$

$$\frac{d}{dr}\left[K_n\left(\frac{\sqrt{10}}{h}r\right)\right] = \frac{n}{r}K_n\left(\frac{\sqrt{10}}{h}r\right) - \frac{\sqrt{10}}{h}K_{n+1}\left(\frac{\sqrt{10}}{h}r\right)$$

$$\frac{d^2}{dr^2}\left[I_n\left(\frac{\sqrt{10}}{h}r\right)\right] = \left[\frac{n(n-1)}{r^2} + \frac{10}{h^2}\right]I_n\left(\frac{\sqrt{10}}{h}r\right) - \frac{\sqrt{10}}{h}\frac{1}{r}I_{n+1}\left(\frac{\sqrt{10}}{h}r\right)$$

$$\frac{d^2}{dr^2}\left[K_n\left(\frac{\sqrt{10}}{h}r\right)\right] = \left[\frac{n(n-1)}{r^2} + \frac{10}{h^2}\right]K_n\left(\frac{\sqrt{10}}{h}r\right) + \frac{\sqrt{10}}{h}\frac{1}{r}K_{n+1}\left(\frac{\sqrt{10}}{h}r\right)$$

Effect of an Acoustic Medium on the Dynamic Buckling of Plates[1]

By F. L. DIMAGGIO,[2] NEW YORK, N. Y.

The effect of a surrounding fluid on the dynamic buckling of an elastic plate under suddenly applied compressive stresses in its middle plane is studied. Assuming an infinite plate supported at regular intervals and a semi-infinite acoustic medium, exact and approximate solutions are obtained. By a numerical example, it is shown that for steel plates in water, with dimensions usually encountered in ship structures, the compressibility of water can be neglected.

Introduction

THE hulls of ships consist principally of flat plates extending continuously over a number of supporting elements. The buckling and postbuckling behavior of such plates when subjected to compressive loading in their middle planes is therefore of practical interest.

If water were not present, the response of a section of plating between supports could be considered as representative. The dynamic buckling of such plates in vacuo has been studied by Zizicas.[3]

This paper is concerned with the modifying effect of the water outside the hull. The problem is idealized by considering an infinite plate, on one side of which is an infinite body of acoustic fluid. It is assumed that the hydrostatic pressures are large enough to prevent cavitation during the time considered, but the effect of this component of the lateral pressure on the plate is otherwise not taken into account. Furthermore, the actual loading process is idealized by assuming an initial state of uniform compressive stress in the middle plane of the plate. This is not physically possible since time is required for such a state to establish itself. This assumption corresponds to that made by Zizicas[3] and by Hoff,[4] who studied the dynamic buckling of finite columns. They justified the assumption on the fact that the time required for a compression wave to travel between supports is many times smaller than the fundamental period of lateral vibrations.

An infinite elastic plate is referred to a rectangular co-ordinate-

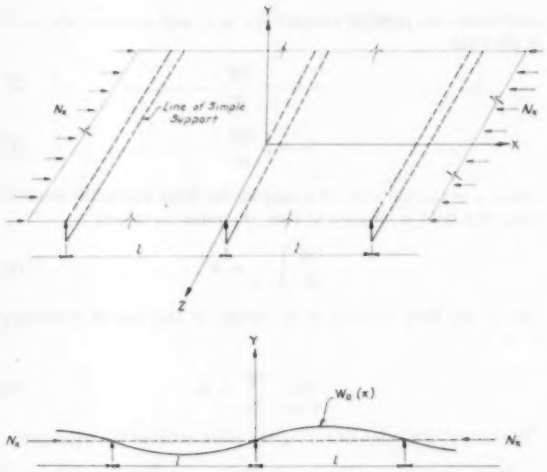

FIG. 1

system, Fig. 1. It is assumed to have a small initial curvature independent of z. At equal intervals l on the x-axis it is supported along lines parallel to the z-axis. An infinite body of acoustic fluid, i.e., one whose motions conform to the linear theory of waves of expansion, occupies the space $y \geq 0$. It is assumed that at time $t = 0$, the plate is in a uniform state of compressive stress N_x. A mathematical study is made of the dynamic response of the plate for $t > 0$ if the plate stress N_x is greater than the buckling stress and remains constant with time.

By means of Laplace transformation, the fluid-velocity potential is eliminated between the simultaneous differential equations which couple the response of the plate and fluid. The resulting transform of the plate displacement is inverted by integration in the complex plane, yielding residues and branch integrals. It is shown that the contribution of the residues represents the asymptotic solution for large values of t.

One purpose of this paper is to explore the possibility of making simplifying assumptions in actual physical problems. It is first found that if the compressibility of the fluid is neglected, the effect of the fluid is entirely accounted for by adding a "virtual mass" of fluid to the actual mass of the plate. This incompressible solution is always a lower bound for the exact solution. For certain combinations of the nondimensional parameters of the problem it is shown that the residues of the transform solution can be well approximated by the incompressible solution.

A solution valid for small values of t only is obtained by means of an approximation previously employed by Bleich and Mindlin.[5]

By a numerical example, it is shown that for steel plates in water, with dimensions usually encountered in ship structures, the

---

[1] The results presented in this paper are based on a dissertation submitted in partial fulfillment of the requirements for the degree of Doctor of Philosophy, Columbia University, June, 1954. The investigation was sponsored by the Office of Naval Research under contract Nonr 266(08).

[2] Instructor in Civil Engineering and Engineering Mechanics, Columbia University.

[3] "Dynamic Buckling of Thin Elastic Plates," by G. A. Zizicas, Trans. ASME, vol. 74, 1952, pp. 1257–1266.

[4] "The Dynamics of the Buckling of Elastic Columns," by N. J. Hoff, Trans. ASME, vol. 73, 1951, pp. 68–74.

Contributed by the Applied Mechanics Division and presented at the Diamond Jubilee Annual Meeting, Chicago, Ill., November 13–18, 1955, of THE AMERICAN SOCIETY OF MECHANICAL ENGINEERS.

Discussion of this paper should be addressed to the Secretary, ASME, 29 West 39th Street, New York, N. Y., and will be accepted until July 10, 1956, for publication at a later date. Discussion received after the closing date will be returned.

NOTE: Statements and opinions advanced in papers are to be understood as individual expressions of their authors and not those of the Society. Manuscript received by ASME Applied Mechanics Division June 25, 1955. Paper No. 55—A-35.

[5] "Response of an Elastic Cylindrical Shell to a Transverse, Step Shock Wave," by R. D. Mindlin and H. H. Bleich, Trans. ASME, vol. 75, 1953, pp. 189–195.

nondimensional parameters are such that the compressibility of the water can be neglected; the "virtual-mass" concept is sufficient to study the motion.

A Formal Solution by Laplace Transform

(*a*) *Equations Governing Motion of Plate and Fluid.* The velocity potential $\phi(x, y, t)$, governed by the equation

$$\frac{\partial^2\phi}{\partial x^2} + \frac{\partial^2\phi}{\partial y^2} = \frac{1}{c^2}\frac{\partial^2\phi}{\partial t^2} \quad [1]$$

determines the particle velocity $v(x, y, t)$ and pressure $p(x, y, t)$ in the fluid

$$v = -\frac{\partial\phi}{\partial y} \quad [2]$$

$$p = \rho\frac{\partial\phi}{\partial t} \quad [3]$$

where c is the velocity of sound in the fluid and ρ its density. Since the fluid is initially at rest, the pressure is zero

$$\left.\frac{\partial\phi}{\partial t}\right]_{t=0} = 0 \quad [4]$$

and if the fluid velocity is to vanish at the infinite boundary $y = \infty$

$$\lim_{y\to\infty}\frac{\partial\phi}{\partial y} = 0 \quad [5]$$

The lateral deflection $w(x, t)$ of the plate satisfies the equation[4]

$$D\frac{\partial^4(w - w_0)}{\partial x^4} + N_x\frac{\partial^2 w}{\partial x^2} + m\frac{\partial^2 w}{\partial t^2} = -\rho\left.\frac{\partial\phi}{\partial t}\right]_{y=0} \quad [6]$$

and the initial conditions

$$w(x, 0) = w_0(x); \quad \left.\frac{\partial w}{\partial t}\right]_{t=0} = 0 \quad [7]$$

The lateral velocity of a point on the plate must equal the particle velocity of the fluid in that direction at $y = 0$. Thus

$$\frac{\partial w}{\partial t} = -\left.\frac{\partial\phi}{\partial y}\right]_{y=0} \quad [8]$$

The most general periodic initial shape of the plate is

$$w_0(x) = \sum_{n=1}^{\infty} a_n \sin\frac{n\pi}{l}x \quad [9]$$

The corresponding plate displacement and fluid-velocity potential may be taken as

$$w(x, t) = \sum_{n=1}^{\infty}[a_n + w_n(t)]\sin\frac{n\pi}{l}x \quad [10]$$

$$\phi(x, y, t) = \sum_{n=1}^{\infty}\Phi_n(y, t)\sin\frac{n\pi}{l}x \quad [11]$$

Since the equations governing ϕ and w are such that the term $n = k$ of the series [10] is not coupled with terms $n \neq k$ of series [11], the response corresponding to each component of the series representing $w_0(x)$ can be determined separately.

Only a finite number of components of the series [9] will lead to plate displacements in the supercritical range for a given load. For later terms, the load will be below the buckling load. Unless the initial shape is such that the constant a_1 is very small, the first term will be the most important in determining the response.

In this paper, only the response due to

$$w_0(x) = a_1\sin\frac{\pi}{l}x \quad [9a]$$

will be considered. The plate displacement and velocity potential are

$$w(x, t) = [a_1 + w_1(t)]\sin\frac{\pi}{l}x \quad [10a]$$

$$\phi(x, y, t) = \Phi(y, t)\sin\frac{\pi}{l}x \quad [11a]$$

Setting

$$\delta(t) = \frac{w_1}{a_1} \quad [12]$$

$$\gamma^2 = \left(\frac{\pi}{l}\right)^4\frac{D}{m} \quad [13]$$

where γ is the fundamental frequency of lateral vibration of the plate in vacuo, and

$$\alpha = \frac{N_x}{N_E} \quad [14]$$

where N_E is the Euler buckling load, i.e.

$$N_E = \frac{\pi^2 D}{l^2} \quad [15]$$

Equations [1], [4], [5], [6], [7], and [8] become, respectively

$$\frac{\partial^2\Phi}{\partial y^2} - \left(\frac{\pi}{l}\right)^2\Phi = \frac{1}{c^2}\frac{\partial^2\Phi}{\partial t^2} \quad [16]$$

$$\left.\frac{\partial\Phi}{\partial t}\right]_{t=0} = 0 \quad [17]$$

$$\lim_{y\to\infty}\frac{\partial\Phi}{\partial y} = 0 \quad [18]$$

$$\frac{d^2\delta}{dt^2} - \gamma^2(\alpha - 1)\delta + \frac{\rho}{ma_1}\left.\frac{\partial\Phi}{\partial t}\right]_{y=0} = \alpha\gamma^2 \quad [19]$$

$$\delta(0) = \left.\frac{d\delta}{dt}\right]_{t=0} = 0 \quad [20]$$

$$\frac{d\delta}{dt} = -\frac{1}{a_1}\left.\frac{\partial\Phi}{\partial y}\right]_{y=0} \quad [21]$$

To determine the response of the plate, Φ must be eliminated between Equations [19] and [21] which govern the interaction between plate and fluid.

(*b*) *Determination of Laplace Transform of Plate Response.* Noting that the initial value of Φ is arbitrary and can be taken equal to zero, the application of the Laplace transform with t as a variable to Equation [16], in conjunction with Equation [17], yields

$$\frac{d^2\bar{\Phi}}{dy^2} - \left[\left(\frac{\pi}{l}\right)^2 + \left(\frac{s}{c}\right)^2\right]\bar{\Phi} = 0 \quad [22]$$

where $\bar{\Phi}(y, s)$ is the Laplace transform of $\Phi(y, t)$ with respect to t. The solution of Equation [22], satisfying Equation [18], is

$$\bar{\Phi} = A(s)\exp\left(-y\sqrt{\left(\frac{\pi}{l}\right)^2 + \left(\frac{s}{c}\right)^2}\right) \quad [23]$$

[4] If the acoustic medium occupies the space $-\infty \leqslant y \leqslant \infty$, ρ is replaced by 2ρ.

where the square root is to be taken such that

$$\text{Re}\sqrt{\left(\frac{\pi}{l}\right)^2+\left(\frac{s}{c}\right)^2}>0 \quad \ldots\ldots [24]$$

Similarly, Equations [21] and [20] yield, upon transformation

$$-a_1 s^2\bar{\delta}\left[\frac{\bar{\Phi}(0,s)}{\dfrac{d\bar{\Phi}}{dy}\Big]_{y=0}}=s\bar{\Phi}(0,s) \quad \ldots\ldots [25]$$

where $\bar{\delta}(s)$ is the Laplace transform of the plate response $\delta(t)$. From Equation [23]

$$\left[\frac{\bar{\Phi}(0,s)}{\dfrac{d\bar{\Phi}}{dy}\Big]_{y=0}}=-\frac{1}{\sqrt{\left(\frac{\pi}{l}\right)^2+\left(\frac{s}{c}\right)^2}} \quad \ldots\ldots [26]$$

with the restriction on the radical of Equation [24]. Finally, transforming Equation [19] and taking into account Equations [20], [25], and [26], the plate response transform is obtained as

$$\bar{\delta}(s)=\frac{\alpha\gamma^2}{s}\left[\frac{1}{s^2+\dfrac{\rho}{m}\dfrac{s^2}{\sqrt{\left(\frac{\pi}{l}\right)^2+\left(\frac{s}{c}\right)^2}}-\gamma^2(\alpha-1)}\right] \quad \ldots [27]$$

(c) *Inversion of Plate-Response Transform.*

Setting

$$\frac{s}{\gamma}=\lambda \quad \ldots\ldots [28]$$

in Equation [27], the inversion integral of the nondimensional plate response is

$$\delta(\tau)=\frac{1}{2\pi i}\int_{Br_1}\frac{\alpha e^{\lambda\tau}d\lambda}{\lambda\left[\lambda^2+\dfrac{\rho c}{m\gamma}\dfrac{\lambda^2}{\sqrt{\lambda^2+\left(\frac{\pi c}{l\gamma}\right)^2}}-(\alpha-1)\right]} \quad \ldots\ldots [29]$$

where τ, defined by

$$\tau=\gamma t \quad \ldots\ldots [30]$$

is a nondimensional time variable. Equation [24] defining the branch of the integrand to be chosen becomes, using Equation [28]

$$\text{Re}\sqrt{\lambda^2+\left(\frac{\pi c}{l\gamma}\right)^2}>0 \quad \ldots\ldots [31]$$

Consider the contour AB . . . H shown in Fig. 2, where the dotted lines indicate branch cuts and the arcs AB, DE, and GH are of infinite radius. Let $G(\lambda)$ denote the integrand of the integral in Equation [29]. By the residue theorem and Jordan's lemma, $\delta(\tau)$ of Equation [29] may be evaluated as

$$\frac{1}{2\pi i}\int_{Br_1}G(\lambda)d\lambda=\frac{1}{2\pi i}\int_{Br_2}G(\lambda)d\lambda+\Sigma R \quad \ldots\ldots [32]$$

where Br_2 indicates the paths BCD and EFG and ΣR means the sum of the residues of the poles of the pertinent branch of $G(\lambda)$.

The operations indicated in Equation [32] are carried out elsewhere.[7] It is found that

[7] See PhD dissertation by author having same title as this paper mentioned in footnote 1.

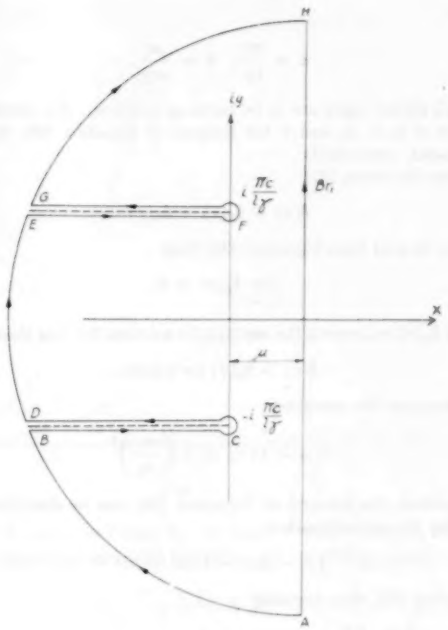

FIG. 2

$$\Sigma R\equiv\delta_R(\tau)=\frac{\alpha}{\alpha-1}\left\{\left(\frac{1}{1-\dfrac{1}{2(\alpha-1)}\dfrac{\rho c}{m\gamma}\dfrac{\xi_1^2}{\left|\left[\xi_1+\left(\frac{\pi c}{l\gamma}\right)^2\right]^{3/2}\right|}}\cosh\sqrt{\xi_1}\tau\right)-1\right\} \quad \ldots\ldots [33]$$

where ξ_1 is that positive real root[8] of the cubic equation

$$\xi^3+\left[\left(\frac{\pi c}{l\gamma}\right)^2-\left(\frac{\rho c}{m\gamma}\right)^2-(2)(\alpha-1)\right]\xi^2+\left[(\alpha-1)^2-2(\alpha-1)\left(\frac{\pi c}{l\gamma}\right)^2\right]\xi+(\alpha-1)^2\left(\frac{\pi c}{l\gamma}\right)^2=0 \quad \ldots\ldots [34]$$

which satisfies the equation

$$\xi+\frac{\rho c}{m\gamma}\frac{\xi}{\sqrt{\left|\xi+\left(\frac{\pi c}{l\gamma}\right)^2\right|}}=\alpha-1 \quad \ldots\ldots [35]$$

Also

$$\frac{1}{2\pi i}\int_{Br_2}G(\lambda)d\lambda\equiv\delta_R(\tau)=-\frac{2ab}{\pi}\int_0^\infty e^{-u\tau}\,\text{Re}\left\{\frac{e^{i\alpha\tau}|u^{1/2}|(ia-u)\left(\sqrt{\sqrt{\frac{u^2}{4}+a^2}-\frac{u}{2}}+i\sqrt{\sqrt{\frac{u^2}{4}+a^2}+\frac{u}{2}}\right)}{b^2(ia-u)^4+u(2ai-u)[(\alpha-1)^2+(ai-u)^4-2(\alpha-1)(ai-u)^2]}\right\}du \quad [36]$$

[8] It is shown in reference of footnote 7 that Equation [34] always has two positive real roots.

where

$$a = \frac{\pi c}{l\gamma}; \quad b = \frac{\rho c}{m\gamma} \quad \ldots\ldots [37]$$

and all square roots are to be taken as positive. For particular values of a, b, α, and τ the integral of Equation [36] can be evaluated numerically.

From Equation [32]

$$\delta(\tau) = \delta_R(\tau) + \delta_E(\tau) \quad \ldots\ldots [38]$$

It can be seen from Equation [36] that

$$\lim_{\tau \to \infty} \delta_E(\tau) = 0 \quad \ldots\ldots [39]$$

Thus $\delta_R(\tau)$ represents the asymptotic solution for long times

$$\delta(\tau) \doteq \delta_R(\tau) \text{ for } \tau \text{ large} \quad \ldots\ldots [40]$$

Whenever the condition

$$2(\alpha - 1) << \left(\frac{\pi c}{l\gamma}\right)^2 \quad \ldots\ldots [41]$$

is satisfied, the integral of Equation [36] can be simplified by making the approximation

$$(ai - u)^4 + (\alpha - 1)^2 - 2(\alpha - 1)(ai - u)^2 \doteq (ai - u)^4 \quad \ldots [42]$$

Equation [36] then becomes

$$\delta_E = -\frac{2ab}{\pi} \int_0^\infty e^{-u\tau} u^{1/2} \operatorname{Re} \left\{ \frac{e^{iu\tau}\left(\sqrt{\sqrt{\frac{u^2}{4} + a^2} - \frac{u}{2}} + i\sqrt{\sqrt{\frac{u^2}{4} + a^2} + \frac{u}{2}}\right)}{(ai - u)^2[b^2 + u(2ai - u)]} \right\} du \quad \ldots\ldots [43]$$

Evaluating the real part of the expression in braces, Equation [43] may be rewritten as

$$\delta_E = -\frac{2ab}{\pi} \int_0^\infty e^{-u\tau} u^{1/2} \frac{f_3(f_1 \cos a\tau - f_2 \sin a\tau) - f_4(f_1 \sin a\tau + f_2 \cos a\tau)}{f_3^2 + f_4^2} du \quad \ldots\ldots [44]$$

where

$$f_1(u) = \sqrt{\sqrt{\frac{u^2}{4} + a^2} - \frac{u}{2}} \quad \ldots\ldots [45]$$

$$f_2(u) = \sqrt{\sqrt{\frac{u^2}{4} + a^2} + \frac{u}{2}} \quad \ldots\ldots [46]$$

$$f_3(u) = u^5 - (9a^2 + b^2)u^3 + (2a^4 + 3a^2b^2)u \quad \ldots\ldots [47]$$

$$f_4(u) = 5au^4 - (7a^3 + 3ab^2)u^2 + b^2a^2 \quad \ldots\ldots [48]$$

Approximate Solutions

(*a*) ***Incompressible Fluid.*** If the fluid is assumed to be incompressible, the Laplace transform of the plate response, $\bar{\delta}_i(s)$, is obtained from Equation [27] by letting c approach ∞. Thus

$$\bar{\delta}_i(s) = \frac{\alpha\gamma^2}{s\left[s^2 + \frac{\rho l}{m\pi} s^2 - \gamma^2(\alpha - 1)\right]}$$

The corresponding plate response becomes

$$\delta_i(\tau) = \frac{\alpha}{\alpha - 1}\left[\cosh \sqrt{\frac{\alpha - 1}{1 + \frac{\rho l}{m\pi}}}\, \tau - 1\right] \quad \ldots\ldots [49]$$

But the right-hand side of Equation [49] is the solution of the differential equation of motion of this plate in vacuo if the actual mass of the plate is replaced by an equivalent mass m_E given by

$$m_E = m + \frac{\rho l}{\pi} \quad \ldots\ldots [50]$$

Thus the effect of an incompressible fluid on the response of the plate is entirely accounted for by adding to the mass of the plate a term usually called "virtual mass" of fluid. In the present case this virtual mass is $\rho l/\pi$.

It can be shown[7] that this incompressible solution is always a lower bound for the exact solution.

(*b*) ***Approximation Valid for Certain Values of Parameters.*** In the following it is shown that the incompressible solution is an excellent approximation to the long-term solution for certain values of the nondimensional parameters of the problem.

Assume the positive real root ξ_1 of Equation [35] is such that

$$\xi_1 \ll \left(\frac{\pi c}{l\gamma}\right)^2 \quad \ldots\ldots [51]$$

Then

$$\xi_1 \doteq \frac{\alpha - 1}{1 + \frac{\rho l}{m\pi}} \quad \ldots\ldots [52]$$

and the long-term solution of Equation [36] becomes

$$\delta_R \doteq \frac{\alpha}{\alpha - 1}\left[\cosh \sqrt{\frac{\alpha - 1}{1 + \frac{\rho l}{m\pi}}}\, \tau - 1\right] \quad \ldots\ldots [53]$$

which is exactly the incompressible solution of Equation [49]. Thus, whenever

$$\frac{\alpha - 1}{1 + \frac{\rho l}{m\pi}} \ll \left(\frac{\pi c}{l\gamma}\right)^2 \quad \ldots\ldots [54]$$

the response of the plate after a sufficiently long time is well approximated by the incompressible solution.

(*c*) ***Solution Valid for Small t Only.*** Instead of eliminating Φ between Equations [19] and [21] by use of Laplace transforms, the procedure[8] is adopted to find a solution valid for t small. Φ is expanded into a Fourier series

$$\Phi(y, t) = \sum_s F_s(y) e^{i\xi_s \frac{ct}{l}} \quad \ldots\ldots [55]$$

where

$$\xi_s = ks\pi/2 \quad \ldots\ldots [56]$$

and k is a number which fixes the interval of expansion ($2l/kc$).

The term corresponding to $s = 0$ in Equation [55], representing a fluid motion without pressure, is taken equal to zero. Then from Equation [16]

$$F_s'' + \frac{1}{l^2}(\xi_s^2 - \pi^2)F_s = 0 \quad \ldots\ldots [57]$$

Let

$$\beta_s = +\sqrt{1 - \left(\frac{\pi}{\xi_s}\right)^2} \quad \ldots\ldots [58]$$

[8] Footnote 5, sec. A3.

where β_s is real and positive if $\xi_s > \pi$. The solution of Equation [57] for outgoing waves is

$$F_s = A_s e^{-i\beta_s \xi_s \frac{y}{l}} \quad \text{[59]}$$

Hence, during $0 \leq t \leq 2l/kc$

$$\Phi = \sum_s A_s e^{-i\frac{\xi_s \beta_s}{l}\left(y - \frac{c}{\beta_s} t\right)} \quad \text{[60]}$$

$$\left.\frac{\partial \Phi}{\partial t}\right]_{y=0} = i\frac{c}{l}\sum_s A_s \xi_s e^{i\frac{\xi_s c}{l} t} \quad \text{[61]}$$

$$-\left.\frac{\partial \Phi}{\partial y}\right]_{y=0} = \frac{i}{l}\sum_s A_s \xi_s \beta_s e^{i\frac{\xi_s c}{l} t} \quad \text{[62]}$$

The interval of expansion is now chosen small enough (k large enough) such that

$$\beta_s \doteq 1 \text{ for all } s \quad \text{[63]}$$

To this approximation, then, from Equations [61] and [62]

$$\left.\frac{\partial \Phi}{\partial t}\right]_{y=0} = -c\left.\frac{\partial \Phi}{\partial y}\right]_{y=0} \quad \text{[64]}$$

Equation [16] now becomes, using Equation [21]

$$\ddot{\delta} + \frac{\rho c}{m\gamma}\dot{\delta} - (\alpha - 1)\delta = \alpha \quad \text{[65]}$$

where dots indicate differentiation with respect to the nondimensional time τ of Equation [30].

Although this equation of motion no longer contains the parameter k, its validity depends on the approximation of Equation [63]. Thus the solution of Equation [65] may be expected to describe only the early response of the plate

$$\delta_v = \frac{\alpha}{\alpha - 1}\left[e^{-\frac{\rho c}{2m\gamma}\tau}\left(\cosh\sqrt{\left(\frac{\rho c}{2m\gamma}\right)^2 + (\alpha - 1)}\,\tau + \frac{\frac{\rho c}{2m\gamma}}{\sqrt{\left(\frac{\rho c}{2m\gamma}\right)^2 + (\alpha - 1)}}\sinh\sqrt{\left(\frac{\rho c}{2m\gamma}\right)^2 + (\alpha - 1)}\,\tau\right) - 1\right] \quad \text{[66]}$$

Numerical Example

The exact and approximate expressions for the plate response derived in the preceding two sections are evaluated numerically in this section for the following values of the nondimensional parameters

$$\frac{\pi c}{l\gamma} = 20; \quad \frac{\rho c}{m\gamma} = 60; \quad \alpha = 2 \quad \text{[67]}$$

These parameters correspond roughly to a steel plate $^1/_2$ in. thick ($m = 0.633$ lb sec^2/ft^3, $\nu = 0.3$) supported every 34 in., salt water ($\rho = 1.99$ lb sec^2/ft^4, $c = 5000$ fps), and an axial stress which is twice the buckling stress.

The frequency γ, given by Equation [13], is 261 radians/sec, which, when substituted into Equation [30], gives the nondimensional time as $\tau = 261\,t$. Thus $\tau = 1$ corresponds to 3.8 millisec.

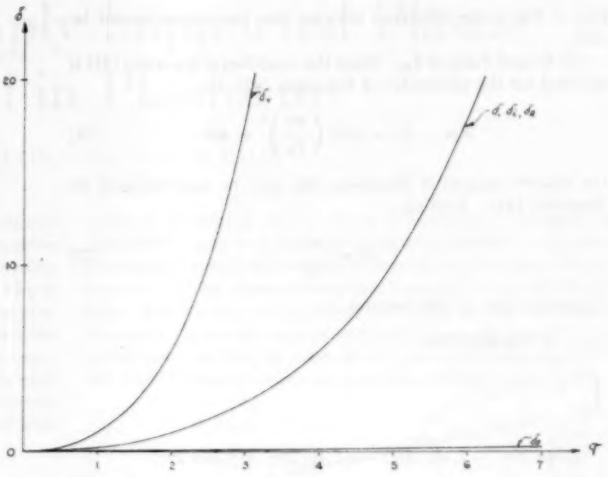

Fig. 3

(*a*) *Response in Vacuo, δ_v.* If water were not present, the response δ_v is obtained from Equation [49] by setting $\rho = 0$

$$\delta_v = \frac{\alpha}{\alpha - 1}\left[\cosh\sqrt{\alpha - 1}\,\tau - 1\right] \quad \text{[68]}$$

which, for the parameters of Equation [67], becomes

$$\delta_v = 2[\cosh\tau - 1] \quad \text{[69]}$$

δ_v is plotted versus τ in Fig. 3.

(*b*) *Incompressible Solution, δ_i.* If water is assumed to be incompressible, the plate response is obtained from Equation [49] using the parameters of Equation [67]

$$\delta_i = 2[\cosh 0.5\tau - 1] \quad \text{[70]}$$

and is plotted in Fig. 3. Note that $\delta_i(2\tau) = \delta_v(\tau)$. The equivalent mass m_E of Equation [50] is, in this case

$$m_E = 4m \quad \text{[71]}$$

(*c*) *Exact Solution, δ: (1) Contribution of Residues, δ_R.* For the parameters of Equation [67], Equation [34] becomes

$$\xi^3 - 3202\xi^2 - 799\xi + 400 = 0 \quad \text{[72]}$$

from which the positive root which satisfies Equation [35] is obtained as

$$\xi_1 = 0.2500586 \quad \text{[73]}$$

and substituted into Equation [33] to obtain δ_R

$$\delta_R = 2[1.000234\cosh 0.5000586\tau - 1] \quad \text{[74]}$$

It is seen that, except for extremely small values of τ, δ_R of Equation [74] is closely approximated by δ_i of Equation [70]. This could have been predicted since the parameters of Equation [67] satisfy the condition of Equation [54]; i.e.

$$\frac{\alpha - 1}{1 + \frac{\rho l}{m\pi}} = \frac{1}{4} \ll \left(\frac{\pi c}{l\gamma}\right)^2 = 400 \quad \text{[75]}$$

In Fig. 4 both δ_i and δ_R are plotted for very small τ. The plot shows that δ_R is well approximated by δ_i for $\tau > 0.1$. On the

plot of Fig. 3 the difference between the two curves cannot be seen.

(2) *Branch Integral* δ_B. Since the condition of Equation [41] is satisfied for the parameter of Equation [67], i.e.

$$2(\alpha - 1) = 2 \ll \left(\frac{\pi c}{l\gamma}\right)^2 = 400 \quad [76]$$

the branch integral of Equation [36] may be approximated by Equation [44]. Letting

$$\bar{u} = \frac{u}{10} \quad [77]$$

Equations [44] to [48] become

$$\delta_B(\tau) = -0.00052065 \int_0^\infty e^{-10\bar{u}\tau} \bar{u}^{1/4} \frac{\bar{f}_2}{\bar{f}_4}(f_1 \cos 20\tau - f_2 \sin 20\tau) - (f_1 \sin 20\tau + f_2 \cos 20\tau) \frac{\bar{f}_3}{\bar{f}_4} \bar{f}_3 + \bar{f}_4 \, d\bar{u} \quad [78]$$

$$f_1(\bar{u}) = \sqrt{\sqrt{25\bar{u}^2 + 400} - 5\bar{u}} \quad [79]$$

$$f_2(\bar{u}) = \sqrt{\sqrt{25\bar{u}^2 + 400} + 5\bar{u}} \quad [80]$$

$$\bar{f}_3(\bar{u}) = f_3(\bar{u})/4{,}640{,}000 = 0.021552\bar{u}^3 - 1.5517\bar{u}^2 + 10\bar{u} \quad [81]$$

$$\bar{f}_4(\bar{u}) = f_4(\bar{u})/4{,}640{,}000 = 0.21551\bar{u}^4 - 5.8621\bar{u}^2 + 6.2069 \quad [82]$$

For each value of τ considered, the integral of Equation [78] has been evaluated numerically by Simpson's rule. As a check, the value of $\delta_B(0)$ was also computed. From Equations [20] and [38]

$$\delta_B(0) = -\delta_R(0) \quad [83]$$

Using Equation [83], the true value of $\delta_B(0)$ for the parameters of Equation [67] is obtained as

$$\delta_B(0) = -0.000468 \quad [84]$$

The numerical integration of Equation [78] yielded

$$\delta_B(0) = -0.000474 \quad [85]$$

which represents an error of 1.3 per cent.

The computed values of δ_B are added to δ_R to obtain the exact response δ. A plot of δ versus τ is shown in Fig. 4 for small values of τ. On the plot of Fig. 3 the difference between δ, δ_i, and δ_R cannot be seen. Fig. 4 shows that the exact solution δ differs considerably from the incompressible solution δ_i in the very early stages of the motion. It rapidly approaches the asymptotic solution δ_R after a short time; i.e., $\tau > 0.1$. It is seen from Equations [70] and [74] and Fig. 4 that δ_i is a lower bound for δ.

(d) *Solution Valid for Short Times,* δ_S. For the parameters of Equation [67], Equation [66] becomes

$$\delta_S = 2[0.00027754e^{-80.016667} + 0.99972245e^{0.016666217} - 1] \quad [86]$$

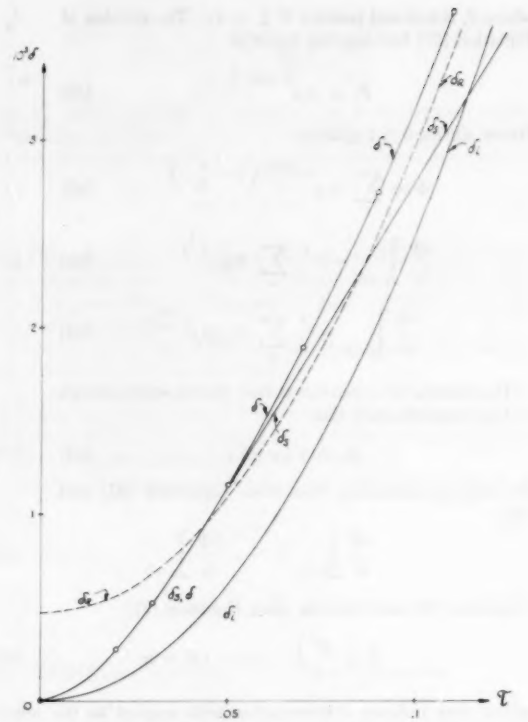

FIG. 4

where the hyperbolic functions have been expressed as exponentials. δ_s is plotted versus τ in Figs. 3 and 4. From Fig. 4 it is seen that δ_s is an excellent approximation to the exact solution δ for $\tau \leq 0.05$, after which the two curves diverge rapidly.

Whenever the nondimensional parameters of the problem satisfy the condition of Equation [54], the behavior will be similar to that obtained in the foregoing. For such cases, the nondimensional response, after a short time, is well approximated by the incompressible solution. It is found that the parameters corresponding to other plate dimensions occurring in ships satisfy Condition [54] provided the buckling parameter is not too large. In the interval during which the incompressible solution is not applicable, it is seen from this example that the plate deflection is of the same order of magnitude as the initial deflection. If the initial curvature is small, this interval will not be of interest.

Thus it may be concluded that, for moderate overloads and small initial curvature, the time at which the hull plating of ships attains critical deflections can be determined from the incompressible solution; i.e., by considering the buckling in vacuo of the plate with an equivalent mass m_s given by Equation [50].

ACKNOWLEDGMENT

The author wishes to thank Prof. H. H. Bleich of Columbia University for his helpful advice in the solution of this problem.

Buckling of Simply Supported Plates Tapered in Planform

By BERTRAM KLEIN,[1] LOS ANGELES, CALIF.

Design curves are presented for determining the elastic buckling loads of simply supported flat plates of isosceles trapezoidal planform and loaded in compression along the parallel edges. Shear loads are assumed to act along the sloping edges so that any ratio of axial loads may act along the parallel edges of the given plate. Isosceles triangular plates are included as a special limiting case, and the range of the values of the various geometric and load parameters presented in the curves is considered large enough to cover practically all conditions of the type treated which are encountered in practice.

Nomenclature

The following nomenclature is used in the paper:

a = coefficient
A = matrix
b_1, b_2 = plate dimensions
b = $(b_1 + b_2)/2$
B = matrix
D = plate flexural rigidity
f, F = functions
h = plate width
h_1 = distance
k = numerical index corresponding to number of half-waves in transverse direction
M = moment acting along edge of plate
N_x, N_y = axial load, lb/in., acting in direction of corresponding axis
N_1, N_2 = axial loads, lb/in., acting on parallel edges of plate
n = numerical index or normal direction
p = geometric parameter
r_1 = (b_1/h); $r_2 = (b_2/h)$
t = tangential direction
w = plate deflection
x, y = co-ordinates
β = eigenvalue
ν = Poisson's ratio
φ, ψ = angles
ρ = parameter
θ = semiangle of plate taper

Introduction

Plates used in structural design are seldom exactly rectangular in shape. In fact in many practical designs plates appear trapezoidal as depicted in Fig. 1. It is of interest to determine the initial buckling load of such flat plates when loaded in axial compression as shown. It is seen that some of the load is assumed to be taken out by shear of constant intensity along the sloping sides. For the sake of simplicity the plate and its loading are assumed to have one axis of symmetry, i.e., the y-axis. It is further assumed that all edges of the plate are simply supported and that the material remains elastic everywhere under load.

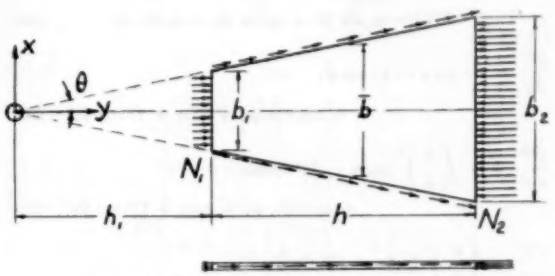

Fig. 1 Trapezoidal Plate and Loading

Method of Solution

The problem is solved by the method of collocation (1, 2).[2] The first step in this approach, as in energy methods (3), is the assumption of a deflected shape as the buckling configuration. However, in the method of collocation, no great restrictions exist as regards the nature of the functions selected; the functions need not be integrable in closed form, form an orthogonal set, satisfy the boundary conditions exactly all over, etc. Next the necessary derivatives of the chosen functions are calculated and then evaluated numerically at as many points as needed to determine the unknown generalized coefficients appearing in the functions. The results are substituted into the governing differential equation (or equations) for buckling and into boundary-condition equations (if necessary) to yield a set of equations. In contrast to energy methods, no integrations need be carried out unless, of course, integrals appear in the equations. Further differentiations also are unnecessary. The eigenvalue matrix form defining the buckling load is obtained directly from the original set of equations as defined.

Notice that physically the differential equation is satisfied exactly at certain points for the assumed shape. If this assumed shape happens to be the exact shape, the exact solution to the given differential equation is obtained. Otherwise the solution is approximate. The power of this philosophy lies in the fact that it may be possible to find functions which are close to the exact shape in certain regions of the structure. Then the results are accurate regardless of large errors in unexplored regions. In energy methods, care must be taken to choose functions which are reasonable all over the plate. Likewise, satisfying the boundary conditions accurately only at certain places or in an approximate manner may be quite sufficient for accurate solutions by the

[1] Senior Structures Engineer, Aerophysics Department, North American Aviation Inc., Downey Calif.; formerly, Research Engineer, Department of Engineering, University of California.

Contributed by the Applied Mechanics Division and presented at the Diamond Jubilee Annual Meeting, Chicago, Ill., November 13–18, 1955, of The American Society of Mechanical Engineers.

Discussion of this paper should be addressed to the Secretary, ASME, 29 West 39th Street, New York, N. Y., and will be accepted until July 10, 1956, for publication at a later date. Discussion received after the closing date will be returned.

Note: Statements and opinions advanced in papers are to be understood as individual expressions of their authors and not those of the Society. Manuscript received by ASME Applied Mechanics Division, October 18, 1954. Paper No. 55—A-39.

[2] Numbers in parentheses refer to the Bibliography at the end of the paper.

method of collocation, but not necessarily by energy methods. In conclusion, it should be stated that the energy technique serves as a powerful tool when it is used to derive differential equations of equilibrium not attainable by direct methods (4).

Assumed Deflection Function and Its Derivatives at Points of Collocation

It is felt that the following function represents a reasonable estimate of the deflected shape at buckling of the plate shown in Fig. 1

$$w = F(y)\cos\left(\frac{\pi k x}{2y}\cot\theta\right), \quad k = 1, 3, 5, \ldots\ldots \quad [1]$$

It is shown in the Appendix that this function satisfies the boundary conditions exactly along the sloping lines only at certain points and only exactly at $x = 0$ along the parallel edges. $F(y)$ and certain of its derivatives are

$$F(y) = a_1 \sin\psi_1 + a_2 \sin\psi_2 + a_3 \sin\psi_3 \ldots\ldots [2a]$$

$$\frac{dF}{dy} = \frac{\pi}{h}[a_1(n-1)\cos\psi_1 + a_2 n\cos\psi_2 + a_3(n+1)\cos\psi_3] \ldots [2b]$$

$$\frac{d^2F}{dy^2} = -\left(\frac{\pi}{h}\right)^2[a_1(n-1)^2\sin\psi_1 + a_2 n^2\sin\psi_2 + a_3(n+1)^2\sin\psi_3] \ldots [2c]$$

$$\frac{d^4F}{dy^4} = \left(\frac{\pi}{h}\right)^4[a_1(n-1)^4\sin\psi_1 + a_2 n^4\sin\psi_2 + a_3(n+1)^4\sin\psi_3] \ldots [2d]$$

where

$$\psi_1 = (n-1)\pi\left(\frac{y-h_1}{h}\right), \quad \psi_2 = n\pi\left(\frac{y-h_1}{h}\right)$$

$$\psi_3 = (n+1)\pi\left(\frac{y-h_1}{h}\right), \quad n = 2, 3, 4, \ldots$$

The three points chosen for collocation are

$$\left(\frac{y-h_1}{h}\right) = \frac{1}{3}, \frac{1}{2}, \text{ and } \frac{2}{3}$$

on the y-axis. Values of $F(y)$ and its derivatives at these points are for $n = 2$ at

$$\left(\frac{y-h_1}{h}\right) = \frac{1}{3}$$

$$\left.\begin{aligned} F &= \frac{\sqrt{3}}{2}(a_1 + a_2) \\ \frac{y\,dF}{dy} &= \left(h_1 + \frac{h}{3}\right)\left(\frac{\pi}{h}\right)\left(\frac{a_1}{2} - a_2 - 3a_3\right) \\ \frac{y^2 d^2F}{dy^2} &= -\left(h_1 + \frac{h}{3}\right)^2\left(\frac{\pi}{h}\right)^2\frac{\sqrt{3}}{2}(a_1 + 4a_2) \\ \frac{y^4 d^4F}{dy^4} &= \left(h_1 + \frac{h}{3}\right)^4\left(\frac{\pi}{h}\right)^4\frac{\sqrt{3}}{2}(a_1 + 16a_2) \end{aligned}\right\} \ldots [3]$$

At $\left(\frac{y-h_1}{h}\right) = \frac{1}{2}$

$$\left.\begin{aligned} F &= (a_1 - a_2) \\ \frac{y\,dF}{dy} &= \left(h_1 + \frac{h}{2}\right)\frac{\pi}{h}(-2a_2) \\ \frac{y^2 d^2F}{dy^2} &= -\left(h_1 + \frac{h}{2}\right)^2\left(\frac{\pi}{h}\right)^2(a_1 - 9a_2) \\ \frac{y^4 d^4F}{dy^4} &= \left(h_1 + \frac{h}{3}\right)^4\left(\frac{\pi}{h}\right)^4\frac{\sqrt{3}}{2}(a_1 - 81a_2) \end{aligned}\right\} \ldots [4]$$

and at $\left(\frac{y-h_1}{h}\right) = \frac{2}{3}$

$$\left.\begin{aligned} F &= \frac{\sqrt{3}}{2}(a_1 - a_3) \\ \frac{y\,dF}{dy} &= \left(h_1 + \frac{2h}{3}\right)\left(\frac{\pi}{h}\right)\left(\frac{-a_1}{2} - a_2 + 3a_3\right) \\ \frac{y^2 d^2F}{dy^2} &= -\left(h_1 + \frac{2h}{3}\right)^2\left(\frac{\pi}{h}\right)^2\frac{\sqrt{3}}{2}(a_1 - 2a_2) \\ \frac{y^4 d^4F}{dy^4} &= \left(h_1 + \frac{2h}{3}\right)^4\left(\frac{\pi}{h}\right)^4\frac{\sqrt{3}}{2}(a_1 - 16a_2) \end{aligned}\right\} \ldots [5]$$

Similar expressions may be written for values of n other than 2.

From the expressions derived in the Appendix, one may write the following derivatives of w at $x = 0$

$$\left.\begin{aligned} \frac{\partial^4 w}{\partial x^4} &= F(y)\left(\frac{\rho}{y}\right)^4 \\ \frac{\partial^4 w}{\partial x^2 \partial y^2} &= \left[\frac{-6F}{y^2} + \frac{4}{y}\left(\frac{dF}{dy}\right) - \left(\frac{d^2F}{dy^2}\right)\right]\left(\frac{\rho}{y}\right)^2 \\ \frac{\partial^4 w}{\partial y^4} &= \frac{d^4F}{dy^4} \\ \frac{\partial^2 w}{\partial x^2} &= -F(y)\left(\frac{\rho}{y}\right)^2 \\ \frac{\partial^2 w}{\partial y^2} &= \frac{d^2F}{dy^2} \end{aligned}\right\} \ldots [6]$$

where

$$\frac{\rho}{y} = \frac{\pi k\cot\theta}{2y}$$

Buckling Criterion

The differential equation for the buckling of any constant-thickness flat plate under axial load is the well-known biharmonic equation

$$\frac{\partial^4 w}{\partial x^4} + 2\frac{\partial^4 w}{\partial x^2 \partial y^2} + \frac{\partial^4 w}{\partial y^4} + \frac{N_x}{D}\frac{\partial^2 w}{\partial x^2} + \frac{N_y}{D}\frac{\partial^2 w}{\partial y^2} = 0 \ldots [7]$$

N_x and N_y being assumed positive when causing compression.

In the present instance, use of equilibrium considerations leads to, see Fig. 2

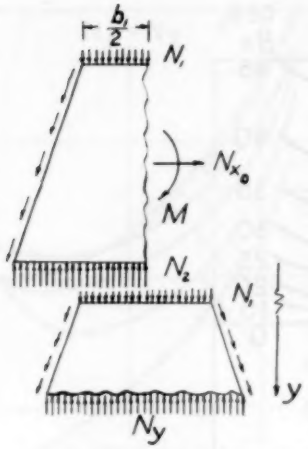

FIG. 2 EXPLODED VIEW OF PLATE

$$\left.\begin{aligned} N_y &= \left\{ r_1 \left[1 - \frac{(y-h_1)}{h} \right] N_1 + r_2 \frac{(y-h_1)}{h} N_2 \right\} \frac{\cot\theta}{(2y/h)} \\ N_x &= -(r_2 N_2 - r_1 N_1) \frac{\tan\theta}{2} - \frac{3}{2} r_1 r_2 (N_2 - N_1) \left[\frac{1}{2} - \frac{(y-h_1)}{h} \right] \end{aligned}\right\} \quad \ldots [8]$$

along the axis of collocation, i.e., the y-axis. Notice that there is no shear since this is an axis of symmetry.

Substitution of Equations [6] into Equation [7] results in

$$\left(\frac{y}{\rho}\right)^4 \frac{d^4F}{dy^4} - 2\left(y^2 \frac{d^2F}{dy^2} - 4y\frac{dF}{dy} + 6F\right)\left(\frac{1}{\rho^2}\right) + N_y \left(\frac{y}{\rho}\right)^2 \frac{1}{D}\left(\frac{y}{\rho}\right)^2 \frac{d^2F}{dy^2} - N_x \left(\frac{y}{\rho}\right)^2 \frac{F}{D} + F = 0 \quad \ldots [9]$$

The following set of three simultaneous equations is obtained by substituting Equations [8] and Equations [4] to [6], one at a time, into Equation [9] and collecting like terms:

At

$$\frac{(y-h_1)}{h} = \frac{1}{3}$$

$$\left.\begin{aligned} &\left\{ \frac{1}{2}\left[\left(\frac{p_1}{k}\right)^2 + 1\right]^2 + \frac{8\tan\theta}{\pi k^2}\left(\frac{p_1}{\sqrt{3}} - \frac{3\tan\theta}{\pi}\right)\right\} a_1 + \left\{ \frac{1}{2}\left[\left(\frac{2p_1}{k}\right)^2 + 1\right]^2 \right. \\ &\left. - \frac{8\tan\theta}{\pi k^2}\left(\frac{2p_1}{\sqrt{3}} + \frac{3\tan\theta}{\pi}\right)\right\} a_2 - \frac{48\, p_1 \tan\theta}{\sqrt{3}\,\pi k^2} a_3 \\ &- \left[r_1 N_1 \left(\frac{1}{3k^2} + \frac{p_1}{8p_1}\right) + r_2 N_2 \left(\frac{1}{6k^2} - \frac{r_2}{8p_1}\right)\right] \frac{p_1^2 h^2}{k^2 \pi^2 2D} a_1 - \left[r_1 N_1 \left(\frac{4}{3k^2} + \frac{p_4}{8p_1}\right) \right. \\ &\left. + r_2 N_2 \left(\frac{2}{3k^2} - \frac{r_2}{8p_1}\right)\right] \frac{p_1^2 h^2}{k^2 \pi^2 D} a_2 = 0 \end{aligned}\right\} \quad \ldots [10]$$

At

$$\frac{(y-h_1)}{h} = \frac{1}{2}$$

$$\left.\begin{aligned} &\left\{\left[\left(\frac{p_2}{k}\right)^2 + 1\right]^2 - \frac{48\tan^2\theta}{\pi 2k^2}\right\} a_1 - \left\{\left[\left(\frac{3p_2}{k}\right)^2 + 1\right]^2 - \frac{48\tan^2\theta}{\pi 2k^2}\right\} a_2 \\ &- \frac{32 p_2}{\pi k^2}\tan\theta\, a_3 - \left[r_1 N_1 \left(\frac{1}{2k^2} + \frac{\tan\theta}{2p_2}\right) + r_2 N_2 \left(\frac{1}{2k^2} - \frac{\tan\theta}{2p_2}\right)\right] \frac{p_2^2 h^2}{k^2\pi^2 D} a_1 \\ &+ \left[r_1 N_1 \left(\frac{9}{2k^2} + \frac{\tan\theta}{2p_2}\right) + r_2 N_2 \left(\frac{9}{2k^2} - \frac{\tan\theta}{2p_2}\right)\right] \frac{p_2^2 h^2}{k^2\pi^2 D} a_3 = 0 \end{aligned}\right\} \quad \ldots [11]$$

and at

$$\left(\frac{y-h_1}{h}\right) = \frac{2}{3}$$

$$\left.\begin{aligned} &\left\{\frac{1}{2}\left[\left(\frac{p_2}{k}\right)^2 + 1\right]^2 - \frac{8\tan\theta}{\pi k^2}\left(\frac{p_2}{\sqrt{3}} + \frac{3\tan\theta}{\pi}\right)\right\} a_1 - \left\{\frac{1}{2}\left[\left(\frac{2p_2}{k}\right)^2 + 1\right]^2 \right. \\ &\left. + \frac{8\tan\theta}{\pi k^2}\left(\frac{2p_2}{\sqrt{3}} - \frac{3\tan\theta}{\pi}\right)\right\} a_2 + \frac{48 p_2 \tan\theta}{\sqrt{3}\,\pi k^2} a_3 \\ &- \left[r_1 N_1 \left(\frac{1}{6k^2} - \frac{r_1}{8p_2}\right) + r_2 N_2 \left(\frac{1}{3k^2} + \frac{p_2}{8p_2}\right) \frac{p_2^2 h^2}{k^2 2D}\right] a_1 + \left[r_1 N_1 \left(\frac{2}{3k^2} - \frac{r_1}{8p_2}\right) \right. \\ &\left. + r_2 N_2 \left(\frac{4}{3k^2} + \frac{p_2}{8p_2}\right) \frac{p_2^2 h^2}{k^2 \pi^2 D}\right] a_2 = 0 \end{aligned}\right\} \quad \ldots [12]$$

where

$$p_1 = r_1 + \frac{2}{3}\tan\theta, \quad p_2 = r_1 + \frac{4}{3}\tan\theta, \quad p_3 = r_1 + \tan\theta = \frac{b}{h}$$

$$p_4 = r_2 + 2\tan\theta, \quad p_5 = r_1 - 2\tan\theta, \quad \text{and} \quad r_2 = r_1 + 2\tan\theta$$

Similar equations to Equations [10] to [12] may be written for values of n other than 2.

Equations [10] to [12] may be written in matrix form as

$$(A + \beta B)a = 0 \quad \ldots [13]$$

where

$$\beta = \frac{N_y h^2}{\pi^2 D}$$

if the buckling condition is based on N_x and h. This form corresponds to a standard eigenvalue problem in which β may be found by determining the characteristic equation and subsequently its lowest positive root or by any equivalent method. Notice that to be perfectly rigorous, both n and k should be varied in determining the lowest value of β.

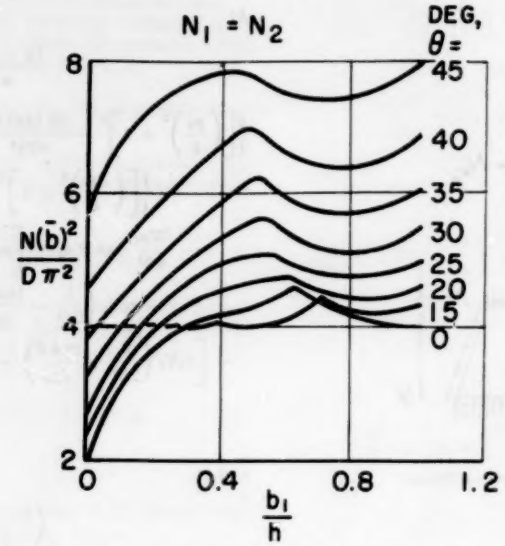

FIG. 3 BUCKLING LOAD VERSUS b_1/h FOR VARIOUS θ: $N_1 = N_2$

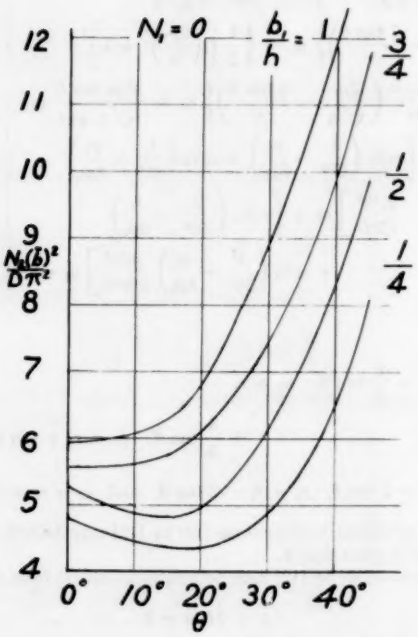

FIG. 4(a) BUCKLING LOAD VERSUS θ FOR VARIOUS b_1/h: $N_1 = 0$

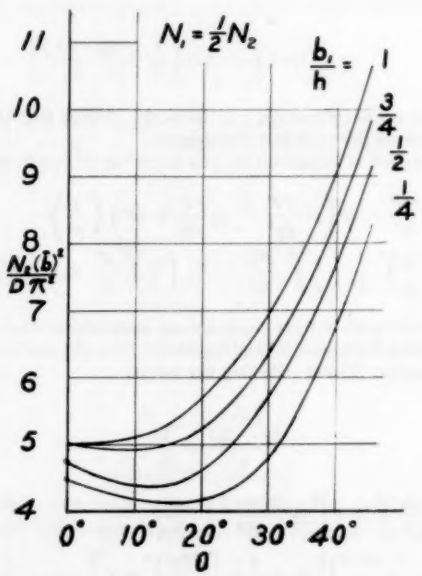

FIG. 4(b) BUCKLING LOAD VERSUS θ FOR VARIOUS b_1/h: $N_1 = {}^1/_2N_2$

CALCULATIONS AND RESULTS

As discernible from Equations [10] to [12] β is a function of the three basic parameters r_1, θ, and N_1/N_2. In order to allow enough variation for a comprehensive coverage, the calculations are carried out for the following multiplicity of combinations of the three parameters: $r_1 = 1$, 0.75, 0.5, 0.25, and 0, each for the angles; $\theta = 0°$, 15°, 30°, and 45°; and each for the loading conditions $N_1/N_2 = 0$, 0.5, 1.0, and 2.0.

Notice that two special cases included are the isosceles triangle obtained when $r_1 = 0$ but $\theta \neq 0$, and the rectangular plate obtained when $\theta = 0$.

The results of the calculations are plotted in Figs. 3 to 5. As seen, the buckling load is based on N_2 and $\bar{b}$. The term $\bar{b}$ is used instead of h in order to keep the values of β from becoming excessively large for small values of r_1, and to obtain values of β which are approximately equal for small values of θ. In Figs. 3 and 5,

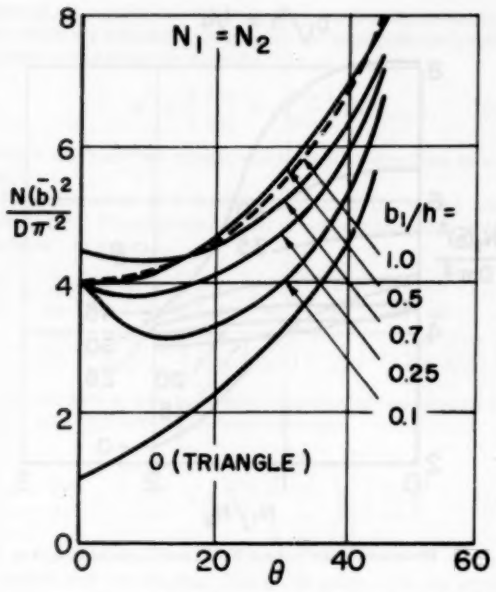

FIG. 4(c) BUCKLING LOAD VERSUS θ FOR VARIOUS b_1/h: $N_1 = N_2$

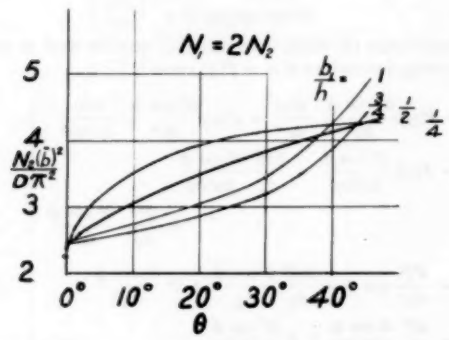

FIG. 4(d) BUCKLING LOAD VERSUS θ FOR VARIOUS b_1/h: $N_1 = 2N_2$

the curves labeled $\theta = 20°$, 25°, 35°, and 40° are obtained by cross-plotting the curves in Figs. 4(*a* to *d*). Curves similar to Fig. 3 and Figs. 4(*a* to *d*) can be drawn for any ratio of $N_1/N_2 > 0$ by cross-plotting the curves in Figs. 5(*a* to *d*), accordingly.

ACCURACY OF RESULTS

In the course of the calculations, it was found that in most cases omitting Equation [11] and setting $a_4 = 0$ had no perceptible effect upon β. Therefore it is concluded that the function $F(y)$ is sufficiently accurate. However, there is no simple way of testing the accuracy of the remaining part of w. In order to make such a test one would have to assume

$$w = \sum_n \sum_k a_{nk} \sin(\psi_n) \cos\left(\frac{k\pi}{2}\frac{x}{y}\cot\theta\right)$$

or some other complicated set of functions, and collocate off the y-axis. Furthermore, more careful satisfaction of the boundary conditions would be in order. The amount of work would be quite excessive compared to the slight gain of accuracy.

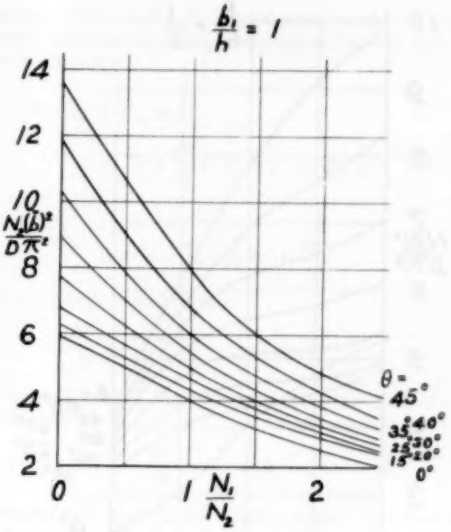

FIG. 5(a) BUCKLING LOAD VERSUS N_1/N_2 FOR VARIOUS θ: $b_1/h = 1$

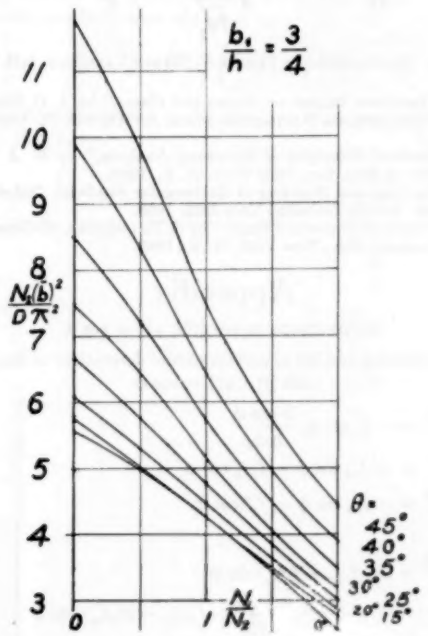

FIG. 5(b) BUCKLING LOAD VERSUS N_1/N_2 FOR VARIOUS θ: $b_1/h = 3/4$

In conclusion, it may be said that, from the nature of the shapes of the curves, it is believed that the present results are accurate enough for practical purposes although possibly not mathematically accurate at all points.

BIBLIOGRAPHY

1 "Approximations to Functions and to the Solution of Linear Differential Equations," by R. A. Fraser, W. P. Jones, and S. W. Skan, British Report and Memoranda No. 1799, 1937.

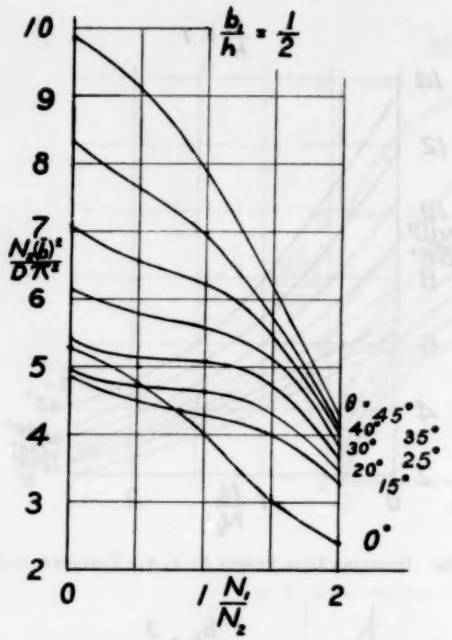

FIG. 5(c) BUCKLING LOAD VERSUS N_1/N_2 FOR VARIOUS θ: $b_1/h = 1/2$

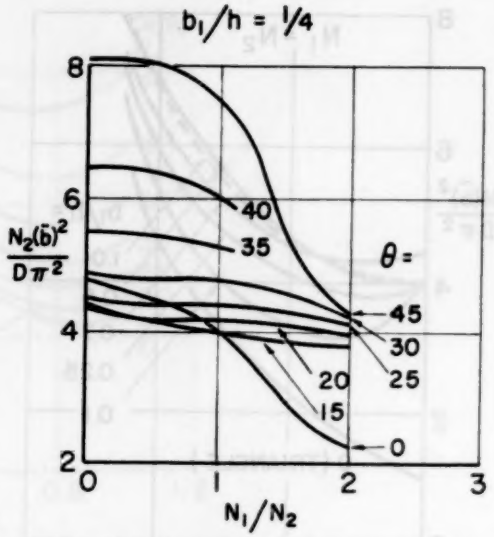

FIG. 5(d) BUCKLING LOAD VERSUS N_1/N_2 FOR VARIOUS θ: $b_1/h = 1/4$

2 "Transverse Impact on Beams and Plates," by A. C. Eringen, JOURNAL OF APPLIED MECHANICS, Trans. ASME, vol. 75, 1953, pp. 461–468.

3 "Minimal Principles of Structural Analysis," by N. J. Hoff, John Wiley & Sons, Inc., New York, N. Y., 1954.

4 "Bending and Buckling of Rectangular Sandwich Plates," by N. J. Hoff, NACA Technical Note 2225, 1950.

5 "Theory of Plates and Shells," by S. Timoshenko, McGraw-Hill Book Company, Inc., New York, N. Y., 1940.

Appendix

DERIVATIVES OF $\cos [f(x, y)] = \cos \phi$

The following is a list of certain partial derivatives of the function $\cos [f(x, y)] = \cos \phi$

$$\left.\begin{aligned}
\frac{\partial \cos\phi}{\partial x} &= -f_x \sin\phi, \quad \frac{\partial \cos\phi}{\partial x \partial y} \\
&= -f_{xy}\sin\phi - f_x f_y \cos\phi \\
\frac{\partial^2 \cos\phi}{\partial x^2} &= -f_{xx}\sin\phi - f_x^2 \cos\phi \\
\frac{\partial^3 \cos\phi}{\partial x^2 \partial y} &= (-f_{xxy} + f_x^2 f_y)\sin\phi \\
&\quad + (-f_{xx}f_y - 2f_x f_{xy})\cos\phi \\
\frac{\partial^3 \cos\phi}{\partial x^3} &= (-f_{xxx} + f_x^3)\sin\phi - 3f_x f_{xx}\cos\phi \\
\frac{\partial^4 \cos\phi}{\partial x^2 \partial y^2} &= (f_x^2 f_{yy} - f_{xxyy} + 4f_x f_y f_{xy} + f_y^2 f_{xx})\sin\phi \\
&\quad + (f_x^2 f_y^2 - 2f_{xy}^2 - f_{xx}f_{yy} - 2f_{xxy}f_y \\
&\quad - 2f_{yyx}f_x)\cos\phi \\
\frac{\partial^4 \cos\phi}{\partial x^4} &= (-f_{xxxx} + 6f_x^2 f_{xx})\sin\phi \\
&\quad + (f_x^4 - 4f_x f_{xxx} - 3f_{xx}^2)\cos\phi
\end{aligned}\right\} \quad \ldots [14]$$

Certain derivatives involving partials with respect to y may be obtained by replacing x by y in the foregoing equations.

DERIVATIVES OF w

Leibnitz's rule for chain differentiation may be used to write the following derivatives of $w = F(y)\cos\phi$

$$\left.\begin{aligned}
\frac{\partial^2 w}{\partial x^2} &= F(y)\frac{\partial^2 \cos\phi}{\partial x^2}, \quad \frac{\partial^4 w}{\partial x^4} = F(y)\frac{\partial^4 \cos\phi}{\partial x^4}, \quad \frac{\partial^4 w}{\partial x^2 \partial y^2} \\
&= F(y)\frac{\partial^4 \cos\phi}{\partial x^2 \partial y^2} + \frac{2dF}{dy}\frac{\partial^3 \cos\phi}{\partial x^2 \partial y} \\
&\quad + \frac{d^2F}{dy^2}\frac{\partial^2 \cos\phi}{\partial x^2} \\
\frac{\partial^2 w}{\partial y^2} &= \frac{d^2F}{dy^2}\cos\phi + \frac{2dF}{dy}\frac{\partial \cos\phi}{\partial y} + F\frac{\partial^2 \cos\phi}{\partial y^2} \\
\frac{\partial^2 w}{\partial x \partial y} &= \frac{dF}{dy}\frac{\partial \cos\phi}{\partial x} + F\frac{\partial^2 \cos\phi}{\partial x \partial y} \\
\frac{\partial^4 w}{\partial y^4} &= \frac{d^4F}{dy^4}\cos\phi + \frac{4d^3F}{dy^3}\frac{\partial \cos\phi}{\partial y} + \frac{6d^2F}{dy^2}\frac{\partial^2 \cos\phi}{\partial y^2} \\
&\quad + \frac{4dF}{dy}\frac{\partial^3 \cos\phi}{\partial y^3} + F\frac{\partial^4 \cos\phi}{\partial y^4}
\end{aligned}\right\} \quad \ldots [15]$$

In the present instance

$$f = \frac{\pi k \cot\theta}{2}\frac{x}{y} = \frac{\rho x}{y}$$

The only derivatives of f which do not vanish at $x = 0$, the axis of collocation, are

$$f_x = \frac{\rho}{y}, \quad f_{xy} = \frac{-\rho}{y^2}, \quad \text{and} \quad f_{xyy} = \frac{2\rho}{y^3}$$

Furthermore, $\sin\phi = 0$ at $x = 0$. Equations [6] can now be derived by direct substitution.

BOUNDARY CONDITIONS

It is seen directly that the assumed function for w satisfies exactly deflection boundary conditions along all edges of the plate.

However, as regards moment boundary conditions, further considerations are necessary. In general, one may write the bending moment acting along the edge of a plate as

$$M = \left(\frac{\partial^2 w}{\partial n^2} + \nu \frac{\partial^2 w}{\partial t^2}\right) D \quad \ldots\ldots\ldots\ldots [16]$$

where n and t are the normal and tangential directions at any point.

If the boundary is a straight edge, then the second term vanishes (5). Therefore there is left to consider the value of the first term. In general

$$\frac{\partial^2 w}{\partial n^2} = \frac{\partial}{\partial n}\left(\frac{\partial w}{\partial n}\right) = \frac{\partial}{\partial y}\left(\frac{\partial w}{\partial n}\right)\frac{\partial y}{\partial n} + \frac{\partial}{\partial x}\left(\frac{\partial w}{\partial n}\right)\frac{\partial x}{\partial n}$$
$$= \frac{\partial^2 w}{\partial y^2}\left(\frac{\partial y}{\partial n}\right)^2 + 2\frac{\partial^2 w}{\partial x \partial y}\left(\frac{\partial x}{\partial n}\right)\left(\frac{\partial y}{\partial n}\right) + \frac{\partial^2 w}{\partial x^2}\left(\frac{\partial x}{\partial n}\right)^2$$

The last term is seen to be zero since $\partial^2 w/\partial x^2$ vanishes on all edges. Also $(\partial y/\partial n)^2$ can be factored to give

$$\frac{\partial^2 w}{\partial n^2} = \left[\frac{\partial^2 w}{\partial y^2} + 2\frac{\partial^2 w}{\partial x \partial y}\left(\frac{\frac{\partial x}{\partial n}}{\frac{\partial y}{\partial n}}\right)\right]\left(\frac{\partial y}{\partial n}\right)^2 \quad \ldots\ldots [17]$$

Consider now the sloping edges of the plate. For the upper edge (taken according to Fig. 1)

$$\frac{\left(\frac{\partial x}{\partial n}\right)}{\left(\frac{\partial y}{\partial n}\right)} = -\frac{\cos\theta}{\sin\theta} = -\cot\theta$$

Substitution of this result and the expressions for the two derivative terms, calculated according to Equations [14] and [15], into Equation [17] yields

$$\frac{\partial^2 w}{\partial n^2} = [F(-f_{yy} + 2f_{xy}\cot\theta) + 2\frac{dF}{dy}(-f_y + f_x\cot\theta)]\sin\left(\frac{k\pi}{2}\right)\sin^2\theta$$

where

$$f_y = -\frac{\rho x}{y^2}, \text{ and } f_{yy} = \frac{2\rho x}{y^3}$$

Further simplification finally yields

$$\frac{M}{D} = \frac{\pi k}{y}\left(\frac{dF}{dy} - \frac{F}{y}\right)\sin\left(\frac{k\pi}{2}\right) \quad \ldots\ldots\ldots [18]$$

According to this result, the moment vanishes along the sloping edges wherever

$$\frac{dF}{dy} - \frac{F}{y} = 0$$

To determine such a point, one draws a tangent line from the origin of co-ordinates to the deflection curve for $x = 0$. Notice that this point usually lies near the region of maximum deflection.

Lastly consider the moments along the parallel edges. From the previous considerations, the result is

$$\frac{M}{D} = -2\left(\frac{\rho}{y}\right)\left(\frac{x}{y}\right)\sin\left(\frac{\rho x}{y}\right) \quad \ldots\ldots\ldots [19]$$

It is seen that the moment vanishes at $x = 0$ and remains fairly small in that region.

Creep Stresses and Deflections of Columns

By T. H. LIN[1]

A direct method (no iteration is involved) of calculating stresses and deflection of a pin-ended column with creep is shown. The relaxation moment in a particular time interval is treated as an additional initial curvature of the column. This method is applicable to stress-strain-time relationship obtained directly from test data without the necessity of making restrictive assumptions. An illustrative example is shown and the results are compared to those obtained by iteration method (10)[2] and test data. Stress distributions across different sections at different instants are shown. The stress distribution at mid-section deviates considerably from being linear as the creep deflection becomes large.

Nomenclature

The following nomenclature is used in the paper:

A = area, constant
B = constant
b = width of section
a_n, b_n = Fourier constants
e = base of natural logarithm, total strain (compressive strain is taken to be positive)
E = Young's modulus of elasticity
h = depth of section
K = constant, curvature
L = length of column
M = bending moment
P = thrust
t = time
x = distance along line joining hinged ends of column
y_0 = initial deflection
y = deflection
ϵ = creep strain (compressive strain is taken as positive)
η = distance from neutral axis
σ = stress (compressive stress is taken as positive)
Δ = denotes incremental value

Subscript 0 denotes neutral axis of geometrical section.

Introduction

Recent increase in the use of structures under elevated temperatures has made the creep problem increasingly important. Rational design of columns with creep is not only of theoretical interest but also of practical need. A number of studies have been made for columns with viscoelasticity in the past few years. For linearly viscoelastic columns, Rosenthal and Baer (1) in 1951 showed the analysis of column deflection involving only transient creep. Hilton (2) in 1951 showed the creep collapse of viscoelastic columns with initial curvature. Lin (3) in 1953 applied Laplace transformation to simplify the calculation of viscoelastic columns of rectangular cross section.

It has been shown that the stress-strain-time relationship of aluminum alloy 75S-T and Nimonic alloy 75 under elevated temperatures at constant stress can be quite closely represented by mechanical models (3). Columns with small initial curvature have nearly constant stress before the deflection is excessive. Hence the viscoelastic column should give a first approximation to the actual column with small deflection. The use of linearly viscoelastic analysis for a metal column is closer to the actual case than for metal beams because the variation of stress across the section of a beam is far more than that in a column. However, the error involved in the assumption of linear viscoelasticity, in certain cases, may be considerable. The linear viscosity represents only a special case of general inelastic behavior and does not reproduce closely the creep characteristics of real materials (4).

In order to represent the nonlinear behavior of the actual materials, Kempner (5) in 1954 showed the analysis of creep buckling of columns with nonlinear viscoelasticity. To reduce the complexity of the equations, Kempner analyzed the column with H-section and assumed that the original shape of the structure was maintained at all times. This assumption necessarily will introduce error, as the actual column deflection with initial sinusoidal curvature may deviate from the sine curve. His analysis will be more lengthy for columns of rectangular sections.

Other simplified stress-strain-time relationships have been used in the study of creep in columns. In 1947 Marin (6) showed an analysis involving only the minimum rate of creep, neglecting the elastic strain and the transient creep. This analysis is only valid where the transient creep and elastic strain are negligible.

Libove, in 1952 and 1953, showed the analyses of columns of H-section (7) and columns of rectangular sections (8) with initial curvature. The stress-strain-time relationship of the material was represented by the equation (9)

$$e = \sigma/E + Ae^{B\sigma}t^k$$

Shanley's engineering hypothesis of creep (10) was assumed. This hypothesis assumes mainly that the strain rate under constant stress is a function only of the stress and the strain and not of the path of attaining this stress and strain. Libove used the simplifying assumption that the deflected shape remains at all times sinusoidal. This introduces error, as the equilibrium condition is not satisfied at all sections of the column.

Higgins (11) showed a more realistic approach by analyzing the creep deflection of columns with iteration method. He used the same stress-strain-time relationship and Shanley's engineering hypothesis as Libove. Higgins' analysis satisfies the equilibrium and compatibility conditions at all sections. Although the particular stress-strain-time relationship used does not involve the recovery effect (12) of the material, yet the iteration method given can be applied to other stress-strain-time relationships. The iteration method to satisfy the equilibrium conditions and the stress-strain-time relationships is necessarily lengthy. An IBM card-program calculator with a floating decimal setup was used.

The foregoing shows briefly previous work done in this field.

[1] Professor of Aeronautical Engineering, University of Detroit, and Visiting Professor of University of California at Los Angeles.

[2] Numbers in parentheses refer to the Bibliography at the end of the paper.

Contributed by the Applied Mechanics Division and presented at the Diamond Jubilee Annual Meeting, Chicago, Ill., November 13–18, 1955, of The American Society of Mechanical Engineers.

Discussion of this paper should be addressed to the Secretary, ASME, 29 West 39th Street, New York, N. Y., and will be accepted until July 10, 1956, for publication at a later date. Discussion received after the closing date will be returned.

Note: Statements and opinions advanced in papers are to be understood as individual expressions of their authors and not those of the Society. Manuscript received by ASME Applied Mechanics Division, January 24, 1955. Paper No. 55—A–43.

The present paper gives a direct method of calculating the stresses and deflections with the equilibrium and compatibility conditions satisfied at all sections.

Mathematical Analysis

The uniaxial strain rate under uniaxial stress at elevated temperature is a function of the stress, time, and total creep strain, and the history of loading. After following a stress-time curve, the material, at some condition of stress and strain, will have a strain rate under constant stress. If the material is given an instantaneous change in stress $\Delta\sigma$, the instantaneous strain increment $\Delta\epsilon$ will be $\Delta\sigma/E$, where E is the elastic modulus of the material at the particular temperature (13). For the following analysis, the smooth stress-time curve of different fibers of the column is represented by infinitesimal steps. Each step consists of a constant stress period of time dt followed by an instantaneous increment of stress $d\sigma$, Fig. 1 (7).

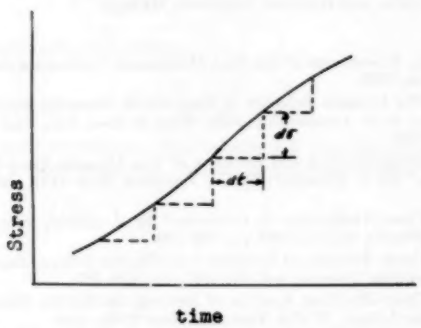

Fig. 1 Approximation of a Smooth Stress History by a Series of Infinitesimal Steps

With the rate of strain under constant stress denoted by φ

$$de = \varphi dt + \frac{d\sigma}{E} \quad [1]$$

$$\sigma = E(e - \epsilon)$$

$$\Delta\sigma = E(\Delta e - \Delta\epsilon) \quad [2]$$

Instead of considering the equilibrium conditions for the total load and total moment at each section, the equilibrium conditions for the incremental load and moment are considered

$$\Delta P = \int \Delta\sigma dA = E\int(\Delta e - \Delta\epsilon)dA \quad [3]$$

$$\Delta M = \int \Delta\sigma\eta dA = E\int(\Delta e - \Delta\epsilon)\eta dA \quad [4]$$

With the condition that plane before loading remains plane during loading

$$e = e_0 + K\eta$$

$$\Delta e = \Delta e_0 + \Delta K\eta \quad [5]$$

For column under constant load P

$$\Delta P = 0$$

$$\int(\Delta e - \Delta\epsilon)dA = \int(\Delta e_0 + \eta\Delta K - \Delta\epsilon)dA = 0$$

$$\Delta e_0 A + \Delta K\int\eta dA = \int\Delta\epsilon dA$$

Let η be zero at the geometrical neutral axis of the section

$$\int\eta dA = 0 \quad [6]$$

$$\Delta e_0 A = \int\Delta\epsilon dA \quad [7]$$

$$\Delta M = E\int[(\Delta e_0 + \eta\Delta K) - \Delta\epsilon]\eta dA = EI\Delta K - E\int\Delta\epsilon\eta dA \quad [8]$$

$$M = -P(y + y_0) \quad [9]$$

$$\Delta M = -P\Delta y \quad [10]$$

The curvature is assumed to be small

$$\Delta K = \frac{d^2\Delta y}{dx^2} \quad [11]$$

From Equations [8], [10], and [11]

$$-P\Delta y = EI\frac{d^2\Delta y}{dx^2} - E\int\Delta\epsilon\eta dA \quad [12]$$

where the term on the left-hand side is the external moment increment, and the terms on the right-hand side are the incremental moment due to incremental curvature and the relaxation moment due to creep in a given-time interval Δt

$$\frac{d^2\Delta y}{dx^2} + \frac{P}{EI}\Delta y = \frac{1}{I}\int\Delta\epsilon\eta dA \quad [13]$$

$\Delta\epsilon$ varies from one section to another. Hence the right-hand term is a function of x. Rewriting Equation [13]

$$\frac{d^2\Delta y}{dx^2} + \frac{P}{EI}\Delta y = \frac{-P}{EI}\left[\frac{-E}{P}\int\Delta\epsilon\eta dA\right] \quad [14]$$

This equation is analogous to the equation for elastic columns with initial curvature (14, 15) and can be readily solved. For elastic columns

$$\frac{d^2y}{dx^2} + \frac{P}{EI}y = \frac{-P}{EI}y_0 \quad [15]$$

where y_0 is the initial curvature.

Comparing Equation [14] with Equation [15], the bracket term is equivalent to initial deflection in elastic columns.

Let

$$\left[\frac{-E}{D}\int\Delta\epsilon\eta dA\right]$$

be represented by Fourier series

$$\Sigma\Delta a_n \sin\frac{n\pi x}{L} \quad [16]$$

and

$$\Delta y = \Sigma\Delta b_n \sin\frac{n\pi x}{L} \quad [17]$$

It has been shown in [14] that

$$\Delta b_n = \frac{\Delta a_n}{\frac{P_{cr_n}}{P} - 1}$$

where

$$P_{cr_n} = \frac{n^2\pi^2 EI}{L^2} \quad [18]$$

From Equations [17], [18], and [11], ΔK is obtained. From Equations [7] and [5] Δe at different parts in the column can be calculated.

In the calculation of deflection-time curve of the column, the initial stress distributions at different sections are calculated as for elastic columns with initial curvature (15). From the stress-strain-time relationship of the material at the particular tem-

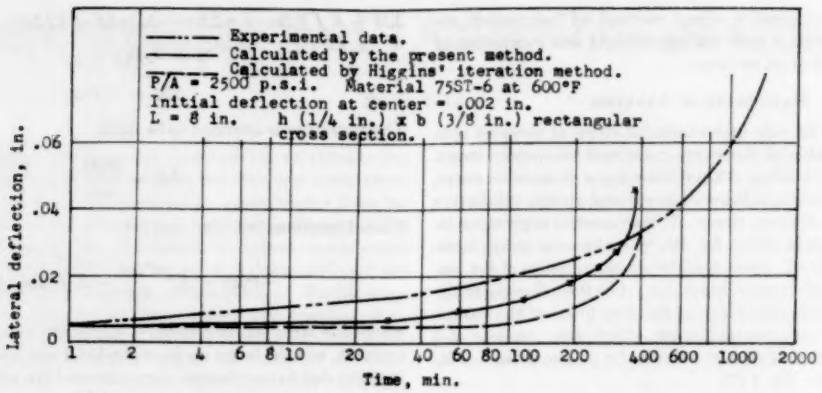
Experimental data.
Calculated by the present method.
Calculated by Higgins' iteration method.
P/A = 2500 p.s.i. Material 75ST-6 at 600°F
Initial deflection at center = .002 in.
L = 8 in. h (1/4 in.) x b (3/8 in.) rectangular cross section.
Lateral deflection, in.
.06
.04
.02
0
1 2 4 6 8 10 20 40 60 80 100 200 400 600 1000 2000
Time, min.

FIG. 2 COMPARISON OF PRESENT METHOD, EXPERIMENTAL DATA, AND HIGGINS' ITERATION METHOD

perature, $\Delta\epsilon$'s for the first time interval are calculated at different points on different sections. The more points and sections used, the more accurate will be the results. Suitable numbers of points and sections can be chosen for the desirable degree of accuracy. Then $\int \Delta\epsilon dA$ and $\int \Delta\epsilon\eta dA$ for different sections are obtained by graphical integration. The Fourier coefficients Δa_n of

$$\left[\frac{-E}{P}\int \Delta\epsilon\eta dA\right]$$

versus x-curve are calculated by harmonic analysis. Then Δb_n and Δy are obtained by Equations [17] and [18]. ΔK's are found by Equation [11] and $\Delta\epsilon$'s at different points are calculated by Equations [5] and [7].

The total strain minus the creep strain gives the elastic strain and hence the stress at the particular point. With the stress and the history of the stress-strain-time path known, the incremental creep strain $\Delta\epsilon$ for the next time interval can be obtained either empirically by stressing the material following the same stress-time history, or by using some stress-strain-time relationship. With $\Delta\epsilon$ known, the process is repeated. By repeating the same process for successive time intervals the stress distribution and deflections of the column at different sections at different instants can be calculated.

The detailed procedure is shown in an illustrative example in the Appendix. The result is shown in Fig. 2 and seems to check well with Higgins' iteration method. The stress distributions at the center section at different instants are shown in Fig. 3; it is seen that the distribution deviates considerably from being linear as the deflection grows. This method is much shorter and no iteration is involved. With the deflection-time curve of the column known, the life of the column can be determined.

ACKNOWLEDGMENT

The author wishes to express his thanks to the Engineering Research Council and the University Research Committee, University of Detroit, for providing time and assistance in preparation of this paper.

BIBLIOGRAPHY

1 "An Elementary Theory of Creep Buckling of Columns," by D. Rosenthal and H. W. Baer, Proceedings of the First U. S. Congress of Applied Mechanics, June, 1951.

2 "Creep Collapse of Visco-Elastic Columns With Initial Curvature," by H. H. Hilton, *Journal of the Aeronautical Sciences*, vol. 19, 1952, pp. 844–846.

3 "Stresses in Columns With Time-Dependent Elasticity," by T. H. Lin, Proceedings of the First Midwestern Conference on Solid Mechanics, 1953.

4 "The Inelastic Behavior of Engineering Materials and Structures," by A. M. Freudenthal, John Wiley & Sons, Inc., New York, N. Y., 1950.

5 "Creep Bending and Buckling of Non-Linearly Visco-Elastic Columns," by J. Kempner, NACA Technical Note 3137, January, 1954.

6 "Creep Deflections in Columns," by J. Marin, *Journal of Applied Physics*, vol. 18, 1947, pp. 103–109.

7 "Creep Buckling of Columns," by Charles Libove, *Journal of the Aeronautical Sciences*, vol. 19, 1952, pp. 459–467.

8 "Creep Buckling Analysis of Rectangular-Section Columns," by Charles Libove, NACA Technical Note 2956, 1953.

9 "Weight-Strength Analysis of Aircraft Structures," by F. R. Shanley, McGraw-Hill Book Company, Inc., New York, N. Y., 1952.

10 "Analysis of Stress-Strain-Time Relations From the Engineering Viewpoint," by F. R. Shanley, Pty No. P-68, The Rand Corporation, March 4, 1949.

11 "Effect of Creep on Column Deflection," by T. P. Higgins, Jr., Preprint No. 385, Institute of the Aeronautical Sciences, 1952.

12 "The Creep Deflections of Beams and Columns," by Y. H. Pao and J. Marin, Preprint No. 406, Institute of the Aeronautical Sciences, 1953.

13 "Bending of Beams With Creep," by E. P. Popov, *Journal of Applied Physics*, vol. 20, 1949, pp. 251–256.

14 "On the Analysis of Experimental Observations in Problems of Elastic Stability," by R. V. Southwell, Proceedings of the Royal Society of London, series A, vol. 135, 1932, pp. 601–616.

15 "Inelastic Column Buckling," by T. H. Lin, *Journal of the Aeronautical Sciences*, vol. 17, 1950, pp. 159–172.

Appendix

A column with the same material and dimensions as calculated by Higgins (11) is analyzed in order to compare the results with those obtained by Higgins. The column is made of aluminum alloy 75S-T6 at 600 F with the following dimensions

Column length, $L = 8$ in. (pin ended)
Depth, $h = 1/4$ in.
Width, $b = 3/8$ in.

Initial curvature is taken as single sine curve with an amplitude of 0.002 in.

$$y_0 = 0.002 \sin \frac{\pi x}{L}$$

$$P_{cr} = \frac{\pi^2 EI}{L^2}$$

$$I = \frac{1}{12} bh^3$$

$$E = 5.2 \times 10^6 \text{ psi at } 600 \text{ F (10)}$$

$$F_{cr} = \frac{P_{cr}}{bh} = \frac{\pi^2 \times 5.2 \times 10^6 \times \frac{1}{12}\left(\frac{1}{4}\right)^3}{8^2} = 4170 \text{ psi}$$

The compressive stress on the column $f_c = 2500$ psi.

This initial deflection is magnified (14, 15) under load at zero time to

$$b_1 = \frac{0.002}{1 - \frac{2500}{4170}} = 0.005 \text{ in.}$$

$$f = \frac{P}{A} \pm \frac{(Py)\eta}{I} = \frac{P}{A}\left(1 \pm \frac{y\eta}{\rho^2}\right)$$

where ρ is radius of gyration

$$\rho^2 = \frac{1}{12}\left(\frac{1}{4}\right)^2 = \frac{1}{192}$$

The same stress-strain-time relationship and Shanley's engineering hypothesis as that used by Higgins and Libove is used here. Taking a time interval of $^1/_2$ hr, with constant stress within this interval, the creep strain $\Delta\epsilon$ at $\eta = 0, \pm h/4$, and $\pm h/2$ on three sections $x = L/6$, $L/3$, and $L/2$ are calculated; then $\int \Delta\epsilon dA$ and $\int \Delta\epsilon\eta dA$ were obtained. Obviously, these integrals can be more accurately determined by calculating more points on the section. Then

$$\left[\frac{-E}{p} \int \Delta\epsilon\eta dA\right]$$

for these sections were found. Using three terms in Fourier series, from Equations [16] and [18], Δa_1, Δa_2, and Δa_3, and hence Δb_1 to Δb_3 were calculated. Then ΔK and Δe are found at three sections. From Δe and $\Delta\epsilon$, the stress increments at these sections were readily calculated. With the stresses at the sections known, the process is repeated. These calculations are summarized in Table 1 and plotted in Figs. 2 and 3.

The discrepancy between the calculated and test results, Fig. 2, is mainly caused by (*a*) the error involved in the stress-strain-time relationship of the material owing to some range of scatter of test data (9); (*b*) the error in the determination of the amplitude of the first harmonic of the initial curvature of the column, and (*c*) the error in evaluating the first harmonic of the relaxation moments at different time intervals. Owing to the unavoidable imperfection of the material, the geometrical shape of the column does not give the total effective initial curvature, which deter-

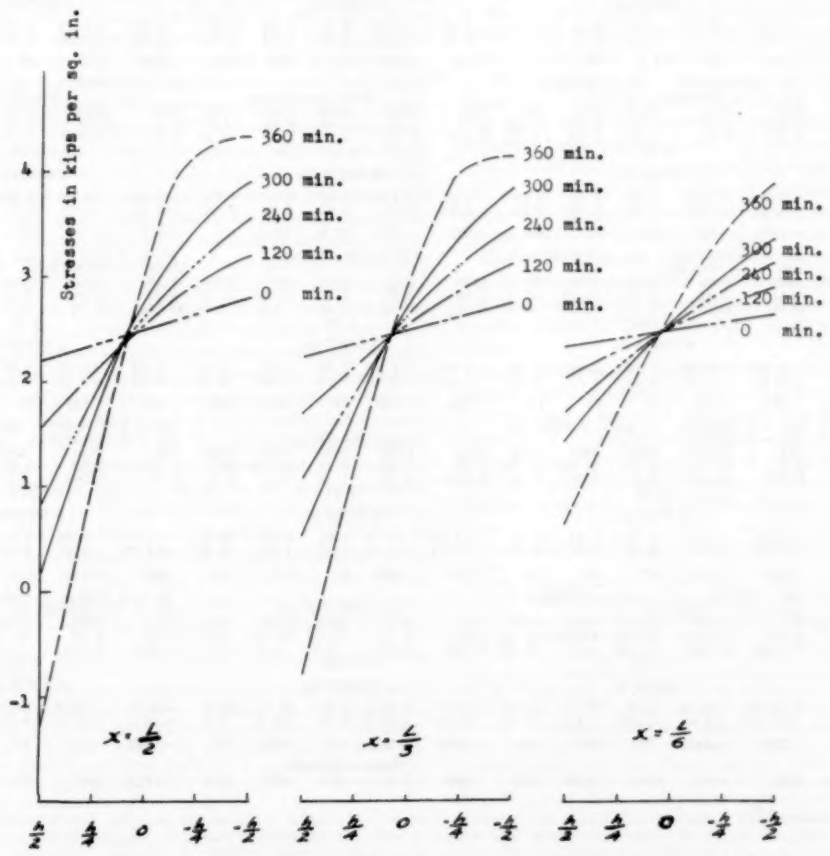

FIG. 3 STRESS DISTRIBUTION AT DIFFERENT INSTANTS

mines the deflection-time relation of the column. This effective initial curvature in terms of different harmonics can be obtained from load-deflection tests as given by Southwell (14). This will reduce the second error. The third error can be easily reduced by either including more terms in the sine series or by using a harmonic analyzer.

TABLE 1 CALCULATION OF CREEP STRESSES AND DEFLECTIONS OF A 758-T6 COLUMN AT 600 F

	$x = \frac{L}{6}$						$x = \frac{L}{3}$						$x = \frac{L}{2}$					
	$\eta = \frac{h}{2}$	$\eta = \frac{h}{4}$	$\eta = 0$	$\eta = \frac{-h}{4}$	$\eta = \frac{-h}{2}$		$\eta = \frac{h}{2}$	$\eta = \frac{h}{4}$	$\eta = 0$	$\eta = \frac{-h}{4}$	$\eta = \frac{-h}{2}$		$\eta = \frac{h}{2}$	$\eta = \frac{h}{4}$	$\eta = 0$	$\eta = \frac{-h}{4}$	$\eta = \frac{-h}{2}$	
	$\Delta a_1 = 0.001543$ in. $\Delta a_2 = 0.0000156$ in. $\Delta a_3 = -0.0000046$ in.						Time 0–30 min						$\Delta b_1 = 0.0023$ in. $\Delta b_2 = 0.0000011$ in. $\Delta b_3 = -0.0000011133$ in. $\delta_{30} = 0.0074$ in.					
(1.1) σ	2350	2425	2500	2575	2650	2240	2370	2500	2630	2760			2200	2350	2500	2650	2800	
(1.2) $\Delta\epsilon \times 10^6$	2.18	2.52	2.90	3.36	3.86	1.75	2.27	2.90	3.72	4.77			1.63	2.17	2.90	3.87	5.16	
(1.3) $\Delta\gamma \times 10^6$			2.955					3.04							3.05			
(1.4) $-\frac{E}{P}\int \eta\Delta\epsilon dA$			0.00063 in.					0.00120 in.							0.00132 in.			
(1.5) $\Delta\epsilon \times 10^6$ [a]	0.71	1.82	2.955	4.04	5.17	−0.80	1.12	3.04	5.00	6.92			1.38	0.76	3.05	5.30	7.48	
(1.6) (1.5) − (1.4)	−1.47	−0.70	0.055	0.68	1.31	−2.55	−1.05	0.14	1.28	2.15			−3.01	−1.41	0.15	1.43	2.32	
(1.7) $\frac{E(1.6)}{10^5}$	−76.5	−36.5	2.9	35.4	68	−132.5	−54.6	7.3	66.6	112			−1565	−73.3	7.8	74.4	120.6	
	$\Delta a_1 = 0.001646$ in. $\Delta a_2 = 0.0000065$ in. $\Delta a_3 = 0.0000845$ in.						Time 30–60 min						$\Delta b_1 = 0.00245$ in. $\Delta b_2 = 0$ $\Delta b_3 = 0.0000208$ in. $\delta_{60} = 0.00975$ in.					
(2.1) σ = (1.1) + (1.7)	2274	2389	2505	2610	2718	2107	2315	2507	2697	2872			2043	2277	2508	2724	2921	
(2.2) $\Sigma\epsilon \times 10^6$	2.18	2.52	2.90	3.36	3.86	1.75	2.27	2.90	3.72	4.77			1.63	2.17	2.90	3.87	5.16	
(2.3) $\Delta\epsilon \times 10^6$	1.00	1.26	1.70	2.18	2.85	0.62	1.09	1.70	2.60	3.74			0.50	1.00	1.70	2.96	4.42	
(2.4) $\Delta\epsilon_0 \times 10^6$			1.77					1.87							3.035			
(2.5) $-\frac{E}{P}\int \eta\Delta\epsilon dA$			0.00087 in.					0.00135 in.							0.00173 in.			
(2.6) $\Delta\epsilon \times 10^6$	−0.64	0.565	1.77	2.975	4.18	−2.31	−0.21	1.87	3.96	6.05			−2.785	−0.375	2.035	4.445	6.855	
(2.7) (2.6) − (2.3)	−1.64	−0.695	0.07	0.795	1.33	−2.93	−1.30	0.17	1.36	2.31			−3.285	−1.375	0.335	1.485	2.435	
(2.8) $\frac{E(2.7)}{10^5}$	−85.3	−36.3	3.6	41.3	69.2	−152	−67.6	8.8	70.7	120			−171	−71.5	17.4	77.2	126.4	
	$\Delta a_1 = 0.00274$ in. $\Delta a_2 = -0.000125$ in. $\Delta a_3 = -0.000073$ in.						Time 60–120 min						$\Delta b_1 = 0.0041$ in. $\Delta b_2 = -0.00000781$ in $\Delta b_3 = -0.00000084$ in. $\delta = 0.01385$ in					
(3.1) σ = (2.1) + (2.8)	2189	2353	2507	2651	2787	1955	2247	2516	2768	2992			1872	2206	2525	2801	3047	
(3.2) $\Sigma\epsilon \times 10^6$	3.18	3.78	4.60	5.54	6.71	2.37	3.36	4.60	6.32	8.51			2.13	3.17	4.60	6.83	9.58	
(3.3) $\Delta\epsilon \times 10^6$	0.74	1.20	1.76	2.62	3.61	0.50	0.90	1.84	3.66	6.4			0.28	0.80	1.85	3.58	6.88	
(3.4) $\Delta\epsilon_0 \times 10^6$			1.91					2.45							2.37			
(3.5) $-\frac{E}{P}\int \eta\epsilon dA$			0.00145 in.					0.00244 in.							0.00254 in.			
(3.6) $\Delta\epsilon \times 10^6$	−2.00	−0.04	1.91	3.86	5.82	−4.33	−0.94	2.45	5.84	9.24			−5.44	−1.53	2.37	6.27	10.18	
(3.7) (3.6) − (3.3)	−2.74	−1.24	0.15	1.24	2.21	−4.73	−1.84	0.61	7.18	2.84			−5.72	−2.33	0.52	2.69	3.30	
(3.8) $\frac{E(3.7)}{10^5}$	−142	−64	7.8	65	115	−246	−96	32	113	147			−297	−122	27	240	172	
	$\Delta a_1 = 0.00286$ in. $\Delta a_2 = 0.000200$ in. $\Delta a_3 = -0.000095$ in.						Time 120–180 min						$\Delta b_1 = 0.00427$ in. $\Delta b_2 = 0.0000143$ in. $\Delta b_3 = -0.0000048$ in. $\delta_{180} = .01813$					
(4.1) (3.1) + (3.8)	2047	2289	2515	2715	2902	1709	2151	2548	2881	3139			1569	2084	2552	2941	3219	
(4.2) $\Sigma\epsilon \times 10^6$	3.92	4.98	6.36	8.16	10.32	2.77	4.26	6.44	9.98	14.91			2.41	3.97	6.45	1041	16.46	
(4.3) $\Delta\epsilon \times 10^6$	0.39	0.64	1.27	2.10	3.35	0.13	0.48	1.42	3.40	6.30			0.10	0.36	1.57	4.09	7.40	
(4.4) $\Delta\epsilon_0 \times 10^6$			1.46					2.05							2.36			
(4.5) $-\frac{E}{P}\int \eta\Delta\epsilon dA$			0.00122 in.					0.00250 in.							0.00304 in.			
(4.6) $\Delta\epsilon \times 10^6$	−2.66	−0.60	1.46	3.52	5.58	−5.08	−1.52	2.05	5.62	9.18			−5.88	−1.76	2.36	6.48	10.60	
(4.7) (4.6) − (4.3)	−3.05	−1.24	0.19	1.42	2.23	−5.21	2.00	0.63	2.22	2.88			−5.98	−2.12	0.79	2.39	3.20	
(4.8) $\frac{E(4.7)}{10^5}$	−159	−645	9.9	74	116	−271	−104	32.8	115	150			−311	−110	41.1	124	166	
	$\Delta a_1 = 0.00352$ in. $\Delta a_2 = 0.000052$ in. $\Delta a_3 = -0.000143$ in.						Time 180–240 min						$\Delta b_1 = 0.00525$ in. $\Delta b_2 = 0.00000372$ in. $\Delta b_3 = -0.00000352$ in. $\delta_{240} = 0.02338$ in.					
(5.1) σ = (4.1) + (4.8)	1888	2225	2525	2789	3018	1438	2047	2581	2996	3280			1258	1974	2593	3065	3385	
(5.2) $\Sigma\epsilon \times 10^6$	4.41	5.62	7.63	10.26	13.67	2.90	4.74	7.86	13.38	21.21			2.51	4.33	8.02	16.80	27.06	
(5.3) $\Delta\epsilon \times 10^6$	0.14	0.50	1.11	2.40	4.10	0.044	0.23	1.33	4.0	7.5			0.034	0.17	1.35	4.05	8.55	
(5.4) $\Delta\epsilon_0 \times 10^6$			1.52					2.36							2.37			
(5.5) $-\frac{E}{P}\int \eta\Delta\epsilon dA$			0.00164 in.					0.00317 in.							0.00343 in.			
(5.6) $\Delta\epsilon \times 10^6$	−3.26	−0.87	1.52	3.94	6.30	−6.61	−2.13	2.36	6.85	11.33			−7.73	−2.68	2.37	7.42	12.47	
(5.7) (5.6) − (5.3)	−3.40	−1.37	0.41	1.51	2.20	−6.65	−2.36	1.03	2.85	3.83			−8.07	−2.85	1.02	3.37	3.92	
(5.8) $\frac{E(5.7)}{10^5}$	−177	−71	21	78	114	−346	−123	54	148	199			−419	−148	53	175	204	
	$\Delta a_1 = 0.00525$ in. $\Delta a_2 = 0.000494$ in. $\Delta a_3 = 0.000150$ in.						Time 240–300 min						$\Delta b_1 = 0.0082$ in. $\Delta b_2 = 0.0000353$ in. $\Delta b_3 = 0.00000267$ in. $\delta_{300} = 0.02792$ in.					
(6.1) (5.1) + (5.8)	1711	2154	2546	2867	3132	1092	1924	2635	3144	3488			839	1826	2646	3240	4289	
(6.2) $\Sigma\epsilon \times 10^6$	4.55	6.12	8.74	12.66	17.77	2.94	4.97	9.19	0.738	2871			2.54	4.50	9.37	20.94	35.61	
(6.3) $\Delta\epsilon \times 10^6$	0.075	0.415	1.4	2.70	4.95	0.023	0.14	1.45	5.5	9.7			0.01	0.093	1.6	6.9	14.3	
(6.4) $\Delta\epsilon_0 \times 10^6$			1.73					3.01							3.79			
(6.5) $-\frac{E}{P}\int \eta\Delta\epsilon dA$			0.0022 in.					0.00442 in.							0.00590 in.			
(6.6) $\Delta\epsilon \times 10^6$	−5.62	−1.95	1.73	5.41	9.08	−10.49	−3.74	3.01	9.76	16.51			−12.76	−4.48	3.79	12.06	20.34	
(6.7) (6.6) − (6.3)	−5.70	−2.37	0.33	2.71	4.13	−10.51	−3.88	1.56	4.26	6.81			−12.77	−4.57	2.19	5.16	6.04	
(6.8) $\frac{E(6.7)}{10^5}$	−296	−126	17	141	215	−546	−202	81	221	354			−663	−238	114	268	314	
	$\Delta a_1 = 0.0108$ in. $\Delta a_2 = -0.000351$ in. $\Delta a_3 = 0.000468$ in.						Time 300–360 min						$\Delta b_1 = 0.0188$ in. $\Delta b_2 = 0.0000334$ in. $\Delta b_3 = -0.0000086$ in. $\delta = 0.04680$ in.					
(7.1) σ = (6.1) + (6.9)	1415	2028	2563	3008	3347	546	1722	2716	3365	3842			176	1583	2760	3508	3903	
(7.2) $\Sigma\epsilon \times 10^6$	4.63	6.54	10.14	15.36	22.72	2.96	5.11	10.64	22.88	38.41			2.55	4.59	10.97	27.84	49.91	
(7.3) $\Delta\epsilon \times 10^6$	0.0425	0.140	1.20	3.70	9.00	0.008	0.076	1.60	9.0	31.4			0.004	0.059	2.00	12.6	35.4	
(7.4) $\Delta\epsilon_0 \times 10^6$			2.16					5.80							7.60			
(7.5) $-\frac{E}{P}\int \eta\Delta\epsilon dA$			0.00312 in.					0.00966 in.							0.01258 in.			
(7.6) $\Delta\epsilon \times 10^6$	−15.19	−6.52	2.16	10.84	19.51	−25.9	−10.1	5.8	21.7	37.5			−28.6	−10.5	7.60	25.7	43.8	
(7.7) (7.6) − (7.3)	−15.23	−6.66	0.96	7.14	10.51	−25.9	−10.2	4.2	12.7	6.1			−28.6	−10.6	5.60	13.1	8.4	
(7.8) $\frac{E(7.7)}{10^5}$	−792	−246	50	372	546	−1246	−530	218	660	317			−1488	−551	291	681	436	
							Time = 360 min											
(8.1) σ = (7.1) + (7.8)	623	1682	2613	3380	3893	−800	1192	2934	4025	4159			−1312	1037	3051	4189	4339	

[a] $\Delta K = \Sigma - \frac{n^2\pi^2}{L^2}\Delta b_n \sin\frac{n\pi x}{L}$

$\Delta\epsilon = \Delta\epsilon_0 + \eta\Delta K$

A Theory of the Yield Point and the Transition Temperature of Mild Steel

By F. FORSCHER,[1] PITTSBURGH, PA.

Experimental results indicate the dependence of the yield-point phenomenon of mild steel on temperature, strain rate, duration of stress, and stress state. This paper proposes a yield criterion which can account for these variables. The theory is developed on the basis of a "structural" model, by which the behavior of microscopic and submicroscopic elements is idealized. The theory postulates as yield criterion a critical number of relaxation centers (active Frank-Read sources) or, equivalently, a critical size of relaxation centers. The transition-temperature phenomenon is considered to be the result of an inhibition of yielding (upper yield point) by means of geometry, temperature and/or strain rate. A relation is given which expresses its dependence on the state of stress and strain rate.

Introduction

EXPERIMENTAL evidence indicates that the yield point in mild steel is not only a function of stress but also a function of time and temperature. This paper proposes a new criterion for yielding of polycrystalline mild steel based on a mechanism of local breakdown. The theory could be classified as structural, rating somewhere between the "atomistic" theory of dislocations and the "macroscopic" theory of the homogeneous, elastic, or plastic body. Structural theories have the advantage that they are able to deal with the external variables (stress, duration of stress, and temperature) and the metallurgical variables (grain size, structure, and composition) in a manner that is a better approximation to reality than either atomistic theories or macroscopic theories; their disadvantage is a loss of generality since they apply to only those materials whose structural behavior they approximate. The major difficulty resides in the setting up of the structural model that can be considered to represent the real material and also lends itself to mathematical representation and manipulations. To this end the real conditions must be idealized by eliminating the less important and retaining the pertinent features of the physical process. The object of the following development of the theory is thus twofold: (*a*) The idealized mechanism of yielding should be in agreement with the present knowledge of the yield process, both from the atomistic and the phenomenological point of view; (*b*) the mathematical conclusions should be in agreement with test results. In particular it is desired to account for the temperature and strain-rate dependence of the yield phenomenon, the yield delay time, the triaxiality effect, and their mutual interactions. It is also intended to show that a necessary but not sufficient condition for the occurrence of the "transition-temperature phenomenon" is the inhibition of the upper yield point by means of temperature, strain rate, and/or geometry.

The Structural Model and Its Mathematical Representation

We assume that in a polycrystalline material under external load the total internal resistance equals the external load, as demanded by the equilibrium condition, but that the individual grains are not subject to a homogeneous stress. When some subgrains reach the limit of their resistance to slip (σ_0), they are no longer able to carry their share of the total load, causing a redistribution of internal resistance (local stress) (1, 2, 3, 4).[2] Localized yielding as well as the resulting redistribution of stress is not only dependent on external load but also on time and temperature (see Appendix). The work-hardening capacity of the yielding subgrains will determine how much of their share of the total load is shifted to neighboring subgrains. A material of high work-hardening capacity will effect a gradual redistribution of stress, tending toward an equalization of internal resistance across all subgrains. A material of low work-hardening capacity, on the other hand, will cause relatively large local increases in stress in the neighborhood of the slipped subgrain. Thus this type of material will make the internal stress distribution increasingly heterogeneous (4, 8). An increase in external load will cause further and faster yielding in localized regions along a surface of maximum shear stress. Eventually, yielding will be catastrophic along surfaces of maximum shear stress. Mild steel is considered to be typical of this type of material.

The proposed theory attempts a mathematical formulation of the foregoing process, taking into account the time and temperature dependence of the redistribution of internal resistance. This is accomplished by the introduction of the concept of relaxation centers.

A relaxation center is thought to be a submicroscopically small, approximately lens-shaped region of matter in which a high degree of disorder has been introduced into the lattice. The deformation of the material is assumed to be highly time and temperature sensitive and is therefore designated as quasiviscous (2).[3] The boundary with the elastic (ordered) lattice is a fuzzy undefinable surface. This and its assumed very small size make

[1] LSR Metallurgy Section, Atomic Power Division, Westinghouse Electric Corporation.

Contributed by the Applied Mechanics Division and presented at the Diamond Jubilee Annual Meeting, Chicago, Ill., November 13–18, 1955, of The American Society of Mechanical Engineers.

Discussion of this paper should be addressed to the Secretary, ASME, 29 West 39th Street, New York, N. Y., and will be accepted until July 10, 1956, for publication at a later date. Discussion received after the closing date will be returned.

Note: Statements and opinions advanced in papers are to be understood as individual expressions of their authors and not those of the Society. Manuscript received by ASME Applied Mechanics Division, February 11, 1955. Paper No. 55—A-42.

[2] Numbers in parentheses refer to the Bibliography at the end of the paper.

[3] The postulation of quasiviscous relaxation centers within the matrix of elastic material constitutes a "two-component system." Zener (2) in a detailed discussion of such systems states that the coexistence of both types of regions is necessary in order to interpret the observed mechanical behavior of metals. One remarkable feature of the two-component system is the large magnitude of the anelastic effects which may be produced by an almost negligible amount of quasiviscous material (i.e., the region affected by an active Frank-Read source). Another remarkable feature of the two-component system is the building up of higher stresses within the elastic matrix as the stress relaxes within the viscous region. This localization of stress may lead to slip nucleation and/or to fracture nucleation. Still another feature of the two-component system is the variety of types of relaxation spectra (2) it may have. However, with the assumption of identical relaxation centers and the relaxation time given by the Arrhenius equation, the relaxation spectrum degenerates to a single line.

it apparent that the macroscopic concept of stress concentration is not applicable to the state of stress at its boundary. For the purpose of this analysis relaxation centers may be considered as active Frank-Read sources (5). The latter point of view constitutes a link to the atomistic theories (6, 7).

The local low work-hardening capacity is exaggerated by the assumption that a formed relaxation center carries no stress at all. The subsequent strengthening of relaxation centers by diffusing atoms is neglected. This assumption is in contradiction to the known effect of aging on the yield phenomenon. It follows that the developed equations will only apply to loading times and temperatures for which the effect of aging can be neglected.[4]

The average time that is needed for the development of a relaxation center and thus for the stress to shift from the relaxing material to the neighboring elastic material is here defined by an Arrhenius-type equation of relaxation time

$$\tau = \tau_0 e^{Q/RT} \quad [1]$$

The assumption of a single temperature-dependent relaxation time implies that all relaxation centers are of equal size (λ^3).

The planes of relaxation centers lie in the planes of the shear-stress components; the number of relaxation centers per square inch in a given plane will be a function of the magnitude of the shear-stress component in this plane. Thus the development of relaxation centers can be described mathematically (see Appendix) by a tensor-point function n_{ij} similar to the stress deviator σ_{ij}. The dimensions of each component of the relaxation-center tensor are "number of relaxation centers per unit cross-sectional area."

A mathematically simpler model can be formulated if we consider that only the second invariant of the deviatory stress (a scalar-point function) is responsible for the formation of relaxation centers. Therefore an "effective stress" σ is defined as the square root of a second invariant by the well-known relation of the principal stresses

$$\sigma = \{1/2[(\sigma_1 - \sigma_3)^2 + (\sigma_2 - \sigma_3)^2 + (\sigma_3 - \sigma_1)^2]\}^{1/2} \quad [2]$$

The corresponding scalar-point function of the relaxation-center density tensor is defined by n, number of relaxation centers per unit volume.[5] The density of relaxation centers per unit volume now varies with the effective stress, time, and temperature and Equations [9a] and [10a] of the Appendix become

$$dn = a n d\sigma + \frac{1}{\tau} e^{a(\sigma - \sigma_0)} dt \quad [3]$$

$$n = \frac{t - t_0}{\tau} e^{a(\sigma - \sigma_0)} \quad [4]$$

where a and σ_0 are material constants. It appears from Equation [4] that, in order to evaluate the point function n, a given stress-time relationship must be substituted. As a first approximation to the early portion of the stress-strain curve, the stress is a linear function of time. Thus

$$\sigma = Et\dot{\epsilon} \quad [5]$$

[4] For slower loading and higher temperatures the predictions of the theory must be modified to allow for the aging effects; keeping this in mind it is possible to predict in which manner experimental results under such conditions should differ from the predictions of the theory.

[5] The reformulation of n in terms of a scalar variable implies isotropic susceptibility to development of relaxation centers.

where $\dot{\epsilon}$ is a constant strain rate and E is Young's modulus. This relation is substituted into Equation [4] to give

$$n = \frac{\sigma - \sigma_0}{\dot{\epsilon} E \tau} e^{a(\sigma - \sigma_0)} \quad [6]$$

Any other experimentally conditioned stress-time relationship can be handled similarly.

Criterion for Yielding

It is postulated that a critical density of relaxation centers; namely, n_y, is the limit of the internal stability of the material; that is, yielding sets in suddenly in the region where n_y has been reached. If we consider that relaxation centers form not randomly within a unit volume but adjacent to each other, then the yield condition $n = n_y$ implies the existence of a critical size instead of a critical density of relaxation centers. The two interpretations of the proposed yield condition are mathematically equivalent. The choice of interpreting n as a measure of density or as measure of size is left to the preference of the reader. Throughout most of the paper the viewpoint is adopted that n is a measure of relaxation-center density, because of its applicability to the mathematical concept of a point function.

The yield condition $n = n_y$ thus becomes a parameter characteristic of the grain size and/or the metallurgical structure. It might be assumed that the "mean ferrite path" (8) is related to n_y; however, more experimental data are needed to establish such a relationship. *It is also interesting to note that the proposed yield criterion is not a condition limiting the stress to a fixed value, but that an internal (structural) condition, that develops mainly during the stress application, determines the instant of yielding.*

From Equation [4] we find

$$n_y = \frac{t - t_0}{\tau} e^{a(\sigma_y - \sigma_0)} \quad [7]$$

where σ_y is the effective yield stress, Equation [2]. The effect of triaxiality of stress on yielding is contained in Equation [7] through σ_y.

Since every relaxation center introduces a small but finite amount of anelastic deformation (2) it appears that the yield condition $n = n_y$ also implies a limiting amount of anelastic strain. Experimental evidence to this effect is reported in the literature (9).

For the special case of a simple tension test of constant stress rate Equation [7] becomes

$$n_y = \frac{\sigma_y - \sigma_0}{\dot{\epsilon} E \tau} e^{a(\sigma_y - \sigma_0)} \quad [8]$$

If we let

$$X = a(\sigma_y - \sigma_0) \quad [9]$$

we can write the yield condition for the special case of constant stress rate as

$$a\dot{\epsilon} E \tau n_y = X e^X \quad [10]$$

The relationship of Equation [10] between stress, temperature, and strain rate is graphically solved for X in Fig. 1.

An estimate of the numerical value of n_y can be gained by the following simplified argument: If n is the number of relaxation centers per unit volume, then $1/n$ is the average elastic volume that surrounds each relaxation center. As n increases the elastic volume decreases. If we assume that this elastic volume asso-

ciated with each relaxation center has a physically fixed lower limit of the size of a block or subgrain (0.5μ to 5μ), we find for n_y between 10^{10} to 10^{13} relaxation centers per cubic centimeter.

Stress-Gradient Effect

The yield condition ($n = n_y$) includes the physical condition that a finite region of material is involved. Experiments leading to this conclusion are reported in the literature (10, 11, 12). Mathematically, we must postulate that a scalar-point function n reaches a critical value, but actually it implies a region in which n_y can be physically accommodated. This is particularly apparent when we consider n_y as a measure of size instead of a measure of density.

The steeper the stress gradient at the edge of a notch, the more difficult is the formation of n_y relaxation centers within the small stress region. Under this condition, the maximum stress at the root of the notch will have exceeded the yield stress for the case of simple tension. The excess will be larger the steeper the stress gradient and the faster the stress application. This effect is independent of the effect of triaxiality which also raises the yield-point stress in accordance with Equations [2] and [7].

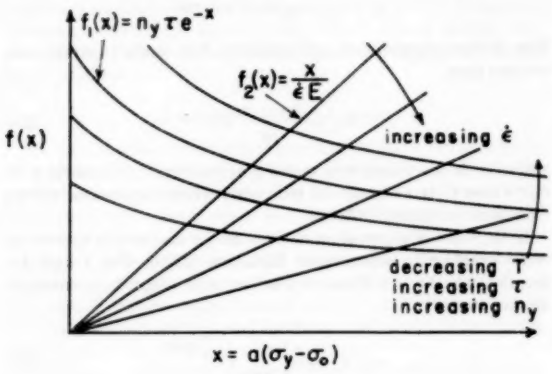

Fig. 1

Temperature and Strain-Rate Effects

Strain rate $\dot{\epsilon}$ entered into the theoretical consideration through the special case of a linear stress-time relation, Equation [5]. In a general case (i.e., a notch) an effective stress-time relation would have to be found and substituted into Equation [4].

We shall restrict ourselves to the simple tensile test under constant strain rate assuming validity of Equation [5], in which case Equation [10] applies.

The temperature effect on the yield point is found from $\partial X/\partial T$ at $\dot{\epsilon} = \text{const}$. Noting that $\tau = \tau_0 e^{Q/RT}$ we find

$$-\frac{Q}{RT^2} X e^X = \frac{\partial X}{\partial T} e^X (1 + X) \quad \ldots\ldots [11]$$

$$\frac{\partial(\ln X)}{\partial\left(\frac{1}{T}\right)} = \frac{Q}{R} \frac{1}{1 + X} \quad \ldots\ldots [12]$$

The strain-rate effect on the yield point is found from $\partial X/\partial \dot{\epsilon}$ at $T = \text{const}$. We find

$$\frac{\partial X}{\partial \dot{\epsilon}} = \frac{1}{\dot{\epsilon}} \frac{1}{1 + X} \quad \ldots\ldots [13]$$

or

$$\frac{\partial X}{\partial(\ln \dot{\epsilon})} = \frac{X}{1 + X} \quad \ldots\ldots [14]$$

which approaches unity as X increases.

Equation [14] shows good agreement with experimental results reported by G. I. Taylor (14). The equivalence of strain rate and temperature can be shown if

$$\frac{\partial X}{\partial \dot{\epsilon}} d\dot{\epsilon} = \frac{\partial X}{\partial T} (-dT) \quad \ldots\ldots [15]$$

Thus, when the change in yield stress due to an increase in strain rate $d\dot{\epsilon}$ equals the change in yield stress due to a temperature drop dT

$$\frac{1}{\dot{\epsilon}} \frac{X}{1 + X} d\dot{\epsilon} = + \frac{Q}{RT^2} \frac{X}{1 + X} dT$$

Integration between proper limits leads to

$$T_1 \left(1 - T_2 \frac{R}{Q} \ln \frac{\dot{\epsilon}_1}{\dot{\epsilon}_2}\right) = T_2 \quad \ldots\ldots [16]$$

where

$$\dot{\epsilon}_2 > \dot{\epsilon}_1$$

$$T_2 > T_1$$

This relation is identical with the velocity modified temperature proposed by MacGregor and Fisher (15).

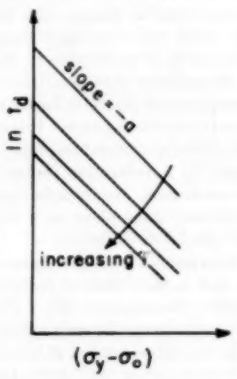

Fig. 2

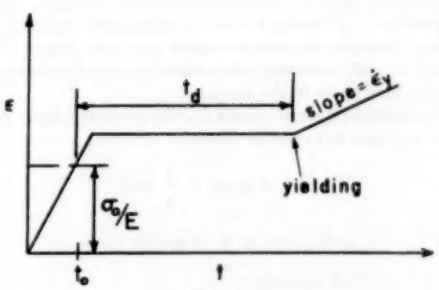

Fig. 3

Yield-Delay Phenomenon

Kramer (16) has reported the slip-delay phenomenon found earlier by Gensamer (17), in a number of body-centered cubic single crystals. Clark and Wood (9, 13, 18, 19) and others (20

have investigated the yield-delay phenomenon in polycrystalline mild steel. The results are schematically shown in Fig. 2. The delay time is here defined at $t_d = t - t_0$, and nearly corresponds to the horizontal portion of the strain-time diagram, Fig. 3. From Equation [7] we can write

$$n_y e^{-a(\sigma_y - \sigma_0)} \tau_0 e^{Q/RT} = t - t_0 = t_d \quad [17]$$

Therefore

$$\frac{d\sigma_y}{d(\ln t_d)} = -\frac{1}{a} \quad [18]$$

The yield-delay experiment establishes the material constant a as the slope of the $(\ln t_d)$ versus $(\sigma_y - \sigma_0)$ plot.

If the stress is rapidly brought up to a level slightly above the elastic limit, relaxation centers will be activated at a slow rate and the yield process is only slowly getting under way. At these stress levels we expect the delay time to show large scatter (18).

Brittle Fracture

The problem of "brittle" fracture in usually ductile mild-steel specimens and structures has met with considerable interest during the past two decades (3, 24, 25, 26, 27). It was exactly this problem which gave the impetus to the present paper on the yield phenomenon in mild steel, based on the hypothesis that the heterogeneous yield and the transition-temperature phenomenon have a common origin (27). Ferritic steel is not unique with respect to the transition-temperature phenomenon; other metals, notably of body-centered cubic structure (tungsten, molybdenum, vanadium) behave in a similar manner (22, 23).[6]

If a material, like steel, shows a highly temperature and rate-sensitive yield behavior it is reasonable to expect that an externally imposed deformation rate could exceed an inherently possible rate of propagation of plastic deformation. Such external conditions would lead to brittle fracture. It is expected that some plastic deformation develops, macroscopically at the root of a notch or microscopically in relaxation centers, but that for the enforced external conditions, the plastic response is not fast enough, so that fracture takes place in a brittle manner, i.e., without appreciable plastic deformation.

Localization of deformation is a basic feature of the concept of relaxation centers and is also believed to be at the root of the transition-temperature phenomenon (8). The development of fracture nuclei, as a consequence of such minute plastic deformation, may lead to a "micromechanism of fracture" (21, 28).

The theoretical formulation of "brittle fracture" is based on the condition that yielding is delayed long enough for a critical number (or critical size), m_f, fracture nuclei to be formed; where m, analogous to n, is assumed to be a scalar-point function of dimension, "number of fracture nuclei per unit volume." The quantity m_f will be strongly dependent on the distribution and shape of a hard phase in the matrix.

The increase in fracture-nuclei density per unit volume may be written analogus to Equation [3] as

$$dm = bmdp + \frac{1}{\tau} e^{bp} dt \quad [19]$$

where $$p = {}^1/_3(\sigma_1 + \sigma_2 + \sigma_3) \text{ for } t > t_0 \quad [20]$$

and b is a material constant.

Hence

$$m = \frac{t - t_0}{\tau} e^{bp}$$

$$\text{if } m = 0 \text{ at } t = t_0 \quad [21]$$

[6] References added in proof of this statement.

These equations assume that the rate of formation of fracture nuclei is governed by the rate of relaxation of shear stress which in turn is controlled by the relaxation time τ. In fact, this implies that fracture and flow (yield) should show the same activation energy which is in agreement with results and conclusions reported in the literature (24, 25, 29).

It follows from these equations that the brittle fracture here discussed will always be associated with some plastic deformation. But it should be pointed out that ideal brittle fracture can occur when a nominal fracture stress (σ_f) is reached before the elastic limit (σ_0) (30, 31). This condition is not considered in this paper.

If yielding does not interfere, brittle fracture under constant stress would have a delay time of the type shown in a stress-rupture experiment. Here it has to be remembered that the aging effect can only be neglected for short delay times. The time needed to develop the critical number of fracture nuclei m_f is given by

$$t_f - t_0 = m_f \tau e^{-bp} \quad [22]$$

Similarly, the time needed to develop n_y relaxation centers is given by

$$t_y - t_0 = n_y \tau e^{-a(\sigma_y - \sigma_0)}$$

The shorter phenomenon will govern. For constant stress rate we also have

$$m_f = \frac{p_f - p_0}{\dot{p}\tau} e^{bp_f} \quad [23]$$

where p_f is the volumetric stress p at fracture. In general $p = C_t\sigma$ where C_t is a measure of triaxiality which can assume values from zero to infinity (32, 33).

If the state of stress of an element in the material is known we could graphically superimpose Equation [23] on Fig. 1 and determine whether yielding or fracture will occur in a constant stress-rate test

$$m_f = \text{const} \frac{C_t}{\tau\dot{p}} X e^{\frac{b}{a} C_t X} \quad [24]$$

where $X = a(\sigma - \sigma_0)$ as previously defined.

If the variation of fracture stress with temperature is known it could be introduced into Equation [23] and the relationship of temperature versus strain rate to reach fracture be derived. A common assumption is a constant fracture stress

$$\left(\frac{b}{a} C_t X = \text{const}\right)$$

In this case Equation [24] becomes

$$m_f = \text{const } e^{\text{const}} e^{-Q/RT} \frac{1}{\dot{p}} \quad [25]$$

and

$$\ln \dot{p} = \text{const} - \frac{Q}{R} \frac{1}{T} \quad [26]$$

Equation [26] is represented in Fig. 4. The sloping line is separating ductile yield (lower left region) from brittle fracture (upper right region) and thus represents "ductility transition temperature" (34, 35) as a function of stress rate. The line would degenerate into a band if the relaxation time τ is not unique, respectively, if the relaxation centers are not identical in size. Such a relation has been reported (24, 32); furthermore, MacGregor and Grossman (33) report the triaxiality effect as a shifting of this line.

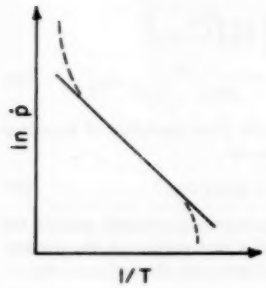

FIG. 4

The physical mechanism sets an upper and lower limit to this relationship, which is indicated with a dashed line in Fig. 4. At the high-temperature side (upper left end of the line) the equation becomes invalid because of the disappearance of the elastic limit and the speed of the aging phenomenon. The dashed line indicates that above a certain temperature brittle fracture will not occur regardless of how high the stress rate. At the low-temperature side (lower right end of the line) the equation becomes invalid because the fracture stress is reached before the elastic limit has been reached. It also indicates that below a certain temperature brittle fracture will occur regardless of how slow the material is stressed.

SUMMARY AND CONCLUSIONS

We may consider a real polycrystalline metal to consist mainly of regions of ordered crystalline material separated by disordered, quasiviscous regions. The relative proportion of these regions and their distribution and shape will greatly effect the mechanical behavior of this "two-component material." Their shape, location, proportion, and relative strength, in turn, is affected in a complicated way by chemical composition, temperature, heat-treatment, aging, precipitation, recrystallization (thermal and chemical energy), and by elastic and plastic deformation and the state of stress (mechanical energy).

In this paper we have focused our attention on one type of these quasiviscous regions, called "relaxation centers" (which also may be considered active Frank-Read sources), and have idealized their properties by assuming equal size and a certain time-and-temperature-dependent response to stress, but neglecting aging as well as history effects upon their properties. The proposed relaxation centers are assumed not to exist in the unstressed material but to be generated by the application of stress. The rate of their formation is roughly proportional to their number present as a consequence of the decrease of the available area over which the applied shear stress can be exerted. This mechanism is applied to the interpretation of the heterogeneous yield phenomenon in mild steel, and the yield criterion is expressed as the presence of a critical number (n_y) of relaxation centers per unit volume. The time, stress, and temperature dependence of the relaxation-center density per unit volume is given by

$$n = \frac{t - t_0}{\tau} e^{\alpha(\sigma - \sigma_0)}$$

where

$$\tau = \tau_{00} e^{Q/RT}$$

and α, σ_0, τ, n_y are material constants. A known stress-time relationship (for a single-stroke experiment) will eliminate either time or stress from this equation. The foregoing expression does not distinguish between increasing number of relaxation centers or the growing of one (larger) region of relaxed material. From the latter point of view the yield criterion $n = n_y$ implies a critical size of the relaxation center.

The paper presents a theoretical derivation and correlation of the strain-rate effect, temperature effect, the yield-delay phenomenon, the triaxiality, and their interaction on the yield point. Volume-constant relaxation centers, generated during the loading in tension, are subject to an additional tensile stress, exerted by the surrounding dilating matrix, and are thought to give rise to fracture nuclei. Relaxation centers are thus qualitatively related to the generation of fracture nuclei. By analogy a critical fracture-nuclei density, or equivalently, a critical fracture-nuclei size, is assumed to be the criterion of brittle fracture. This leads to a new interpretation of the transition-temperature phenomenon—its stress-state and strain-rate dependence. The theory also predicts a fracture-delay time similar to the yield-delay time.

ACKNOWLEDGMENT

The author wishes to acknowledge his indebtedness to Prof. A. M. Freudenthal and Prof. M. Gensamer for their joint sponsorship, advice, comments, and many helpful discussions in relation to theoretical and experimental work performed by the author, during 1951 and part of 1952, while an instructor at Columbia University, Department of Civil Engineering.

This paper is a portion of a thesis submitted in partial fulfillment of the requirements for the degree of Doctor of Philosophy, in the Faculties of Political Science, Philosophy, and Pure Science, Columbia University, 1953.

BIBLIOGRAPHY

1 "Flow and Fracture of Solids," by A. Nadai, McGraw-Hill Book Company, Inc., New York, N. Y., 1951.

2 "Elasticity and Anelasticity of Metals," by C. Zener, The University of Chicago Press, Chicago, Ill., 1948.

3 "The Inelastic Behavior of Engineering Materials and Structures," by A. M. Freudenthal, John Wiley & Sons, Inc., New York, N. Y., 1950.

4 "Faults in a Material Which Yields to Shear Stress While Retaining Its Volume Constancy," by G. I. Taylor, Proceedings of the Royal Society of London, series A, vol. 145, 1934, p. 1.

5 Oral communication by T. A. Read.

6 "Dislocation Theory of Yielding and Strain Aging of Iron," by A. H. Cottrell and B. A. Bilby, Proceedings of the Physical Society, vol. 62A, 1949, p. 49.

7 "Dislocation Collision and the Yield Point of Iron," by A. N. Holden, Trans. AIME, vol. 4, 1952, p. 184.

8 "Strength and Ductility," by M. Gensamer, Campbell Memorial Lecture 1945, Trans. ASM, vol. 36, 1946, pp. 30–60.

9 "A Study of the Mechanism of the Delayed Yield Phenomenon," by T. Vreeland, D. S. Wood, and D. S. Clark, Trans. ASM, vol. 45, 1953, p. 620.

10 "The Tensile Properties of Iron Crystals and the Influence of Crystal Size Upon the Tensile Properties of Iron," by C. A. Edwards and L. B. Pfeil, *Journal of the Iron and Steel Institute*, vol. 112 (2), 1925, p. 79.

11 "The Yield of Mild Steel With Particular Reference to the Effect of Size of Specimens," by J. L. M. Morrison, Proceedings of The Institution of Mechanical Engineers, vol. 142 (3), 1940, p. 193.

12 Proceedings of Conference on "Brittle Fracture in Mild Steel Plates," by E. Orowan, N. F. Mott, et al., British Iron and Steel Research Association, Bristol, October, 1945.

13 "Delayed Yield in Annealed Steels of Very Low Carbon and Nitrogen Content," by D. S. Wood and D. S. Clark, Trans. ASM, vol. 44, 1952, p. 726.

14 "Testing of Material at High Rates of Loading," by G. I. Taylor, Institution of Civil Engineers, vol. 25–26, 1946, p. 486.

15 "Tension Tests at Constant True Strain Rates," by C. W. MacGregor and J. C. Fisher, JOURNAL OF APPLIED MECHANICS, Trans. ASME, vol. 67, 1945, p. A-217.

16 "Delay Time for the Initiation of Slip in Metal Single Crystals," by I. R. Kramer and R. Maddin, *Journal of Metals*, vol. 4, 1952, pp. 197–203.

17 "Yield Point of Single Crystals of Iron Under Static Loads," by M. Gensamer and R. F. Mehl, Trans. AIME, vol. 131, 1938, p. 372.

18 "The Time Delay for the Initiation of Plastic Deformation at Rapidly Applied Constant Stress," by D. S. Clark and D. S. Wood, Proceedings of the ASTM, vol. 49, 1949, p. 717.

19 "The Influence of Temperature Upon the Time Delay for Yielding in Annealed Mild Steel," Trans. ASM, vol. 43, 1951, p. 571.
20 "The Delayed Yielding of Mild Steel," by J. Gibson, submitted by J. F. Baker, British NCRE Report 158E, July, 1950.
21 "The Micromechanism of Fracture," by C. Zener, ASM Publication, Fracturing of Metals, 1948, p. 7.
22 "Effects of Temperature on the Tensile Properties of Annealed Tungsten," by P. G. Shewnon, Westinghouse Research Report, September, 1952.
23 "Effects of Temperature on the Flow and Fracture Characteristics of Molybdenum," by J. H. Bechtold, Westinghouse Scientific Paper 1707, November, 1952.
24 "The Problem of Fracture," by H. H. Hollomon, A Report of the Welding Research Council, American Welding Society, 1946.
25 "Report on the Fracture of Metals," by M. Gensamer, et al., *The Welding Journal*, vol. 26 (8), Research Supplement, 1947.
26 "Behavior of Metals at Low Temperatures," by R. M. Brick, J. R. Low, and C. H. Lorig, ASM Publication, 1953.
27 "Notch Brittleness and Ductile Fracture in Metals," by E. Orowan, J. F. Nye, and W. D. Cairns, Report No. 8, Strength and Testing of Materials, Part 1, H. M. Stationery Office, London, England, 1952.
28 "The Micromechanism of Fracture in Tension Impact Test," by W. H. Bruckner, *The Welding Journal*, vol. 29 (9), Research Supplement, 1950, p. 467-s.
29 "On the Effect of Plastic Extension and Compression on the Fracture of Metals," by D. J. McAdam, G. W. Geil, and W. J. Jenkins, Proceedings of the ASTM, vol. 47, 1947, p. 554.
30 "A Statistical Theory of Fracture," by J. C. Fisher and J. H. Hollomon, Trans. AIME, vol. 171, 1947, p. 546.
31 "A Statistical Distribution Function of Wide Applicability," by W. Weibull, JOURNAL OF APPLIED MECHANICS, Trans. ASME, vol. 73, 1951, pp. 293–297.
32 "A Comparison of the Brittle Transition Temperatures as Determined by the Charpy Impact and the MIT Slow Bend Test," by C. W. MacGregor and J. Grossman, *Welding Journal*, vol. 27, Research Supplement, 1948, p. 160-s.
33 "Quantitative Effect of Combined Stress Ratios on Brittle Transition Temperature of SAE-1020 Steel," by C. W. MacGregor and J. Grossman, Ibid., 1948, p. 12-s.
34 "Comparison of Notch Tests and Brittleness Criteria," by C. J. Osborn, et al., *The Welding Journal*, vol. 28 (1), Research Supplement, 1949, p. 24-s.
35 "Evaluating Notch Toughness," by R. W. Vanderbeck and M. Gensamer, Ibid., vol. 29 (1), Research Supplement, 1950, p. 37-s.

Appendix

It is assumed that relaxation centers of constant magnitude λ^2 form in planes on which the shear-stress component has increased beyond the threshold stress σ_0. The density of relaxation centers per unit area in such planes n_{ij} will increase with increasing stress, time, and temperature. Thus

$$n_{ij} = f(\sigma_{ij}, t, T)$$

$$dn_{ij} = \frac{\partial n_{ij}}{\partial \sigma_{ij}}\, d\sigma_{ij} + \frac{\partial n_{ij}}{\partial t}\, dt + \frac{\partial n_{ij}}{\partial T}\, dT \quad \ldots\ldots [27]$$

Explicit expressions for the partial derivatives are now developed.

Let n_i be the total possible number of relaxation centers per unit area; i.e., $\lambda^2 n_i = 1$. After formation of n_{ij} relaxation centers per unit area, the actual stress-carrying area is reduced, and the actual shear stress (σ_L = local shear stress) is increased over the nominal shear stress. Their relationship is expressed by

$$\sigma_L = \frac{\sigma_{ij}}{\lambda^2(n_i - n_{ij})} \quad \ldots\ldots [28]$$

where $n_{ij} \ll n_i$, and hence

$$\lambda^2(n_i - n_{ij}) \approx 1 \quad \ldots\ldots [29]$$

The local shear-stress increment $d\sigma_L$ is the differential

$$d\sigma_L = \frac{\partial \sigma_L}{\partial \sigma_{ij}}\, d\sigma_{ij} + \frac{\partial \sigma_L}{\partial n_{ij}}\, dn_{ij} = \frac{d\sigma_{ij}}{\lambda^2(n_i - n_{ij})} + \frac{\sigma_{ij}}{\lambda^2(n_i - n_{ij})^2}\, dn_{ij} \quad \ldots\ldots [30]$$

Another relationship between the three variables of Equation [28], independent of the foregoing, is

$$d\sigma_L = d\sigma_{ij} + \text{const}\, dn_{ij} \quad \ldots\ldots [31]$$

In other words, the local shear-stress increment equals the nominal shear-stress increment plus that portion of the nominal stress which is shifted to the local stress by relaxation of dn_{ij} relaxation centers.

Rewriting Equation [31]

$$dn_{ij} = \text{const}\, d(\sigma_L - \sigma_{ij})$$

Substituting the expression for the local shear-stress leads to

$$dn_{ij} = \text{const}\, d\sigma_{ij}\left(\frac{1}{\lambda^2(n_i - n_{ij})} - \frac{1}{\lambda^2 n_i}\right) \approx \text{const}\, n_{ij} d\sigma_{ij} \quad \ldots [32]$$

The first of the partial derivatives of Equation [27] is therefore

$$\frac{\partial n_{ij}}{\partial \sigma_{ij}} = \text{const}\, n_{ij}$$

The time dependence of n_{ij} is assumed to be an adaptation of the hyperbolic sine law

$$\frac{\partial n_{ij}}{\partial t} = \text{const}\, V_0 e^{-Q/RT} \sinh\,[\text{const}\,(\sigma_{ij} - \sigma_0)] = \frac{1}{\tau} \sinh\,[\text{const}\,(\sigma_{ij} - \sigma_0)] \quad \ldots\ldots [33]$$

Since only isothermal processes are considered here, the third term in Equation [27] becomes identically equal to zero.

The total differential of n_{ij} becomes now

$$dn_{ij} = \text{const}\, n_{ij} d\sigma_{ij} + \frac{1}{\tau} \sinh\,[\text{const}\,(\sigma_{ij} - \sigma_0)]dt \quad \ldots [34]$$

Equation [34] can be modified by neglecting $e^{-(\sigma_{ij} - \sigma_0)}$ in comparison to $e^{(\sigma_{ij} - \sigma_0)}$. This leads to

$$dn_{ij} = \text{const}\, n_{ij} d\sigma_{ij} + \frac{1}{\tau}\, e^{\text{const}\,(\sigma_{ij} - \sigma_0)}\, dt \quad \ldots\ldots [35]$$

For Equation [27] to be an exact differential the two constants in Equation [35] must be identical. Hence

$$n_{ij} = \frac{t - t_0}{\tau}\, e^{a(\sigma_{ij} - \sigma_0)} + \text{const} \quad \ldots\ldots [36]$$

This implies that in the mathematical idealization of the process the point function n_{ij} is assumed to be independent of the sequence of events but not of the timing of the sequence. For any sequence of stress going from σ_0 to σ, and corresponding time lasting from t_0 to t, there is a relaxation-center density associated with it which may be calculated according to Equation [36]. The constant in this equation is dependent on the history of the specimens before time t_0 and will be assumed to be zero.

With any density n_{ij} is associated a unique quantity of dissipated energy W_D. This follows from the definition of the relaxation-center properties. These regions are assumed to be the only ones that dissipate energy and hence a unique number of such regions dissipates a corresponding amount of energy.

Comparison of Slip-Line Solutions With Experiment[1]

By E. G. THOMSEN,[2] BERKELEY, CALIF.

Plane-strain and axially symmetric approximate solutions for a perfect plastic are compared with experimental results obtained from the extrusion of a billet of commercially pure aluminum. The extrusion process was carried out at room temperature under essentially negligible external wall friction with a reduction of area of 87.8 per cent. It is found that the plane-strain solution is in good agreement with the experimental results, if a constant $k = s/2 = 20{,}000$ psi (maximum shear stress for Tresca's criterion) is substituted in the plane-strain solution. The flow stress ($s \cong 40{,}000$ psi) was determined from a property test for the aluminum billet, at a strain equivalent to the uniform deformation in the extrusion (i.e., same area reduction without shear deformation). It is found that the Haar and von Karman yield condition is not valid for the present case, and further that the axially symmetric solution demonstrates no real advantage over the simpler plane-strain solution in predicting the stress distribution in an axially symmetric extrusion problem.

Introduction

THE successful prediction of forming loads and stress and strain distribution involved in the forming of metal objects is of scientific as well as of technological interest. While a significant amount of theoretical work has been done in obtaining solutions for specific forming operations, surprisingly little has been reported in the literature of experimental verification of these solutions. Hence potentially valuable information has remained largely in the realm of theoretical speculation and only rarely has been considered by the production engineer as an alternative to costly trial-and-error methods. As the size of forming equipment grows and new metals and alloys are being used in forming problems (as witnessed by the new U. S. heavy-press program and the cold forming of steel), the need for accurate prediction becomes more and more urgent as an element in the reduction of development costs. It would seem, therefore, to be of paramount practical importance that the existing theories on plastic flow of metals be verified experimentally, in order that it can be determined which of them is useful and which should remain as merely interesting mathematical exercises.

Progress has been made recently in devising an experimental method for studying plastic flow of a metal in certain steady-state forming operations (1).[3] This method is called visioplasticity and consists of determining particle-velocity vectors during steady-state motion by stepwise deformation processes in an actual forming operation. The method was applied to the extrusion of axially symmetric shapes, i.e., solid bars and tubes of lead (2, 3, 4) and, more recently, to the extrusion of commercially pure aluminum bars (5). For these cases, when the metals were subjected to essentially frictionless extrusion processes, it was possible to determine stress, strain, and strain-rate distribution within the plastically flowing metal, provided the forming load was known. It was later shown (6), however, that prior knowledge of the actual forming load was not an essential since such forming load could be obtained with good precision from the mechanical properties of the metal and from the strain distribution within the billet. Up to this time the visioplasticity method has been purposely limited to extrusion problems with essentially no external friction and to axially symmetric shapes in order to make a reasonably complete exploration with comparable results. It is the belief of the author, however, that the method of visioplasticity can be used for other forming operations such as rolling and drawing, under conditions of high external friction and for shapes formed under conditions of plane strain.

To the extent to which the present experimental information permits and for the limited experiments performed, it may be concluded that:

1 The particle-velocity vector patterns for both lead and aluminum are identical; i.e., these patterns appear to be uniquely determined by boundary conditions alone and are independent of the properties of the metals being deformed.

2 The stress and strain-rate distributions are dependent only on the boundary conditions if compared on a suitable dimensionless basis regardless of the work-hardening or strain-rate characteristics of the metals.

3 The extrusion pressure for lead is a strong function of the extrusion speed, while for aluminum it is dependent only on the state of deformation until steady state is reached and is essentially independent of extrusion speed.

These conclusions have important theoretical implications because they appear to permit generalization of forming problems and the adoption of a suitable constant flow stress characterizing a particular metal and the rate under which the deformation is being carried out. These are precisely the conditions assumed in the theory of perfectly plastic solids and the solution of forming problems given by the Hencky-Prandtl shear nets (7). Hence it is the purpose of this paper to demonstrate, through comparison of slip-line solutions with experimental results obtained from an aluminum extrusion, that the perfectly plastic solid may be a suitable model for solving forming problems.

Discussion of Theory and Results

The axial-stress distribution in a 4.3-in. round billet extruded into a 1.5-in-diam solid bar of 1100-0(28-0) commercially pure aluminum is shown in Fig. 1. The axial-stress distribution is given for various constant distances $z = 0.2$ to $z = 1.8$ in., where z is the upstream distance in the billet from the orifice. The

[1] The investigation presented in this paper was carried out under joint sponsorship of the University of California under faculty research and the National Science Foundation under Research Grant G-1002.

[2] Professor of Mechanical Engineering, College of Engineering, University of California. Mem. ASME.

Contributed by the Applied Mechanics Division and presented at the Diamond Jubilee Annual Meeting, Chicago, Ill., November 13–18, 1955, of The American Society of Mechanical Engineers.

Discussion of this paper should be addressed to the Secretary, ASME, 29 West 39th Street, New York, N. Y., and will be accepted until July 10, 1956, for publication at a later date. Discussion received after the closing date will be returned.

Note: Statements and opinions advanced in papers are to be understood as individual expressions of their authors and not those of the Society. Manuscript received by ASME Applied Mechanics Division, May 4, 1955. Paper No. 55—A-51.

[3] Numbers in parentheses refer to the Bibliography at the end of the paper.

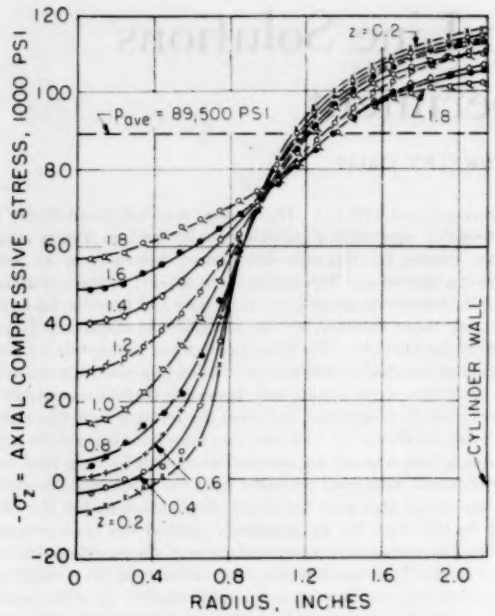

FIG. 1 EXPERIMENTALLY DETERMINED AXIAL COMPRESSIVE STRESS DISTRIBUTION FOR VARIOUS z-DISTANCES UPSTREAM FROM THE ORIFICE DURING STEADY-STATE EXTRUSION OF A 4.3-IN. BILLET INTO A 1.5-IN-DIAM SOLID BAR OF 1100-0 ALUMINUM AT ROOM TEMPERATURE UNDER CONDITION OF NEGLIGIBLE WALL FRICTION

axial-stress distribution of Fig. 1 was obtained by integrating equations of the form

$$\frac{\partial \sigma_z}{\partial r} = \frac{2}{3}\,\bar{\sigma}\left[\frac{\partial}{\partial r}\left(\frac{\dot{\epsilon}_z - \dot{\epsilon}_r}{\dot{\bar{\epsilon}}}\right) - \left(\frac{\dot{\epsilon}_r - \dot{\epsilon}_\theta}{r\dot{\bar{\epsilon}}}\right) - \frac{1}{2}\,\frac{\partial}{\partial z}\left(\frac{\dot{\gamma}_{zr}}{\dot{\bar{\epsilon}}}\right)\right] \quad \ldots\ldots [1]$$

where $\dot{\epsilon}_z$, $\dot{\epsilon}_r$, $\dot{\epsilon}_\theta$, and $\dot{\gamma}_{zr}$ are the axially symmetric normal and shear-strain-rate components and $\dot{\bar{\epsilon}}$ is the effective strain rate which were obtained from the experimentally determined velocity-vector gradients on a meridian plane of the billet. The effective stress $\bar{\sigma}$ was obtained from a stress-strain curve of the aluminum under investigation for the logarithmic equivalent effective strain to which the metal was subjected at each point under investigation. For a full discussion of the method employed the reader is referred to the references cited previously and, in particular, to reference (5) in which the aluminum-extrusion experiment is discussed in detail.

By use of the so-called Lévy-Mises plasticity equations for axial symmetry

$$\left.\begin{aligned} \dot{\epsilon}_z &= \frac{3}{2}\,\frac{\dot{\bar{\epsilon}}}{\bar{\sigma}}\,(\sigma_z + p) \\ \dot{\epsilon}_r &= \frac{3}{2}\,\frac{\dot{\bar{\epsilon}}}{\bar{\sigma}}\,(\sigma_r + p) \\ \dot{\epsilon}_\theta &= \frac{3}{2}\,\frac{\dot{\bar{\epsilon}}}{\bar{\sigma}}\,(\sigma_\theta + p) \\ \dot{\gamma}_{zr} &= 3\,\frac{\dot{\bar{\epsilon}}}{\bar{\sigma}}\,\tau_{zr} \end{aligned}\right\} \quad \ldots\ldots [2]$$

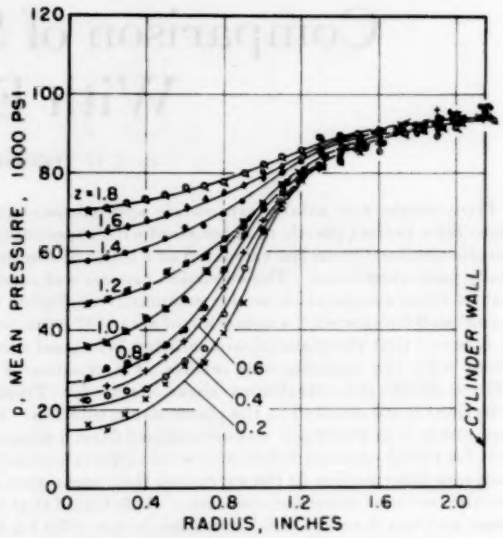

FIG. 2 EXPERIMENTALLY DETERMINED MEAN PRESSURE DISTRIBUTION UNDER SAME EXTRUSION CONDITION AS GIVEN IN FIG. 1

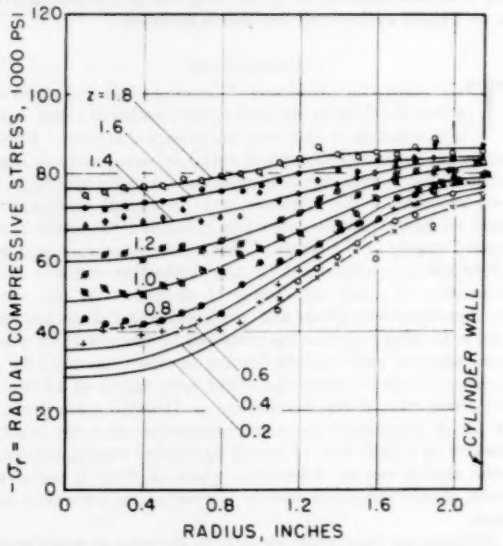

FIG. 3 EXPERIMENTALLY DETERMINED RADIAL COMPRESSIVE STRESS DISTRIBUTION UNDER SAME EXTRUSION CONDITION AS GIVEN IN FIG. 1

the mean pressure

$$p = -\frac{1}{3}\,(\sigma_z + \sigma_r + \sigma_\theta)$$

radial stress σ_r, and hoop stress σ_θ can be determined from the experimental strain rates and the known axial stress σ_z. These calculated stress distributions are shown in Figs. 2 to 4, inclusive. The calculated points are shown by symbols for all curves except σ_r and σ_θ near the orifice where appreciable scatter occurred, which may be attributed to the difficulty of obtaining accurate strain measurements because of high particle velocities. While it is not possible to clearly confirm the stress distributions in these

figures, substantial confirmation has been obtained from hardness measurements in the deformed billet and from residual stress measurements in the extruded bar, which were recently reported (8) and from the forming pressure, which was calculated from the work of deformation, utilizing only mechanical properties and experimental strain distributions previously referred to (6). In the following paragraphs it will be assumed that the experimental stress distributions are correct and that these stresses may be used as a criterion for comparison of theoretical solutions.

The analytical solutions are usually restricted to plane-strain problems, although approximate solutions can be obtained for axially symmetric problems as will be shown subsequently. In these solutions it is assumed that the material is perfectly plastic and deforms only under a constant shearing stress whenever the yield condition is exceeded; in regions of a body where the yield condition is not satisfied, the metal remains perfectly rigid. Hence this method of analysis strives for the determination of a line of demarcation between the perfectly plastic material and that which remains absolutely rigid. Under these conditions the stresses are as given by Hencky (9) and in the terminology of Hill (10)

$$\left.\begin{aligned} \sigma_z &= -p - k \sin 2\phi \\ \sigma_r &= -p + k \sin 2\phi \\ \tau_{zr} &= k \cos 2\phi \end{aligned}\right\} \quad \ldots\ldots\ldots\ldots [3]$$

where σ_z and σ_r are the two-dimensional axial and radial-stress components, respectively, τ_{zr} is the shearing-stress component, k is a constant critical shearing stress, and ϕ is the counterclockwise angular rotation of an α slip line from the z-axis. The α and β slip lines—also called first and second shear lines by other writers (11)—are networks of orthogonal lines of maximum shear and represent the solutions of the statical equilibrium equations. Along these slip lines the following conditions for plane strain hold

$$\left.\begin{aligned} p + 2k\phi &= \text{const along an } \alpha \text{ slip line} \\ p - 2k\phi &= \text{const along a } \beta \text{ slip line} \end{aligned}\right\} \quad \ldots\ldots [4]$$

$$\left.\begin{aligned} du - v d\phi &= 0 \text{ along an } \alpha \text{ slip line} \\ dv - u d\phi &= 0 \text{ along a } \beta \text{ slip line} \end{aligned}\right\} \quad \ldots\ldots [5]$$

where

$$p = -\frac{1}{2}(\sigma_z + \sigma_r) = -\sigma_\theta$$

is the mean pressure and u and v are velocity components along the α and β slip lines, respectively. Hence a complete solution for a perfectly plastic material under conditions of plane strain is given by a network of slip lines known as the Hencky-Prandtl net previously referred to, which must satisfy Equations [4] and [5] everywhere in the plastic metal inclusive of the boundary. The most useful method for getting such solutions is by transforming Equations [4] into finite-difference equations, and in this form they permit numerical integration. Several solutions to extrusion problems were obtained by this method by Hill (10) and other possible solutions are discussed by Prager and Hodge (11). The unique solution evidently cannot be determined from theory alone and requires some additional experimental facts.

Another method which is appreciably faster than the numerical method has been used for the specific extrusion problem under discussion by the use of a newly designed mechanical slip-line integrator. This integrator utilizes the properties of the Hencky-Prandtl net and will be discussed in a future paper. A possible

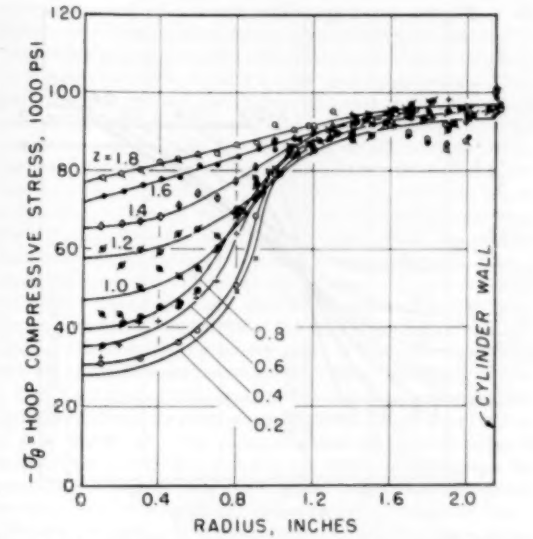

FIG. 4 EXPERIMENTALLY DETERMINED HOOP COMPRESSIVE STRESS DISTRIBUTION UNDER SAME EXTRUSION CONDITION AS GIVEN IN FIG. 1

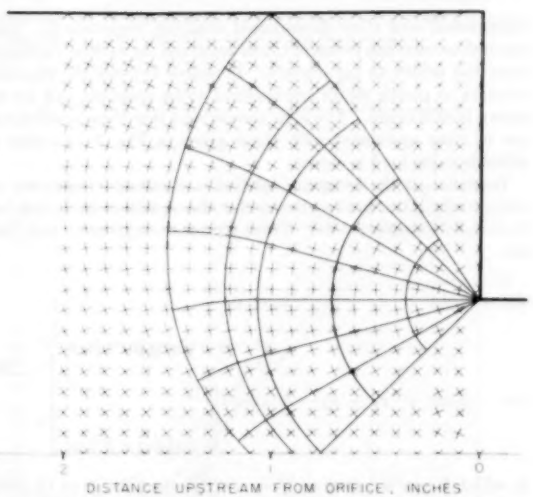

FIG. 5 MAXIMUM SHEAR DIRECTIONS OF A 4.3-IN-DIAM BILLET EXTRUDED INTO A 1.5-IN-DIAM BAR

(a—Solid lines are slip lines from a plane-strain solution for a perfectly plastic solid. b—Crosses are calculated points of aluminum extrusion under conditions as given in Fig. 1.)

solution obtained with this integrator is given by the solid lines in Fig. 5. This solution satisfies Equations [4] and [5] and is of the same pattern as previously obtained by Hill (10) for the general case. In addition to these slip lines the experimentally determined principal shear directions are plotted as crosses on the same figure. It is at once evident that close agreement in slip directions between theory and experiment exists but that the extent of plastic deformation is more extensive than predicted by the theory.

The slip-line network can now be used to calculate the mean pressure p_2 by use of Equations [4] and the results are shown in Fig. 6. The subscript 2 and later subscript 3 used for the pressure have the meaning that the pressure was obtained for the two-

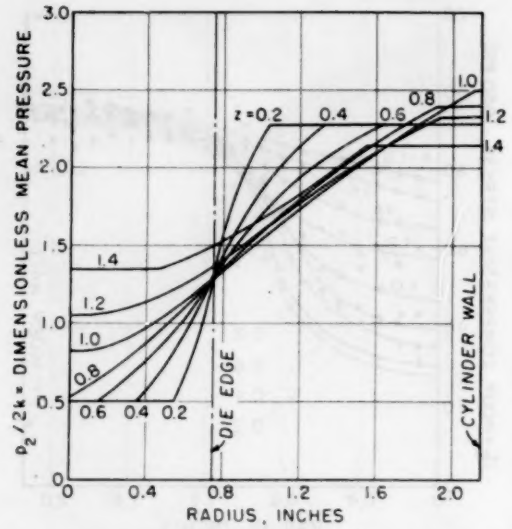

FIG. 6 DIMENSIONLESS MEAN PRESSURE DISTRIBUTION FOR A PERFECTLY PLASTIC SOLID UNDER EXTRUSION CONDITION OF PLANE STRAIN

dimensional and three-dimensional analysis, respectively. The mean dimensionless pressure ratios are given for various locations from the orifice as parameters. Pressures beyond the slip-line network or plastic sector are assumed to be constant and are so shown in this figure. It will be shown later that these predictions are in close agreement with those given in Fig. 2, provided a suitable value for k is chosen.

Inasmuch as the foregoing solution is obtained for the case of plane strain, it is of interest to examine also equations applicable for the axially symmetric case. These equations as given by Hill (10) are

$$\left.\begin{aligned} dp_2 + 2k\,d\phi + (\sigma_\theta + p_2 - k\cot\phi)\frac{dr}{r} &= 0 \text{ along an } \alpha \text{ line} \\ dp_2 - 2k\,d\phi + (\sigma_\theta + p_2 - k\tan\phi)\frac{dr}{r} &= 0 \text{ along a } \beta \text{ line} \end{aligned}\right\} \quad \ldots[6]$$

in which k now is based on Tresca's criterion, i.e., $k = {}^1/_2$ yield strength. The solving of these equations depends on successful elimination of σ_θ from Equations [6]. Such a method was suggested by Haar and von Karman (12), who assumed that $\sigma_\theta + p_2 = \pm k$, where $p_2 = -{}^1/_2(\sigma_z + \sigma_r)$. Hencky later used this relationship for the problem of indentation of a plane surface by a flat punch by assuming that the plane-strain slip lines are also those for the axially symmetric case. Ishlinsky (13) has improved the Hencky solution by a numerical solution but also used the Haar and von Karman yield condition in eliminating σ_θ. The slip-line pattern obtained in this manner by Ishlinsky appears to differ from the plane-strain solution only slightly and hence the plane-strain solution may be accepted as a good approximation. This, however, does not prove that the Haar and von Karman yield condition is correct and hence such solutions heretofore have had little value, as pointed out by Hill[1] (10).

Since experimentally determined stresses are now available for the extrusion problem it is possible to test the Haar and von Karman yield condition. Accordingly, the experimental deviator stresses $\sigma_\theta + p$ are shown plotted in Fig. 7 (with z as parameters) as functions of r. It is to be noted that p in the latter equation refers to

$$p = -\frac{1}{3}(\sigma_z + \sigma_\theta + \sigma_r)$$

It is seen that in spite of appreciable scatter of points near the orifice a definite trend exists. The deviator stresses in magnitude have values of approximately —10,000 psi on the axis and diminish to approximately zero at the cylinder wall. Hence the plastic metal appears to be deformed under axially symmetric conditions in the region below the die opening but approaches plane-strain conditions in the region near the wall. It is evident at once that no single value of the deviator stress $\sigma_\theta + p$ exists throughout the section. For purposes of calculating the axially symmetric stresses, however, a constant value of $\frac{3}{2}\sigma_\theta' = \sigma_\theta + p_2 = -10{,}000$ psi will be assumed.

In order to calculate the stresses for the axially symmetric case it is necessary to assume an appropriate value for k. It was shown elsewhere (6) that the effective stress for the aluminum billet in the deformed metal at the orifice varied from approximately 40,000 psi on the extrusion axis to nearly 50,000 psi at the die corner. Hence the rise of the flow stress from an initial yield-point stress of approximately 5000 psi for the undeformed metal to these high values in the deformed state indicates appreciable work hardening. It is, therefore, the choice of a proper flow stress which will determine whether or not agreement between theory and experiment can be achieved.

It was shown (6) that an effective flow stress $\bar{\sigma} \cong 40{,}000$ psi as obtained from a stress-strain curve equivalent to uniform deformation in the billet, i.e., an effective strain

$$\bar{\epsilon}_a = 2\log_e\left(\frac{4.3}{1.5}\right) = 2.1$$

yielded good agreement between the plane-strain solution and experimental results at a particular section $z = 0.8$ in. in the billet. The value of k was chosen in this case in accordance with the von Mises criterion, i.e., $k = \bar{\sigma}/\sqrt{3}$. As will be shown subsequently, however, better agreement is achieved between theory and experiment if Tresca's criterion is chosen, namely, $k = \bar{\sigma}/2 \cong 20{,}$-

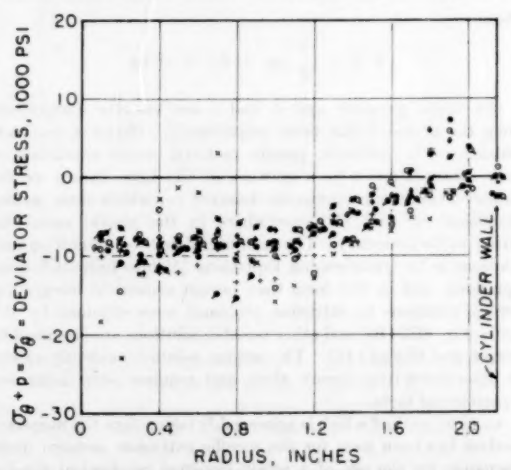

FIG. 7 EXPERIMENTALLY DETERMINED HOOP DEVIATOR STRESS DISTRIBUTION UNDER SAME EXTRUSION CONDITION AS GIVEN IN FIG. 1

000 psi. Selecting this value of k for the axially symmetric solution, the following equation may be written

$$\frac{3}{2}\sigma_\theta' = \sigma_\theta + p_3 = -10{,}000 \text{ psi} = -\frac{k}{2}$$

Substitution of this condition into Equations [6] permits the evaluation of the dimensionless mean pressures. It was found that the plane-strain plastic sector given in Fig. 5 is applicable, since in traveling around a closed path along α and β slip lines the initial value of the mean pressure is approximately regained. The dimensionless mean pressures evaluated in this manner are shown in Fig. 8 as functions of r with z again as the parameters. Comparison of this pressure distribution with that of the plane-strain solution given in Fig. 6, reveals the following differences. The pressures p_3 are generally higher than p_2 for all z-sections but the shapes of the pressure curves are comparable. In the region below the orifice, i.e., from $r = 0$ to $r = 0.75$ in. in which the largest values of $\sigma_\theta + p_3$ were shown to exist by the experimental data, the differences between p_2 and p_3 are least. Near the cylinder wall, however, where the deformation process approaches that of plane straining, the differences are greatest. It appears from these observations, therefore, that little is accomplished by using the more complicated analysis of the axially symmetric case and that, as will be shown, the proper choice of k for the plane-strain solution yields good agreement between theory and experiment.

Figs. 9 and 10 show the mean pressure and axial-stress distribution obtained from the plane-strain solutions using constant values of $k = 20{,}000$ psi. The range of values of the experimental stresses from $z = 0.2$ to $z = 1.4$ in. are shown as dotted lines for comparison. It is at once evident that under these conditions the agreement between theory and experiment, except for minor differences, is good. It appears, therefore, that the plane-strain solution is a powerful tool for evaluating forming stresses, provided that a proper flow stress can always be found. Hence further investigations in other metals and other forming operations should be carried out with a view of establishing general rules for the determination of suitable flow stresses.

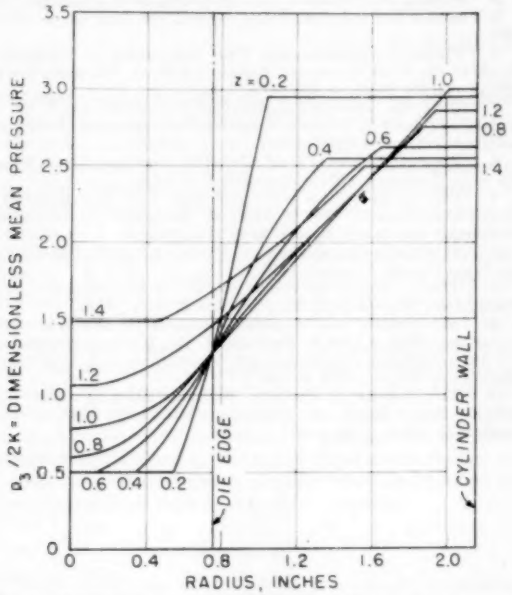

FIG. 8 DIMENSIONLESS MEAN PRESSURE DISTRIBUTION FOR A PERFECTLY PLASTIC SOLID UNDER EXTRUSION CONDITION OF AXIAL SYMMETRY

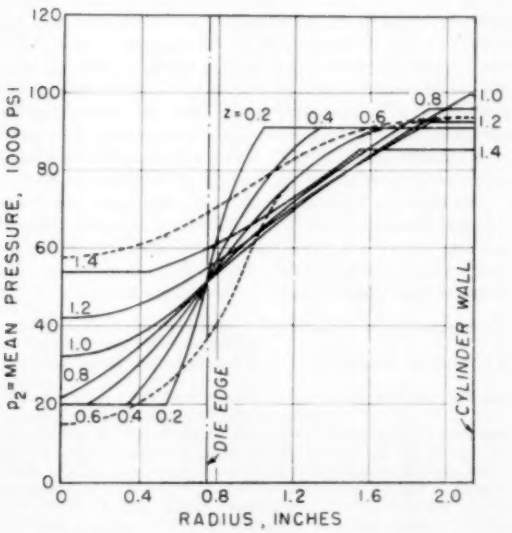

FIG. 9 COMPARISON OF EXPERIMENTALLY AND THEORETICALLY DETERMINED MEAN PRESSURES

(a—Solid curves are obtained from plane-strain analysis of a perfectly plastic solid. b—Dotted curves are experimentally determined values taken from Fig. 2 for $z = 0.2$ in. and 1.4 in.)

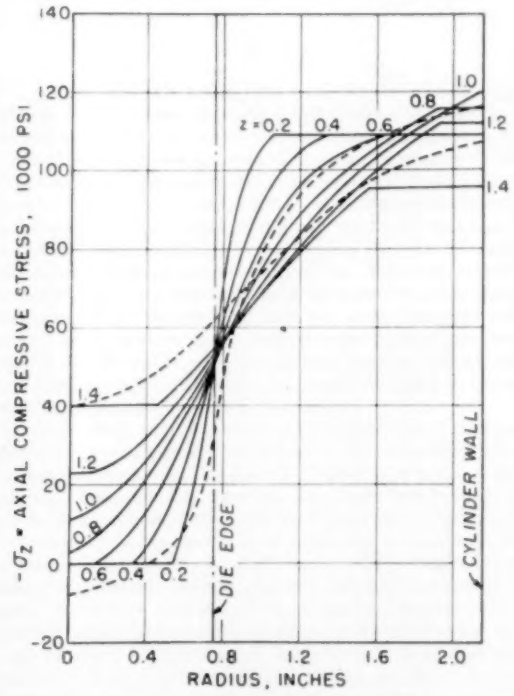

FIG. 10 COMPARISON OF EXPERIMENTALLY AND THEORETICALLY DETERMINED AXIAL STRESSES

(a—Solid curves are obtained from plane-strain analysis of a perfectly plastic solid. b—Dotted curves are experimentally determined values taken from Fig. 1 for $z = 0.2$ in. and 1.4 in.)

Conclusions

1 Theoretical solutions for a plane-strain and an axially symmetric extrusion problem were examined and it was found that the axially symmetric solution shows little advantage over the simpler plane-strain solution.

2 The plane-strain solution yields mean pressures and axial stresses which are in good agreement with experimental results.

3 The choice of a proper flow stress in order to permit prediction of forming loads from a plane-strain solution appears to be the most important property of the metal which must be determined.

4 Selecting $k = \bar{\sigma}/2$, where $\bar{\sigma}$ is equal to the flow stress of the aluminum under investigation at an equivalent uniform strain in a property test, yielded good correlation between theory and experiment.

5 The perfectly plastic solid appears to be a suitable model for solving forming problems.

Acknowledgment

The author wishes to thank the National Science Foundation and the University of California for making funds available for this investigation. He also wishes to thank Mr. T. Jordan, a graduate student in the College of Engineering, for his assistance with the integration of the plane-strain extrusion problem.

BIBLIOGRAPHY

1 "Experimental Stress Determination Within a Metal During Plastic Flow," by E. G. Thomsen and J. T. Lapsley, Jr., Proceedings of the Society of Experimental Stress Analysis, vol. 11, 1954, p. 59.

2 "An Experimental Investigation of the Mechanics of Plastic Deformation of Metals," by E. G. Thomsen, C. T. Yang, and J. B. Bierbower, University of California Publication in Engineering, vol. 5, no. 4, 1954, p. 89.

3 "An Experimental Study of Metal Extrusions at Various Strain Rates," by J. Frisch and E. G. Thomsen, Trans. ASME, vol. 76, 1954, pp. 599–606.

4 "A New Approach to Metal-Forming Problems—Experimental Stress Analysis for a Tubular Extrusion," by E. G. Thomsen, Trans. ASME, vol. 77, 1955, pp. 515–522.

5 "Stresses and Strains in Cold Extruding 2S-O Aluminum," by E. G. Thomsen and J. Frisch, Trans. ASME, vol. 77, 1955, pp. 1343–1353.

6 "Plasticity Equations and Their Application to Working of Metals in the Work Hardening Range," by E. G. Thomsen, Trans. ASME, vol. 78, 1956, pp. 407–412.

7 "Über die Hencky-Prandtlschen Kurven-scharen," by C. Carathéodory and E. Schmidt, *Zeitschrift für angewandte Mathematik und Mechanik*, vol. 5, 1925, p. 147.

8 "Residual Stresses in Cold Extruded Aluminum," by J. Frisch and E. G. Thomsen, ASME Paper No. 55—A-27.

9 "Über einige statisch bestimmte Fälle des Gleichgewichts in Plastischen Körpern," by H. Hencky, *Zeitschrift für angewandte Mathematik und Mechanik*, vol. 3, 1923, p. 241.

10 "The Mathematical Theory of Plasticity," by R. Hill, Clarendon Press, Oxford, England, 1950.

11 "Theory of Perfectly Plastic Solids," by W. Prager and P. G. Hodge, John Wiley & Sons, Inc., New York, N. Y., 1951.

12 "Zur Theorie der Spannungszustände in plastischen und sandartigen Medien," by A. Haar and T. von Karman, Nachrichten von der Königlichen Gesellschaft der Wissenschaften zu Göettingen, Math. Phys. Klasse, 1909, p. 204.

13 "The Problem of Plasticity With the Axial Symmetry and Brinell's Test," by A. J. Ishlinsky, *Prikladnaia Mathematika i Mekhanika*, vol. 8, 1944, p. 201.

Analysis of Creep in Rotating Disks Based on the Tresca Criterion and Associated Flow Rule

By A. M. WAHL,[1] EAST PITTSBURGH, PA.

An analysis of creep deformations in rotating disks based on the Tresca criterion and the associated flow rule is presented. Assuming steady-state creep conditions and a creep rate equal to a function of stress times a function of time, the method is applied to the following cases: (*a*) Disk with constant thickness and constant temperature, (*b*) disk with variable thickness and constant temperature, and (*c*) disk with variable thickness and variable temperature. In many cases, the equations can be expressed in closed form. Comparison is made with test results on rotating disks at elevated temperature as reported in a previous paper. Based on certain stress-creep-rate relations, the method is also applied to the problem of calculating the transient change in stress when the stress distribution changes from an initial to a steady-state condition during the starting period. It is suggested that the simplification effected by the use of these methods may be of value for design purposes pending the development of more accurate methods based on test results.

Introduction

THIS paper may be considered a sequel to a previous paper (1)[2] in which the results of some long-time spin tests on 12 per cent chrome-steel disks at 1000 F were compared with the theoretical values using two methods of analysis. One of these methods (designated as Method 1 in what follows) was based on the Mises criterion (which is commonly used at present)[3] and the other (designated here as Method 2) on the Tresca (maximum-shear) criterion. The latter method, however, was combined with the flow rule associated with the Mises criterion in plasticity theory. It was found that Method 1 gave creep deformations much too low compared to average test values while Method 2 gave much better results. Both of these methods, however, require numerical integration of the differential equations involved and hence are rather cumbersome for practical use.

Recently Prager (2) and Koiter (3) have discussed the considerable simplification obtained by using the Tresca criterion and its associated flow rule for certain problems involving plastic flow. In the present paper the Tresca criterion and its associated flow rule (designated here as Method 3) are applied to the problem of calculating creep deformations and stresses in rotating disks operating at elevated temperatures. The results show a considerable simplification in the analysis; in many cases, where steady-state conditions are involved, the equations for stress and creep deformation may be expressed in closed form (even for variable-thickness disks), no numerical integrations being required. In addition, comparison with test data indicates that Method 3 is better in certain cases than the previously used one utilizing the Mises criterion (Method 1). Only disks with central holes are discussed in this paper.

Because of the simplification realized by using the Tresca criterion and its associated flow rule it is possible to treat many cases such as disks with radially variable temperature and the transient condition on starting (where the stress distribution relaxes from an initial to the steady-state condition). These become rather complicated if Method 1 is used.

In this paper, for simplicity, the creep rate $\dot{\epsilon}$ at a given temperature is assumed to be equal to a function of stress multiplied by a function of time, i.e.

$$\dot{\epsilon} = F(\sigma)f(t)$$

It is realized that this assumption does not always hold true; however, in many cases creep data obtained under essentially constant stress may be represented with sufficient approximation for engineering work in this manner. For example, recently Bailey (4) has made the assumption that the creep rate is the product of a power function of stress multiplied by a power function of strain. By integration of this expression it may be shown that this is equivalent to assuming the creep rate equal to $F(\sigma)f(t)$, both functions in this case being power functions (5). Moreover, Johnson (6) states that a creep-rate function of the form $F(\sigma)f(t)$ is "most descriptive of the experimental data for many materials particularly at moderate or lower stresses in the primary stages of creep." No attempt is made here to justify the use of this function for all materials; it is used here because it results in rather simple expressions for stress in certain cases.

In the previous paper (1) the opinion was expressed that the differences between test and theoretical results obtained by using the Mises criterion might be due to effects of anisotropy of the material. Since that time, however, some tests have been made by one of the authors of the paper mentioned (M. J. Manjoine) using tension-creep specimens cut in a direction perpendicular to the plane of the disk (the axial direction). These tests showed average creep rates in the axial direction about 20 to 40 per cent greater than those obtained in the tangential direction. This amount of anisotropy does not appear to be sufficient to account for the relatively large differences obtained between average test results and those calculated using the Mises criterion. In the present paper, effects of anisotropy will be neglected.

The various methods discussed in this paper may be defined as follows.

Method 1. This involves the use of the stress-creep-rate rela-

[1] Advisory Engineer, Mechanics Department, Westinghouse Research Laboratories. Fellow ASME.

[2] Numbers in parentheses refer to the Bibliography at the end of the paper.

[3] See references (3 to 8), inclusive, of the previous paper (1); also see article listed in reference (5) of this paper.

Contributed by the Applied Mechanics Division and presented at the Diamond Jubilee Annual Meeting, Chicago, Ill., November 13–18, 1955, of The American Society of Mechanical Engineers.

Discussion of this paper should be addressed to the Secretary, ASME, 29 West 39th Street, New York, N. Y., and will be accepted until July 10, 1956, for publication at a later date. Discussion received after the closing date will be returned.

Note: Statements and opinions advanced in papers are to be understood as individual expressions of their authors and not those of the Society. Manuscript received by ASME Applied Mechanics Division, May 31, 1955. Paper No. 55—A-46.

tions based on the Mises criterion and its associated flow rule as was done in (1).

Method 2. This method utilizes the Tresca (maximum-shear) criterion with the flow rule associated with the Mises criterion as discussed in (1).

Method 3. This method which is developed in this paper assumes stress-strain-rate relations corresponding to the Tresca criterion and its associated flow rule. The application of this method to the various cases is discussed in Sections 2 to 5.

The following rotating-disk cases are analyzed using Method 3. Other cases could also be analyzed in a similar way. In all cases it is assumed that the disk has a central hole or bore of diameter considerably greater than the thickness, as was the case for the disks tested, and that axial stresses are negligible (thin disk). Note that Cases I to III below are restricted to steady-state conditions (where the stress does not change with time). This means that the initial transient condition is neglected in these cases.

Case I. Disk having constant thickness and constant temperature—steady-state conditions.

Case II. Disk having variable thickness and constant temperature—steady-state conditions.

Case III. Disk with variable thickness and variable temperature—steady-state conditions.

Case IV. Disk with constant thickness and temperature, considering the transient condition during starting where the initial distribution changes to the steady-state condition.

2. Case I. Constant Thickness and Constant Temperature Disk—Steady-State Condition

For the constant thickness rotating disk, Fig. 1*b*, operating under steady-state conditions, in the previous paper (1) the tangential, radial, and axial strain rates $\dot{\epsilon}_t$, $\dot{\epsilon}_r$, $\dot{\epsilon}_z$ were taken in the following form

$$\left.\begin{aligned} \frac{\dot{w}}{r} &= \dot{\epsilon}_t = F(s)f(t)\left[\frac{\sigma_t - \sigma_r/2}{s}\right] \\ \frac{d\dot{w}}{dr} &= \dot{\epsilon}_r = F(s)f(t)\left[\frac{\sigma_r - \sigma_t/2}{s}\right] \\ \dot{\epsilon}_z &= -(\dot{\epsilon}_t + \dot{\epsilon}_r) \end{aligned}\right\} \quad \ldots\ldots\ldots [1]$$

where σ_r and σ_t are radial and tangential stresses, Fig. 1, $\dot{w}$ = radial deformation rate $(dw)/(dt)$ at radius r, and $F(s)$ = function of equivalent or effective stress s. In (1), $F(s)$ was taken as a power function of s

For Method 2, s is taken equal to σ_t while if Method 1 is used, the expression for s becomes

$$s = \sqrt{\sigma_t^2 - \sigma_r\sigma_t + \sigma_r^2} \quad \ldots\ldots\ldots [2]$$

It should be noted, however, that the terms in the square brackets of Equations [1] as used in (1) correspond to the flow rule associated with the Mises criterion (2, 3).

The equilibrium condition to be satisfied by a rotating disk of constant thickness is

$$\frac{d}{dr}(r\sigma_r) - \sigma_t + \frac{\gamma\omega^2 r^2}{g} = 0 \quad \ldots\ldots\ldots [3]$$

In this γ = weight per unit volume, g = gravitational acceleration, ω = angular velocity.

In (1) Equations [1] and [3] were solved by a numerical integration method.

If we now assume the flow rule associated with the Tresca criterion (Method 3), $\dot{\epsilon}_r = 0$ and $\dot{\epsilon}_t = -\dot{\epsilon}_z$ assuming that $\sigma_t > \sigma_r > 0$ in Equations [1]. This latter inequality is fulfilled in the present

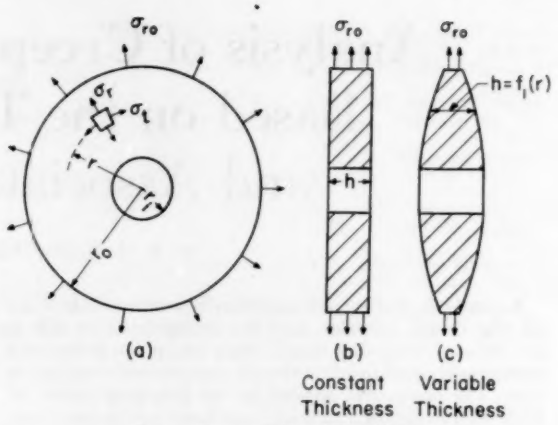

Fig. 1 Rotating Disk With Hole

case except right at the inside diameter where $\sigma_r = 0$ and at the outside diameter if σ_r at that point is zero. On this basis, $\dot{\epsilon}_t$ is taken independent of σ_r and Equations [1] reduce to

$$\left.\begin{aligned} \dot{\epsilon}_t &= \frac{\dot{w}_i}{r} = F(\sigma_t)f(t) \\ \frac{d\dot{w}}{dr} &= \dot{\epsilon}_r = 0 \\ \dot{\epsilon}_z &= -\dot{\epsilon}_t \end{aligned}\right\} \quad \ldots\ldots\ldots [4]$$

Integrating the second of these equations we obtain $\dot{w} = \dot{w}_i$ where $\dot{w}_i$ is the radial deformation rate at the inside diameter. Hence

$$\dot{\epsilon}_t = \dot{w}/r = \dot{w}_i/r$$

The tests of (1) indicate that the assumption $\dot{\epsilon}_r = 0$ as used in Equations [4] is approximately fulfilled except near the inside or outside diameter of the disk. It seems probable that the degree of approximation of this assumption near the inner diameter would depend to some extent on the ratio of disk thickness to hole diameter in a manner not yet explored. (In the case of the disks tested this ratio was 2.5.) Also for holes of small diameter relative to thickness, the condition of zero axial stress would not be fulfilled near the bore.

Power-Function Stress-Creep-Rate Relation. Taking

$$F(\sigma_t) = K\sigma_t^n$$

and using the first of Equations [4] we may solve for σ_t giving

$$\sigma_t = \left[\frac{\dot{w}_i}{Kf(t)}\right]^{1/n} r^{-1/n} \quad \ldots\ldots\ldots [5]$$

Integrating Equation [3], between the limits r_i and r_o, Fig. 1*a*

$$r\sigma_r\Big]_{r_i}^{r_o} = \int_{r_i}^{r_o} \sigma_t dr - \frac{\gamma\omega^2}{3g}(r_o^3 - r_i^3) \quad \ldots\ldots\ldots [6]$$

If a load giving a stress σ_{r_o} acts at the outside radius of the disk, while no load acts on the inside, Equation [6] may be integrated by substituting Equation [5] for σ_t under the integral sign. Integrating and solving for $\dot{w}_i/[Kf(t)]$ the latter may be substituted in Equation [5] giving

$$\sigma_t = \left(\frac{n-1}{n}\right)\left(\frac{\sigma_{r_o}(r_o - r_i)}{r_o^{\frac{n-1}{n}} - r_i^{\frac{n-1}{n}}}\right) r^{-1/n} \quad \ldots\ldots\ldots [7]$$

In this the average tangential stress σ_{tav} is

$$\sigma_{tav} = \frac{\gamma\omega^2(r_o^3 - r_i^3)}{3g(r_o - r_i)} + \frac{r_o\sigma_{ro}}{r_o - r_i} \quad \ldots\ldots\ldots\ldots [8]$$

Substituting Equation [7] in Equation [3] and integrating we obtain

$$\sigma_r = \frac{\sigma_{tav}(r_o - r_i)}{r}\left[\frac{r^{\frac{n-1}{n}} - r_i^{\frac{n-1}{n}}}{r_o^{\frac{n-1}{n}} - r_i^{\frac{n-1}{n}}}\right] - \frac{\gamma\omega^2(r^3 - r_i^3)}{3gr} \quad \ldots [9]$$

In Fig. 2 a comparison is made between the calculated radial and tangential stress distributions obtained using Methods 1 and 2 and those obtained using Method 3, Equations [7] and [9]. These stress values apply to the disks tested in (1). Note that the radial stress distribution is practically the same for all methods.

The tangential creep strain for any value of σ_t can be found by integrating $\dot{\epsilon}_t$, Equation [4], with respect to time.

Exponential Stress-Creep-Rate Relation. Taking

$$F(\sigma_t) = K\exp\left(\frac{\sigma_t}{\sigma_o}\right)$$

in the first of Equations [4] we obtain

$$\frac{\dot{w}_i}{rKf(t)} = \exp\left[\frac{\sigma_t}{\sigma_o}\right] \quad \ldots\ldots\ldots\ldots [9a]$$

In this K and σ_o are constants.

Solving for σ_t/σ_o

$$\frac{\sigma_t}{\sigma_o} = \ln\left(\frac{\dot{w}_i}{rKf(t)}\right) \quad \ldots\ldots\ldots\ldots [10]$$

Substituting this in Equation [3] and proceeding as before we obtain

$$\sigma_t = \sigma_o\left[\frac{\ln\frac{r_o}{r} - \frac{r_i}{r_o}\ln\frac{r_i}{r}}{1 - \frac{r_i}{r_o}}\right] + \sigma_{tav} - \sigma_o \quad \ldots\ldots [11]$$

In this σ_{tav} is given by Equation [8].

Substituting Equation [11] into Equation [3] and integrating, the expression for σ_r becomes

$$\sigma_r = \frac{\sigma_o r_o}{r_o - r_i}\left[\left(\ln\frac{r_o}{r} + 1\right) + \frac{r_i}{r}\left(\ln\frac{r_i}{r_o} - 1\right) + \frac{r_i}{r_o}\left(\ln\frac{r}{r_i} - 1 + \frac{r_i}{r}\right)\right] + \left(1 - \frac{r_i}{r}\right)(\sigma_{tav} - \sigma_o) - \frac{\gamma\omega^2(r^3 - r_i^3)}{3gr} \quad \ldots\ldots [12]$$

If the constant σ_o in the expression for creep rates is chosen so that the strain rates agree at 25,000 and at 30,000 psi with those given by the power-function relation for $n = 6$, the results for σ_t and σ_r are practically the same as those given for Method 3 in Fig. 2. This would be expected since within this range of stress the power and exponential functions agree closely.

Comparison With Test Results. In Figs. 3 to 5, a comparison of the creep deformations calculated by the various methods is shown compared with the scatter bands obtained by spin tests on three disks as discussed in (1). The curves for Methods 1 and 2 shown on these figures are the same as those given in (1) while the

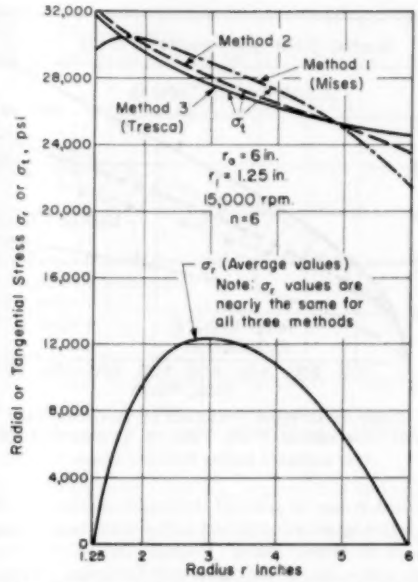

FIG. 2 COMPARISON OF STRESS DISTRIBUTIONS IN ROTATING DISK CALCULATED BY DIFFERENT METHODS FOR POWER-FUNCTION RELATION ($n = 6$)

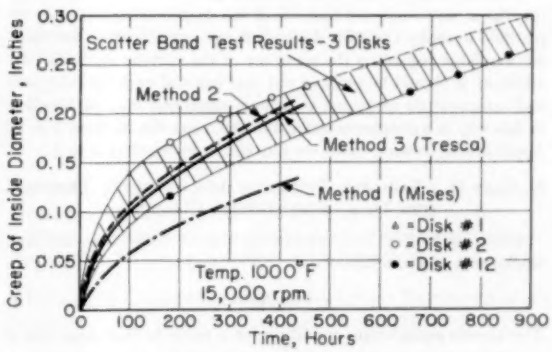

FIG. 3 CREEP ON INSIDE DIAMETER OF ROTATING DISK VERSUS TIME AND COMPARISON WITH VARIOUS THEORETICAL METHODS (For method of making tests see reference 1.)

curves for Method 3 were calculated on the basis of Equations [4] and [7] using the test data for the material given in (1). Account was taken of the slight increase in stress due to the expansion of the disk as the creep progressed in the same manner as was done in (1).

Reference to Fig. 4 indicates that the creep deformations at the outside diameter as calculated by Method 3 are high compared to the test values, particularly in the later stages of the spin tests. However, as far as the deformations at the inside diameter are concerned, Fig. 3, the results obtained using Method 3 are rather close to average test results up to around 400 hr. (Because of lack of tension-creep data at true stresses around 32,000 psi for times around 500 to 900 hr the curves of Fig. 3 were not extended beyond about 400 hr.) Also as shown in Fig. 5 the tangential creep-strain distributions obtained using Method 3 lie within the scatter band of the test values.

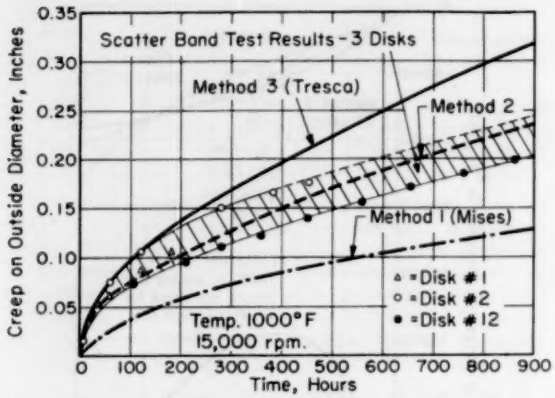

FIG. 4 CREEP ON OUTSIDE DIAMETER OF ROTATING DISK VERSUS TIME AND COMPARISON WITH VARIOUS THEORETICAL METHODS
(For method of making tests see reference 1.)

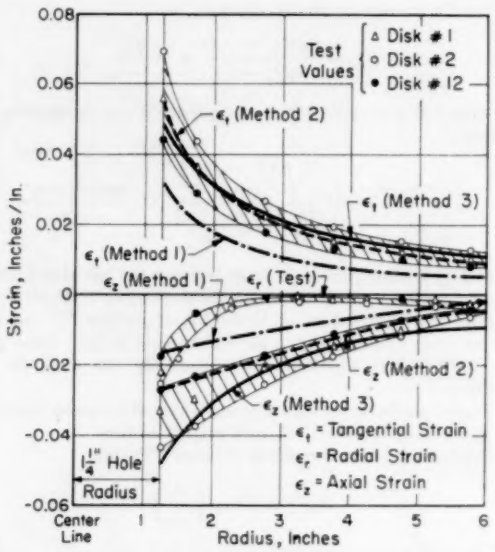

FIG. 5 CREEP-STRAIN DISTRIBUTIONS ALONG RADIUS AFTER 180 HR COMPARED WITH CALCULATED VALUES USING VARIOUS METHODS
(Crosshatched regions show scatter bands of test results.)

In general, it may be said that the results calculated by Method 3 are in better agreement with test values than those calculated on the basis of the Mises criterion (Method 1) which yields much too low creep values, i.e., on the unsafe side for design. Method 2 as indicated in the previous paper (1) probably gives the best overall agreement with test values. However, as stated in (1), further test data are required before general conclusions may be drawn as to the best method for practical use; in view of this uncertainty it is the author's opinion that use of the simpler Method 3 may be justified in many cases for design purposes until further test data are available regarding the accuracy of the various methods. In addition, it should be pointed out that cases of variable thickness and temperature and also transient conditions may be handled in this way in a simpler manner than by using the Method 1 or 2. Applications to such cases are illustrated in Sections 3 to 5.

3 CASE II. VARIABLE THICKNESS AND CONSTANT TEMPERATURE DISK—STEADY-STATE CONDITION

Referring to Fig. 1(*c*), assume $\sigma_t > \sigma_r > 0$ and that the disk thickness h is a function of r

$$h = f_1(r) \quad [13]$$

The known equilibrium condition for a variable thickness disk is

$$\frac{d}{dr}(rh\sigma_r) - h\sigma_t + \frac{\gamma\omega^2 hr^2}{g} = 0 \quad [14]$$

Assume again that no stress or loading acts on the inside diameter of the disk and that a radial stress σ_{r_o} acts at the outside diameter. Then integrating Equation [14]

$$r_o h_o \sigma_{r_o} = \int_{r_i}^{r_o} h\sigma_t dr - \frac{\gamma\omega^2}{g}\int_{r_i}^{r_o} hr^2 dr \quad [15]$$

where

h_o = thickness at outside diameter

Let σ_{tav} = average tangential stress across section, A = area of cross section, and

$$I_o = \int_{r_i}^{r_o} hr^2 dr$$

equals moment of inertia of cross section about disk axis. Then

$$\sigma_{tav} = \frac{1}{A}\int_{r_i}^{r_o} h\sigma_t dr \quad [16]$$

$$\sigma_{tav} = \frac{r_o h_o \sigma_{r_o}}{A} + \frac{\gamma\omega^2 I_o}{gA} \quad [16a]$$

Power-Function Stress-Creep-Rate Relation. Using Method 3 and taking a power-function stress-creep-rate relation

$$\dot{\epsilon}_i = K\sigma_i^n f(t)$$

(as was done in Case I), we substitute Equation [5] for σ_i in Equation [14] and integrate from r_i to r_o. This gives

$$\int_{r_i}^{r_o} h\sigma_t dr = \sigma_{tav}A = \left[\frac{\dot{w}_i}{Kf(t)}\right]^{1/n}\int_{r_i}^{r_o} hr^{-1/n} dr \quad [17]$$

Solving for

$$\left[\frac{\dot{w}_i}{Kf(t)}\right]^{1/n}$$

and substituting in Equation [5], the tangential stress becomes

$$\sigma_t = \frac{\sigma_{tav}Ar^{-1/n}}{\int_{r_i}^{r_o} hr^{-1/n} dr} \quad [18]$$

The radial stress σ_r is obtained by integrating Equation [14] using Equation [18]. For no radial stress at the inside diameter

$$\sigma_r = \frac{1}{rh}\left[\int_{r_i}^{r} h\sigma_t dr - \frac{\gamma\omega^2 I}{g}\right] \quad [19]$$

where

$$I = \int_{r_i}^{r} hr^2 dr$$

equals moment of inertia about axis of section out to a radius r.

If we assume, for example, $h = cr^m$ as a power function of the radius, Equations [18] and [19] become

$$\sigma_t = \frac{\alpha\sigma_{tav}Ar^{-1/n}}{c(r_o^{\alpha} - r_i^{\alpha})} \quad [20]$$

$$\sigma_r = \frac{1}{cr^{m+1}}\left[\frac{\sigma_{tav}A(r^\alpha - r_i^\alpha)}{r_o^\alpha - r_i^\alpha} - \frac{\gamma\omega^2 I}{g}\right] \quad [20a]$$

In these $\alpha = (mn + n - 1)/n$. As before, the creep strains can be obtained by integrating the first of Equations [4] with respect to time.

Exponential Stress-Creep-Rate Relation. We assume an exponential stress-creep-rate relation

$$\dot{\epsilon}_t = Kf(t)\exp\left(\frac{\sigma_t}{\sigma_o}\right)$$

Using Equation [10] in Equation [16] and integrating, we obtain

$$\ln\left[\frac{\dot{w}_i}{Kf(t)}\right] = \frac{\sigma_{tav}}{\sigma_o} + \frac{1}{A}\int_{r_i}^{r_o} h \ln r\, dr \quad [21]$$

Substituting this in Equation [10] the expression for tangential stress becomes

$$\sigma_t = \sigma_{tav} + \frac{\sigma_o}{A}\int_{r_i}^{r_o} h \ln r\, dr - \sigma_o \ln r \quad [22]$$

To obtain the radial stress σ_r, Equation [22] is substituted in Equation [19] and the integration carried out. Assuming, for example

$$h = f_1(r) = cr^m$$

Equation [22] becomes

$$\sigma_t = \sigma_{tav} + \frac{\sigma_o cB_1}{A(m+1)} - \sigma_o \ln r \quad [23]$$

where

$$B_1 = r_o^{m+1}\ln r_o - r_i^{m+1}\ln r_i + \frac{r_i^{m+1} - r_o^{m+1}}{m+1} \quad [23a]$$

Using Equation [23] in Equation [19]

$$\sigma_r = \frac{1}{r^{m+1}}\left[\left(\sigma_{tav} + \frac{\sigma_o cB_1}{A(m+1)}\right)\left(\frac{r^{m+1} - r_i^{m+1}}{m+1}\right) - \frac{\sigma_o B_2}{m+1} - \frac{\gamma\omega^2 I}{gc}\right] \quad [24]$$

where

$$B_2 = r^{m+1}\left(\ln r - \frac{1}{m+1}\right) - r_i^{m+1}\left(\ln r_i - \frac{1}{m+1}\right)$$

These equations are restricted to the case where $\sigma_t > \sigma_r > 0$.

4 Case III. Variable Thickness Disk With Variable Temperature—Steady State

In this case we assume that both stress and temperature are constant in time (steady state) while the temperature is a function of the radius r. As an example, to illustrate the method, we will assume that the creep rate of the material for constant stress can be expressed as the product of functions of stress, temperature, and time. For simplicity it is further assumed that both temperature and thickness variations in the radial directions are not too great so that the condition $\sigma_t > \sigma_r > 0$ holds. (If this is not the case the analysis becomes more complicated.) Under these conditions the tangential creep rate $\dot{\epsilon}_t$ in Equations [4] can be expressed as

$$\frac{\dot{w}_i}{r} = \dot{\epsilon}_t = F(\sigma_t)f(t)\phi(r) \quad [25]$$

(The term $\phi(r)$ is assumed to take into account the effects of radial variation in temperature.)

Using an exponential function for $F(\sigma_t)$ we obtain

$$\dot{\epsilon}_t = \frac{\dot{w}_i}{r} = Kf(t)\phi(r)\exp\left(\frac{\sigma_t}{\sigma_o}\right) \quad [26]$$

Solving this for σ_t

$$\sigma_t = \sigma_o \ln\frac{\dot{w}_i}{Kf(t)} - \sigma_o \ln[r\phi(r)] \quad [27]$$

Proceeding as before by substituting this in Equation [16] and integrating, an expression for

$$\ln\left[\frac{\dot{w}_i}{Kf(t)}\right]$$

is found; this may be substituted in Equation [27] giving

$$\sigma_t = \sigma_{tav} + \frac{\sigma_o}{A}\int_{r_i}^{r_o} h \ln[r\phi(r)]dr - \sigma_o \ln[r\phi(r)] \quad [28]$$

Here h is a function of r and σ_{tav} is calculated using Equation [16a].

The expression for σ_r may be obtained as before, using this in Equation [19] and integrating.

If a power-function relation is assumed for $F(\sigma_t)$, the expression for $\dot{\epsilon}_t$ becomes

$$\dot{\epsilon}_t = \frac{\dot{w}_i}{r} = K\sigma_t^n f(t)\phi(r) \quad [29]$$

Proceeding as before, the following expression for σ_t may be derived

$$\sigma_t = \frac{A\sigma_{tav}[r\phi(r)]^{-1/n}}{\int_{r_i}^{r_o} h[r\phi(r)]^{-1/n}\, dr} \quad [30]$$

The stress σ_r may be obtained as before and in this way we may determine whether or not the condition $\sigma_t > \sigma_r > 0$ holds.

The creep strains at any radius r can be obtained from Equation [26] or [29] and integrating with respect to time.

5 Case IV. Transient Change of Stress Distribution on Starting, for Disk With Constant Thickness and Temperature

The previous calculations (Cases I to III) were all based on the assumption of a steady-state stress distribution. However, when the disk is first brought up to speed it may be expected that stress distribution will be nearly elastic if the stresses are low enough and hence will differ from the steady-state condition. In addition for higher stress there may be some plastic yielding or creep near the inside diameter while bringing the disk up to speed. This will result in a tangential stress distribution along the radius as shown by the full line for $t = 0$ in Fig. 6, which refers to the disk tested in (1). After a time this stress distribution changes to the steady state as indicated.

Soderberg (7) has developed a rather complicated method of calculating this transient change in stress distribution based on the Mises criterion. In this paper, we will utilize the Tresca criterion and associated flow rule to develop a simpler approximate method which may yield at least a fair estimate of the time required for the stress distribution to change from the initial to the final steady-state value.

We now assume that the total tangential strain ϵ_t is the sum of a plastic strain ϵ_{tp} due to creep and an elastic strain. In an incre-

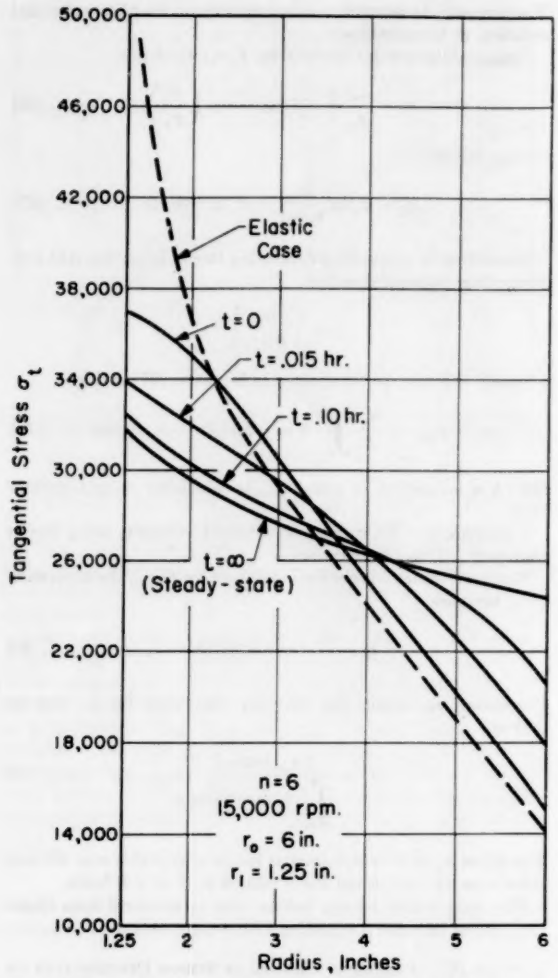

FIG. 6 CHANGE IN TANGENTIAL-STRESS DISTRIBUTION WITH TIME DURING TRANSIENT PERIOD FOR ROTATING DISK

ment of time $\Delta t = t_o - t_i$, the change in tangential strain $\Delta\epsilon_t$ then becomes

$$\Delta\epsilon_t = \frac{\Delta w}{r} = \frac{\Delta\sigma_t}{E} - \nu\frac{\Delta\sigma_r}{E} + \Delta\epsilon_{tp} \quad [31]$$

In this equation $\Delta\sigma_t$ and $\Delta\sigma_r$ are the increments of change in tangential and radial stresses, respectively, in time Δt, ν = Poisson's ratio, E = modulus of elasticity, and $\Delta\epsilon_{tp}$ is the plastic strain occurring in time Δt.

In this case, we assume that the plastic-strain rate $\dot{\epsilon}_{tp}$ in the increment Δt can be expressed approximately as follows

$$\dot{\epsilon}_{tp} = K\sigma_t^n t^m \quad [32]$$

(This assumption should be considered as a very rough approximation when the stress changes with time since recovery and other effects are neglected, but it is used here for simplicity.)

A further assumption is made that the stress σ_t does not change too much during the time increment Δt so that in applying Equation [32] we can use an average stress

$$\sigma_{ta} = \sigma_t + \frac{\Delta\sigma_t}{2}$$

in the increment Δt as a basis for calculating $\Delta\epsilon_{tp}$. Hence in time Δt, using σ_{ta} for σ_t in Equation [32]

$$\Delta\epsilon_{tp} = \int_{t_i}^{t_o} K\sigma_{ta}^n t^m\, dt \quad [33]$$

On the basis of the flow rule associated with the Tresca criterion the plastic component of radial strain $\Delta\epsilon_{rp}$ will be zero provided $\sigma_t > \sigma_r > 0$ as is the case for the disk of Fig. 1(*b*), except right at the inner edge. Using Equation [33] in Equation [31]

$$\Delta\epsilon_t = \frac{\Delta w}{r} = \frac{\Delta\sigma_t}{E} - \nu\frac{\Delta\sigma_r}{E} + \int_{t_i}^{t_o} K\sigma_{ta}^n t^m\, dt \quad [34a]$$

$$\Delta\epsilon_r = \frac{d(\Delta w)}{dr} = \frac{\Delta\sigma_r}{E} - \nu\frac{\Delta\sigma_t}{E} \quad [34b]$$

where Δw = increment of radial deflection at radius r in time Δt.

Integrating the second of these equations between r_i and r we have

$$\Delta w = \int_{r_i}^{r}\frac{\Delta\sigma_r dr}{E} - \int_{r_i}^{r}\nu\frac{\Delta\sigma_t}{E}dr + \Delta w_i \quad [35]$$

In this Δw_i = radial deflection increment at $r = r_i$, Fig. 1(*a*). Also from the equilibrium condition, Equation [3], for constant thickness, by integration

$$\Delta\sigma_r = \frac{1}{r}\int_{r_i}^{r}\Delta\sigma_t\, dr \quad [36]$$

Assuming only a small change in σ_t during the time increment Δt, as an approximation in Equation [34*a*], we write

$$\sigma_{ta}^n = \sigma_t^n\left(1 + \frac{n\Delta\sigma_t}{2\sigma_t}\right)$$

Using this it is possible to eliminate Δw between Equations [34*a*] and [35] and solve for $\Delta\sigma_t$. Putting

$$\Delta w_i = r_i\Delta\epsilon_{ti}$$

where $\Delta\epsilon_{ti}$ is the increment of strain at the inside diameter in time Δt and, using Equation [36], we obtain

$$\Delta\sigma_t = \frac{E\Delta\epsilon_{ti}r_i}{r\phi_1} - \frac{E\Delta\epsilon_{ti}}{\phi_1}\left(\frac{\sigma_t}{\sigma_{ti}}\right)^n + \frac{1}{r\phi_1}\int_{r_i}^{r}\Delta\sigma_r dr \quad [37]$$

In this

$$\Delta\epsilon_{ti} = \frac{K\sigma_{ti}^n}{m+1}(t_o^{m+1} - t_i^{m+1}) \quad [38]$$

σ_{ti} = steady-state value of stress at inside diameter calculated from Equation [7]

$$\phi_1 = \frac{nE\Delta\epsilon_{ti}}{2\sigma_{ti}}\left(\frac{\sigma_t}{\sigma_{ti}}\right)^{n-1} + 1 \quad [39]$$

Note that σ_t here is the initial value of σ_t at time $t = t_i$. The final value at $t = t_o$ is $\sigma_t + \Delta\sigma_t$.

Also from equilibrium

$$\int_{r_o}^{r_i}\Delta\sigma_t dr = 0$$

Using Equation [37] in this and integrating we may solve for $\Delta\epsilon_{ti}$. Substituting this value in Equation [37] and using Equation [36] for $\Delta\sigma_r$ we obtain

$$\Delta\sigma_t = \psi(r) + \psi_1(r) \quad [40]$$

$$\psi(r) = \frac{E\Delta\epsilon_{tsi}}{\phi_1}\left[\frac{\Sigma_1}{r\Sigma_2} - \left(\frac{\sigma_t}{\sigma_{tsi}}\right)^n\right] \quad [41]$$

$$\psi_1(r) = \frac{1}{r\phi_1}\left[B - \frac{\Sigma_3}{\Sigma_2}\right] \quad [42]$$

where

$$B = \int_{r_i}^{r}\frac{dr}{r}\int_{r_i}^{r}\Delta\sigma_t\,dr; \quad \Sigma_1 = \int_{r_i}^{r_o}\left(\frac{\sigma_t}{\sigma_{tsi}}\right)^n\frac{dr}{\phi_1};$$

$$\Sigma_2 = \int_{r_i}^{r_o}\frac{dr}{r\phi_1}; \quad \Sigma_3 = \int_{r_i}^{r_o}\frac{B\,dr}{r\phi_1}$$

Equations [41] and [42] may be utilized to solve the problem in the following manner: An increment of strain $\Delta\epsilon_{tsi}$, Equation [38], is chosen corresponding to an increment of time $\Delta t = t_o - t_i$ where $t_i = 0$ at the start of the process. (This increment should be chosen small enough so that the stress increments $\Delta\sigma_t$ are small compared to the stresses σ_t.) The initial stress distribution σ_t as a function of r may be taken as the elastic distribution except that some allowance for yielding near the inside diameter may have to be made. In general, the term $\psi_1(r)$ will be small compared to the term $\psi(r)$ on the right side of Equation [40] so that for a first approximation $\Delta\sigma_t$ can be taken equal to $\psi(r)$. Then using the assumed $\Delta\epsilon_{tsi}$ values and the known σ_t and σ_{tsi} values, the value of $\psi(r)$ is computed by means of numerical integration using Equation [41]. Using these $\psi(r)$ values for $\Delta\sigma_t$ in Equation [42], by numerical integration a first approximation to $\psi_1(r)$ is computed, and from this a new set of $\Delta\sigma_t$ values using Equation [40]. From these new $\Delta\sigma_t$ values, a new set of $\psi_1(r)$ values is obtained using Equation [42]. In general, this process converges rapidly.

Having the $\Delta\sigma_t$ values for the first increment Δt, new σ_t values can be computed which are valid at time $t = \Delta t$. Using these new σ_t values, the process can be repeated for a new increment of time Δt which may be different from the first increment; thus new $\Delta\sigma_t$ values are obtained. This process is illustrated in the following example.

Example Calculation for Transient Period After Starting. This method is applied to the rotating-disk tests described in (1). We start out with an initial σ_t distribution plotted against the radius as shown by the full lines marked $t = 0$ in Fig. 6. To obtain this curve approximately, the tangential elastic strains near the bore were computed and, from the stress-strain diagram at the given temperature, the corresponding stresses could be obtained using the Tresca criterion. To compensate for the reduced stresses near the bore, the tangential stresses in the remaining elastic portions of the disk were increased slightly. This method is believed sufficiently accurate for our purpose since the exact shape of the $t = 0$ curve is not important. The curve for $t = \infty$ (steady state) is the same as that obtained using Method 3 in Fig. 2, which assumes $n = 6$. (The elastic-stress distribution is shown by the dashed line.)

To obtain the first approximation we assume $E\Delta\epsilon_{tsi} = 10{,}600$ psi corresponding to $\Delta t = 0.015$ based on $E = 25 \times 10^6$ psi and a creep-time relation as follows

$$\epsilon_{tsi} = 0.002\left(\frac{\sigma_{tsi}}{29{,}000}\right)^6 \quad (t^{0.5})$$

This relation is based on average tensile-creep data for the first few hours. Using this value of $E\Delta\epsilon_{tsi}$ and taking $\psi_1(r)$ equal to zero in Equation [40], the first approximation $\psi(r)$ to the $\Delta\sigma_t$ values can be obtained by numerical integration as indicated in Table 1. (The initial σ_t values are given by the curve marked $t = 0$ in Fig. 6, σ_{tsi} being 31,900 psi.) The calculations for this first approximation $\psi(r)$ are indicated in Table 1.

To obtain the next approximation for $\Delta\sigma_t$, we take $\psi(r) = \Delta\sigma_t$ in Equation [42] and calculate $\psi_1(r)$ by numerical integration. These values are then used in Equation [40] to obtain new $\Delta\sigma_t$ values, designated as $(\Delta\sigma_t)_2$. The method of doing this is indicated in Table 2.

TABLE 1 CALCULATION[a] OF FIRST APPROXIMATION $(\Delta\sigma_t)_1 = \psi(r)$

r	σ_t	σ_t/σ_{tsi}	$(\sigma_t/\sigma_{tsi})^6$	ϕ_1[b]	$\frac{1}{\phi_1}(\sigma_t/\sigma_{tsi})^6$	$(dr/\phi_1)(\sigma_t/\sigma_{tsi})^6$	$\frac{1}{r\phi_1}$	$\frac{dr}{r\phi_1}$	$\psi(r)$[c]
1.25	37000	1.16	2.44	3.10	0.788		0.258		−3670
2.00	35000	1.095	1.72	2.57	0.67	0.546	0.194	0.170	−3550
3.00	30500	0.957	0.77	1.80	0.426	0.550	0.184	0.189	−1160
4.00	25000	0.784	0.23	1.293	0.178	0.302	0.193	0.189	1640
5.00	20300	0.637	0.07	1.11	0.061	0.120	0.180	0.186	2600
6.00	15200	0.476	0.01	1.02	0.01	0.035	0.163	0.171	2900
						$\Sigma_1 = 1.553$		$\Sigma_2 = 0.905$	

[a] From $t = 0$ to $t = 0.015$ hr; $\sigma_{tsi} = 31{,}900$ psi.
[b] ϕ_1 is obtained from Equation [39] taking $n = 6$.
[c] $\psi(r)$ is obtained from Equation [41].

TABLE 2 CALCULATION OF SECOND APPROXIMATION $(\Delta\sigma_t)_2$

r	$\psi(r)$[a]	$\int_{r_i}^{r}\Delta\sigma_t dr$	$\frac{1}{r}\int_{r_i}^{r}\Delta\sigma_t dr$	B[b]	$\frac{B}{r\phi_1}$	$\frac{B\,dr}{r\phi_1}$	$\psi_1(r)$[c]	$(\Delta\sigma_t)_2$[d]	$\sigma_t-(\Delta\sigma_t)_2$
1.25	−3670	0	0	0	0		650	−3020	33980
2.00	−3550	−2700	−1350	−500	−97	−36	390	−3160	31840
3.00	−1160	−5050	−1680	−2010	−370	−234	90	−1070	29430
4.00	1640	−4810	−1200	−3450	−665	−520	−180	1460	26460
5.00	2600	−2690	−540	−4320	−780	−720	−330	2270	22570
6.00	2900	0	0	−4590	−748	−760	−340	2560	17760
						$-2270 = \Sigma_3$			

[a] Values of $\psi(r)$ and $r\phi_1$ obtained from Table 1.
[b] $B = \int_{r_i}^{r}\frac{dr}{r}\int_{r_i}^{r}\Delta\sigma_t dr$.
[c] $\psi_1(r)$ is obtained from Equation [42].
[d] $(\Delta\sigma_t)_2 = \psi(r) + \psi_1(r)$ from Equation [40].

Using the values $(\Delta\sigma_i)_2$ in the next to the last column of Table 2 for $\Delta\sigma_i$ in Equation [42] and repeating the process, a second approximation for $\psi_1(r)$ and a third approximation for $\Delta\sigma_i$ can be obtained. This will usually be quite close to $(\Delta\sigma_i)_2$. The values of σ_i for $t = 0.015$ hr are then $\sigma_i - (\Delta\sigma_i)_2$ where σ_i is given by the first column of Table 1. This new curve for $t = 0.015$ hr is indicated in Fig. 6. Now this σ_i curve may be used in the same way to get a new σ_i curve for a new value of t, i.e., $0.015 + \Delta t$, and the whole process repeated starting with the σ_i curve for $t = 0.015$. In calculating $\Delta\epsilon_{i_{ss}}$, Equation [38] may be used taking $t_i = 0.015$ and $t_s = 0.015 + \Delta t$. Results obtained in this way for $t_s = 0.1$ and $\Delta t = 0.085$ are given in Fig. 6. These results indicate that for the case considered the initial tangential stress approaches the steady-state condition within a very short time. Thus errors made by assuming a steady condition are small in this case.

6 Summary and Conclusions

For calculating stress distributions and creep deformations in rotating disks with central holes and operating at elevated temperatures, the procedure discussed in the present paper, involving use of the Tresca criterion with the associated flow rule (Method 3), appears to offer advantages in regard to simplicity and ease of calculation, both for the transient and steady-state conditions. In the latter case, for creep rates which may be written as

$$\dot{\epsilon} = F(\sigma)f(t)$$

(where $F(\sigma)$ is either a power or exponential function) the results may be expressed in closed form by relatively simple equations both for the constant thickness case and for certain variable thickness cases. Expressions are also given for the variable temperature case which apply if certain restrictions are met.

Comparison with available creep data on disks spun at elevated temperature (1) indicates that Method 3, besides being simpler, also gives results generally in closer agreement with test data than the commonly used method involving application of the Mises criterion and its associated flow rule (Method 1). (Incidentally, the latter criterion may yield too low creep values, i.e., on the unsafe side.) The best over-all agreement with test results is found using Method 2. However, further test data on other materials and under other conditions are needed before general conclusions can be drawn.

The method discussed here also appears to offer considerable simplification in the calculation where transient conditions are to be handled. As an illustration, equations are developed on the basis of certain assumptions for calculating the constant thickness disk during the initial starting period where the stress distribution changes from the initial to the steady-state value.

In view of the lack of test data concerning the accuracy of more complicated methods such as those involving use of the Mises criterion, it is the author's belief that, until additional test results become available, the simpler Method 3 as discussed here may provide useful design data, particularly for cases where the use of the more complicated Method 2 is not warranted. It is realized, of course, that this method may eventually have to be modified in the light of future developments. At present, the available test data, reference (1), appear to favor the use of Method 2, however.

Acknowledgment

The author is indebted to Mr. R. E. Peterson of the Research Laboratories for his suggestions and interest in this project and to Mr. M. J. Manjoine for additional test data on the material. The support given this work by Mr. R. P. Kroon of the Aviation Gas Turbine Division is also appreciated.

BIBLIOGRAPHY

1 "Creep Tests of Rotating Disks at Elevated Temperature and Comparison With Theory," by A. M. Wahl, G. O. Sankey, M. J. Manjoine, and E. Shoemaker, Journal of Applied Mechanics, Trans. ASME, vol. 76, 1954, pp. 225–235.

2 "On the Use of Singular Yield Conditions and Associated Flow Rules," by William Prager, Journal of Applied Mechanics, Trans. ASME, vol. 75, 1953, pp. 317–320.

3 "Partially Plastic Thick-Walled Tubes," by W. T. Koiter, Biezeno Anniversary Volume, Haarlem, Holland, 1953, p. 232.

4 "Creep Relationships and Their Application to Pipes, Tubes, and Cylindrical Parts Under Internal Pressure," by R. W. Bailey, Proceedings of the Institution of Mechanical Engineers, vol. 164, 1951, p. 425.

5 "Recent Advances in Theories of Creep of Engineering Materials," by F. K. G. Odquist, *Applied Mechanics Reviews*, vol. 7, 1954, p. 517.

6 "Creep Under Complex Stress Systems at Elevated Temperatures," by A. E. Johnson, Proceedings of the Institution of Mechanical Engineers, vol. 164, 1951, p. 433.

7 "Interpretation of Creep Tests for Machine Design," by C. R. Soderberg, Trans. ASME, vol. 58, 1936, pp. 733–743.

Plastic Deformation of Semi-Infinite Beams Subject to Transverse Impact Loading at the Free End

By M. F. CONROY,[1] NEWTON, MASS.

The object of this paper is to consider the plastic deformation of semi-infinite beams subject to dynamic transverse loading at the free end. The type of loading considered is that of a constant bending moment, together with a transverse force the magnitude of which is inversely proportional to the square root of time. Part 1 of the paper consists of a plastic-rigid analysis of the problem, based on the plastic-rigid analysis of infinite beams under transverse, constant velocity, impact loading developed by the author.[2] Part 2 of the paper consists of an elastic-plastic solution of the problem, based on a theoretical analysis of the plastic deformation of infinite beams subject to transverse, constant-velocity impact loading developed by H. F. Bohnenblust.[3] Specific problems are considered for which the deflection solutions obtained by elastic ideally plastic and rigid ideally plastic analyses are compared.

Nomenclature

The following nomenclature is used in the paper:

- x = distance along beam
- y = deflection
- K = $\partial^2 y/\partial x^2$, curvature of deflection curve
- m = mass per unit length of beam
- E = Young's modulus
- I = moment of inertia of cross section
- M = bending moment
- Q = shearing force
- t = time
- M_0 = limit value of M for elastic bending

Introduction

An elastic-plastic analysis of the deformation of infinite beams subject to dynamic, transverse, constant-velocity loading has been developed by H. F. Bohnenblust.[3] A plastic-rigid analysis of the same problem has been developed by the author.[2] These papers consider both the case of ideal plasticity and the case of a work-hardening material. A further investigation of the solutions obtained in these analyses indicates that similar types of solutions can be obtained for the problem of the plastic deformation of semi-infinite beams subject to dynamic transverse loading at the free end, when the loading consists of a constant bending moment and a transverse force of magnitude inversely proportional to the square root of time. Under this type of loading the free end of the beam moves at a constant velocity, say, V_1. This accounts for the similarity of the solutions obtained here to those derived in the references cited.[2,3]

In the present analysis, as in the papers mentioned, the bending moment of the beam is assumed to depend on the curvature of the deflection curve according to a nonlinear relation $M(K)$, that is obtained from the stress-strain curve of the material. As in the case of the usual elastic analysis, both the shear displacements of the cross sections and the rotary kinetic energy of the beam are neglected. The beam is assumed to extend infinitely in one direction only and to be initially at rest. At $t = 0$ the beam is loaded at the free end, $x = 0$, with a constant bending moment, $M(0)$, and a transverse force $Q(0)$, of magnitude inversely proportional to the square root of time. The results presented here concerning this problem are, of course, also valid for a beam of finite length l, with fixed end at $x = l$, until such time as the disturbance propagated from $x = 0$ reaches $x = l$.

Since much of the analysis presented here is analogous to the analyses previously developed,[2,3] some details which are discussed in those papers have not been repeated here.

1 Plastic-Rigid Solution

The plastic deformation of semi-infinite beams will be considered when a plastic-rigid type of analysis is adopted, rather than the elastic-plastic type of analysis. That is, we will assume here that elastic strains are negligible compared to plastic strains and so the elastic material can be considered to be rigid. It is expected that this type of analysis will be satisfactory for problems involving large strains. In general, problems in which elastic strains can be neglected are much easier to handle than the corresponding elastic-plastic problem. However, while such a simplification occurs here for the case of an ideally plastic material, no such simplification results for the case of a work-hardening material.

The beam is assumed to extend infinitely in one direction, say, the positive x-direction, and to be initially at rest. At $t = 0$ the beam is loaded at the free end, $x = 0$, with a constant bending moment $M(0)$ and a transverse force $Q(0)$ which varies inversely as the square root of time. In particular, we have

$$\left.\begin{aligned} M(0) &= M_0 - A' \\ Q(0) &= \frac{A}{\sqrt{t}} \end{aligned}\right\} \quad \ldots\ldots\ldots\ldots [1]$$

where A and A' are arbitrary constants. The equation of motion of the beam is

---

[1] Assistant Professor of Mathematics, Department of Mathematics, Boston College, Newton, Mass.

[2] "Plastic-Rigid Analysis of Long Beams Under Transverse Impact Loading," by M. F. Conroy, JOURNAL OF APPLIED MECHANICS, Trans. ASME, vol. 74, 1952, pp. 465–470.

[3] "The Behavior of Long Beams Under Impact Loading," by P. E. Duwez, D. S. Clark, and H. F. Bohnenblust, JOURNAL OF APPLIED MECHANICS, Trans. ASME, vol. 72, 1950, pp. 27–34.

Contributed by the Applied Mechanics Division and presented at the Diamond Jubilee Annual Meeting, Chicago, Ill., November 13–18, 1955, of THE AMERICAN SOCIETY OF MECHANICAL ENGINEERS.

Discussion of this paper should be addressed to the Secretary, ASME, 29 West 39th Street, New York, N. Y., and will be accepted until July 10, 1956, for publication at a later date. Discussion received after the closing date will be returned.

NOTE: Statements and opinions advanced in papers are to be understood as individual expressions of their authors and not those of the Society. Manuscript received by ASME Applied Mechanics Division, November 17, 1954. Paper No. 55—A-49.

$$\frac{\partial Q}{\partial x} + m\frac{\partial^2 y}{\partial t^2} = 0 \quad \ldots\ldots [2]$$

Now, it has been shown[3] that, under the assumption $y = tf(\eta)$, where $\eta = x^2/4t$, this equation of motion can be put in the form

$$S''(\eta) + m\frac{dK}{dM}S(\eta) = 0 \quad \ldots\ldots [3]$$

where $S = 2\sqrt{t}\,Q$ and $(dK)/(dM)$ depends upon the particular bending-moment-curvature relationship of the material. Once $S(\eta)$ has been determined so as to satisfy this equation together with appropriate boundary conditions, the shear force, bending moment, curvature, and deflection distributions along the beam may be obtained by means of integration. The results of these integrations have been presented.[3]

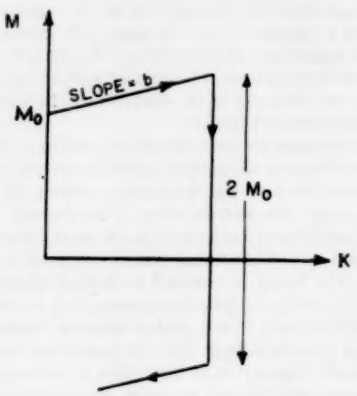

FIG. 1

Let us assume that the material of the beam obeys the plastic-rigid bending moment-curvature relationship of Fig. 1. In this case $S(\eta)$ is composed of sections of curves of the form

$$\left.\begin{array}{lll} \text{I} & S = -B(\eta - \eta_1) & 0 \le \eta \le \eta_1 \\ \text{II} & S = -C\sin\sqrt{\dfrac{m}{b}}\,(\eta - \eta_1) & \eta_1 \le \eta \le \eta_2 \\ \text{III} & S = D(\eta - \eta_2) & \eta_2 \le \eta \le \eta_3 \end{array}\right\} \ldots [4]$$

etc.

We have alternate rigid and plastic regions, the number of such regions depending upon the particular problem. The unknowns appearing in the solution, B, C, D, η_1, η_2, η_3, etc., are determined by imposing on the solution a set of conditions analogous to that used in previous work.[3] Conditions [1] and [3] therein are not necessary for the present problem, and Conditions [7] and [8] are replaced by the conditions

$$\frac{1}{2}\int_0^{\eta_1}\frac{S}{\sqrt{\eta}}\,d\eta = M_0 - M(0) \quad \ldots\ldots [5]$$

and

$$S(0) = 2A$$

The continuity conditions on S and S' have been discussed[3] for both the case of a work-hardening material, Fig. 1, and the case of an ideally plastic material, Fig. 2. Also, as noted before,[3] in plastic-rigid analysis the last region of the solution must be the straight-line region $S(\eta) = 0$.

Case of Ideal Plasticity. The bending-moment-curvature relationship of the material is assumed to be that of Fig. 2. It has been shown before[3] that, in the case of such an ideally plastic material, plastic hinges form instead of finite plastic regions. A consideration of the solution obtained for the problem of an infinite beam subject to a constant-velocity impact[3] suggests that, in the case of a rigid ideally plastic material, $S(\eta)$ consists of two regions and Equation [4] assumes the form

$$\left.\begin{array}{ll} S = -B(\eta - \eta_1) & 0 \le \eta \le \eta_1 \\ \text{Plastic hinge} & \eta = \eta_1 \\ S = 0 & \eta > \eta_1 \end{array}\right\} \quad \ldots\ldots [6]$$

This solution satisfies the necessary continuity conditions and,

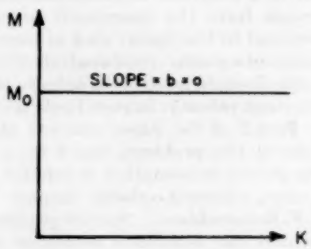

FIG. 2

once $Q(0)$ and $M(0)$ have been prescribed by fixing A and A' in Equation [1], B and η_1 may be determined from Equation [5]. It is found by imposing the conditions that

$$\left.\begin{array}{l} \eta_1 = \dfrac{9}{16}\left(\dfrac{A'}{A}\right)^2 \\ \text{and} \\ B = \dfrac{32}{9}\dfrac{A^3}{A'^2} \end{array}\right\} \quad \ldots\ldots [7]$$

Equations [6] and [7] completely determine $S(\eta)$ for a rigid ideally plastic semi-infinite beam, initially straight and at rest, and subject to a load at the free end of the type of Equation [1] in which $0 \le A' \le 2M_0$. Q, K, M, and y can be obtained from $S(\eta)$ by means of integration as previously shown.[3] It is also clear from these equations[3] that the free end of the beam moves with the constant velocity

$$V_1 = \frac{8A^2}{3mA'}$$

Since $\eta_1 = \dfrac{x_1^2}{4t} = \text{const}$, the plastic hinge at $\eta = \eta_1$ occurs physically at $x = x_1$ and moves outward along the beam, its distance from $x = 0$ being proportional to $\sqrt{t}$.

When $A' = 2M_0$, and hence $M(0) = -M_0$, the solution obtained is also that for an infinite beam[2] subject to a prescribed constant-velocity impact at $x = 0$. In this case plastic hinges appear at $x = 0$ and at $x = \pm x_1$.

Case of a Work-Hardening Material. The bending-moment-curvature relationship of the material is as shown in Fig. 1. $S(\eta)$ is composed of sections of curves of the form given by Equation [4]. Both $S(\eta)$ and $S'(\eta)$ must be everywhere continuous because the shear-force and bending-moment distributions are continuous along the beam. The last region of the solution must be the straight-line region $S = 0$, and the boundary conditions of Equa-

tion [5] must be satisfied. Moreover, in the case of a solution having more than three regions, the change in bending moment over every rigid region, except the first and last, must be $2M_0$. This is clear from the bending-moment-curvature relationship. However, as was demonstrated before,[2] it appears impossible to obtain a solution of the form of Equation [4] for which all of these conditions are satisfied, and yet have $S(\eta)$ be composed of a finite number of regions. Calculations have been carried out[2] which indicate that the number of regions may become infinite in the case of the plastic-rigid analysis for a work-hardening material. For this reason there is difficulty in obtaining a plastic-rigid solution analytically in the case of a work-hardening material. The form of $S(\eta)$, however, in the case of a plastic-rigid work-hardening material is that of Equation [4] where the unknown constants appearing in the solution are determined by imposing the conditions just cited.

2 Elastic-Plastic Solution

Now let us consider an elastic-plastic analysis of the deformation of semi-infinite beams when subject to dynamic transverse loading at the free end of the type given by Equation [1], where A and A' are arbitrary constants.

Bohnenblust[2] has shown that, under the assumption $y = tf(\eta)$ where $\eta = x^2/4\sqrt{\frac{EI}{m}}\,t$, Equation [2] can be written in the form

$$S''(\eta) + EI\,\frac{dK}{dM}\,S(\eta) = 0$$

where $(dK)/(dM)$ depends upon the bending-moment-curvature relationship of the material, and

$$S(\eta) = \frac{2}{EI}\left(\frac{EI}{m}\right)^{3/4}\sqrt{t}\,Q$$

Q, K, M, V_1, y may be obtained by means of integration, once $S(\eta)$ has been determined so as to satisfy the foregoing equation and the boundary conditions of the problem. The results of these integrations are given elsewhere.[2]

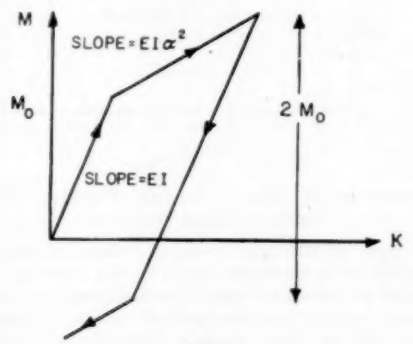

Fig. 3

Let us assume that the bending-moment-curvature relationship of the material is as shown in Fig. 3. In the case of a work-hardening material α is nonzero; in the case of an ideally plastic material $\alpha = 0$. For this particular bending-moment-curvature relation, $(dK)/(dM)$ is either

$$\frac{1}{EI} \quad \text{or} \quad \frac{1}{EI\alpha^2}$$

and, as shown by Bohnenblust, $S(\eta)$ is composed of sections of curves of the following form

$$\left.\begin{array}{lll} \text{I} & S = -B\sin(\eta - \eta_1) & 0 \le \eta \le \eta_1 \\ \text{II} & S = -C\sin\left(\frac{1}{\alpha}\right)(\eta - \eta_1) & \eta_1 \le \eta \le \eta_2 \\ \text{III} & S = D\sin(\eta - \eta_2) & \eta_2 \le \eta \end{array}\right\} \quad \ldots [8]$$

where, however, the number of regions is not necessarily three, but depends upon the particular problem. The unknowns of the solution, in this case $B, C, D, \eta_1, \eta_2, \eta_3$, are determined by imposing the following conditions on $S(\eta)$: (1) Continuity of S at η_2; (2) continuity of S' at η_1; (3) continuity of S' at η_2; (4) $M = M_0$ at η_3; (5) $S(0) = (2a^2/EI)A$; and (6)

$$M_0 - M(0) = \frac{EI}{2a^2}\int_0^{\eta} \frac{S(\eta)}{\sqrt{\eta}}\,d\eta$$

where

$$\left(a^2 = \sqrt{\frac{EI}{m}}\right)$$

Similar continuity and bending-moment conditions are imposed on solutions consisting of more than three regions. The change in bending moment over every elastic region, except the first and last, must equal $2M_0$.

Special Cases of Elastic-Plastic Solution

Elastic Beam. In the case of an elastic beam under impact, $|M(\eta)| < M_0$ for all η. Equation [8] takes the form

$$S(\eta) = -B\sin(\eta - \eta_1) \qquad 0 \le \eta \quad \ldots\ldots [9]$$

B and η_1 are determined by imposing the free-end boundary conditions

$$S(0) = \frac{2a^2}{EI}\,A = B\sin\eta_1$$

and

$$M(0) = M_0 - A' = \frac{-EI}{2a^2}\int_0^{\infty} \frac{-B\sin(\eta - \eta_1)}{\sqrt{\eta}}\,d\eta \quad \ldots [10]$$

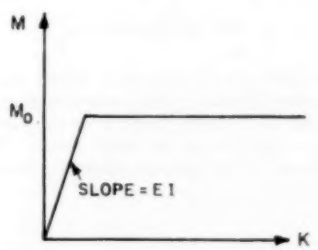

Fig. 4

Now, given A and A', it is clear that B and η_1 can be readily determined from Equations [9] and [10]. Q, K, M, y, and y' can then be obtained from $S(\eta)$, as shown by Bohnenblust.[2]

Case of Ideal Plasticity. In the case of a beam made of an elastic ideally plastic material having a bending-moment-curvature relationship of the type shown in Fig. 4, Equations [8] assume the form

$$\begin{array}{ll} S(\eta) = -B\sin(\eta - \eta_1) & 0 \le \eta \le \eta_1 \\ \text{Plastic hinge} & \eta = \eta_1 \\ S(\eta) = D\sin(\eta - \eta_1) & \eta \ge \eta_1 \end{array}$$

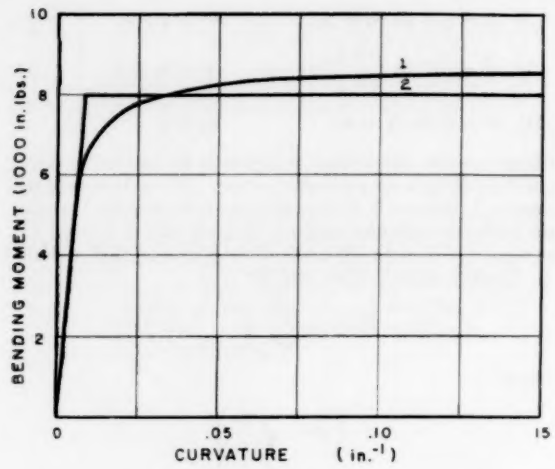

FIG. 5

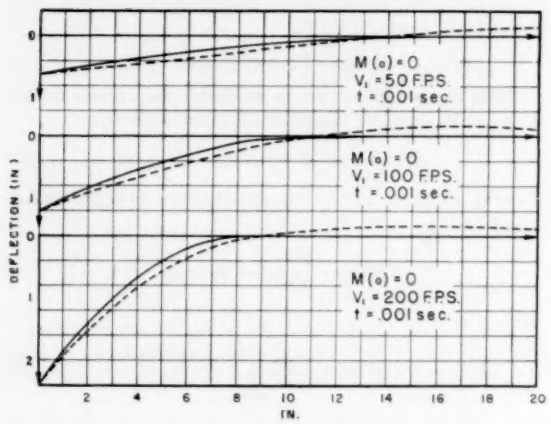

FIG. 6(*a*), (*b*), AND (*c*)

As mentioned before, in the case of an ideally plastic material, plastic hinges form instead of finite plastic regions. $S'(\eta)$ may be discontinuous at a plastic hinge, since the curvature of the beam may be discontinuous at these points. The unknown constants B, D, and η_1 may be determined from the following conditions

$$(1)\quad S(0) = \frac{2a^2}{EI} A$$

$$(2)\quad \frac{-EI}{2a^2} D \int_{\eta_1}^{\infty} \frac{\sin(\eta - \eta_1)}{\sqrt{\eta}}\, d\eta = M_0$$

$$(3)\quad \frac{-EI}{2a^2}\left[\int_0^{\eta_1} \frac{-B \sin(\eta - \eta_1)}{\sqrt{\eta}}\, d\eta + \int_{\eta_1}^{\infty} \frac{D \sin(\eta - \eta_1)}{\sqrt{\eta}}\, d\eta\right] = M(0)$$

Again, once $S(\eta)$ is completely determined, M, Q, K, and y can be immediately obtained.[3]

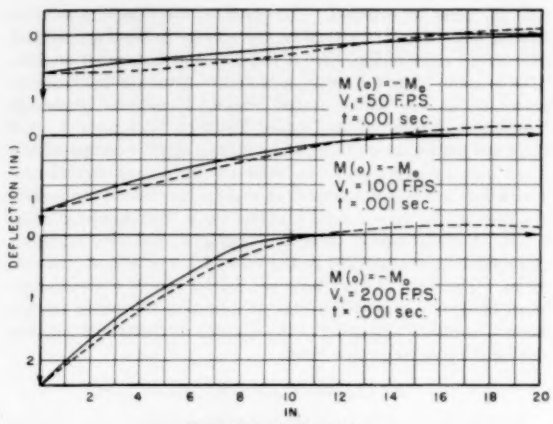

FIG. 7(*a*), (*b*), AND (*c*)

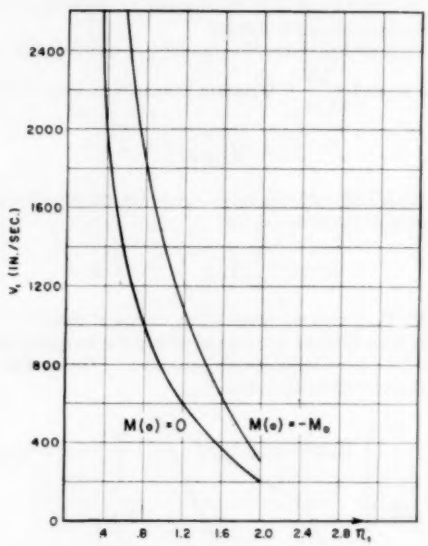

FIG. 8

3 COMPARISON OF ELASTIC IDEALLY PLASTIC AND RIGID IDEALLY PLASTIC SOLUTIONS

In the recent literature on the subject of the plastic deformation of beams subject to transverse impact loading, a number of problems have been solved by means of a rigid-plastic analysis. No comparison seems to have been made of the solutions obtained in this way with the more accurate elastic-plastic solutions, although Lee and Symonds[4] set up a criterion for the use of the rigid-plastic analysis in the case of finite beams. The lack of such comparisons is due to the absence of the elastic-plastic solutions of most of these problems. It seems worth while, then, since we have here both the elastic-plastic and rigid-plastic solutions of a class of problems, to cite a few examples and observe the corresponding elastic-plastic and rigid-plastic solutions. Because the problems discussed in the recent literature pertain to an ideally plastic material, the numerical work presented here will be re-

[4] "Large Plastic Deformations of Beams Under Transverse Impact," by E. H. Lee and P. S. Symonds, JOURNAL OF APPLIED MECHANICS, Trans. ASME, vol. 74, 1952, pp. 308–314.

stricted to the comparison of elastic ideally plastic and rigid ideally plastic solutions. The establishment of a criterion for the use of the more convenient rigid ideally plastic solution requires some modification of the Lee-Symonds criterion due to the fact that the beams discussed here are of infinite length. The author has not obtained such a criterion for infinite beams.

Bohnenblust, Duwez, and Clark[3] have shown that the bending moment-curvature curve for a cold-rolled low-carbon-steel beam $^3/_8$ in. wide and 1 in. deep is, as shown by curve 1, in Fig. 5. It was also shown that the bending moment and curvature at the elastic limit are 8000 in-lb and 0.853×10^{-2}/in., respectively. The numerical examples considered here pertain to such beams.

The approximate elastic ideally plastic bending moment-curvature curve taken for the computation is shown by curve 2 in Fig. 5. The approximate rigid ideally plastic bending-moment-curvature curve taken for the computations is shown by Fig. 2, where $M_0 = 8000$ in-lb.

In the first example a semi-infinite beam is subject to a dynamic transverse loading at the free finite end ($x = 0$) consisting of a zero bending moment and a transverse force of such a magnitude that the point $x = 0$ moves with a constant velocity of 50 fps. Both the rigid ideally plastic and elastic ideally plastic deflection curves are shown in Fig. 6(a) for $t = 0.001$ sec. The problem is repeated for impact velocities of 100 and 200 fps. The elastic ideally plastic and rigid ideally plastic solutions for the deflection curves are shown in Figs. 6(b) and 6(c). The Fresnel integrals encountered in the calculation of the elastic ideally plastic solutions can be evaluated with the aid of a table of integrals by C. M. Sparrow.[5]

In the second example a semi-infinite beam is subject to a dynamic transverse loading at the free finite end ($x = 0$) consisting of a bending moment, $M(0) = -M_0$. As before, the transverse force applied at this end is first of such a magnitude that the point $x = 0$ moves with a constant velocity of 50 fps. Then impact velocities of 100 and 200 fps are considered. The elastic ideally plastic and rigid ideally plastic solutions of these problems are shown in Fig. 7.

The manner in which η_1 varies with V_1 in the elastic ideally plastic solutions is shown in Fig. 8.

Acknowledgment

The author wishes to express her gratitude to Prof. P. S. Symonds of Brown University for his valuable suggestions.

---

[5] "Table of Fresnel Integrals," by C. M. Sparrow, Edwards Bros., Ann Arbor, Mich., 1934.

On the Ideally Plastic Indentation of Inset Rectangular Bands[1]

By E. W. ROSS, JR.,[2] WATERTOWN, MASS.

One of the limit design theorems of ideal plasticity is applied to find an upper bound on the initial indentation pressure for the case where a flat, smooth die is pushed into an inset band of rectangular cross section. The dependence of the upper bound on the clearance and width of the band is given, and a possible extension to asymmetrically inset bands is suggested.

Introduction

IN this paper we consider a rectangular band of ductile material partially set into a rigid encasement and indented by a flat, smooth die as shown in Fig. 1. We shall find an upper bound on the pressure which the die must exert in order to initiate permanent indentation. This problem is an idealization of the rotating-band engraving process in interior ballistics. The coordinate system and pertinent dimensions to be used are shown in Fig. 2. We assume $b \geqslant a$ throughout this paper.

Several results on a related problem are already in the literature. Hill[3] has shown that the average pressure to initiate plastic indentation cannot exceed $(2 + \pi)k$, k being the yield stress in pure shear, when L is very large (i.e., in plane strain) and $D/a \geqslant 0.707$. Shield and Drucker[4] have shown that the indentation pressure for this problem must exceed $5k$. The principal value of the present result is in indicating for what geometries these plane-strain bounds are inaccurate and in providing a better estimate of the indentation pressure for those cases.

We shall use one of the limit design theorems of ideal plasticity theory to give an upper bound on the indentation pressure for any values of L/a, H/a, and D/a. The die is assumed to be smooth, flat, and lubricated so no shear stress acts on the face $y = 0$, $|z| \leqslant L$, $|x| \leqslant a$. We assume that the band is glued or otherwise completely restrained on its inset faces so that $v_x = v_y = v_z = 0$ on the surface $y = -D$, $|z| \leqslant L$ and on the surfaces $|z| = L$, $-D \leqslant y \leqslant -H$. The band material is taken to obey Tresca's yield criterion, and work hardening is neglected.

We shall first present a rather inelegant version of the limit-design theorem to be used, then obtain the upper bound.

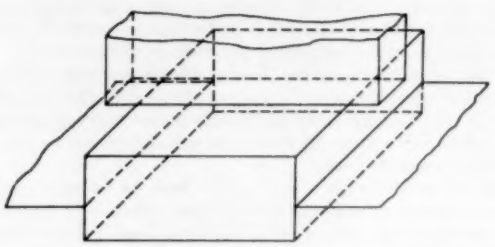

FIG. 1 INSET BAND AND DIE

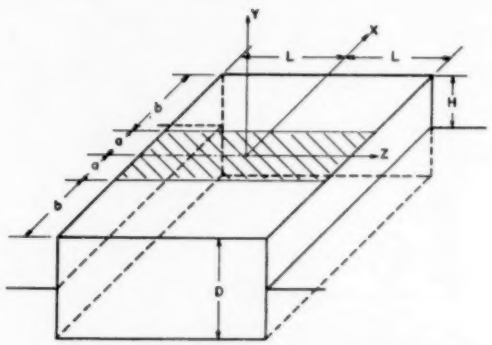

FIG. 2 CO-ORDINATE SYSTEM AND DIMENSIONS
(Loaded area is shown shaded.)

Limit-Design Theorem

Detailed statements and proofs of the two limit-design theorems can be found in the works of Prager and Hodge[5] and Drucker, Prager, and Greenberg.[6] Some additional comments are made by Shield,[7] and Shield and Drucker.[4]

We shall consider the assemblage consisting of the band and die; the band is assumed to be composed of an elastic-ideally plastic material, and the die is taken as rigid and subject to uniform pressure from above. It is clear that the boundary conditions on this assemblage obey the restrictions under which the limit-design theorems are effective; i.e., at all boundary points either the stress components are prescribed or the velocity components are zero.

A kinematically admissible velocity state is defined as a set of velocity components satisfying all conditions on velocities at the boundary of the assemblage and the incompressibility condition at all interior points. We can calculate a die pressure correspond-

---

[1] This work was done at Watertown Arsenal, Watertown, Mass., and originally appeared as Watertown Arsenal Laboratory Report No. 760/525.

[2] Mathematician, Watertown Arsenal Laboratory.

[3] "The Plastic Yielding of Notched Bars Under Tension," by R. Hill, *Quarterly Journal of Mechanics and Applied Mathematics*, vol. 2, 1949, pp. 40–52.

[4] "The Application of Limit Analysis to Punch-Indentation Problems," by R. T. Shield and D. C. Drucker, JOURNAL OF APPLIED MECHANICS, Trans. ASME, vol. 75, 1953, pp. 453–460.

Contributed by the Applied Mechanics Division and presented at the Diamond Jubilee Annual Meeting, Chicago, Ill., November 13–18, 1955, of THE AMERICAN SOCIETY OF MECHANICAL ENGINEERS.

Discussion of this paper should be addressed to the Secretary, ASME, 29 West 39th Street, New York, N. Y., and will be accepted until July 10, 1956, for publication at a later date. Discussion received after the closing date will be returned.

NOTE: Statements and opinions advanced in papers are to be understood as individual expressions of their authors and not those of the Society. Manuscript received by ASME Applied Mechanics Division, February 11, 1955. Paper No. 55—A-52.

[5] Theory of Perfectly Plastic Solids," by W. Prager and P. G. Hodge, Jr., John Wiley & Sons, Inc., New York, N. Y., 1951.

[6] "Extended Limit Design Theorems for Continuous Media," by D. C. Drucker, W. Prager, and H. J. Greenberg, *Quarterly of Applied Mathematics*, vol. 9, 1952, pp. 381–389.

[7] "The Plastic Indentation of a Layer by a Flat Punch," by R. T. Shield, *Quarterly of Applied Mathematics*, vol. 13, 1955, pp. 27–46.

ing to any kinematically admissible velocity state by equating the external work rate to the internal dissipation rate (assuming all strain rates to be plastic strain rates). The limit-design theorem that we shall use says that the die pressure found in this way is not less than the true die pressure required to initiate indentation.

When a kinematically admissible set of velocities has been chosen, the internal dissipation rate is given (for a material obeying Tresca's yield condition and flow rule) by

$$\text{Internal dissipation rate} = \int_V 2k \max |\dot{\epsilon}| \, dV \quad \ldots\ldots [1]$$

where $\max |\dot{\epsilon}|$ denotes the absolutely largest principal component of the plastic strain rates derived from the velocity state, k is the yield stress in pure shear and the integral is extended over the whole assemblage. If there are surfaces in the assemblage across which there are tangential velocity discontinuities involving plastic dissipation, then the expression

$$\int_{S_D} k \Delta v \, dS_D$$

must be added to the right side of Equation [1]; Δv is the magnitude of the velocity jump, and this integral is extended over all discontinuity surfaces.

An Upper Bound on the Initial Indentation Pressure

We begin by choosing the velocity state shown in Fig. 3.

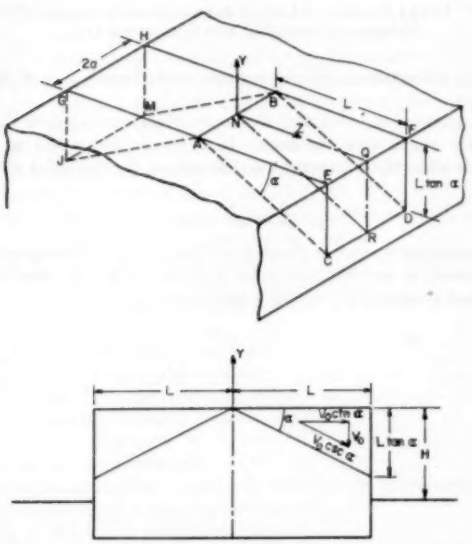

Fig. 3 Velocity Field for Narrow Bands, Showing Cross Section of Band Under Die

This may be described analytically as $v_x = v_y = v_z = 0$ everywhere except

$$\left.\begin{aligned} v_x &= 0 \\ v_y &= -V_0 \\ v_z &= V_0 \operatorname{ctn} \alpha \end{aligned}\right\} \text{ in zone } A\text{-}B\text{-}D\text{-}C\text{-}E\text{-}F \quad \ldots\ldots [2]$$

and

$$\left.\begin{aligned} v_x &= 0 \\ v_y &= -V_0 \\ v_z &= -V_0 \operatorname{ctn} \alpha \end{aligned}\right\} \text{ in zone } A\text{-}B\text{-}G\text{-}H\text{-}J\text{-}M \quad \ldots\ldots [3]$$

where V_0 is the downward velocity of the die. This state satisfies the incompressibility condition and all the velocity boundary conditions, provided

$$L \tan \alpha \leqslant H \quad \ldots\ldots [4]$$

All the internal energy dissipation takes place in the discontinuity surfaces *A-B-D-C*, *A-B-M-J*, *G-J-A*, *B-M-H*, *A-C-E*, and *B-F-D*. If we equate the internal dissipation rate and external work rate, using Equation [1], we find that the average pressure on the die is not less than k times

$$F(G;\ \alpha) = \frac{1}{\cos \alpha}\left[\frac{G}{2} + \frac{1}{\sin \alpha}\right] \quad \ldots\ldots [5]$$

where $G = L/a$. $F(G;\ \alpha)$ has a minimum with respect to α when α satisfies

$$\frac{G}{2} \sin^3 \alpha + 2 \sin^2 \alpha - 1 = 0 \quad \ldots\ldots [6]$$

This state with α given by Equation [6] (for any G this equation gives only one nonnegative value for $\sin \alpha$, and we must have $0 \leqslant \alpha \leqslant \pi/2$, hence no ambiguity in α-value is possible) will not be kinematically admissible unless α also satisfies Equation [4]. Where it fails to do so, the best value of α which makes the state kinematically admissible is given by

$$\alpha = \tan^{-1}\left(\frac{C}{G}\right) \quad \ldots\ldots [7]$$

where $C = H/a$. Thus, by the limit design theorem $kF\ (G;\ \alpha)$, with α given by Equation [6] or [7] as appropriate, is an upper bound on the indentation pressure for any value of D/a. When α is given by Equation [7] we can show the explicit dependence of F on G and C by

$$F = \frac{C}{G} + \frac{G}{C} + \frac{1}{2} C \sqrt{1 + \left(\frac{G}{C}\right)^2} \quad \ldots\ldots [8]$$

For wider bands (larger values of G), an upper bound better than Equation [5] is given by a velocity state (Fig. 4) combining the best kinematically admissible state so far found for plane

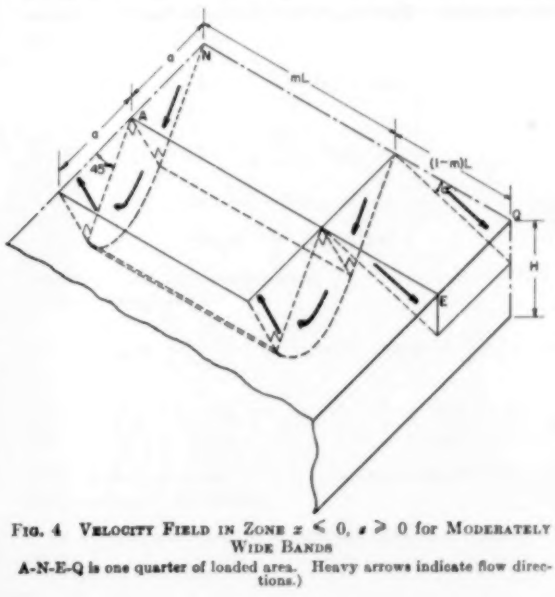

Fig. 4 Velocity Field in Zone $x \leqslant 0$, $z \geqslant 0$ for Moderately Wide Bands

A-N-E-Q is one quarter of loaded area. Heavy arrows indicate flow directions.)

strain ($G \to \infty$) near the middle of the band with the state used above near the end faces. The state near the middle of the band is the familiar one given by Hill.[3] The dissipation calculation shows that the die pressure equals or exceeds k times

$$Q(G; m, \alpha) = (2 + \pi)m + \frac{1 - m}{\sin \alpha \cos \alpha} + \frac{G}{2}\frac{(1-m)^2}{\cos \alpha} + \frac{\sqrt{2}}{G}\left(\frac{1}{2} + \frac{\pi}{8}\right) \quad [9]$$

where we must have

$$(1 - m)G \tan \alpha \leqslant C \quad [10]$$

in order for the velocity state to be kinematically admissible.

The values of m and α were found so as to minimize $Q(G; m, \alpha)$ subject to the constraining Condition [10]. By the limit-design theorem $kQ(G; m, \alpha)$ with these values of m and α is an upper bound on the initial indentation pressure.

The behavior of these upper bounds as functions of G and C is shown in Fig. 5. The bounds given by Equation [5], shown by solid lines, are valid for all values of D/a. The bounds given by Equation [9], shown by broken lines, are valid only for $D/a \geqslant 0.707$ because this velocity state violates the boundary condition $v_y = 0$ on $y = -D$, $|x| \leqslant L$ when $D/a < 0.707$. The solid line labeled "opt" gives the value of F from Equation [5] when α takes on the best possible value for each G, i.e., the value of α found from Equation [6]. The broken line labeled "opt" gives the value of Q from Equation [9] when α and m take on the best possible values for each G; it turns out that these optimum values are

$$\alpha \approx 37.2° \text{ (for all } G)$$

$$m \approx 1 - 2.442/G$$

and Condition [10] shows this bound is valid for $C \geqslant 1.85$, provided that $D/a \geqslant 0.707$. In general it is seen that the upper bound increases with band width and increases whenever it is affected by a decrease in band clearance. This is the qualitative behavior that one expects of the true average indentation pressure. Further, the bounds for wide bands (i.e., broken curves) all approach the plane-strain upper bound, $2 + \pi$, as $G \to \infty$.

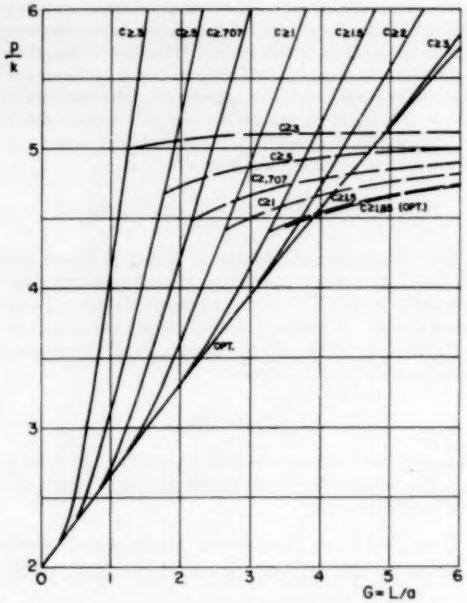

FIG. 5 UPPER BOUNDS ON INITIAL INDENTATION PRESSURE (P) FOR BANDS OF WIDTH ($2L$) AND CLEARANCE (H)

We mention in conclusion that only trivial extensions of these velocity states seem necessary in order to get useful upper bounds when the encasement is different on the two sides of the band.

ACKNOWLEDGMENT

The author wishes to thank the Office, Chief of Ordnance for permission to publish this paper and the reviewers, who contributed a number of valuable suggestions.

Stiffness of Curved Circular Tubes With Internal Pressure

By P. G. KAFKA[1] and M. B. DUNN,[1] SEATTLE, WASH.

A method is presented for computing the flexibility factor for plane pipe lines with internal-pressure effects considered. Formulas for the first and second approximation to both the flexibility and the stress-intensification factors are given. Comparisons of the second approximations with experimental results are also made.

Nomenclature

The following nomenclature is used in the paper:

- a = radius of pipe bend, in.
- b = mean radius of pipe section, in.
- $D = \frac{Eh^3}{12(1-\nu^2)}$ plate stiffness, in-lb
- E = modulus of elasticity, psi
- h = shell thickness, in.
- k = flexibility factor
- I = moment of inertia of pipe section, in.[4]
- M = applied bending moment, in-lb
- M_θ = bending moment per unit length on meridian, lb
- M_φ = bending moment per unit length on parallel, lb
- N_θ = normal force per unit length in parallel direction, lb/in.
- N_φ = normal force per unit length in meridional direction, lb/-in.
- P = internal pressure, psi
- r_0 = radius of curvature of parallel, in.
- r_1 = radius of curvature of meridian, in.
- r_2 = radius of curvature of surface in plane normal to meridian plane and containing r_1, in.
- v = displacement tangential to surface in meridional plane; positive in direction of positive φ, in.
- w = displacement normal to surface; positive in direction of inward normal, in.
- β = stress-intensification factor
- ϵ_θ = strain in parallel direction
- ϵ_φ = strain in meridional direction
- θ = angle subtended by arc of parallel
- ν = Poisson's ratio
- σ = bending stress, psi
- φ = angle between r_2 and axis of rotation in meridional plane
- χ_θ = change in principal curvature $1/r_2$
- χ_φ = change in principal curvature $1/r_1$

Introduction

When a plane pipe line, consisting of both straight and curved sections, is analyzed by simple beam theory as an indeterminate system under applied thermal loadings, the computed support reactions are greater than actually would be measured in an experiment. Th. von Karman (1)[2] showed that the apparent decrease in stiffness in such a case is due to an ovalization of the pipe in the curved sections. The effect of the ovalization is to reduce the stiffness parameter EI of the curved pipe to a fictitious value

$$(EI)' = \frac{EI}{k} \quad (k > 1)$$

The number k has been named the flexibility factor.

The ovalization also yields a stress distribution different from that computed by the simple formula $\sigma = My/I$ of beam theory. It is found that the maximum bending stress is given by

$$\sigma_{max} = \beta \frac{Mb}{I}$$

where β is a stress-intensification factor (2).

In the formulas for k and β given by von Karman and subsequent investigators the influence of internal pressure on the ovalization has not been considered.[3] This influence is small for rather heavy pipes as used in industry, in general. For very thin tubes, however, as used in aeronautical applications, neglect of the pressure influence leads to a gross overestimation of the flexibility and stress-intensification factors. It is for this reason that an extension of von Karman's work is considered necessary.

Analysis

Timoshenko (3) relates the membrane forces and bending moments in a shell which is a surface of revolution to the strains of the middle surface and changes in curvature, respectively, in the well-known relations

$$\left.\begin{aligned} N_\varphi &= \frac{Eh}{1-\nu^2}\left[\epsilon_\varphi + \nu\epsilon_\theta\right] \\ N_\theta &= \frac{Eh}{1-\nu^2}\left[\epsilon_\theta + \nu\epsilon_\varphi\right] \end{aligned}\right\} \quad \ldots\ldots\ldots\ldots [1]$$

$$\left.\begin{aligned} M_\varphi &= -D\left[\chi_\varphi + \nu\chi_\theta\right] \\ M_\theta &= -D\left[\chi_\theta + \nu\chi_\varphi\right] \end{aligned}\right\} \quad \ldots\ldots\ldots\ldots [2]$$

(See Fig. 1 and the nomenclature.)

He further gives

$$\epsilon_\varphi = \frac{1}{r_1}\frac{dv}{d\varphi} - \frac{w}{r_1}, \quad \epsilon_\theta = \frac{v}{r_2}\cot\varphi - \frac{w}{r_2} \quad \ldots\ldots [3]$$

$$\chi_\varphi = \frac{1}{r_1}\frac{d}{d\varphi}\left(\frac{v}{r_1} + \frac{dw}{r_1 d\varphi}\right), \quad \chi_\theta = \left(\frac{v}{r_1} + \frac{1}{r_1}\frac{dw}{d\varphi}\right)\frac{\cot\varphi}{r_2} \quad \ldots [4]$$

in which the strains and changes in curvature are related to the displacements of the surface.

---

[1] Structural Engineer, Boeing Airplane Company.

Contributed by the Applied Mechanics Division and presented at the Diamond Jubilee Annual Meeting, Chicago, Ill., November 13–18, 1955, of The American Society of Mechanical Engineers.

Discussion of this paper should be addressed to the Secretary, ASME, 29 West 39th Street, New York, N. Y., and will be accepted until July 10, 1956, for publication at a later date. Discussion received after the closing date will be returned.

Note: Statements and opinions advanced in papers are to be understood as individual expressions of their authors and not those of the Society. Manuscript received by ASME Applied Mechanics Division, April 21, 1955. Paper No. 55—A-32.

[2] Numbers in parentheses refer to the Bibliography at the end of the paper.

[3] Except in reference (12).

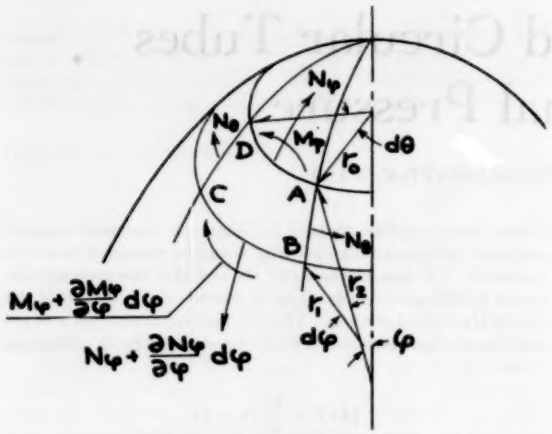

FIG. 1 FORCES AND MOMENTS ACTING ON AN ELEMENT OF A SURFACE OF REVOLUTION

Consider a curved tube, which is a portion of a surface of revolution (torus), subtending the angle θ. Under applied end moments M, the angle is increased to $\theta + \Delta\theta$, Fig. 2. This bending action superimposed upon the effect of the displacements v and w will cause an additional longitudinal strain $\rho(\theta)$, and an additional change in curvature $\psi(\theta)$, in the plane of the bend.

Thus, for the torus deformed by the bending action, we get with (see Fig. 3)

$$r_0 = a + b \sin \varphi \approx a$$

$$r_1 = b$$

$$r_2 = \frac{a + b \sin \varphi}{\sin \varphi} = \frac{a}{\sin \varphi} + b \approx \frac{a}{\sin \varphi}, \; a \gg b$$

and the assumption that r_1 may be considered constant with negligible error, the relations

$$\epsilon_\varphi = \frac{1}{b}\left(\frac{dv}{d\varphi} - w\right), \quad \epsilon_\theta = \frac{\sin \varphi}{a}(v \cot \varphi - w) + \rho(\theta) \ldots [3a]$$

$$\chi_\varphi = \frac{1}{b^2}\frac{d}{d\varphi}\left(v + \frac{dw}{d\varphi}\right),$$

$$\chi_\theta = \frac{\cos \varphi}{ab}\left(v + \frac{dw}{d\varphi}\right) + \psi(\theta) \ldots\ldots [4a]$$

The functions $\rho(\theta)$ and $\psi(\theta)$ are now computed.

Before deformation due to the end moment M, an elementary parallel sector was of length

$$dS_0 = (a + b \sin \varphi)d\theta$$

After deformation the length becomes

$$dS_1 = (a_1 + b \sin \varphi)(d\theta + \Delta d\theta)$$

If it is assumed that the tube center line is the neutral axis, we have

$$ad\theta = a_1(d\theta + \Delta d\theta)$$

Thus the additional strain due to M is

$$\rho(\theta) = \frac{dS_1 - dS_0}{dS_0} = \frac{b \sin \varphi}{a + b \sin \varphi}\frac{\Delta d\theta}{d\theta} \approx \frac{b \sin \varphi}{a}\frac{\Delta d\theta}{d\theta} \ldots\ldots [5]$$

The curvature of the shell sector in the parallel plane was originally

$$\Gamma_0 = \frac{d\theta}{dS_0} \approx \frac{d\theta}{ad\theta}$$

After deformation due to M the curvature is

$$\Gamma_1 = \frac{d\theta + \Delta d\theta}{dS_1} \approx \frac{d\theta + \Delta d\theta}{ad\theta[1 + \rho(\theta)]}$$

The change in curvature is

$$\Gamma_1 - \Gamma_0 = \frac{d\theta + \Delta d\theta}{ad\theta[1 + \rho(\theta)]} - \frac{1}{a} = \frac{1}{a}\frac{\Delta d\theta}{d\theta}$$

(approx.)

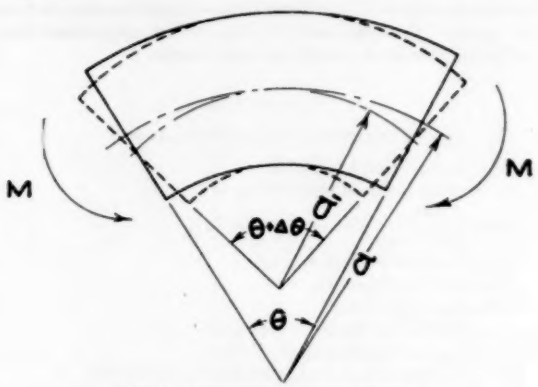

FIG. 2 ELEMENT OF CURVED TUBE

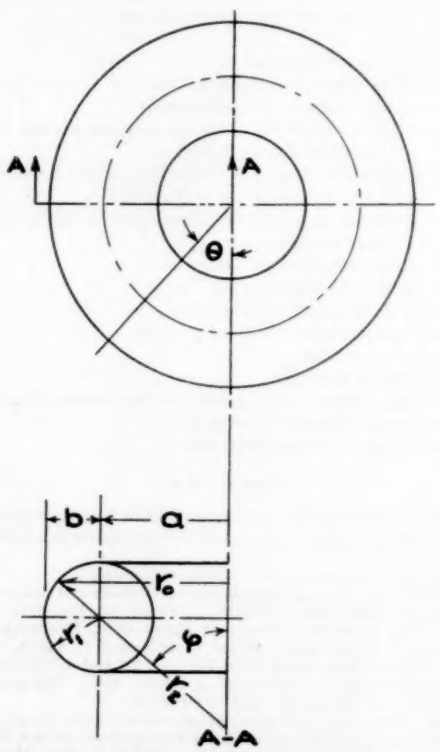

FIG. 3 GEOMETRY OF TORUS

From differential geometry

$$\frac{1}{r_2} = \frac{\sin \varphi}{r_0}$$

so that the change in χ_θ due to M is

$$\psi(\theta) = (\Gamma_1 - \Gamma_0) \sin \varphi = \frac{\sin \varphi}{a} \frac{\Delta d\theta}{d\theta} \quad [6]$$

Having now obtained the relations between strains, changes in curvature, and the deformations, Equations [1] and [2] will be solved for the unknowns v and w by the energy method. The problem is greatly simplified by introducing the following assumptions which are usually used in shell problems:

1 In the meridional direction the middle surface of the shell is inextensible, and a filament in this direction (AB, Fig. 1) is distorted by pure bending only. The strain caused by N_φ is thus neglected.

2 In the parallel direction the middle surface is extensible, and a filament in this direction (AD, Fig. 1) is distorted by normal forces only. Thus the strain caused by M_θ is neglected.

By assumption 1, $\epsilon_\varphi = 0$. Hence from Equation [3]

$$w = \frac{dv}{d\varphi} \quad [7]$$

Consider an arc of curved tube subtending the angle $d\theta$. When the angle is increased to $d\theta + \Delta d\theta$, the strain energy per unit area is as follows:

Due to normal forces—from Equations [1], [3a], [5], [7], and assumptions 1 and 2

$$V_N = \frac{1}{2} N_\theta \epsilon_\theta = \frac{Eh}{2(1-\nu^2)} \epsilon_\theta^2 = \frac{Eh}{2(1-\nu^2)a^2} \left(v \cos \varphi - \frac{dv}{d\varphi} \sin \varphi + b \sin \varphi \frac{\Delta d\theta}{d\theta} \right)^2 \quad [8]$$

Due to bending—from Equations [2], [4a], [6], [7], and assumptions 1 and 2

$$V_B = \frac{1}{2} M_\varphi \chi_\varphi = -\frac{D}{2b^2} \left\{ \frac{1}{b^2} \left(\frac{dv}{d\varphi} + \frac{d^3v}{d\varphi^3} \right) + \frac{\nu}{a} \left[\left(v + \frac{d^2v}{d\varphi^2} \right) \frac{\cos \varphi}{b} + \frac{\Delta d\theta}{d\theta} \sin \varphi \right] \right\} \left(\frac{dv}{d\varphi} + \frac{d^3v}{d\varphi^3} \right) \quad [9]$$

The energy stored in the tube wall per unit length then is approximately

$$V = \int_0^{2\pi} bV_N d\varphi + \int_0^{2\pi} bV_B d\varphi \quad [10]$$

As the tube cross section deforms and becomes ovalized, any internal pressure P will do a work $P\Delta A$ per unit length, if ΔA is the change in cross-section area.

Finally, the work done by the applied end moments per unit length of tube is

$$\frac{1}{2} \frac{M \Delta d\theta}{a d\theta} \quad [11]$$

The energy stored in the system, which must be minimized, is

$$V' = V - P\Delta A \quad [12]$$

It is now necessary to find a series expression for v, which satisfies the assumed boundary conditions. The deformation is considered symmetrical about two axes, from which it follows that the tangential displacements at points 1, 2, 3, 4 of Fig. 4 are zero. Thus $v = 0$ at these points.

A trigonometric series which satisfies this requirement is

$$v = \sum_1^\infty C_K \sin 2K\varphi \quad [13]$$

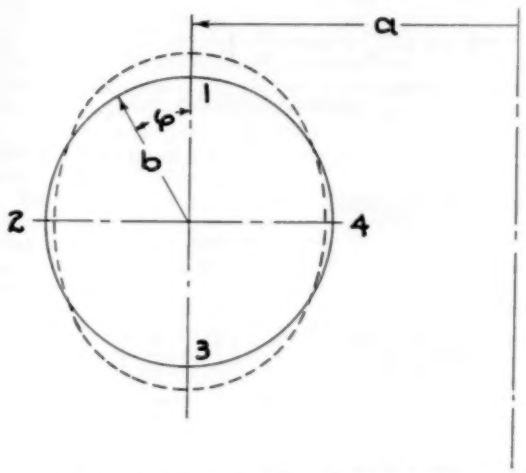

FIG. 4 DEFORMATION OF TUBE CROSS SECTION

The substitution of Equation [13] in [9] and [10], and the expression of ΔA as a function of v, gives V' as a function of the C_K's. Equations

$$\frac{\partial V'}{\partial C_K} = 0, \quad K = (1, 2, 3, \ldots) \quad [14]$$

are a set of simultaneous equations which determine the C_K's. Once the C_K's are found in terms of the other parameters, the requirement that external work equals internal energy gives

$$V' = \frac{1}{2} M \frac{\Delta d\theta}{a d\theta} \quad [15]$$

from which $(\Delta d\theta)/(d\theta)$ is found as a function of M.

Consider next a straight tube of identical cross section and length as the curved tube and with the same moment M acting on the ends. Assuming a membrane theory for the stresses in the straight tube and no distortion of the cross section, the rotation per unit length would be

$$\frac{\Delta_0 d\theta}{a d\theta} = \frac{1-\nu^2}{EI} M, \quad I = \pi b^3 h \quad [16]$$

The ratio

$$\frac{\Delta d\theta}{\Delta_0 d\theta} = k$$

found from Equations [15] and [16], is by definition the flexibility factor.

The outline of the solution is completed by expressing ΔA as a function of the C_K's.

By the analysis of Appendix 1

$$\Delta A = -2\pi \sum_1^\infty (4K^4 - K^2) C_K^2 \quad [17]$$

First Approximation of Flexibility Factor

Series [13] is restricted to its first term

$$v = C_1 \sin 2\varphi$$

and $\Delta A = -6\pi C_1^2$. Equation [12] becomes

$$V' = \frac{Ehb}{2a^2(1-\nu^2)} \int_0^{2\pi} \left[C_1(\sin 2\varphi \cos\varphi - 2\cos 2\varphi \sin\varphi) + b \sin\varphi \frac{\Delta d\theta}{d\theta} \right]^2 d\varphi + \frac{D}{2b} \int_0^{2\pi} \left[-\frac{36C_1^2}{b^2} \cos^2 2\varphi - \frac{18\nu C_1^2}{ab} \sin 2\varphi \cos 2\varphi \cos\varphi + \frac{6\nu C_1}{a} \frac{\Delta d\theta}{d\theta} \sin\varphi \cos 2\varphi \right] d\varphi + 6\pi P C_1^2$$

Equation [14] yields

$$C_1 = -\frac{B}{A} \frac{\Delta d\theta}{d\theta}$$

where

$$A = \frac{5}{2} \frac{Ehb}{a^2(1-\nu^2)} + \frac{36D}{b^2}\left(\frac{1}{b} + \frac{4\nu}{15a\pi}\right) + 12P$$

$$B = \frac{3}{2} \frac{Ehb^2}{a^2(1-\nu^2)} + \frac{4D\nu}{\pi ab}$$

Substituting C_1 in Equation [15] we get

$$\Delta d\theta = \frac{M d\theta}{\pi\left[\frac{Ehb^3}{a(1-\nu^2)} - \frac{aB^2}{A}\right]}$$

From Equation [16]

$$\Delta_\varphi d\theta = \frac{1-\nu^2}{\pi b^3 hE} M\, ad\,\theta$$

The flexibility factor given by the first approximation then is

$$k_1 = \frac{\Delta d\theta}{\Delta_\varphi d\theta} = \frac{1}{1 - \frac{(1-\nu^2)a^2B^2}{Eb^3hA}} \quad \text{..... [18]}$$

For $\nu = 0$ and $P = 0$ this becomes

$$k = \frac{10 + 12\frac{h^2a^2}{b^4}}{1 + 12\frac{h^2a^2}{b^4}}$$

which is the factor obtained by von Karman (1).

Second Approximation of Flexibility Factor

Taking two terms of Series [13] we have

$$v = C_1 \sin 2\varphi + C_2 \sin 4\varphi$$

and

$$\Delta A = -6\pi C_1^2 - 120\pi C_2^2$$

Following the analysis procedure we obtain the results

$$C_1 = -\rho_1 \frac{\Delta d\theta}{d\theta}$$

$$C_2 = -\rho_2 \frac{\Delta d\theta}{d\theta}$$

where

$$\rho_1 = \frac{a_{12}b_2 + a_{22}b_1}{a_{11}a_{22} - a_{12}^2}$$

$$\rho_2 = \frac{a_{12}b_1 + a_{11}b_2}{a_{11}a_{22} - a_{12}^2}$$

$$a_{11} = \frac{5}{2}\frac{Ehb\pi}{a^2(1-\nu^2)} + \frac{36\pi D}{b^3} + \frac{144\nu D}{15ab^2} + 12\pi P$$

$$a_{12} = \frac{5}{4}\frac{Ehb\pi}{a^2(1-\nu^2)} + \frac{96}{7}\frac{\nu D}{ab^2}$$

$$a_{22} = \frac{17}{2}\frac{Ehb\pi}{a^2(1-\nu^2)} + 3600\frac{\pi D}{b^3} + \frac{1600}{7}\frac{D\nu}{ab^2} + 240\pi P$$

$$b_1 = \frac{3}{2}\frac{Ehb^2\pi}{a^2(1-\nu^2)} + \frac{4D\nu}{ab}$$

$$b_2 = \frac{8\nu D}{ab}$$

The flexibility factor turns out to be

$$k_2 = \frac{1}{1 + \frac{a^2(1-\nu^2)}{\pi Ehb^3}(a_{11}\rho_1^2 + a_{22}\rho_2^2 - 2a_{21}\rho_1\rho_2 - 2b_1\rho_1 - 2b_2\rho_2)} \quad \text{..... [19]}$$

Bending Stress in Curved Tube

Because of cross-section ovalization the maximum bending stress is no longer given by the formula Mb/I. In this section the maximum longitudinal stress $(N_\theta/h)_{max}$ will be computed and divided by Mb/I to obtain a stress-intensification factor β.

By Equations [3a] and [5] the longitudinal strain is

$$\epsilon_\theta = \frac{1}{a}(v\cos\varphi - w\sin\varphi + b\frac{\Delta d\theta}{d\theta}\sin\varphi)$$

Using Equation [7] and the first approximation for v, the corresponding stress is

$$\sigma_\theta = \frac{E\epsilon_\theta}{1-\nu^2} = \frac{E}{a(1-\nu^2)}\frac{\Delta d\theta}{d\theta}\left(b\sin\varphi - \frac{2B}{A}\sin^3\varphi\right)$$

However, by Equation [16]

$$M = \frac{EI}{a(1-\nu^2)}\frac{\Delta_\varphi d\theta}{d\theta} = \frac{EI}{a(1-\nu^2)}\frac{\Delta d\theta}{d\theta}\frac{1}{k_1}$$

so that

$$\frac{Mk_1}{I} = \frac{E}{a(1-\nu^2)}\frac{\Delta d\theta}{d\theta}$$

and

$$\sigma_\theta = \frac{Mk_1}{I}\left(b\sin\varphi - \frac{2B}{A}\sin^3\varphi\right)$$

The maximum bending stresses are (see Appendix 2)

$$\sigma_{\theta\,max} = \frac{Mb}{I}k_1\left(1 - \frac{2B}{Ab}\right), \quad \text{if } \frac{6B}{A} < b$$

$$\sigma_{\theta max} = \frac{2}{3}\frac{Mb}{I}k_1\sqrt{\frac{bA}{6B}}, \quad \text{if } \frac{6B}{A} > b$$

Without ovalization the maximum bending stress would be Mb/I. Hence the stress-intensification factor for the first approximation is

$$\left.\begin{aligned} \beta_1 &= k_1\left(1-\frac{2B}{Ab}\right) \quad \text{for} \quad \frac{6B}{A} < b \\ \beta_1 &= \frac{2}{3}\,k_1\sqrt{\frac{bA}{6B}} \quad \text{for} \quad \frac{6B}{A} > b \end{aligned}\right\} \quad \ldots\ldots [20]$$

For $P = 0$, $\nu = 0$, Equations [20] become

$$\beta_1 = \frac{12\lambda^2 - 2}{12\lambda^2 + 1}, \quad \text{for} \quad \lambda > 1.472$$

$$\beta_2 = \frac{(12\lambda^2 + 10)^{3/2}}{9(12\lambda^2 + 1)}, \quad \text{for} \quad \lambda < 1.472$$

where

$$\lambda = \frac{ha}{b^2}$$

which are the Hovgaard factors (2).

Analysis of the second approximation of the stress-intensification factor yields the relations

$$\left.\begin{aligned} \beta_2 &= 1 + \frac{4\rho_2 - 2\rho_1}{b}, \quad \text{for} \quad 60\rho_2 + b > 6\rho_1 \\ \beta_2 &= k_2\sqrt{z}\left[1 - \frac{2z\rho_1}{b} - \frac{\rho_2}{b}\,(20z - 24z^2)\right], \\ &\qquad \text{for} \quad 60\rho_2 + b < 6\rho_1 \end{aligned}\right\} \quad \ldots [21]$$

where

$$z = \frac{3\rho_1 + 30\rho_2 - \sqrt{(3\rho_1 + 30\rho_2)^2 - 120b\rho_2}}{120\rho_2}$$

The maximum bending stress can be computed by the usual simple bending formula and multiplied by β to get the true value. To this stress must be added the longitudinal stress due to internal pressure and normal forces induced by the support reactions of the pipe system.

The transverse stress is

$$\sigma_\varphi = \frac{N_\varphi}{h} \pm \frac{6M_\varphi}{h^2}$$

and can be obtained from Equations [1], [2], [3], [4] and the values of v and w computed in the analysis.

Comparison Between Theory and Experiment

Tests conducted by the author's company made available some limited experimental data by means of which the results of the theory have been experimentally confirmed.

Plane U-type expansion loops consisting of two quarter-bends, one half-bend, and short-tangent sections, were made up of seam-welded tube.

Diameters were 3 in. and 3.5 in.; thicknesses 0.016 in. and 0.020 in., respectively. The material was 18-8 stainless-steel sheet, titanium stabilized, specification AISI 321, and the bends were manufactured by forming half-sections in a hammer die, and fusion-welding them together. Owing to this construction the welding seams fell in the plane of the bend and not on the neutral axis. The tubes finally were annealed for stress relieving.

One end of the expansion loop was held fixed, while the other end was displaced along the axis of the tangent sections; both ends could be restrained against rotation or else left free to rotate at will.

Stresses were measured by means of electric strain gages (SR4) distributed, both in the longitudinal and the transverse direction, along two sections near the center of the loops, on the outside only.

Pressurizing was accomplished by means of compressed air. The pressure was applied first, then the strain gages were balanced to read zero, and finally the end was displaced through application of suitable loads.

Load-deflection curves were obtained at 0, 25, 50, 100, 200, 250 psig.

Experimental values of the flexibility factor were inferred from the load-deflection curves, by comparison with the theoretical load-deflection relations, with unspecified k factor. Care was taken to exclude load conditions which would cause any buckling of the loops out of their planes or local buckling of the tubes.

Longitudinal and transverse stresses were obtained directly from strain-gage readings and the longitudinal stress-intensification factors were inferred from them.

Figs. 5, 6, 7 show the comparison of flexibility factor and stress-intensification factor as reduced from the experiments, with the values predicted by the theory. The calculated values are based on the second approximation, since the first approximation did not give satisfactory agreement, as might be expected for such thin-walled tubes.

The comparison indicates fair agreement between theory and experiment, the agreement improving with increasing pressure. The loops appear to be less flexible than the theory would predict, so that little gain in accuracy could be expected from a third-approximation calculation, or a correction for hoop strain, as suggested in reference (4). The discrepancy could be due to the stiffening effect of the welding seams, which is certainly significant for such thin walls. More tests would be desirable, using seamless tubes, but the consistency of trends shown in Figs. 5, 6, 7 seems to indicate that the theory accounts for all major factors which influence the stiffening phenomena.

The theory is based on the assumption, among others, that the ratio a/b is large. It was shown in reference (5) that reasonably accurate results are obtained even for a/b as small as 2.2. For very thin tubes $a/b = 5$ is probably a safe lower limit.

BIBLIOGRAPHY

1 "Über die Formänderung dünnwandiger Rohre, insbesondere federnder Ausgleichrohre," by T. von Karman, *Zeitschrift des Vereins deutscher Ingenieure*, vol. 55, 1911, pp. 1889–1895.

2 "Elastic Deformation of Pipe Bends," by W. Hovgaard, *Journal of Mathematics and Physics*, M.I.T., vol. 6, 1926, pp. 69–118.

"Deformation of Plane Pipes," ibid., vol. 7, 1927–1928, pp. 198–238.

"Further Research on Pipe Bends," ibid., vol. 7, 1927–1928, pp. 239–297.

"Tests on High-Pressure Pipe Bends," ibid., vol. 8, 1929, pp. 293–344.

3 "Theory of Plates and Shells," by S. Timoshenko, McGraw-Hill Book Company, Inc., New York, N. Y., 1940.

4 "Experiments on Short-Radius Pipe Bends," by N. Gross, Proceedings of The Institution of Mechanical Engineers, series B, vol. 1B, no. 10, 1952–1953, pp. 465–479.

5 "The Flexibility of Short-Radius Pipe Bends," by N. Gross and H. Ford, loc. cit.

6 "Properties of Thin-Walled Curved Tubes of Short-Bend Radius," by T. E. Pardue and Irwin Vigness, Trans. ASME, vol. 73, 1951, pp. 77–87.

7 "Bending of Curved Thin Tubes," by L. Beskin, Journal of Applied Mechanics, Trans. ASME, vol. 67, 1945, pp. A-1–A-7.

8 "Bourdon Tubes and Bending of Thin Curved Tubes," by M. Tueda, Kyoto Imp. University, Memoirs, July, 1934, February, 1936.

9 "Bending of Curved Tubes," by R. A. Clark and E. Reissner, *Advances in Applied Mechanics*, vol. 2, Academic Press, New York, N. Y.

10 "On the Theory of Thin Elastic Shells," by E. Reissner, Contributions to Applied Mechanics, Reissner Anniversary, 1949.

11 "Elastic Properties of Curved Tubes," by Irwin Vigness, Trans. ASME, vol. 65, 1943, pp. 105–120.

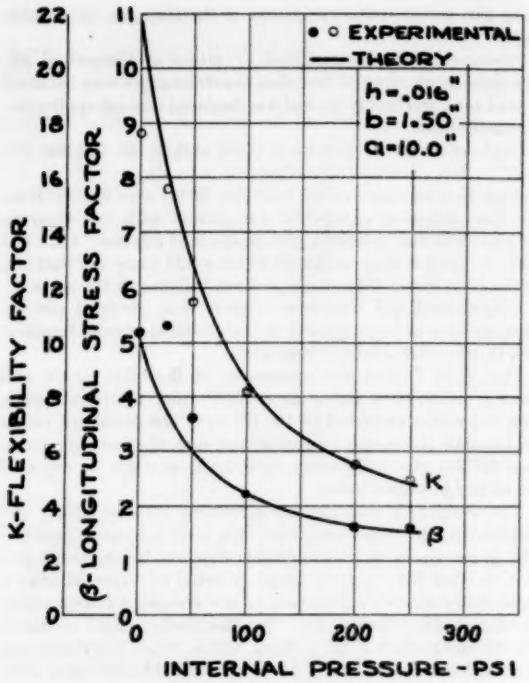

Fig. 5

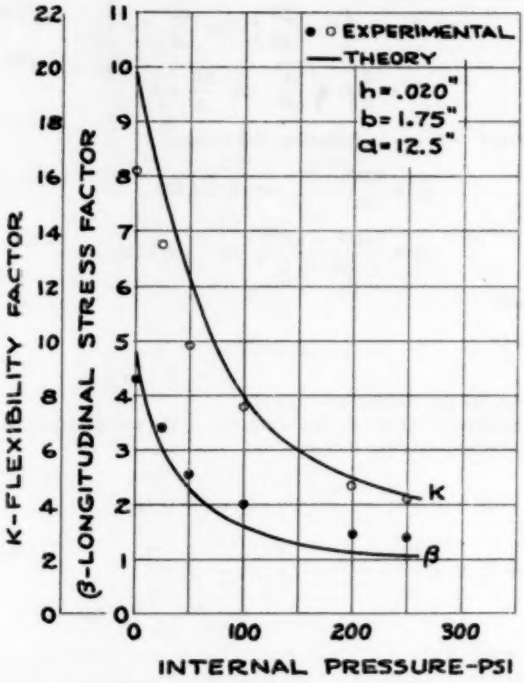

Fig. 6

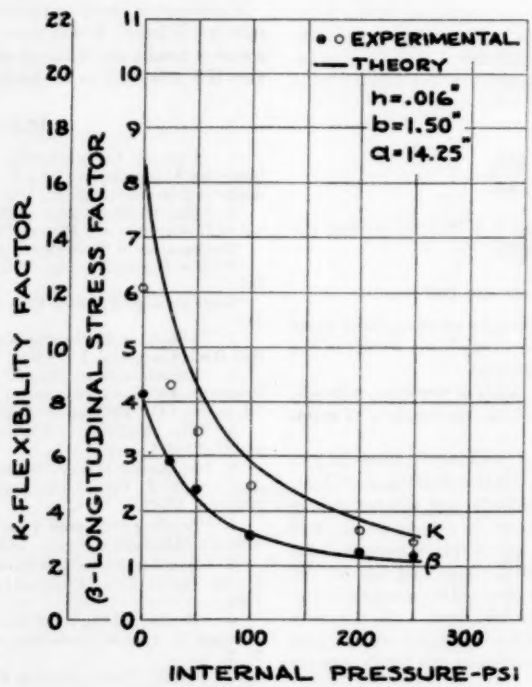

Fig. 7

FIGS. 5, 6, 7 VARIATION OF FLEXIBILITY AND LONGITUDINAL STRESS-INTENSIFICATION FACTORS WITH INTERNAL PRESSURE

12 "Étude de la Déformation et des Tensions Internes des Tuyaux a Ligne Moyenne Plane, Soumis a des Efforts Extèrieurs et a une Pression Interne," by J. Barthélemy, Bulletin de l'Association Technique Maritime, 1947.

Appendix 1

DERIVATION OF EQUATION [17] FOR CHANGE IN TUBE CROSS-SECTION AREA

Referring to Fig. 8, points A and B are displaced in the ovalization to points A' and B' as shown. The change in cross-section

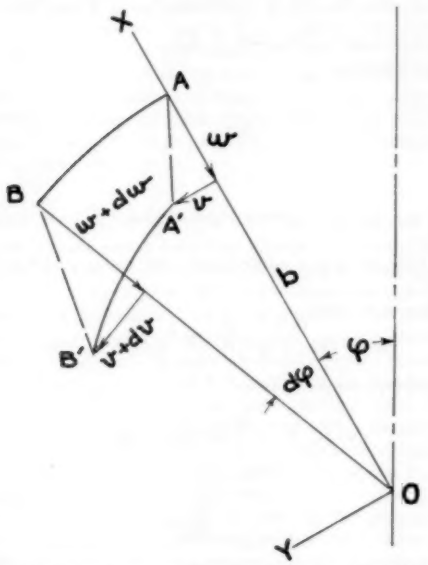

FIG. 8 DISTORTION OF AN ELEMENT OF TUBE CROSS SECTION

area is the area of the quadrilateral $ABB'A'$, and is negative when w is positive.

Auxiliary co-ordinate axes x and y are established as shown. The co-ordinates of points A, B, B', A' are

$$A[b,\ 0]$$

$$B[b\cos\varphi,\quad b\sin d\varphi]$$

$$B'\{[b-(w+dw)-(v+dv)\tan d\varphi]\cos d\varphi,$$
$$[b-(w+dw)]\sin d\varphi+(v+dv)\cos d\varphi\}$$

$$A'[b-w,\ v]$$

The area sought is the sum of triangles ABB' and $AB'A'$

$$-d(\Delta A)=\frac{1}{2}\begin{vmatrix}x_A & y_A & 1\\ x_B & y_B & 1\\ x_{B'} & y_{B'} & 1\end{vmatrix}+\frac{1}{2}\begin{vmatrix}x_A & y_A & 1\\ x_{B'} & y_{B'} & 1\\ x_{A'} & y_{A'} & 1\end{vmatrix}$$

$$=\frac{1}{2}\begin{vmatrix}x_A & y_A & 1\\ x_B-x_{A'} & y_B-y_{A'} & 0\\ x_{B'} & y_{B'} & 1\end{vmatrix}$$

Taking $\cos d\varphi = 1$, $\sin d\varphi = \tan d\varphi = d\varphi$ and neglecting differentials of higher order, this reduces to

$$-d(\Delta A)=\frac{1}{2}\left(2bw-v\frac{dw}{d\varphi}+w\frac{dv}{d\varphi}-w^2-v^2\right)d\varphi$$

For complete inextensionality it is required that $AB = A'B'$ or $\overline{AB}^2 = \overline{A'B'}^2$.

Now $\overline{AB}^2 = b^2d\varphi^2$

$$\overline{A'B'}^2=(dw+vd\varphi)^2+(bd\varphi+wd\varphi-dv)^2$$

Equating these expressions, expanding, and using the relation

$$w=\frac{dv}{d\varphi}=v'$$

we get

$$-v^2=2vv''+v''^2$$

Substituting this in the ΔA equation, along with $w = v'$, we get

$$-d(\Delta A)=\frac{1}{2}(2bv'+vv''+v''^2)\,d\varphi$$

$$-\Delta A=\frac{1}{2}\int_0^{2\pi}(2bv'+vv''+v''^2)\,d\varphi$$

Substituting $v=\sum_1^\infty C_K\sin 2K\varphi$ from Equation [13] and carrying out the integration we obtain

$$\Delta A=-2\pi\sum_1^\infty(4K^4-K^2)C_K^2 \qquad \text{[17]}$$

Appendix 2

COMPLETE ANALYSIS OF STRESS-INTENSIFICATION FACTORS FOR FIRST AND SECOND APPROXIMATIONS

For the first approximation we have

$$\sigma_\theta=\frac{M}{I}\,k_1\left(b\sin\varphi-\frac{2B}{A}\sin^3\varphi\right)$$

For a maximum

$$\frac{d\sigma_\theta}{d\varphi}=0\quad\text{or}\quad\left(b-\frac{6B}{A}\sin^2\varphi\right)\cos\varphi=0$$

Hence either

$$\cos\varphi=0,\ \text{i.e.,}\ \varphi=\frac{\pi}{2},\quad\text{or}\quad\sin^2\varphi=\frac{bA}{6B}$$

For a maximum

$$\frac{d^2\sigma_\theta}{d\varphi^2}<0$$

or

$$-\sin\varphi\left(b-\frac{6B}{A}\sin^2\varphi\right)-2\sin\varphi\cos^2\varphi\,\frac{6B}{A}<0$$

If

$$\sin^2\varphi=\frac{bA}{6B}$$

then

$$-2\left(1-\frac{bA}{6B}\right)\sqrt{\frac{bA}{6B}}<0,\quad\text{or}\quad\frac{bA}{6B}<1,\quad\text{or}\quad\frac{6B}{A}>b$$

If $\cos\varphi = 0$, then

$$-b + \frac{6B}{A} < 0, \quad \text{or} \quad \frac{6B}{A} < b$$

Consequently, for

$$\frac{6B}{A} > b$$

$$\sigma_{\theta\,\max} = \frac{2}{3}\frac{Mb}{I}k_1\sqrt{\frac{bA}{6B}}$$

and

$$\beta_1 = \frac{2}{3}k_1\sqrt{\frac{bA}{6B}}$$

For

$$\frac{6B}{A} < b$$

$$\sigma_{\theta\,\max} = \frac{Mb}{I}k_1\left(1 - \frac{2B}{Ab}\right)$$

and

$$\beta_1 = k_1\left(1 - \frac{2B}{Ab}\right)$$

For the second approximation we have

$$\sigma_\theta = -\frac{M}{I}k_2\left[2\rho_1\sin^2\varphi + \rho_2(20\sin^2\varphi - 24\sin^5\varphi) - b\sin\varphi\right]$$

$$\frac{d\sigma_\theta}{d\varphi} = 0 = [6\rho_1\sin^2\varphi + \rho_2(60\sin^2\varphi - 120\sin^4\varphi) - b]\cos\varphi$$

Hence either $\cos\varphi = 0$ or

$$\sin^2\varphi = z = \frac{3\rho_1 + 30\rho_2 \pm \sqrt{(3\rho_1 + 30\rho_2)^2 - 120b\rho_2}}{120\rho_2}$$

For reality it must be

$$3\rho_1 + 30\rho_2 \geqslant \sqrt{120b\rho_2}$$

On the other hand, $z \leqslant 1$ or

$$3\rho_1 + 30\rho_2 \leqslant 120\rho_2 \pm \sqrt{(3\rho_1 + 30\rho_2)^2 - 120b\rho_2}$$

Put

$$3\rho_1 + 30\rho_2 = \alpha, \quad \text{and} \quad \sqrt{120b\rho_2} = \gamma$$

then

$$\alpha \pm \sqrt{\alpha^2 - \gamma^2} \leqslant \frac{\gamma^2}{b}$$

Taking the plus sign, we obtain

$$\sqrt{\alpha^2 - \gamma^2} \leqslant \frac{\gamma^2}{b} - \alpha, \quad \text{or} \quad \gamma^2 - 2\alpha b + b^2 \geqslant 0$$

Therefore

$$60\rho_2 + b \geqslant 6\rho_1$$

Consequently, the solution

$$z_+ = \frac{3\rho_1 + 30\rho_2 + \sqrt{\alpha^2 - \gamma^2}}{120\rho_2}$$

implies the condition $60\rho_2 + b \geqslant 6\rho_1$.
The solution

$$z_- = \frac{3\rho_1 + 30\rho_2 - \sqrt{\alpha^2 - \gamma^2}}{120\rho_2}$$

implies the condition $60\rho_2 + b \leqslant 6\rho_1$.

For a maximum

$$\frac{d^2\sigma}{d\varphi^2} < 0$$

Thus

$$\frac{d^2\sigma}{d\varphi^2} = [6\rho_1\sin^2\varphi + \rho_2(60\sin^2\varphi - 120\sin^4\varphi) - b]\sin\varphi - \left[12\rho_1\sin\varphi + \rho_2(120\sin\varphi - 480\sin^3\varphi)\right]\cos^2\varphi < 0$$

If $\cos\varphi = 0$, then

$$6\rho_1 - 60\rho_2 - b < 0 \quad \text{or} \quad 60\rho_2 + b > 6\rho_1$$

The maximum stress becomes

$$\sigma_{\theta\,\max} = -\frac{M}{I}k_2(2\rho_1 - 4\rho_2 - b)$$

and

$$\beta_2 = 1 + \frac{4\rho_2 - 2\rho_1}{b}$$

If $\sin^2\varphi = z_+$, then

$$-(1 - z_+)\left[12\rho_1\sqrt{z_+} + \rho_2(120\sqrt{z_+} - 480\,z_+\sqrt{z_+})\right] < 0$$

or

$$-[\rho_1 + \rho_2(10 - 40z_+)] < 0$$

This gives the condition

$$+\sqrt{(3\rho_1 + 30\rho_2)^2 - 120b\rho_2} < 0$$

Since the positive square root cannot be less than zero, the z_+ solution does not give a maximum.

The z_- solution gives the maximum and is associated with the condition

$$60\rho_2 + b < 6\rho_1$$

The stress-intensification factor in this case is found to be

$$\beta_2 = k_2\sqrt{z_-}\left[1 - \frac{2\rho_1 z_-}{b} - \frac{\rho_2}{b}(20z_- - 24z_-^2)\right]$$

A Study of Axisymmetric Vibrations of Cylindrical Shells as Affected by Rotatory Inertia and Transverse Shear[1]

By T. C. LIN[2] and G. W. MORGAN[3]

An analysis is presented of the problem of the propagation of axisymmetric waves in an elastic circular tube. The theory includes the effects of rotatory inertia and transverse shear in the same manner as does Timoshenko's theory of the vibrations of bars. These effects are of importance for waves at high frequencies; they tend to decrease the velocity of propagation and introduce an additional mode due to shear.

Introduction

THIS paper presents the first step in the authors' study of the propagation of axisymmetric pressure waves through elastic circular tubes filled with compressible fluid over a wide range of frequencies. To proceed with the analysis of this problem it is necessary to formulate the equations of motion for the tube. Since the complete three-dimensional equations of elasticity are too complicated to admit analytical treatment, it is important to determine approximate equations which are adequate for the purpose of the investigation. Since the presence of the fluid affects the equations of motion for the tube only by the introduction of the terms representing the pressure and the shearing stress which the fluid exerts on the tube wall, a convenient procedure is to begin by studying the propagation of waves in an empty tube, particularly since this problem is itself an interesting one. We therefore direct our attention to this problem in the present paper and reserve the study of waves in the presence of a fluid for a later paper.

Our main purpose here is to develop an analysis which will be valid for a wide range of frequency, particularly for high frequencies. This is accomplished by taking account of two effects which become increasingly important as the frequency is increased; these are the inertia connected with the rotation of the elements of the tube wall, and the influence of shear strain on the bending terms. These factors have been neglected in previous treatments of the problem (1, 2, 3, 4, 5, 6)[4] and are here taken into account in the same manner as in Timoshenko's theory for the vibrations of bars (7, 8).

[1] The results in this paper were obtained in the course of research sponsored by the Office of Naval Research, under Contract 562(07).

[2] Formerly, Research Associate in Applied Mathematics, Brown University, Providence, R. I.

[3] Associate Professor of Applied Mathematics, Brown University, Providence, R. I.

[4] Numbers in parentheses refer to the Bibliography at the end of the paper.

Contributed by the Applied Mechanics Division and presented at the Diamond Jubilee Annual Meeting, Chicago, Ill., November 13–18, 1955, of The American Society of Mechanical Engineers.

Discussion of this paper should be addressed to the Secretary, ASME, 29 West 39th Street, New York, N. Y., and will be accepted until July 10, 1956, for publication at a later date. Discussion received after the closing date will be returned.

Note: Statements and opinions advanced in papers are to be understood as individual expressions of their authors and not those of the Society. Manuscript received by ASME Applied Mechanics Division, January 31, 1955. Paper No. 55—A-59.

Basic Equations

A cylindrical co-ordinate system (r, θ, x) with the x-axis directed along the axis of the cylindrical tube is used. For axisymmetric vibrations it is stipulated that the displacements of the shell wall are independent of θ and that there are no displacements in the θ-direction. It is also assumed that the thickness h of the wall is small compared with its mean undeformed radius a.

Consider an infinitesimal element of the wall contained between two axial planes, angle $d\theta$ apart, and between two cross-sectional planes, distance dx apart, as shown in Fig. 1. Let t de-

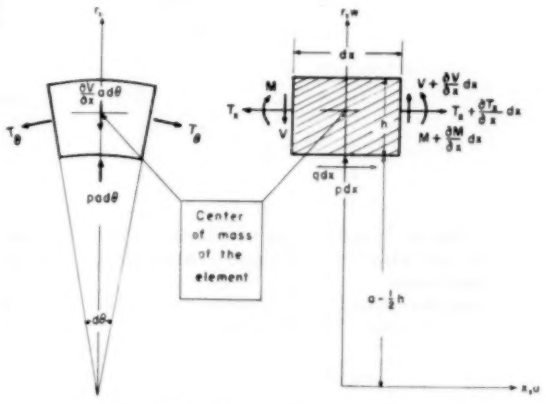

Fig. 1 An Element of Cylindrical Shell

note time and let $u(r, x, t)$ and $w(r, x, t)$ denote the axial and the radial displacements, respectively, of a point on the wall. Further, let $r = r_0$ denote the radial co-ordinate of the centroid of the intersection of the element with a plane $x = \text{const}$; more exactly, r_0 gives the limiting co-ordinate of the centroid as $d\theta$ approaches zero, that is

$$r_0 = \frac{1}{ah} \int_{a-\frac{1}{2}h}^{a+\frac{1}{2}h} r^2 dr = a\left(1 + \frac{h^2}{12a^2}\right) \quad \ldots\ldots [1]$$

The motion is approximated by assuming the following expressions for u and w

$$\left.\begin{aligned} u(r, x, t) &= u_0(x, t) + (r_0 - r)\alpha(x, t) \\ w(r, x, t) &= w_0(x, t) \end{aligned}\right\} \quad \ldots\ldots [2]$$

Thus it is assumed that the axial displacement u is such that radial lines remain straight, α representing the angular rotation of a radial line about $r = r_0$, and that the radial displacement w is independent of r.

In general, the strain-displacement relations are

$$\left.\begin{aligned}
\epsilon_x &= \frac{\partial u}{\partial x} \\
\epsilon_\theta &= \frac{1}{r}\frac{\partial v}{\partial \theta} + \frac{w}{r} \\
\epsilon_r &= \frac{\partial w}{\partial r} \\
\gamma_{xr} &= \frac{\partial u}{\partial r} + \frac{\partial w}{\partial x} \\
\gamma_{x\theta} &= \frac{1}{r}\frac{\partial u}{\partial \theta} + \frac{\partial v}{\partial x} \\
\gamma_{r\theta} &= \frac{\partial v}{\partial r} - \frac{v}{r} + \frac{1}{r}\frac{\partial w}{\partial \theta}
\end{aligned}\right\} \quad \ldots\ldots\ldots [3]$$

where the ϵ and γ quantities are the tensile and shearing strains, respectively, and v is the displacement in the θ-direction. For the present case, because of axial symmetry, $v = \partial/\partial\theta = 0$. Making use of this and Equations [2], one obtains from Equations [3] the following expressions for the strains

$$\left.\begin{aligned}
\epsilon_x &= \frac{\partial u_0}{\partial x} + (r_0 - r)\frac{\partial \alpha}{\partial x} \\
\epsilon_\theta &= \frac{w_0}{r} \\
\gamma_{xr} &= \frac{\partial w_0}{\partial x} - \alpha \\
\epsilon_r &= \gamma_{x\theta} = \gamma_{r\theta} = 0
\end{aligned}\right\} \quad \ldots\ldots\ldots [4]$$

The Expressions [2] and [4] may be expected to be valid whenever $h \ll a$ and when h is small compared with the wave length λ of the disturbance.

By using Equations [3], the stresses can be found from the stress-strain relations. They are given by

$$\left.\begin{aligned}
\sigma_x &= \frac{E}{1-\nu^2}(\epsilon_x + \nu\epsilon_\theta) \\
\sigma_\theta &= \frac{E}{1-\nu^2}(\epsilon_\theta + \nu\epsilon_x) \\
\tau_{xr} &= G\gamma_{xr}
\end{aligned}\right\} \quad \ldots\ldots\ldots [5]$$

where σ_x and σ_θ denote the axial and the hoop tensile stresses, respectively, and τ_{xr} the shearing stress acting in the radial direction on a plane x = const. E, G, and ν are Young's modulus of elasticity, the modulus of rigidity, and Poisson's ratio, respectively. The first two of Equations [5] are based on the assumption that the radial tensile stress σ_r is much smaller than σ_x and σ_θ, which may be expected to be the case when $h \ll a$.

The equations of motion for the infinitesimal element can now be set up in terms of the translation of its center of mass and its rotation about an axis which passes through the center of mass and is perpendicular to a bisecting radius of the element, Fig. 1. The desired differential equations are then obtained by allowing $d\theta$ and dx to approach zero. In the following it is simpler, though less rigorous, to imagine the limiting process carried out and to write down the differential equations directly. This is done by keeping in mind that in the limiting process the axis of rotation moves to the limiting position defined by $r = r_0$. It is first necessary to find the resultant forces on the element and the resultant moment about $r = r_0$. Let T_x, V, and M denote, respectively, the resultant tensile and shear forces and resultant moment about $r = r_0$ acting on the plane x = const per unit length of undeformed mean circumference, and let T_θ denote the resultant tensile force acting on the plane θ = const per unit length of the undeformed cylinder. Then

$$\left.\begin{aligned}
T_x &= \frac{1}{a}\int_{a-\frac{1}{2}h}^{a+\frac{1}{2}h} \sigma_x r\, dr \\
T_\theta &= \int_{a-\frac{1}{2}h}^{a+\frac{1}{2}h} \sigma_\theta\, dr \\
M &= \frac{1}{a}\int_{a-\frac{1}{2}h}^{a+\frac{1}{2}h} (r_0 - r)\sigma_x r\, dr \\
V &= \frac{1}{a}\int_{a-\frac{1}{2}h}^{a+\frac{1}{2}h} \tau_{xr} r\, dr
\end{aligned}\right\} \quad \ldots\ldots\ldots [6]$$

Substituting Equations [5] into [6] and using [4] one obtains

$$\left.\begin{aligned}
T_x &= \frac{Eh}{1-\nu^2}\left[\frac{\partial u_0}{\partial x} + \nu\frac{w_0}{a}\right] \\
T_\theta &= \frac{Eh}{1-\nu^2}\left[\frac{w_0}{h}\ln\left(\frac{2a+h}{2a-h}\right) + \nu\frac{\partial u_0}{\partial x} + \frac{\nu h^2}{12a}\frac{\partial \alpha}{\partial x}\right] \\
M &= \frac{Eh^3}{12(1-\nu^2)}\left[\left(1 - \frac{h^2}{12a^2}\right)\frac{\partial \alpha}{\partial x} + \frac{\nu w_0}{a^2}\right]
\end{aligned}\right\} \quad \ldots\ldots [7]$$

and

$$V = Gh\left[\frac{\partial w_0}{\partial x} - \alpha\right] \quad \ldots\ldots\ldots\ldots [7a]$$

The foregoing expression for V is based on our approximation to the shear strain γ_{xr} given in Equations [4], which is independent of r. A more accurate account can be taken of V by appealing to the relation

$$V = KGH\left[\frac{\partial w_0}{\partial x} - \alpha\right] \quad \ldots\ldots\ldots\ldots [8]$$

where K is the "shear constant" which depends on the shape of the cross section. An experimental value for a rectangular cross section was determined by Filon and is 8/9 (8). It will be assumed that, with $h \ll a$, this is a good approximation in the present case.

Using Fig. 1 the differential equations of motion can now be obtained. They are

$$\left.\begin{aligned}
\rho_t h\frac{\partial^2 u_0}{\partial t^2} &= \frac{\partial T_x}{\partial x} + q \\
\rho_t h\frac{\partial^2 w_0}{\partial t^2} &= \frac{\partial V}{\partial x} - \frac{T_\theta}{a} + p \\
\rho_t I_0\frac{\partial^2 \alpha}{\partial t^2} &= \frac{\partial M}{\partial x} + V + \frac{1}{2}qh\left(1 + \frac{h}{6a}\right)
\end{aligned}\right\} \quad \ldots\ldots [9]$$

where ρ_t is the density of the tube material, p and q are the pressure and shearing stresses per unit area of the undeformed mean surface of the tube exerted on the wall by the fluid inside the tube. I_0 is the limiting value as $d\theta$ approaches zero of $1/(ad\theta)$ times the moment of inertia of the cross-sectional area of the element about an axis which passes through the centroid of the area and is perpendicular to the bisecting radius of the area. It is given by

$$I_0 = \frac{1}{a}\int_{a-\frac{1}{2}h}^{a+\frac{1}{2}h}(r-r_0)^2 r\,dr$$

which, on using Equation [1], becomes

$$\left.\begin{aligned} I_0 &= I\left(1-\frac{h^2}{12a^2}\right) \\ \text{where} \qquad I &= \frac{h^3}{12} \end{aligned}\right\} \quad \ldots\ldots\ldots\ldots [10]$$

The third Equation [9] introduces the rotatory inertia $\rho_t I_0$.

It will be of interest in the following to examine the role played by various physically meaningful quantities in determining the phase velocity of a disturbance. For this purpose it is convenient to identify the contributions of the various terms in the basic equations by introducing the artificial tracers A, C, F, and H into the system [7] as follows

$$\left.\begin{aligned} T_x &= \frac{Eh}{1-\nu^2}\left[C\frac{\partial u_0}{\partial x}+\nu\frac{w_0}{a}\right] \\ T_\theta &= \frac{Eh}{1-\nu^2}\left[H\frac{w_0}{h}\ln\left(\frac{2a+h}{2a-h}\right)\right. \\ &\qquad \left. +\nu\frac{\partial u_0}{\partial x}+F\frac{\nu h^2}{12a}\frac{\partial\alpha}{\partial x}\right] \\ M &= \frac{Eh^3}{12(1-\nu^2)}\left[\left(1-\frac{h^2}{12a^2}\right)A\frac{\partial\alpha}{\partial x}+F\frac{\nu w_0}{a^2}\right] \end{aligned}\right\} \quad \ldots [11]$$

Each tracer is set equal to 1 when the corresponding physical quantity is to be taken into account, but it is set equal to zero when the corresponding quantity is to be neglected. Here A traces the conventional bending term; C, the axial strain; F, the curvature effects coupled with Poisson's ratio; and H, the hoop strain.

Substituting Equations [8] and [11] into [9], and using [10], one obtains the following three differential equations for the three unknowns u_0, w_0, and V

$$\left.\begin{aligned} L\rho_t h\frac{\partial^2 u_0}{\partial t^2} &= \frac{Eh}{1-\nu^2}\left[C\frac{\partial^2 u_0}{\partial x^2}+\frac{\nu}{a}\frac{\partial w_0}{\partial x}\right]+q \\ D\rho_t h\frac{\partial^2 w_0}{\partial t^2} &= \frac{\partial V}{\partial x}-\frac{Eh}{1-\nu^2}\left[H\frac{w_0}{ah}\ln\left(\frac{2a+h}{2a-h}\right)\right. \\ &\quad \left.+\frac{\nu}{a}\frac{\partial u_0}{\partial x}+F\frac{\nu h^2}{12a^2}\left(\frac{\partial^2 w_0}{\partial x^2}-\frac{1}{KGh}\frac{\partial V}{\partial x}\right)\right]+p \\ N\rho_t I\left(1-\frac{h^2}{12a^2}\right)\frac{\partial^2}{\partial t^2}\left(\frac{\partial w_0}{\partial x}-\frac{V}{KGh}\right) &= \frac{EI}{1-\nu^2}\left[\left(1-\frac{h^2}{12a^2}\right)A\frac{\partial^2}{\partial x^2}\left(\frac{\partial w_0}{\partial x}-\frac{V}{KGh}\right)\right. \\ &\quad \left.+F\frac{\nu}{a^2}\frac{\partial w_0}{\partial x}\right]+V+\frac{1}{2}qh\left(1+\frac{h}{6a}\right) \end{aligned}\right\} \quad \ldots [12]$$

In Equations [12] three additional tracers L, D, and N for terms due to inertia in the axial and radial directions, and the rotatory inertia, respectively, are introduced.

The terms

$$\frac{V}{KGh} \quad \text{and} \quad \frac{1}{KGh}\frac{\partial V}{\partial x}$$

introduce the effect of shear strain into the second and third of Equations [12]. It will be seen later that this effect is important only in the third of Equations [12]. The omission of these terms would be tantamount to the replacement of α in Equations [9] and [11] by $\partial w_0/\partial x$, as is usually done in the theory of bending. In that case Equation [8] would become superfluous since we would then have six Equations [9] and [11] for the six unknowns u_0, w_0, V, T_x, T_θ, and M. The effect of shear strain can be removed in Equations [12] by allowing K to approach infinity in such a manner that V, as given by Equation [8], remains finite when α approaches $\partial w_0/\partial x$.

Velocity—Frequency Relation

It is convenient to introduce dimensionless variables and parameters as follows

$$\left.\begin{aligned} p^* &= \frac{ap}{\rho_t c_1^2 h} \\ q^* &= \frac{aq}{\rho_t c_1^2 h} \\ V^* &= \frac{V}{\rho_t c_1^2 h} \\ t^* &= \frac{c_1 t}{a} \\ u^* &= \frac{u_0}{a} \\ w^* &= \frac{w_0}{a} \\ x^* &= \frac{x}{a} \\ h^* &= \frac{h}{a} \\ \xi &= \frac{1}{12}h^{*2} \\ \eta &= \frac{2}{(1-\nu)K} \end{aligned}\right\} \quad \ldots\ldots\ldots\ldots [13]$$

where

$$c_1^2 = \frac{E}{\rho_t(1-\nu^2)} \quad \ldots\ldots\ldots\ldots [14]$$

Using Equations [13], [14], and the relation

$$E/G = 2(1+\nu) \quad \ldots\ldots\ldots\ldots [15]$$

and neglecting terms containing second and higher powers of ξ, one obtains from Equations [12] the following equations in dimensionless form

$$\left.\begin{aligned} & L\frac{\partial^2 u^*}{\partial t^{*2}}-C\frac{\partial^2 u^*}{\partial x^{*2}}-\nu\frac{\partial w^*}{\partial x^*}-q^*=0 \\ & D\frac{\partial^2 w^*}{\partial t^{*2}}+F\nu\xi\frac{\partial^2 w^*}{\partial x^{*2}}+H(1+S\xi)w^*+\nu\frac{\partial u^*}{\partial x^*} \\ & \qquad -(1+F\nu\xi\eta)\frac{\partial V^*}{\partial x^*}-p^*=0 \\ & \xi\left[N\frac{\partial^2 w^*}{\partial t^{*2}\partial x^*}-A\frac{\partial^2 w^*}{\partial x^{*2}}-F\nu\frac{\partial w^*}{\partial x^*}\right] \\ & \qquad -\xi\eta\left[N\frac{\partial^2 V^*}{\partial t^{*2}}-A\frac{\partial^2 V^*}{\partial x^{*2}}\right]-V^* \\ & \qquad -\frac{1}{2}q^*h^*\left(1+\frac{1}{6}h^*\right)=0 \end{aligned}\right\} \quad \ldots [16]$$

In the second of equations [16] another tracer S denoting a curvature correction to the hoop strain is introduced. The parameters η and ν may conveniently be used as tracers for the effect of shear strain and the influence of Poisson's ratio, respectively, although their values are not unity.

Eliminating u^* and V^* and neglecting terms containing ξ^2, one obtains the following equation in w^*

$$\left[1 + \xi\eta\left(N\frac{\partial^2}{\partial t^{*2}} - A\frac{\partial^2}{\partial x^{*2}}\right)\right]\left[\left(L\frac{\partial^2}{\partial t^{*2}} - C\frac{\partial^2}{\partial x^{*2}}\right)\left(D\frac{\partial^2 w^*}{\partial t^{*2}} + Hw^* - p^*\right) + \nu^2\frac{\partial^2 w^*}{\partial x^{*2}}\right] - \xi\left(L\frac{\partial^2}{\partial t^{*2}} - C\frac{\partial^2}{\partial x^{*2}}\right)\left[\left(N\frac{\partial^2}{\partial t^{*2}} - A\frac{\partial^2}{\partial x^{*2}} - 2F\nu\right)\frac{\partial^2 w^*}{\partial x^{*2}} - HSw^*\right] = 0 \quad \ldots\ldots [17]$$

Here we have also assumed that the influence of the shear stress which the fluid exerts on the wall is very small and have therefore neglected all terms containing q^*.

For the case of sinusoidal waves one may write

$$\left.\begin{aligned} u^* &= U^* e^{i(mx^* - \omega^* t^*)} \\ w^* &= W^* e^{i(mx^* - \omega^* t^*)} \\ p^* &= P^* e^{i(mx^* - \omega^* t^*)} \end{aligned}\right\} \quad \ldots\ldots [18]$$

where U^*, W^*, and P^* are the amplitudes of the waves, and ω^* and m are dimensionless parameters related to the circular frequency ω and the phase velocity c for the propagated wave by the following equations

$$\left.\begin{aligned} \omega^* &= \frac{a\omega}{c_1} \\ c^* &= \frac{c}{c_1} \\ m &= \frac{\omega^*}{c^*} \end{aligned}\right\} \quad \ldots\ldots [19]$$

On using Equations [18] and [19], [17] yields the following relations between m and ω^*, or c^* and ω^*

$$[1 - \xi\eta(N\omega^{*2} - Am^2)]\left[(L\omega^{*2} - Cm^2)\left(D\omega^{*2} - H + \frac{P^*}{W^*}\right) - \nu^2 m^2\right] - \xi(L\omega^{*2} - Cm^2)[HS - (N\omega^{*2} - Am^2 + 2F\nu)m^2] = 0 \quad \ldots\ldots [20]$$

and

$$c^{*2}[c^{*2} - \xi\eta\omega^{*2}(Nc^{*2} - A)]\left[(Lc^{*2} - C)\left(D\omega^{*2} - H + \frac{P^*}{W^*}\right) - \nu^2\right] - \xi(Lc^{*2} - C)(HSc^{*4} - N\omega^{*4}c^{*2} + A\omega^{*4} - 2F\nu\omega^{*2}c^{*2}) = 0 \quad \ldots\ldots [21]$$

From Equation [21] it is seen that, with the tracers D and H equal to 1, the ratio of the contributions of inertia in the radial direction and hoop strain is ω^{*2}. Therefore, when $\omega^* = 1$, the two terms cancel each other. The axial and the radial motions of the tube are coupled through the presence of Poisson's ratio ν. If the terms due to ν are neglected, Equation [21] reduces to the following two equations

$$\left.\begin{aligned} &Lc^{*2} - C = 0 \\ &c^{*2}[c^{*2} - \xi\eta\omega^{*2}(Nc^{*2} - A)]\left(D\omega^{*2} - H + \frac{P^*}{W^*}\right) - \xi(HSc^{*4} - N\omega^{*4}c^{*2} + A\omega^{*4}) = 0 \end{aligned}\right\} \quad \ldots [22]$$

The first of these gives the phase velocity for longitudinal vibrations, the second for radial vibrations including rotary motion.

For the empty tube $P^* = 0$; Equation [21] may then be written as a quadratic equation in ω^{*2}, the coefficients of which are polynomials in c^{*2}

$$A_0 + A_1\omega^{*2} + A_2\omega^{*4} = 0 \quad \ldots\ldots [23]$$

where

$$\left.\begin{aligned} A_0 &= (CH - \nu^2 + CHS\xi)c^{*4} - HL(1 + S\xi)c^{*6} \\ A_1 &= (ACH\eta - A\nu^2\eta - 2CF\nu)\xi c^{*2} - (CD - 2FL\nu\xi + CHN\xi\eta + AHL\xi\eta - \nu^2\xi\eta)c^{*4} + L(D + HN\xi\eta)c^{*6} \\ A_2 &= AC\xi - (AL + CN + ACD\eta)\xi c^{*2} + (LN + CDN\eta + ALD\eta)\xi c^{*4} - DLN\xi\eta c^{*6} \end{aligned}\right\} \quad \ldots [24]$$

For a given value of c^* the corresponding values of ω^{*2} can be obtained from Equation [23] by solving the quadratic equation with the coefficients given by Equations [24].

To find the values of c^* corresponding to a given value of ω^*, it is convenient to write Equation [21] in the form

$$B_0 + B_1c^{*2} + B_2c^{*4} + B_3c^{*6} = 0 \quad \ldots\ldots [25]$$

where

$$\left.\begin{aligned} B_0 &= AC\xi\omega^{*4} \\ B_1 &= (ACH\eta - A\nu^2\eta - 2CF\nu)\xi\omega^{*2} - (AL + CN + ACD\eta)\xi\omega^{*4} \\ B_2 &= (CH - \nu^2 + CHS\xi) - (CD - 2FL\nu\xi + CHN\xi + AHL\xi\eta - \nu^2\xi\eta)\omega^{*2} + (LN + CDN\eta + ADL\eta)\xi\omega^{*4} \\ B_3 &= -HL(1 + S\xi) + L(D + HN\xi\eta)\omega^{*2} - DLN\xi\eta\omega^{*4} \end{aligned}\right\} \quad \ldots [26]$$

If we take account of all the physical quantities in the equations, the tracers A, C, D, F, H, L, N, and S have the value of unity, and Equations [23] and [24] yield the following relation between c^* and ω^* in terms of the parameters ξ, η, and ν

$$\xi(1 - c^{*2})^2(1 - \eta c^{*2})\omega^{*4} + c^{*2}(1 - c^{*2})[(\eta - \nu^2\eta - 2\nu)\xi - (1 + \xi\eta)c^{*2}]\omega^{*2} + c^{*4}[1 + \xi - \nu^2 - (1 + \xi)c^{*2}] = 0 \quad \ldots [27]$$

Examination of the coefficients [24] shows that, since $\xi \ll 1$ and $\nu < 1/2$, the S-terms in A_0 may be neglected without materially affecting the $c^* - \omega^*$ relation. Similarly, a more detailed examination will show that the F-terms in A_1 may also be omitted. These approximations permit us to set up simplified expressions for T_θ and M, to replace the original expressions in Equations [11], for the study of wavelike deformations. They are obtained by dropping terms containing F, and by substituting

$$Hw_0/a \text{ for } (Hw_0/h)\ln[(2a + h)/(2a - h)]$$

(i.e., by retaining only the first term in the expansion for the logarithm), in Equations [11]

$$\left.\begin{aligned} T_x &= \frac{Eh}{1-\nu^2}\left[C\frac{\partial u_0}{\partial x} + \nu\frac{w_0}{a}\right] \\ T_\theta &= \frac{Eh}{1-\nu^2}\left[H\frac{w_0}{a} + \nu\frac{\partial u_0}{\partial x}\right] \\ M &= \frac{EI_0}{1-\nu^2}A\frac{\partial \alpha}{\partial x} \end{aligned}\right\} \quad \ldots\ldots [28]$$

The use of Equations [28] in the preceding analysis leads to the following equation in place of Equation [27]

$$\xi(1-c^{*2})^2(1-\eta c^{*2})\omega^{*4} + c^{*2}(1-c^{*2})[(1-\nu^2)\xi\eta - (1+\xi\eta)c^{*2}]\omega^{*2} + c^{*4}(1-\nu^2-c^{*2}) = 0 \quad [29]$$

Equation [29] may, of course, be obtained also directly from Equations [23] and [24] by putting $F = S = 0$.

It will be seen that for practically interesting values of ξ, ($h/a \leq$ say $1/8$), c^{*2} has a minimum value which is approximately given by

$$c^{*2}_{\min} = 2(1-\nu^2)^{1/2}\xi^{1/2}$$

so that the remaining ξ-terms in the coefficient of ω^{*2} in Equation [29] are also negligible. Since this further approximation does not, however, lead to any further simplification to the expressions for T_x, T_θ, and M, and since it does not substantially facilitate numerical computation, we have retained the terms in the following.

We shall only look for unattenuated waves, for which both ω and c, or ω^* and c^* are real. The sign of the ratio c/ω or c^*/ω^* will then indicate the direction of propagation. In discussing the relation between c^* and ω^* it is therefore sufficient to study only the positive real values of c^* and ω^*. From Equations [23] to [26] it is seen that for a given positive real value of c^* there are at most two positive real values of ω^*, and for a given positive real value of ω^*, there are at most three positive real values of c^*. Therefore for a given frequency there exist at most three modes of vibration.

From Equations [29] the limiting values of c^{*2} and ω^{*2} can be obtained

$$\left.\begin{aligned} &c^{*2} = 1-\nu^2, \text{ at } \omega^{*2} = 0 \\ &c^{*2} = 1, 1, \text{ and } 1/\eta, \text{ at } \omega^{*2} = \infty \\ &\omega^{*2} = 1 \text{ and } 1/\xi\eta, \text{ at } c^{*2} = \infty \end{aligned}\right\} \quad \ldots\ldots [30]$$

It is of interest to find the minimum value of c^*. For $c^{*2} \ll 1$, and recalling that $\xi \ll 1$, Equation [29] may be written approximately as

$$\xi\omega^{*4} - c^{*4}\omega^{*2} + (1-\nu^2)c^{*4} = 0$$

Substituting

$$\xi = \frac{1}{12}h^{*2}$$

one finds from this a minimum of c^{*2} and its corresponding value of ω^{*2} given, respectively, by

$$\left.\begin{aligned} c^{*2}_{\min} &= \left(\frac{1-\nu^2}{3}\right)^{1/2}h^* \\ \omega^{*2} &= 2(1-\nu^2) \end{aligned}\right\} \quad \ldots\ldots [31]$$

or dimensionally, on using Equations [19], [13], and [14]

$$\left.\begin{aligned} c^2_{\min} &= \frac{1}{3^{1/2}(1-\nu^2)^{1/2}}\frac{Eh}{\rho_f a} \\ \omega^2 &= \frac{2E}{\rho_f a^2} \end{aligned}\right\} \quad \ldots\ldots [31a]$$

By means of Equations [31] more accurate expressions for $c^2_{\min}$ and its corresponding value of ω^2 are obtained from Equations [29] by iteration. They are

$$\left.\begin{aligned} c^2_{\min} &= \frac{1}{3^{1/2}(1-\nu^2)^{1/2}}\frac{Eh}{\rho_f a}\left[1-\frac{1}{2}\left(\frac{1}{1-\nu^2}+\eta\right)\left(\frac{1-\nu^2}{3}\right)^{1/2}\frac{h}{a}\right] \\ \omega^2 &= \frac{2E}{\rho_f a^2}\left[1-\frac{\nu^2}{3^{1/2}(1-\nu^2)^{1/2}}\frac{h}{a}\right] \end{aligned}\right\} \quad \ldots [32]$$

It is interesting that $c_{\min}$ is essentially proportional to $(Eh/\rho_f a)^{1/2}$ and occurs approximately at $\omega^2 = 2E/\rho_f a^2$. Thus, keeping all other parameters fixed, the minimum phase velocity decreases as the radius a increases and it occurs at lower frequencies.

Equation [29] can be used to compute curves showing the variation of c^* with ω^* for various values of h^* or ξ. Two such curves are shown in Fig. 2. For $\omega^* < 1$ only the "first" mode occurs. The dimensionless phase velocity c^* of the first mode is

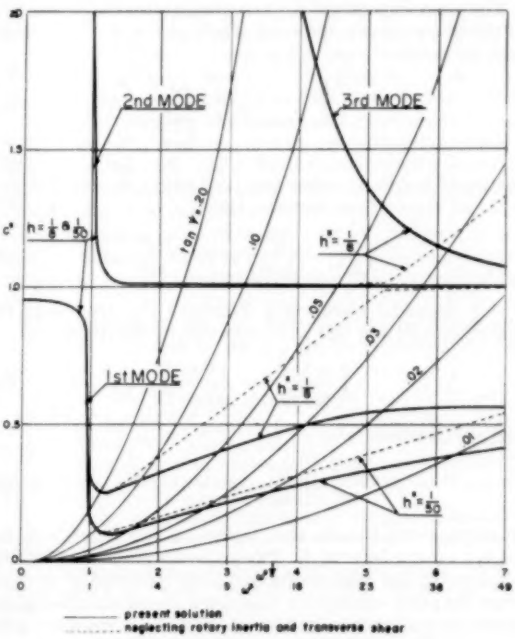

$h/a = 1/8$ and $1/20$
$\nu = 0.3$ and $K = 5/6$

FIG. 2 PHASE VELOCITY VERSUS FREQUENCY

always less than 1. It decreases from $(1-\nu^2)^{1/2}$ to an approximate minimum value

$$\left(\frac{1-\nu^2}{3}\right)^{1/4}h^{*1/2}$$

as ω^* varies from zero to approximately $2^{1/4}(1-\nu^2)^{1/8}$, and then increases to a limiting value $\eta^{-1/2}$ as ω^* increases to infinity. The dimensionless phase velocity c^* of the second and third modes are always greater than 1. For the second mode c^* starts at $\omega^* = 1$. It decreases at first very rapidly from ∞ to a value a little above 1 as ω^* increases, and then approaches 1 asymptotically as ω^* approaches ∞. The third mode exists for $\omega^* \geq (\xi\eta)^{-1/2}$ with c^* becoming infinite as ω^* approaches its minimum value. With increasing ω^*, c^* decreases monotonically to 1.

When both the rotatory inertia and shear-strain effects are neglected, Equation [29] reduces to

$$\xi(1-c^{*2})\omega^{*4} - c^{*4}(1-c^{*2})\omega^{*2} + c^{*4}(1-\nu^2-c^{*2}) = 0 \quad \text{[33]}$$

This may be obtained from Equations [23] and [24] by putting $F = S = N = \eta = 0$ and $A = C = D = H = L = 1$. Since the coefficients of ω^{*4} and ω^{*2} differ from those of Equation [29], it may be expected that the effects of rotatory inertia and shear strain will be important at high frequencies. To demonstrate this importance the variations of c^* with ω^* given by Equation [33] are also shown in Fig. 2. It is seen that for $h/a = 1/8$ a change in c^* of the order of 15 per cent is obtained in the region $2 < \omega^* < 4$. For $h/a = 1/20$ the change is 15 per cent in the region $10 < \omega^* < 20$.

Strain and Amplitude Ratios

The mean value of the strain ratio $\epsilon_\theta/\epsilon_x$ over the cross section of the tube is equal to the value of $\epsilon_\theta/\epsilon_x$ at $r = r_0$. From Equations [4] and [13]

$$\left(\frac{\epsilon_\theta}{\epsilon_x}\right)_{r=r_0} = \frac{a}{r_0}\frac{w^*}{\dfrac{\partial u^*}{\partial x^*}} \quad \text{[34]}$$

Setting $q^* = 0$ for an empty tube, and setting the tracers $C = L = 1$, one obtains from Equation [16]

$$\left(\frac{\partial^2}{\partial t^{*2}} - \frac{\partial^2}{\partial x^{*2}}\right)u^* = \nu\frac{\partial w^*}{\partial x^*} \quad \text{[35]}$$

For a sinusoidal wave, using Equations [1], [18], and [19], Equations [34] and [35] yield, respectively, the strain ratio

$$\left(\frac{\epsilon_\theta}{\epsilon_x}\right)_{r=r_0} = \frac{c^{*2}-1}{\nu(1+\xi)} \quad \text{[36]}$$

and the amplitude ratio

$$\frac{W^*}{U^*} = \frac{\omega^*}{\nu c^*}(c^{*2}-1)e^{i\pi/2} \quad \text{[37]}$$

It is interesting to note that $(\epsilon_\theta/\epsilon_x)_{r=r_0} > 0$ for $c^* > 1$, and $(\epsilon_\theta/\epsilon_x)_{r=r_0} < 0$ for $c^* < 1$. Physically this means that both the mean radial and axial strains are either compressive or tensile when the phase velocity $c > c_1$ as in the second and third modes, while one is compressive and the other tensile, or vice versa, when $c < c_1$ as in the first mode. The factor $e^{i\pi/2}$ in Equation [37] indicates that there is a phase lag of $\pi/2$ between the axial and radial displacements of the tube wall. To study the ratio W^*/U^* the relation between c^* and ω^* given by Equation [21] must be used. For an empty tube $P^* = 0$ and Equation [21] may be replaced by [29]. Equations [36] and [37] are valid so long as q^* is zero.

From Equation [36], neglecting ξ, one has at $r = r_0$

$$|\epsilon_\theta| \leq |\epsilon_x| \text{ for } (1-\nu)^{1/2} \leq c^* \leq (1+\nu)^{1/2}$$

$$|\epsilon_\theta| \geq |\epsilon_x| \text{ for } c^* \leq (1-\nu)^{1/2} \text{ or } c^* \geq (1+\nu)^{1/2}$$

Using the curves in Fig. 2 and Equation [37], the type of vibration which occurs for different ranges of c^* (and hence ω^*) can be determined. When $c^* \approx 1$, $W^*/U^* \approx 0$, giving mainly axial motion. When $c^* \gg 1$

$$W^*/U^* \approx \frac{\omega^* c^*}{\nu} e^{i\pi/2}$$

Since this occurs for $\omega^* \geq 1$, the motion is predominantly one in the radial direction. When $c^* \ll 1$

$$W^*/U^* \approx -\frac{\omega^*}{\nu c^*} e^{i\pi/2}$$

Since this occurs for $\omega^* > 0.7$ approximately, the motion is again primarily radial.

So far as the dimensionless velocity c^* is concerned, the relative importance of the various terms for different ranges of values of ω^* can be conveniently determined from Equations [23] and [24]. For $\omega^* \ll 1$, only A_0 of Equation [23] is of importance, and from Equation [24] it is seen that the terms in A_0 are due to (*a*) axial strain C; (*b*) hoop strain H; (*c*) axial inertia L; and (*d*) Poisson's effect ν. For $\omega^* \gg 1$, A_2 of Equation [23] is of importance, and from Equation [24] it is seen that the terms in A_2 are due to (*a*) conventional bending A, as in a beam; (*b*) axial strain C; (*c*) radial inertia D; (*d*) axial inertia L; (*e*) rotatory inertia N; and (*f*) the shear strain η.

Limitation of the Theory

The foregoing theory is based on the assumption that the thickness h of the tube is small compared with both the radius and the wave length $\lambda = 2\pi c/\omega$. Let

$$\frac{h}{\lambda} \leq \Gamma \ll 1 \quad \text{[38]}$$

It follows from Equations [19] that

$$\frac{c^*}{\omega^*} \geq \frac{h^*}{2\pi\Gamma} \quad \text{[39]}$$

If one writes

$$\psi = \tan^{-1}\frac{c^*}{\omega^*} \quad \text{[40]}$$

it follows that

$$\psi_{\min} = \tan^{-1}\frac{h^*}{2\pi\Gamma} \quad \text{[41]}$$

Therefore, in the c^* versus ω^* diagram, the theory may be expected to be valid in the region where $\psi > \psi_{\min}$. From Equation [41] it is seen that for a given Γ, $\psi_{\min}$ decreases with h^*. Hence the smaller the ratio h/a, the larger is the region $\psi > \psi_{\min}$.

Comparison With Previous Results

1 As a special case of the problem, neglecting terms due to (*a*) rotatory inertia, (*b*) shear strain, (*c*) bending, (*d*) curvature correction to hoop tension, and (*e*) curvature effect coupled with Poisson's ratio, and considering only terms due to (*a*) axial strain, (*b*) inertia in the radial direction, (*c*) inertia in the axial direction, (*d*) hoop strain, and (*e*) Poisson's effect, one has for an empty tube

$$\left.\begin{aligned} P^* = N = \eta = A = S = F = 0 \\ C = D = L = H = 1 \end{aligned}\right\} \quad \text{[42]}$$

On using Equations [42], [20] reduces to

$$(\omega^{*2} - m^2)(\omega^{*2} - 1) - \nu^2 m^2 = 0 \quad \ldots\ldots [43]$$

Writing

$$\left.\begin{aligned} \nu' &= \frac{\nu}{1-\nu} \\ c_2^2 &= G/\rho \end{aligned}\right\} \quad \ldots\ldots [44]$$

and using Equations [13], [14], [15], and [19], one obtains from Equation [43]

$$\frac{\omega^2 R^2}{c_2^2}\left[\frac{\omega^2 R^2}{c_2^2} - 2(1+\nu')(1+m^2)\right] + 4(1+2\nu')m^2 = 0 \quad [45]$$

This checks with the axisymmetric case of Rayleigh's (1) solution for vibrations of empty tubes. The ω/c_2, E, ν', and m of Equation [45] correspond, respectively, to Rayleigh's k, a, N, and h.

2 As another special case, neglecting terms due to (*a*) rotatory inertia, (*b*) shear strain, (*c*) curvature correction to hoop strain, and (*d*) curvature effect coupled with Poisson's ratio, one has

$$\left.\begin{aligned} P^* = N = \eta = S = F = 0 \\ A = C = D = L = H = 1 \end{aligned}\right\} \quad \ldots\ldots [46]$$

Substitution of Equations [46] into [20] yields

$$(\omega^{*2} - m^2)[\omega^{*2} - 1 - \xi m^4] - \nu^2 m^2 = 0 \quad \ldots\ldots [47]$$

This checks with the axisymmetric case of Naghdi's and Berry's solution (4). The ξ, ω^{*2} and m of Equation [47] correspond, respectively, to their k, γp^2, and $i\lambda$.

Using Kennard's (3) simplified equations of motion, Naghdi and Berry (4) obtain another relation between m and ω^*. In terms of the notation of the present paper this relation for the axisymmetric case can be written as

$$(\omega^{*2} - m^2)\left[\omega^{*2} - 1 - \xi\frac{2+\nu}{2(1-\nu)} - \xi m^4\right] - \nu^2 m^2 = 0 \quad [48]$$

where the torsional vibration parameter of (4) has been set equal to zero. Equations [47] and [48] differ only in the constant terms inside the bracket. Since $\xi \ll 1$, and $0 < \nu < \frac{1}{2}$, the difference is negligible.

3 As a limiting case, letting the radius a of the tube approach infinity, using Equations [13] and [19], and putting $\lambda = 2\pi c/\omega$, one obtains from Equations [20]

$$\left.\begin{aligned} c^2 &= c_1^2 \\ \frac{\eta}{12}\left(\frac{h\omega}{c_1}\right)^4 - \left[1 + \left(\frac{1+\eta}{3}\right)\left(\frac{\pi h}{\lambda}\right)^2\right]\left(\frac{h\omega}{c_1}\right)^2 &+ \frac{4}{3}\left(\frac{\pi h}{\lambda}\right)^4 = 0 \end{aligned}\right\} \quad [49]$$

These equations apply to the vibrations of an infinite plate. The first equation gives the velocity for vibrations which take place in the plane of the plate. The second equation gives the $\omega - \lambda$ relation for the straight-crested flexural waves in an infinite plate, and it checks with the solution given by Mindlin (9). The c_1^2 and c_1^2/η in Equations [49] correspond, respectively, to c_p^2 and $\kappa^2 c_s^2$ of Equation [46] in (9).

For $h/\lambda \ll 1$, Equation [49] yields

$$\left.\begin{aligned} \omega^2 &= \frac{4\pi^4 h^2 c_1^2}{3\lambda^4}\left[1 - \frac{\pi^2}{3}(1+\eta)\frac{h^2}{\lambda^2}\right] \\ \omega^2 &= \frac{12 c_1^2}{\eta h^2}\left[1 + \frac{\pi^2}{3}(1+\eta)\frac{h^2}{\lambda^2}\right] \end{aligned}\right\} \quad \ldots\ldots [50]$$

In Equations [50], c_1 is given by Equation [14]. In the case of a bar, on assuming plane stress, Equation [14] is replaced by $c_1^2 = E/\rho_1$. The first of Equations [50] then checks with Timoshenko's (8) solution for the flexural vibrations of prismatic bars. The parameters ω, λ, η, h^2, and c_1^2 correspond, respectively, to P_{ω}, $2L$, $E/\lambda c$, $12k^2$, and $\alpha^2/12$ of (8). The second of Equations [50] gives the frequency of thickness shear vibrations in terms of wave length. It has a much higher value than that for the flexural waves.

Discussion and Conclusion

The effects of rotatory inertia and transverse shear are of importance at high frequencies. They tend to lower the velocity of propagation and introduce an additional mode in the velocity-frequency diagram.

The limit of the velocity for the second mode, as the frequency becomes very large, is made finite; it should be noted, however, that the results for very large ω are possibly not reliable because in this range the condition $h \ll \lambda$ is violated.

Since the effects in question do not vanish with decreasing h/a, they cannot be investigated by retaining higher-order terms in a theory of thin shells based on power-series expansion in h/a without retaining higher-order terms in h/λ.

The minimum phase velocity of the "first" mode is essentially equal to

$$(hE/a\rho_1)^{1/2}/[3(1-\nu^2)]^{1/4}$$

and it occurs approximately at $\omega^2 = 2E/a^2\rho_1$. Thus, keeping all the other parameters fixed, the minimum phase velocity decreases as the radius a increases and it occurs at lower frequencies. Without changing the frequency, the minimum phase velocity may be reduced by using a thinner tube with the same radius.

The motion is mainly axial when $c \approx c_1$, and becomes primarily radial when $c \ll c_1$ or $c \gg c_1$. For the second and third modes the mean radial and axial strains over a cross section are either compressive or tensile, while for the first mode one is compressive and the other tensile, or vice versa.

The accuracy of the present theory may be improved by using additional terms in the power series for the displacements and by considering moments of higher orders in the equations of equilibrium.

The present theory may be extended to include various modes of torsional vibrations by using a similar expression for v as is used for u.

BIBLIOGRAPHY

1 "The Theory of Sound," by Lord J. Rayleigh, Dover Publications, New York, N. Y., 1945, p. 404.

2 "A Strain-Energy Expression for Thin Cylindrical Shells," by H. H. Bleich and F. DiMaggio, Journal of Applied Mechanics, Trans. ASME, vol. 75, 1953, pp. 448–449.

3 "The New Approach to Shell Theory: Circular Cylinders," by E. H. Kennard, Journal of Applied Mechanics, Trans. ASME, vol. 75, 1953, pp. 33–40.

4 "On the Equations of Motion of Cylindrical Shells," by P. M. Naghdi and J. G. Berry, Journal of Applied Mechanics, Trans. ASME, vol. 76, 1954, pp. 160–166.

5 "Frequencies and Modes of Cylindrical Shells," by M. L. Baron and H. H. Bleich, Journal of Applied Mechanics, Trans. ASME, vol. 76, 1954, pp. 178–184.

6 "The Propagation of Elastic Waves in Thin Walled Cylindrical Shells," by M. C. Junger and F. J. Rosato, *Journal of the Acoustical Society of America*, vol. 26, 1954, pp. 709–713.

7 "On the Correction for Shear of the Differential Equation for Transverse Vibrations of Prismatic Bars," by S. P. Timoshenko, *Philosophical Magazine*, series 6, vol. 41, 1921, pp. 744–746.

8 "On the Transverse Vibrations of Bars of Uniform Cross Section," by S. P. Timoshenko, *Philosophical Magazine*, series 6, vol. 43, 1922, pp. 125–131.

9 "Influence of Rotatory Inertia and Shear on Flexural Motions of Isotropic Elastic Plates," by R. D. Mindlin, Journal of Applied Mechanics, Trans. ASME vol. 73, 1951, pp. 31–38

On the Wake Energy of Moving Cascades[1]

By N. H. KEMP[2] and W. R. SEARS[3]

The rate of transfer of energy to the vortex-wake pattern is calculated for isolated thin airfoils and cascades of thin airfoils in unsteady flow. This part of the work parallels earlier investigations by Garrick (7)[4] and Keller (1). Application is made to the elementary two-row stages treated in an investigation (2) of the induction effects due to relative motion of the blade rows. The results show that the energy transferred to the wake pattern is a small fraction of the work absorbed by the rotor. Cross-induced contributions for a two-row stage may be negative but are small. By far the greatest contribution to the wake energy is that due to the circulation fluctuations induced in a blade row by the relative motion of the adjacent downstream row.

Nomenclature

The following nomenclature is used in the paper:

A = coefficient of vortex sheet, Equation [13]
b = axial distance between centers of stator and rotor rows (Fig. 4)
b' = axial distance between trailing edge of stator row and leading edge of rotor row (Fig. 4)
B_m = coefficient of trailing vortex-sheet, Equation [15]
c = blade semichord (Fig. 4)
C_m = Fourier coefficient of quasi-steady circulation, Equations [7], [31], [32]
$_0C_L$ = steady lift coefficient
d = pitch of blades in direction of rotation (Fig. 4)
E = average energy per unit length and width transferred to wake of a blade as a result of interference of blades of same row
E_* = average energy per unit length and width transferred to wake of a blade as a result of interference of blades of adjacent row
H_m = steady bound vortex-distribution function, Equation [33]
J_n = Bessel function of first kind
$J = J_0 - iJ_1$
K_n = modified Bessel function of second kind
$K_V/100$ = ratio of wake power to rotor power, Equation [35a]
P_p—see Equation [30]
Q_{pm}—see Equation [28]
$\Re$—real part
t = time
t' = constant time lag between occurrences at consecutive blades
U = rotational speed of rotor, positive down
V = speed of flow relative to blade
w = upwash normal to vortex sheet
x = co-ordinate along blade from center, positive toward trailing edge
$X = x - Vt$
α = angle of stagger of blades (Fig. 4)
β = angle between rotor and stator blades
β' = angle defined in Fig. 3
γ = strength of bound-vortex distribution, positive clockwise
ϵ = strength of wake-vortex distribution, positive clockwise
$\lambda = \mu c/V$
$\mu_s = (2\pi V_s/d_r)e^{i(\pi/2 - \alpha_s)}$
$\mu_r = (2\pi V_r/d_s)e^{-i(\pi/2 - \alpha_r)}$
ν = circular frequency of motion in time $\nu_s = 2\pi U/d_r$, $\nu_r = 2\pi U/d_s$
ρ = air density
ϕ = velocity potential
$\Delta\phi = \phi_{\text{bottom}} - \phi_{\text{top}}$
σ = solidity $2c/d$
ω = reduced frequency $\nu c/V$
Γ = circulation, positive clockwise
ψ_m = induced velocity factor, Equation [18]
τ = dimensionless time lag, Vt'/d
$\Omega = \nu d/V$

Postsubscripts

s = stator
r = rotor

Presubscripts

0 = steady quantities
q = quasi-steady quantities
t = time-dependent quantities

Superscripts

s = stator
r = rotor
(k, n) = kth, nth blade

Introduction

The blades of a typical turbomachine stage move through a field of flow disturbed by neighboring blade rows, and therefore experience periodic fluctuations of such quantities as angle of attack and relative speed. One result is that the circulation around such blades fluctuates in a periodic manner about some mean value, and, in accordance with the laws of fluid flow, wakes of vortexes are shed at their trailing edges and are carried downstream by the flow. The production of these vortex wakes represents an expenditure of energy, i.e., a transfer of energy from more useful forms into the kinetic energy of the vortex-wake pattern downstream. It is important in the design and development of turbomachinery to make an evaluation of this energy transfer in comparison with other "losses."

This problem was attacked by C. Keller (1), who calculated the energy transfer for a single row of blades in terms of the percentual

[1] This work was partially supported by the U. S. Air Force, Air Research and Development Command, Office of Scientific Research, under contract AF 33 (038)-21406.

[2] Advanced Research Engineer, Research Laboratory, AVCO Manufacturing Corporation, Everett, Mass. Formerly Group Leader, Analytical Engineering, United Aircraft Corporation, Research Department, East Hartford, Conn.

[3] Director, Graduate School of Aeronautical Engineering, Cornell University, Ithaca, N. Y.

[4] Numbers in parentheses refer to Bibliography at end of paper.

Contributed by the Applied Mechanics Division and presented at the Diamond Jubilee Annual Meeting, Chicago, Ill., November 13–18, 1955, of The American Society of Mechanical Engineers.

Discussion of this paper should be addressed to the Secretary, ASME, 29 West 39th Street, New York, N. Y., and will be accepted until July 10, 1956, for publication at a later date. Discussion received after closing date will be returned.

Note: Statements and opinions advanced in papers are to be understood as individual expressions of their authors and not those of the Society. Manuscript received by ASME Applied Mechanics Division, March 23, 1955. Paper No. 55—A-33.

fluctuation of blade circulation. The magnitude of this fluctuation, however, was not estimated in his paper.

Basically, the theory of the present paper is the same as Keller's. The present work differs from his principally in the fact that the circulation fluctuations are calculated according to the approximations of thin-airfoil theory. In this sense the paper is a continuation of an earlier one by the same authors (2). Two cases are considered, viz., (*a*) the general case of a single cascade of blades experiencing periodic disturbances, and (*b*) the case of an elementary compressor stage consisting of two rows of blades in relative motion. In the first case the results are given in terms of the Fourier constants of the *quasi-steady* circulation, which is a quantity describing essentially the periodic geometrical situation encountered by the blades. The second case is the same one for which the unsteady blade forces were calculated in reference (2). Here the results involve the *quasi-steady* circulations of both rows of blades. As numerical examples, these results are applied to the particular stages treated in reference (2), where the fluctuations of *quasi-steady* circulation arise solely from the interference effects of the adjacent blade row.

As in reference (2), the first step is to replace the rotating cascade by an infinite two-dimensional one. It should be emphasized that the wake pattern involved here consists entirely of vortexes with their axes lying in the radial direction; i.e., it is a case of plane flow. In a real turbomachine there are also trailing vortexes, whose axes are normal to the radial direction, due to radial variations of circulation, and the energy represented by them is probably important. These are not the concern of the present investigation.

Wake Energy of an Airfoil

The kinetic energy of any two-dimensional flow, per unit depth, is (1, 3)

$$T = \frac{1}{2}\rho \int_A \phi \frac{d\phi}{dn}\, dA \qquad [1]$$

where ρ is the mass density, ϕ the velocity potential, A a surface bounding the flow, and $\partial\phi/\partial n$ the derivative of ϕ in the direction normal to this surface, i.e., the normal velocity component, taken positive in the direction out of the fluid. Applying this well-known formula to a plane vortex sheet in an infinite body of fluid, one has for the energy per unit width

$$T = \frac{1}{2}\rho \int w \Delta\phi\, dx \qquad [2]$$

where now the integral is taken along the sheet (which lies in the x-direction), $\Delta\phi$ is the potential jump across the sheet, $\phi_{\text{bottom}} - \phi_{\text{top}}$, and w is the fluid velocity normal to the sheet, positive upward.

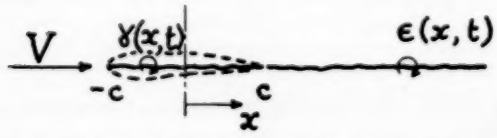

Fig. 1 Airfoil and Wake in Unsteady Motion Represented as Vortex Sheets

Consider now the case of a thin airfoil with its trailing wake, Fig. 1. In the familiar thin-airfoil theory both the airfoil and its wake are approximated by plane vortex sheets, whose strengths are $\gamma(x, t)$ and $\epsilon(x, t)$, respectively. From the definition of ϕ as the line integral of the velocity, it follows that the expression for $\Delta\phi(x, t)$ in this case is simply

$$\Delta\phi(x, t) = -\Gamma(t) - \int_c^x \epsilon(\xi, t) d\xi \qquad [3]$$

where $\Gamma(t)$ denotes the circulation about the airfoil, i.e.

$$\int_{-c}^{c} \gamma(\xi, t) d\xi$$

Furthermore, the wake strength $\epsilon(x, t)$ and the circulation $\Gamma(t)$ are related by the condition that the rate of shedding of vortexes at the trailing edge is $-d\Gamma/dt$, i.e. (4)

$$-\Gamma'(t) = V\epsilon(c, t) \qquad [4]$$

(where the prime denotes differentiation) and the condition that the free vortexes are carried rearward with the speed V, i.e. (4)

$$-\Gamma'\left(t - \frac{x - c}{V}\right) = V\epsilon(x, t) \qquad [5]$$

Upon substitution of Equation [5] into Equation [3], the following simple formula is obtained for the potential jump across the wake

$$\Delta\phi(x, t) = -\Gamma\left(t - \frac{x - c}{V}\right) \qquad [6]$$

Thus the jump at x is determined by the value of the circulation at an earlier instant, the instant at which the part of the wake now at x was created at the trailing edge.

In the present study it will be assumed that the circulation of each airfoil consists of a steady part plus a periodic fluctuation, and this will be expressed in Fourier-series form. It is easiest to express the instantaneous state of affairs at any blade in terms of its "quasi-steady" circulation ${}_q\Gamma(t)$, which is the circulation it would have, as a result of the instantaneous flow conditions encountered, in the absence of any effects of its vortex wake (4). Thus, in a cascade, ${}_q\Gamma(t)$ accounts for all the induced effects of neighboring blade rows and of members of the blade's own row, and is simply calculated by application of steady-flow airfoil theory with no attention to the vortexes shed by the blade in question. Since ${}_q\Gamma(t)$ is assumed to be periodic, let it be expressed in a Fourier series

$${}_q\Gamma(t) = \sum_{m=1}^{\infty} C_m e^{im\nu t} + {}_0\Gamma \qquad [7]$$

where ν is real and positive[5] and the constant ${}_0\Gamma$ represents the steady or average circulation.

The theory of thin airfoils in unsteady motion relates ${}_q\Gamma(t)$ to the total circulation $\Gamma(t)$ and, by Equation [5], to the wake-vortex strength $\epsilon(x, t)$; viz., corresponding to Equation [7] (4, 5)

$$\Gamma(t) = \sum_{m=1}^{\infty} C_m e^{-im\omega} S(m\omega) e^{im\nu t} + {}_0\Gamma \qquad [8]$$

where ω denotes the reduced frequency $\nu c/V$ and $S(\omega)$ is a combination of modified Bessel functions of the second kind

$$S(\omega) \equiv \{i\omega[K_0(i\omega) + K_1(i\omega)]\}^{-1} \qquad [9]$$

$S(\omega)$ is plotted in Fig. 3 of reference (6) and tabulated in reference (5).

Equations [6] and [8] provide an expression for $\Delta\phi(x, t)$ for use in the calculation of the wake energy for any periodic case. It is necessary now to work out the normal velocity at the vortex wake, w, and to do this one must sum up the effects of all blades, wakes, and rows. It is clear that the energy formula, Equation [2], is nonlinear, so that wake energies cannot be simply summed

[5] Complex notation will be used throughout; the real part is always implied, unless otherwise stated.

up. Such summation or superposition is permissible, however, in calculating $\Delta\phi$ (as has been done in the foregoing) and w.

Before going on, it will be mentioned that the calculation of wake energy for an isolated airfoil in oscillatory motion is a much easier matter, since, far behind the airfoil, the velocity w is simply related to ϵ. The integral in Equation [2] takes on an especially simple form. This type of calculation has been used (7) to calculate the drag or thrust of oscillating airfoils.

Velocities Induced by Wakes

In this section a general expression will be derived for the velocity induced by the vortex wakes of a cascade of blades, far downstream of the blades. The cascade is sketched in Fig. 2. The blades are numbered both ways from $n = 0$ as shown and $x^{(n)}$ is the co-ordinate measured in the free-stream direction from the center of the nth blade; d is the circumferential spacing, and α the angle of swirl relative to the cascade.

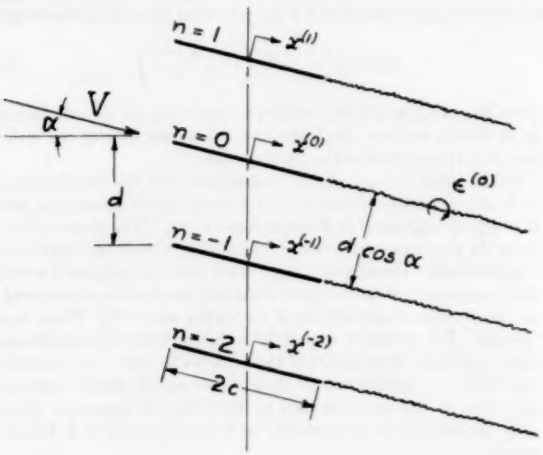

Fig. 2 Cascade of Thin Airfoils and Trailing Wakes

Now the formulas of the preceding section describe the wake of any one of these blades in terms of its co-ordinate $x^{(n)}$ and the time. To relate the events at various blades with respect to a common time scale, it will be assumed that there is some constant time lag t' between any occurrence at successive blades. In other words, any event occurring at time t at the $(n + k)$th blade is repeated at time $t + kt'$ at the nth blade. This implies, in particular, that if $\epsilon^{(n)}(x^{(n)}, t)$ describes the strength of the nth wake, the $(k + n)$th wake strength is exactly

$$\left.\begin{aligned}\epsilon^{(k+n)}(x^{(k+n)}, t) &= \epsilon^{(n)}(x^{(k+n)}, t + kt') \\ &= \epsilon^{(n)}(x^{(k+n)} - Vkt', t)\end{aligned}\right\} \quad \ldots\ldots [10]$$

Thus the wake pattern consists of identical, periodic wakes shifted in the stream direction relative to one another. The velocity induced by such an arrangement will now be evaluated. It will be necessary to describe all the wakes in terms of the co-ordinate $x^{(0)}$, say; this is easily done since

$$x^{(k)} = x^{(0)} + kd \sin \alpha \quad \ldots\ldots [11]$$

Furthermore, since any wake configuration, in the present approximation, is steady relative to a co-ordinate system transported with the stream, it is convenient to adopt such a system here, i.e.

$$X^{(0)} = x^{(0)} - Vt \quad \ldots\ldots [12]$$

Consider first the sinusoidal vortex sheet of Fig. 3 whose strength is

$$\epsilon(X) = -Ae^{-i\nu X} \quad \ldots\ldots [13]$$

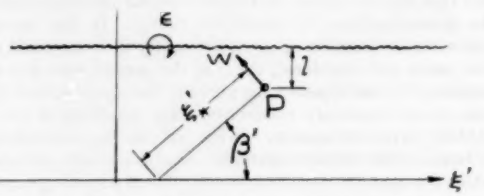

Fig. 3 Calculation of Velocity Induced at a Point P, Near a Plane Vortex Sheet of Sinusoidal Strength

where A is a complex constant. Let l be the perpendicular distance from the sheet to a point P, positive as sketched. The velocity w at P in the direction shown is

$$w = \frac{i}{2} Ae^{-i\nu X} e^{-\nu|l|} \left\{\begin{array}{l} e^{i\beta'} \text{ when } l > 0 \\ \cos \beta' \text{ when } l = 0 \\ e^{-i\beta'} \text{ when } l < 0 \end{array}\right\} \quad \ldots\ldots [14]$$

The strength of an airfoil's vortex wake follows from Equations [5] and [8]. For the wake of the zeroth blade

$$\epsilon^{(0)}(x^{(0)}, t) = -\sum_{m=1}^{\infty} B_m e^{im\nu(t - x^{(0)}/V)}$$

$$= -\sum_{m=1}^{\infty} B_m e^{-im\nu X^{(0)}/V} \quad \ldots\ldots [15]$$

where B_m denotes $im\nu C_m S(m\omega)/V$. Similarly, the strength of the kth wake is, from Equations [10], [11], and [12]

$$\epsilon^{(k)}(x^{(k)}, t) = \epsilon^{(0)}(x^{(k)}, t + kt')$$

$$= -\sum_{m=1}^{\infty} B_m e^{-im\nu(X^{(0)} + kd \sin \alpha - kVt')/V} \quad \ldots [16]$$

Thus, far downstream from the cascade, each vortex wake consists of a superposition of sinusoidal wakes of the same form as Equation [13], and Equations [14] can be used to calculate the velocity induced by any one of these.

Velocity Induced at Zeroth Wake. The velocity $w^{(0)}$ induced by all the wakes at the zeroth wake and normal to it is found by use of Equations [14] with $\beta' = 0$. The distance from the kth wake is $l_k = kd \cos \alpha$; the result is

$$w^{(0)} = \frac{i}{2} \sum_{m=1}^{\infty} B_m e^{-im\nu X^{(0)}/V} \sum_{k=-\infty}^{\infty} \exp\left\{-\frac{m\nu}{V}\left[|kd \cos \alpha| - ik(Vt' - d \sin \alpha)\right]\right\} \quad \ldots\ldots [17]$$

The series over k is a geometric series and can be summed. Its value is

$$\frac{\sinh (m\Omega \cos \alpha)}{\cosh (m\Omega \cos \alpha) - \cos [m\Omega(\tau - \sin \alpha)]} = \psi_m \quad \ldots [18]$$

where Ω denotes $\nu d/V$ and τ denotes Vt'/d. The final expression for the normal velocity at the zeroth wake is therefore

$$w^{(0)} = -\frac{1}{2} \sum_{m=1}^{\infty} \frac{m\omega}{c} C_m S(m\omega) \psi_m e^{-im\omega X^{(0)}/c} \quad \ldots [19]$$

The functions ψ_m approach unity as the spacing d approaches infinity for any m, and the difference $\psi_m - 1$ for each term represents the effect of the wakes of the other blades. This function also appears in the work of Keller (1), where it is denoted by F, with the argument of the hyperbolic and circular functions being h/l and a/l, respectively. Keller has plotted F in his Fig. 8 and tabulated it in his Chart I for various values of h/l and a/l.

Wake Energy of a Single Cascade

Formula [19] makes it possible to calculate at this point the kinetic energy in the vortex wakes of any single cascade of airfoils. Equations [6] and [8] give the potential jump and Equation [19] the normal velocity at the zeroth wake, for substitution in the energy formula, Equation [2]. The calculation is carried out far downstream of the blades, where Equation [19] applies, and can be expressed in the $X^{(0)}$ co-ordinate system. It is only necessary to integrate over one full wave length of the periodic wake; in fact, the *average* energy transfer per unit length of wake, per blade (per unit radial distance), is the quantity of interest; it is

$$E = \rho \frac{\omega}{4\pi c} \int_0^{2\pi c/\omega} w^{(0)} \Delta\phi dX^{(0)} \quad \ldots\ldots\ldots [20]$$

It must be remembered that real parts of complex quantities are implied in all the foregoing analysis. Upon multiplying $w^{(0)}$ and $\Delta\phi$ it is necessary to work out the product of real parts by use of one of the formulas

$$\Re\{w^{(0)}\}\Re\{\Delta\phi\} = \Re\left\{w^{(0)} \frac{1}{2} [\Delta\phi + \overline{\Delta\phi}]\right\}$$

$$= \Re\left\{\frac{1}{2} [w^{(0)} + \overline{w^{(0)}}]\Delta\phi\right\} \quad \ldots\ldots [21]$$

where $\Re$ denotes the real part and the bar denotes a complex conjugate. Thus, upon multiplication, one has two double summations, but these reduce to a single summation when the integration is carried out, by virtue of the formulas

$$\frac{\omega}{2\pi c} \int_0^{2\pi c/\omega} e^{-ik\omega X^{(0)}/c} dX^{(0)} = \left\{\begin{matrix} 0 & k \neq 0 \\ 1 & k = 0 \end{matrix}\right\} \quad \ldots [22]$$

It should also be noticed that the constant term in Equation [7] does not contribute to E.

The result is

$$E = \frac{1}{8} \rho \frac{\omega}{c} \sum_{m=1}^{\infty} m|C_m|^2|S(m\omega)|^2\psi_m \quad \ldots\ldots [23]$$

After multiplication by the wave length $2\pi c/\omega m$ to give the average energy in one wave length of the wake, each term of this result may be compared with equation [26] of Keller (1). It can be shown that Keller's result and the present one are identical, with the amplitude of the fluctuating circulation, called by Keller $\Delta\Gamma/2$, here taken to be $|C_m S(\omega m)|$, according to the theory of thin airfoils in nonsteady flow. While Keller only estimated the size of $\Delta\Gamma/2$, use of nonsteady theory makes it possible to calculate this quantity, if the nonsteady velocity field operating on a blade is known. (See reference 2, for example.)

The Fourier coefficients C_m describe the quasi-steady conditions encountered by a blade; ψ_m involves the geometry of the flow and the blade-to-blade lag time t'; and S is a tabulated function. Equation [23] would be applicable, for example, in a case of cascade-blade flutter. Unfortunately, in most other applications the velocity component $w^{(0)}$ in Equation [2] will involve contributions from other sources than the wakes of the single cascade; for example, it will often include the same disturbance velocities that cause the circulation to be unsteady in the cascade. The analysis is consequently more complicated.

In the next section a typical case, namely, that of an elementary stage consisting of rotor and stator, will be treated.

Wake Energy of Elementary Stage

The application of the present theory, to an elementary turbomachine stage, consisting of a stator cascade followed by a rotor cascade moving relative to it, Fig. 4, is straightforward in principle but involves lengthy calculations. The stage of Fig. 4 has arbitrary chords, pitches, and staggers, and arbitrary axial

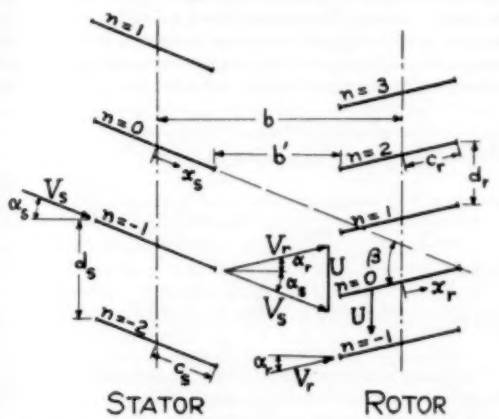

Fig. 4 Notation and Configuration of Elementary Turbomachine Stage

distance between the rows. The stator blades lie nearly in the direction of the entering stream V_s, as is consistent with thin-airfoil approximations, while the rotor blades bear the same relationship to their relative-stream vector V_r. It is easy to verify that the rotor wakes lie (in first approximation) in the direction of V_r as sketched. This is the configuration studed in reference (2).

If, as in reference (2), the only unsteady effects present are those due to the relative motion of these two rows, the circular frequencies of periodic quantities pertaining to the stator and rotor blades are, respectively

$$\nu_s = 2\pi U/d_r \quad \text{and} \quad \nu_r = 2\pi U/d_s \quad \ldots\ldots [24]$$

These correspond to the frequencies at which the blades of the adjacent row are seen to pass an observer sitting on one of the blades. Furthermore, the lag times t_s' and t_r' for the stator and rotor are just d_s/U and $-d_r/U$; i.e., the dimensionless time lags τ are

$$\tau_s = V_s/U \text{ and } \tau_r = -V_r/U \quad \ldots\ldots [25]$$

Let the stator and rotor quasi-steady circulations be expressed as

$${}_q\Gamma^s = \sum_{m=1}^{\infty} C_m{}^s e^{i\nu_s m t} + {}_0\Gamma^s$$

and

$${}_q\Gamma^r = \sum_{m=1}^{\infty} C_m{}^r e^{i\nu_r m t} + {}_0\Gamma^r \quad \ldots\ldots [26]$$

The potential jumps across the wakes of both families are then expressed in the same terms by Equations [6] and [8]. The self-induced normal velocities, i.e., those induced at a wake-vortex sheet by the sheets of its own family, are still given in each case, by Equation [19]. Thus for each cascade there is a self-induced energy transfer which is given by Equation [23] with the respective geometrical parameters, frequency, and time lag inserted.

The cross-induced contributions, however, must also be calculated. The cross-induced velocity component is calculated by use of Equation [14] with summation over the Fourier components of the wakes and over the infinity of wakes. The appropriate values of β' are, Fig. 4, $\beta(=\alpha_s + \alpha_r)$ for the calculation of velocities *at* the rotor wakes and $-\beta$ for the velocities *at* the stator wakes. The cross-induced velocities are, of course, periodic, and it is found convenient to express them in Fourier-series form. The result is, for the cross-induced normal velocity component at the zeroth stator wake due to the rotor wakes[6]

$$w_{s_0}^{(0)} = \sum_{p=1}^{\infty}\sum_{m=1}^{\infty}\left[\frac{C_m{}^r S(m\omega_r)e^{-im\omega\tau}}{d_r\cos\alpha_r}Q^r{}_{pm}(+) - \frac{\overline{C_m{}^r}S(m\omega_r)e^{im\omega\tau}}{d_r\cos\alpha_r}Q_{pm}{}^s(-)\right]e^{ip\nu_2 X_2^{(0)}/V_2} \quad [27]$$

where

$$Q_{pm}{}^s(\pm) \equiv \frac{pd_sV_r}{md_rV_s}\left\{1+\cot^2\beta\left[1\pm\frac{pd_sV_r}{md_rV_s}\sec\beta\right]^2\right\}^{-1}. \quad [28]$$

An analogous formula, which may be obtained from this one by an interchange of subscripts, gives the cross-induced velocity $w_{r_0}^{(0)}$ at the rotor wakes due to the stator wakes.

Use of Equation [27], together with the expression for the potential jump across the stator wake (cf. Equations [6] and [8]), in the energy expression, Equation [20], finally leads to the result

$$E_s{}^s = \frac{-\rho}{4d_r\cos\alpha_r}\sum_{m=1}^{\infty}\sum_{p=1}^{\infty}C_m{}^r S(m\omega_r)e^{-im\omega\tau} \times [P_p{}^s Q_{pm}{}^s(+) - \overline{P_p{}^r}Q_{pm}{}^s(-)] \quad [29]$$

This is the average energy in a stator wake due to the velocities induced by the rotor wakes, per unit length and width. The coefficients $P_p{}^s$ are defined by

$$P_p{}^s = C_p{}^s S(p\omega_s)\exp\left[-i\pi\sigma_r p\left(\frac{bU}{V_s c_r\cos\alpha_s}+\frac{U}{V_r}\right)\right] \quad [30]$$

The analogous formula for the average energy $E_s{}^r$ in a rotor wake due to stator-induced velocities is obtained by interchanging all subscripts and superscripts s and r in Equations [29] and [30]. The total "cross-induced" energy, per unit length and width, is the sum of $E_s{}^s$ and $E_s{}^r$. The Fourier coefficients $C_n{}^r$ and $C_n{}^s$, it will be recalled, describe the periodic quasi-steady situations encountered by the rotor and stator blades, respectively. $S(\omega)$ is a tabulated function, and all other symbols in Equations [29] and [30] refer to the geometry of the configuration. The characteristic frequencies ν and lag times τ, it must be remembered, have already been put equal to their values (Equations [24] and [25]) for the case when the only fluctuations are due to inter-row interference.

Application to Stages of Reference (2). As numerical examples, the theory of this section will now be applied to the elementary stator-rotor stages considered in reference (2), using the results obtained there by an approximate analysis of aerodynamic interference between rows. The stages considered there are of the type of Fig. 4. The calculations of reference (2) were based on the assumption that the steady part of the circulation about any blade ${}_0\Gamma$ is large compared to the fluctuating part ${}_t\Gamma(t)$. The steady part ${}_0\Gamma$ is due to the blade's angle of attack and all the steady induction effects of other blades, while ${}_t\Gamma(t)$ includes all the effects due to relative motion of the cascades. On the basis of this assumption, an approximate calculation was carried out, the numerical results of which confirmed the basic assumption regarding the relative magnitudes of ${}_0\Gamma$ and ${}_t\Gamma(t)$.

This analysis leads to the following results for the Fourier constants C_m of the quasi-steady circulation functions for the stator and rotor:

Stator

$$C_m{}^s = {}_0\Gamma^r J(m\lambda_s)\frac{\pi\sigma_s d_s}{d_r}e^{-ia_{sr}}\exp\left\{-\pi m\sigma_r \times\left[\frac{b}{c_r}\left(1+i\tan\alpha_r-\frac{iU}{V_r\cos\alpha_s}\right)-\frac{iU}{V_r}\right]\right\}H_m{}^r \quad [31]$$

Rotor

$$C_m{}^r = -{}_0\Gamma^s J(m\lambda_r)\frac{\pi\sigma_r d_r}{d_s}e^{ia_{sr}m}\exp\left\{\frac{-\pi m\sigma_r d_r}{d_s} \times\left[\frac{b}{c_r}\left(1+i\tan\alpha_r-\frac{iU}{V_r\cos\alpha_s}\right)-\frac{iU}{V_r}\right]\right\}H_m{}^s - \sum_{k=1}^{\infty}J(k\omega_r)\frac{\pi\sigma_r d_r}{d_s}e^{ia_{sr}m}\left[P_k{}^s Q_{mk}{}^r(-) - \overline{P_k{}^s}Q_{mk}{}^r(+)\right] \quad [32]$$

Here $P_k{}^s$ is defined in Equation [30]. $Q_{mk}{}^r(\pm)$ may be obtained from Equation [28] by interchanging the subscripts r and s. $J(z)$ denotes

$$J_0(z) - iJ_1(z)$$

and

$$H_m{}^r \equiv J_0(\pi m\sigma_r e^{-i(\pi/2-\alpha_r)}) + \sum_{n=1}^{\infty}(-i)^n\frac{A_{n+1}{}^r - A_{n-1}{}^r}{A_0{}^r + A_1{}^r} J_n(\pi m\sigma_r e^{-i[\pi/2-\alpha_r]}) \quad [33]$$

The coefficients $H_m{}^s$ are exactly the same as $H_m{}^r$ but with all subscripts and superscripts r replaced by s, and vice versa. In these coefficients the symbols $A_n{}^r$ and $A_n{}^s$ appear, for various n; these are the coefficients of the "Glauert series" describing the steady circulation distributions of rotor and stator blades, respectively. Thus the steady circulation or chordwise lift distributions are expressed in the form

$$\gamma(x) = 2V\left[A_0\frac{1-\cos\theta}{\sin\theta}+2\sum_{n=1}^{\infty}A_n\sin n\theta\right] \quad [34]$$

where either a superscript r or s is to be added to appropriate symbols and θ denotes $\cos^{-1}(x/c)$.

In reference (2) two typical circulation distributions were considered, viz., a flat-plate case, for which all the A_n are zero except A_0, and an elliptical distribution for which all the coefficients are zero except A_1. For these special cases, it will be noted, the coefficients $H_m{}^r$ and $H_m{}^s$ are especially simple. Actually, only the elliptical distribution was assumed for the stator blades, while both cases were investigated for the rotor blades.

At this point it is only necessary to substitute the foregoing values written out for $C_m{}^r$ and $C_m{}^s$ into Equations [23] and [29], in the appropriate combinations, in order to evaluate the self-induced and cross-induced energies for both rotor and stator.

Numerical Results. In order to calculate numerical values it is

[6] The details are given in reference (8).

convenient to work with nondimensional quantities. Following Keller, the rate of energy production in the wake will be normalized with the rate of energy input to the rotor of the elementary compressor stage. E is the energy per unit length of wake, and V is the rate at which the wake is produced. Therefore EV represents the power input to the wake. The steady power per blade necessary to turn the rotor is the component of rotor lift in the direction of motion, ${}_0\Gamma^r\rho V_r \cos \alpha_r$, times the rotor speed U. Thus the ratio of wake power to rotor power may be written, using Keller's notation

$$\frac{K_V}{100} = \frac{EV}{{}_0\Gamma^r\rho V_r U \cos \alpha_r} \quad \text{[35a]}$$

Actually, for calculation, it is further convenient to write this as

$$\frac{K_V/100}{{}_0C_L} = \frac{EV^2c}{{}_0\Gamma} \frac{1}{{}_0\Gamma^r\rho V_r U \cos \alpha_r} \quad \text{[35b]}$$

so that the various parameters appear on the right only as ratios of the same kind of physical quantities, instead of combinations like $\Gamma/(Ud)$. It is in the form of Equation [35b] that the power ratio was calculated for the case of a representative compressor stage.

Since the purpose of the calculations was to obtain an estimate of the size of the energy in the wake, they were carried out for only one simple cascade, for two different types of steady-state loading. The geometrical parameters were chosen to be typical of present-day compressors, viz.

$$\sigma_r = \sigma_s = 1, \quad d_r/d_s = 1, \quad \alpha_s = \alpha_r = 45°, \quad b'/c_r = 0.2$$

Here

$$b' = b - c_r \cos \alpha_r - c_s \cos \alpha_s$$

is the separation of the two rows of blades (Fig. 4). The ratio of steady-state circulations was fixed by assuming that the stage produced no net turning of the flow. Since the turning produced by a stage is proportional to ${}_0\Gamma/d$, the condition of no net turning is

$${}_0\Gamma^s/d_s = -{}_0\Gamma^r/d_r \quad \text{or} \quad {}_0\Gamma^s/{}_0\Gamma^r = -d_s/d_r$$

The circulation ratio is thus related to the spacing ratio, and is equal to -1 for the stage under consideration.

It remains only to specify the coefficients A_n of the chordwise lift distribution on the rotor and stator blades, which are defined in Equation [34] and appear in the H-functions of Equation [33]. To investigate the effect of a variation in this lift distribution, two cases were considered:

(a) Lift distribution on both stator and rotor blades is the "elliptical" distribution $4VA_1 \sin \theta$ so that

$$A_n{}^r = A_n{}^s = 0, \quad n \neq 1$$

(b) Lift distribution on stator blades is elliptical as in case (a), but on the rotor blades it is "flat-plate"

$$\gamma^r = 2A_0{}^r \left(\frac{1 - \cos \theta}{\sin \theta}\right)$$

so that

$$A_n{}^r = 0, \quad n \geq 1$$

With the data just given, the quantity

$$(K_V/100)/{}_0C_L$$

was calculated for both rotor and stator blades from Equation [35b], using the energy expressions in Equations [23] and [29] and the quasi-steady circulation coefficients from Equations [31] and [32]. In order to reduce the numerical work for this estimate, only the first two terms in each of the summations were kept; i.e., the summation indexes m, p, and k took on the values 1, 2 only. The results are summarized in Table 1.

TABLE 1 RESULTS OF CALCULATIONS

	Case (a)	Case (b)
Stator wake: $(K_V{}^s/100)/{}_0C_L{}^s$	0.00017	0.0069
Rotor wake: $(K_V{}^r/100)/{}_0C_L{}^r$	0.0000042	0.000046

Discussion

In view of the fact that the steady-state lift coefficients of the blades will usually be somewhat less than 1, Table 1 shows that the power in the vortex wakes is a very small fraction of the power necessary to turn the rotor. Keller (1) obtained values of K_V between 0.004 and 0.010 for various configurations when he assumed the amplitude of the circulation fluctuation to be 10 per cent of the steady-state circulation. A calculation of this circulation ratio for the cases of Table 1 confirms[7] the fact that it is substantially less than 10 per cent except for the stator blades in Case (b), where the value obtained for K_V does, in fact, agree with Keller's values.

An interesting feature of the energy calculations is brought out by Table 1. The energy in the stator wake is about 100 times as large as that in the rotor wake. This is primarily a reflection of the fact that the stator nonsteady circulation is about 10 times that of the rotor. Since the energy is the product of induced velocity and wake strength, it varies as the square of the nonsteady circulation.

Actually, this large difference in circulation and energy is not dependent on the function of the blades as "rotor" or "stator" but on their relative position *upstream* and *downstream*. A blade will always have a considerably larger nonsteady circulation and energy loss induced by motion of the adjacent *downstream* row than by motion of the adjacent *upstream* row. The reason for this is seen in the importance of the velocity field at the *trailing* edge of a blade in determining the circulation. The formula for the circulation of a blade in a given upwash field (Munk's first integral formula) clearly shows the heavy weight given to the upwash at the trailing edge. Put another way, the circulation is determined by application of the Kutta condition at the trailing edge, so the upwash there is decisive in its determination. Applying this idea to a turbomachine stage, one sees that the circulation fluctuations induced by the downstream neighbor of a row will usually be larger than those induced by the row upstream. (In reference (2), however, it was found that the lift fluctuations induced by upstream and downstream neighboring rows are of about the same magnitude.)

Detailed consideration of the wake-energy calculations indicates the possibility of some approximations to simplify them. In the first place, the factor ψ_m is very close to unity for all the configurations studied here and in reference (2), and probably for all typical cascades, and can be put equal to 1. Since $\psi_m - 1$ represents the effect of the wakes of all other blades in a cascade on the velocity induced at the wake of a given blade, this means that only the velocity induced by its own wake need be considered.

Also, for upstream blades, the cross-induced energy is only a few per cent of the self-induced energy. Although this cross-induced energy may actually be negative, thus representing a recapture by the upstream blade of some of the energy lost by the downstream blade, it is so small as to be negligible and its calculation seems unnecessary.

For the downstream blades, however, the self-induced and cross-induced energies are of the same order. This is because of

[7] See reference (2), table 2, p. 597.

the large size of the upstream wakes relative to the downstream ones, as just discussed. Again, some of the cross-induced terms are negative, representing energy recapture. Therefore, in order to find the energy in the wakes of the downstream blades, it seems necessary to obtain both the self-induced and cross-induced energies.

In practical application to multistage machines, however, any typical blade row has both upstream and downstream neighbors; it seems justifiable to neglect the influence of the former entirely and to take the wake-energy transfer to be approximately equal to the self-induced component due to induction of the downstream row. Combining this conclusion with the approximation $\psi_m \approx 1$ suggested in the foregoing, one arrives at a greatly simplified procedure for the estimation of wake energy, viz.:

1 Determine the magnitude of circulation fluctuations due to the adjacent downstream blade row, e.g., by the approximate methods of reference (2). These data are most conveniently expressed by the Fourier coefficients C_m.

2 Calculate the wake energy by use of Equation [23] with $\psi_m = 1$. The resulting formula is recognized to be just the expression for wake energy of an isolated airfoil experiencing periodic circulation fluctuations. It is therefore a generalization of a formula given by Garrick (7) for the oscillating airfoil.

Conclusions

An evaluation has been made of the transfer of energy into kinetic energy of the vortex wakes in the case of unsteady two-dimensional flow in cascades of thin airfoils. In particular, the analysis has been applied to the elementary two-row stages treated in reference (2), where the unsteady effects due to aerodynamic interactions between the blade rows were calculated approximately.

The general conclusions of the investigation are as follows:

1 The magnitude of the energy transfer, in the numerical examples studied, is small, amounting to less than 1 per cent of the energy absorbed by the rotor.

2 The results of an earlier investigation by Keller (1) are generally verified. Keller's work concerned only a single row of blades and also left the magnitude of the circulation fluctuation undetermined.

3 For a two-row stage, the cross-induced energy transfer may be negative, but in the present example it is always very small. The energy transfer of the upstream row, moreover, is many times as great as that of the downstream row, because of the disparity of the magnitudes of the respective induced circulation fluctuations.

4 In view of item 3, it is suggested that in practical applications the wake-energy transfer for a typical row of a multistage machine be estimated by use of isolated-airfoil formulas, approximating to the circulation fluctuations by neglecting all induced effects except those resulting from the adjacent downstream blade row.

BIBLIOGRAPHY

1 "Energy Losses on High-Speed Turbo-Machines Resulting From Irregular Flow to the Runner Wheel," by C. Keller, Escher-Wyss News, March-April, 1935, p. 40. Also "Kinetic Energy Losses Behind Blade Grids as a Result of Periodic Variation in the Circulation," RTP Translation No. 1883, British MAP; translated from Mitteilung Nr. 2 aus dem Institut für Aerodynamik Eidgenössische Technische Hochschule, Zurich, Switzerland, 1934.

2 "Aerodynamic Interference Between Moving Blade Rows," by N. H. Kemp and W. R. Sears, *Journal of the Aeronautical Sciences*, vol. 20, September, 1953, pp. 585–597.

3 "Hydrodynamics," by H. Lamb, Cambridge University Press, Cambridge, England, 1932, p. 46; also Dover Publications, New York, N. Y., 1945.

4 "Airfoil Theory for Non-Uniform Motion," by Th. von Karman and W. R. Sears, *Journal of the Aeronautical Sciences*, vol. 5, August, 1938, pp. 379–390.

5 "On the Lift and Circulation of Airfoils in Some Unsteady-Flow Problems," by N. H. Kemp, *Journal of the Aeronautical Sciences*, vol. 19, October, 1952, pp. 713.

6 "Some Aspects of Non-Stationary Airfoil Theory and Its Practical Application," by W. R. Sears, *Journal of the Aeronautical Sciences*, vol. 8, January, 1941, pp. 104–108.

7 "Propulsion of a Flapping and Oscillating Airfoil," by I. E. Garrick, NACA Report 567, May, 1936.

8 "Nonsteady Aerodynamic Effects in Axial-Flow Turbomachines," by N. H. Kemp, PhD thesis, Cornell University, June, 1953.

A Suction Device Using Air Under Pressure

By L. F. WELANETZ,[1] SYOSSET, N. Y.

An analysis is made of the suction holding power of a device in which a fluid flows radially outward from a central hole between two parallel circular plates. The holding power and the fluid flow rate are determined as functions of the plate separation. The effect of changing the proportions of the device is investigated. Experiments were made to check the analysis.

Introduction

IT IS a popular trick to place the hole in a spool of thread above and close to a small piece of paper, then to blow gently through the spool. If the conditions are correct, the piece of paper will be attracted to, rather than repelled from, the end of the spool. This phenomenon results from the fact that the air, in flowing radially outward between the end of the spool and the paper, has a high velocity and a correspondingly low pressure, in fact, less than atmospheric. The purpose of this analysis is to investigate the characteristics of this device with the view that it may serve as a suction-restraining device when applied in new product designs. It is assumed that it would be used to hold a thin sheet or membrane in close proximity to a flat plane, but separated therefrom by a thin film of air.

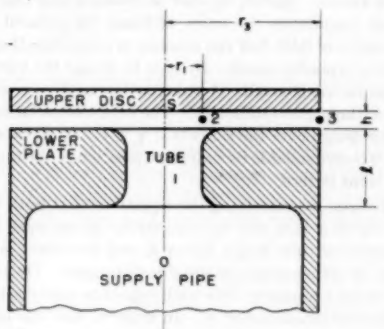

FIG. 1 SUCTION DEVICE

For purposes of analysis the device is assumed to have the form shown in Fig. 1. The air is assumed to flow from a reservoir at 0, where its velocity is practically zero and its pressure is p_0, through the circular tube to 1, from which point it flows radially outward between the plane end of the tube and the thin sheet or disk. At 3 the flow emerges into the atmosphere, at which point the pressure is the ambient pressure p_a. By using the general energy equation of steady flow and accounting for the various energy losses along the path, it is possible to derive the equations describing the characteristics of the device.

Development of the Flow Equations

As the fluid flows through the system it may suffer energy losses at different sections. In going from the reservoir 0 into the tube an entrance loss may occur. However, with a well-rounded entrance, this loss is negligibly small.[2] It will be assumed here that the entrance can be suitably rounded. In passing through the tube a pipe-friction loss is incurred. For turbulent flow this may be written in the form

$$E_{\text{pipe}} = \frac{flQ^2}{4\pi^2 r_1^5}$$

where

f = pipe-friction factor
l = length of tube
Q = volume rate of flow
r_1 = radius of tube

As will be seen later, much of the range of operation of the device would be in the turbulent region, in which case the pipe-friction factor is substantially constant and dependent upon the relative roughness of the tube.[3] For very rough pipes, $f = 0.06$. For small tubes this is a reasonable and conservative estimate.

The flow at entrance to a tube requires some appreciable length of tube to develop fully to that type which characterizes steady, uniform pipe flow.[4] Even for turbulent flow the minimum length is about 25 diam. For laminar flow it may be much greater. In the device under consideration it is desirable to make the tube as short as possible; for example, of length equal to tube radius. Under these conditions the foregoing estimates of pipe-energy loss may be greatly in error. It is believed that this is not serious because the loss is small in any case and, furthermore, it is probably less than estimated.

The possibility of energy loss at the point of transition from pipe flow to radially outward flow between the plates should be considered. For the smaller values of plate separation h, which will be seen later to be the more important condition, the flow is converging. The limiting value is

$$h = r_1/2$$

It is common experience[5] that losses in converging flow can generally be made low by careful shaping of the channel. In the case under consideration rounding of the exit edges of the tube provides a suitable channel shape. Therefore it is considered justifiable to neglect transition loss here.

The radially outward flow between the parallel plates is similar to one-dimensional flow between infinitely wide parallel plates. For friction-loss calculations the diameter of an equivalent pipe is taken as[6]

$$D_{\text{equiv}} = 4\,\frac{\text{cross-section area of flow}}{\text{wetted perimeter}}$$

$$= 4\,\frac{2\pi r h}{4\pi r} = 2h$$

[1] Chief Engineer, Plans and Analysis, Fairchild Camera and Instrument Corporation. Mem. ASME.

Contributed by the Applied Mechanics Division and presented at the Diamond Jubilee Annual Meeting, Chicago, Ill., November 13–18, 1955, of THE AMERICAN SOCIETY OF MECHANICAL ENGINEERS.

Discussion of this paper should be addressed to the Secretary, ASME, 29 West 39th Street, New York, N. Y., and will be accepted until July 10, 1956, for publication at a later date. Discussion received after the closing date will be returned.

NOTE: Statements and opinions advanced in papers are to be understood as individual expressions of their authors and not those of the Society. Manuscript received by the Applied Mechanics Division, June 26, 1955. Paper No. 55—A-38.

[2] "Hydraulics," by R. L. Dougherty, McGraw-Hill Book Company, Inc., New York, N. Y., 1937, p. 221.

[3] "Elementary Mechanics of Fluids," by Hunter Rouse, John Wiley & Sons, Inc., New York, N. Y., 1947, pp. 204, 205.

[4] Ibid., pp. 188, 189.

[5] Ibid., pp. 215, 216.

where

r = radius of any annular flow cross section
h = parallel-plate separation

Since the cross-section area of flow varies along the flow path, the energy-loss equation is expressed in incremental form as

$$\Delta E = \frac{f \Delta r Q^2}{16\pi^2 r^3 h^3}$$

where ΔE = energy loss occurring in the pipe length Δr.

By integration, the energy loss through the outer portion of radial distance between the plates is

$$_rE_2 = \frac{fQ^2}{16\pi^2 h^3}\left(\frac{1}{r} - \frac{1}{r_2}\right) \quad [1]$$

The total energy loss between the plates is

$$_2E_2 = \frac{fQ^2}{16\pi^2 h^3}\left(\frac{1}{r_1} - \frac{1}{r_2}\right) \quad [2]$$

Substitution of the energy-loss terms in the general energy equation for steady-flow results, by rearrangement, in the following equations which permit the determination of the pressure p at any radius r between the plates

$$\frac{p_a - p}{\rho} = \frac{Q^2}{8\pi^2 h^2}\left[\left(\frac{1}{r^2} - \frac{1}{r_2^2}\right) - \frac{f}{2h}\left(\frac{1}{r} - \frac{1}{r_2}\right)\right] \quad [3]$$

and

$$\frac{p_0 - p_a}{\rho} = \frac{Q^2}{8\pi^2 h^2}\left[\frac{1}{r_2^2} + \frac{2fl h^2}{r_1^5} + \frac{f}{2h}\left(\frac{1}{r_1} - \frac{1}{r_2}\right)\right] \quad [4]$$

from which

$$\frac{p_a - p}{p_0 - p_a} = \frac{\left(\frac{1}{r^2} - \frac{1}{r_2^2}\right) - \frac{f}{2h}\left(\frac{1}{r} - \frac{1}{r_2}\right)}{\frac{1}{r_2^2} + \frac{2fl h^2}{r_1^5} + \frac{f}{2h}\left(\frac{1}{r_1} - \frac{1}{r_2}\right)} \quad [5]$$

It has been assumed that the density ρ of the fluid is constant.

For the region $r_1 \leqslant r \leqslant r_2$ the total force is

$$P_1 = \int_{r_1}^{r_2} (p_a - p)\, 2\pi r dr \quad [6]$$

It is positive if it tends to force the disk against the end of the tube. For the region $0 \leqslant r \leqslant r_1$ the total force is that required to deflect the stream flow from an axial direction to radially outward. It is

$$P_2 = -\rho Q V_1 = -\frac{\rho Q^2}{\pi r_1^2} \quad [7]$$

where V_1 = velocity of the fluid in the tube 1.

Substituting Equation [5] in Equation [6], and Equation [4] in Equation [7] and adding the results gives the following equation for the total force on the disk

$$P = \frac{2\pi(p_0 - p_a)\left[\ln \frac{r_2}{r_1} - \frac{r_2^2 - r_1^2}{2r_2^2} - \frac{f}{2h}\left(r_2 - r_1 - \frac{r_2^2 - r_1^2}{2r_2}\right) - \frac{4h^2}{r_1^2}\right]}{\left[\frac{1}{r_2^2} + \frac{2fl h^2}{r_1^5} + \frac{f}{2h}\left(\frac{1}{r_1} - \frac{1}{r_2}\right)\right]} \quad [8]$$

This equation may be simplified by using the following dimensionless terms:

Total-force factor, $\psi = \dfrac{P}{\pi r_2^2 (p_0 - p_a)}$

Tube-radius factor, $\gamma = r_1/r_2$

Tube-length factor, $\lambda = l/r_2$

Plate-separation factor, $\eta = h/r_2$

The dimensionless equation is

$$\psi = -\frac{\eta(1 - \gamma^2 + \ln \gamma^2) + \frac{f}{2}(1 - \gamma)^2 + \frac{8\eta^3}{\gamma^2}}{\eta + \frac{2f\lambda\eta^3}{\gamma^4} + \frac{f}{2}\left(\frac{1 - \gamma}{\gamma}\right)} \quad [9]$$

Using Equation [4] a dimensionless equation may also be written for flow rate as

$$\chi = \frac{Q}{\pi r_2^2 \sqrt{(p_0 - p_a)/\rho}} = \sqrt{\frac{8\eta^3}{\eta + \frac{2f\lambda\eta^3}{\gamma^4} + \frac{f}{2}\left(\frac{1 - \gamma}{\gamma}\right)}} \quad [10]$$

Effect of Variation of Dimensions

The magnitude of the friction factor f can be controlled only to a limited extent; that is, by care in creating and maintaining smooth flow boundaries the value of f may be reduced below a maximum value of 0.06, but the amount of reduction that can be guaranteed is probably small. By care in design the tube-length factor λ can be made small. A value as low as $\lambda = 1$ should be attainable without great difficulty. The tube-radius factor γ may be varied by design over the range $0 < \gamma < 1$. The plate-separation factor η is controllable by fixing the position of the upper disk. The lower limit is zero.

It may be seen by examining the equations that both the total force and the flow rate will be reduced by an increase in either friction factor f or tube-length factor λ, and that there is no optimum value of either which is greater than zero. On the other hand, this is not necessarily true with regard to tube-radius factor γ and plate-separation factor η. In order to find the maximum value of total-force factor ψ it should be possible to differentiate ψ partially with respect to γ and also to η, equate the derivatives to zero, to solve the two resulting equations simultaneously for the values of γ and η at which the maximum occurs, and finally to obtain the maximum of ψ by substitution of these values in the original equation for ψ. However, the resulting equations are so unwieldy as to preclude the possibility of using the foregoing rational method of solution. Therefore the method was adopted of choosing series of arbitrary values for the four independent variables, calculating the corresponding values of ψ, and also of flow-rate factor χ, and plotting the results as a family of curves. These curves are shown in Figs. 2 and 3.

In Fig. 2 is plotted a family of curves of total-force factor ψ as a function of plate-separation factor η for various values of tube-radius factor γ, for a constant value of friction factor f and for a tube length l equal to its radius $r_1(\lambda = \gamma)$. It will be noted that for small values of plate-separation factor η, the total-force factor ψ is negative. This means that the total force acts in such a direction as to blow the upper disk away from the lower plate.

It is noted in passing also that for small values of total-force factor ψ the curves are nearly linear. Thus, if the upper disk is retained in its position by a resilient support or is freely floating, the conditions are favorable for the establishment of a natural

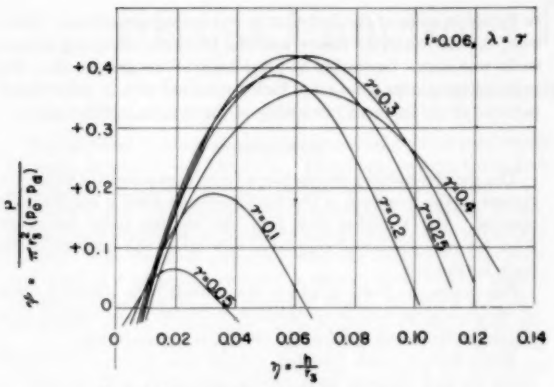

FIG. 2 SUCTION HOLDING-CHARACTERISTICS

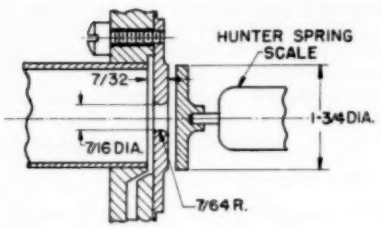

FIG. 4 TEST APPARATUS

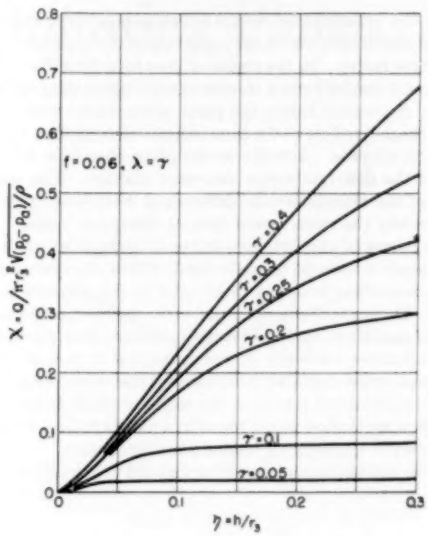

FIG. 3 FLOW-RATE CHARACTERISTICS

vibration condition subjected only to the viscous damping of the flowing fluid.

As the plate separation is increased, the total force tending to force the upper disk back against the lower plate increases to a maximum. For higher values of plate separation this force again decreases. The magnitude of the total-force factor ψ depends on the tube-radius factor γ, the maximum occurring between $\gamma = 0.25$ and 0.30.

EXPERIMENTAL VERIFICATION

In order to determine the accuracy of the derived results, apparatus was constructed and tests were run using air as the fluid. The orifice plate and disk were made as shown in Fig. 4. The pressure in the large pipe ($p_0 - p_a$) was measured by a corner tap as shown. The flow rate was measured by a thin-plate orifice. The force on the disk was measured by a Hunter spring scale. The plate separation was measured by the combination of a micrometer screw on the spring-scale support and the dial gage on the spring scale. The air flow was varied from 0.04 to 0.63 cfs. The plate separation was varied between zero and 1/8 in. The maximum pressure occurring in the large pipe was 1 psi at which time the plate separation was 0.004 in. and the flow rate was 0.10 cfs.

The results of several tests are shown in Fig. 5. This is a graph of total-force factor ψ versus flow-rate factor χ. The curve shown is for the derived function with $\gamma = 0.25$, $\lambda = \gamma$, and $f =$

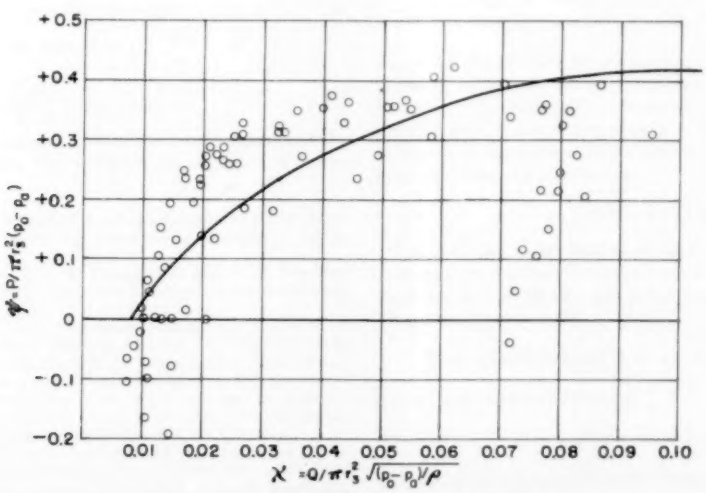

FIG. 5 CHARACTERISTICS DETERMINED BY TESTS

0.06. The experimental results follow generally the curve of the derived characteristics for the region up to the maximum value of total-force factor. In the region of zero total-force factor the experimental results have a steeper characteristic than the derived curve. Somewhat before the point of maximum total-force factor on the derived curve the tests indicate that the flow-rate factor ceases to increase. Actually as the plate separation is increased further the flow-rate factor decreases slightly. The maximum value of the experimentally determined total-force factor is approximately the same as the derived maximum value.

The failure of the flow-rate factor to increase as predicted by the analysis is believed to be the result of flow separation occurring at the transition from the small tube to the space between the plates. During the tests, operation in the region of, and beyond, the point of maximum total-force factor produced a high pitched sound. The calculated velocities at the transition area were subsonic. Flow separation may also be the cause of the steepness of the trend of the experimental results in the region of small flow-rate factor since flow separation would result in a narrower flow channel, and effectively it represents a smaller plate separation.

In the test apparatus the upper disk did not exhibit a tendency to flutter in spite of the fact that it was spring-supported. However, it was relatively heavy and the frictional damping apparently was high. Operation at plate separations greater than the point of maximum total-force factor required care in adjustment because of the inherent instability of the system in this region.

Conclusions

The suction-holding device has a force characteristic which increases as the flow rate of the fluid increases until a maximum is reached. For a higher flow rate the holding force decreases. Also, for very small and very large flow rates, the direction of the force is reversed.

For maximum holding power the central tube should have a diameter 0.25 to 0.30 times the disk diameter. The central tube should be short and well formed to reduce energy losses.

Tests with a short, rounded, central tube with diameter 0.25 times the disk diameter gave general agreement with the analysis for the smaller values of plate separation. The predicted maximum total-force factor was obtained. The predicted flow rates at large plate separations were not obtained, probably because of flow separation.

Stress Functions for Rotating Plates

By P. G. HODGE, JR.,[1] BROOKLYN, N. Y.

The general theory of two-dimensional bodies subjected to body forces is well known. However, except for a few examples in which gravity is the body force, and various examples of rotationally symmetric rotating disks, comparatively little appears to have been done with this theory. The present paper applies the theory to the general case of a thin plate rotating about an axis in its plane. As specific examples, a circular plate rotating about a diameter, and a triangular plate rotating about a side are considered. For the case of a long thin triangle, the result is shown to reduce to that previously obtained by using an extension of beam theory.

Basic Theory

LET us consider a thin plate of uniform thickness t rotating about an axis lying in its plane. Co-ordinates are chosen so that the y-axis is parallel to the axis of rotation and at a distance b from it, Fig. 1. We assume that the boundary of the plate can be represented by two continuous and piecewise continuously differentiable functions

$$y = h_1(x), \quad y = h_2(x)$$

where $h_1(x) \leq h_2(x)$. In particular, we rule out the possibility of a finite vertical boundary.

Assuming conditions of plane stress, the only stress components to be considered are σ_x, σ_y, and τ_{xy}. These must satisfy the equilibrium equations

$$\partial\sigma_x/\partial x + \partial\tau_{xy}/\partial y - \rho\omega^2(b - x) = 0$$

$$\partial\sigma_y/\partial y + \partial\tau_{xy}/\partial x = 0 \quad \ldots\ldots[1]$$

and the compatibility relation[2]

$$\nabla^2(\sigma_x + \sigma_y) = -(1 + \nu)\rho\omega^2 \quad \ldots\ldots[2]$$

In order to reduce Equations [1] and [2] to a single equation, we first define the body force potential V by

$$V = -\rho\omega^2(x^2/2 - bx) \quad \ldots\ldots[3]$$

A stress function φ is then defined by

$$\left.\begin{aligned} \sigma_x = \partial^2\varphi/\partial y^2 + V, \; \sigma_y = \partial^2\varphi/\partial x^2 + V \\ \tau_{xy} = -\partial^2\varphi/\partial x\partial y \end{aligned}\right\} \quad \ldots\ldots[4]$$

The substitution of Equations [4] into the equilibrium equations yields an identity, while the compatibility equation is transformed into

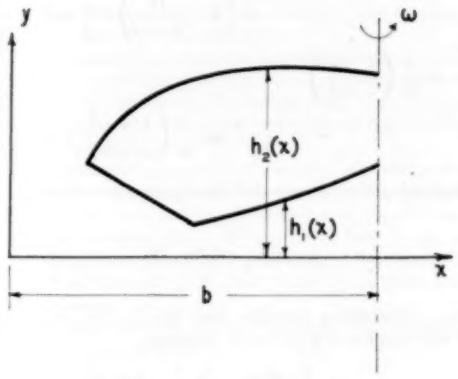

Fig. 1 Rotating Plate

$$\nabla^4\varphi = (1 - \nu)\rho\omega^2 \quad \ldots\ldots[5]$$

Along the edges of the plate no loads are applied so that the resulting normal and shear stresses must vanish. Thus, if α_1 and α_2 represent the inclinations of the bottom and top edges of the plate

$$N_k = \sigma_x \sin^2\alpha_k + \sigma_y \cos^2\alpha_k - 2\tau_{xy} \sin\alpha_k \cos\alpha_k = 0$$

$$T_k = (\sigma_x - \sigma_y) \sin\alpha_k \cos\alpha_k + \tau_{xy}(\sin^2\alpha_k - \cos^2\alpha_k) = 0, \; k = 1, 2$$

It is readily verified that these equations are equivalent to

$$\sigma_x \tan\alpha_k = \tau_{xy} = \sigma_y \cot\alpha_k$$

along the edge. Finally, since $\tan\alpha_k$ represents the slope, we may write the boundary conditions in the form

$$\left.\begin{aligned} \sigma_x h_1'(x) = \tau_{xy} = \sigma_y/h_1'(x) \text{ on } y = h_1(x) \\ \sigma_x h_2'(x) = \tau_{xy} = \sigma_y/h_2'(x) \text{ on } y = h_2(x) \end{aligned}\right\} \quad \ldots\ldots[6]$$

Therefore the solution of the problem is reduced to the determination of a solution of Equations [5] which satisfies the Boundary Conditions [6]. Since no boundary conditions are specified on the axis of the plate $x = b$, such a solution will be valid only in the sense of Saint Venant; i.e., at a reasonable distance from the axis of rotation.

Circular Plate

For a circular plate rotating about a diameter it is convenient to choose the y-axis as the axis of rotation, so that $b = 0$. Further, we may evidently use polar co-ordinates to advantage. Thus from Equation [3]

$$V = -(\rho\omega^2/2)r^2\cos^2\vartheta = -(\rho\omega^2/4)r^2(1 + \cos 2\vartheta)$$

Any stress function of the form

$$\varphi = [\rho\omega^2(1 - \nu)/64](\varphi_1 + r^4) \quad \ldots\ldots[7]$$

where φ_1 is biharmonic will satisfy Equations [5]. In terms of φ_1, the boundary conditions may be written

---

[1] Associate Professor of Applied Mechanics, Department of Aeronautical Engineering, Polytechnic Institute of Brooklyn. Mem. ASME.

[2] "Theory of Elasticity," by S. Timoshenko and J. N. Goodier, McGraw-Hill Book Company, Inc., New York, N. Y., second edition, 1951, section 16.

Contributed by the Applied Mechanics Division and presented at the Diamond Jubilee Annual Meeting, Chicago, Ill., November 13–18, 1955, of The American Society of Mechanical Engineers.

Discussion of this paper should be addressed to the Secretary, ASME, 29 West 39th Street, New York, N. Y., and will be accepted until July 10, 1956, for publication at a later date. Discussion received after the closing date will be returned.

Note: Statements and opinions advanced in papers are to be understood as individual expressions of their authors and not those of the Society. Manuscript received by ASME Applied Mechanics Division, January 24, 1955. Paper No. 55—A-5.

$$\left.\begin{aligned}
\text{on } r = a, \quad \sigma_r &= \frac{1}{r}\frac{\partial \varphi}{\partial r} + \frac{1}{r^2}\frac{\partial^2 \varphi}{\partial \vartheta^2} + V \\
&= -\frac{1-\nu}{64}\rho\omega^2\left[\frac{1}{r}\frac{\partial \varphi_1}{\partial r} + \frac{1}{r^2}\frac{\partial^2 \varphi_1}{\partial \vartheta^2} + \left(4 - \frac{16}{1-\nu}\right)r^2\right] = 0 \\
\tau_{r\vartheta} &= -\frac{\partial}{\partial r}\left(\frac{1}{r}\frac{\partial \varphi}{\partial \vartheta}\right) \\
&= -\frac{1-\nu}{64}\rho\omega^2\frac{\partial}{\partial r}\left(\frac{1}{r}\frac{\partial \varphi_1}{\partial \vartheta}\right) = 0
\end{aligned}\right\} \quad \ldots [8]$$

We may integrate the second of these equations on $r = a$ to obtain

$$\text{on } r = a, \quad \frac{\partial \varphi_1}{\partial r} = \frac{\varphi_1}{a} \quad \ldots [9a]$$

Further, substituting Equation [9a] into [8] we may integrate twice with respect to ϑ on $r = a$, obtaining

$$\text{on } r = a, \quad \varphi_1 = \left(\frac{16}{1-\nu} - 4\right)a^4 - \frac{16}{3}\frac{a^4}{1-\nu}\cos 2\vartheta \quad \ldots [9b]$$

In each case the constants of integration have been set equal to zero since they do not affect the stress components.

Any biharmonic function can be written as the real or imaginary part of a complex function

$$f(z) + \bar{z}g(z) \quad \ldots [10]$$

where f and g are analytic. Applying this to functions

$$f = z^n = r^n e^{in\vartheta} = r^n(\cos n\vartheta + i \sin n\vartheta)$$

$$\bar{z}g = \bar{z}z^{n+1} = r^{n+2}(\cos n\vartheta + i \sin n\vartheta)$$

we obtain four sets of solutions

$$r^n \cos n\vartheta, \quad r^n \sin n\vartheta, \quad r^{n+2}\cos n\vartheta, \quad r^{n+2}\sin n\vartheta$$

In view of the Boundary Conditions [9] we are led to a function of the form

$$\varphi_1 = A + Br + Cr^2 + (Dr^2 + Er^4)\cos 2\vartheta$$

The constants are easily evaluated from Equations [9] and the condition that the stresses be finite, and the resulting stress function is

$$\varphi_1 = \frac{1}{2}\left(\frac{16}{1-\nu} - 4\right)(a^4 + a^2r^2) + \frac{8}{3(1-\nu)}(r^4 - 3a^2r^2)\cos 2\vartheta$$

Finally, the stresses are then found to be

$$\left.\begin{aligned}
\sigma_r &= \rho\omega^2\left[\frac{1+\cos 2\vartheta}{4} - \frac{1-\nu}{16}\right](a^2 - r^2) \\
\sigma_\vartheta &= \rho\omega^2\left[\frac{1-\cos 2\vartheta}{4}(a^2 - r^2) + \frac{1-\nu}{16}(3r^2 - a^2)\right] \\
\tau_{r\vartheta} &= \frac{1}{4}\rho\omega^2(r^2 - a^2)\sin 2\vartheta
\end{aligned}\right\} \quad \ldots [11]$$

While Equations [11] were obtained only from the stress-boundary conditions on the outer edge of the plate, they also satisfy the boundary conditions on the axis. Owing to symmetry, these latter may be written

$$\text{at } \vartheta = \pi/2, \quad v = 0$$
$$\text{at } r = 0, \quad u \text{ and } v \text{ single valued}$$

where u and v represent the radial and tangential displacements, respectively. It is readily verified that the displacements

$$\left.\begin{aligned}
u &= \frac{\rho\omega^2}{E}\left[\left(\frac{3-2\nu-\nu^2}{16} + \frac{1+\nu}{4}\cos 2\vartheta\right)a^2r - \left(\frac{1-\nu^2}{16} + \frac{1+\nu}{12}\cos 2\vartheta\right)r^3\right] \\
v &= -\frac{\rho\omega^2(1+\nu)}{12E}(3a^2r - 2r^3)\sin 2\vartheta
\end{aligned}\right\} \quad \ldots [12]$$

satisfy these boundary conditions and are related to the stress components (Equations [11]) according to Hooke's law.[3] Therefore Equations [11] and [12] represent the complete solution for a circular plate rotating about a diameter.

Of some interest is the maximum speed at which the plate can rotate and still be wholly elastic. If the Mises yield criterion is adopted, then this will be the maximum speed for which

$$3J_2 = \sigma_r^2 - \sigma_r\sigma_\vartheta + \sigma_\vartheta^2 + 3\tau_{r\vartheta}^2 \leq Y^2 \quad \ldots [13]$$

everywhere in the plate. Here Y is the yield stress in simple tension. Without computing $3J_2$ in full detail, it is evident that the resulting expression will be a quadratic in r^2. Collecting only the coefficient of $(r^2)^2$, we obtain

$$(\rho^2\omega^2/256)[64 + 8(1-\nu)(3\cos 2\vartheta - 2) + 7(1-\nu)^2]$$

Evidently this term is positive for all real ϑ; hence $3J_2$ may be represented as a function of r^2 by a parabola which is convex upward. Therefore the maximum value of $3J_2$ will occur at one of the end points of the interval, $r^2 = a^2$ or $r^2 = 0$. Each of these extreme values turns out to be independent of θ, and the latter is readily verified to be the larger. Therefore Inequality [13] will be satisfied everywhere if and only if

$$3J_2(0, \vartheta) = (\rho^2\omega^4a^4/256)[64 - 8(1-\nu) + (1-\nu)^2] \leq Y^2$$

Finally, then, the maximum speed for fully elastic behavior is given by

$$\omega_m\sqrt{\frac{\overline{\rho a^2}}{Y}} = 4[64 - 8(1-\nu) + (1-\nu)^2]^{-1/4} \quad [14]$$

Triangular Plate

As a second example we consider a triangular plate rotating about one of its sides, Fig. 2. In this case it is convenient to take the origin at the opposing vertex. The two sides are then given by

$$h_1(x) = Sx, \; h_2(x) = Tx \quad \ldots [15]$$

where $S = \tan \alpha_1$, $T = \tan \alpha_2$.

We choose a stress function of the form

$$\varphi = [\rho\omega^2(1-\nu)/24](\varphi_1 + y^4) \quad \ldots [16]$$

where φ_1 is biharmonic, in order to satisfy Equation [5]. We seek a polynomial solution, and it is easily shown that all boundary conditions on polynomials higher than the sixth degree are homogeneous and hence such terms are excluded. The most general polynomial of the fifth degree is obtained from taking the real and imaginary parts of the functions z^n, $\bar{z}\,z^{n-1}$, $n = 2, 3, 4, 5$. The resulting function may be written

[3] Footnote 2, chapter 4.

$$\varphi_1 = A(x^4 - 6x^2y^2 + y^4) + B(x^4 - y^4) + Cx^3y + Dxy^3 + Ex^3 + Fx^2y + Gxy^2 + Hy^3 + Ix^2 + Jxy + Ky^2 \quad \ldots\ldots [17]$$

The stress components are now easily computed from Equations [16] and [4] and the arbitrary constants determined from Equations [15] and [6].

Since the resulting expressions become algebraically complicated we shall here limit ourselves to a right triangular plate rotating about one side. Then $S = 0$ and the boundary conditions become

$$\left.\begin{array}{l} \text{on } y = 0, \quad \sigma_y = \tau_{xy} = 0 \\ \text{on } y = Tx, \quad T\sigma_x = \tau_{xy} = \sigma_y/T \end{array}\right\} \quad \ldots\ldots [18]$$

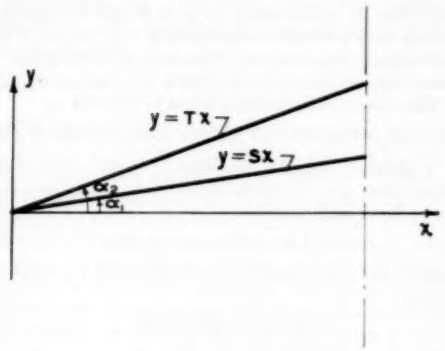

FIG. 2 TRIANGULAR PLATE

When Equations [18] are used to evaluate the constants in Equation [17] the resulting stress components are found to be

$$\left.\begin{array}{l} \sigma_x = \dfrac{\rho\omega^2}{4T(3+T^2)}\,[-(7+2T^2+\nu T^2)Tx^2 \\ \quad + 6(1+\nu T^2)xy + 2T(1-3\nu)y^2 - 4b(3+T^2)(y-Tx)] \\ \tau_{xy} = \dfrac{\rho\omega^2}{4T}\,\dfrac{1+\nu T^2}{3+T^2}\,(2Txy - 3y^2) \\ \sigma_y = -\dfrac{\rho\omega^2}{4}\,\dfrac{1+\nu T^2}{3+T^2}\,y^2 \end{array}\right\} \quad [19]$$

Here again it is desirable to find the maximum elastic speed. In general, this would involve finding the maximum value of J_2 which is of the fourth degree in x and y. However, at least when $T < \sqrt{2}$, it can be shown as indicated in the Appendix that the maximum value of J_2 occurs on the bottom edge, $y = 0$. Since σ_x is then the only nonvanishing stress component, Equation [13] reduces to

$$\sigma_x \leq Y$$

Setting $y = 0$ in the first Equation [19] and evaluating the relative maximum as a function of x we find

$$(\sigma_x)_{\max} = \rho\omega^2 b^2\,\frac{3+T^2}{7+(2+\nu)T^2}$$

Therefore the maximum allowable elastic speed is given by

$$\omega_m \sqrt{\frac{\rho b^2}{Y}} = \sqrt{\frac{7+(2+\nu)T^2}{3+T^2}} \quad \ldots\ldots [20]$$

COMPARISON WITH BEAM THEORY

In a previous paper[4] the problem of a long rotating triangular plate (T small) was solved by an extension of simple beam theory. There it was assumed that plane sections normal to the bottom edge of the plate remained plane and normal to the deformed bottom edge. We can now use the present theory to assess the limits of the validity of that assumption.

We first observe that normals to the bottom edge must remain normal for all small elastic deformations. Indeed, since one of the boundary conditions is zero shearing stress along the bottom edge, it follows from Hooke's law that the shear strain is zero and right angles remain right.

To investigate the assumption of planarity, we must first compute the displacement from Hooke's law.[5] In this example we cannot satisfy the boundary condition that $u = 0$ on the axis $y = b$, so that the solution given by Equations [19] is not exact. However, Equations [19] are still a solution in the sense of Saint Venant and will become increasingly close to the exact solution away from the axis.

For definiteness we have assumed that the boundary conditions against rigid body motion are

$$u(b, 0) = v(b, 0) = \partial u/\partial y(b, 0) = 0 \quad \ldots\ldots [21]$$

Further, we have taken Poisson's ratio to be $1/2$ since this leads to particularly simple expressions. The resulting displacements are

$$\left.\begin{array}{l} u = (\rho\omega^2/36ET)[-7Tx^3 + 9x^2y + Txy^2 - 7y^3 \\ \quad + 18bTx^2 - 36bxy + 6bTy^2 + 27b^2y - 11Tb^2] \\ v = (\rho\omega^2/36ET)[-3x^2 + 7Tx^2y - 3xy^2 - Ty^3 \\ \quad + 18bx^2 - 12bTxy + 6by^2 - 27b^2x + 12b^2] \end{array}\right\} \quad [22]$$

Within the limits of small strain theory the deformation from plane of an originally vertical element will depend only upon the horizontal displacement u. The section would remain plane only if u were linear in y; hence the nonlinear y-terms are a measure of the variation from a plane. To obtain a definite measure, let us compare the displacements at the top surface, $y = Tx$. From the first Equation [22] the exact top surface displacement is

$$u_E = (\rho\omega^2/36E)(x-b)(2x^2 - 16bx + 11b^2 - 6T^2x^2) \quad [23a]$$

On the other hand, if terms in y^2 and y^3 are neglected, the approximate top surface displacement is

$$u_A = (\rho\omega^2/36E)(x-b)(2x^2 - 16bx + 11b^2) \quad [23b]$$

It follows that the error depends only upon the last term in Equation [23a] and becomes vanishingly small for sufficiently small T.

A convenient dimensionless measure of the error is obtained by dividing the error by the displacement at the tip. Thus we define

$$\chi = \left|\frac{u_E - u_A}{u(0,0)}\right| = (6/11)T^2(x/b)^2(1 - x/b) \quad \ldots\ldots [24]$$

The maximum value of this function occurs at $x = (2/3)b$ and is given by

$$\chi_{\max} = 24T^2/297 \quad \ldots\ldots [25]$$

Therefore, even for $T = 1$ the error is less than 10 per cent while for $T = 1/3$ it is less than 1 per cent.

---

[4] "Stress Distributions in Nonsymmetric Rotating Rays," by P. G. Hodge, Jr., JOURNAL OF APPLIED MECHANICS, Trans. ASME, vol. 77, 1955, pp. 311–316.

[5] Footnote 2, chapter 3.

If the maximum elastic speed is desired, the results of the beam-theory approach are even more applicable. From footnote 4, the maximum elastic speed is given by

$$\omega_m' \sqrt{\rho b^2/Y} = \sqrt{7/3} \quad \ldots\ldots [26]$$

Comparison with Equation [20] shows that for $\nu = 1/3$ the approximate solution is exact for all T for which Equation [20] is valid. If we consider a range of Poisson's ratio, then even for $T = 1$ the error is less than 2 per cent for $\nu = 0$ and less than 1 per cent for $\nu = 1/2$. Therefore the beam-theory approach used[4] appears to have considerable merit even for plates with considerable slope.

Appendix

The proof that the maximum value of J_2 occurs on the bottom edge of the plate for $T^2 < 2$ is carried out by first showing that $\partial J_2/\partial y$ is negative on the bottom edge and positive on the top edge for all $0 < x < b$. It follows that the maximum value of J_2 must certainly occur on an edge unless J_2 has two relative minima and a relative maximum in $0 < y < Tx$; i.e., at least three extrema. A necessary condition that this be so is that $\partial^3 J_2/\partial y^3 = 0$ has a root in the interior. However, we can show that $\partial^3 J_2/\partial y^3$ is always negative and hence the maximum occurs on the boundary.

For simplicity we consider only the value $\nu = 1/3$, although the method is general. Further, we make a change of variable defined by

$$y = Tpx \quad \ldots\ldots [27]$$

The bottom surface is then given by $p = 0$ and the top surface by $p = 1$, so that the remarks of the preceding paragraph apply with y replaced by p. It then follows from Equation [19] that the stress components are

$$\left.\begin{aligned} \sigma_x &= (\rho\omega^2/12)[(-7 + 6p)x^2 + 12b(1 - p)x] \\ \sigma_y &= (\rho\omega^2/12)[-p^2T^2x^2] \\ \tau_{xy} &= (\rho\omega^2/12)[pT(2 - 3p)x^2] \end{aligned}\right\} \quad \ldots [28]$$

Since $J_2 = (1/3)(\sigma_x^2 - \sigma_x\sigma_y + \sigma_y^2 + 3\tau_{xy}^2)$

$$\frac{\partial J_2}{\partial p} = \frac{1}{3}\left[(2\sigma_x - \sigma_y)\frac{\partial \sigma_x}{\partial p} + (2\sigma_y - \sigma_x)\frac{\partial \sigma_y}{\partial p} + 6\tau_{xy}\frac{\partial \tau_{xy}}{\partial p}\right]$$

On $p = 0$ it is readily verified that

$$(\partial J_2/\partial p) = -(\rho^2\omega^4x^2/36)(12b - 7x)(2b - x)$$

which is obviously less than zero for all $0 < x < b$. Similarly, on $p = 1$

$$(\partial J_2/\partial p) = (\rho^2\omega^4x^3/108)[(-3 + 7T^2 + T^4)x + 3(2 - T^2)b]$$

The sign of this function will depend upon the sign of the linear function in brackets. This in turn is positive at $x = b$ for all T, and positive at $x = 0$ for $T^2 < 2$. Therefore, for $T^2 < 2$, $\partial J_2/\partial p$ is positive on the top edge.

Next, since J_2 is decreasing at $p = 0$ and increasing at $p = 1$, J_2 can have a relative maximum in $0 < p < 1$ only if $\partial J_2/\partial p$ has three roots in that interval. This, in turn, implies that $\partial^2 J_2/\partial p^2$ change sign at least twice and hence $\partial^3 J_2/\partial p^3$ has at least one root. This last quantity is easily found to be given by

$$\partial^3 J_2/\partial p^3 = (\rho^2\omega^4T^2x^3/36)[(2T^2 - 54)px - (15x + 6b)]$$

which is certainly negative provided $T^2 < 27$. Therefore the maximum value of J_2 occurs on either the top or bottom edge.

On $p = 0$, we easily find

$$J_2 = (\rho^2\omega^4/432)(-7x^2 + 12bx)^2$$

The maximum value is readily found to occur at $x = 6b/7$ and to be given by

$$(J_2)_{m1} = 3\rho^2\omega^4b^4/49 \quad \ldots\ldots [29]$$

On $p = 1$, we obtain

$$J_2 = (\rho^2\omega^4/432)x^4(1 + T^2)^2$$

This function increases with x; hence its maximum occurs at $x = b$

$$(J_2)_{m2} = (1 + T^2)^2\rho^2\omega^4b^4/432$$

Evidently $(J_2)_{m2}$ is less than $(J_2)_{m1}$ provided only that $T^2 < 29/7$. Therefore, for $\nu = 1/3$, the maximum value occurs at $(6b/7, 0)$ and is given by Equation [29].

High-Frequency Extensional Vibrations of Plates[1]

By T. R. KANE[2] and R. D. MINDLIN[3]

The equations of generalized plane stress are applicable to the extensional vibrations of plates only for the low modes of motion of thin plates. In this paper equations are derived which are applicable to both low and high modes of thin plates and to low modes of thick plates. As an example, the equations are solved for the case of axially symmetric vibrations of a circular disk and comparisons are made with the theory of generalized plane stress and with experiments.

1 Introduction

EXTENSIONAL vibrations of thin plates are described satisfactorily by the equations of generalized plane stress provided the wave lengths, or distances between nodes, are large in comparison with the thickness of the plate. In terms of frequencies, that is to say that the theory of generalized plane stress gives good results for frequencies which are much lower than the frequency of the first mode of thickness vibration of the plate. The essential reason for the limitation of the equations of generalized plane stress is the absence, in them, of the phenomenon of coupling between extensional and thickness modes of motion.

Consider, for example, the radial vibrations of a circular disk. As the radius of the disk diminishes, the frequency of the fundamental mode of vibration increases without limit, according to the equations of generalized plane stress. This is illustrated by Curve I in Fig. 1. However, it is apparent that, in a disk whose diameter is considerably smaller than its thickness (i.e., a rod) there must be a mode of, essentially, thickness vibration whose frequency is much lower than that of the radial vibration. In a real disk, the coupling between the thickness and radial vibrations affects both the mode shapes and the frequencies to a very marked degree even at frequencies well below the fundamental frequency of thickness vibration.

It is the purpose of this paper to describe the derivation of a set of differential equations and boundary conditions which take into account coupling between extensional motions and the first mode of thickness vibration and to give the solution for the axially symmetric vibrations of a circular disk as an illustrative example, followed by a comparison with experimental measurements. The scheme adopted for the derivation of the equations is intended to exhibit the nature of the approximations by which

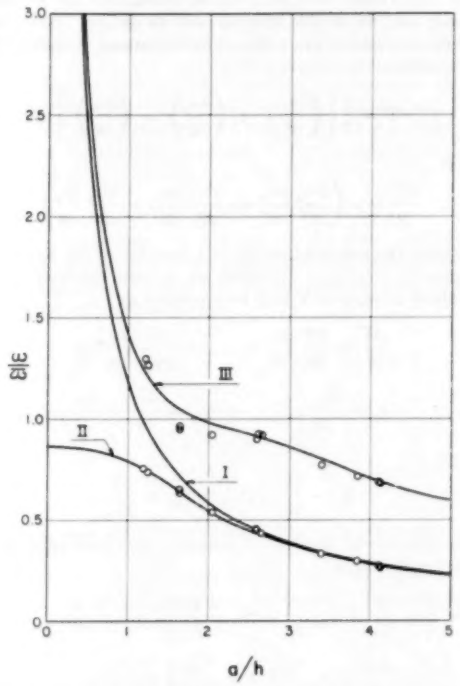

Fig. 1 Curves II and III Show Frequencies of First Two Modes of Axially Symmetric, Extensional Vibrations of Circular Disk According to Equations of This Paper
(Circled points are from experimental data obtained with barium-titanate disks at Bell Telephone Laboratories. Curve I shows frequencies of first mode according to theory of generalized plane stress.)

the three-dimensional theory is reduced to a two-dimensional one without carrying the reduction so far as to arrive at the theory of generalized plane stress. An alternative course is to start with the equations of generalized plane stress and add correction terms, as was done by E. Reissner (1)[4] in a related investigation aimed at obtaining improved expressions for the variation of stress through the thickness of the plate. The equations derived in the present paper are not applicable to that problem.

2 Three-Dimensional Equations

It is useful to review a derivation of a few of the classical equations of the linear theory of elasticity, arranged in such a manner as to serve as a guide in the derivation of the plate equations.

The law of conservation of energy (considering only mechanical effects) states that the rate of increase of energy in a body is equal to the rate at which work is done by the external forces. Thus, omitting body forces

[1] This investigation was supported by the Office of Naval Research, the Signal Corps Engineering Laboratories, and Bell Telephone Laboratories, Inc.

[2] Assistant Professor of Mechanical Engineering, University of Pennsylvania, Philadelphia, Pa. Assoc. Mem. ASME.

[3] Professor of Civil Engineering, Columbia University, New York, N. Y. Mem. ASME.

Contributed by the Applied Mechanics Division and presented at the Diamond Jubilee Annual Meeting, Chicago, Ill., November 13–18, 1955, of The American Society of Mechanical Engineers.

Discussion of this paper should be addressed to the Secretary, ASME, 29 West 39th Street, New York, N. Y., and will be accepted until July 10, 1956, for publication at a later date. Discussion received after the closing date will be returned.

Note: Statements and opinions advanced in papers are to be understood as individual expressions of their authors and not those of the Society. Manuscript received by ASME Applied Mechanics Division, April 8, 1955. Paper No. 55—A-50.

[4] Numbers in parentheses refer to the Bibliography at the end of the paper.

$$\iiint \left(\frac{\partial T}{\partial t} + \frac{\partial V}{\partial t}\right) dxdydz = \iint \left(\bar{X}\frac{\partial u_x}{\partial t} + \bar{Y}\frac{\partial u_y}{\partial t} + \bar{Z}\frac{\partial u_z}{\partial t}\right) dS \quad [1]$$

where T and V are the kinetic and potential energy-densities, respectively, and $\bar{X}$, $\bar{Y}$, $\bar{Z}$ (2) and u_x, u_y, u_z are the rectangular components of the surface traction and displacement, respectively. The triple integral is taken throughout the volume of the body and the double integral over its surface. Note that if the time derivatives are replaced by variations, Equation [1] is the variational equation of motion.[5]

Now $$T = \frac{\rho}{2}\left[\left(\frac{\partial u_x}{\partial t}\right)^2 + \left(\frac{\partial u_y}{\partial t}\right)^2 + \left(\frac{\partial u_z}{\partial t}\right)^2\right] \quad [2]$$

so that

$$\frac{\partial T}{\partial t} = \rho\left(\frac{\partial^2 u_x}{\partial t^2}\frac{\partial u_x}{\partial t} + \frac{\partial^2 u_y}{\partial t^2}\frac{\partial u_y}{\partial t} + \frac{\partial^2 u_z}{\partial t^2}\frac{\partial u_z}{\partial t}\right) \quad [3]$$

Also, since the potential energy is a function of the components of strain (ϵ_x, . . ., γ_{yz}, . . .) which are, in turn, functions of time, the rate of increase of V may be expressed as

$$\frac{\partial V}{\partial t} = \frac{\partial V}{\partial \epsilon_x}\frac{\partial \epsilon_x}{\partial t} + \ldots + \frac{\partial V}{\partial \gamma_{yz}}\frac{\partial \gamma_{yz}}{\partial t} + \ldots \quad [4]$$

Now $$\epsilon_x = \frac{\partial u_x}{\partial x}, \ldots, \qquad \gamma_{yz} = \frac{\partial u_z}{\partial y} + \frac{\partial u_y}{\partial z}, \ldots \quad [5]$$

and (3)

$$\sigma_x = \frac{\partial V}{\partial \epsilon_x}, \ldots, \qquad \tau_{yz} = \frac{\partial V}{\partial \gamma_{yz}}, \ldots \quad [6]$$

Hence the rate of increase of potential energy-density may be written in the form

$$\left.\begin{aligned}\frac{\partial V}{\partial t} &= \left(\sigma_x\frac{\partial}{\partial x} + \tau_{yz}\frac{\partial}{\partial y} + \tau_{zz}\frac{\partial}{\partial z}\right)\frac{\partial u_x}{\partial t} + \ldots + \ldots \\ &= \frac{\partial}{\partial x}\left(\sigma_x\frac{\partial u_x}{\partial t} + \tau_{yz}\frac{\partial u_y}{\partial t} + \tau_{zz}\frac{\partial u_z}{\partial t}\right) + \ldots + \ldots \\ &\quad - \left(\frac{\partial \sigma_x}{\partial x} + \frac{\partial \tau_{yz}}{\partial y} + \frac{\partial \tau_{zz}}{\partial z}\right)\frac{\partial u_x}{\partial t} - \ldots - \ldots\end{aligned}\right\} \quad [7]$$

By integration by parts

$$\iiint\left[\frac{\partial}{\partial x}\left(\sigma_x\frac{\partial u_x}{\partial t} + \tau_{yx}\frac{\partial u_y}{\partial t} + \tau_{zx}\frac{\partial u_z}{\partial t}\right) + \ldots\right] dxdydz$$
$$= \iint\left[(\sigma_x l + \tau_{xy}m + \tau_{xz}n)\frac{\partial u_x}{\partial t} + \ldots + \ldots\right] dS$$
$$= \iint\left(\bar{X}\frac{\partial u_x}{\partial t} + \bar{Y}\frac{\partial u_y}{\partial t} + \bar{Z}\frac{\partial u_z}{\partial t}\right) dS$$

where l, m, n are the direction cosines of the outward drawn normal to S. Hence, substituting Equations [3] and [7] in [1], the law of conservation of energy reduces to

$$\iiint\left[\left(\frac{\partial \sigma_x}{\partial x} + \frac{\partial \tau_{yx}}{\partial y} + \frac{\partial \tau_{zx}}{\partial z} - \rho\frac{\partial^2 u_x}{\partial t^2}\right)\frac{\partial u_x}{\partial t} + \ldots + \ldots\right] dxdydz = 0 \quad [8]$$

Since this must hold for all volumes, the integrand must vanish, and, since the integrand must vanish for all velocities, the quantities in parentheses must vanish. This leads to three stress equations of motion of the type

$$\frac{\partial \sigma_x}{\partial x} + \frac{\partial \tau_{yx}}{\partial y} + \frac{\partial \tau_{zx}}{\partial z} = \rho\frac{\partial^2 u_x}{\partial t^2} \quad [9]$$

In an isotropic elastic body (3)

$$2V = \lambda(\epsilon_x + \epsilon_y + \epsilon_z)^2 + 2G(\epsilon_x^2 + \epsilon_y^2 + \epsilon_z^2) + G(\gamma_{yz}^2 + \gamma_{zx}^2 + \gamma_{xy}^2) \quad [10]$$

where λ and G are Lamé's constants of elasticity. Hence the stress-strain relation, from Equations [6] and [10], is

$$\left.\begin{aligned}\sigma_x &= (\lambda + 2G)\epsilon_x + \lambda(\epsilon_y + \epsilon_z) \\ \sigma_y &= (\lambda + 2G)\epsilon_y + \lambda(\epsilon_z + \epsilon_x) \\ \sigma_z &= (\lambda + 2G)\epsilon_z + \lambda(\epsilon_x + \epsilon_y) \\ (\tau_{yz}, \tau_{zx}, \tau_{xy}) &= G(\gamma_{yz}, \gamma_{zx}, \gamma_{xy})\end{aligned}\right\} \quad [11]$$

Substituting these in Equation [9] and using Equations [5], there result the displacement equations of motion

$$\left.\begin{aligned}G\nabla^2 u_x + (\lambda + G)\frac{\partial e}{\partial x} &= \rho\frac{\partial^2 u_x}{\partial t^2} \\ G\nabla^2 u_y + (\lambda + G)\frac{\partial e}{\partial y} &= \rho\frac{\partial^2 u_y}{\partial t^2} \\ G\nabla^2 u_z + (\lambda + G)\frac{\partial e}{\partial z} &= \rho\frac{\partial^2 u_z}{\partial t^2}\end{aligned}\right\} \quad [12]$$

where $$e = \frac{\partial u_x}{\partial x} + \frac{\partial u_y}{\partial y} + \frac{\partial u_z}{\partial z}$$

Boundary conditions appropriate to these equations of motion are obtained from Neumann's uniqueness theorem (4). By this theorem it is shown that, subject to the usual restrictions as to continuity, single valuedness, singularities and behavior at infinity, it is sufficient to specify, at each point of the boundary, one member of each of the three products appearing in the integrand of

$$\iint\left(\bar{X}\frac{\partial u_x}{\partial t} + \bar{Y}\frac{\partial u_y}{\partial t} + \bar{Z}\frac{\partial u_z}{\partial t}\right) dS \quad [13]$$

or their equivalents referred to co-ordinates normal and tangential to the surface.

3 Plate-Stress Equations of Motion

Consider a plate bounded by planes $z = \pm h$ and a right cylindrical surface intersecting the middle plane in a closed curve C. The components of displacement in the plate are assumed to be given to sufficient approximation by

$$\left.\begin{aligned}u_x &= v_x(x, y, t) \\ u_y &= v_y(x, y, t) \\ u_z &= zh^{-1}v_z(x, y, t)\end{aligned}\right\} \quad [14]$$

These expressions are substituted into Equations [8], which are integrated with respect to z between limits $\pm h$. The integrations are carried out explicitly wherever possible. Then, following the procedure leading from Equations [8] to [9], there result the plate-stress equations of motion

$$\left.\begin{aligned}\frac{\partial N_x}{\partial x} + \frac{\partial N_{xy}}{\partial y} + F_x &= 2\rho h\frac{\partial^2 v_x}{\partial t^2} \\ \frac{\partial N_{xy}}{\partial x} + \frac{\partial N_y}{\partial y} + F_y &= 2\rho h\frac{\partial^2 v_y}{\partial t^2} \\ \frac{\partial R_x}{\partial x} + \frac{\partial R_y}{\partial y} - N_z + hF_z &= \frac{2}{3}\rho h^3\frac{\partial^2 v_z}{\partial t^2}\end{aligned}\right\} \quad [15]$$

[5] See reference (4), p. 167.

where

$$(N_x, N_y, N_s, N_{xy}) = \int_{-h}^{h} (\sigma_x, \sigma_y, \sigma_s, \tau_{xy})dz \quad \ldots\ldots [16]$$

$$(R_x, R_y) = \int_{-h}^{h} (\tau_{xz}, \tau_{xy})zdz \quad \ldots\ldots [17]$$

$$(F_x, F_y, F_z) = [\tau_{xz}, \tau_{xy}, \sigma_z]_{z=h} - [\tau_{xz}, \tau_{xy}, -\sigma_z]_{z=-h} \quad \ldots [18]$$

N_x, N_y, and N_{xy} are the usual forces per unit of length which appear in the elementary theory of plates acted upon by forces in the middle plane (5). N_s is $2h$ times the average transverse stress. R_x and R_y are components of "pinching" shear. They play a role, in the last of Equations [15], analogous to that of the components of transverse shear force, Q_x and Q_y, in the corresponding equation of the theory of flexure of plates (6). F_x, F_y, and F_z are the components of surface traction. They play the role in Equations [15] that is played by body forces in the three-dimensional theory.

The first two of Equations [15] are identical with those of the theory of generalized plane stress, but none of the terms of the third equation appears in that theory.

4 Plate-Displacement Equations of Motion

The relations between the plate-stresses (N_x, N_y, N_s, N_{xy}, R_x, R_y) and the plate-displacements (v_x, v_y, v_z) are obtained, as in the three-dimensional theory, from the potential energy-density V. In order to improve the results, the thickness strain, ϵ_z, in Equation [10] is replaced by $\kappa\epsilon_z$ where κ is a constant which plays a role analogous to that of the square root of the constant k' in Timoshenko's theory of beams (7). Thus

$$2V = \lambda(\epsilon_x + \epsilon_y + \kappa\epsilon_z)^2 + 2G(\epsilon_x^2 + \epsilon_y^2 + \kappa^2\epsilon_z^2) + G(\gamma_{yz}^2 + \gamma_{xz}^2 + \gamma_{xy}^2) \quad \ldots [19]$$

The motivation for the introduction of κ, with the concomitant, fictitious anisotropy, is discussed in Section 7.

Using Equations [19] and [6], there results

$$\left.\begin{aligned} \sigma_x &= (\lambda + 2G)\epsilon_x + \lambda(\epsilon_y + \kappa\epsilon_z) \\ \sigma_y &= (\lambda + 2G)\epsilon_y + \lambda(\epsilon_x + \kappa\epsilon_z) \\ \sigma_z &= (\lambda + 2G)\kappa^2\epsilon_z + \lambda\kappa(\epsilon_x + \epsilon_y) \\ (\tau_{yz}, \tau_{xz}, \tau_{xy}) &= G(\gamma_{yz}, \gamma_{xz}, \gamma_{xy}) \end{aligned}\right\} \quad \ldots\ldots [20]$$

The Expressions [5] for the strains in terms of the displacements are now inserted in Equations [20], following which the Approximations [14] are used to replace the displacements u_x, u_y, u_z. The resulting expressions for the stresses in terms of v_x, v_y, v_z are inserted in the right-hand sides of Equations [16] and [17] and the integrations are performed, with the results

$$\left.\begin{aligned} N_x &= 2h\left[(\lambda + 2G)\frac{\partial v_x}{\partial x} + \lambda\frac{\partial v_y}{\partial y} + \kappa\lambda\frac{v_z}{h}\right] \\ N_y &= 2h\left[(\lambda + 2G)\frac{\partial v_y}{\partial y} + \lambda\frac{\partial v_x}{\partial x} + \kappa\lambda\frac{v_z}{h}\right] \\ N_s &= 2h\left[\kappa^2(\lambda + 2G)\frac{v_z}{h} + \kappa\lambda\left(\frac{\partial v_x}{\partial x} + \frac{\partial v_y}{\partial y}\right)\right] \\ N_{xy} &= 2hG\left(\frac{\partial v_y}{\partial x} + \frac{\partial v_x}{\partial y}\right) \\ R_x &= \frac{2h^3G}{3}\frac{\partial v_z}{\partial x}, \qquad R_y = \frac{2h^3G}{3}\frac{\partial v_z}{\partial y} \end{aligned}\right\} \quad \ldots [21]$$

The displacement equations of motion are now obtained by substituting Equations [21] into [15], with the result

$$\left.\begin{aligned} G\nabla_1^2 v_x + (\lambda + G)\frac{\partial e_1}{\partial x} + \frac{\kappa\lambda}{h}\frac{\partial v_z}{\partial x} + \frac{F_x}{2h} &= \rho\frac{\partial^2 v_x}{\partial t^2} \\ G\nabla_1^2 v_y + (\lambda + G)\frac{\partial e_1}{\partial y} + \frac{\kappa\lambda}{h}\frac{\partial v_z}{\partial y} + \frac{F_y}{2h} &= \rho\frac{\partial^2 v_y}{\partial t^2} \\ G\nabla_1^2 v_z - \frac{3\kappa\lambda e_1}{h} - \frac{3\kappa^2}{h^2}(\lambda + 2G)v_z + \frac{3F_z}{2h} &= \rho\frac{\partial^2 v_z}{\partial t^2} \end{aligned}\right\} \quad \ldots [22]$$

where

$$e_1 = \frac{\partial v_x}{\partial x} + \frac{\partial v_y}{\partial y}, \qquad \nabla_1^2 = \frac{\partial^2}{\partial x^2} + \frac{\partial^2}{\partial y^2}$$

It may be observed that Equations [22] degenerate to those of generalized plane stress if the third equation is ignored and if v_z, in the first two, is replaced by its value, in terms of v_x and v_y, obtained from the third of Equations [21] by setting $N_z = 0$, and $\kappa = 1$. See p. 497, Bibliography (4).

5 Boundary Conditions

Boundary conditions, on the edge of the plate, sufficient to assure a unique solution of Equations [22], are obtained by substituting Equation [14] into [13] and performing the integration with respect to z, with the result

$$\oint_C \left(\bar{X}_1\frac{\partial v_x}{\partial t} + \bar{Y}_1\frac{\partial v_y}{\partial t} + \frac{\bar{Z}_1}{h}\frac{\partial v_z}{\partial t}\right)ds \quad \ldots\ldots [23]$$

where s is measured along the edge of the plate

$$\left.\begin{aligned} \bar{X}_1 &= N_x l + N_{xy} m \\ \bar{Y}_1 &= N_{xy} l + N_y m \\ \bar{Z}_1 &= R_x l + R_y m \end{aligned}\right\} \quad \ldots\ldots [24]$$

and l and m are the direction cosines of the outward drawn normal to the edge.

The integrand of Expression [23] may be referred to co-ordinates n, s, normal and tangential to the edge, by means of the transformations

$$\left.\begin{aligned} v_n &= v_x l + v_y m \\ v_s &= v_y l - v_x m \\ N_n &= N_x l^2 + N_y m^2 + 2N_{xy} lm \quad \ldots\ldots \\ N_{ns} &= (N_y - N_x)lm + N_{xy}(l^2 - m^2) \\ R_n &= R_x l + R_y m \end{aligned}\right\} \quad \ldots\ldots [25]$$

with the result that Equation [23] becomes

$$\oint_C \left(N_n\frac{\partial v_n}{\partial t} + N_{ns}\frac{\partial v_s}{\partial t} + \frac{R_n}{h}\frac{\partial v_z}{\partial t}\right)ds \quad \ldots\ldots [26]$$

The first two products in Expression [26] are identical with those occurring in the theory of generalized plane stress but it is seen that an additional boundary condition is required for Equations [22]; namely, either the shear R_n or the velocity $\partial v_z/\partial t$ must be specified.

6 Alternative Procedure

The results in Sections 3, 4, and 5 were obtained by inserting the Approximations [14] into equations at several stages of the development outlined in Section 2. This type of exposition was adopted in order to emphasize the relations between corresponding equations in the three-dimensional and plate theories. Alternatively, the approximations may be inserted directly into Equation [1] and the integration with respect to z performed once and for all. The plate equations then follow logically (except for the arbitrary introduction of κ) by a procedure analogous to that in the remainder of Section 2. One advantage of this method is

the appearance of explicit expressions for the kinetic-energy density of the plate

$$T^* = \rho h\left[\left(\frac{\partial v_x}{\partial t}\right)^2 + \left(\frac{\partial v_y}{\partial t}\right)^2 + \frac{1}{3}\left(\frac{\partial v_z}{\partial t}\right)^2\right]$$

and the potential energy-density of the plate

$$2V^* = \lambda h(e_x + e_y + \kappa e_z)^2 + 2Gh(e_x^2 + e_y^2 + \kappa^2 e_z^2) + Gh\left(\frac{h^2}{3}\gamma_{yz}^2 + \frac{h^2}{3}\gamma_{zx}^2 + \gamma_{xy}^2\right)$$

where

$$e_x = \frac{\partial v_x}{\partial x} \qquad \gamma_{yz} = \frac{1}{h}\frac{\partial v_z}{\partial y}$$

$$e_y = \frac{\partial v_y}{\partial y} \qquad \gamma_{zx} = \frac{1}{h}\frac{\partial v_z}{\partial x}$$

$$e_z = \frac{v_z}{h} \qquad \gamma_{xy} = \frac{\partial v_y}{\partial x} + \frac{\partial v_x}{\partial y}$$

are the components of plate strain. Also, the relations

$$N_x = \frac{\partial V^*}{\partial e_x}, \ldots, \qquad R_y = \frac{\partial V^*}{\partial \gamma_{yz}}$$

are found.

In addition, a rigorous proof of the theorem on uniqueness of solutions may be developed along the lines described in a previous paper (8) on flexural motions of plates.

7 Determination of κ

The constant κ was inserted in the expression for the strain energy in order to overcome a difficulty inherent in approximate equations of the type described here. In the present case the source of the difficulty is the assumption of a particular (linear) functional dependence, on z, of the thickness displacement u_z. This can be correct only at one frequency. At low frequencies the thickness stresses, τ_{zz}, τ_{xy}, σ_z, and the thickness inertia $\rho\partial^2 u_z/\partial t^2$ are small and, accordingly, the thickness displacement follows the extensional stresses, σ_x, σ_y, as in statical deformation. Since the extensional stresses are essentially independent of z, at low frequencies, the best assumption for u_z in this range, is proportionality to z. This is the assumption used in Equation [14]. However, as the frequency increases, a range is reached where strong coupling exists between extensional motions in the plane of the plate and the first mode of pure thickness vibration of the plate, in which u_z varies as $\sin(\pi z/2h)$. For this range it would be preferable to start with the assumption

$$u_z = v_z(x, y, t)\sin(\pi z/2h)$$

but then the low-frequency results would be in error. A two-term approximation could be used, at the expense of increased order of the differential equations. Alternatively, the factor κ can be introduced and its value fixed so that the frequency of the first thickness mode, at which the important coupling occurs, is correct despite the incorrect distribution of displacement. At low frequencies, all the terms containing κ are negligible so that the equations reduce to the appropriate form of generalized plane stress.

The value of κ is chosen, then, by equating the frequency of pure thickness vibration, obtained from the plate equations of motion, Equations [22], with the corresponding frequency obtained from the three-dimensional equations.

In Equations [22] let

$$\left.\begin{aligned} v_x = v_y = F_x = F_y = F_z = 0 \\ v_z = C\exp(i\bar{\omega}t)\end{aligned}\right\} \quad [27]$$

Then the first two of Equations [22] are satisfied identically and the third yields

$$\bar{\omega}^2 = \frac{3\kappa^2}{h^2}\frac{\lambda + 2G}{\rho} \quad [28]$$

It may be observed that no such frequency is contained in the equations of generalized plane stress. It is, in fact, the presence of such a mode of vibration in Equations [22] that makes them applicable to much higher frequencies than those accommodated by the equations of generalized plane stress.

The frequency, corresponding to Equation [28], obtained from the three-dimensional equations is

$$\bar{\omega}^2 = \frac{\pi^2}{4h^2}\frac{\lambda + 2G}{\rho} \quad [29]$$

Equating [28] and [29], we find

$$\kappa^2 = \pi^2/12 \quad [30]$$

8 Free Vibrations

In the case of free vibrations, the equations of motion, Equations [22], take a simple and revealing form when expressed in terms of the potentials of the dilatation and rotation in the plane of the plate.

Let

$$\left.\begin{aligned} v_x &= \frac{\partial\varphi}{\partial x} + \frac{\partial H}{\partial y} \\ v_y &= \frac{\partial\varphi}{\partial y} - \frac{\partial H}{\partial x}\end{aligned}\right\} \quad [31]$$

Then, introducing a time factor $\exp(i\omega t)$ (omitted in the sequel), Equations [22] are satisfied, in the absence of surface tractions, if

$$\left.\begin{aligned} c_2^2\nabla_1^2 H + \omega^2 H &= 0 \\ c_1^2\nabla_1^2\varphi + \omega^2\varphi + (\kappa\lambda/\rho h)v_z &= 0 \\ c_2^2\nabla_1^2 v_z + (\omega^2 - 3\kappa^2 c_1^2/h^2)v_z - (3\kappa\lambda/\rho h)\nabla_1^2\varphi &= 0\end{aligned}\right\} \quad [32]$$

where

$$c_1^2 = (\lambda + 2G)/\rho, \quad c_2^2 = G/\rho \quad [33]$$

Eliminating v_z between the second and third of Equations [32], the equation governing φ is found to be

$$(\nabla_1^2 + \delta_1^2)(\nabla_1^2 + \delta_2^2)\varphi = 0 \quad [34]$$

where

$$\left.\begin{aligned} \delta_i^2 &= \frac{3\kappa^2}{2\beta h^2}\left[(\alpha + \beta)\frac{\omega^2}{\bar{\omega}^2} - 1 - (-1)^i\psi\right], \quad i = 1, 2 \\ \psi &= \left\{\left[(\alpha + \beta)\frac{\omega^2}{\bar{\omega}^2} - 1\right]^2 + 4\alpha\beta\frac{\omega^2}{\bar{\omega}^2}\left(1 - \frac{\omega^2}{\bar{\omega}^2}\right)\right\}^{1/2} \\ \alpha &= \frac{c_1^2}{c_3^2}, \quad \beta = \frac{c_2^2}{c_3^2}, \quad c_3^2 = \frac{4G(\lambda + G)}{\rho(\lambda + 2G)} = \frac{E}{\rho(1 - \nu^2)}\end{aligned}\right\} \quad [35]$$

in which E is Young's modulus and ν is Poisson's ratio.

Hence there are three independent displacement potentials: φ_1, φ_2, and H (where $\varphi_1 + \varphi_2 = \varphi$). They are governed by the three equations

$$\left.\begin{aligned} (\nabla_1^2 + \delta_1^2)\varphi_1 &= 0 \\ (\nabla_1^2 + \delta_2^2)\varphi_2 &= 0 \\ (\nabla_1^2 + \delta_3^2)H &= 0\end{aligned}\right\} \quad [36]$$

where $\delta_i^2 = \omega^2/c_i^2$. It may be seen that there are three phase velocities in this theory, given by ω/δ_i, $i = 1, 2, 3$. The velocity, $\omega/\delta_3 = c_3$, of the rotation, is the same as in the theory of generalized plane stress; but there are two dilatational velocities (ω/δ_1 and ω/δ_2) as opposed to only one (c_3) in the theory of generalized plane stress. Furthermore, the two dilatational velocities are dispersive, whereas c_3 is not. Examination of the expressions for δ_1 and δ_2 shows that δ_1 is always real but δ_2 is real for $\omega/\bar{\omega} > 1$ and imaginary for $\omega/\bar{\omega} \ll 1$. Hence, an important change in the vibration spectrum of the plate occurs at the frequency $\bar{\omega}$. This is why the appropriate choice of the value of κ is essential.

The plate displacements are expressed in terms of the three potentials by

$$\left.\begin{aligned} v_x &= \frac{\partial\varphi_1}{\partial x} + \frac{\partial\varphi_2}{\partial x} + \frac{\partial H}{\partial y} \\ v_y &= \frac{\partial\varphi_1}{\partial y} + \frac{\partial\varphi_2}{\partial y} - \frac{\partial H}{\partial x} \\ v_z &= \sigma_1\varphi_1 + \sigma_2\varphi_2 \end{aligned}\right\} \quad \ldots\ldots\ldots [37]$$

where

$$\sigma_i = \frac{h(\lambda + 2G)}{\kappa\lambda}\left(\delta_i^2 - \frac{\omega^2}{c_1^2}\right), \quad i = 1, 2 \ldots\ldots [38]$$

The expression for v_z in terms of φ_1 and φ_2 comes from the second of Equations [32] and the first two of Equations [36].

9 Symmetrical Vibrations of a Circular Disk

In this case the variables are expressed in terms of polar coordinates r, θ, by means of the relations $x = r\cos\theta$, $y = r\sin\theta$ and the transformation Equations [25]. For symmetrical vibrations, $H = 0$ and $\varphi = \varphi(r)$, so that Equations [36] reduce to

$$\left(\frac{d^2}{dr^2} + \frac{1}{r}\frac{d}{dr} + \delta_i^2\right)\varphi_i = 0, \quad i = 1, 2 \ldots\ldots [39]$$

The solutions of Equation [39], for a solid disk, are

$$\varphi_1 = A_1 J_0(\delta_1 r), \qquad \varphi_2 = A_2 J_0(\delta_2 r) \ldots\ldots [40]$$

where J is the Bessel function of the first kind and A_1 and A_2 are constants. Hence

$$\left.\begin{aligned} v_r &= -A_1\delta_1 J_1(\delta_1 r) - A_2\delta_2 J_1(\delta_2 r) \\ v_\theta &= 0 \\ v_z &= A_1\sigma_1 J_0(\delta_1 r) + A_2\sigma_2 J_0(\delta_2 r) \end{aligned}\right\} \quad \ldots\ldots [41]$$

We consider the case of a free edge $r = a$. The appropriate components of edge traction are, from Equations [25], [26], and [21]

$$\left.\begin{aligned} N_r &= 2h\left[(\lambda + 2G)\frac{dv_r}{dr} + \lambda\frac{v_r}{r} + \kappa\lambda\frac{v_z}{h}\right] \\ N_{r\theta} &= 0 \\ R_r &= \frac{2Gh^2}{3}\frac{dv_z}{dr} \end{aligned}\right\} \quad \ldots [42]$$

A unique solution is obtained by setting these equal to zero at $r = a$. This results in a pair of simultaneous,[6] homogeneous equations in A_1 and A_2. The determinant of the coefficients, when equated to zero, yields the frequency equation

$$\frac{\beta}{\alpha} - \frac{\eta\gamma}{\xi}\frac{J_0(\xi\gamma)}{J_1(\xi\gamma)} = \frac{\xi^2 - 2\eta}{1 - 2\eta}\left[\frac{\beta}{\alpha} - \eta\gamma\frac{J_0(\gamma)}{J_1(\gamma)}\right] \ldots [43]$$

where

$$\xi = \delta_2/\delta_1, \qquad \gamma = \delta_1 a$$

$$\eta = \frac{\omega^2}{2c_1^2\delta_1^2} = \beta\frac{\omega^2}{\bar{\omega}^2}\left[(\alpha + \beta)\frac{\omega^2}{\bar{\omega}^2} - 1 + \psi\right]^{-1} \ldots [44]$$

From the last two of Equations [44], noting that $\bar{\omega} = \pi c_1/2h$

$$\frac{a}{h} = \frac{\gamma\bar{\omega}}{\pi\omega}\sqrt{8\eta} \ldots\ldots [45]$$

The frequency spectrum may be computed from Equations [43], [44], and [45] in the following manner: First, it is noted that α and β depend only on Poisson's ratio ν, while ξ and η depend only on ν and $\omega/\bar{\omega}$. Hence a choice of ν and $\omega/\bar{\omega}$ reduces Equation [43] to a transcendental equation in γ only. For each root, γ, of this equation, there corresponds a value of a/h in accordance with Equation [45]. Thus, for a given material and thickness, a sequence of disk diameters is found that will vibrate at a given frequency. Then the frequency is changed and a new set of diameters is calculated in the same manner. The process is repeated until sufficient data are obtained to enable curves to be drawn of $\omega/\bar{\omega}$ versus a/h. Results of such computations for the first two modes ($\nu = 0.3$) are shown in Table 1 and illustrated by Curves II and III in Fig. 1.

[6] It may be observed that for boundary conditions $v_r = 0$, $R_r = 0$ (analogous to a simply supported edge in the theory of flexure) the two modes of motion represented by φ_1 and φ_2 are not coupled and Equation [43] is replaced by the two simpler equations $J_1(\delta_1 a) = 0$ and $J_1(\delta_2 a) = 0$.

TABLE 1 COMPUTED FREQUENCIES OF FIRST TWO MODES OF VIBRATION OF CIRCULAR DISK

	First Mode									
a/h	0	0.496	0.98	1.43	1.81	2.24	2.88	3.88	5	
$\omega_1/\bar{\omega}$	0.863	0.85	0.8	0.7	0.6	0.5	0.4	0.3	0.235	
	Second Mode									
a/h	0.473	0.67	0.81	0.925	1.1	1.47	2.30	3.09	3.43	4.11	4.94
$\omega_2/\bar{\omega}$	3.0	2.0	1.7	1.5	1.3	1.1	0.95	0.85	0.80	0.70	0.60

TABLE 2 EXPERIMENTAL DATA

	1 diam, cm	2 thickness, cm	3 a/h	4 $\omega_1/2\pi$, kc	5 $\omega_2/2\pi$, kc	6 ω_1/ω	7 $\omega_2/\bar{\omega}$
1	2.68	0.648	4.14	121.1	301.5	0.276	0.686
2	2.63	0.640	4.11	123.4	306.5	0.278	0.690
3	2.16	0.564	3.84	150.4	363.6	0.298	0.720
4	2.16	0.637	3.39	150.1	345.4	0.336	0.773
5	2.17	0.638	3.39	149.7	345.8	0.336	0.774
6	2.16	0.729	2.97	....	....	....	....
7	1.58	0.596	2.66	208.3	438.0	0.436	0.920
8	1.59	0.612	2.60	208.5	422.0	0.449	0.910
9	1.58	0.604	2.62	208.7	436.6	0.443	0.926
10	1.58	0.580	2.72	....	....	....	....
11	1.31	0.639	2.05	237.6	410.5	0.534	0.922
12	1.05	0.636	1.65	285.4	430.0	0.638	0.962
13	1.05	0.637	1.64	280.0	427.0	0.648	0.956
14	0.783	0.629	1.25	334.0	572.0	0.739	1.265
15	0.777	0.636	1.22	338.6	579.0	0.757	1.295

10 Discussion of Disk Frequencies

The interpretation of the results for the disk is facilitated by a study of several limiting cases.

Low Frequency, Large Diameter. For $\omega/\bar{\omega} \ll 1$, the first and third of Equations [44] reduce, approximately, to

$$\xi^2 = -\bar{\omega}^2/\alpha\beta\omega^2, \qquad \eta = 1/2\alpha$$

Hence Equation [43] reduces to

$$\gamma \frac{J_0(\gamma)}{J_1(\gamma)} = 2\beta = \frac{\lambda + 2G}{2(\lambda + G)} = 1 - \nu \quad [46]$$

and Equation [45] reduces, for large a/h, to

$$\frac{a}{h} = \frac{2\bar{\omega}c_3\gamma}{\pi\omega c_1}$$

or

$$\omega = \frac{\gamma}{a}\sqrt{\frac{E}{\rho(1-\nu^2)}} \quad [47]$$

That is, the frequencies are given by Equation [47], in which γ are the roots of Equation [46]. This is exactly the solution of the equations of generalized plane stress. Hence, for the low frequencies of thin plates, the present equations, as they should, give the same results as the equations of generalized plane stress. Accordingly, the lower right-hand portions of Curves I and II in Fig. 1 are essentially identical. See p. 498, reference (4).

Intermediate Frequency, Small Diameter. In this case $a/h \ll 1$. Hence, from Equation [45], $\gamma \ll 1$. Now, for small x

$$\frac{xJ_0(x)}{J_1(x)} \backsimeq 2 \quad [48]$$

Hence Equation [43] reduces to

$$\left(\frac{\beta}{\alpha} - \frac{2\eta}{\xi^2}\right)(1 - 2\eta) = (\xi^2 - 2\eta)\left(\frac{\beta}{\alpha} - 2\eta\right) \quad [49]$$

or

$$\left(\frac{\omega^2}{\bar{\omega}^2} - \frac{1-\beta}{\alpha-\beta}\right)(\delta_1^2 - \delta_2^2) = 0 \quad [50]$$

This equation has only one real, positive root

$$\frac{\omega}{\bar{\omega}} = \sqrt{\frac{1-\beta}{\alpha-\beta}} \quad [51]$$

which is the ordinate of the first mode, illustrated by Curve II in Fig. 1 at $a/h = 0$.

Equation [51] can be rewritten in the form

$$\omega = \frac{\pi}{2h}\sqrt{\frac{E}{\rho}} \quad [52]$$

This will be recognized as the limiting value of the exact solution for the longitudinal vibration of a thin rod in its fundamental mode. It seems remarkable that a plate theory should contain such a result; that is, at least for the fundamental mode, the equations are valid for a plate so thick that, in comparison, its diameter is negligibly small. Of course this remarkable property is not held by the second mode, since only one thickness mode is contained in the theory. For $a/h \to 0$, the second mode should couple with a second thickness mode and approach thrice the frequency of Equation [52] as a limit. In the present theory the second radial mode does, however, couple with the first thickness mode. This is evidenced, in Fig. 1, by the slight reversal of curvature of Curve III in the neighborhood of $\omega/\bar{\omega} = 1$. This effect becomes more pronounced with the higher radial modes at large values of a/h. In fact, for large a/h and $\omega/\bar{\omega} > 1$, coupling occurs, in addition, with overtones of the first thickness mode; i.e., with motions characterized by multiple circular nodes as distinguished from nodal planes. These curves are not shown in Fig. 1, but they are very similar to those found for the high-frequency flexural vibrations of a disk (9).

High Frequency, Small Diameter. Although, for very small diameters, only the lowest mode is correct for intermediate frequencies, the theory again gives good results for very high frequencies. For $\omega/\bar{\omega} \gg 1$, the first and third of Equations [44] give, approximately

$$\xi^2 = \beta/\alpha, \qquad \eta = \beta/2\alpha \quad [53]$$

Hence Equation [43] reduces to

$$\frac{\xi\gamma J_0(\xi\gamma)}{J_1(\xi\gamma)} = \frac{2\beta}{\alpha} = \frac{2G}{\lambda + 2G} = \frac{1-2\nu}{1-\nu} \quad [54]$$

and Equations [44] yield

$$\omega = \frac{\xi\gamma}{a}\sqrt{\frac{\lambda + 2G}{\rho}} \quad [55]$$

Accordingly, the frequencies are given by Equation [55], in which $\xi\gamma$ are the roots of Equation [54]; but this is exactly the solution of the three-dimensional equations for the radial vibrations of an infinite rod. Thus there are two ranges of frequencies of a thin rod which are contained, exactly, in the plate theory.

Intermediate Frequency, Large Diameter. In this case, for $a/h \to \infty$, Equation [45] gives $\gamma \to \infty$. Hence one solution of Equation [43] is $\xi^2 = 0$, that is, $\omega = \bar{\omega}$. Thus the solution contains, as one of the frequencies of vibration of an infinite plate, the correct frequency of the fundamental thickness mode. This, of course, is to be expected, in view of the procedure by which the value of κ was chosen.

11 Experimental Investigation

Frequency measurements were performed[7] on 15 barium-titanate disks with diameters, thicknesses, and ratios a/h shown in columns 1, 2, 3 of Table 2.

After the disks were lapped, spotted, gold-plated, and polarized, their resonant frequencies were measured by applying the output of a tunable oscillator to a frequency counter, the frequency of oscillation being controlled by the disk under test. These frequencies are recorded in columns 4 and 5 of Table 2.

The frequencies $\omega_1/2\pi$, of the fundamental mode of vibration, were obtained without difficulty for all the disks except numbers 6 and 10, both of which appeared to be mechanically defective. The frequencies of the second mode were more difficult to measure as it was necessary not only to locate resonances, but also to evaluate their relative strengths. The frequencies recorded in column 5 are thus to be considered less reliable than those in column 4.

To compare the experimental results with those predicted by the theory, the ratios $\omega/\bar{\omega}$ were computed for each disk, using for ω the experimental values and for $\bar{\omega}$ (see Equations [28], [29], [30])

$$\bar{\omega} = \frac{\pi}{2h}\left(\frac{\lambda + 2G}{\rho}\right)^{1/2} = \frac{\pi}{2h}\left[\frac{2G(1-\nu)}{\rho(1-2\nu)}\right]^{1/2}$$

with[8]

[7] At Bell Telephone Laboratories.

[8] The values of the elastic constants were supplied by W. P. Mason and the density by L. Egerton.

$\nu = 0.3$
$G = 49.3 \times 10^{10}$ dynes/cm^2
$\rho = 5.33$ gm/cm^3

The results are recorded in columns 6 and 7 of Table 2 and are plotted as circles in Fig. 1.

As may be seen, the agreement between theory and experiment is good, especially for the first mode of motion. For diameter-to-thickness ratios less than 3, the theory furnishes a considerably better description than the theory of generalized plane stress. For $a/h = 0$, there is, of course, ample confirmation, by experiments with thin rods, of the predicted value of the frequency of the first mode.

BIBLIOGRAPHY

1 "On the Calculation of Three-Dimensional Corrections for the Two-Dimensional Theory of Plane Stress," by E. Reissner, Proceedings of the Fifteenth Semi-Annual Eastern Photoelasticity Conference, Addison-Wesley Press, Inc., Cambridge, Mass., 1942, pp. 23–31.

2 "Theory of Elasticity," by S. Timoshenko and J. N. Goodier, McGraw-Hill Book Company, Inc., New York, N. Y., second edition, 1951, p. 214.

3 Reference (2), p. 148.

4 "Theory of Elasticity," by A. E. H. Love, Cambridge University Press, fourth edition, Cambridge, England, 1927, p. 176.

5 "Theory of Plates and Shells," by S. Timoshenko, McGraw-Hill Book Company, Inc., New York, N. Y., 1940, p. 299.

6 Reference (5), p. 86.

7 "Vibration Problems in Engineering," by S. Timoshenko, D. Van Nostrand Company, Inc., New York, N. Y., second edition, 1937, p. 338.

8 "Influence of Rotatory Inertia and Shear on Flexural Motions of Isotropic, Elastic Plates," by R. D. Mindlin, JOURNAL OF APPLIED MECHANICS, Trans. ASME, vol. 73, 1951, pp. 31–38.

9 "Axially Symmetric Flexural Vibrations of a Circular Disk," by H. Deresiewicz and R. D. Mindlin, JOURNAL OF APPLIED MECHANICS, Trans. ASME, vol. 77, 1955, pp. 86–88.

Propagation of a Sudden Rotary Disturbance in an Elastic Plate in Plane Stress[1]

By J. N. GOODIER[2] and W. E. JAHSMAN[3]

Detailed results are found for two plane-stress problems of an elastic plate with a hole from which a symmetrical disturbance is propagated. In the first a uniform shear stress is suddenly applied and maintained at the hole. In the second a uniform (rotary) velocity is suddenly applied and maintained. The subsequent motion is entirely rotary and involves shear stress only. The problems are mathematically analogous to those of symmetrical pressure and radial velocity at the hole, already solved by Kromm, and his analysis is followed. The existence of a similar analogy in the statical cases is well known.

Introduction

THE problem of finding the motion of an elastic plate following sudden rise of pressure in a hole (as a plane-stress problem), or sudden imposition of a "radial" velocity at the hole, was solved by A. Kromm[4] in 1948, who gives detailed results as curves in dimensionless variables. The operational method used incorporates devices of a special nature, reducing the original differential equation in the radial displacement to an integral equation of Volterra's first kind, amenable to numerical solution.

The problem of "rotary" motion—caused by sudden application of (in-plane) shear loading uniformly round the hole, or sudden imposition of a rotary velocity at the hole—turns out to be closely analogous, and is worked out here by Kromm's method. The results appear in Figs. 2, 3, 4, 5.

The Equation of Rotary Motion

The dynamical equations corresponding to plane stress in polar co-ordinates are (with u for radial, v for tangential displacement)

$$\left.\begin{aligned} \frac{\partial \sigma_r}{\partial r} + \frac{1}{r}\frac{\partial \tau_{r\theta}}{\partial \theta} + \frac{1}{r}(\sigma_r - \sigma_\theta) &= \rho \frac{\partial^2 u}{\partial t^2} \\ \frac{\partial \tau_{r\theta}}{\partial r} + \frac{1}{r}\frac{\partial \sigma_\theta}{\partial \theta} + \frac{2}{r}\tau_{r\theta} &= \rho \frac{\partial^2 v}{\partial t^2} \end{aligned}\right\} \quad \ldots [1]$$

The accelerations have been linearized by restriction to sufficiently small velocity and displacement. The Hooke's law relations

$$\left.\begin{aligned} \frac{\partial u}{\partial r} &= \frac{1}{E}(\sigma_r - \nu\sigma_\theta), \quad \frac{1}{r}\frac{\partial v}{\partial \theta} + \frac{u}{r} = \frac{1}{E}(\sigma_\theta - \nu\sigma_r), \\ \frac{\partial v}{\partial r} &- \frac{v}{r} + \frac{1}{r}\frac{\partial u}{\partial \theta} = \frac{1}{G}\tau_{r\theta} \end{aligned}\right\} \quad \ldots [2]$$

complete a set of five equations in the displacements u, v, and the stress components σ_r, σ_θ, $\tau_{r\theta}$, Fig. 1. E, G, ν, ρ are Young's modulus, the shear modulus, Poisson's ratio, and density.

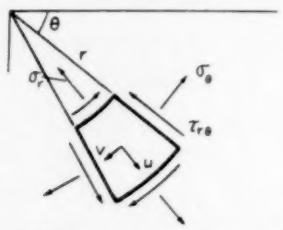

Fig. 1 Stress and Displacement Notation in Polar Co-Ordinates

Purely rotary motion is possible, characterized by $u = 0$; v, σ_r, σ_θ, $\tau_{r\theta}$ are independent of θ.

It follows from Equations [2] that $\sigma_r = \sigma_\theta = 0$. The first of Equations [1] is identically satisfied, and the second gives

$$\frac{\partial^2 v}{\partial r^2} + \frac{1}{r}\frac{\partial v}{\partial r} - \frac{v}{r^2} = \frac{1}{c_2^2}\frac{\partial^2 v}{\partial t^2}, \quad c_2^2 = \frac{G}{\rho} \quad \ldots [3]$$

The problem is reduced to the solution of this equation for v under the appropriate initial and boundary conditions. Kromm reduced his problem of symmetrical radial motion to an equation of the same form with u instead of v, c_1^2 $[= E/\rho(1-\nu^2)]$ instead of c_2^2.

The plate is here taken as infinite, and initially at rest and unstrained. Two cases are considered, involving distinct boundary conditions at the hole $r = a$. They are as follows:

(a) A shear stress τ_0 is suddenly applied and maintained at the hole, at $t = 0$. Thus

$$(\tau_{r\theta})_{r=a} = -\tau_0, \quad t > 0 \quad \ldots [4]$$

(b) A sudden rotary velocity v_0 is imparted and maintained at the hole. Thus

$$\left(\frac{\partial v}{\partial t}\right)_{r=a} = v_0, \quad t > 0 \quad \ldots [5]$$

The initial conditions in each case are

$$(v)_{t=0} = 0, \quad (\partial v/\partial t)_{t=0} = 0, \quad r > a \quad \ldots [6]$$

Solution by Kromm's Method[4]

In view of the initial conditions [6], Equation [3] yields as the equation for $V(r, s)$, the Laplace transform

---

[1] The results reported here were obtained in the course of research under a contract (N6onr-251 Task Order 12, Project NR-064-241) between the Office of Naval Research and Stanford University.

[2] Professor of Engineering Mechanics, Stanford University, Stanford, Calif. Mem. ASME.

[3] Specialist, Mechanical Engineering Analysis, Knolls Atomic Power Laboratory, General Electric Company, Schenectady, N. Y.; formerly, Research Assistant, Stanford University, Stanford, Calif.

[4] "Zur Ausbreitung von Stosswellen in Kreislochscheiben," by A. Kromm, *Zeitschrift für angewandte Mathematik und Mechanik*, vol. 28, no. 4, 1948, pp. 104–114; vol. 28, no. 10, 1948, pp. 297–303.

Contributed by the Applied Mechanics Division and presented at the Diamond Jubilee Annual Meeting, Chicago, Ill., November 13–18, 1955, of The American Society of Mechanical Engineers.

Discussion of this paper should be addressed to the Secretary, ASME, 29 West 39th Street, New York, N. Y., and will be accepted until July 10, 1956, for publication at a later date. Discussion received after the closing date will be returned.

Note: Statements and opinions advanced in papers are to be understood as individual expressions of their authors and not those of the Society. Manuscript received by ASME Applied Mechanics Division, January 24, 1955. Paper No. 55—A-47.

$$\int_0^\infty v(r, t)e^{-st}\,dt \text{ of } v(r, t)$$

$$V'' + \frac{1}{r}V' - \left(\frac{s^2}{c_2^2} + \frac{1}{r^2}\right)V = 0 \quad \ldots\ldots\ldots [7]$$

Primes indicate differentiation with respect to r.

The solution satisfying the transform of the boundary condition [4] is

$$V(r, s) = \frac{\tau_0 c_2}{Gs^2}\,\frac{K_1(sr/c_2)}{K_2(sa/c_2)} \quad \ldots\ldots\ldots [8]$$

where $K_1()$, $K_2()$ are modified Bessel functions of the second kind. The general solution of Equation [7] would contain also the modified Bessel function of the first kind $I_1(sr/c_2)$, but this is discarded here to insure regularity of the solution for $v(r, t)$ as r becomes infinite.

It is convenient to introduce new variables defined by

$$\left.\begin{aligned} r. = r/a, \quad t. = c_2 t/a, \quad s. = as/c_2, \\ v. = Gv/\tau_0 a, \quad V. = Gc_2 V/\tau_0 a^2, \\ v. = \partial v./\partial t. = (G/c_2\tau_0)\partial v/\partial t, \quad \tau_{r\theta} = \tau_{r\theta}/\tau_0 \end{aligned}\right\} \ldots [9]$$

It follows that

$$V. = \int_0^\infty v.e^{-s.t.}dt. \quad \ldots\ldots\ldots [10]$$

Then Equation [8] becomes

$$V.(r., s.) = \frac{1}{s.^2}\,\frac{K_1(s.r.)}{K_2(s.)} \quad \ldots\ldots\ldots [11]$$

The transforms of $\tau_{r\theta}$ and of the particle velocity $\partial v/\partial t$ can now be found, using for $\tau_{r\theta}$ the transform of the third of Equations [2] with $u = 0$. In terms of the new variables [9] the results are

$$L[\tau_{r\theta}] = -\frac{1}{s.}\,\frac{K_2(s.r.)}{K_2(s.)}, \quad L[\dot{v}.] = \frac{1}{s.}\,\frac{K_1(s.r.)}{K_2(s.)} \quad \ldots [12]$$

where $L[\ ]$ symbolizes "Laplace transform of," as in Equation [10].

So far the procedure has been a straightforward application of the transform method. The problem is solved if the function $v.(r., t.)$ can be found which has the right-hand side of Equation [11] for its Laplace transform—that is, if the inverse of this transform can be found. It has not been found in tables of transforms and the inversion integral seems to offer no aid toward a form suitable for numerical evaluation. Following the method devised by Kromm for the closely analogous problem of radial motion, we multiply the first of Equations [12] by $e^{s.}K_2(s.)$

$$L[\tau_{r\theta}]\cdot e^{s.}K_2(s.) = -s.^{-1}e^{s.}K_2(s.r.) \quad \ldots\ldots\ldots [13]$$

The advantage of this lies in the fact that the inverses of the functions $e^{s.}K_2(s.)$ and $(e^{s.}/s.)K_2(s.r.)$ can be found, as Kromm shows. On the left of Equation [13] we have a product of two transforms. It therefore represents the transform of a convolution integral. Thus if

$$e^{s.}K_2(s.) = L[k(t.)], \quad s.^{-1}e^{s.}K_2(s.r.) = L[f_1(r., t.)] \quad \ldots [14]$$

we can take the inverses of the two sides of Equation [13] and write

$$\int_0^{t.} \tau_{r\theta}(r., x)k(t. - x)dx = -f_1(r., t.) \quad \ldots\ldots\ldots [15]$$

Similarly, the second of Equations [12] may be written

$$L[\dot{v}.]\cdot e^{s.}K_2(s.) = s.^{-1}e^{s.}K_1(s.r.) \quad \ldots\ldots\ldots [16]$$

and if

$$s.^{-1}e^{s.}K_1(s.r.) = L[f_2(r., t.)] \quad \ldots\ldots\ldots [17]$$

we can write

$$\int_0^{t.} \dot{v}.(r., x)k(t. - x)dx = f_2(r., t.) \quad \ldots\ldots\ldots [18]$$

Numerical results for $\tau_{r\theta}$ and $\dot{v}.$, from which the curves in Figs. 2, 3, 4, 5 were plotted, were obtained from the integral Equations [15] and [18]. This required evaluation of the three functions $k(t.)$, $f_1(r., t.)$, and $f_2(r., t.)$ so far defined only by their transforms in Equations [14] and [17]. Inversion of these transforms is effected by the Schläfli integral representation[5] of $K_n(z)$

$$K_n(z) = \frac{\Gamma(1/2)}{\Gamma(n + 1/2)}\left(\frac{z}{2}\right)^n \int_1^\infty e^{-zt}(t^2 - 1)^{n-1/2}\,dt. \quad [19]$$

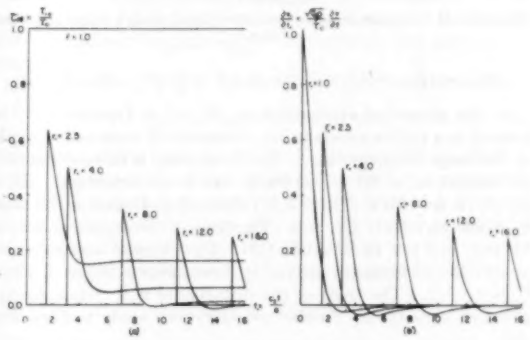

FIG. 2 SHEAR STRESS τ_θ SUDDENLY APPLIED AT HOLE ($r. = 1$) AND MAINTAINED

(Time variations of (*a*) shear stress, (*b*) particle velocity at several locations.)

after suitable manipulation in each case. For instance, to find $f_1(r., t.)$ from its transform $s.^{-1}e^{s.}K_2(s.r.)$, $K_2(s.r.)$ is written in the form of Equations [19] and multiplied by $e^{s.}$ to give

$$e^{s.}K_2(s.r.) = \frac{1}{3}\,r.^2 s.^2 \int_1^\infty e^{-s.(r.t.-1)}(t^2 - 1)^{3/2}\,dt$$

Changing the variable of integration to $\tau = r.t. - 1$ and integrating by parts leads to

$$e^{s.}K_2(s.r.) = \frac{s.}{r.^2}\int_{r.-1}^\infty e^{-s.\tau}(\tau + 1)\sqrt{(\tau + 1)^2 - r.^2}\,d\tau$$

Changing the lower limit to zero, with a zero value of the integrand in $0 < \tau < r. - 1$, it follows that $s.^{-1}e^{s.}\cdot K_2(s.r.)$ is the transform of

$$f_1(r., t.) = \begin{cases} 0 \text{ when } t. < r. - 1 \\ \dfrac{1}{r.^2}(t. + 1)\sqrt{(t. + 1)^2 - r.^2} \text{ when } t. > r. - 1 \end{cases}$$

The other two functions are

$$f_2(r., t.) = \begin{cases} 0 \text{ when } t. < r. - 1 \\ \dfrac{1}{r.}\sqrt{(t. + 1)^2 - r.^2} \text{ when } t. > r. - 1 \end{cases}$$

[5] "Treatise on the Theory of Bessel Functions," by G. N. Watson, The Macmillan Co., New York, N. Y., second edition, 1945, p. 172.

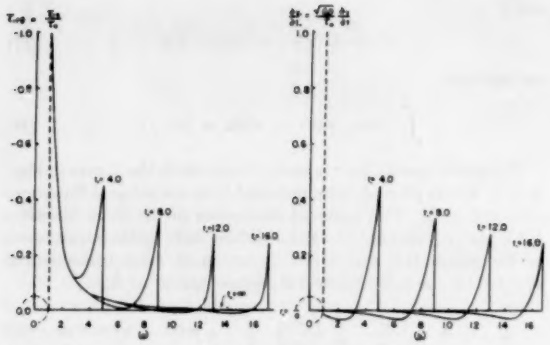

FIG. 3 SHEAR STRESS τ_0 SUDDENLY APPLIED AT HOLE ($r. = 1$) AND MAINTAINED
(Variation of (a) shear stress, (b) particle velocity along a radius at several times.)

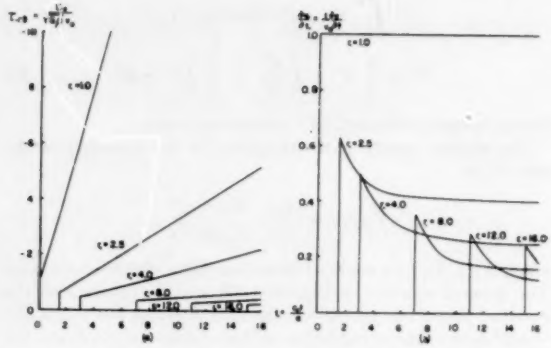

FIG. 4 ROTARY VELOCITY v_0 SUDDENLY APPLIED AT HOLE ($r. = 1$) AND MAINTAINED
(Time variation of (a) shear stress, (b) particle velocity at several locations.

$$k(t.) = [2(t. + 1)^2 - 1][(t. + 1)^2 - 1]^{-1/2} \quad \text{when } t. > 0$$

In the numerical evaluations, $\tau_{.r\theta}(r., x)$ in Equation [15] is treated as stepwise constant in a succession of short subintervals of the range of integration. The integration is thereby reduced to integration of $k(t. - x)$ itself, which is elementary. Since $f_1(r., t.)$ is zero for $t. < r. - 1$, it follows from Equation [15] that $\tau_{.r\theta}$ is also zero for $t. < r. - 1$. The range of integration is reducible to $r. - 1$ to $t.$ in Equation [15]. The physical interpretation is that the disturbance arrives at dimensionless radius $r.$ when $t. = r. - 1$. The front of the disturbance is therefore propagated at velocity c_2. Similar considerations apply to Equation [18].

DISCUSSION OF RESULTS

Figs. 3(a, b) show the propagation of a disturbance due to shear stress τ_0 suddenly applied at the hole, then maintained. Fig. 3(a) shows the stress distribution with respect to the radial co-ordinate at various times. For $t. = 4.0$, for instance, the vertical line is the wave front. The stress behind the front is represented by the catenarylike curve ascending on the left to —1 at the hole (representing the applied shear stress). At later times $t. = 8.0$, $t. = 12.0$, $t. = 16.0$, the front is found further out (moving with velocity c_2), and the height is diminishing. The heights follow the law[4] ($\tau_{.r\theta}$) front $= -1/\sqrt{r}$. This follows at once from Equation [15] considered for $t. = r. - 1 + \epsilon$, and taken to a limit as $\epsilon \to 0$.

Fig. 3(b) shows the particle velocity $\partial v./\partial t.$ in a similar fashion. Behind the fronts the velocity falls off, to the left, and becomes negative in the neighborhood of the hole. At $t. = 4.0$ its value at the hole is negative, but small. When $t. = 8.0$ the value at the hole is imperceptible, and remains so, indicating local quiescence. The stress in the quiescent region is represented by the horizontal parts of the curves in Fig. 2(a). These curves show the time history at fixed points $r. = 2.5$, $r. = 4.0$, etc. At $r. = 2.5$, for instance, we find the sudden rise of stress, followed (to the right) by a fall, then a slight rise to a steady value—which is the statical value given by $\tau_{r\theta}/\tau_0 = 1/r^2$. Accordingly, it has become very small at $r. = 12$. By contrast, the wave-front stress is still very much in evidence, diminishing only as $1/\sqrt{r}$. Fig. 2(b) shows the particle velocities rising suddenly at, for instance, $r. = 2.5$, quickly falling to negative values and climbing back to zero. As far as the curves actually drawn show, quiescence is reached by the time the wave front has gone a distance of about $6a$ past the point in question.

[4] This, and following results of the same nature, are also obtained for nonsymmetrical propagation (including symmetry as a special case) by the method of characteristics, in a forthcoming paper.

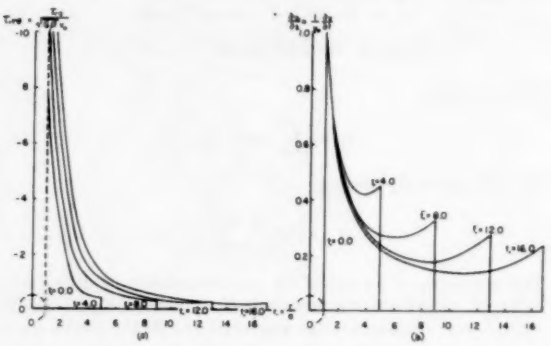

FIG. 5 ROTARY VELOCITY v_0 SUDDENLY APPLIED AT HOLE ($r. = 1$) AND MAINTAINED
(Variation of (a) shear stress, (b) particle velocity along a radius at several times.)

The quiescence as to velocity and associated statical stress values represent in a finite plate a temporary local equilibrium which will in due course be disturbed by an incoming wave reflected from the outer boundary.

The effects of a rotary velocity suddenly applied and maintained at the hole (boundary condition [5]) are shown in Figs. 4 and 5. Unlike the preceding curves for the stress problem, these were obtainable by a simple adaptation from Kromm's results for the pressure problem. If we make our $v.(= c_2 v/a v_0$, v_0 being the imposed velocity) analogous to Kromm's dimensionless radial velocity $\bar{u} = c_1 u/a v_0$, it turns out by Equations [2] that our dimensionless shear stress

$$\tau_{.r\theta} = c_2 \tau_{r\theta}/v_0 G$$

becomes analogous to Kromm's

$$(c_1/v_0)[(1 - \nu^2)/E](\sigma_r - \sigma_\theta)$$

The curves of Figs. 4 and 5 show that after the wave front passes a given neighborhood, the neighborhood soon settles down to a quasi-static state corresponding to a static displacement at the hole of magnitude $v_0 t$. Again, the ordinates at the wave front diminish as $1/\sqrt{r}$, the fronts themselves traveling with velocity c_2.

Effect of Hub Radius on the Vibrations of a Uniform Bar[1]

By W. E. BOYCE,[2] PROVIDENCE, R. I.

Methods are discussed for obtaining upper and lower bounds on the frequencies of a uniform beam, rotating at a constant speed about an axis at one end, and vibrating transversely to the plane of rotation. Previous results are extended to include the case of a nonzero hub radius. Bounds on the first two frequencies are given for several ratios of hub radius to beam length. These show that the frequencies depend almost linearly on the hub radius for various rotational speeds.

Introduction

THE problem under consideration is that of determining the frequencies of vibration of a uniform beam, rotating at constant angular speed about an axis at one end perpendicular to the axis of the beam, and vibrating transversely to the plane of rotation. Previous work on the problem has utilized the assumption of a zero hub radius; that is, the constraining device at the fixed end was assumed to be so small that the boundary conditions could be applied at the axis of rotation. In practice this is not the case and the purpose of this paper is to investigate the effect on the frequency of vibration produced by considering a nonzero hub radius.

Derivation of Equations

Let the transverse displacement of the beam be denoted by $u(s, t)$. Then the differential equation of motion may be written

$$EI\frac{\partial^4 u}{\partial s^4} - \frac{mA\Omega^2}{2}\frac{\partial}{\partial s}\left[(l^2 - s^2)\frac{\partial u}{\partial s}\right] = -mA\frac{\partial^2 u}{\partial t^2} \quad [1]$$

where E is Young's modulus, I the moment of inertia of the cross section about the principal axis parallel to the plane of rotation, m the mass per unit volume, A the cross-sectional area, Ω the angular speed of rotation in radians per second, and l the length of the beam. Removal of the time-dependent factor $\exp i\lambda t$ and normalization to a beam of unit length transforms Equation [1] into

$$w^{iv} - \frac{\alpha^2}{2}[(1 - x^2)w']' = \beta^2 w \quad [2]$$

where

$$\alpha^2 = mAl^4\Omega^2/EI, \quad \beta^2 = mAl^4\lambda^2/EI$$

w is the normalized displacement function, and primes and roman numerals denote differentiation with respect to x.

Assuming the fixed end to be elastically supported, the boundary conditions there are

$$w(\delta) = 0, \quad w'(\delta) - \epsilon w''(\delta) = 0 \quad [3]$$

Here ϵ is a positive constant depending on the degree of elastic support, while δ is a small positive number which is the ratio of the hub radius of the restraining mechanism to the length of the beam.

If the other end is free, the boundary conditions there are

$$w''(1) = 0, \quad w'''(1) = 0 \quad [4]$$

The portion of the beam for $0 \leq x \leq \delta$ is assumed to be rigid.

The eigenvalues β now clearly depend on the three parameters α, δ, ϵ. In a previous paper (1)[3] upper and lower bounds for the first two frequencies, $\beta^{(1)}$ and $\beta^{(2)}$, were determined as functions of α and ϵ, δ being taken to be zero. In the current work the effect on these bounds produced by a variation in δ is studied.

Variational Theorems

Before proceeding further, it is convenient to state without proof several well-known results which will be useful later. The eigenvalues β of the boundary-value problem, Equations [2], [3], [4], can be characterized by a minimum principle involving functionals of the following form

$$D(w, t) = \int_\delta^1 \left[w''t'' + \frac{\alpha^2}{2}(1 - x^2)w't'\right]dx + \frac{1}{\epsilon}w'(\delta)t'(\delta) \quad [5]$$

$$H(w, t) = \int_\delta^1 wt\,dx \quad [6]$$

The notation $D(w)$ will be used to denote $D(w, w)$ and similarly for $H(w)$. The following minimum principle can then be proved.

Let W be the class of functions w having continuous first derivatives, piecewise continuous second derivatives, and satisfying $w(\delta) = 0$. Then of all functions w belonging to W, that one which minimizes $D(w)$, subject to the side conditions $H(w) = 1$ and $H(w, w^{(i)}) = 0$, $i = 1, \ldots, n-1$, is the nth eigenfunction of the System [2], [3], [4]. The minimum value of $D(w)$ is the corresponding nth eigenvalue, ordered in increasing size, and denoted by $\beta^{(n)2}$. The functions $w^{(i)}$, $i = 1, \ldots, n-1$ are the first $n-1$ eigenfunctions.

Courant's maximum-minimum principle (2) can then be used to establish the Rayleigh-Ritz-Galerkin technique for the calculation of upper bounds for eigenvalues. This procedure makes use of a trial function

$$w = a_1\varphi_1 + \ldots + a_n\varphi_n$$

[1] This research has been supported by the United States Air Force through the Office of Scientific Research of the Air Research and Development Command. The material in this paper forms part of a thesis submitted in partial fulfillment of the requirements for the degree of Doctor of Philosophy at Carnegie Institute of Technology.

[2] Research Associate, Division of Applied Mathematics, Brown University.

Contributed by the Applied Mechanics Division and presented at the Diamond Jubilee Annual Meeting, Chicago, Ill., November 13–18, 1955, of The American Society of Mechanical Engineers.

Discussion of this paper should be addressed to the Secretary, ASME, 29 West 39th Street, New York, N. Y., and will be accepted until July 10, 1956, for publication at a later date. Discussion received after the closing date will be returned.

Note: Statements and opinions advanced in papers are to be understood as individual expressions of their authors and not those of the Society. Manuscript received by ASME Applied Mechanics Division, April 11, 1955. Paper No. 55—A-44.

[3] Numbers in parentheses refer to the Bibliography at the end of the paper.

where the φ_i are members of W and the a_i are undetermined constant coefficients. Inserting w into the minimum principle (disregarding the orthogonality requirements) and minimizing with respect to the a_i leads to an algebraic nth-order eigenvalue problem. This gives rise to an nth-degree polynomial characteristic equation having n real roots. It can be shown (3) that each successive root is an upper bound to the corresponding eigenvalue, up to the nth.

Finally Courant-Hilbert (4) give the following useful result. Let $\varphi_1, \ldots, \varphi_n$ be functions belonging to W and satisfying

$$H(\varphi_i) = 1, \quad H(\varphi_i, \varphi_j) = 0, \; i \neq j$$

Then

$$\beta^{(1)2} + \ldots + \beta^{(n)2} = \min_{\varphi_i} [D(\varphi_1) + \ldots + D(\varphi_n)]$$

where the minimum is taken over all admissible sets of functions.

Variation of $\beta^{(n)}$ With δ

Qualitatively, the variation of $\beta^{(n)}$ as a function of δ may be expressed quite simply. If all other parameters are held fixed and δ is increased, then $\beta^{(n)}$ does not decrease; conversely, if δ is decreased, then $\beta^{(n)}$ does not increase.

The proof depends on the maximum-minimum characterization of $\beta^{(n)}$. Admissible functions for the problem associated with a beam of hub radius δ may be extended into the region $0 \leq x \leq \delta$ so as to become admissible functions for the problem associated with a beam of zero hub radius. By proper manipulation it can be shown that the eigenvalues of the latter problem are no larger than those of the former. An extension of the proof for the general case is obvious. A detailed discussion will not be given since these results are not so useful as those to be given later.

Precise determination of the eigenvalues is generally possible only at the price of extended numerical calculations, so the quantitative relation between $\beta^{(n)}$ and δ is best ascertained approximately by means of upper and lower bounds on $\beta^{(n)}$ which can be found with comparative ease.

Numerous methods are available which give upper bounds on the eigenvalues. The Rayleigh-Ritz-Galerkin technique is perhaps the simplest when bounds on only the first few eigenvalues are desired.

A method for finding lower bounds originates in the variational representation of $\beta^{(n)}$, that is

$$\beta^{(n)2} = \min_{w \in W} \int_\delta^1 \left[w''^2 + \frac{\alpha^2}{2}(1 - x^2)w'^2 \right] dx + \frac{1}{\epsilon}[w'(\delta)]^2 \quad \ldots\ldots [7]$$

under the side restrictions

$$H(w) = 1 \text{ and } H(w, w^{(i)}) = 0, \quad i = 1, \ldots, n-1$$

The right-hand side of Equation [7] can be broken into two parts and each considered as a separate minimum problem. First let

$$\mu^{(n)2} = \min_{w \in W} \int_\delta^1 w''^2 dx + \frac{1}{\epsilon}[w'(\delta)]^2 \ldots\ldots [8]$$

subject to the conditions $H(w) = 1$ and orthogonality conditions of the usual form, but involving the eigenfunctions of this problem. By familiar methods of the calculus of variations, it can be shown that Equation [8] is equivalent to the boundary-value problem

$$w^{iv} = \mu^2 w$$

$$w(\delta) = 0, \quad w'(\delta) - \epsilon w''(\delta) = 0$$

$$w''(1) = 0, \quad w'''(1) = 0$$

Introducing the new variable

$$s = \frac{x - \delta}{1 - \delta}$$

this boundary-value problem becomes

$$\frac{d^4w}{ds^4} = \mu^2(1 - \delta)^4 w$$

$$w(0) = 0, \quad \frac{dw}{ds}(0) - \epsilon \frac{d^2w}{ds^2}(0) = 0$$

$$\frac{d^2w}{ds^2}(1) = 0, \quad \frac{d^2w}{ds^3}(1) = 0$$

whose eigenvalues have been tabulated for certain values of ϵ (1). The successive values of $\mu^{(n)2}$ can then be found at once.

Now let

$$\nu^{(n)2} = \min_{w \in W} \int_\delta^1 \frac{\alpha^2}{2}(1 - x^2)w'^2 dx \ldots\ldots [9]$$

subject to the conditions $H(w) = 1$ and orthogonality conditions analogous to the previous ones. Again employing the methods of variational calculus, the differential equation

$$[(1 - x^2)w']' + 2\frac{\nu^2}{\alpha^2} w = 0$$

results, together with the natural boundary condition that w have less than a logarithmic singularity at $x = 1$ and the assigned boundary condition that $w(\delta) = 0$.

If

$$2\frac{\nu^2}{\alpha^2} = \rho(\rho + 1)$$

then the differential equation is Legendre's equation and the solutions are Legendre functions $P_\rho(x)$, which may be written as infinite power series in x. For $\delta = 0$ the series terminate and the solutions are the odd Legendre polynomials, the even polynomials being eliminated by the boundary condition at $x = 0$. In this case ρ is an odd integer. For $\delta \neq 0$, but small, the series do not terminate and the solutions are Legendre functions whose orders differ slightly from the odd positive integers. In this case the values of ρ and hence of ν^2 may be found from a study of the zeros of $P_\rho(x)$.

To find the value of ρ corresponding to a given value of δ, it is necessary to determine the order of the Legendre function which vanishes at $x = \delta$. First, write $P_\rho(x)$ as a power series

$$P_\rho(x) = 1 + \sum_{n=1}^{\infty} a_n \rho^n$$

whose coefficients are functions of x. Gray (5) has given expressions for the expansion coefficients a_n which are valid for small ρ. Since values of ρ near the odd positive integers are of interest, it is convenient to write

$$\rho = n + \sigma \ldots\ldots [10]$$

where n is an odd positive integer and σ is small. Then, by the recurrence formula for Legendre functions

$$P_{n+\sigma}(x) = \frac{2n - 1 + 2\sigma}{n + \sigma} x P_{n-1+\sigma}(x) - \frac{n - 1 + \sigma}{n + \sigma} P_{n-2+\sigma}(x)$$

$P_\rho(x)$ may be expressed in terms of $P_\sigma(x)$, for which the series expansion in terms of σ is valid. Truncating the series at a suitable term, substituting the proper value of x, and solving the resulting polynomial equation yields the desired value of σ and hence of ρ.

The characterization of the sum of the first n eigenvalues, previously given, states that for all values of n

$$\beta^{(1)2} + \ldots + \beta^{(n)2} = \min_{\varphi_i} [D(\varphi_1) + \ldots + D(\varphi_n)] \ldots [11]$$

where the set φ_i is orthonormalized and each of its members belongs to W. Then

$$\beta^{(1)2} + \ldots + \beta^{(n)2} \geq \min_{\varphi_i} \left\{ \int_\delta^1 \varphi_1''^2 dx + \frac{1}{\epsilon} [\varphi_1'(\delta)]^2 + \ldots + \int_\delta^1 \varphi_n''^2 dx + \frac{1}{\epsilon} [\varphi_n'(\delta)]^2 \right\}$$

$$+ \min_{\varphi_i} \left\{ \int_\delta^1 \frac{\alpha^2}{2} (1 - x^2)\varphi_1'^2 dx + \ldots + \int_\delta^1 \frac{\alpha^2}{2} (1 - x^2)\varphi_n'^2 dx \right\}$$

The first term on the right is the sum of the first n eigenvalues $\mu^{(1)2}, \ldots, \mu^{(n)2}$ of a uniform nonrotating beam, while the second term is the sum of the first n eigenvalues $\nu^{(1)2}, \ldots, \nu^{(n)2}$ of the Legendre equation. Hence

$$\beta^{(1)2} + \ldots + \beta^{(n)2} \geq \mu^{(1)2} + \ldots + \mu^{(n)2} + \nu^{(1)2} + \ldots + \nu^{(n)2} \ldots [12]$$

Upper and lower bounds can now be found for each eigenvalue in turn. For $n = 1$, Inequality [12] becomes

$$\beta^{(1)2} \geq \mu^{(1)2} + \nu^{(1)2} \ldots [13]$$

This is a relation of a sort first given by Southwell (6). In his development Southwell does not mention boundary conditions, but adds the finiteness requirement at $x = 1$ as an additional restriction. It is seen here to arise as a natural boundary condition. The Southwell method may be extended in the following way so as to provide lower bounds for the higher frequencies.

For $n = 2$, Inequality [12] becomes

$$\beta^{(1)2} + \beta^{(2)2} \geq \mu^{(1)2} + \mu^{(2)2} + \nu^{(1)2} + \nu^{(2)2}$$

Denoting by $\beta^{*(1)2}$ the upper bound for $\beta^{(1)2}$ found from the Rayleigh-Ritz-Galerkin process, a lower bound for $\beta^{(2)2}$ is given by the inequality

$$\beta^{(2)2} \geq \mu^{(1)2} + \mu^{(2)2} + \nu^{(1)2} + \nu^{(2)2} - \beta^{*(1)2} \ldots [14]$$

This stepwise procedure may be continued indefinitely, though presumably with decreasing accuracy and increasing labor required for the computation of the successive upper bounds.

This technique is applicable to a rather general class of problems, as it is valid whenever the basic minimum principles hold. Its practical utility depends to a large extent upon the ease with which the subsidiary problems may be solved. Another aspect of the problem at hand has already been approached in this manner (1).

Numerical Calculation and Conclusions

Upper and lower bounds have been computed for $\beta^{(1)}$ and $\beta^{(2)}$ for the case $\epsilon = 0$ for several values of α^2. This corresponds to a beam cantilevered at the fixed end and rotating at various speeds. The boundary conditions at $x = \delta$ then are $w(\delta) = 0$, and $w'(\delta) = 0$; the boundary term in $D(w)$ vanishes. Also, the admissible functions for the minimum principle must be subject to the further restriction $w'(\delta) = 0$. The values of δ used in the computations are $\delta = 0.005, 0.01, 0.02, 0.05$, and 0.10. The case $\delta = 0$ has been considered earlier (1).

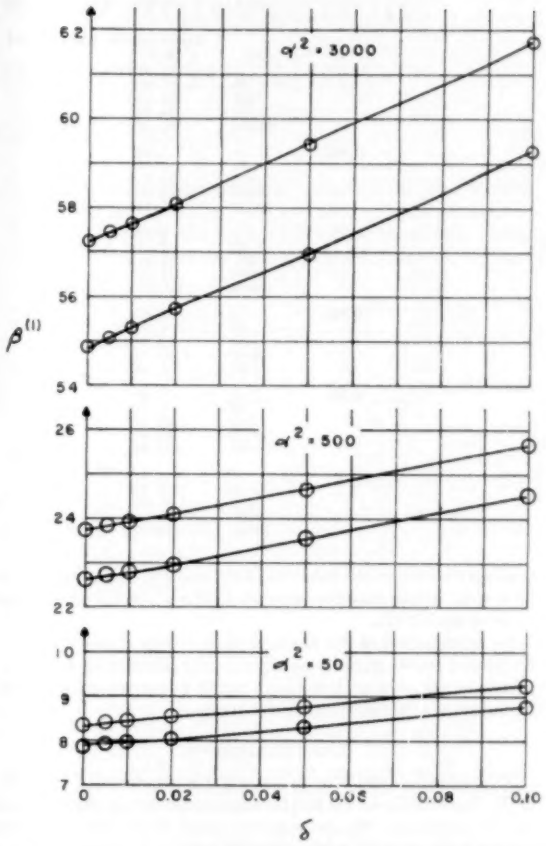

Fig. 1 Variation of Frequency $\beta^{(1)}$ With the Hub Radius δ for Fixed Values of Rotation Parameter α^2

(For each value of α^2 upper and lower curves correspond to upper and lower bounds on $\beta^{(1)}$, respectively.)

The Rayleigh-Ritz-Galerkin technique has been used to compute upper bounds with

$$w = (x - \delta)^4 + a(x - \delta)^4 - 2[2a(1 - \delta) + 5(1 - \delta)^2] (x - \delta)^3 + 2[3a(1 - \delta)^3 + 10(1 - \delta)^3](x - \delta)^2$$

as the trial function. The parameter a is determined from the minimizing condition which yields upper bounds on the first two frequencies.

Lower bounds were computed from Equations [13] and [14] as outlined in the preceding section. The series for $P_\sigma(x)$ was cut off at the second-degree term, yielding a cubic equation in σ for the first eigenvalue and a fifth-degree equation for the second eigenvalue. These were solved by iteration and ρ then found from Equation [10]. The results appear in Table 1. In addition, there is a typical graph of $\beta^{(1)}$ versus δ for fixed values of α^2, Fig. 1.

A study of the tabulated data reveals that $\beta^{(1)}$ and $\beta^{(2)}$ depend on δ in a very nearly linear fashion, at least for $0 \leq \delta \leq 0.10$. This is

TABLE 1 UPPER AND LOWER BOUNDS FOR $\beta^{(1)}(\alpha,\delta)$ AND $\beta^{(2)}(\alpha,\delta)$

δ	α^2	Lower bound for $\beta^{(1)}$	Upper bound for $\beta^{(1)}$	Per cent of gap to mean	Lower bound for $\beta^{(2)}$	Upper bound for $\beta^{(2)}$	Per cent of gap to mean
0	0	3.516	3.516	...	22.034	22.725	3.089
	50	7.897	8.375	5.875	27.887	29.024	3.994
	500	22.635	23.736	4.749	58.604	61.667	5.094
	3000	54.885	57.253	4.223	134.981	142.393	5.344
	10000	100.062	104.285	4.133	244.177	257.688	5.384
0.005	0	3.551	3.551	...	22.256	22.935	3.005
	50	7.936	8.414	5.847	28.098	29.222	3.922
	500	22.724	23.827	4.738	58.854	61.904	5.051
	3000	55.093	57.463	4.211	135.452	142.843	5.312
	10000	100.439	104.665	4.120	244.998	258.474	5.366
0.01	0	3.587	3.587	...	22.481	23.171	3.023
	50	7.976	8.454	5.819	28.311	29.444	3.924
	500	22.813	23.916	4.724	59.107	62.162	5.038
	3000	55.302	57.671	4.194	135.928	143.325	5.298
	10000	100.818	105.046	4.108	245.828	259.315	5.340
0.02	0	3.661	3.661	...	22.942	23.620	2.912
	50	8.058	8.535	5.749	28.748	29.865	3.811
	500	22.993	24.100	4.701	59.620	62.651	4.957
	3000	55.724	58.096	4.167	136.887	144.237	5.229
	10000	101.583	105.810	4.076	247.498	260.901	5.272
0.05	0	3.895	3.895	...	24.414	25.164	3.025
	50	8.310	8.791	5.625	30.141	31.323	3.846
	500	23.538	24.674	4.712	61.220	64.344	4.975
	3000	56.994	59.426	4.177	139.830	147.378	5.256
	10000	103.886	108.215	4.081	252.605	266.362	5.301
0.10	0	4.340	4.340	...	27.202	28.004	2.905
	50	8.782	9.256	5.255	32.782	34.031	3.738
	500	24.530	25.678	4.572	64.148	67.460	5.033
	3000	59.297	61.732	4.023	145.056	153.085	5.386
	10000	108.058	112.383	3.923	261.611	276.254	5.444

in sharp contrast to the behavior of $\beta^{(1)}$ and $\beta^{(2)}$ as functions of ϵ, for $\delta = 0$; in that case the variation of β was concentrated in the range of small ϵ (1).

An examination of the slopes of these curves shows that, as a function of α^2, the slopes remain practically constant for small and moderate values of α^2, but have a nearly linear dependence on α for values of α^2 larger than several hundred.

Acknowledgments

The author would like to express his appreciation to Prof. G. H. Handelman for his helpful suggestions during the course of this investigation. He also wishes to thank Miss Carol Trammell for her help with the computational work.

BIBLIOGRAPHY

1 "Vibrations of Rotating Beams of Constant Section," by William E. Boyce, R. C. DiPrima, and G. H. Handelman, Proceedings of the Second U. S. National Congress of Applied Mechanics, 1954.

2 "Methods of Mathematical Physics, Vol. 1," by R. Courant and D. Hilbert, Interscience Publishers, Inc., New York, N. Y., 1953, p. 405.

3 "Eigenwertprobleme und ihre numerische Behandlung," by Lothar Collatz, Chelsea Publishing Company, New York, N. Y., 1948, p. 236.

4 Loc. cit., R. Courant and D. Hilbert, p. 459.

5 "Legendre Functions of Fractional Order," by Marion C. Gray, *Quarterly of Applied Mathematics*, vol. 11, 1953, pp. 311–318.

6 "The Vibrations of a Spinning Disc," by H. Lamb and R. V. Southwell, Proceedings of the Royal Society of London, series A, vol. 99, 1921, pp. 272–280.

A Method of Stepwise Integration in Problems of Impact Buckling

By A. F. SCHMITT,[1] LAFAYETTE, IND.

The equations for the dynamic buckling of an axially impacted column are discussed. A method is presented for the calculation of approximate load and deflection variations in problems of high-velocity impact. The method may be extended for cases wherein the stresses exceed the elastic limit. Results of calculations are presented for two cases. In one of these, agreement with a previous exact solution is found to be good.

Introduction

THE analyses available in the literature for the problem of dynamic-column instability may be divided into two classes: (*a*) Those in which an impulsive load of constant-known magnitude is applied for a specified period (1, 2).[2] (*b*) Those in which the ends of the column are assumed to be displaced axially at a uniform rate (3). In each case referred to, the speed of propagation of longitudinal waves is assumed to be instantaneous so that the load is uniform throughout the column at any given time. In addition, elastic behavior is assumed.

In the course of an experimental program testing the dynamic failure of structural elements, another analysis was sought to explain the results obtained in the impact buckling of columns. The analyses referred to proved inadequate in applications employing impact velocities in excess of 20 fps upon columns of usual proportions.

Analysis

In the axial impact of a mass on a slightly bowed column, Fig. 1, the end of the column is displaced axially at a nonuniform rate. For many practical problems the ratio of impacting mass to specimen mass is great enough so that the impacting mass velocity may be taken constant. The column load then builds up by a series of reflections, the longitudinal wave traveling back and forth in the column. The result at each column station is a load which is stepwise increasing with time. An increment in particle velocity is related to an increment in stress level by (4)

$$\Delta V = \Delta \int_0^{\sigma} \frac{d\sigma}{\sqrt{\rho E_t}} \quad \ldots\ldots [1]$$

where ρ is the material density and E_t is the tangent modulus. In the elastic range this relation becomes

$$\Delta V = \frac{\Delta \sigma}{\sqrt{\rho E}} \quad \ldots\ldots [1a]$$

ΔV, the particle velocity increment, is equal to the relative velocity between the impacting mass and the impacted column end. While the load-time history is similar at each column station, differences exist due to the finite velocity of travel of the longitudinal waves, Fig. 1.

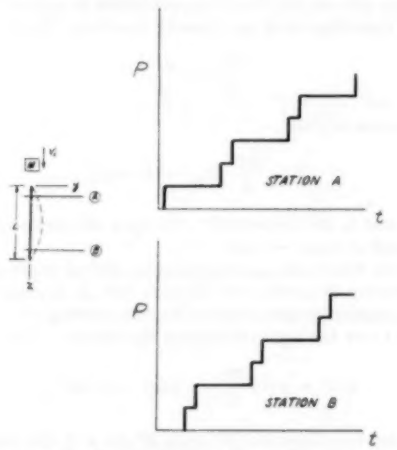

Fig. 1 Load-Time Histories at Two Stations of an Axially Impacted Column

Under the usual assumptions of small displacements and uniform properties, and neglecting rotary and shear inertias, the differential equation for the lateral deflections y at station x of an axially loaded column is

$$EI \frac{\partial^4 y}{\partial x^4} + \frac{\partial}{\partial x}\left(P \frac{\partial y}{\partial x}\right) + \rho A \frac{\partial^2 y}{\partial t^2} = EI \frac{\partial^4 y_0}{\partial x^4} \quad \ldots\ldots [2]$$

where EI is the flexural stiffness and A the cross-sectional area; y_0 is the initial imperfection and P is the axial load. Rewritten this becomes

$$EI \frac{\partial^4 y}{\partial x^4} + P \frac{\partial^2 y}{\partial x^2} + \frac{\partial y}{\partial x} \frac{\partial P}{\partial x} + \rho A \frac{\partial^2 y}{\partial t^2} = EI \frac{\partial^4 y_0}{\partial x^4} \quad \ldots [3]$$

The term $\partial P/\partial x$ is zero at all points of the column except the longitudinal wave front where it is very great. Then at the wave front, since in general $\partial y/\partial x$ is not zero, the other terms likewise must be large. The wave front is thus a constant source of new traveling flexural waves. The situation has been well described by Taub (5).

The problem of traveling flexural waves may be dismissed by the observation that the velocity of propagation of longitudinal waves is great enough in comparison with those of flexural waves so that the lateral deflections are (practically) excited simultaneously at each station rather than successively, thus resulting in standing flexural waves. This is equivalent to the assumption of a uniform column load at all stations; i.e., $\partial P/\partial x = 0$ everywhere.

---

[1] Instructor of Aeronautical Engineering, Purdue University.

[2] Numbers in parentheses refer to the Bibliography at the end of the paper.

Contributed by the Applied Mechanics Division and presented at the Diamond Jubilee Annual Meeting, Chicago, Ill., November 13–18, 1955, of The American Society of Mechanical Engineers.

Discussion of this paper should be addressed to the Secretary, ASME, 29 West 39th Street, New York, N. Y., and will be accepted until July 10, 1956, for publication at a later date. Discussion received after the closing date will be returned.

Note: Statements and opinions advanced in papers are to be understood as individual expressions of their authors and not those of the Society. Manuscript received by ASME Applied Mechanics Division, December 20, 1954. Paper No. 55—A-37.

Return now to the picture of the stepwise load build-up at each station. The height of each load increment per wave cycle is

$$\Delta P = 2A\Delta\sigma = \frac{2AE}{a}\left(V_i - \frac{d\delta}{dt}\right)$$

where V_i is the impact velocity, a is the velocity of longitudinal wave travel, and δ is the axial displacement of the impacted end of the column. Since the period of one wave cycle is $\Delta t = 2L/a$, one has

$$\frac{\Delta P}{\Delta t} = \frac{AE}{L}\left(V_i - \frac{d\delta}{dt}\right) \quad \ldots\ldots\ldots\ldots [4]$$

If now the velocity of impact is small enough so that the load increments ΔP are fine, then it is permissible to approximate the stepwise load-time curve by a smooth function. Thus let

$$\frac{\Delta P}{\Delta t} \doteq \frac{dP}{dt}$$

and integrate to yield

$$P = \frac{AE}{L}\left[V_i t - (\delta - \delta_0)\right] \quad \ldots\ldots\ldots\ldots [5]$$

where δ and δ_0 are, respectively, the axial displacements of the column end at time $t = t$ and $t = 0$.

This last step is also accomplished by letting the longitudinal wave velocity a become very large so that Δt approaches zero. This assumption is again compatible with putting $\partial P/\partial x = 0$.

Assume now the deflected form of the column. Let

$$y(x) = y \sin\frac{\pi x}{L}; \qquad y_0(x) = y_0 \sin\frac{\pi x}{L} \quad \ldots\ldots\ldots [6]$$

Substituted into Equation [3], with $\partial P/\partial x = 0$, this yields

$$\left.\begin{aligned} &\frac{d^2y}{d\tau^2} + \Omega\left(1 - \frac{P}{P_e}\right)y = \Omega y_0 \\ &\text{where} \\ &\Omega = \pi^2\left(\frac{a}{V_i}\right)^2 \epsilon_e^2 \\ &P_e = \frac{\pi^2 EI}{L^2} \end{aligned}\right\} \quad \ldots\ldots\ldots [7]$$

and the independent variable is now

$$\tau = \frac{V_i}{L\epsilon_e}\, t$$

Here

$$\epsilon_e = \frac{P_e}{AE}$$

Further, with the assumed shape, one may evaluate

$$\delta - \delta_0 = \frac{\pi^2}{4L}(y^2 - y_0^2)$$

Substituted into Equation [5] and then Equation [7] one gets

$$\frac{d^2f}{d\tau^2} + \Omega[(1-\tau)f - e + \frac{1}{4}(f^3 - e^3f)] = 0 \quad \ldots\ldots [8]$$

where f and e are y and y_0, respectively, nondimensionalized by the radius of gyration of the cross section.

Equation [8] was obtained by Hoff (3) and was solved in series form. The solution there obtained showed that the motion of a column loaded as assumed—uniform displacement of the ends at a moderate rate—is composed of two movements. The motion is that of the steady outward bowing experienced in a static test with an oscillatory motion superposed.

The foregoing analysis is valid only so long as the use of a smooth curve to replace the stepwise load variation is permissible. An approximate index of the range of validity of this analysis is the number of cycles (N) of the impact wave which may occur between the time of impact and the time at which the static Euler load is reached. If P_i is the load developed at initial impact then the number of cycles required is given by

$$N = P_e/2P_i$$

since the axial load increases by $2P_i$ per cycle due to reflections of the wave. Now for columns of practical size and proportions impacted at velocities of 10 mph or more, N will seldom exceed 4 or 5 and will be more nearly 1 or 2. Consequently, any analysis which explains behavior in this range cannot avoid the stepwise nature of the loading. In addition, the stresses are certain to exceed the elastic limit and account must be taken of this fact. To handle the problem of a traveling step load, an integration of the partial differential equation, Equation [2], would appear necessary.

The foregoing difficulties may be avoided and the major result—knowledge of the load-displacement-time relationship in the early loading stages—obtained by the following approximate method.

Assume that any one load step, as it leaves the end of the column, instantly covers the full column length for a period equal to the time this wave would require to travel the column length. A reflection then occurs and again the new total load is applied to the entire column for a like period. Envisioning this action it seems not implausible to assume a half-sine-wave shape, thus reducing the problem to a step-by-step integration of an ordinary differential equation with constant coefficients. In addition, the sine-wave shape is that shape for which the critical load is lowest. Thus, for monotonically increasing loading, the resulting deflections will form an upper bound to the actual column action.

For columns wherein the elastic limit is exceeded, the method encounters no difficulty provided an effective elastic modulus is used where appropriate. Here, however, the use of a half-sine-wave deflected shape may be open to question as plastic columns tend to kink. The possible use of other deflected forms is subject to investigation.

Now adopt the scheme for solution just described. During the period of travel of any one load increment Equation [7] applies (since $\partial P/\partial x = 0$) and has, moreover, constant coefficients. The solutions for the mid-column displacement and velocity at the end of the nth traverse of the longitudinal wave in terms of the corresponding quantities at the end of the n-1st passage are

$$\begin{aligned} y_n = {} & y_{n-1}\cos\omega_n\lambda_n(t_n - t_{n-1}) \\ & + \frac{y_{n-1}'}{\omega_n\lambda_n}\sin\omega_n\lambda_n(t_n - t_{n-1}) \\ & + \frac{y_0}{\lambda_n^2}\left[1 - \cos\omega_n\lambda_n(t_n - t_{n-1})\right] \quad \ldots\ldots [9] \end{aligned}$$

$$\begin{aligned} y_n' = {} & -y_{n-1}\omega_n\lambda_n\sin\omega_n\lambda_n(t_n - t_{n-1}) \\ & + y_{n-1}'\cos\omega_n\lambda_n(t_n - t_{n-1}) \\ & + \frac{y_0\omega_n}{\lambda_n}\sin\omega_n\lambda_n(t_n - t_{n-1}) \quad \ldots\ldots [10] \end{aligned}$$

where

$$\lambda = \sqrt{1 - P/P_e}$$

$$\omega t = \sqrt{\Omega}\,\tau$$

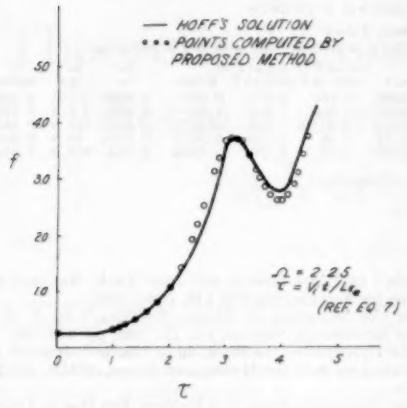

FIG. 2 LATERAL MID-SPAN DEFLECTION OF AN IMPACTED ELASTIC COLUMN VERSUS TIME BY TWO METHODS

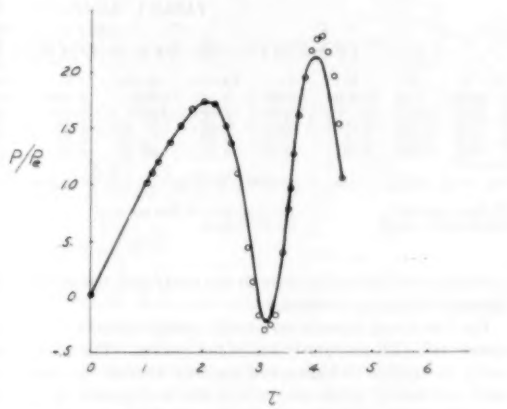

FIG. 3 COLUMN-LOAD VARIATION VERSUS TIME AS COMPUTED BY TWO METHODS

and t is real time. The quantities λ_n and ω_n are the quantities associated with the load P_n and which quantities will vary with the effective modulus of the material. Note, that when $P/P_e > 1$, the parameter λ is imaginary and the appropriate changes from trigonometric to hyperbolic functions must be made.

The method of calculation is now clear. Begin with assumed values of the initial imperfection (y_0) and initial velocity (y_0', probably zero). With the load P_1 corresponding to the stress level of the first wave down the column one evaluates all the parameters ω_1, λ_1, and the sonic velocity a_1. Put $t_{n-1} = t_0 = 0$ and $t_n = t_1 = L/a_1$. Solve Equations [9] and [10] for y_1 and y_1'. These are approximate values of the mid-span deflection and velocity at the end of the first wave passage. The wave is now assumed to be completely reflected, the stress increment being given by Equations [1] or [1a], and resulting in a load P_2. Again all parameters are evaluated and $t_n - t_{n-1}$ is put equal to L/a_2 so that y_2 and y_2' may be computed. The process is repeated; the deflections and velocities thus found forming approximations to the true column behavior.

One additional point: At the end of each period t_n, for n even, before computing the new load P_{n+1}, one computes

$$\Delta V = V_i - d\delta/dt = V_i - \pi^2 y_n y_n'/2L$$

This same value of ΔV also applies for the wave reflection immediately following when n goes from odd to even.

EXAMPLES

Two problems are worked by the method: First an impact problem wherein the stresses are entirely elastic owing to the great slenderness ratio and low impact velocity. The second is a high-velocity impact on a column of usual proportions wherein the stresses quickly exceed the elastic limit.

Case 1. The same problem was taken for calculation as was used by Hoff (3) so that the solutions might be compared. The results are shown in Figs. 2 and 3. The parameters could be obtained by impact at a velocity of 0.256 ips upon a steel column of slenderness ratio 370. Hoff's solution, which is exact under the assumptions discussed in obtaining Equation [8], is shown by the solid line. The circles represent points calculated by the stepwise method proposed herein. It should be noted that the points shown represent only a few of those calculated. In all, over 300 traverses of the longitudinal wave (and as many points) were calculated to cover the range of nondimensional time shown. Lest it be thought that this number of steps represents a formidable work barrier, it should be reported that all the work was performed by a slow-speed digital computer in less than 2 hr.

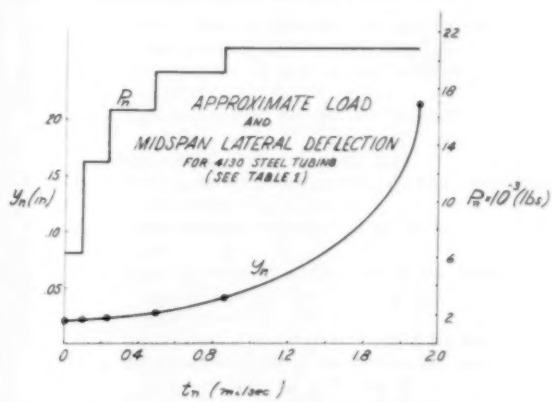

FIG. 4 COLUMN BEHAVIOR UNDER HIGH-VELOCITY IMPACT AS COMPUTED BY PROPOSED METHOD

In comparing solutions it may be seen that the solution by the proposed method swings above Hoff's while the load is increasing. This overshoot ultimately causes the axial load to undershoot Hoff's on the first swing, in turn producing a lower deflection on the first oscillation in the deflection.

Case 2. A complete calculation for a steel-tube column similar to those tested in an experimental program is shown in Table 1. The results are plotted in Fig. 4. In this case the impact velocity was great enough to produce a load which exceeded the Euler load and stresses which went above the yield stress after only a few reflections of the longitudinal wave. Note that in the table corrections are applied to P_e, ω, and a for the reduction in effective modulus. The values of $\Delta\sigma$ were calculated with the aid of a plot of Equation [1] prepared for the particular alloy and not shown here.

CONCLUSIONS

A method of stepwise integration has been presented to permit

TABLE 1 SAMPLE CALCULATIONS y VERSUS t; P VERSUS t

4130 Chrome-Molybdenum Alloy-Steel Tube

$D = 1^1/_4$; $t = 0.058$; $L/\rho = 50$; $P_e = 24{,}850$ lb; $\omega = 1890$ sec^{-1}; $y_0 = 0.02$ in.; $y_0' = 0$; $V_i = 207.5$ ips

n	σ	P_n, lb	E_t	P_{en}	P_n/P_{en}	a_n, ips	λ_n	ω_n, sec^{-1}	T_n, milsec	y_{n-1}	$\cos \omega\lambda T$ or $\cosh \omega\lambda T$	$\sin \omega\lambda T$ or $\sinh \omega\lambda T$	$E/\lambda_n{}^3$	y_n, in.	y_n', ips	t_n, milsec	ΔV
1	30K	6520	30×10^6	24800	0.262	200K	0.860	1890	0.105	0.0200	0.986	0.170	0.027	0.0201	1.9	0.105	207.5
2	60K	13000	16	13240	0.984	146K	0.128	1380	0.144	0.0201	0.999	0.025	1.22	0.0206	7.3	0.249	207.5
3	77K	16700	5.5	4560	3.67	85.6K	1.63(i)	809	0.245	0.0206	1.05	0.326	0.0075	0.0274	19.8	0.495	207.5
4	89K	19300	2.5	2070	9.30	56.8K	2.84	537	0.370	0.0274	1.16	0.590	0.0025	0.0398	49.8	0.864	207.5
5	97K	21000	0.30	250	84.6	20.0K	9.15	189	1.05	0.0398	3.17	3.00	0.0002	0.213	365.0	1.910	207.5

$P_{en} = (E_t/E)P_e$ $\quad a_n = 200{,}000\sqrt{E_t/E}$ ips $\quad \omega_n = \omega\sqrt{E_t/E}$ sec^{-1} $\quad \lambda_n{}^2 = 1 - (P_n/P_{en})$

E_t from material stress-strain curve $\quad$ $\Delta\sigma$ from plot of Equation [1] for 4130 steel $\quad$ $t_n = \Sigma T_n$

calculation of approximations to the loads and deflections in the dynamic buckling of columns.

For low-speed impacts on purely elastic columns the solution agrees well with previously computed results. The method may easily be applied to high-speed impacts wherein the stresses exceed the elastic range and where the assumption of infinitely great longitudinal wave velocity may not be appropriate.

BIBLIOGRAPHY

1 "Impact Buckling of Thin Bars in the Elastic Range Hinged at Both Ends," by Carel Koning and Josef Taub, National Advisory Committee for Aeronautics, TM 748, June, 1934.

2 "On the Dynamics of Elastic Buckling," by J. H. Meier, *Journal of Aeronautical Sciences*, vol. 12, 1945, pp. 433–440.

3 "The Dynamics of the Buckling of Elastic Columns," by N. J. Hoff, JOURNAL OF APPLIED MECHANICS, Trans. ASME, vol. 73, 1951, pp. 68–74.

4 "The Permanent Strain in a Uniform Bar Due to Longitudinal Impact," by M. P. White and LeVan Griffis, Office of Scientific Research and Development, Report No. 742, 1942.

5 "Impact Buckling of Thin Bars in the Elastic Range for Any End Condition," by J. Taub, National Advisory Committee for Aeronautics, TM 749, July, 1934.

Theoretical Considerations of Combined Thermal and Mass Transfer From a Vertical Flat Plate

By E. V. SOMERS,[1] EAST PITTSBURGH, PA.

In free-convective processes involving both thermal and mass transfer, since the driving force for the fluid motion has its source solely in the density difference from ambient, it is necessary to consider the thermal and mass-transfer processes simultaneously in solving any given problem. The present problem involves evaporation and condensation phenomena associated with free-convective thermal and mass transfer from a wetted isothermal vertical flat plate to a gas at an ambient temperature and mass concentration different from that on the plate. This problem presents itself in the practical case of vaporization cooling of equipment without forced circulation of the ambient gas.

Nomenclature

The following nomenclature is used in the paper:

A = dimensionless coefficient of Nusselt-Grashof correlations

a_i = coefficients of power series representing velocity profile (u/u_x)

b_i = coefficients of power series representing diffusion concentration profile (g)

C = relative concentration of diffusing species in boundary layer, Equation [2]

C_0 = value of C at the wall ($y = 0$)

C_s = value of C at the free-stream edge of the boundary layer ($y = \delta'$)

C', C_0' = $C' = \dfrac{C}{1 - C}$ $\quad C_0' = \dfrac{C_0}{1 - C_0}$

c_p = specific heat at constant pressure of gas in boundary layer, Btu/lb deg F

d_i = coefficients of power series representing thermal profile ($\theta = T/T_s$)

D = diffusion coefficient of evaporating species, (ft²/hr)

f = $f(\eta) = u/u_x$

g = $g(\eta') = C/C_0$, concentration ratio

g_x = gravitational acceleration constant, (ft/hr²)

h = thermal convection coefficient, Equation [50], Btu/hr ft deg F

h_v = mass-convection coefficient, Equation [44], fph

k = ratio of boundary-layer thicknesses, δ'/δ, mass over momentum

k' = ratio of boundary-layer thicknesses, δ''/δ, energy over momentum

m_1 = mass per molecule of species one, the evaporating or condensing species (lb/molecule)

m_2 = mass per molecule of species two, the nonevaporating or noncondensing species (lb/molecule)

N = total number of molecules per unit volume (molecule/ft³)

N_0 = total number of molecules per unit volume at the wall ($y = 0$)

N_s = total number of molecules per unit volume at the free-stream edge of the boundary layer ($y = \delta$)

N_1 = total number of species one molecule per unit volume

N_2 = total number of species two molecules per unit volume

p = static pressure of gas mixture, psf

p_s = static pressure of gas mixture at the free-stream edge of boundary layer, psf

p_0 = vapor pressure of species one at the wall, ($y = 0$), psf

p_{1s} = vapor pressure of species one at the free-stream edge of boundary layer, ($y = \delta$), psf

T = temperature of gas, deg R

T_0 = temperature of gas at the wall, ($y = 0$), deg R

T_s = temperature of gas at the free-stream edge of the boundary layer, ($y = \delta''$), deg R

u = velocity of gas parallel to the plate, fph

u_x ~ maximum velocity of gas parallel to plate, fph

v = velocity of gas normal to the plate, fph

v_0 = velocity of gas normal to plate at wall, ($y = 0$), fph

x = distance co-ordinate parallel to plate, ft

y = distance co-ordinate perpendicular to plate, ft

α = dimensionless coefficient in Nusselt-Grashof correlation, Equation [3]

β = $\dfrac{m_1}{m_2} - 1$, Equation [17]

γ_s = thermal diffusivity of gas at free-stream edge of boundary layer, ($y = \delta$)(ft²/hr)

δ = momentum boundary-layer thickness, ft

δ' = diffusion boundary-layer thickness, ft

δ'' = thermal boundary-layer thickness, ft

η, η', η'' = $\eta = \omega y/x^{1/4}$, Pohlhausen variables for momentum, diffusion, and thermal boundary layers, respectively

θ = $\theta(\eta'') = \dfrac{T}{T_s}$ temperature ratio

κ = $\dfrac{\delta''}{\delta'} \dfrac{\mathrm{Pr}}{\mathrm{Sc}} \kappa'$

κ' = $\sqrt{1 + \dfrac{3C_0'}{2}} - 1$

K = Boltzmann constant, lb ft/molecule deg F

λ = thermal conductivity of gas, Btu/hr ft deg R

---

[1] Research Engineer, Mechanics Department, Westinghouse Research Laboratories.

Contributed by the Applied Mechanics Division and presented at the Diamond Jubilee Annual Meeting, Chicago, Ill., November 13–18, 1955, of The American Society of Mechanical Engineers.

Discussion of this paper should be addressed to the Secretary, ASME, 29 West 39th Street, New York, N. Y., and will be accepted until July 10, 1956, for publication at a later date. Discussion received after the closing date will be returned.

Note: Statements and opinions advanced in papers are to be understood as individual expressions of their authors and not those of the Society. Manuscript received by ASME Applied Mechanics Division, October 20, 1954. Paper No. 55—A-48.

μ = dynamic viscosity of gas, lb/hr ft
ν = kinematic viscosity of gas, ft²/hr
ν_e = kinematic viscosity of gas at free-stream edge of boundary layer, ($y = \delta$), ft²/hr
ρ = gas density, pcf
ρ_0 = gas density at wall, ($y = 0$) pcf
ρ_1 = gas density of species one, pcf
ρ_2 = gas density of species two, pcf
ρ_{10}, ρ_{1e} = gas density of species one at the wall, ($y = 0$), and at free-stream edge of boundary layer, ($y = \delta$), respectively, pcf
ω = Pohlhausen proportionality constant
$\mathrm{Gr}_x = \dfrac{g_x x^3}{D^2} \dfrac{T_0 - T_e}{T_e}$
$\mathrm{Gr}_{ex} = \dfrac{g_x x^3}{D^2} C_0 \left(1 - \dfrac{m_1}{m_2}\right)$
$\mathrm{Gr}_x' = \dfrac{g_x x^3}{D^2}$, here buoyancy force is assumed to be a maximum, so that in evaluating Equations [10] and [22] Spalding assumes $\rho - \rho_e \sim \rho$ and $T_e - T \sim T_e$, respectively, replacing $\dfrac{T_0 - T_e}{T_e}$ by 1.0 in Gr_x
$\mathrm{Nu}_x = \dfrac{h_x}{\lambda}$
$\mathrm{Nu}_{ex} = \dfrac{h_x x}{D}$
$\mathrm{Pr} = \dfrac{c_p \mu}{\lambda}$
$\mathrm{Sc} = \dfrac{\mu}{\rho D}$

Introduction

For Schmidt and Prandtl numbers equaling 1 and at low concentrations of the diffusing gas, Nusselt (1)[3] has given the following relationship for the mass transfer

$$\mathrm{Nu}_{ex} = A(\mathrm{Gr}_x + \mathrm{Gr}_{ex})^{1/4} \quad [1]$$

where A is a constant. Recently, Spalding (2) has derived a relationship for a vertical flat plate with high concentration and temperature differences existing across the boundary

$$\mathrm{Nu}_{ex} = A(\mathrm{Gr}'_x)^{1/4} \quad [2]$$

where A is a variable depending on the concentration difference and Schmidt number of the process. The result reported here is

$$\mathrm{Nu}_{ex} = A(\mathrm{Gr}_x + \alpha \mathrm{Gr}_{ex})^{1/4} \quad [3]$$

where both A and α are functions of the concentration difference, ratio of the ambient and plate temperatures, and Prandtl and Schmidt numbers. For concentrations ranging from low to moderate and for values of the temperature ratio near one, the value of A changes slowly and the value of α can be approximated by $\sqrt{\mathrm{Pr/Sc}}$.

Development of Controlling Equations

The following equations are of importance in the thermal mass-transfer process: Equation of state; continuity equation; momentum equation; diffusion equation; and energy equation (3). Following Pai, each of these will be discussed separately, considering their application to the model, a vertical isothermal flat plate wetted with a liquid at temperature T_0 and at vapor pressure p_0, exposed to a nonmoving gas at ambient temperature T_e and at ambient vapor pressure p_{1e} for the diffusing component, and at pressure p_e. In the vicinity of the plate where thermal and concentration gradients exist, there arises an unbalanced force giving rise to free-convective motion. In this region the Prandtl boundary assumptions (4) are assumed to be valid.

Equation of State. The pressure across the boundary layer is assumed constant, and Dalton's law of partial pressures is valid. We let

N = total number molecules per unit volume
N_1 = total number molecules per unit volume, species one
N_2 = total number molecules per unit volume, species two

where species one represents the evaporating or condensing fluid, and species two represents the nonevaporating or noncondensing fluid. At any point in the boundary layer

$$N = N_1 + N_2 \quad [4]$$

The relative concentration of both species is given by

$$C = \frac{N_1}{N}, \qquad 1 - C = \frac{N_2}{N} \quad [5]$$

With m_1 and m_2 representing the weight per molecule of the two species the gas density can be determined from Equations [4] and [5]

$$\rho = \left\{ \begin{matrix} \rho_1 + \rho_2 \\ m_1 N_1 + m_2 N_2 \\ C m_1 N + (1 - C) m_2 N \end{matrix} \right\} \quad [6]$$

The equation of state is given by

$$p = NKT \quad [7]$$

with N_e and T_e representing the ambient conditions

$$\rho = \frac{N_e T_e}{T} [C m_1 + (1 - C) m_2] \quad [8]$$

Continuity Equation. For two-dimensional steady flow, the equation of continuity, expressing the condition for conservation of mass, is given by

$$\frac{\partial(\rho u)}{\partial x} + \frac{\partial(\rho v)}{\partial y} = 0 \quad [9]$$

Momentum Equation. The equations of motion of the mixture are identical with the Navier-Stokes equations for the steady case, from which it follows that

$$\rho \left(u \frac{\partial u}{\partial x} + v \frac{\partial u}{\partial y} \right) = \mu \frac{\partial^2 u}{\partial y^2} - g_x(\rho - \rho_e) \quad [10]$$

From Equation [8] we evaluate $(\rho - \rho_e)/\rho$ with $C_e = 0$

$$\frac{\rho - \rho_e}{\rho} = 1 - \frac{T}{T_e} \left[1 + C \left(\frac{m_1}{m_2} - 1 \right) \right]^{-1} \quad [11]$$

If the analysis is limited to values of $T/T_e \sim 1.0$ and $C(m_1/m_2 - 1) \ll 1.0$

$$\frac{\rho - \rho_e}{\rho} \sim \left(1 - \frac{T}{T_e}\right) + C \left(\frac{m_1}{m_2} - 1 \right) \frac{T}{T_e} \quad [12]$$

If $C = C_0$ at the wall (vaporization in this case), with $C = \varphi C_0$

$$\frac{\rho - \rho_e}{\rho} \sim \left(1 - \frac{T}{T_e}\right) + \varphi C_0 \frac{T}{T_e} \left(\frac{m_1}{m_2} - 1 \right) \quad [13]$$

For C_e unequal to zero, especially in the case of condensation with $C_e > C_0$

[3] Numbers in parentheses refer to Bibliography at end of paper.

$$\frac{\rho - \rho_e}{\rho} \sim \left(1 - \frac{T}{T_e}\right) + g(C_0 - C_e)\frac{T}{T_e}\left(\frac{m_1}{m_2} - 1\right) \quad [14]$$

where

$$g = \frac{C - C_e}{C_0 - C_e}$$

We will use Equation [13] in the analysis realizing that C_0 can be used in all cases to represent the concentration difference between the wall and the outer edge of the boundary layer, subject to the restrictions

$$\frac{T}{T_e} \sim 1.0 \text{ and } C_0\left(\frac{m_1}{m_2} - 1\right) \ll 1.0$$

The equation of motion now becomes

$$u\frac{\partial u}{\partial x} + v\frac{\partial u}{\partial y} = \gamma\frac{\partial^2 u}{\partial y^2} - g_x\left[\left(1 - \frac{T}{T_e}\right) - gC_0\frac{T}{T_e}\left(1 - \frac{m_1}{m_2}\right)\right] \quad [15]$$

Note that for vaporization using a coolant of heavier molecular weight from that of the ambient gas, with $T_0 > T$, $m_1 > m_2$, and $C_0 > 0$, the thermal and mass forces in the boundary layer oppose each other.

Diffusion Equation. The diffusion equation for the evaporating or condensing species, applicable in the boundary layer, can be written as

$$\frac{\partial}{\partial x}(\rho_1 u) + \frac{\partial}{\partial y}(\rho_1 v) = D\frac{\partial^2}{\partial y^2}(\rho_1) \quad [16]$$

This equation reasonably assumes to be zero all diffusion coefficients other than that for species one diffusing into species two; e.g., the thermal diffusing coefficients and the diffusive drag-coefficients equal zero (5). Substituting into Equation [16], Equations [5] and [9], the latter being the continuity equation, we obtain

$$u\frac{\partial C}{\partial x} + v\frac{\partial C}{\partial y} = D\left(\frac{\beta C + 1}{N}\right)\frac{\partial^2}{\partial y^2}(CN) \quad [17]$$

where $\beta = (m_1/m_2 - 1)$. When the concentration C is small so that $T_e/T \sim 1.0$, and $(\beta C + 1) \sim 1.0$, Equation [17] can be approximated by

$$u\frac{\partial C}{\partial x} + v\frac{\partial C}{\partial y} = D\frac{\partial^2 C}{\partial y^2} \quad [18]$$

Energy Equation. The energy equation for a two-dimensional steady boundary-layer flow, with negligible expansion and viscous dissipation effects, can be written as (3, 5)

$$\rho c_p\left[u\frac{\partial T}{\partial x} + v\frac{\partial T}{\partial y}\right] = \lambda\frac{\partial^2 T}{\partial y^2} \quad [19]$$

Integrated Forms of Controlling Equation

The solution to the thermal mass-transfer problem is derived by considering simultaneously the partial differential equations for momentum, diffusion, and energy transfer, reducing them to three simultaneous nonlinear ordinary differential equations by the Pohlhausen transformation (6).

However, the solution requires excessive numerical computation, and a better approach is obtained by using the von Karman-Pohlhausen approximate method which employs integrated forms of the three transfer equations. The dependent variables u, C, and T, occurring in the integrands, are approximated by polynomials which afford direct integration of the equations. The resulting three simultaneous equations are then solved algebraically for the three parameters introduced into the polynomials, and the approximate solutions of u, C, and T are obtained.

The integral equations are obtained by integrating each of the three equations over the thickness of the boundary layer. We have the following results for our particular problem:

Momentum

$$\frac{d}{dx}\int_0^\delta \rho u^2 dy = g_x\int_0^\delta \rho\left(\frac{T - T_e}{T_e}\right)dy + g_x C_0\left(1 - \frac{m_1}{m_2}\right)\int_0^\delta \rho\frac{T}{T_e}g\,dy - \mu\left(\frac{\partial u}{\partial y}\right)_{y=0} \quad [20]$$

Diffusion

$$\frac{d}{dx}\int_0^{\delta'} ug\frac{T_e}{T}(\beta C_0 g + 1)dy = v_0\frac{T_e}{T_0}(\beta C_0 + 1) - D\left[(1 - \beta^2 C_0^2)\left(\frac{\partial\left(g\frac{T_e}{T}\right)}{\partial y}\right)_{y=0} - 2\int_0^{\delta'}\beta C_0 g\left(\frac{\partial}{\partial y}(\beta C_0 g + 1)\frac{\partial}{\partial y}\left(g\frac{T_e}{T}\right)dy\right)\right] \quad [21]$$

Energy

$$\frac{d}{dx}\int_0^{\delta''}\rho T u\left(1 - \frac{T_e}{T}\right)dy = -\frac{\lambda}{c_p}\left(\frac{\partial T}{\partial y}\right)_{y=0} - v_0\rho_0(T_e - T_0) \quad [22]$$

The boundary-layer thicknesses are designated as δ, δ', and δ'', indicating that they may not be identical; for our problem we will later see that either $\delta = \delta' > \delta''$ or $\delta = \delta'' > \delta'$; i.e., either the energy transfer or the mass transfer occurs entirely within the momentum boundary layer.

From continuity considerations at the wall, the diffusion velocity at the wall v_0 can be determined to be

$$v_0 = -D\left(\frac{C_0}{1 - C_0}\right)\left(\frac{\partial g}{\partial y}\right)_{y=0} = -DC_0'\left(\frac{\partial g}{\partial y}\right)_{y=0} \quad [23]$$

Solution of Transfer Equations

The solution of the transfer equations consists of two steps: (*a*) Representing the dependent variables u, g, and T by polynomials and fitting the polynomials to the boundary conditions; (*b*) integrating the equations and solving the resulting algebraic equations. An illustration of the boundary-layer profiles developed along a vertical wetted wall is shown in Fig. 1.

Polynomial Representation of Velocity, Concentration, and Temperature Profiles. From the Pohlhausen transformation, $\eta = \omega(y/x^{1/4})$, reducing the three partial differential equations to three ordinary differential equations, as mentioned in the preceding section, it is found that

$$\frac{u}{u_x} = g(\eta), \quad g = g(\eta), \quad \frac{T}{T_e} = \theta(\eta) \quad [24]$$

where u_x is a function of x only, varying with a velocity value within the boundary, e.g., the maximum velocity. The function η can now be represented by y/δ, where δ will contain the variation of η with x. For u, g, and T, we will use the respective boundary-layer thickness δ, δ', and δ'' in η. Representing

$$\frac{u}{u_x} = f(\eta), \quad g = g(\eta'), \quad \text{and} \quad \frac{T}{T_s} = \theta(\eta'')$$

means that the three profiles retain geometrically similarity as the flow proceeds downstream.

We will approximate each of the dependent variables f, g, and θ by a polynomial of argument y/δ (or y/δ', y/δ'' as the case may be)

$$\left.\begin{aligned} \frac{u}{u_x} &= \sum_{i=0}^{n} a_i (y/\delta)^i \\ g &= \sum_{i=0}^{n} b_i (y/\delta')^i \\ \theta &= \sum_{i=0}^{n} d_i (y/\delta'')^i \end{aligned}\right\} \quad \ldots\ldots\ldots\ldots [25]$$

The boundary conditions applicable to the polynomials are:

Momentum

$$\left.\begin{aligned} &u(0) = 0 \\ &u(\delta) = 0 \\ &\frac{\partial^m u(\delta)}{\partial y^m} = 0 \qquad (m = 1, 2, \ldots n-2) \end{aligned}\right\} \quad \ldots\ldots [26]$$

Diffusion

$$\left.\begin{aligned} &g(0) = 1.0 \\ &g(\delta') = 0 \\ &\frac{\partial^m g(\delta')}{\partial y^m} = 0 \qquad (m = 1, 2, \ldots n-2) \\ &(\beta C_0 + 1) D \left(\frac{\partial^2 \left(g \frac{T_s}{T} \right)}{\partial y^2} \right)_{y=0} = v_0 \frac{T_s}{T_0} \left(\frac{\partial g}{\partial y} \right)_{y=0} \end{aligned}\right\} \quad \ldots [27]$$

Energy

$$\left.\begin{aligned} &\frac{T(0)}{T_s} = \frac{T_0}{T_s} \\ &\frac{T(\delta'')}{T_s} = 1.0 \\ &\frac{\partial^m \left(\frac{T(\delta'')}{T_s} \right)}{\partial y^m} = 0 \qquad (m = 1, 2, \ldots n-2) \\ &\frac{\lambda}{\rho_0 c_p} \frac{\partial^2 \left(\frac{T}{T_s} \right)}{\partial y^2} = v_0 \left(\frac{\partial \left(\frac{T}{T_s} \right)}{\partial y} \right)_{y=0} \end{aligned}\right\} \quad \ldots [28]$$

For simple calculation only the polynomial terms through $n = 3$ are retained. The accuracy of such an approximation has been good in past applications (2, 4). With this approximation we obtain the following from Equations [25] through [28]

$$\left.\begin{aligned} \frac{u}{u_x} &= \left[\left(\frac{y}{\delta} \right) - 2 \left(\frac{y}{\delta} \right)^2 + \left(\frac{y}{\delta} \right)^3 \right] \\ g &= 1.0 - \left[\frac{3}{2+\kappa'} \left(\frac{y}{\delta'} \right) + \frac{3\kappa'}{2+\kappa'} \left(\frac{y}{\delta'} \right)^2 - \frac{1+2\kappa'}{2+\kappa'} \left(\frac{y}{\delta'} \right)^3 \right] \end{aligned}\right\} \quad \ldots [29]$$

$$\left.\begin{aligned} \frac{T}{T_s} &= \frac{T_0}{T_s} + \left(\frac{T_s - T_2}{T_s} \right) \left[\frac{3}{2+\kappa} \left(\frac{y}{\delta''} \right) + \frac{3\kappa}{2+\kappa} \left(\frac{y}{\delta''} \right)^2 - \frac{1+2\kappa}{2+\kappa} \left(\frac{y}{\delta''} \right)^3 \right] \end{aligned}\right\} \quad \ldots [29] \text{ (continued)}$$

where

$$\kappa' = \sqrt{1 + \frac{3C_0'}{2}} - 1, \quad \kappa = \frac{\delta''}{\delta'} \frac{\mathrm{Pr}}{\mathrm{Sc}} \kappa', \quad C_0' = \frac{C_0}{1 - C_0}$$

For use in the energy equation with T/T_s approximately equal to 1.0, we obtain

$$1 - \frac{T_s}{T} \sim \frac{T_0 - T_s}{T_s} \left\{ 1.0 - \left[\frac{3}{2+\kappa} \left(\frac{y}{\delta''} \right) + \frac{3\kappa}{2+\kappa} \left(\frac{y}{\delta} \right)^2 - \frac{1+2\kappa}{2+\kappa} \left(\frac{y}{\delta} \right)^3 \right] \right\} \quad \ldots [30]$$

The three profiles to be substituted in the three integral equations contain four unknown parameters u_x, δ, δ', and δ''. A convenient assumption to reduce the number of unknowns to three is that either $\delta = \delta'$ or $\delta = \delta''$; this is a reasonably good assumption, since the motion has its source in a density difference caused by either a concentration or temperature difference.

Solution of the Integral Equations. In the solution of the momentum equation, the effect of density change on both the inertia term and the mass-transfer convective-force term are neglected and ρ can be approximated in the thermal convective-force term by $(\rho_s T_s)/T$. We also assume $T_s/T \sim 1.0$, in the integrals and derivatives and in the integral form of the diffusion equation. In the energy equation $\rho \sim (\rho_s T_s)/T$ as in the momentum equation.

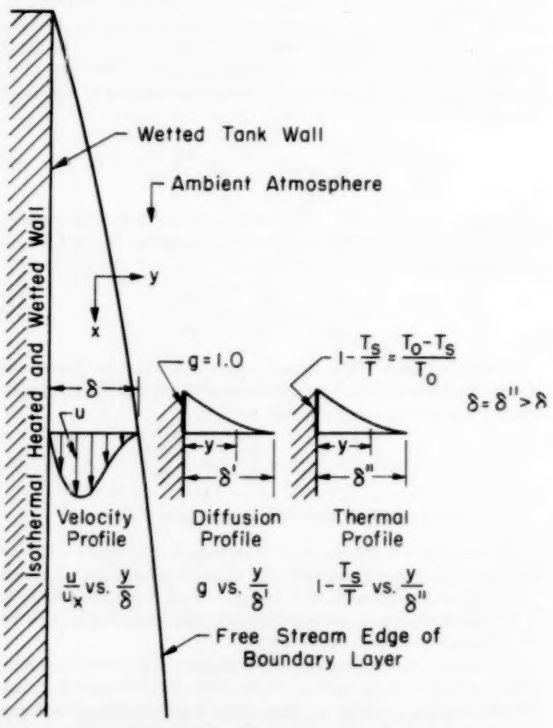

FIG. 1 BOUNDARY-LAYER PROFILES

Two separate solutions of the equations are possible—the first, assuming $\delta = \delta' > \delta''$; the second, assuming $\delta = \delta'' > \delta'$. These follow

Momentum. The integral equation is

$$\frac{d}{dx}\int_0^\delta u^2 dy = g_x \int_0^\delta \left(1 - \frac{T_s}{T}\right) dy + g_x C_0 \left(1 - \frac{m_1}{m_2}\right) \int_0^\delta g dy - \frac{\mu}{\rho_s}\left(\frac{\partial u}{\partial y}\right)_{y=0} \quad [31]$$

Substituting Equations [29] and [30] in [31] and performing the indicated operations we obtain for $\delta = \delta' > \delta''$

$$\frac{1}{105}\frac{d}{dx}(u_x^2\delta) = -\nu_s \frac{u_x}{\delta} + g_x \left(\frac{T_0 - T_s}{T_s}\right)\delta'' M_1 + g_x C_0 \left(1 - \frac{m_1}{m_2}\right)\delta M_2 \quad [32]$$

where

$$M_1 = \frac{3}{2} - \frac{3}{2+\kappa}\left(\frac{3}{4} + \frac{\kappa}{3}\right)$$

$$M_2 = \frac{1}{2} - \frac{1}{12}\left(\frac{3}{2+\kappa}\right)$$

while for $\delta = \delta'' > \delta'$

$$\frac{1}{105}\frac{d}{dx}(u_x^2\delta) = -\nu_s \frac{u_x}{\delta} + g_x \left(\frac{T_0 - T_s}{T_s}\right)\delta M_1 + g_x C_0 \left(1 - \frac{m_1}{m_2}\right)\delta' M_2 \quad [33]$$

Diffusion. The integral equation is

$$\frac{d}{dx}\int_0^{\delta'} u g dy = v_0 \frac{T_s}{T_0} - D\left(\frac{\partial g}{\partial y}\right)_{y=0} \quad [34]$$

Substitutions and operations similar to these for the momentum equation yield for $\delta = \delta' > \delta''$

$$\frac{1}{105}\frac{d}{dx}\left[\left(5.5 - \frac{3}{2+\kappa'}\right)u_x\delta\right] = \frac{3}{2+\kappa'}\left(1 + C_0'\frac{T_s}{T_0}\right)\frac{D}{\delta} \quad [35]$$

while for $\delta = \delta'' > \delta'$

$$\frac{d}{dx}\left[\left(M_3 - \frac{3}{2+\kappa'}M_4\right)u_x\delta'\right] = \frac{3}{2+\kappa'}\left(1 - C_0'\frac{T_s}{T_0}\right)\frac{D}{\delta'} \quad [36]$$

where

$$\left.\begin{aligned} M_3 &= k\left(\frac{3}{20} - \frac{2}{15}k + \frac{1}{28}k^2\right) \\ M_4 &= k\left(\frac{1}{30} - \frac{1}{30}k + \frac{1}{105}k^2\right) \end{aligned}\right\}, \quad k = \frac{\delta'}{\delta}$$

In the foregoing

$$C_0' = \frac{C_0}{1 - C_0}$$

per Equation [23], accounting for the convective velocity due to the diffusion of the nonevaporating or noncondensing species toward the wall. Considering our many assumptions of $C_0 \ll 1.0$, as in Equations [12], [21], and [34], C_0' cannot assume high values, e.g., $C_0 > 0.3$, without introducing error in the result.

Energy. The integral equation is

$$\frac{d}{dx}\int_0^{\delta''} u\left(1 - \frac{T_s}{T}\right)dy = \frac{T_0 - T_s}{T_s}\frac{T_s}{T_0}v_0 - \frac{\lambda}{\rho_s c_p}\left(\frac{\partial\left(\frac{T}{T_s}\right)}{\partial y}\right)_{y=0} \quad [37]$$

Substituting Equations [29] and [30] in Equation [37], we obtain for $\delta = \delta' > \delta''$

$$\frac{d}{dx}\left[\left(M_5 - \frac{3}{2+\kappa}M_6\right)u_x\delta''\right] = \frac{3}{2+\kappa}\left[1 + \frac{2+\kappa}{2+\kappa'}\frac{\delta''}{\delta}\frac{\mathrm{Pr}}{\mathrm{Sc}}C_0'\frac{T_s}{T_0}\right]\frac{\gamma_s}{\delta''} \quad [38]$$

where

$$\left.\begin{aligned} M_5 &= k'\left(\frac{3}{20} - \frac{2}{15}k' + \frac{1}{28}k'^2\right) \\ M_6 &= k'\left(\frac{1}{30} - \frac{1}{30}k' + \frac{1}{105}k'^2\right) \end{aligned}\right\}, \quad k' = \frac{\delta''}{\delta}$$

while for $\delta = \delta'' > \delta'$

$$\frac{1}{105}\frac{d}{dx}\left[\left(5.5 - \frac{3}{2+\kappa}\right)u_x\delta\right] = \frac{3}{2+\kappa}\left[1 + \frac{2+\kappa}{2+\kappa'}\frac{\delta}{\delta'}\frac{\mathrm{Pr}}{\mathrm{Sc}}C_0'\frac{T_s}{T_0}\right]\frac{\gamma_s}{\delta} \quad [39]$$

For a particular problem, we can consider that in which a fluid of heavy molecular weight evaporates into or condenses from a lighter gas mixture with the Prandtl number less than 1 and the Schmidt number greater than 1. Since the ratio of the Schmidt number to Prandtl number indicates to some degree the ratio of δ''/δ', we can conclude that the thermal boundary-layer thickness δ'' is larger than the mass-transfer boundary layer δ'. It follows that $\delta = \delta'' > \delta'$. We now have three equations, Equations [33], [36], and [39], in which u_x, δ, and δ' are unknowns. These equations can be reduced to a set of three algebraic equations substituting for u_x, δ, and δ'

$$\left.\begin{aligned} u_x &= \alpha_1 x^{1/2} \\ \delta &= \alpha_2 x^{1/4} \\ \delta' &= \alpha_3 x^{1/4} \end{aligned}\right\} \quad [40]$$

These substitutions, arising from the Pohlhausen transformation discussed briefly at the beginning of this section, yield the following

$$\frac{1}{84}\alpha_1^2\alpha_2 = -\gamma_s\frac{\alpha_1}{\alpha_2} + g_x M_1 \alpha_2\left[\frac{T_0 - T_s}{T_s} + C_0\left(1 - \frac{m_1}{m_2}\right)\frac{\alpha_3}{\alpha_2}\frac{M_2}{M_1}\right] \quad [41]$$

$$\frac{3}{4}\left(M_4 - \frac{3}{2+\kappa'}M_4\right)\alpha_1\alpha_3 = \frac{3}{2+\kappa'}\left(1 + C_0'\frac{T_s}{T_0}\right)\frac{D}{\alpha_3} \quad [42]$$

$$\frac{1}{140}\left(5.5 - \frac{3}{2+\kappa}\right)\alpha_1\alpha_2 = \frac{3}{2+\kappa}\left(1 + \frac{2+\kappa}{2+\kappa}\frac{\mathrm{Pr}}{\mathrm{Sc}}\frac{\alpha_2}{\alpha_3}C_0'\frac{T_s}{T_0}\right)\frac{\gamma_s}{\alpha_2} \quad [43]$$

$$\alpha_1 = \frac{\left(\frac{3}{2+\kappa'}\right)\left(1 + C_0'\frac{T_s}{T_0}\right) D}{\frac{3}{4}\left(M_3 - \frac{3}{2+\kappa'} M_4\right)} \frac{1}{\alpha_3^2} \text{ (Equation [42])} \ldots [44]$$

$$\left\{\frac{4}{189}\left[\frac{\left(1 + C_0'\frac{T_s}{T_0}\right) D \left(\frac{3}{2+\kappa'}\right)}{\left(M_3 - \frac{3}{2+\kappa'} M_4\right)}\right]^2\right\} + \left\{\frac{4}{3}\left[\frac{\gamma_s\left(1 + C_0'\frac{T_s}{T_0}\right) D \left(\frac{3}{2+\kappa'}\right)}{\left(M_3 - \frac{3}{2+\kappa'} M_4\right)}\right]\left(\frac{\alpha_3}{\alpha_2}\right)^2\right\} \alpha_3^2 - \left\{g_s M_1\left[\frac{T_0 - T_s}{T_s} + C_0\left(1 - \frac{m_1}{m_2}\right)\left(\frac{\alpha_3}{\alpha_2}\right)\left(\frac{M_2}{M_1}\right)\right]\right\} \alpha_3^4 = 0$$

(Equations [41] and [44]) . . [45]

Equation [45] can be solved for α_3 retaining $\alpha_3/\alpha_2 = \delta'/\delta = k$

$$\alpha_3 = \sqrt[4]{\frac{\frac{4}{189}\left[\frac{\left(1 - C_0'\frac{T_s}{T_0}\right) D \left(\frac{3}{2+\kappa'}\right)}{\left(M_3 - \frac{3}{2+\kappa'} M_4\right)}\right]^2 + \frac{4}{3}\left[\frac{\nu_s\left(1 + C_0'\frac{T_s}{T_0}\right) D \left(\frac{3}{2+\kappa'}\right)}{\left(M_3 - \frac{3}{2+\kappa'} M_4\right)}\right] k^2}{g_s M_1\left[\frac{T_0 - T_s}{T_s} + C_0\left(1 - \frac{m_1}{m_2}\right) k \frac{M_1}{M_2}\right]}} \ldots [46]$$

From Newton's law of convective transfer and Fourier's law of conductive transfer

$$h_s(\rho_{10} - \rho_{1s}) = -D\left(\frac{\partial \rho_1}{\partial y}\right)_{y=0} \ldots [47]$$

Since ρ is given by Equation [14] for low concentrations, we can approximate

$$\left(\frac{\partial \rho_1}{\partial y}\right)_{y=0} \text{ by } -DN_0(C_0 - C_s)\left(\frac{\partial g}{\partial y}\right)_{y=0}$$

and $(\rho_{10} - \rho_{1s})$ by $N_0(C_0 - C_s)$

and obtain from Equations [29] and [46]

$$h_x = \frac{D}{\delta'}\left(\frac{3}{2+\kappa'}\right) = \frac{D}{\alpha_3 x^{1/4}}\left(\frac{3}{2+\kappa'}\right)$$

$$\frac{h_x x}{D} = \sqrt[4]{\frac{\left(\frac{3}{2+\kappa'}\right)^4 M_1}{\frac{4}{189}\left[\frac{\left(1 + C_0'\frac{T_s}{T_0}\right)\left(\frac{3}{2+\kappa'}\right)}{M_3 - \frac{3}{2+\kappa'} M_4}\right]^2 + \frac{4}{3}\left[\frac{\text{Sc}\left(1 + C_0'\frac{T_s}{T_0}\right)\left(\frac{3}{2+\kappa'}\right)}{\left(M_3 - \frac{3}{2+\kappa'} M_4\right)}\right] k^2}} \sqrt[4]{\text{Gr}_x + \alpha \text{Gr}_{xx}} \ldots [48]$$

$$\text{Gr}_x = \frac{g_s x^3}{D^2}\frac{T_0 - T_s}{T_s}, \qquad \text{Gr}_{xx} = \frac{g_s x^3}{D^2} C_0\left(1 - \frac{m_1}{m_2}\right)$$

The Nusselt-Grashof correlation of Equation [48] requires an additional equation defining k, which can be obtained by solving Equations [42] and [43] simultaneously

$$\left(1 + \frac{2+\kappa}{2+\kappa'}\frac{1}{k}\frac{\text{Pr}}{\text{Sc}} C_0'\frac{T_s}{T_0}\right) k^2 - \frac{1}{140}\left[\frac{5.5(2+\kappa)}{3} - 1\right]\left[\frac{\left(1 + C_0'\frac{T_s}{T_0}\right)\frac{\text{Pr}}{\text{Sc}}\left(\frac{3}{2+\kappa'}\right)}{\frac{3}{4}\left(M_3 - \frac{3}{2+\kappa'} M_4\right)}\right] = 0 \ldots [49]$$

recalling that

$$\kappa = \frac{1}{k}\frac{\text{Pr}}{\text{Sc}}\left(\sqrt{1 + \frac{3C_0'}{2}} - 1\right), \qquad \kappa' = k\frac{\text{Sc}}{\text{Pr}}\kappa$$

The form of Equation [48] is that given in Equation [3], where

$$\alpha\left(\frac{\text{Pr}}{\text{Sc}}, C_0', \frac{T_s}{T_0}\right) = k\frac{M_2}{M_1}$$

The foregoing refers to the mass transfer; a similar consideration of the thermal transfer follows

$$h(T_0 - T_s) = -\lambda\left(\frac{\partial T}{\partial y}\right)_{y=0} \ldots [50]$$

From Equations [29], [46], and [48]

$$h = \frac{\lambda}{\delta'}\left(\frac{3}{2+\kappa}\right) = \frac{\lambda}{\alpha_3 x^{1/4}}\frac{3}{2+\kappa}$$
$$\frac{hx}{\lambda} = \frac{2+\kappa'}{2+\kappa} k \frac{h_x x}{D} \ldots [51]$$

For very low concentrations $C_0' \sim 0$ and $\text{Pr} = \text{Sc} = 1.0$, we obtain $k(M_2/M_1) = 1.0$ and $\kappa = \kappa' = 0$. The fourth-root constant term

$$A(C_0', T_s/T_0, \text{Sc}, \text{Pr}) = 0.380$$

the same result as that obtained by Nusselt (1)

$$\text{Nu}_{xx} = 0.380 \sqrt[4]{\text{Gr}_x + \text{Gr}_{xx}} \ldots [52]$$

Since $\text{Nu}_x = \text{Nu}_{xx}$ with these assumptions, the calculated results are comparable with those for thermal convection only. The thermal-convection results, determined by several methods of calculation, are

Pohlhausen's method	$A = 0.359$	$\text{Pr} = 0.733$

(Adjusted to $\text{Pr} = 1.000$ by a factor of $\text{Pr}^{1/4}$, Pohlhausen's constant is $A = 0.388$.)

Lorenz's method (4)	$A = 0.412$	$\text{Pr} = 1.000$
Squire's method (4)	$A = 0.382$	$\text{Pr} = 0.733$
	$A = 0.429$	$\text{Pr} = 1.000$

Pohlhausen's method obtains an exact solution of the thermal-convection equations resulting from a reduction of the partial differential equations for momentum and energy to ordinary differential equations by the transformation

$$\eta = \omega\frac{y}{x^{1/4}}$$

Pohlhausen worked the problem for air at a Prandtl number of

0.733. Lorenz's method (in 1881) applied to an extremely simplified model, yields an approximately correct value of A. Squire's method obtains an approximate solution as contained in this report. Squire used a second-degree polynomial for T/T_s and a third-degree polynomial for u/u_s.

McAdams (7) lists several experimental values for short vertical plates submerged in air (Pr = 0.733); these values range between $A = 0.353$ for Hilpert's data (7) to $A = 0.442$ for King's data (7).

For values of Sc/Pr near 1.0, covering most gaseous problems, $k \sim (\mathrm{Pr/Sc})^{1/3}$ and $M_2/M_1 \sim 1.0$; accordingly, we can rewrite Equation [48] with this approximation and obtain

$$\mathrm{Nu}_{zz} = A\left(C_0', \frac{T_s}{T_0}, \mathrm{Sc}, \mathrm{Pr}\right)\sqrt[4]{\mathrm{Gr}_x + \left(\frac{\mathrm{Pr}}{\mathrm{Sc}}\right)^{1/3}\mathrm{Gr}_{zz}} \quad [53]$$

Numerical Results for a Cooling Problem

For a cooling or heating problem, it is desirable to estimate the range of variation of the coefficient

$$A\left(C_0', \frac{T_s}{T_0}, \mathrm{Sc}, \mathrm{Pr}\right)$$

in Equation [53], and that of α in Equation [48]. In a particular application, the wall of a heated tank containing Freon-11 (CCl_3F) is to be cooled by wetting the walls with pentachlorodiphenol ($C_{12}H_5Cl_5$). The Prandtl and Schmidt numbers arising from the use of these fluids are approximately 0.9 and 1.2, respectively. The Prandtl-Schmidt ratio is approximately 0.75, and the square root of 0.75 is 0.867. For a value of T_s/T_0 of 0.9, the values of A and α are given in Table 1.

TABLE 1 VALUES OF α AND A VERSUS C_0

For $T_s/T_0 = 0.9$, Sc = 1.2, and Pr = 0.9

C_0	k	α	A
0.0	0.867	0.867	0.394
0.1	0.875	0.876	0.379
0.2	0.879	0.883	0.355
0.3	0.889	0.889	0.333

The approximation used to obtain Equation [53] is good since $\sqrt{\mathrm{Pr/Sc}} = 0.867$. The range of variablity of

$$A(C_0', T_s/T_0, \mathrm{Sc}, \mathrm{Pr})$$

in Table 1 shows that for the conditions listed in the foregoing, all of the values lie within 8.5 per cent of

$$A = 0.363 \quad [54]$$

Thus, for a wide range of values of C_0, we can represent the vertical-flat-plate mass transfer for the two fluids, Freon-11 and pentachlorodiphenol, by the approximate formula

$$\mathrm{Nu}_{zz} = 0.363\sqrt[4]{\mathrm{Gr}_x + 0.87\mathrm{Gr}_{zz}} \quad [55]$$

Summary

For combined thermal and mass transfer on a vertical flat plate, it has been shown for gases that

$$\left.\begin{aligned}\mathrm{Nu}_{zz} &= A\left(C_0', \frac{T_s}{T_0}, \mathrm{Sc}, \mathrm{Pr}\right)\sqrt[4]{\mathrm{Gr}_x + \alpha\mathrm{Gr}_{zz}}\\ \mathrm{Nu}_x &= \frac{2+\kappa'}{2+\kappa}\,\mathrm{k}\,\mathrm{Nu}_{zz}\end{aligned}\right\} \quad [56]$$

The parameter A is reasonably constant over a range of variation $0 < C_0 < 0.3$, for $0.9 < T_s/T_0 < 1.0$, and the value α can be replaced with $\sqrt{\mathrm{Pr/Sc}}$, yielding

$$\left.\begin{aligned}\mathrm{Nu}_{zz} &\simeq A\sqrt[4]{\mathrm{Gr}_x + \left(\frac{\mathrm{Pr}}{\mathrm{Sc}}\right)^{1/3}\mathrm{Gr}_{zz}}\\ \mathrm{Nu}_x &\simeq \frac{2+\kappa'}{2+\kappa}\sqrt{\frac{\mathrm{Pr}}{\mathrm{Sc}}}\,\mathrm{Nu}_{zz}\end{aligned}\right\} \quad [57]$$

BIBLIOGRAPHY

1 "Wärmeübergang, Diffusion, and Verdunstung," by W. Nusselt, *Zeitschrift für angewandte Mathematik und Mechanik*, vol. 10, 1930, pp. 105–121; also, NACA TM 1367, March, 1954.

2 "Mass Transfer in Laminar Flow," by D. B. Spalding, Proceedings of the Royal Society of London, January, 1954, pp. 78–104.

3 "The Laminar Jet Mixing of Two Compressible Fluids," by S. I. Pai, Inst. Fluid Dynamics and Applied Mathematics, University of Maryland Technical Report BTI, February 11, 1952.

4 "Modern Developments in Fluid Dynamics," by S. Goldstein, Oxford University Press, London, England, vol. 1, 1938, pp. 116–118, 156–163; vol. 2, 1938, pp. 641–643.

5 "Thermodynamics of Irreversible Processes I. Simple Fluid, II. Fluid Mixtures," by C. Eckart, *Physical Review*, vol. 58, 1940, pp. 267–275.

6 "Das Temperatur und Geschwindigkeitsfeld von einer Wärme abgebenden senkrechten Platte bei natürlicher Konvektion," by E. Schmidt and W. Beckmann, *Techn. Mechanik und Thermodynamik*, vol. 1, 1930, p. 391.

7 "Heat Transmission," by W. H. McAdams, McGraw-Hill Book Company, Inc., New York, N. Y., second edition, 1942, pp. 248–249.

Some Dynamic Properties of Oil-Film Journal Bearings With Reference to the Unbalance Vibration of Rotors

By A. C. HAGG[1] and G. O. SANKEY,[2] EAST PITTSBURGH, PA.

Some dynamic properties of oil films have been determined experimentally and their significance in the problem of unbalance vibration and critical speeds of rotor systems is illustrated by an example. It is shown that oil films have an important role in the unbalance-vibration behavior of rotor systems, particularly the vibration magnification at resonance.

Nomenclature

The following nomenclature is used in the paper; some of the quantities are shown in Fig. 1.

W = static load, lb
F = rotating load, lb
N = journal speed, rpm
ω = vibration frequency, rad/sec, $\omega = \frac{\pi N}{30}$
R = journal radius, in.
C = radial clearance, in.
L = axial length of bearing, in.
a = length of pivoted pad in direction of motion, in.
ϵ = journal eccentricity, in.
μ = viscosity of lubricant in reyns, lb sec/in.^{2}
P = static load per unit projected area, psi
S = $\left(\frac{R}{C}\right)^2 \frac{\mu N}{P}$, sec/min
φ = angle between rotating load and displacement, rad
K_1 = minimum film elasticity, lb/in.
K_2 = maximum film elasticity, lb/in.
B_1 = minimum film damping, lb sec/in.
B_2 = maximum film damping, lb sec/in.
$\left(\frac{C}{W}\right) K$ = dimensionless film elasticity
$\left(\frac{C}{W}\right) B\omega$ = dimensionless film damping

Introduction

The usual calculated unbalance vibration and critical speeds of rotor systems often bear little resemblance to the observed vibration. The defects in the calculations stem from simplifying assumptions with respect to complex and uncertain rotor-support characteristics. Until the advent of rapid computers it was probably impractical to consider more representative support conditions even had they been known. However, with the lifting of the computing barrier, it seems appropriate to reconsider this aspect of rotor systems.

In machines, such as modern turbines and generators, the journal-center motion with respect to the bearing is usually greater than the motion of other nonrotating parts. Consequently, it seems plausible that a substantial move toward a more realistic system would involve the dynamic properties of the oil film which is the first element of rotor support. In pursuit of this view some dynamic tests of oil-film journal bearings have been carried out for the case of a rotating load at the frequency of journal rotation; that is, the case corresponding to unbalance vibration. The dynamic oil-film properties obtained are used in an example of rotor unbalance vibration given later.

Attention has been centered on bearings which are subjected to a static load by the rotor they support and, indeed, normally designed on this basis alone. The dynamic load is superimposed on the static load.

This case is one in the area of dynamically loaded bearings (1), (2);[3] however, with the object of a better understanding of unbalance-vibration problems, we are obliged to resolve the dynamic oil-film reaction into displacement-force and velocity-force components which are elastic and damping forces, respectively. We have also considered only the fundamental harmonics of journal motion, and thus our treatment is a linear one.

The experiments of Stone and Underwood (2) are related in part to the present work in that vibration diagrams were obtained from which vibration amplitude and phase can be estimated. This permits a calculation of oil-film elasticity and damping for their case of a full (360-deg) bearing with dynamic load only, and certain comparisons are made later.

Almost 30 years ago Stodola (3) considered the elasticity of oil films and suggested that "critical disturbances" would be introduced in an otherwise rigid rotor system. Since that time it has become not uncommon to ascribe to oil films, at least in part, the observed reduction in critical speeds under those calculated on the basis of simple support at the bearings (4). The role of oil-film damping in unbalance vibration and particularly in limiting vibration magnification at critical speeds was suggested more recently (5). However, it appears probable that engineers concerned with rotor-vibration problems have had for a long time a qualitative awareness of the benefits of oil-film damping.

Design of Tests and Apparatus

The dynamic oil-film properties were determined from measurements of the forced vibration of a journal mass contained by the bearing. Referring to Fig. 1, and for displacements of the journal mass m from the position of static equilibrium up to about one half of the minimum film thickness in the direction of motion, we assume

[1] Section Manager, Mechanics Department, Westinghouse Research Laboratories. Mem. ASME.
[2] Research Engineer, Mechanics Department, Westinghouse Research Laboratories.

Contributed by the Applied Mechanics Division and presented at the Diamond Jubilee Annual Meeting, Chicago, Ill., November 13–18, 1955, of The American Society of Mechanical Engineers.
Discussion of this paper should be addressed to the Secretary, ASME, 29 West 39th Street, New York, N. Y., and will be accepted until July 10, 1956, for publication at a later date. Discussion received after the closing date will be returned.
Note: Statements and opinions advanced in papers are to be understood as individual expressions of their authors and not those of the Society. Manuscript received by ASME Applied Mechanics Division, November 29, 1954. Paper No. 55—A-45.

[3] Numbers in parentheses refer to the Bibliography at the end of the paper.

$$\left.\begin{aligned} m\ddot{x} + B_1\dot{x} + K_1x &= F\cos(\omega t + \varphi) \\ m\ddot{y} + B_2\dot{y} + K_2y &= F\sin(\omega t + \varphi) \end{aligned}\right\} \quad [1]$$

where the x-y co-ordinates correspond to the major and minor axes of the journal locus. The quantities B_1, B_2, and K_1 and K_2 are damping and elastic constants of the oil film and are the desired dynamic properties. The quantity F is a rotating force directed at an angle φ with respect to the journal displacement as shown.

The steady-state solution of Equations [1] gives x and y as harmonic functions of time.

At $y = 0$, $x = x_0$, $\varphi = \varphi_1$; and at $x = 0$, $y = y_0$, $\varphi = \varphi_2$; and we obtain

$$K_1 = \frac{F\cos\varphi_1}{x_0} + m\omega^2 \quad [2]$$

$$B_2 = \frac{F\sin\varphi_1}{y_0\omega} \quad [3]$$

$$K_2 = \frac{F\cos\varphi_2}{y_0} + m\omega^2 \quad [4]$$

$$B_1 = \frac{F\sin\varphi_2}{x_0\omega} \quad [5]$$

A cross section of the test machine is shown in Fig. 2. The test bearing with a nominal diameter of 3 in. is mounted vertically in a rigid frame which, in turn, is securely bolted to a bedplate. The journal mass is axially supported by the drive motor through a direct-connected flexible shaft and is statically loaded through ball bearings and isolating springs by a lever system and weights. The rotating force is obtained by an unbalance weight in the journal.

Vibration measurements of the journal are made by the wattmeter method, which is widely used in rotor balancing. In this arrangement a phase-reference sine-wave generator with an angularly adjustable stator is coupled to the test machine and energizes the current coil of the wattmeter. The potential coil of the wattmeter is connected to an electromagnetic pickup unit applied through graphite brushes to the vibrating journal. The wattmeter which indicates electrical power can be made to read zero with high sensitivity by angular adjustment of the generator stator. The stator position so obtained indicates the phase angle of the vibration. By switching to a second-generator winding, 90 deg displaced from the phase-reference winding, the amplitude of vibration is indicated. The wattmeter indicates only the fundamental harmonic of the journal motion corresponding to journal speed; thus the force functions determined from the vibration measurements are the linear components.

Oil is supplied to the test bearing with regulated temperature and a gage pressure of 12 to 15 psi. The vibration measurements are made after equilibrium conditions have been reached as indicated by bearing and oil-drain temperatures. During the warm-up period axial adjustments of the rotor unbalance weight and other small trim weights are made to obtain the same motion at each end of the journal. A survey of the journal motion is also made to locate the angular positions of maximum and minimum vibration[4] corresponding to the minimum and maximum properties, respectively, and the x-y co-ordinates of Fig. 1.

Following a consistent set of vibration measurements the test machine and oil supply were shut down quickly and a thermocouple was inserted in a journal well; rotor temperature was subsequently determined by extrapolation of time-temperature readings. The average oil-film temperature was assumed to be very nearly the rotor temperature. The viscosity-temperature characteristics of the lubricant was determined by the Ostwald viscometer.

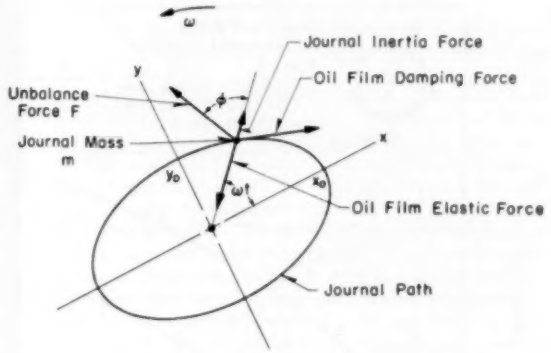

FIG. 1 JOURNAL-FORCE EQUILIBRIUM

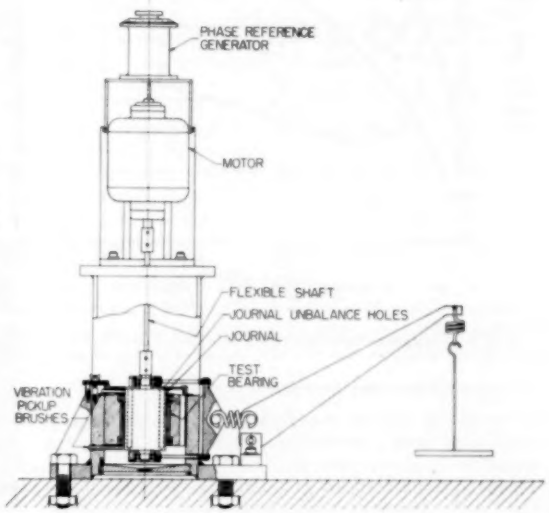

FIG. 2 BEARING-TESTING MACHINE

TEST RESULTS

The oil-film elastic and damping properties are given for a 150-deg partial bearing which is widely used in the support of horizontal rotors, and for a pivoted-pad bearing now often applied to the higher-speed machines where stability is difficult or impossible to achieve with plain bearings.

The elasticity and damping may be put in dimensionless form through previous considerations (3, 6) as follows

$$K = \left(\frac{W}{\epsilon}\right) f(S) \quad [6]$$

where W is the static load on the bearing, ϵ is the static journal eccentricity, and S is the well-known Sommerfeld variable

$$\left(\frac{R}{C}\right)^2 \frac{\mu N}{P}$$

[4] The displacement of a brush follower on a vibrating journal is similar to the action of a flat-faced follower on a rotating cam; thus a direct indication of the journal displacement in line with the brush is obtained only along the x and y-axes (Fig. 1).

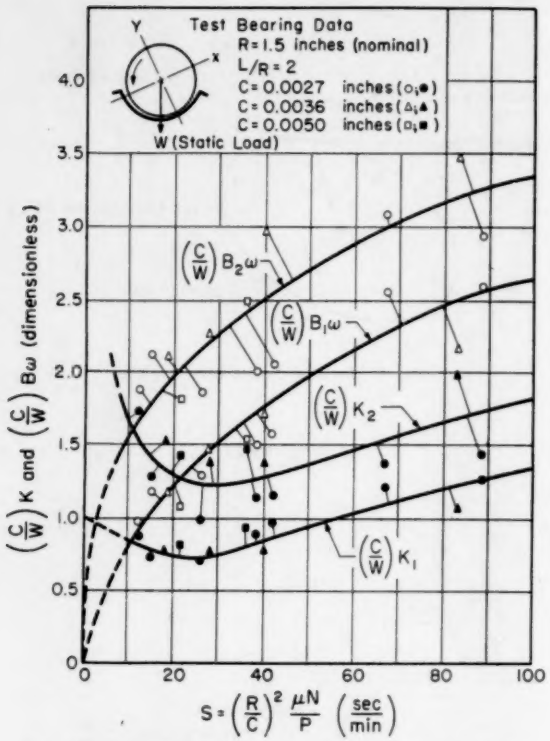

FIG. 3 DYNAMIC PROPERTIES OF 150-DEG PARTIAL BEARING

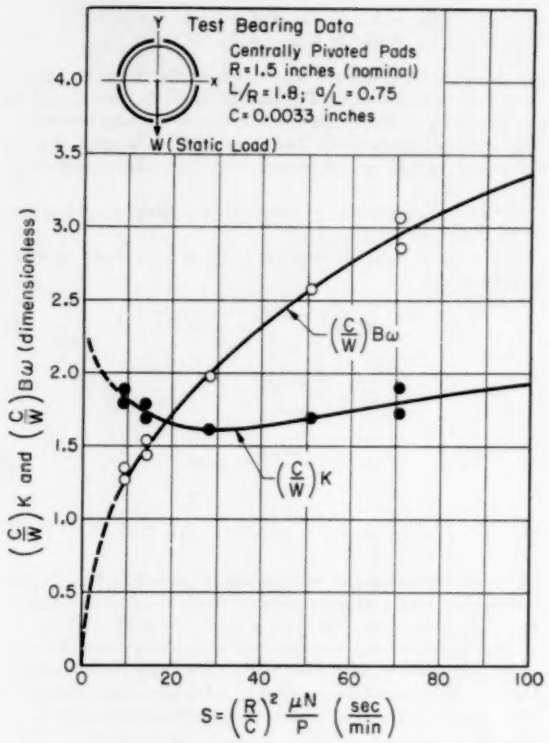

FIG. 4 DYNAMIC PROPERTIES OF PIVOTED-PAD BEARING

The eccentricity ϵ may be written

$$\epsilon = C\left(\frac{\epsilon}{C}\right) = Cf'(S)$$

where C is the radial bearing clearance, and Equation [6] becomes

$$\left(\frac{C}{W}\right)K = f_1(S) \quad \ldots\ldots\ldots\ldots\ldots\ldots [7]$$

where $(C/W)K$ is the dimensionless film elasticity. Similarly, the dimensionless damping is $(C/W)B\omega$, and

$$\left(\frac{C}{W}\right)B\omega = f_2(S) \quad \ldots\ldots\ldots\ldots\ldots\ldots [8]$$

The maximum and minimum values of the elasticity and damping for the 150-deg bearing are given in the dimensionless form in Fig. 3. The maximum values are in the direction of the minor axis (y) of the journal path, and the minimum values are in the direction of the major axis (x). The curve for minimum elasticity is carried over to the value $(C/W)K_1 = 1$ at $S = 0$. The value of K_1 for this end condition is the "pendulum" unit-force component along the clearance circle, and it is the elastic spring constant involved in the suggestion of Hummel (7) that the horizontal natural frequency ω_n of a rigid rotor supported by the half-bearing is approximately

$$\omega_n = \sqrt{\frac{g}{C}} \text{ (radians per sec)}$$

where g is the gravitational acceleration and C is the radial bearing clearance. The value for $(C/W)K_2$ is estimated to rise to the journal and bearing-contact elasticity as S approaches zero. The dimensionless damping is zero at $S = 0$, because $(C/W)\omega = 0$. With increasing values of S both damping and elasticity should approach constant positive slopes.

The properties of the pivoted-pad bearing are given in Fig. 4 for the case where the static load is applied midway between two pads. The journal path was found to be very nearly a circle caused apparently by the disposition of the oil-film reactions at 45 deg with respect to the static load and, consequently, elasticity and damping are each given by a single curve. The properties of the pivoted-pad bearing tested do not differ appreciably from those of the 150-deg bearing. This might be inferred from the analysis of Boyd and Raimondi (8).

It may be mentioned that when the static load is numerically in excess of the rotating load, tests indicate that the properties are not changed appreciably by removal of the two pads opposite the static load. This may not be true for small diametral clearances below the usual practice of about 0.002 in. per in. of bearing diameter.

In the higher ranges of S the oil-film damping force for either bearing tested appears to approach a value of about twice the corresponding elastic force. This agrees with elasticity and damping values estimated from the diagrams of Stone and Underwood (2) (their Fig. 13 for 1000 rpm) for their full bearing and zero static load. These are $B_1\omega = B_2\omega = 100{,}000$ lb per in., and $K_1 = K_2 = 50{,}000$ lb per in., approximately.

All of the test parameters except bearing diameter were varied over a considerable range, and most of these could be controlled or measured with high accuracy. Small errors in clearance and in vibration measurements, particularly phase, are probably unavoidable in tests of this kind, and these may account for the

scatter in the test results which is most prominent in the case of K_2 and B_2 for the 150-deg bearing. The scatter does not appear to be systematic; however, it may not be unreasonable to expect inaccuracies in the curve values of Figs. 3 and 4 of some 10 to 20 per cent for bearing sizes near those tested. For very large bearings the errors may be greater, although the data have been used with apparent success for 14 and 16-in. bearings.

It may be noted that the elasticity K and the damping $B\omega$ are evidently proportional to bearing diameter for geometrically similar bearings with design conditions of R/C, P, and S held constant. This compares with a static load capacity proportional to bearing diameter squared, and suggests that the influence of oil films on unbalance vibration would be more noticeable with the heavier rotors.

The oil-film properties are, of course, quite sensitive to bearing clearance, and it seems possible that this may be a significant factor in the variation in unbalance sensitivity of otherwise identical machines.

Influence of Oil Films on Unbalance Vibration

The Holzer-type calculation of Myklestad (9) for the bending vibration of beams or rotors has been extended to systems with damped-elastic supports by Miller (10). This method carried out on a digital computer is now in use for unbalance-vibration calculations which include the oil-film properties.

A comparison of calculated and observed unbalance vibration of a machine rotor is shown in Fig. 5. The case is typical of the heavier rotors and it is probably sufficient to show the powerful effect of oil films in limiting vibration magnification at resonance, and to show the reduction in the critical speeds. The rotor weight of 90,000 lb was supported by 16 × 16-in. bearings. From Fig. 3 the values

$$K_2 = B_2\omega = 6 \times 10^6 \text{ lb per in.}$$

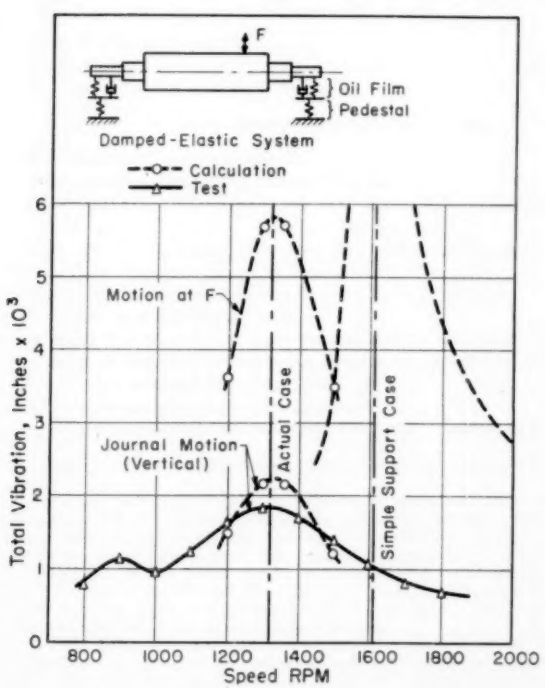

Fig. 5 Rotor Unbalance Vibration

were taken for conditions corresponding to 1000 to 1500 rpm. The measured pedestal flexibility in the vertical direction was 13.5×10^6 lb per in.

A background vibration run with the rotor as balanced was made prior to the run with a test unbalance; the results of Fig. 5 are the net vibration vector lengths caused by a 45 lb-in. unbalance which is a sizable unbalance. The agreement between observed and calculated journal vibration is quite good, but not unusual as compared to other cases studied including calculations and tests at higher modes. The actual vertical critical speed at 1310 rpm is appreciably below the value of 1615 rpm calculated on the basis of simple support of the rotor at the bearings, although some of this reduction is caused by pedestal flexibility. The peak in the test curve shown at about 900 rpm is the vertical component of the vibration resonance in the x-direction, and is adequately explained on the basis of the reduced oil-film properties in the x-direction.

It is particularly significant that the oil-film damping accounts for the very low and practical level of vibration at the critical speeds. Finite vibration amplitudes obtained along the length of the rotor are a basis for judgment of internal machine clearances; they are also helpful in interpretations of vibration measurement at and near the journals.

It may be mentioned that in any given case of rotor vibration the calculated journal motion affords a check on the assumption of linear oil-film properties. Excessive journal vibration would naturally increase the oil-film forces over those determined on a linear basis. Present practice involves repeat calculations in some cases utilizing upper and lower values of oil-film constants.

In contrast to oil-film bearings, the damping in ball or roller bearings is very small. The critical speeds of rotors supported by these bearing types would be severe in most cases and probably destructive unless extreme measures were taken with respect to balancing, or separate damping devices were added to the system.

Conclusions

The elastic and damping properties of oil films for the case of unbalance vibration have been evaluated on a linear basis; addition of these oil-film properties to a rotor system yields a more realistic calculation of unbalance vibration and of critical speeds. The oil-film damping explains the relative ease with which rotors may pass through critical speeds with low vibration amplitudes.[8] Bearing proportions for low unbalance-vibration levels at resonance is a complementary and perhaps new design concept that may deserve more attention.

Acknowledgments

The authors are grateful to Messrs. M. Rashevsky and D. F. Miller for preparing and supplying the data for Fig. 5, and to Mr. P. C. Warner for verifying the dimensionless elasticity and damping parameters.

BIBLIOGRAPHY

1 "Analysis and Lubrication of Bearing," by M. C. Shaw and E. Macks, McGraw-Hill Book Company, Inc., New York, N. Y., 1949, p. 189 and pp. 201–208. Note selected references.

2 "Load-Carrying Capacity of Journal Bearings," by J. M. Stone and A. F. Underwood, *SAE Quarterly Transactions*, vol. 1, 1947, p. 56.

3 "Kritische Wellenstörung infolge der Nachgiebigkeit bes Oelpolsters im Lager," by A. Stodola, *Schweizeriche Bauzeitung*, vol. 85, 1925, pp. 265–266.

4 "Recent Improvements in Turbine-Generators," by Stuart L. Henderson and C. Richard Soderberg, Trans. AIEE, vol. 47, 1928, p. 566; see also "Effect of Flexibility of Support Upon Critical

[8] Friction of a surrounding medium can be an important factor in some cases. Such effects for a turbine or generator rotor appear to be negligible compared to oil-film damping.

Speeds of High-Speed Rotors," by Frank C. Linn and M. A. Prohl, Trans. SNAME, vol. 59, 1951, p. 537.

5 "Some Vibration Aspects of Lubrication," by A. C. Hagg, *Lubrication Engineering*, vol. 4, August, 1948, pp. 166–169.

6 "Influence of Oil-Film Journal Bearings on the Stability of Rotating Machines," by A. C. Hagg, JOURNAL OF APPLIED MECHANICS, Trans. ASME, vol. 68, 1946, pp. A-211–A-220.

7 "Kritische Drehzahlen als Folge der Nachgiebigkeit des Schmiermittels im Lager," by C. Hummel, *Forschungsarbeiten, VDI*, Heft 287, 1926.

8 "An Analysis of the Pivoted-Pad Journal Bearing," by John Boyd and Albert A. Raimondi, *Mechanical Engineering*, vol. 75, 1953, p. 380.

9 "New Method of Calculating Natural Modes of Uncoupled Bending Vibrations," by N. O. Myklestad, *Journal of the Aeronautical Sciences*, vol. 11, 1944, p. 153.

10 "Forced Lateral Vibration of Beams on Damped Flexible End Supports," by D. F. Miller, JOURNAL OF APPLIED MECHANICS, Trans. ASME, vol. 75, 1953, pp. 167–172.

Design Data and Methods

It is important that the data contained in technical papers be made readily available to designing engineers. In order to satisfy these needs of industry, this section of the Journal includes a concise presentation of data and information drawn chiefly from papers previously published by the Applied Mechanics Division of The American Society of Mechanical Engineers.

Computation of Roll Force and Torque in Cold-Rolling by Modern Theory

By P. W. WHITTON,[1] VICTORIA, AUSTRALIA

The full theory for the comparison of calculated roll force and torque with experimental values is outlined. This takes into account the strip elastic compression, the derivation of the yield-stress curves in cold-rolling, and the accurate values for friction coefficient between rolls and strip. Hitherto, the contribution of each of these rolling variables has been found separately. This paper presents the combination of current theory on each. The application of this method yields results within ±5 per cent, a much more accurate comparison than hitherto presented.

Nomenclature[2]

The following nomenclature is used in the paper:

h = thickness of strip, in.
b = width of strip, in.
$\delta = h_1 - h_2$ = reduction in a pass, in.
$r = \frac{h_1 - h_2}{h_1} \times 100$ = percentage reduction in a pass
L = length of arc of contact, in.
e = distance along arc of contact from exit, in.
P = roll force, either total or per inch width (tons or tons per in.)
T = roll torque, either total or per inch width (tons in. or tons in. per in.)
R = radius of undeformed roll, in.
R^1 = radius of deformed roll, in.
μ = coefficient of friction between roll surface and material
ϕ = angle between normal to an element in contact arc and line joining roll centers, radians
k^* = yield stress in tension, tons per sq in.
k = yield stress with inhibited spread = $1.15k^*$, tons per sq in.
k = mean yield stress in a pass, tons per sq in.
σ = tension acting on strip, tons per sq in.
s = radial pressure at any point in the contact arc, tons per sq in.
p = vertical pressure at any point in contact arc, tons per sq in.
f = horizontal force on an element of unit width, tons per in.
ν = Poisson's ratio
E = Young's modulus, tons per sq in.
C = a constant depending on elastic properties of rolls = $\frac{8(1-\nu^2)}{\pi E} = 1.67 \times 10^{-4}$ for steel rolls, in. and ton units

Suffixes

0 denotes value when no tensions are applied
1 or — denotes entry
2 or + denotes exit
n denotes neutral point
f denotes value before rolling

Introduction

Over the past 10 years the increased attention paid to the calculation of the cold-rolling variables has been aimed at the accurate design of mill plant and planning of pass schedules to meet the demands of industry for higher and higher production. The theories take as their object the computation of roll force and torque for a specified reduction of strip thickness by cold-rolling. This requires not only the geometrical properties of a pass, i.e., the initial and final thickness of the strip and the roll radius, but also a knowledge of the yield stress of the deformed metal, the elastic distortion of the work roll, and the value of the coefficient of friction between the rolls and strip. In addition, it is now generally recognized that to obtain agreement between practical values and theory, it is essential to take into account the contribution of the elastically deformed strip at the entrance to, and exit from, the roll gap.

It has been necessary to carry out searching investigations into each of the physical requirements named, in order to insure agreement between theory and practice, and the research has now reached a stage where this agreement can be obtained within ±5 per cent. While various theories have been published—von Karman (1),[3] Orowan (2), Ford and Bland (3), Cook and Parker

[1] Senior Lecturer in Mechanical Engineering, Melbourne University.

[2] The ton unit used here is the *long ton*, equivalent to 2240 lb. Numerical values of stresses are given in tons per square inch, rather than pounds, in order to avoid confusion that would arise in conversion when the references given were consulted by readers.

Discussion of this paper should be addressed to the Secretary, ASME, 29 West 39th Street, New York, N. Y., and will be accepted until July 10, 1956, for publication at a later date. Discussion received after the closing date will be returned.

Note: Statements and opinions advanced in papers are to be understood as individual expressions of their authors and not those of the Society. Manuscript received by ASME Applied Mechanics Division, June 3, 1955.

[3] Numbers in parentheses refer to the Bibliography at the end of the paper.

(4)—they have necessarily been presented "piecemeal." The object of this paper is thus to combine the separate parts to obtain the roll force and torque, with and without tensions applied, easily and accurately. To do this, it is necessary to consider separately the basic theory of rolling reduction, and to add to it the determination of the elastic contributions of strip and roll, the accurate yield stress of the strip at all points in the arc of contact, and the long-sought-after values of friction coefficient between roll and strip under the conditions encountered.

Hitherto, calculation has been based on speed, combined with an accuracy within 10 per cent for the roll force and 14 per cent for the torque (Ford and Ellis, reference 5). Ford and Whitton (6), examining a new method of determining friction between roll and strip, recently showed that an accuracy of ±5 per cent can be obtained when measured and calculated values are compared. The steps required are now shown fully, so that accurate and fairly rapid calculation is possible by those concerned in the rapidly widening cold-rolling industry.

The Basic Theory

Selection of the basic theory to determine the roll force and torque has as its main considerations that (*a*) accuracy must not be sacrificed for speed if the best check of theory and practice is to be obtained, and (*b*) the theory should be as simple as possible within the same limitations.

The theory selected is that of Ford and Bland (3) for rolling with tensions which they describe as an approximation to the homogeneous compression theory of Orowan (2). The theory is corrected by a paper of Bland and Sims (7) for passes in which heavy back tensions are applied to the strip. Previously, the theory had yielded values of roll force lower than the experimental for these passes, especially on annealed strip, Fig. 1.

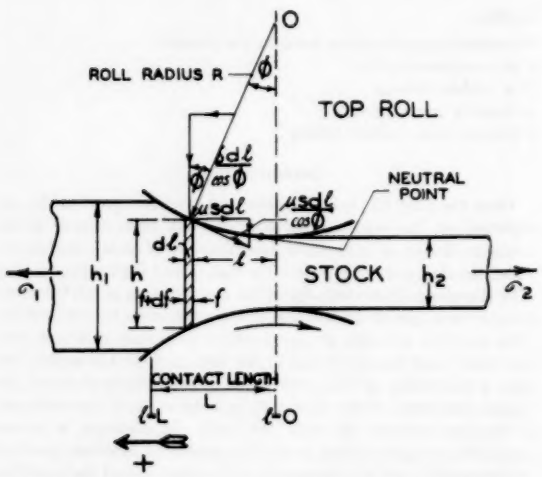

Fig. 1 Forces and Stresses Acting Upon an Elemental Vertical Section of Strip Between Rolls

It is difficult to say whether the results yielded by this theory are more accurate than those of von Karman (1) or Orowan (2), since they all give almost identical results over the practical range of cold-rolling. A comparison with the experimental data so far published leads to the conclusion that there is little to choose between them. The theory chosen is certainly simpler in its calculation method and is selected for this reason. Ford and Bland (3) give the expression for the normal roll pressure, with tensions as

$$s^+ = \frac{kh}{h_2}\left(1 - \frac{\sigma_2}{k_2}\right)e^{\mu H} \quad \text{and}$$

$$s^- = \frac{kh}{h_1}\left(1 - \frac{\sigma_1}{k_1}\right)e^{\mu(H_1 - H)} \quad \ldots\ldots [1]$$

denoting s on the exit side by s^+ and at entry by s^- and

$$H = 2\sqrt{\frac{R^1}{h_2}}\tan^{-1}\sqrt{\frac{R^1}{h_2}}\,\phi \quad \ldots\ldots [2]$$

These expressions give values of roll force lower than the experimental, but the "no-tension" expressions obtained by putting σ_1, and σ_2 equal to 0, have been proved accurate when these expressions are integrated over the contact arc, i.e.

$$s_0^+ = \frac{kh}{h_2}e^{\mu H} \quad \text{and} \quad s_0^- = \frac{kh}{h_1}e^{\mu(H_1 - H)} \quad \ldots\ldots [1a]$$

denoting the no-tension case with suffix 0.

The correction due to Bland and Sims (7) takes as its starting point the equation

$$\frac{df}{d\phi} = 2sR^1(\sin\phi \pm \mu\cos\phi) \quad \ldots\ldots [3]$$

This is the same as Bland and Ford's equation [22], and Orowan's equation [27] from Orowan's "homogeneous compression theory" (2). It connects the normal roll pressure s at any point on the arc of contact with the horizontal force f on the corresponding plane element of unit width, perpendicular to the direction of rolling, Fig. 1. Bland and Sims (7) obtain the expressions for s

$$s^+ = \left(\frac{kh}{h_2} - \sigma_2\right)e^{\mu H}$$

$$s^- = \left(\frac{kh}{h_1} - \sigma_1\right)e^{\mu(H_1 - H)} \quad \ldots\ldots [4]$$

The new equations are obtained from a proved s_0 and deduction of $(s_0 - s)$ from Orowan's original equation. It is then possible to obtain from the following equations of Ford and Bland the total roll force and torque inserting the foregoing values for s

$$\text{Roll force } P = R^1\int_0^{\phi_1} s\,d\phi \quad \ldots\ldots [5]$$

and

$$\text{Roll torque } T = RR^1\left[\int_0^{\phi_1} s\phi\,d\phi + \frac{\sigma_1 h_1 - \sigma_2 h_2}{2R^1}\right] \quad \ldots [6]$$

using point-to-point summation.

Strip Elasticity

It is not proposed to set out fully the theory of the elastic contribution of the rolled strip to the total roll force, roll torque, and roll radius. This has been dealt with in detail by Ford and Bland (8). It is sufficient to indicate the expressions used and modification required to the foregoing theory. The method applies to passes of over about 5 per cent reduction. The elastic zones on the entry and exit sides of the roll gap not only contribute to the roll force directly, but they cause horizontal compressive stresses on the section of the strip in the plastic arc, thus modifying the effective back and front tensions.

(*a*) *Initial Elastic Compression Zone*

Pe_1 = elastic contribution to the roll force of this zone

$$= \frac{(1-\nu^2)}{4E} h_1 \sqrt{\frac{R^1}{h_1 - h_2}} (k_1 - \sigma_1)^2 \quad [7]$$

where

σ_1 = applied back tension

$$\sigma_1' = \sigma_1 - \frac{2\mu Pe_1}{h_1} \quad [8]$$

σ_1' is thus the effective back tension and is used in calculations for the plastic zone. Term $(2\mu Pe_1)/h_1$ is the compressive stress set up in the strip at entry due to elastic compression. The contribution of this zone to both roll force and torque is, for normal passes, very small and usually can be neglected. (See Appendix.)

(*b*) *Elastic Recovery Zone*

Pe_2 = elastic contribution to the roll force in this zone

$$= \frac{2}{3} (k_2 - \sigma_2) \sqrt{\frac{R^1 h_2}{E} (1-\nu^2)(k_2 - \sigma_2)} \quad [9]$$

where

σ_2 = applied front tension

$$\sigma_2' = \sigma_2 - \frac{2\mu Pe_2}{h_2} \quad [10]$$

σ_2' is thus the effective front tension, and is used in calculations for the plastic zone. Term $(2\mu Pe_2)/h_2$ is the compressive stress set up in the strip at exit due to elastic recovery.

(*c*) *Effect on the Roll Torque.* The effect of the elastic compression zone at entry is to retard the roll due to the friction forces acting in the elastic arc, and thus makes a positive contribution to the roll torque given by $\mu R\ Pe_1$. This effect is negligible. The effect in the recovery zone at exit is to help the roll to turn, thus making a negative contribution of $\mu R\ Pe_2$. A tension on the strip is produced which opposes any applied front tension. The torque due to the plastic zone is thus increased, but since the elastic friction forces make a negative contribution of $\mu R\ Pe_2$, the applied torque is little changed.

The roll torque is thus, in practice, altered little by elastic forces. Modification to R^1 the deformed roll radius, however, has an indirect effect on this value.

(*d*) The deformed roll radius is directly affected due to the increase in the effective contact arc of strip and roll. It is quoted as

$$R^1 = R\left[1 + \frac{2cP}{[\sqrt{\delta'} + \sqrt{\delta_2}]}\right] \quad [11]$$

where

δ = draft $h_1 - h_2$

$$\delta_2 = \frac{h_2 (1-\nu^2)(k_2 - \sigma_2)}{E} \quad [12]$$

$\delta_r = \nu(1+\nu)(h_2\sigma_2 - h_1\sigma_1)$

δ' = reduction in pass allowing for elastic recovery

$= \delta + \delta_2 + \delta_r$

When elastic recovery is neglected, Equation [11] reduces to Hitchcock's (9) well-known formula for deformed roll radius.

The complete theory outlined is illustrated by a fully worked check calculation shown in the Appendix, using the practical observations of Whitton (10).

The experimental roll force P is used in determining the deformed roll radius R^1.

Friction Between Rolls and Strip

All the rolling theories make the attempt to assess the frictional contribution of the forces between roll and strip to the total roll force and torque. The roll force is made up of the force to deform the metal from its initial thickness to its final thickness, which is that due to the yield stress of the deformed metal, plus the force due to the friction between roll and strip. The determination of both the yield stress of the metal at each

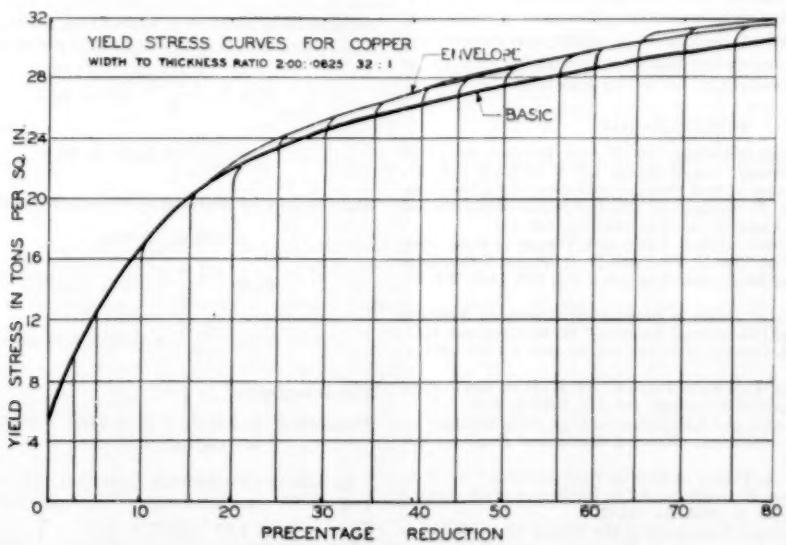

Fig. 2 Yield-Stress Curve for High-Conductivity Copper

point in the roll gap and the contribution due to friction, are thus essential for accurate comparison between theory and practice. Until recently, little was known of the frictional conditions through the arc, and it was necessary to assume a mean value for the coefficient of friction, and to choose a suitable numerical value to facilitate comparison.

In 1953, following a suggestion of Bland in a discussion on a paper to The Institution of Mechanical Engineers (3), a new method was derived, and subsequently tested, for obtaining the mean coefficient of friction between strip and rolls under any lubrication conditions. The values under various practical conditions were reported by Ford and Whitton (6), and the possible variation of μ through the arc of contact was examined by Whitton (10) using this method.

At the present time, it is the only method known which gives the value of μ occurring in cold-rolling under any conditions.

In an unpublished paper, Orowan and Hoff in 1946 attempted to obtain the mean μ by calculation from the roll force and torque. The order of values they obtained was similar to those obtained using the foregoing method, but the values calculated from the roll force differed considerably from those due to the torque. The new method gives repeatable values of μ within about 2 per cent.

Yield-Stress Curve for Metal Rolled

This is most accurately determined by the plane strain-compression method of Watts and Ford (11). The accuracy is estimated by them as within 1 per cent. When the roll force and torque are calculated, the yield stress at each required point in the contact arc is taken from the yield-stress curve at the equivalent reduction (see Appendix).

A typical yield-stress curve is shown in Fig. 2 for high-conductivity copper obtained by this method.

Conclusions

The most accurate and simplest steps essential for the determination of cold-rolling load and torque have been described. Much research by many workers has gone into the establishment of each part, and the practical results obtained over the past 50 years have contributed to the excellent agreement that has now been attained.

Although this stage has been reached, continued work is essential as the rolling of new materials becomes possible and higher production speeds desirable. In making any comparison, it is of the highest importance that every precaution be taken in the practical measurement of the rolling variables.

BIBLIOGRAPHY

1 "On the Theory of Rolling," by Th. von Karman, *Zeitschrift für angewandte Mathematik und Mechanik*, vol. 5, 1952, pp. 139–141.

2 "The Calculation of Roll Pressure in Hot and Cold Flat Rolling," by E. Orowan, Proceedings of The Institution of Mechanical Engineers, London, England, vol. 150, 1943, pp. 140–167.

3 "The Calculation of Roll Force and Torque in Cold Strip Rolling With Tensions," by H. Ford and D. R. Bland, Proceedings of The Institution of Mechanical Engineers, vol. 159, 1948, WE 39, pp. 144–153.

4 "Computation of Loads in Metal Strip Rolling by Methods Involving the Use of Dimensional Analysis," by M. Cook and R. J. Parker, *Journal of the Institute of Metals*, vol. 82, part 3, 1953–1954, p. 129.

5 "Cold Rolling With Strip Tension," by H. Ford and F. Ellis, *Journal of the Iron and Steel Institute*, vol. 171, 1952, p. 239.

6 "Surface Friction and Lubrication in Cold Strip Rolling," by H. Ford and P. W. Whitton, *Chartered Mechanical Engineer*, vol. 1, no. 8, 1954, p. 386.

7 "A Note on the Theory of Rolling With Tensions," by D. R. Bland and R. B. Sims, Proceedings of The Institution of Mechanical Engineers, vol. 167, no. 4, 1953, pp. 371–372.

8 "An Approximate Treatment of the Elastic Compression in Cold Rolling," by H. Ford and D. R. Bland, *Journal of the Iron and Steel Institute*, vol. 171, 1952, p. 245.

9 "Roll Neck Bearings," by J. H. Hitchcock, ASME Research Publication, 1935, Appendix 1.

10 "An Investigation of the Surface Friction in Cold Rolling," by P. W. Whitton, PhD thesis, University of London, London, England, 1953.

11 "An Experimental Investigation of the Yielding of Strip Between Smooth Dies," by A. B. Watts and H. Ford, Proceedings of The Institution of Mechanical Engineers, vol. B1, 1953, p. 10.

Appendix

An example is given of the calculation of roll force and torque for a pass where back tension is applied. Formulas are as quoted in the text.

The experimental data are taken from the work of Whitton (10), and are test No. 116 from Ford and Whitton (6). It is a third pass on copper strip, made with roughened rolls and using no lubricant.

Mean value of μ using the method outlined = 0.113.

Experimental data

Initial thickness of strip = h_f = 0.062 in.
Thickness of strip before pass = h_1 = 0.03 in.
Thickness of strip after pass = h_2 = 0.023 in.
Mean width of strip = b = 2.01 in.
Undeformed roll radius = R = 2.00 in.
Experimental roll force = P_{exp} = 4.77 tons per in. width
Experimental roll torque = T_{exp} = 0.380 ton in. per in. width
Applied back tension = $\sigma_{1\,exp}$ = 5.17 tons per sq in.

The yield-stress curve used for the copper is shown in Fig. 2. The constants for the elastic Formulas [7], [9], [12] are

Young's modulus = E = 6250 tons per sq in.

Poisson's ratio = ν = 0.35

These were selected from tables, and are sufficiently accurate for the calculation of elastic contributions.

$$\text{Percentage reduction before pass} = \frac{0.032}{0.062} = 51.6 \text{ per cent}$$

$$\text{Percentage reduction after pass} = \frac{0.039}{0.062} = 62.9 \text{ per cent}$$

Yield stress at entry = k_1 = 28.8 tons per sq in.
Yield stress at exit = k_2 = 30.4 tons per sq in.

$$\delta_2 = h_2 \frac{(1-\nu^2)}{E}(k_2 - \sigma_2) \quad \ldots\ldots\ldots\ldots\ldots\ldots [12]$$

$$= \frac{1.404}{10^4} \times 0.023 \times 30.4$$

neglecting σ_2 for this and inserting constants

$$= 9.82 \times 10^{-5} \text{ in.}$$

$$\delta_r = \frac{\nu(1+\nu)}{E}(h_2\sigma_2 - h_1\sigma_1) \quad \ldots\ldots\ldots\ldots\ldots\ldots [12]$$

$$= \frac{-7.57}{10^5} \times 0.03 \times 5.17 = \frac{-1.17}{10^5} \text{ in.}$$

This is negligible.

Therefore $\delta' = \delta + \delta_2 + \delta_r = 0.007 + 0.000098 - 0.000012$
$= 0.0071$ in.

In Hitchcock's formula (equation [11]) the constant $C = 1.67 \times 10^{-4}$ for steel rolls. Deformed roll radius = $R' = 2\left[1 + \frac{2 \times 1.67 \times 4.77 \times 10^{-4}}{(\sqrt{0.0071} + \sqrt{9.82 \times 10^{-5}})^2}\right]$ and the experimental

value of roll force is used for this, i.e., 4.77 tons per in. Therefore $R^1 = 2.358$ in.

Pe_1 is Negligible

$$Pe_2 = \frac{2}{3}(k_2 - \sigma_2)\sqrt{\frac{R^1 h_2}{E}(1-\nu^2)(k_2-\sigma_2)} \quad \ldots\ldots\ldots\ldots [9]$$

$$= \frac{1.842}{10^3}(30.4 - \sigma_2)^{3/2}$$

Inserting elastic constants for E and ν, and

$$\frac{2\mu Pe_2}{h_2} = 9.84\, Pe_2$$

Trying a value for Pe_2 of 0.36 ton per in. gives $9.84\, Pe_2 = 3.54$ tons per sq in. and checking

$$Pe_2 = \frac{1.842}{10^3}(30.4 + 3.54)^{3/2} = 0.364 \text{ tons per in.}$$

This is sufficiently accurate. Therefore

$Pe_2 = 0.36$ ton per in.

$\sigma_2' = -3.54$ tons per sq in. ..... [10]

Plastic angle of contact $= \phi_1 = \sqrt{\frac{\delta'}{R^1}} = 0.055$

$$H_1 = 2\sqrt{\frac{R^1}{h_1}}\tan^{-1}\sqrt{\frac{R^1}{h_2}}\,\phi_1 \quad \ldots\ldots\ldots\ldots [2]$$

$$= 10.28$$

The integrals in Equations [5] and [6] are then evaluated. To do this it is necessary to calculate the values of s and $s\phi$ at various points in the plastic arc of contact. This is set out in Table 1.

The yield-stress curve is used to obtain line 13 from line 12 and Equation [4] to give s in lines 14 and 15. The values of s are then plotted against ϕ and the roll force and torque obtained using Equations [5] and [6] as stated, by point-to-point summation. Fig. 3 shows the values of s plotted against ϕ, the angle of contact.

From Fig. 3

$$\int_0^{\phi_1} s\,d\phi = 1.837$$

by graphical integration

$$\text{Plastic roll force} = R^1\int_0^{\phi_1} s\,d\phi \quad \ldots\ldots\ldots [5]$$

$$= 2.358 \times 1.837 = 4.33 \text{ tons per in.}$$

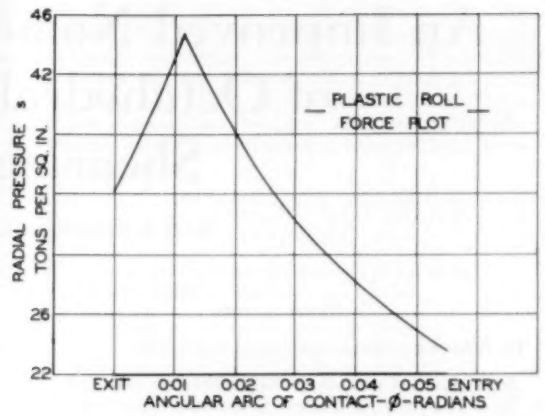

FIG. 3 PLASTIC ROLL-FORCE PLOT

Therefore

$$\text{Calculated roll force} = \text{plastic roll force} + Pe_2$$

$$= 4.33 + 0.36 = 4.69 \text{ tons per in.}$$

$$\text{Error in roll force} = \frac{4.77 - 4.69}{4.77} = 1.7 \text{ per cent low}$$

taken on the experimental value

$$\text{Calculated roll torque} = RR^1\left[\int_0^{\phi_1} s\phi\,d\phi + \frac{\sigma_1 h_1 - \sigma_2 h_2}{2R^1}\right] \quad \ldots [6]$$

$$= 2 \times 2.358\left[0.0455 + \frac{5.17 \times 0.03}{2 \times 2.358}\right]$$

where

$$\int_0^{\phi_1} s\phi\,d\phi = 0.0455$$

by graphical integration. Therefore

$$\text{Calculated roll torque} = 0.369 \text{ ton in. per in.}$$

$$\text{Error in roll torque} = \frac{0.38 - 0.369}{0.38} = 2.9 \text{ per cent low on the}$$

experimental value.

TABLE 1 CALCULATION OF ROLL FORCE AND TORQUE

	Exit point 1	2	3	4	5	6	7	8	9	10	Entry point 11
(1) ϕ	0	0.0055	0.0110	0.0165	0.0220	0.0275	0.0330	0.0385	0.0440	0.0495	0.0550
(2) $\sqrt{\frac{R^1}{h_2}}\,\phi$	0	0.0566	0.111	0.167	0.222	0.278	0.333	0.389	0.445	0.500	0.558
(3) $\tan^{-1}\sqrt{\frac{R^1}{h_2}}\,\phi$	0	0.0556	0.110	0.166	0.218	0.271	0.322	0.371	0.419	0.464	0.508
(4) H	0	1.12	2.23	3.34	4.40	5.48	6.50	7.50	8.45	9.37	10.28
(5) $H_1 - H$	10.28	9.16	8.05	6.94	5.88	4.80	3.78	2.78	1.83	0.91	0
(6) μH	0	0.127	0.252	0.378	0.498						
(7) $\mu(H_1 - H)$	1.16	1.035	0.910	0.785	0.665	0.543	0.427	0.314	0.207	0.103	0
(8) $e^{\mu H}$	1.00	1.13	1.29	1.46	1.64						
(9) $e^{\mu(H_1-H)}$	3.19	2.81	2.48	2.19	1.94	1.72	1.53	1.37	1.23	1.11	1.00
(10) $R^1\phi^2$ in.	0	0.0001	0.0003	0.0006	0.0011	0.0018	0.0026	0.0035	0.0046	0.0058	0.0070
(11) $h = h_2 + R^1\phi^2$	0.0230	0.0231	0.0233	0.0236	0.0241	0.0248	0.0256	0.0265	0.0276	0.0288	0.0300
(12) Total percentage reduction	62.9	62.8	62.4	61.9	61.2	60.0	58.7	57.3	55.5	53.6	51.6
(13) k tons per sq in.	30.4	30.4	30.3	30.2	30.1	29.9	29.7	29.5	29.2	29.0	28.8
(14) s exit	33.9	38.7	44.0	50.2	57.6						
(15) s entry	57.8	51.5	45.6	40.8	36.9	33.6	30.8	28.6	26.6	25.0	23.63

An Improved Nomogram for the Ratios of Octahedral to Maximum Shearing Stresses

By O. P. KHARBANDA,[1] LONDON, ENGLAND

Nomenclature

The following nomenclature is used in the note:

S_1 = principal stress of maximum absolute value, psi
S_2, S_3 = two principal stresses of absolute value less than or equal to the absolute value of S_1, psi
$\alpha = S_2/S_1$ = nondimensional parameter
$\beta = S_3/S_1$ = nondimensional parameter
$\tau_{max} = S_1 - S_3/2$ = maximum shearing stress, psi
τ_{oct} = octahedral shearing stress
$\rho = \tau_{oct}/_{max}$ = nondimensional ratio of octahedral to maximum shearing stress

Nomogram

A nomogram recently published gives the ratio of the octahedral to the maximum shearing stresses for all possible stress distributions. The parameters used are the ratios of the two principal stresses (S_2, S_3) to the one (S_1) of maximum absolute value.

The nomogram is a timesaver for design calculations. However, its use in the present form is not very convenient and, particularly, interpolation is rather difficult. The accompanying nomogram, consisting of three intersecting straight lines, is believed to be more convenient to use and, in addition, interpolation is much easier. The result is readily obtained by a single setting of a straight ruler.

The use and the physical significance of this nomogram as described by Zizicas remain unchanged. The nomenclature used here is identical to the nomenclature in the paper cited.[2]

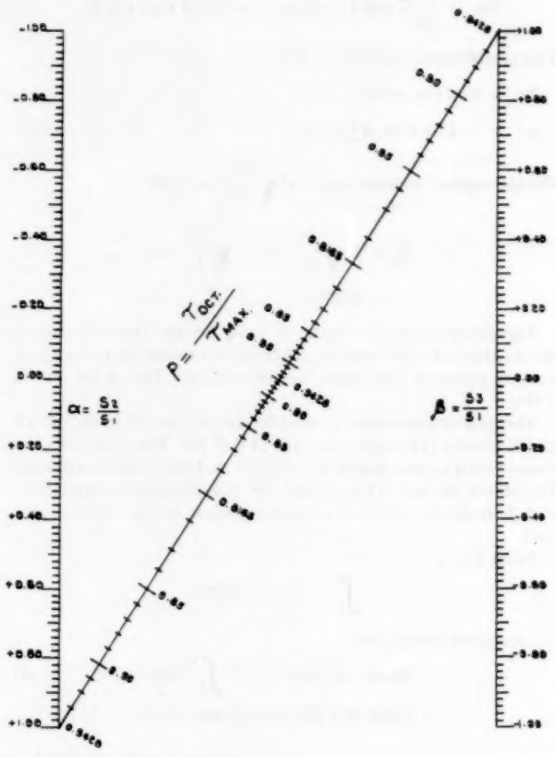

[1] Costain-John Brown, Ltd.

Discussion of this paper should be addressed to the Secretary, ASME, 29 West 39th Street, New York, N. Y., and will be accepted until July 10, 1956, for publication at a later date. Discussion received after the closing date will be returned.

Note: Statements and opinions advanced in papers are to be understood as individual expressions of their authors and not those of the Society. Manuscript received by ASME Applied Mechanics Division, January 3, 1955.

[2] "A Simple Nomogram for the Ratios of Octahedral to Maximum Shearing Stresses and Its Physical Interpretation," by G. A. Zizicas, Journal of Applied Mechanics, Trans. ASME, 1954, p. 291.

Brief Notes*

On the recommendations of the Executive Committee of the ASME Applied Mechanics Division, it has been decided to initiate a section devoted to brief notes on technical matters in mechanics. These notes must not be longer than 750 words (about 2½ double-spaced typewritten pages, including figures) and will be subject to the usual review procedure prior to publication. After approval such notes will be published in the next issue of the Journal. The notes should be submitted to the Secretary of the ASME Applied Mechanics Division.

Transient Temperature Rise in a Semi-Infinite Solid Due to a Uniform Disk Source

By M. M. ATALLA[1] and K. PRESTON, JR.,[1]
NEW YORK, N. Y.

A transient solution is presented for the temperature rise in a semi-infinite solid due to a circular-disk source with a uniform and constant rate of heat flux. The solution is obtained only along the axis of the disk. It is shown that the temperature-time relation at any point along this axis is obtainable from the corresponding well-known one-dimensional solution for a semi-infinite rod by the relation

$$[\theta(z, t)]_{3\text{-dimensional}} = \left[\theta(z, t) - \theta\left(\sqrt{z^2 + a^2}, t\right)\right]_{1\text{-dimensional}}$$

where θ, z, a, and t are the temperature rise, distance from the surface, radius of the heat source, and time, respectively.

Introduction

In the course of a study of the mechanism of the electric arc, the following idealized heat-conduction problem was involved: A plane surface (the anode) is bombarded by a circular beam of electrons of uniform power density. It was desired to obtain the transient temperature distribution in the anode during the electron bombardment. This was done by replacing the electron bombardment by an equivalent heat source on the surface of the anode and by neglecting the variations with temperature of the physical properties of the solid. This solution should be useful for a number of practical applications having the same boundary conditions.

Solution

Consider a semi-infinite solid with thermal conductivity k; specific heat c; and density ρ. Let a circular disk source of radius a and uniform power density Q be suddenly applied on the surface of the solid. The solid is initially at a uniform temperature. The resulting temperature rise is determined by integrating the appropriate Green's function over the disk source. This function gives the temperature rise produced at a point (x, y, z, t) or (r, φ, z, t) for Cartesian or cylindrical co-ordinates, respectively, due to a unit heat source at the point (x', y', z', t') or (r', φ', z', t').

In Cartesian co-ordinates the Green's function[2] for a semi-infinite solid is given by

$$G = \frac{2 \exp\left\{-[(x - x')^2 + (y - y')^2 + (z - z')^2]/4\alpha(t - t')\right\}}{\rho c[4\pi\alpha(t - t')]^{3/2}}$$

where $\alpha = k/\rho c$ and is the thermal diffusivity of the solid.

In cylindrical co-ordinates this function becomes

$$G = \frac{2 \exp\left\{-[r^2 + r'^2 - 2rr' \cos(\varphi - \varphi') + (z - z')^2]/4\alpha(t - t')\right\}}{\rho c[4\pi\alpha(t - t')]^{3/2}}$$

The expression for the desired temperature rise θ is obtained by integrating Green's function over time and space

$$\theta(r, \varphi, z, t) = \int_{\text{time}} \int_{\text{space}} Gr'dr'd\varphi'dz'dt'$$

Unfortunately, an integration for the general solution results in integrals that cannot be evaluated in terms of tabulated functions. The special solution for temperature rise along the z-axis, however, can be obtained readily in terms of error functions. This is done by setting $r = 0$ in the foregoing integral and choosing limits corresponding to the disk source. This gives

$$\theta = \frac{2Q}{\rho c} \int_0^t [4\pi\alpha(t - t')]^{-3/2} dt' \int_0^a \exp\left[-\frac{r'^2 + z^2}{4\alpha(t - t')}\right] r'dr' \int_0^{2\pi} d\varphi'$$

where Q is the power density at the disk source.

By integrating, the following expression for temperature rise is obtained

$$\theta(z, t) = \frac{Q}{k}\left[2\left(\frac{\alpha t}{\pi}\right)^{1/2}\left(e^{-\frac{z^2}{4\alpha t}} - e^{-\frac{a^2+z^2}{4\alpha t}}\right) - z \operatorname{erfc} \frac{z}{(4\alpha t)^{1/2}} + (a^2 + z^2)^{1/2} \operatorname{erfc}\left(\frac{a^2 + z^2}{4\alpha t}\right)^{1/2}\right]$$

It is of interest to compare this solution with the corresponding one-dimensional solution for a semi-infinite rod. In this latter case the temperature rise θ is given by[3]

$$\theta(z, t) = \frac{Q}{k}\left[2\left(\frac{\alpha t}{\pi}\right)^{1/2} e^{-\frac{z^2}{4\alpha t}} - z \operatorname{erfc}\left(\frac{z}{4\alpha t}\right)^{1/2}\right]$$

where z is measured from the end of the rod. From the two foregoing equations it is evident that

$$[\theta(z, t)]_{3\text{-dimensional}} = \left[\theta(z, t) - \theta\left(\sqrt{a^2 + z^2}, t\right)\right]_{1\text{-dimensional}}$$

This states that the temperature distribution on the z-axis in a semi-infinite solid heated by a disk source of radius a and uniform power density Q is equal to the temperature difference between

---

[1] Bell Telephone Laboratories.

* Discussion of papers in Brief Notes should be addressed to the Secretary, ASME, 29 West 39th Street, New York, N. Y., and will be accepted until July 10, 1956, for publication at a later date. Discussion received after the closing date will be returned.

Note: Statements and opinions advanced in papers are to be understood as individual expressions of their authors and not those of the Society. Manuscript received by ASME Applied Mechanics Division, June 9, 1955.

[2] "Conduction of Heat in Solids," by H. S. Carslaw and J. C. Jaeger, Oxford University Press, 1947, p. 291. The Green's function herein is for an "infinite" solid which was multiplied by a factor of 2 for the semi-infinite solid.

[3] "Heat Transfer," by M. Jakob, John Wiley & Sons, Inc., New York, N. Y., vol. 1, 1949, p. 258.

the two points z and $(a^2 + z^2)^{1/2}$ in the one-dimensional case of heating a semi-infinite rod.

The maximum temperature rise at any point along the axis of the heat source is reached asymptotically and is given by

$$\theta(z, \infty) = \frac{Q}{k} [(a^2 + z^2)^{1/2} - z]$$

The Mean Stress Around a Small Opening of Any Shape in a Uniformly Loaded Plate[1]

By J. S. BROCK,[2] WASHINGTON, D. C.

This paper proposes a theorem concerning the mean stress around an opening in a uniform stress field. The theorem states that the mean stress along the free boundary of an opening of any shape in a uniformly loaded plate is equal to the sum of the co-ordinate normal stresses applied to the plate at a great distance from the opening. The theorem is proved by using well-known properties of harmonic functions in conjunction with Green's theorem.

Mean-Stress Theorem

THE object of this note is to propose and prove a theorem concerning the mean stress on the boundary of any hole in a plate which is subjected to a uniform stress field at regions remote from the hole.

Consider an opening of arbitrary shape in an infinite, uniformly loaded plate. Define the mean tangential stress, $\bar{\sigma}_t$, along the free boundary of the opening as

$$\frac{1}{2\pi} \int_0^{2\pi} \sigma_t d\beta$$

where σ_t is the tangential stress at any point on the boundary and β is the curvilinear co-ordinate which takes one around the boundary of the opening. Then the mean stress on the free boundary of any opening (which may be mapped by a rational function) is equal to the sum of the applied normal stresses in mutually perpendicular directions. This theorem may be expressed as follows

$$\frac{1}{2\pi} \int_0^{2\pi} \sigma_t d\beta = S_x + S_y \quad [1]$$

where S_x and S_y are the applied normal stresses at infinity. It will be noted that the theorem requires the stress to be averaged with respect to β rather than the arc length of the opening. This is a convenience since the solution to boundary-value problems in the theory of elasticity gives the stresses as a function of the curvilinear co-ordinates used in the solution.

The theorem can be proved by using the properties of harmonic functions. It is well known that the sum of the normal stresses satisfies Laplace's equation. By using this fact in conjunction with Green's theorem in the plane it can easily be shown that if γ is the boundary of a hole in an infinite plate in which $\sigma_x + \sigma_y$ has no singularities

$$\int_\gamma \frac{d(\sigma_x + \sigma_y)}{dn} ds + \int_\Gamma \frac{d(\sigma_x + \sigma_y)}{dn} ds = 0 \quad [2]$$

where $d/(dn)$ denotes the derivative normal to the boundary; ds is an element of arc length along the boundary; and Γ is the circle at infinity. Now $d(\sigma_x + \sigma_y)/dn$ is zero at infinity and the right-hand integral vanishes; therefore Equation [2] becomes

$$\int_\gamma \frac{d(\sigma_x + \sigma_y) ds}{dn} = 0 \quad [3]$$

which holds when γ is the boundary of the opening and for any boundary which completely encloses the opening.

Assume a curvilinear orthogonal system of co-ordinates as defined by the following mapping function

$$z = c\zeta + \sum_0^k \frac{c_m}{\zeta^m} \quad [4]$$

where

$$z = x + iy; \quad \zeta = e^{\alpha + i\beta}; \quad m = 0, 1, 2, \ldots k$$

Since the mapping function is rational this may appear to be too restricted. However, owing to the freedom in the choice of c_m, it is possible to map regions of arbitrary shape to any desired accuracy. The transformation from the z-plane to the ζ-plane is conformal and isometric, i.e.

$$J_\alpha = J_\beta \text{ or } \frac{dn}{d\alpha} = \frac{ds}{d\beta} \quad [5]$$

Equation [3] becomes

$$\int_\gamma \frac{d(\sigma_x + \sigma_y)}{dn} \frac{dn}{d\alpha} d\beta = \frac{d}{d\alpha} \int_\gamma (\sigma_x + \sigma_y) d\beta = 0 \quad [6]$$

therefore

$$\int_\gamma (\sigma_x + \sigma_y) d\beta = \int_\gamma (\sigma_\alpha + \sigma_\beta) d\beta = \text{const} \quad [7]$$

The value of this constant is evaluated on a circle of large radius where the stresses are everywhere S_x, S_y, T_{xy}. Since the shear stress does not affect the sum of the normal stresses, $\sigma_\alpha + \sigma_\beta = S_x + S_y$ along the circle so that the value of the constant is $2\pi (S_x + S_y)$. Then Equation [7] becomes

$$\frac{1}{2\pi} \int_0^{2\pi} (\sigma_\alpha + \sigma_\beta) d\beta = S_x + S_y \quad [8]$$

On the free boundary of the opening this reduces to Equation [1].

The theorem indicates that a pure shearing stress applied at infinity contributes nothing to the mean stress around the opening. This is evident since a state of pure shear is defined by two normal stresses of equal magnitude but of opposite sign; i.e., $S_x = -S_y$.

Consider the case of pure tension in which $S_x = T_{xy} = 0$, $S_y = T$. The theorem becomes

$$\frac{1}{2\pi} \int_0^{2\pi} \sigma_t d\beta = T \quad [9]$$

This simply signifies that the mean stress around an opening in a field of pure tension is equal to the magnitude of the applied stress. Since the mean stress around an opening is the same regardless of its shape, it is impossible to have an infinite stress concentration except on an infinitesimal length of boundary.

---

[1] The opinions or assertions in this paper are the author's and do not reflect the views of the David Taylor Model Basin or the Navy Department.

[2] Structural Research Engineer, David Taylor Model Basin.

Manuscript received by ASME Applied Mechanics Division, July 1, 1955.

The validity of the theorem may be demonstrated by means of the results of previous solutions for the stresses around common openings. Finally, the theorem, Equation [1] or [9], may be used to check new solutions to boundary-value problems in the theory of elasticity.

Note on Torsion With Variable Twist[1]

By ERIC REISSNER,[2] CAMBRIDGE, MASS.

In a recent paper (1)[3] the author considered anew the problem of determining corrections to the Saint Venant theory of torsion, induced by restraint against warping at the end section of the beam. The present note is intended to furnish some further discussion of these earlier results.

RESTRICTING attention to cylindrical rods of doubly symmetric cross section, the following alternate differential equations and boundary conditions were obtained

$$GC\beta' - E\Gamma\beta''' = T, \qquad \beta'(0) = \beta'''(L) = 0 \ldots\ldots [1]$$

$$GC\beta' - E\Gamma\frac{I_p}{D}\beta''' = T, \qquad \beta'(0) = \frac{T}{GI_p}, \ \beta'''(L) = 0 \ldots [2]$$

In Equations [1] and [2] primes denote differentiation and the meaning of the symbols is as follows:

G = modulus of rigidity
E = modulus of elasticity
T = torque applied at end $z = L$
β = angle of rotation of beam section
$C = I_p - D$ = torsional rigidity
$I_p = \int (x^2 + y^2)dA$ = polar moment of inertia of cross-sectional area A
$D = \int [(\partial\phi/\partial x)^2 + (\partial\phi/\partial y)^2]dA$ = Dirichlet integral over Saint Venant warping function ϕ
$\Gamma = \int \phi^2 dA$

Equations [1] had been obtained by Wagner (2) and Goodier (3) by a different approach and prior to that by Timoshenko (4) for the special case of certain thin-walled open sections.

It was indicated in reference (1) that Equations [2] appear to be more accurate than Equations [1]. The following observation is to be added to this general remark. For the case of thin-walled open sections we have the fact that the torsional rigidity C is small compared to either one of its two components I_p and D. Accordingly, we have for this class of cross sections $I_p \sim D$ and Equations [2] reduce effectively to Equations [1]. This means that for thin-walled *open* sections the practical improvement gained by working with Equations [2] instead of with Equations [1] will in general be negligible. This observation is in agreement with certain interesting results which were recently obtained by Flügge and Marguerre (5). These authors also point out that results equivalent to Equations [1] are not adequate for the treatment of thin-walled *closed* sections, without however offering an alternative such as Equations [2]. Results for closed-section beams with rectangular cross sections were given earlier by H. Reissner (6), H. Ebner (7), and others.

Applying Equations [2]

To illustrate the use of Equations [2] we shall evaluate in what follows the appropriate coefficients for the special case of the thin-walled rectangular section with corner flanges. This case is also considered in [5]. Let a and b be the lateral dimensions of the section, and let the wall thicknesses be t. Let F be area of each of the four corner flanges. The Saint Venant warping function for this case is

$$\left.\begin{aligned} \phi &= \pm\frac{b}{2}\frac{a-b}{b+a}x, \text{ along the } a\text{-sides} \\ \phi &= \pm\frac{a}{2}\frac{b-a}{b+a}y, \text{ along the } b\text{-sides} \end{aligned}\right\} \ldots\ldots [3]$$

We further have

$$\left.\begin{aligned} I_p &= 2\int_{-b/2}^{b/2}[(a/2)^2 + y^2]t\,dy + \\ &\qquad 2\int_{-a/2}^{a/2}[(b/2)^2 + x^2]t\,dx \\ &= \frac{1}{2}ab(a+b)t + \frac{1}{6}(b^3 + a^3)t \end{aligned}\right\} \ldots [4]$$

$$\left.\begin{aligned} D &= 2\int_{-b/2}^{b/2}\left[\frac{a}{2}\frac{b-a}{b+a}\right]^2 t\,dy + \\ &\qquad 2\int_{-a/2}^{a/2}\left[\frac{b}{2}\frac{b-a}{b+a}\right]^2 t\,dx \\ &= \frac{t}{2}\frac{ab(b-a)^2}{b+a} \end{aligned}\right\} \ldots [5]$$

$$\Gamma = 2\int_{-b/2}^{b/2}\left[\frac{a}{2}\frac{b-a}{b+a}y\right]^2 t\,dy + 2\int_{-a/2}^{a/2}\left[\frac{b}{2}\frac{a-b}{a+b}x\right]^2 t\,dx + 4F\left[\frac{ba}{4}\frac{a-b^2}{b+a}\right]$$

$$= \frac{a^2b^2}{4}\left[\frac{a-b}{b+a}\right]^2\left[F + \frac{1}{6}(b+a)t\right] \ldots\ldots [6]$$

In first approximation we have $D \ll I_p$. If we set $C \sim I_p$, then according to Equations [2]

$$\beta' - \frac{E}{G}\frac{\Gamma}{D}\beta''' = \frac{T}{GI_p} \ldots\ldots [2a]$$

and according to Equations [5] and [6]

$$\frac{\Gamma}{D} = \frac{1}{2}\frac{F + \frac{1}{6}t(b+a)}{t(b+a)}ab \ldots\ldots [7]$$

In contrast to this, Equation [1] would assume the form

$$\beta' - \frac{E}{G}\frac{\Gamma}{I_p}\beta''' = \frac{T}{GI_p} \ldots\ldots [1a]$$

with

$$\frac{\Gamma}{I_p} = \frac{1}{2}\frac{F + \frac{1}{6}t(b+a)}{t(b+a)}\left(\frac{ab(b-a)}{(b+a)^2}\right)^2 \ldots\ldots [8]$$

---

[1] Supported by Office of Naval Research under Contract N5-ori-07834, with Massachusetts Institute of Technology, Cambridge, Mass.

[2] Professor of Mathematics, Massachusetts Institute of Technology.

[3] Numbers in parentheses refer to the Bibliography at the end of the paper.

Manuscript received by ASME Applied Mechanics Division, September 22, 1955.

For the sake of comparison we note that when $a = 2b$, then the value of Γ/I_p of Equation [8] is only $^2/_{\pi}$ of the value of Γ/D of Equation [7]. This shows, as it was intended, that for thin-walled *closed*-section beams the more accurate System [2] leads to results which are quite different from what would follow from a use of the System [1].

Wherever the System [1] is applicable there it furnishes effectively the same results as the no more complicated System [2].

BIBLIOGRAPHY

1 "On Non-Uniform Torsion of Cylindrical Rods," by E. Reissner, *Journal of Mathematics and Physics*, vol. 31, 1952, pp. 214–221.

2 "Torsion and Buckling of Open Sections," by H. Wagner, NACA TM 807, 1936.

3 "The Buckling of Compressed Bars by Torsion and Flexure," by J. N. Goodier, Cornell University Eng. Exp. Station, Bulletin No. 27, 1941.

4 "Einige Stabilitätsprobleme der Elastizitätstheorie," by S. Timoshenko, *Zeitschrift für Mathematik und Physik*, vol. 58, 1910, p. 361.

5 "Warping-Restraints in Thin-Walled Rods" (in German), by W. Flügge and K. Marguerre, *Ingenieur-Archiv*, vol. 18, 1950, pp. 23–38.

6 "Flügelkorper ohne äusseres Tragwerk," by H. Reissner, *Zeitschrift für Flugtechnik und Motorluftschiffahrt*, vol. 17, 1926, pp. 384–393.

7 "Die Beanspruchung dünnwandiger Kastenträger auf Drillung bei behinderter Querschnittswölbung," by H. Ebner, Jahresbericht 1933 der Statischen Abteilung der DVL (Sonderdruck aus dem Jahrbuch 1933 der Deutschen Versuchsanstalt für Luftfahrt) III 72–III 90.

Circular-Symmetric Vibrations of Infinitely Long Cylindrical Shells With Equidistant Stiffeners[1]

By M. L. BARON,[2] NEW YORK, N. Y.

TABLES for the determination of the frequencies of circular symmetric free vibrations of an infinitely long cylindrical shell with equidistant stiffeners are presented. It is assumed that the stiffeners are closely spaced with the result that motion of the shell parallel to the axis of the cylinder can be neglected, Fig. 1. Only those oscillations in which the space configuration has the period l (l = spacing of stiffening rings) in the direction of the axis of the cylinder are considered. The results apply for the case where the radii of the ring and of the shell are alike. Allowance was made in the analysis for an additional uniformly distributed mass attached to the shell, but having no elastic resistance, like an insulation. Under the foregoing assumptions, the frequency equation for the free vibrations is obtained in terms of just two parameters κ and ϕ which are functions of the properties of the stiffened shell and the added mass.

Considering radial motions only, the equation of motion of the shell carrying the additional mass Δm per unit of area is

$$\frac{Eh^3}{12(1-\nu^2)}\frac{\partial^4 w}{\partial z^4} = -\frac{Eh}{a^2}w - (m+\Delta m)\frac{\partial^2 w}{\partial t^2} \quad [1]$$

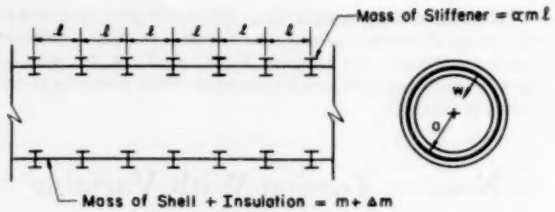

FIG. 1 GEOMETRY OF PROBLEM

where $w(z, t)$ is the radial displacement of a point on the shell. Its free vibrations of frequency Ω are of the form

$$w(z, t) = W(z)\sin \Omega t \quad [2]$$

where for vibrations in which the space configurations have the period l in the direction of the axis of the cylinder

$$W(z) = C_1 \cos \beta z + C_2 \cosh \beta z \quad [3]$$

and

$$\beta^4 = \frac{(m+\Delta m)\,\Omega^2 - Eh/a^2}{\frac{Eh^3}{12(1-\nu^2)}}$$

The boundary conditions of the shell require that the slope of the deflection curve vanishes at the stiffening rings

$$\frac{dw}{dz} = 0 \text{ at } z = l/2 \quad [4]$$

and that the shear at the stiffening rings is in equilibrium with the inertia forces of the stiffener and the forces due to the elasticity of the stiffening ring

$$-\frac{Eh^3}{12(1-\nu^2)}\frac{\partial^3 w}{\partial z^3} = -\frac{\alpha m\, l}{2}\frac{\partial^2 w}{\partial t^2} - \frac{\alpha E h\, l}{2a^2}w \text{ at } z = l/2. \quad [5]$$

Substitution of Equations [2] and [3] into Equations [4] and [5] leads to two homogeneous algebraic equations, the determinant of which when equated to zero gives the frequency equation

$$2\left(\frac{\beta l}{2}\right)^3 + \kappa\left[\left(\frac{\beta l}{2}\right)^4 - \phi\right]\left[\cot\frac{\beta l}{2} + \coth\frac{\beta l}{2}\right] = 0 \quad [6]$$

Once β_i has been determined the shape of the particular mode of vibration may be determined from the relation

$$W_i = C_1\left[\cos\beta_i z + \frac{\sin\beta_i l/2}{\sinh\frac{\beta_i l}{2}}\cosh\beta_i z\right] \quad [7]$$

The tables of values of $\beta_0 l/2$ and $\beta_1 l/2$ permit the computation of the frequencies Ω_0 and Ω_1 of the fundamental and second lowest modes of vibration of the stiffened shell. The value of $\beta l/2$ depends on the two parameters κ and ϕ

$$\phi = \frac{0.75\,\Delta m}{m}\frac{l^4(1-\nu^2)}{a^2h^2} \quad [8]$$

$$\kappa = \frac{\alpha}{1+\frac{\Delta m}{m}} \quad [9]$$

where

l = spacing of stiffener rings

---

[1] The material is an extract of that presented in "Circular Symmetric Vibrations of Infinitely Long Cylindrical Shells With Equidistant Stiffeners," by M. L. Baron, Tech. Report No. 11, Office of Naval Research Contract Nonr 266(08), AFSWP 871, Columbia University, 1954.

[2] Assistant Professor, Department of Civil Engineering and Engineering Mechanics, Columbia University. Assoc. Mem. ASME.

Manuscript received by ASME Applied Mechanics Division, June 3, 1955.

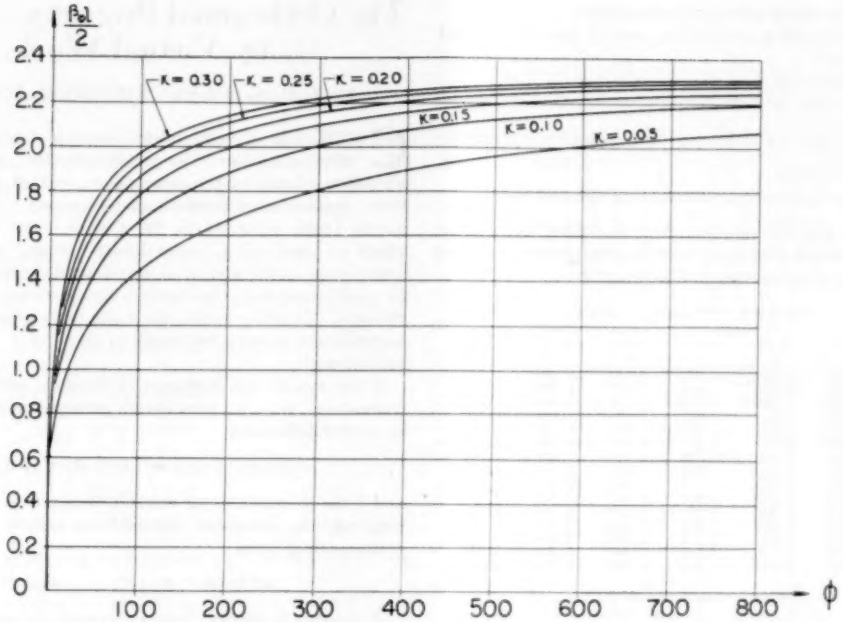

FIG. 2 FREQUENCY PARAMETER $\beta_0 l/2$

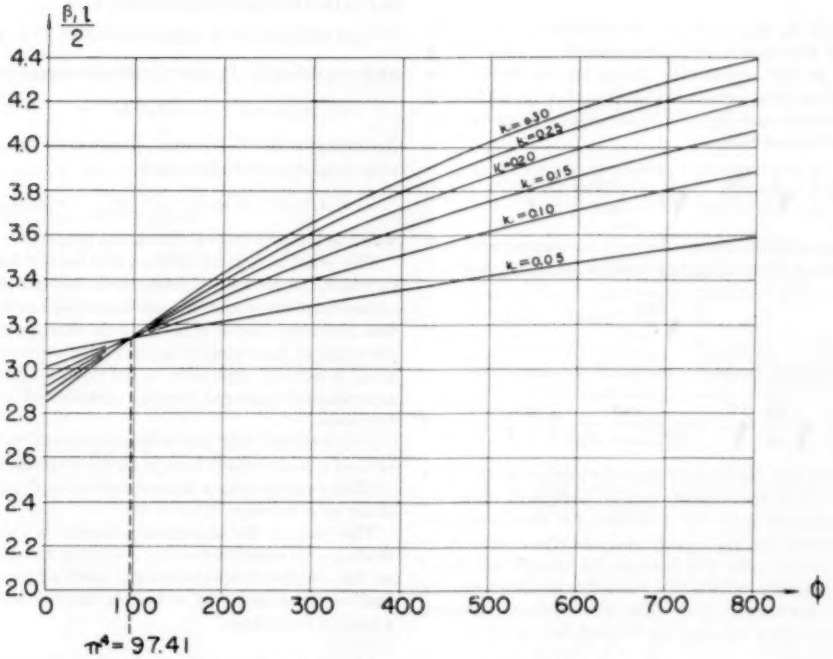

FIG. 3 FREQUENCY PARAMETER $\beta_1 l/2$

m = mass per unit of area of cylindrical shell
Δm = additional mass per unit of area of materials carried by shell
h = shell thickness
a = mean radius of shell
$\alpha = \frac{A_R}{hl}$ = where A_R is the cross-sectional area of ring stiffener
ν = Poisson's ratio
Ω = circular frequency of vibration of stiffened shell

Tables 1 and 2 give the values of $\beta_0 l/2$ and $\beta_1 l/2$, respectively, for each value of $\kappa = 0.05(0.05)\ 0.30$ as ϕ varies between 0 and 1000. The values are plotted in Figs. 2 and 3.

TABLE 1 VALUES OF $\beta_0 l/2$

	κ =					
ϕ	0.05	0.10	0.15	0.20	0.25	0.30
0	0	0	0	0	0	0
5	0.698	0.819	0.896	0.952	0.996	1.031
10	0.829	0.972	1.062	1.127	1.179	1.220
15	0.916	1.073	1.172	1.243	1.298	1.344
20	0.983	1.151	1.255	1.330	1.389	1.436
40	1.163	1.356	1.473	1.557	1.621	1.673
60	1.281	1.487	1.610	1.696	1.761	1.813
80	1.369	1.583	1.708	1.794	1.858	1.908
100	1.441	1.659	1.784	1.868	1.930	1.977
150	1.575	1.795	1.915	1.992	2.047	2.088
200	1.672	1.888	2.000	2.069	2.117	2.151
250	1.746	1.956	2.059	2.121	2.163	2.192
300	1.807	2.007	2.103	2.158	2.195	2.220
400	1.898	2.081	2.162	2.207	2.236	2.256
500	1.964	2.130	2.200	2.238	2.262	2.277
1000	2.134	2.241	2.280	2.300	2.313	2.322

TABLE 2 VALUES OF $\beta_1 l/2$

	κ =					
ϕ	0.05	0.10	0.15	0.20	0.25	0.30
0	3.070	3.012	2.962	2.920	2.883	2.851
100	3.143	3.145	3.146	3.148	3.149	3.149
200	3.217	3.277	3.327	3.368	3.402	3.430
300	3.288	3.403	3.491	3.561	3.618	3.664
400	3.358	3.518	3.637	3.728	3.800	3.859
500	3.425	3.625	3.767	3.873	3.957	4.023
800	3.609	3.893	4.080	4.214	4.316	4.396
1000	3.718	4.040	4.243	4.386	4.492	4.576

The frequencies Ω_0 and Ω_1 of the fundamental and second lowest modes of vibration may be determined by substituting values of $\beta l/2$ in the appropriate frequency equation. The parameter ϕ differs from zero if the shell carries an additional uniformly distributed mass $\Delta m l$, i.e., insulation. The frequency Ω is in this case obtained from

$$\Omega = \frac{1}{a}\sqrt{\frac{Eh}{m + \Delta m}}\sqrt{1 + \frac{\Delta m}{\phi m}\left(\frac{\beta l}{2}\right)^4} \quad \ldots\ldots [10]$$

For shells with no additional mass, $\Delta m = 0$, the parameter $\phi = 0$ and the frequency of the fundamental mode is for all values of κ

$$\Omega_0 = \frac{1}{a}\sqrt{\frac{Eh}{m}} \quad \ldots\ldots [11]$$

while the frequencies of the higher modes are obtained from

$$\Omega = \frac{1}{a}\sqrt{\frac{Eh}{m}}\sqrt{1 + \frac{a^2h^2}{0.75\ (1 - \nu^2)l^4}\left(\frac{\beta l}{2}\right)^4} \quad \ldots\ldots [12]$$

The assumption has been made that the motion of the shell parallel to the axis of the cylinder can be neglected. This assumption is reasonable only if $l < a$ since for these cases the longitudinal motions are very small and contribute very little to the kinetic energy. For the case of the unstiffened shell,[2] the longitudinal motion affects the fundamental frequency by no more than 0.6 per cent if $l \leq a$. The present theory therefore is likely to give excellent values of the frequencies for $l \leq a$.

[2] "Tables for the Frequencies and Modes of Free Vibrations of Infinitely Long Thin Cylindrical Shells," by M. L. Baron and H. H. Bleich, JOURNAL OF APPLIED MECHANICS, Trans. ASME, vol. 76, 1954. Table 1, p. 171.

The Orthogonal Property—A Proof by Virtual Work

By R. P. N. JONES,[1] SHEFFIELD, ENGLAND

CONSIDER a conservative linear system executing free vibrations in one of its principal modes. It is known that all points vibrate in the same phase, so that all points reach their maximum deflection simultaneously. The maximum inertia forces occurring in the system define a set of forces which we may call a "natural-force system," and since these forces occur at the instant of maximum deflection they must be in equilibrium with the elastic forces resulting from those deflections. In other words, the static deflections produced by a natural-force system are equal to those of the corresponding natural mode.

If the system has n-degrees of freedom, with deflection co-ordinates $y_1, y_2 \ldots y_n$, then the rth principal mode will be defined by a set of deflections

$$[y_1, y_2, \ldots y_n] = [A_1^{(r)}, A_2^{(r)}, \ldots A_n^{(r)}] \quad \ldots\ldots [1]$$

and if the co-ordinates are suitably chosen to eliminate dynamic coupling, the associated natural-force system will consist of corresponding forces

$$\omega_r^2\ [m_1A_1^{(r)}, m_2A_2^{(r)}, \ldots\ldots m_nA_n^{(r)}] \quad \ldots\ldots [2]$$

A theorem in statics (Betti's theorem) states that if two sets of forces, P_1 and P_2, say, are applied to a linear elastic system, the work done by the set P_1 over the displacements due to P_2 equals the work done by P_2 over the displacements due to P_1.

Suppose P_1 and P_2 are taken equal to the natural-force system, for the rth and sth modes, respectively. Then the work done by P_1 over the displacements due to P_2 is

$$\omega_r^2\ [m_1A_1^{(r)}A_1^{(s)} + m_2A_2^{(r)}A_2^{(s)} + \ldots\ldots + m_nA_n^{(r)}A_n^{(s)}] \quad \ldots [3]$$

while that done by P_2 over the displacements due to P_1 is

$$\omega_s^2\ [m_1A_1^{(s)}A_1^{(r)} + m_2A_2^{(s)}A_2^{(r)} + \ldots + m_nA_n^{(s)}A_n^{(r)}] \quad \ldots [4]$$

According to Betti's theorem, Expressions [3] and [4] are equals and, if $\omega_r \neq \omega_s$, it follows that

$$m_1A_1^{(r)}A_1^{(s)} + m_2A_2^{(r)}A_2^{(s)} + \ldots + m_nA_n^{(r)}A_n^{(s)} = 0 \quad \ldots [5]$$

which is the well-known orthogonal property.

This proof is more direct than that usually found in textbooks, in which the orthogonal property is derived by a manipulation of the equations of motion, and the author has found the presentation given here useful in bringing the orthogonal property within the scope of more elementary teaching courses. The method of proof is equally applicable to continuous systems in which the natural-force systems become distributed "natural loading functions."

It is evident that the orthogonal property also may be expressed in an invariant form in terms of virtual work as follows:

"The work done by a natural-force system in the displacements of any *other* principal mode is zero."

This form of the orthogonal property is valuable in problems dealing with complex systems involving dynamic coupling—such as the coupled flexural-torsional oscillations of beams—since it enables the property to be written directly without the need for a lengthy derivation.

[1] Lecturer in Applied Mechanics, Post Graduate School in Applied Mechanics, University of Sheffield.

Manuscript received by ASME Applied Mechanics Division, May 31, 1955.

Symmetric Flexural Vibrations of a Clamped Circular Disk[1]

By H. DERESIEWICZ,[2] NEW YORK, N. Y.

The frequency spectrum is computed for the case of free, axially symmetric vibrations of a circular disk with clamped edges, using a theory which includes the effects of rotatory inertia and transverse shear deformation.

THE high-frequency spectrum for symmetric flexural vibrations of a circular disk has been given for the case of a traction-free boundary.[3] The purpose of this note is to present the analogous spectrum for a circular disk with a clamped edge.

The appropriate solutions of the equations of motion are given by Equations [7], [9], and [10].[3] On the clamped boundary $r = a$ these solutions must satisfy the conditions

$$\psi = w = 0 \qquad [1]$$

a requirement which leads to the frequency equations

$$\left.\begin{aligned}(1 - g\beta^2)\Gamma_1 + \beta(g - \beta^2)\Gamma_2 &= 0 \qquad p > \bar{p}\\ (1 + g\beta_1^2)\Gamma_1 + \beta_1(g + \beta_1^2)G_2 &= 0 \qquad p < \bar{p}\end{aligned}\right\} \quad [2]$$

The quantities appearing in Equations [2] are defined in the paper cited.[3]

The complete solution to the problem of a clamped disk is given by Equations [2] of the present note and Equations [14] and [15].[3]

The results of a numerical computation are shown, for the range $0.80 < p/\bar{p} < 1.20$, in Fig. 1 in which the frequency ratio is plotted as a function of the diameter-thickness ratio. It is seen that, as in the case of a free disk, the curves are characteristic of a frequency spectrum arising from the coupling of two infinite systems, namely, the flexural modes and the first thickness-shear mode and its overtones.

The uncoupled modes may be arrived at by considering the boundary conditions

$$\psi = Q_r = 0 \qquad \text{at} \qquad r = a \qquad [3]$$

i.e., those which must be satisfied at a "guided" or "lubricated" edge. If we set, in turn, in Equation [10][3], $A_2, A_1 = 0$, the conditions [3] lead to the frequency equations

$$J_1(\gamma) = 0, \qquad J_1(\beta\gamma) = 0 \qquad [4]$$

respectively. These, together with Equations [14] and [15][3], yield the curves which represent the flexural and thickness-shear families, respectively.

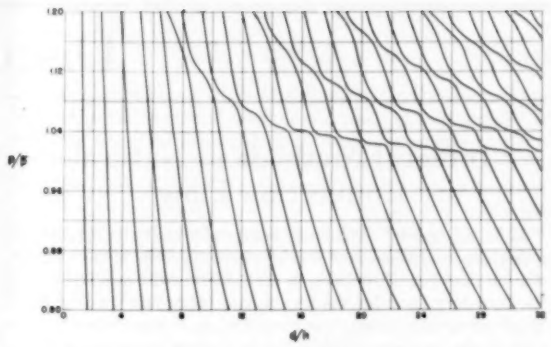

FIG. 1 FREQUENCY SPECTRUM OF SYMMETRIC FLEXURAL VIBRATIONS OF A CLAMPED CIRCULAR DISK, ILLUSTRATING RESULTS OF COUPLING OF FLEXURE AND THICKNESS-SHEAR

(d/h = ratio of diameter to thickness; $p/\bar{p}$ = ratio of resonant frequency of simple thickness-shear vibration of an infinite plate of thickness h; $\nu = 0.312$.)

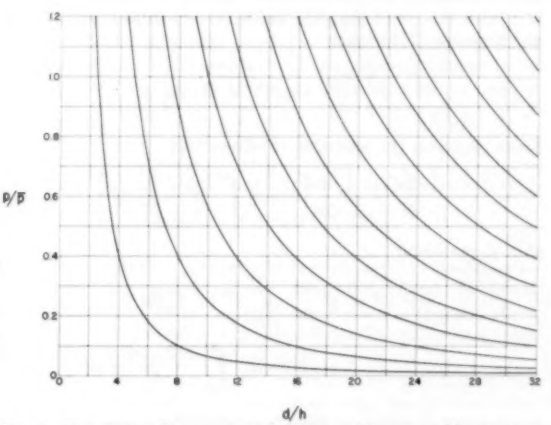

FIG. 2 FREQUENCY SPECTRUM OF SYMMETRIC FLEXURAL VIBRATIONS OF A CLAMPED CIRCULAR DISK ACCORDING TO THE CLASSICAL THEORY OF FLEXURE OF PLATES ($\nu = 0.312$)

The complete spectrum in Fig. 1 is to be compared with that depicted in Fig. 2, which was computed from the relation given by the classical theory[4]

$$d/h = \gamma(\bar{p}/p)^{1/2}[8/3\pi^2(1 - \nu)]^{1/4} \qquad [5]$$

Here the values of γ are given by the roots of the secular equation[5]

$$\Gamma_1 + G_1 = 0 \qquad [6]$$

[1] This investigation was supported by the Office of Naval Research under Contract Nonr-266(09).

[2] Assistant Professor of Mechanical Engineering, Columbia University. Assoc. Mem. ASME.

[3] "Axially Symmetric Flexural Vibrations of a Circular Disk," by H. Deresiewicz and R. D. Mindlin, JOURNAL OF APPLIED MECHANICS, Trans. ASME, vol. 77, 1955, pp. 86–88.

Manuscript received by ASME Applied Mechanics Division, May 10, 1955.

[4] "Theory of Sound," by Lord Rayleigh, Dover Publications, New York, N. Y., 1944, article 217, equations [1] and [4].

[5] Ibid., article 221*a*, equation [5].

Discussion

Integral Methods in Natural-Convection Flow[1]

E. M. Sparrow.[2] The analysis given by the author represents a significant advance over previous investigations of free-convection on nonvertical surfaces, in that the pressure gradient across the boundary layer for the first time is taken into consideration. In all previous analyses,[3] the modification, due to surface inclination, of the buoyancy term in the momentum equation for the x-direction has been made; but the pressure variation across the boundary layer has been ignored.

It is of interest to study the physical meaning of Equations [9] and [42] of the paper and to show their relationship to the conservation-of-momentum principle. To make this study, the full set of boundary-layer assumptions is applied to Equations [1] and [2]; with the result that $\partial^2 u/\partial x^2$ is deleted from Equation [1], and Equation [2] becomes

$$-\frac{1}{\rho}\frac{\partial p}{\partial y} = g\beta(T - T_1)\cos\phi \quad \ldots\ldots [1]$$

From Equation [1], herewith, it follows that

$$\frac{1}{\rho}\frac{\partial p}{\partial x} = g\beta\frac{\partial}{\partial x}\left[\cos\phi\int_y^\delta (T - T_1)dy\right] \quad \ldots\ldots [2]$$

and, in particular

$$\frac{1}{\rho}\frac{\partial p}{\partial x}\bigg|_{y=0} = -g\beta\sin\phi\frac{\partial\phi}{\partial x}\int_0^\delta (T - T_1)dy + g\beta(\cos\phi)\int_0^\delta \frac{\partial(T - T_1)}{\partial x}dy \quad \ldots\ldots [3]$$

Using this last equation, Equation [9] of the paper may be rewritten as follows

$$\nu\frac{\partial^2 u}{\partial y^2}\bigg|_{y=\delta} = g\beta(T_w - T_1)\sin\phi + \nu\frac{\partial^2 u}{\partial y^2}\bigg|_{y=0} - \frac{1}{\rho}\frac{\partial p}{\partial x}\bigg|_{y=0} \quad \ldots\ldots [4]$$

Equation [4], and hence Equation [9] of the paper, state that the net shear force acting on an infinitesimal fluid element located at the edge of the boundary layer equals the net force acting on an infinitesimal fluid element located at the wall. Under the condition that

$$(\partial^2 u/\partial y^2)\big|_{y=\delta}$$

is zero, Equation [4] requires that the net force acting on a fluid element at the wall be zero. But these same conditions are obtained by imposing the x-momentum equation (Equation [1] of the paper), at the edge of the boundary layer and at the wall. So the use of Equation [4] of this discussion with

$$(\partial^2 u/\partial y^2)\big|_{y=\delta}$$

equal to zero is identical to satisfying the x-momentum equation at two places, at the wall and at the edge of the boundary layer. However, no restriction whatsoever is imposed on the momentum at all other points in the boundary layer by the use of Equation [4] of this discussion. Under the circumstance that

$$(\partial^2 u/\partial y^2)\big|_{y=\delta}$$

is not zero, Equation [4] actually is a contradiction of the x-momentum equation at the wall and at the edge of the boundary layer. So it seems plausible that velocity profiles with

$$(\partial^2 u/\partial y^2)\big|_{y=\delta}$$

different from zero should yield poor results.

Equation [42] is obtained from an integral equation into which the polynomial Expressions [11] and [12] have been introduced. This integral equation may be derived in a direct manner by integrating Equation [1] of the paper (with $(\partial^2 u/\partial x^2)$ deleted) from $y = 0$ to $y = \delta$, and by using Equations [2] of this discussion and Equation [4] of the paper. The result is

$$\frac{d}{dx}\int_0^\delta u^2 dy = g\beta\sin\phi\int_0^\delta (T - T_1)dy - \nu\left(\frac{\partial u}{\partial y}\right)\bigg|_{y=0} + \frac{d}{dx}\int_0^\delta dy\left[\int_\delta^y g\beta(T - T_1)\cos\phi dy\right] \quad \ldots\ldots [5]$$

Inspection of foregoing Equation [5] shows that it is an expression of conservation of momentum for an element of boundary layer of dimensions δ by dx. So Equation [5] requires that momentum be conserved across the boundary layer as a whole, but does not require that momentum be conserved locally at any position within the boundary layer.

As is pointed out by the author, the superiority of Equation [5] of this discussion as compared with Equation [4] lies in the fact that the former takes account of momentum changes, while no momentum terms appear in the latter.

It may be noted that the pressure p, which is used throughout the paper, is not the static pressure. Rather, it is the static pressure minus the ambient pressure.

Carl Wagner.[4] In addition to the author's solution for heat transfer from a heated plate facing upward, a solution for heat transfer from a heated plate facing downward seems to be of interest. In accord with the author, the width of the plate is assumed to be small in comparison with its length. At the upper side of a heated plate, fluid flows from the edges to the middle and finally flows upward, whereas at the lower side, fluid approaches the plate from below and passes along the surface of the plate toward the edges. Thus the flow velocity u_1 of the fluid moving along the plate vanishes at the mid-line of the plate

$$u_1 = 0 \text{ at } x = 0 \quad \ldots\ldots [6]$$

where x is the distance from the mid-line of the plate.

---

[1] By Salomon Levy, published in the December, 1955, issue of the Journal of Applied Mechanics, Trans. ASME, vol. 77, 1955, pp. 515–522.

[2] NACA, Lewis Laboratory, Cleveland, Ohio.

[3] "Thermal Convection in Laminar Boundary Layers," by H. J. Merk and J. A. Prins, *App. Sci. Res.*, section A, vol. 4, 1953–1954, part I, pp. 11–24; part II, pp. 195–206; part III, pp. 206–221.

"Heat Transfer by Free Convection From Horizontal Cylinders in Diatomic Gases," by R. Hermann, NACA TM 1366, 1954.

[4] Department of Metallurgy, Massachusetts Institute of Technology, Cambridge, Mass.

Beyond the edges of the plate, the pressure is independent of x and the pressure distribution in the vertical direction is given by the bulk density of the liquid. In view of continuity, the same pressure distribution must be found underneath the plate in the vicinity of the edges. This is possible only if the thickness δ of the boundary layer decreases sharply at the edges

$$\delta \cong 0 \text{ at } x = \pm a \quad [7]$$

where a is half the width of the plate.

Upon substituting Equation [13] of the paper for $\varphi = 0$ in his Equation [14] and introducing the auxiliary variables

$$z = \delta^4[\beta g(T_w - T_1)/1080\alpha\nu a^2]^{1/5} \quad [8]$$

$$\xi = x/a \quad [9]$$

where the symbols have the same meaning as in the paper, it follows that

$$\frac{1}{4}\, z^{1/4} d^2z/d\xi^2 + 1 = 0 \quad [10]$$

In view of Equations [6] to [9] of this discussion the boundary conditions are

$$dz/d\xi = 0 \text{ at } \xi = 0 \quad [11]$$

$$z = 0 \text{ at } \xi = 1 \quad [12]$$

Integrating Equation [10] once and using Equation [11], herewith

$$dz/d\xi = -[32(z_0^{5/4} - z^{5/4})/3]^{1/2} \quad [13]$$

where z_0 is the value of z at $\xi = 0$.

Substituting the auxiliary variable

$$t = (z/z_0)^{1/4} \quad [14]$$

and integrating Equation [13]

$$\xi = \left(\frac{3}{2}\right)^{1/2} z_0^{5/4} \int_t^1 t^2(1 - t^3)^{-1/2}\, dt$$

$$= (6^{1/2}/5)[t(1 - t^3)^{1/4} + 3^{-1/4} F(k, \varphi)]z_0^{5/4} \quad [15]$$

where $F(k, \varphi)$ is Legendre's standard form of the elliptic integral of first kind[5] and

$$k = \frac{1}{2}\,(2 + 3^{1/2})^{1/2} = 0.96593 = \sin 75 \text{ deg} \quad [16]$$

$$\varphi = \cos^{-1}[(3^{1/2} - 1 + t)/(3^{1/2} + 1 - t)] \quad [17]$$

Since $t = 0$ for $\xi = 1$ according to Equations [12] and [14] of this discussion, it follows from Equation [15] that

$$z_0 = 1.824 \quad [18]$$

In view of the foregoing Equations [8] and [9] and Equation [17] of the paper, the local value of the Nusselt number is found to be

$$N_{Nu} = 2a/\delta = 0.426(z_0/z)^{1/4}(N_{Gr}N_{Pr})^{1/5} \quad [19]$$

where half the width of the plate a is used as the characteristic length for the definition of both the local Nusselt number and the Grashof number. The value of $(z_0/z)^{1/4}$ determined by Equations [14] and [15], herewith, varies only slightly except for the vicinity of the edges

x/a	0	0.2	0.4	0.6	0.8
$(z_0/z)^{1/4}$	1.00	1.01	1.03	1.11	1.28

[5] "Tables of Functions," by E. Jahnke and F. Emde, B. G. Teubner, Leipzig, Germany, fourth edition, 1938, p. 59.

The average value of the Nusselt number is found to be

$$N_{Nu(avg)} = 0.50(N_{Gr}N_{Pr})^{1/5} \quad [20]$$

Experimental data compiled by Fishenden and Saunders[6] are in accord with the general result that the rate of heat transfer at the lower side of a heated horizontal plate is proportional to the fifth root rather than the fourth root of the product $N_{Gr}N_{Pr}$. At the upper side of a heated plate, the rate of heat transfer increases somewhat more rapidly for, even at low values of the Grashof number, eddies are formed owing to the instability of a boundary layer having a lower density than the bulk fluid above. The occurrence of eddies under these conditions has been shown especially by Weise.[7]

Author's Closure

The author wishes to thank Mr. Sparrow and Dr. Wagner for their valuable comments. Mr. Sparrow's discussion leads to a better physical understanding of the fundamental equations and boundary conditions. Dr. Wagner gives another example of the value of integral methods by solving the case of a heated horizontal plate facing upward. His solution can be extended to low Prandtl number fluids by numerical methods.

As an additional closing comment the author wishes to point out that Equation [28] assumes that the surface heat flux varies as $N_{Pr}^{-2/3}$ and its application to low Prandtl numbers may be opened to question.[8]

Some Solutions of the Timoshenko Beam Equations[1]

H. N. Abramson.[2] The authors have rendered a valuable service by providing "building blocks" which may be used to form a large number and variety of solutions of the Timoshenko beam equations. The availability of this information will be welcomed by all those who are working with such problems.

Because of the great interest currently being shown in the general problem of transverse impact on elastic beams, some comments of a general nature may be in order. Investigations concerned with this problem seem to be concentrated largely along the paths of (*a*) experimental investigations and (*b*) solutions of the Timoshenko beam equations, both approximate and exact. A crossing of these two paths was presented in a recent paper by Goland, Wickersham, and Dengler,[3] and the resulting discussions[4] brought forth many succulent comments. These discussions serve to point out that there is yet a third path to be followed; that is, investigations also must proceed from the general theory of elasticity to an exact analysis of the problem.

A critical appraisal of the Timoshenko theory, on this basis, was

[6] "An Introduction to Heat Transfer," by M. Fishenden and O. A. Saunders, Clarendon Press, Oxford, England, 1950, pp. 95–97.

[7] "Wärmübergang durch freie Konvektion an quadratischen Platten," by R. Weise, *Forschung auf dem Gebiete des Ingenieurwesens*, vol. 6, 1935, pp. 281–292.

[8] "Liquid-Metals Handbook, Sodium-NaK Supplement," Atomic Energy Commission, July, 1955, p. 54.

[1] By B. A. Boley and C. C. Chao, published in the December, 1955, issue of the Journal of Applied Mechanics, Trans. ASME, vol. 77, pp. 579–586.

[2] Department of Engineering Mechanics, The University of Texas, Austin, Texas. Assoc. Mem. ASME.

[3] "Propagation of Elastic Impact in Beams in Bending," by M. Goland, P. D. Wickersham, and M. A. Dengler, Journal of Applied Mechanics, Trans. ASME, vol. 77, 1955, pp. 1–7.

[4] Ibid., discussion in Journal of Applied Mechanics, Trans. ASME, vol. 77, 1955, pp. 608–610.

given in the now well-known paper of Cremer;[5] however, it must be emphasized that the exact solutions used for this comparison were those for the elastic plate rather than the beam. On the other hand, the exact solution for the case of a beam of solid circular cross section was given by Hudson[6] on the basis of the Pochhammer-Chree solutions of the elastic equations of motion. Hudson purported to show that the resulting frequency equation for flexural wave propagation has only one root so that only one mode of transmission is possible; this result has been carried over into the work of other authors.[7] Here, then, is an area of fundamental disagreement, for the Timoshenko theory predicts not one, but two modes of transmission.

The writer has recently reinvestigated the exact theory in an attempt to reconcile this difference.[8] It has been found that, contrary to Hudson's work, the frequency equation for the Pochhammer-Chree solutions possesses an infinite number of roots and that therefore an infinite number of transmission modes are possible. The lowest mode from the Timoshenko and exact theories show excellent agreement; however, in the second mode, the agreement is not nearly so good. On the basis of both phase and group-velocity studies the two theories show good agreement in the second mode for a rather wide range of wave lengths, extending from infinitely long wave lengths down to those about two or three times the cross-section radius. For shorter wave lengths, the disagreement becomes large since the exact result appears to approach the shear velocity $\sqrt{G/\rho}$ while the Timoshenko result approaches the bar velocity $\sqrt{E/\rho}$; the general shape of the dispersion curves (on the basis of both phase and group velocities) are, however, very similar.

Thus it may be concluded that the Timoshenko theory provides a rather good description of the transverse impact problem, except for extremely short waves, even though all transmission modes above the lowest two are ignored. This agrees with the experimental evidence.

Therefore the range of validity of the Timoshenko theory has been somewhat more clearly defined than heretofore and consequently the results of that theory, such as provided by the present authors, may be employed with fuller knowledge of their applicability.

It is anticipated that the results from the exact theory mentioned briefly in the foregoing, and the accompanying discussion and comparison of the two theories, will be published at an early date.

[5] "Bemerkungen zur Ausbreitung von 'Biegewellen' in Stäben and Platten," by L. Cremer, *Zeitschrift für angewandte Mathematik und Mechanik*, vol. 23, October 5, 1943, pp. 291–295.

[6] "Dispersion of Elastic Waves in Solid Circular Cylinders," by G. E. Hudson, *Physical Review*, vol. 63, 1943, pp. 46–51.

[7] "Stress Waves in Solids," by H. Kolsky, Oxford University Press, 1953, pp. 68–73.

[8] "The Propagation of Flexural Elastic Waves in Solid Circular Cylinders," by H. N. Abramson, PhD Dissertation, The University of Texas, Austin, Texas, June, 1956.

Thin Circular Conical Shells Under Arbitrary Loads[1]

F. V. Pohle.[2] In this paper the author has established, for the conical shell, equations which are similar in form to those for the cylindrical shell given by him.[3] In the form presented here, there is an 8th order equation in w alone, Equation [40], and there are two equations each of the 4th order, Equations [32] and [36]. In the latter two equations only v and w, and u and w, respectively, are involved. Since the equations for the cylindrical shell have been shown to be useful in many practical problems (such as vibration, stress analysis, and stability) the present equations also should prove to be most useful in applications.

The work of Wenk and Taylor[4] may be used as an indication of the utility of the equations. In their work a simplified differential equation was used in the case of axial symmetry. This equation was obtained from a more accurate one, due to Dubois, by dropping one term in the equation. Such an approximation yielded a much more tractable equation for purposes of numerical analysis. It is of interest to observe that this simplified equation is precisely the one which results from the present paper in the case of axial symmetry. Therefore the simplified equation which results from the present paper is placed upon a much firmer theoretical ground since the author has derived his results from clearly stated assumptions. It also should be mentioned that the inclusion of appropriate boundary conditions is essential for applications.

It is unfortunate that the series solution attempted in the paper is not useful in any numerical sense. This is at once evident if any values are substituted into the series; although there is no mathematical question of convergence, there is a very strong practical question of usefulness. The absolute values of the successive terms in the series increase for many terms and no practical use can be made of the series in the form given.

The behavior of the series can be understood more clearly if reference is made to the case of axial symmetry, where it is known that the solutions can be expressed in terms of Bessel functions of (large) complex argument. Since the power-series representation in these cases is known to be inadequate it is not surprising that the series solution obtained converges too poorly for use in applications. In the theory of Bessel functions there are basically three types of expansions: (*a*) Series expansions for reasonably small values of the independent variable; (*b*) asymptotic expansions for large values of the independent variable; and (*c*) expansions for the case when both independent variable and the order of the Bessel function are large in some definite sense.

Since the series solution has proved to be impractical it is natural to attempt the asymptotic expansion and this has been done at the Polytechnic Institute of Brooklyn by the author and the writer. The results are essentially the same as those obtained by Love,[5] and with the same shortcomings. The asymptotic solution as given by Love is not numerically useful for any reasonable range of the parameters involved. This behavior is due to the presence of a parameter $(n/\sin\alpha)^2$ which occurs in the numerators of the successive terms; n is an integer and α is the half-cone angle. Owing to the presence of this parameter the successive numerators increase much more rapidly than the terms which arise from the largeness of the independent variable. The result is that the asymptotic expansion in this form is also of no use. However, it should be noted that for $n = 0$ the solutions do reduce to the appropriate expansions for the Bessel functions.

[1] By N. J. Hoff, published in the December, 1955, issue of the Journal of Applied Mechanics, Trans. ASME, vol. 77, pp. 557–562.

[2] Associate Professor of Applied Mechanics, Department of Aeronautical Engineering and Applied Mechanics, Polytechnic Institute of Brooklyn, Brooklyn, N. Y.

[3] "Boundary-Value Problems of the Thin-Walled Circular Cylinder," by N. J. Hoff, Journal of Applied Mechanics, Trans. ASME, vol. 76, 1954, pp. 343–351.

[4] "Analysis of Stresses at the Reinforced Intersection of Conical and Cylindrical Shells," by E. Wenk and C. E. Taylor, Navy Department, David Taylor Model Basin Report 826, NS 731–038, March, 1953, Eq. (11), p. 3.

[5] "A Treatise on the Mathematical Theory of Elasticity," by A. E. H. Love, Dover Publications, New York, N. Y., fourth edition, 1944, p. 612.

Although Love states[6] that the problem of the conical shell may be considered as completely solved, the present remarks show that this is certainly not the case. It is also of some moment to point out that Love has obtained only four of the required eight solutions. The four solutions which have been obtained arise from four values obtained from a characteristic determinant;[5] these values are distinct. However, there are four additional values which correspond to $m = 0$ as a root of multiplicity 4 and these are not discussed. It is still possible to obtain the appropriate solutions in this case by other methods;[7] the practical results are still the same.

In the search for an appropriate method there are two guides, one of which is physical and the other mathematical. As to the latter it is known that if the limit case of the cylinder is approached correctly the results should reduce to the known results.[3] In the former case it is known from the case of the cylinder that four solutions decay exponentially from each edge and this behavior also should appear in the case of the cone. It is true that the effects do not decay equally away from the edge but the decaying behavior in general is the important fact in the present discussion.

When the three types of solutions to the Bessel equation were discussed it was clear that each of them could be used to clarify the present problem. In the third case both the argument and the order are large and it is to this possibility that we must now turn. It is the most difficult of the three cases and the difficulties, in the case of the Bessel equation, stem from the fact that care must be taken to specify precisely how the independent variable and the order become "large." The parameters in the cone problem are really two. If the displacements are expanded into Fourier series in the circumferential direction the integer n is introduced into the three ordinary differential equations which result; in addition to n, the half-cone angle α also enters. From the form of the equations it can be shown that wherever n occurs it occurs in the form $(n/\sin\alpha)^2$ but α occurs without n in the form $\cot\alpha$. It is necessary to distinguish between the two parameters and of the two, α is clearly the important one since n usually will assume only the first few integral values, but α can range over a significant set of values, including zero. If an expansion is made with respect to the parameter α, then the limit case of $\alpha = 0$ corresponds to the case of the cylinder. For that case all eight solutions are known and in the case of the cone the form of the solutions will be the same. The solutions will then have the correct behavior. Such expansions are now being carried out at the Polytechnic Institute of Brooklyn.

On the Nonlinear Oscillations of Viscoelastic Plates[1]

J. Martinek.[2] Dr. Yeh[2] and the writer have been faced with a problem somewhat similar in nature to the one treated by the author. We have used a different approach toward establishing the plate equations for small oscillations whereby we also included internal viscous-damping effects as well as the effects of thermal damping and the surrounding fluid media. As we are now in the process of studying a similar problem as that of the author, the writer believes it to be worth while to present our reasoning, which differs considerably from his basic assumptions.

It is indeed a pleasure to observe that the analysis in the field of mechanics of continuum is carried out to an ever-increasing amount on the basis of rheology. The writer will refer to the basic equation, a generalization of Alfrey's stress-strain relation used here by the author. At the beginning, the initial state of rheology was characterized by the establishment of relationships among stress, strain, and their time derivatives in form of a series with a number of elasticity and viscosity coefficients E_i, μ_i. This reminds us particularly of the theoretical investigations of the nineteenth century, where the discussions over the number of elastic constants extended over decades, while later it became apparent that the difficulties were located in an entirely different direction, namely, the formal and mathematical complexities encountered during the treatment of practical important problems. On the other hand, the physical meaning of the ever-increasing number of coefficients can only be understood with the greatest difficulty; much less can they be found by experimental investigations. The question after the elastic constants could then finally be limited to two, which according to Lamé was by all means sufficient.

The important question to answer is first of all which one of the two following bodies

The Maxwell body

$$\dot{E}_0 = \frac{1}{2G}\dot{S}_0 + \frac{1}{2\mu}S_0 \qquad [1]$$

or

Jeffreys-Voigt body

$$S_0 = 2G\dot{E}_0 + 2\mu\dot{E}_0 \qquad [2]$$

where Equation [1] renders for the simplest one-axial case

$$\dot{\epsilon}_x = \frac{\partial v_x}{\partial x} = \frac{\dot{\sigma}_x}{E} + \frac{\sigma_x}{Z};\quad E = \frac{mG}{2(m+1)};\quad Z = \frac{2\mu + 3\lambda}{\mu + \lambda}\mu \qquad [3]$$

with

$$\dot{\epsilon}_x = \dot{\epsilon}_{x\text{el}} + \dot{\epsilon}_{x\text{visc}}$$

is acceptable as a basis for the analysis.

In a dual material the Maxwell hypothesis states that to one stress correspond two different strains in one volume element, whereby Equation [2] for the simplest one-axial case states that

$$\sigma_x = 2G\frac{m-1}{m-2}\epsilon_x + (2\mu + \lambda)\dot{\epsilon}_x \qquad [4]$$

in which

$$\sigma_x = \sigma_{x\text{el}} + \sigma_{x\text{visc}}$$

that is, that to one strain ϵ correspond two different stresses in a dual-system body. It is now of importance to investigate which one of these two hypotheses complies more to physical reality and which one is more idealized. For this purpose, let us consider the equation of motion of an infinitesimal tetrahedron element which reads in x-direction

$$\rho dV\left(\frac{\partial^2 x_s}{\partial t^2} - X\right) = dF_n\,[p_{nx} - \sigma_x\cos(x,n) - \tau_{xy}\cos(y,n) - \tau_{xz}\cos(z,n)] \qquad [5]$$

etc., in y and z-directions.

As we have on the left side of Equation [5] a smallness of magnitude of one order higher (third order) than on the right

[6] "A Treatise on the Mathematical Theory of Elasticity," by A. E. H. Love, Dover Publications, New York, N. Y., fourth edition, p. 613.

[7] "Über die Asymptotische Integration von Differentialgleichungen," by W. Sternberg, *Mathematische Annalen*, vol. 81, 1925, pp. 119–186.

[1] By A. C. Eringen, published in the December, 1955, issue of the Journal of Applied Mechanics, Trans. ASME, vol. 77, pp. 563–567.

[2] Staff Scientist, Reed Research Inc., Washington, D. C.

side where a number of terms of second order (dF_n) appear, we are entitled to neglect the left side and arrive so at the surface conditions of the infinitesimal tetrahedron

$$p_{nx} = \sigma_x \cos(x, n) + \tau_{xy} \cos(y, n) + \tau_{xz} \cos(z, n) \ldots [6]$$

etc., in y and z-directions. This equation is valid for elastic as well as for viscous materials and any material which lies in between elastic and viscous. This, however, indicates that the stress relations are almost independent of density and strain velocities. It proves that we have to give our preference to the Maxwell body since two different stresses belonging to a dual material which is elastic and viscous can hardly exist; that is, because of dealing with a material having two characteristics like elasticity and viscosity, we cannot have two different stresses at the same time. So, Equation [3] appears to us physically possible; whereas, the second hypothesis, Equation [4], is physically too much idealized.

It is also interesting to note here that the transition from the Maxwell body (Equations [1] and [3]) and the Jeffreys-Voigt body (Equations [2] and [4]) to bodies of only elastic or only viscous characteristic is quite revealing. While in the case of pure elastic material, Equations [1] and [3], μ has then to go toward infinity ($\mu \to \infty$); in Equations [2] and [4], μ must go to zero ($\mu = 0$). Now the question arises whether a pure elastic material is viscorigid (Maxwell $\mu \to \infty$) or viscoless (Jeffreys-Voigt $\mu = 0$). Also for the case of pure viscous materials, Maxwell's hypothesis predicts elastorigid ($E \to \infty$) and Jeffreys-Voigt a material without elastic characteristic ($E = 0$). In the light of the foregoing description and with additional tests, Fromm has convinced himself that the Maxwell equation, i.e., elastorigid and viscorigid materials ($E \to \infty$, $\mu \to \infty$) deserves priority.

So it is worth while to consider the proposal by C. Torre which suggests we confine ourselves first of all to the Maxwell body of three-tensor relation

$$F(\bar{S}, \dot{\bar{S}}, \dot{\bar{E}}) = 0$$

or in linear form

$$\dot{\bar{E}} = \frac{1}{2G} \dot{\bar{S}}_0 + \frac{1}{2\mu} \bar{S}_0 + \frac{1}{3} \left(\frac{\dot{\sigma}_m}{K_e} + \frac{\sigma_m}{K_v} \right) \bar{J}$$

where $K_e = \dfrac{2}{3} \dfrac{m+1}{m-2} G$

$$K_v = \frac{2}{3} \mu + \lambda$$

$\bar{S}$ .... stress tensor

$\bar{S}_0 = \bar{S} - \sigma_m \bar{J}$ ... deviator of stress

$\sigma_m \bar{J}$ .... spherical tensor

$$\bar{J} = \begin{pmatrix} \bar{i}\bar{i} & 0 & 0 \\ 0 & \bar{j}\bar{j} & 0 \\ 0 & 00 & \bar{k}\bar{k} \end{pmatrix} = \bar{i}\bar{i} + \bar{j}\bar{j} + \bar{k}\bar{k}$$

$$\sigma_m = \frac{1}{3} (\sigma_x + \sigma_y + \sigma_z)$$

$$\bar{S} = \begin{pmatrix} \sigma_x & \tau_{xy} & \tau_{xz} \\ \tau_{yx} & \sigma_y & \tau_{yz} \\ \tau_{zx} & \tau_{xy} & \sigma_z \end{pmatrix} = \begin{matrix} \bar{i}\bar{i}\sigma_x + \bar{i}\bar{j}\tau_{xy} + \bar{i}\bar{k}\tau_{xz} \\ + \bar{j}\bar{i}\tau_{yx} + \bar{j}\bar{j}\sigma_y + \bar{j}\bar{k}\tau_{yz} \\ + \bar{k}\bar{i}\tau_{zx} + \bar{k}\bar{j}\tau_{xy} + \bar{k}\bar{k}\sigma_z \end{matrix}$$

so

$$\bar{S}_0 = \bar{S} - \sigma_m \bar{J} = \bar{i}\bar{i}(\sigma_x - \sigma_m) + \bar{i}\bar{j}\tau_{xy} + \ldots . + \bar{j}\bar{j}(\sigma_y - \sigma_m) + \bar{j}\bar{k}\tau_{yz} + \ldots . + \bar{k}\bar{k}(\sigma_z - \sigma_m)$$

and to postpone the more complicated cases to a later date.

In the Maxwell hypothesis, however, the derivation after the time is of importance since, according to Fromm and Torre's investigations, it gives a rotation of the stress tensor

$$\frac{d\bar{S}}{dt} = \vec{w} \times \bar{S} \ldots \ldots \ldots \ldots \ldots \ldots [7]$$

and the rate of strain as a function of the shearing stresses [with $(\vec{r} \cdot \nabla)(\sigma_x - \sigma_m) = 0$ a quadratic term if taken with equation]

$$\dot{\epsilon}_x = \frac{\partial \dot{w}_x}{\partial x} = \frac{1}{2G} \left[\frac{\partial (\sigma_x - \sigma_m)}{\partial t} + (\tau_{xy}\omega_z - \tau_{xz}\omega_y) \right] + \frac{\sigma_x - \sigma_m}{2\mu} + \frac{1}{3} \left(\frac{\dot{\sigma}_m}{K_e} + \frac{\sigma_m}{K_v} \right) \ldots [8]$$

with ω angular velocity.

That is, even if we consider a pure elastic material ($\mu \to \infty$), Equation [8] is of importance. This was indicated by Torre when he proved that, in case of torsion of a round bar, an elongation of the axis of the bar due to shearing stresses and a change of the cross section of the bar must take place.

Deformation in axial direction

$$w = \frac{1}{\beta_1 c} J_0(i\beta\mu) (A \sin \beta' z + B \cos \beta' z) (1 - \cos \beta_1 c t) \ldots [9]$$

$$\beta'^2 = \beta^2 + \beta_1^2$$

c = propagation velocity of shear waves

β = integration constant which appears when separating variables

whereby the Navier hypothesis about the circular cross section has been improved, which proves that a two-tensor theory $F(\hat{S}, \hat{E}) = 0$ differentiated after time already renders an improvement of the classical linear theory of elasticity. These results have been experimentally confirmed in Germany, France, and Austria. So in the case of copper bars of circular cross section (Paris), an elongation of a maximum of 7 per cent of the original length is observable—which is a first-order effect.

In the spirit of what has been said here, the small oscillations of a plate with internal damping have been investigated by Dr. Yeh and the writer. In addition to viscous damping, we also took into account the heat-conduction effects (thermal damping). Here should begin the final plate equations developed from a body of three tensor form, $F(\bar{S}, \dot{\bar{S}}, \dot{\bar{E}}) = 0$ (Maxwell), without thermal damping, shearing deformation, or rotary inertia, but being elastic and viscous

$$\frac{GD_0}{\mu} \left(\frac{D_1}{3K_v} + \frac{D_0}{\mu} \right) \left(\frac{\partial^2}{\partial x^2} + \frac{\partial^2}{\partial y^2} \right)^2 \dot{w} - \omega_z \left(\frac{2D_1}{3K_v} + \frac{D_0}{2\mu} \right) \left(\frac{\partial^2}{\partial x^2} - \frac{\partial^2}{\partial y^2} \right) \frac{\partial^2 \dot{w}}{\partial x \partial y} + \frac{6G\bar{m}}{\mu^2 h^2} \left(\frac{2D_1}{3K_v} + \frac{D_0}{2\mu} \right) D_0 \ddot{w} = \frac{6G}{\mu^2 h^2} \left(\frac{2D_1}{3K_v} + \frac{D_0}{2\mu} \right) D_0 \ddot{p} \ldots [10]$$

where $D_0 = 1 + T_0 \dfrac{\partial}{\partial t}$, $D_1 = 1 + T_1 \dfrac{\partial}{\partial t}$

$$T_1 = \frac{K_v}{K_e}, \qquad T_0 = \frac{\mu}{G}$$

Equation [10] reduces for pure elastic material with $\omega_z = 0$ to the well-known dynamic equation of motion of a vibrating plate

$$D\Delta\Delta w + \overline{m}\frac{\partial^2 w}{\partial t^2} = p$$

where

$$D = \frac{Eh^3}{12(1-\mu^2)} \quad \text{[11]}$$

In conclusion, it should be pointed out that, besides the foregoing reasons which speak in favor of Maxwell material, another advantage is the fact that, after Duhem in (8), Maxwell material propagates waves, whereas Jeffreys-Voigt material does not.

REFERENCES

1 "Criticism and Extension of Maxwell's Law for Viscoelastic Materials. Torsion of Rods as an Example" (in German), by C. Torre, *Osterreichisches Ingenieur-Archiv*, vol. 8, 1954, pp. 55–76.

2 "Ergänzungen zum Maxwellschen Ansatz für elastisch-zähe stoffe. Verdrehung mit instationärer Spannungsänderung als Beispiel," by C. Torre, *Kolloid Zeitschrift*, vol. 138, 1954, pp. 11–18.

3 "Strukturmodelle und Systematik der Fliessvorgänge," by E. Mewes, *Zeitschrift für angewandte Mathematik und Mechanik*, vol. 32, 1952, pp. 261–262.

4 "On the Dynamical Theory of Gases," by J. C. Maxwell, Philosophical Transactions of the Royal Society of London, England, vol. 157, 1867, pp. 49–88.

5 "Laminar Flow of Newtonian and Maxwellian Fluids" (in German), by H. Fromm, *Zeitschrift für angewandte Mathematik und Mechanik*, vol. 28, 1948, pp. 43–54.

6 "Non-Homogeneous Stresses in Visco-Elastic Media," by T. Alfrey, *Quarterly of Applied Mechanics*, vol. 2, 1944, pp. 113–119. Also "Methods of Representing the Properties of Viscoelastic Materials," by T. Alfrey, *Quarterly of Applied Mechanics*, vol. 3, 1946, pp. 143–150.

7 "Über innere Reibung fester Körper, insbesondere der Metalle," by W. Voigt, *Annalen der Physik*, vol. 47, 1892, pp. 671–693.

8 "Elasticity and Fluid Dynamics," by C. Truesdell, *Journal of Rational Mechanics and Analysis*, vol. 1, 1952, p. 176.

Author's Closure

The author appreciates the interest of J. Martinek in his paper. Even though it is hard to draw a close connection between these comments and the present paper it is believed that the following observations are appropriate: The stress-strain relations of the present paper contain the simple Voigt and simple Maxwell type of models with which he is concerned. It is well known, however, that both of these models are unsatisfactory from the experimental point of view. (See, for instance, "Stress Waves in Solids," by H. Kolsky, Oxford Press, 1953, pp. 111–112.)

The author is doubtful about the validity of the arguments advanced in favor of Maxwell model based on boundary conditions, Mr. Martinek's Equation [6], and about the concluding paragraph of these comments.

Forced Vibration of a Clamped Rectangular Plate in Fluid Media[1]

M. C. Junger.[2] It is of interest to relate the results of this analysis to some of the general principles of acoustics. Thus the much greater value of the transmission coefficient for the case of the plate exposed on both sides to water, as compared to the case where one side is exposed to water and the other to air, is an illustration of the principle of "impedance matching" which is of great practical importance in coupling acoustic systems. The fraction of the sound energy which is reflected at the interface between two media varies with the difference between their respective acoustic impedances.

The present analysis suggests that the plate modes which are excited near their resonant frequencies are mostly responsible for transmitting sound energy (see equation [36] of the paper). This is related to the "coincidence effect" by virtue of which an extended thin plate does not appreciably oppose the transmission of an obliquely incident sound wave if the trace velocity of the sound wave on the plate coincides with the phase velocity of the flexural wave at the frequency in question.[3] It recently has been found that the transmission of sound into a cylindrical shell is also largely dependent on the excitation of the natural modes of the shell.[4] The governing principle which may be formulated is that a thin elastic plate, either flat or curved, of finite or infinite extent, offers little opposition to the transmission of sound if excited in a resonant fashion, i.e., at a frequency where the inertia forces balance the elastic forces. The investigation of this general problem might be carried further by extending Cremer's analysis[3] of the transmission of obliquely incident sound waves to the system here analyzed, i.e., to the case where the plate separates two different media.

Authors' Closure

The authors wish to thank Dr. Junger for his contribution to the paper in relating the results of their analysis to some of the general principles of acoustics. Extension of Cremer's analysis of the transmission of obliquely incident sound waves to the system in this paper would be an interesting topic for future research in which we hope to participate.

Stress Distribution in Square Plates With Hydrostatically Loaded Central Circular Holes[1]

G. Mesmer.[2] As the authors clearly state in their discussion of the neighborhood of the corners, it is only of academic interest to know the real distribution of stresses as they are very small in this region. For completeness, however, some remarks may be in order.

As indicated in Fig. 5 of the paper, there is always one singular point at the external edge at about 60 deg. At this point the stress trajectories must have two singular lines as indicated in Fig. 9. Taking the line $y = 0$ as extreme edge, it follows from the equation of equilibrium that in the immediate vicinity of the singularity the stresses must be of the type $\tau_{xy} = c$, $\sigma_y = 0$, $\sigma_x = -c_1 x + c_2 y$. The inclination of the stress trajectories is then given by

$$\tan 2\varphi = \frac{2\tau}{\sigma_x - \sigma_y} = \frac{y}{-1/2 x + ay} = \frac{y/x}{-1/2 + ay/x}$$

(see Fig. 1 of this discussion). The free parameter a may have any value, describing the different possible types of singularities at the straight edge. The two singular lines $\tan \varphi_0 = y/x$ are given by $\tan \varphi_0 = -a \pm \sqrt{a^2 + 2}$, one sees that the angle 2β

---

[1] By G. C. K. Yeh and Johann Martinek, published in the December, 1955, issue of the Journal of Applied Mechanics, Trans. ASME, vol. 77, pp. 568–572.

[2] Partner, Cambridge Acoustical Associates, Cambridge, Mass. Assoc. Mem. ASME.

[3] "Theorie der Schalldaemmung duenner Waende bei schraegem Einfall," by L. Cremer, *Akustische Zeitschrift*, vol. 7, 1942, p. 81.

[4] "Sound Transmission Through Thin Cylindrical Shells," by P. W. Smith, Jr., Paper No. L-5, was presented at the Spring 1955 Meeting of the Acoustical Society of America, The Pennsylvania State University, University Park, Pa.

[1] By A. J. Durelli and J. Barriage, published in the December, 1955, issue of the Journal of Applied Mechanics, Trans. ASME, vol. 77, 1955, pp. 539–544.

[2] Head, Department of Applied Mechanics, Washington University, St. Louis, Mo.

between the two singular trajectories must be at least 70.3 deg (case of symmetry $a = 0$) or more, up to 90 deg. More difficult however, is the description of the free corner. It seems to be impossible to describe the vicinity of this point by elementary means, and the singularity at this point must be of higher order, as

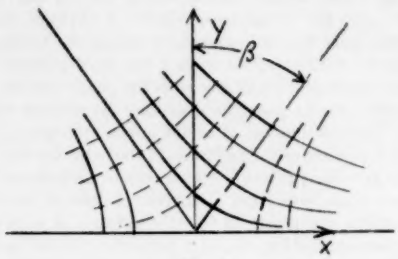

FIG. 1

the curves of σ along the edge (Fig. 5 in the paper) must have horizontal tangents at the corner. Calculations of this point seem not to have been performed as yet. Airy stress functions of the type $x^m y^n$ or of the type $r^n \cos \lambda\varphi$ cannot fulfill the boundary conditions along the two free edges.

There is some doubt whether the fourth singularity apart from the corner is necessary, and additional thoughts about these "academic" questions would be interesting indeed.

AUTHORS' CLOSURE

The authors are very grateful to Professor Mesmer for his pertinent observations. The reasoning behind his considerations about the angle between isostatic asymptotes at singular points on free straight boundaries is correct and can be found developed in detail in Professor Mesmer's book "Spannungsoptik" (Springer, Berlin, 1939), page 33. The authors pointed out that the brittle-coating results near the corner of the square plate may not be very accurate because of the very low state of stress present in the whole region. The sketch of Fig. 9 should be redrawn allowing for larger angles between the asymptotes at the singular points.

In respect to the fourth singular point, the authors wish to state that they cannot visualize the isostatic pattern without this point on the diagonal.

Steady-State Behavior of Systems Provided With Nonlinear Dynamic Vibration Absorbers[1]

N. J. DABROWSKI.[2] The existence of only one resonant frequency is intuitively correct. It is well known that a linear two-degree-of-freedom system has two resonant frequencies, one in which the masses are both in phase with the forcing vibration, the other in which one mass is out of phase. With a nonlinear spring between the masses, one would expect the two masses to be at corresponding points of their cycles only momentarily; that is, their phase relationship would continually be changing. If that is the case, then the distribution of vibrations of the second mass with respect to the first is random, and the resonant frequency of the system is the (suitably modified) resonant frequency of the first mass. That this frequency turns out to be the same as that for a single mass equal to the sum of the two given masses is also reasonable.

AUTHOR'S CLOSURE

The author wishes to invite attention to two possible points of misinterpretation which Mr. N. J. Dabrowski has kindly noted in a personal communication relating to this paper. It was noted that the *Conclusions* as stated applied to the particular type of systems generally described by Fig. 2 and not to those of Fig. 3 or Fig. 4 An inspection of the latter figures reveals a somewhat different behavior from the apparently general remarks made by the author.

The second point is the use of terms "positively" and "negatively" when discussing the results of Equations [16] and [24]. These terms were intended to convey the meanings "positive value" and "negative value," respectively. I agree with Mr. Dabrowski that in discussing limits it is important that ambiguity regarding the direction of change be avoided.

[1] By F. R. Arnold, published in the December, 1955, issue of the JOURNAL OF APPLIED MECHANICS, Trans. ASME, vol. 77, pp. 487–492.

[2] Research and Development Department, Electric Boat Division of General Dynamics Corporation, Groton, Conn.

Book Reviews

Servomechanisms

SERVOMECHANISMS AND REGULATING SYSTEM DESIGN. By Harold Chestnut and Robert W. Mayer. Vol. 2. John Wiley & Sons, Inc., New York, N. Y., 1955. Cloth, 6 × 9 in., xiii and 384 pp., illus., $8.50.

REVIEWED by JOHN A. HRONES[1]

IN their preface the authors state: "Volume II is devoted to the needs of the practicing designer and the advanced graduate student...design steps required to convert the control system parameters into suitable hardware terms are stressed so that dependable, serviceable, and reliable equipment can be obtained." They, however, also indicate in their preface the absence of any treatment of system components as such. Volume 2 is, therefore, concerned with the important analysis considerations leading to some necessary important design decisions where at least some of the realities of the character of the input, power requirements, and the presence of certain nonlinearities have been considered.

Early chapters are devoted to measurement of system characteristics, the influence of the nature of the input on system design, and the selection of the power element, and include a brief and simplified presentation of methods for handling noise. Chapter four deals with compensating networks. Schematics

[1] Professor of Mechanical Engineering, Massachusetts Institute of Technology, Cambridge, Mass. Mem. ASME.

of a considerable number of circuits in wide usage are listed in tabular form accompanied with their frequency-response attenuation characteristics and transfer characteristics.

Chapters five and six deal with the design of the electronics for both d-c and a-c servo systems. Chapters seven through nine are concerned with analysis techniques for systems in which certain types of nonlinearity occur. The following subject matter is discussed:

1 Linearization of systems with small departures from linearity.

2 Linearization of nonlinear elements in which large departures from linearity occur.

Included in the discussion of nonlinearities are saturation, deadband, hysteresis, backlash, and time-varying parameters.

The book is well written and obviously represents the result of mature experience in actual design work. The book is heavily weighted in the direction of frequency-response techniques. It includes illustrations from a number of fields of interest. An excellent bibliography is included. There are no problems. Valuable as the book is, it does not come to grips with the comprehensive problem of design of a complicated system. It leads the way to a block diagram with certain specifications established apparently with the hope always firmly fixed in the mind of the servo man that the boxes can be bought off the shelves of somebody's stockroom.

Hydrodynamics

THE THEORY OF HYDRODYNAMIC STABILITY. By C. C. Lin. Cambridge Monographs on Mechanics and Applied Mathematics. Cambridge University Press, New York, N. Y., 1955. Cloth, 5¼ × 8½ in., xi and 155 pp., fig., $4.25.

REVIEWED BY S. I. PAI[2]

ONE of the most interesting problems in fluid dynamics is the problem of the stability of a laminar flow and its transition to turbulence. This problem is also well known for its controversial nature and there are still many points unsettled, particularly about the relation between the stability of a laminar flow and its transition to turbulence. However, the investigation of the stability of a laminar flow due to infinitesimal disturbances has made great advances both in theory and in experimental results during recent years. It should be welcome by all of the scientists to see a definite survey in book form of this part of the problem by one of the most active workers in this field, Prof. C. C. Lin.

After a general discussion of hydrodynamic stability in chapter 1, the author gives the detailed treatment of the stability of two simplest types of flow by solving the eigenvalue problem associated with the linearized equation governing the disturbances of the exponential time factor. These flows are the Couette flow (chapter 2) which was first solved by G. I. Taylor and the plane Poiseuille flow (chapter 3) which represents the most extensive investigation of stability of parallel flows and which is based on the well-known Heisenberg-Lin theory.

The physical mechanism of instability is discussed in chapter 4 together with a brief account of the behavior of finite disturbance.

The theory of stability of parallel flows (chapter 3) is applicable to the flow which is essentially parallel to one direction such as boundary-layer flows. Thus the stability of flows of many practically important problems may be analyzed. In chapters 5 and 6, the results of stability theory of boundary-layer flow over a flat plate and other nearly parallel flows are discussed including such factors as compressibility, cooling and heating, pressure gradient, suction and injection, and curvature of the boundary.

Chapter 7 gives some examples of stability problems of interest in astrophysics and geophysics such as stability of zonal minds in the atmosphere, convective motion of a fluid heated from below or in the presence of a magnetic field.

Another interesting aspect of problems of hydrodynamic stability is attributable to the mathematical problems raised. Many of the controversial issues in this subject have been mathematical. The author made many valuable contributions to clarify these controversies.

In the last chapter the author gives a valuable analysis of the mathematical aspects for the stability of parallel flows.

There is an extensive bibliography at the end of this book which contains 258 items and which would be of great value to those who want to study further the stability problems or to know many other stability problems which have not been discussed in this book.

In reviewer's opinion, this book is an excellent review of stability theory of laminar flows and is recommended to all engineers and scientists working in the field of fluid dynamics.

[2] Associate Research Professor, Institute for Fluid Dynamics and Applied Mathematics, University of Maryland, College Park, Maryland.

Testing of Materials

DIE PRÜFUNG DER METALLISCHEN WERKSTOFFE. By E. Siebel and N. Ludwig. Vol. 2 of Handbuch der Werkstoffprüfung, edited by Erich Siebel. Springer-Verlag, Berlin, Göttingen, Heidelberg, Germany, 1955. Cloth, 9¾ × 6½ in., xv and 754 pp., 960 figs., DM 118.50.

REVIEWED BY A. ALI KHEIRALLA[3]

THE book under review is volume 2 of the Handbuch der Werkstoffpruefung (Second Edition) and consists of 11 sections written by 19 authorities in the field of mechanical testing.

An introductory section by U. Dehlinger summarizes the microstructural properties of metals and alloys and discusses briefly crystal lattices, transformations, polycrystalline materials, and the atomistic theory of strength.

Then follows a 104-page section on static strength testing by F. Koerber and A. Krisch. Included are the tensile test, the compression test, the buckling test, the bending test, the torsion test, shear and piercing tests, and the testing of materials under multiaxial loading.

The next section by K. Fink, Chr. Rohrbach, and R. Mailaender deals with strength testing under impulsive loading. Homogeneous uniaxial testing as well as inhomogeneous multiaxial impulsive loading is presented.

Fatigue testing forms the subject of section 3 (72 pages) which is divided into three parts dealing with fatigue strength as a material property, influences on technical fatigue strength, and durability of constructions. Included in the discussion are microstresses, damping, fracture characteristics, cold-working, heat-treating, multiaxial loading, size effects, prestressing, residual stresses, understressing, damage, influence of frequency and temperature, notch effects, surface finish, and corrosion.

A section by A. Pomp and K. Bungardt treats of strength testing at high and low temperatures. Tensile, drop, and fatigue as well as hardness and impact testing are discussed.

Hardness determination is the subject of section 5 by W. Hengemuehle. Spherical, conical, and pyramidal indentors, dynamic hardness testing, and hardness at elevated temperature are discussed.

The techniques of technological testing are covered by K. Wellinger in the sixth section while the testing of welds is presented by N. Ludwig in section 7.

[3] Lessells and Associates, Inc., Boston, Mass.

H. Mueller gives a short section on the testing of wire and cable, while miscellaneous tests form the subjects of section 9. Included in the latter are wear, bearing materials, machinability, erosion and corrosion testing.

Section 10 by F. Wever deals with the measurement of physical properties such as specific heat, thermal expansion, thermal conductivity, electrical conductivity, and so on.

A final section by A. Eichinger treats investigations connected with theories of strength.

Altogether, the material is well organized and presented. In some places there is a noticeable paucity of references to relevant American research. This is presumably due to poor liaison in the postwar period. In any case, the book can be well recommended for engineers in industrial research and testing laboratories.

Compressible Fluid Flow

THE DYNAMICS AND THERMODYNAMICS OF COMPRESSIBLE FLUID FLOW. Vol. 2. By Ascher H. Shapiro, Ronald Press Company, New York, N. Y., 1954. Cloth, 6 × 9 in., xi and 1185 pp., figs. 580, $16.

REVIEWED by WILLIAM R. HAWTHORNE[4]

THIS is the second of two volumes on the subject of compressible flow. The first volume, which was reviewed earlier in the Journal,[5] contained four parts dealing with basic principles, one-dimensional analysis, and introduction to two and three-dimensional compressible flow. Volume 2 contains four more parts, devoted to supersonic flow, mixed flow, unsteady motion in one dimension, and boundary layers. The volume maintains the high standard of presentation and clarity shown in Volume 1.

Part 5, on supersonic flow, contains a chapter on axially symmetrical supersonic flow, giving the solutions for flow past a cone and developing the linearized theory. The method of characteristics is also explained for both external and internal axisymmetric flow. The chapter contains useful summaries and comparisons of theoretical and experimental results. Chapter 18 deals with supersonic flow past wings of finite span. There is a discussion of the behavior of the flow over wings of different planform; a similarity rule is derived; linearized solutions are outlined using the method of supersonic source distributions and Büsemann's method of conical fields. Many theoretical results for differing planforms are quoted and some experimental results for comparison with the theory are given. Inevitably this chapter is highly condensed, so that it tends to be more of a summary than a text. However, large numbers of diagrams and references make it a useful chapter. Chapter 19 deals with hypersonic flow and is particularly valuable as a survey of up-to-date work. Similarity laws are derived, oblique shock and simple wave-expansion relations are given, the performance of two-dimensional profiles and bodies of revolution is covered. The chapter is noteworthy for the comparison between the approximate and exact theories and the summary of available experimental results.

[4] Hunsaker Professor of Aeronautics, Massachusetts Institute of Technology, Cambridge, Mass.

[5] The Dynamics and Thermodynamics of Compressible Fluid Flow (review by W. R. Hawthorne), JOURNAL OF APPLIED MECHANICS, Trans. ASME, vol. 77, March, 1955, pp. 159–160.

Part 4 starts with chapter 20 in which the hodograph method for mixed subsonic and supersonic flow is presented. The author applies the hodograph method formally and carefully to source and source vortex flows. He gives Ringleb's 180-deg turn flow in detail. The remainder of the chapter is devoted to a discussion of the limit line. It would have benefited the reader of this discussion if the geometrical and physical interpretations had been presented first. Chapter 21 deals with transonic flow and starts with an exposition of the similarity law which is then applied to shocks, expansions, and airfoils. The flow in nozzles is next examined and Emmons' solution by the relaxation method is presented. The chapter also includes a summary of behavior of airfoils at Mach number unity. Chapter 22 starts with a survey of the experimental confirmation of the transonic similarity law and then deals with the characteristics of wing profiles in the transonic range. There is a section on detached shocks, followed by a section on flow without shocks. The development of shocks is also described.

Part 7 contains three chapters devoted to unsteady one-dimensional flow. Chapter 23 deals with waves of small amplitude and develops solutions by the method of characteristics. This serves as an introduction to chapter 24 in which the solutions for finite disturbances by the method of characteristics are outlined. The presentation is detailed and elegant and includes examples showing the effect of intersections and reflections at open ends with and without flow. Changes in area, fixed and moving boundaries, and temperature discontinuities are also covered. This chapter gives a useful and adequate summary of the methods of calculation and is likely to be of considerable value to the engineer. Chapter 25 deals with moving shock waves. Analytical and graphical (the shock polar) methods are described for both weak and strong shocks. The effects of interferences and various types of reflections are included. There is an analysis of the shock tube and some comparison with experiment.

Part 8 deals with boundary-layer problems, chapter 26 giving the equations and a number of solutions for the laminar boundary layer. Chapter 27 deals similarly with the turbulent boundary layer. The author has achieved a reasonable balance between coverage of theory and experiment, although in the chapter on turbulent boundary layer the theory may occupy more space than it deserves! The volume finishes with chapter 28 which is devoted to a discussion of flow in tubes and to a well-illustrated survey of what is known about the interaction between shocks and boundary layers.

A volume which is intended to acquaint engineers with the latest developments in compressible flow is inevitably likely to arouse some criticism of its coverage. Some might prefer a fuller treatment of wings, others might wish that more attention had been paid to internal aerodynamics; e.g., the flow in turbine and compressor blading. The author has, however, managed to preserve a satisfactory balance and has generally succeeded in maintaining the clarity of his presentation of theoretical material in spite of its condensation. As a reference book for engineers it is likely to be extremely useful. It is not of course a textbook for general use, but for those who have mastered Volume 1, or who are already familiar with some aspect of compressible flow, it is eminently useful and stimulating further reading.

Are you making full use of these ASME Publications?

APPLIED MECHANICS REVIEWS — the magazine that is helping engineers in all parts of the world to survey worldwide advances in applied mechanics and related engineering science in a relatively short time, pinpoint any major developments in their fields in seconds, keep abreast of rapidly expanding scientific frontiers, and have a constant flow of new ideas, some of which have evolved into money-makers for them and their employers.

MONTHLY AMR brings its reader over three hundred reviews of the most significant contributions that have been culled from a thousand sources including seven hundred and fifty engineering periodicals of thirty countries, new technical books in all languages, and reports of industrial research laboratories everywhere. Each review is both a summary and a critical examination of the author's findings written by an expert in the field involved and signed, thus attesting to the authority for the opinion advanced.

Additionally, each number contains a specially prepared progress survey prepared by an international authority summarizing the important factors responsible for advances in a special branch of the field, interpreting the developments, and assessing their prospects. In the column at the right is a sampling of subjects regularly reviewed:

GENERAL: Theoretical and experimental methods, and mechanics. MECHANICS OF SOLIDS: Servomechanisms, governors, gyroscopics; Vibrations, balancing; Wave motion in solids; Impact; Elasticity theory; Experimental stress analysis; Rods, beams, cables, machine elements; Plates, disks, shells, membranes; Buckling problems; Joints and joining methods; Structures; Rheology; Failure, mechanics of solid state; Material test techniques; Mechanical properties of specific materials; Mechanics of forming and cutting. MECHANICS OF FLUIDS: Hydraulics, cavitation, transport; Incompressible flow; Compressible flow, gas dynamics; Wave motion in fluids; Turbulence, boundary layer; Aerodynamics of flight, wind forces; Aeroelasticity; Propellers, fans, turbines, pumps; Flow and flight test techniques. HEAT: Thermodynamics, heat and mass transfer, combustion. MISCELLANEOUS: Acoustics; Ballistics; Soil mechanics, seepage; Micromeritics; Geophysics, meteorology, oceanography; Lubrication, bearings; Marine engineering problems; Biomechanics.

Subscription price to nonmembers, $25; to ASME members, $10

Proceedings, SECOND U. S. NATIONAL CONGRESS OF APPLIED MECHANICS

Makes accessible the findings of original researches and the current approach to important problems by the use of new analytical tools and procedures.

Each of the 99 papers in this 825-page book is an individual treatise which can be studied independently. Collectively they form an invaluable record of recent advances made in connection with significant problems encountered throughout modern applied mechanics including kinematics, dynamics, vibration, wave motion; mechanical properties of material and failure; stress analysis, elasticity, plates and shells; plasticity, fluid flow, aerodynamics, and heat transfer.

Price to nonmembers and ASME members, $9

DESIGN DATA AND METHODS— APPLIED MECHANICS

A collection of original and practical contributions. The data in this publication have been drawn chiefly from the Journal of Applied Mechanics. They include stress and deflection methods applied to circular and rectangular plates; analysis of circular beams; information on hydrostatic testing and variable-section column problems; design data for piping; data on stress concentrations, torsion, helical compression and tension springs, thermal stresses, stresses in pressure vessels, shrink-fitted assemblies, and thick-walled cylinders. There are also numerical solutions of gas flow problems, information on two-dimensional supersonic flow; a chart for oblique shock waves under water; accurate bearing calculations; and methods of treating and solving problems of vibration and of balancing rotating apparatus.

Pub. 1953. Price to nonmembers, $4; to ASME members, $3.20.

The American Society of Mechanical Engineers

29 West 39th Street — New York 18, N. Y.

[redacted]